UNIVERSITÉ DE LORRAINE

AVERTISSEMENT

Ce document est le fruit d'un long travail approuvé par le jury de soutenance et mis à disposition de l'ensemble de la communauté universitaire élargie.

Il est soumis à la propriété intellectuelle de l'auteur. Ceci implique une obligation de citation et de référencement lors de l'utilisation de ce document.

D'autre part, toute contrefaçon, plagiat, reproduction illicite encourt une poursuite pénale.

Contact : ddoc-theses-contact@univ-lorraine.fr

LIENS

Code de la Propriété Intellectuelle. articles L 122. 4
Code de la Propriété Intellectuelle. articles L 335.2- L 335.10
http://www.cfcopies.com/V2/leg/leg_droi.php
http://www.culture.gouv.fr/culture/infos-pratiques/droits/protection.htm

UNIVERSITÉ DE LORRAINE

LRGP LABORATOIRE RÉACTIONS ET GÉNIE DES PROCÉDÉS

SIMPPÉ Ecole Doctorale Sciences et Ingénierie des Molécules Procédés Produits et Énergie

University of Lorraine

Thesis submitted in partial fulfillment of the requirements for the Doctor of Philosophy from University of Lorraine

GENIE DES PROCEDES, DES PRODUITS ET DES MOLECULES

Presentee et soutenue publiquement
le 16 juillet 2019

Study of the separation by organic solvent nanofiltration of diluted solutes using commercial, dense and porous membranes and their derivatives by deposition of polyelectrolyte nanolayers.

Mahbub MORSHED

Composition of the Jury:

Rapporteurs

Bart Van der Bruggen, *Professor, KU Leuven*

Boris Lakard, *Professor,University of Franche-Comte*

Examinateurs:

Eric favre, *Professor, University of Lorraine (UL)*

Murielle Rabiller-Baudry, *Professor,University of Rennes*

Denis ROIZARD, *DR, CNRS,UL (Thesis director)*

Halima Alem, *Asst. professor,UL.(Thesis co-director)*

Scientific Valorization

Scientific articles

N°1. Organic Solvent Nanofiltration (OSN) performance of commercial membranes and their further surface functionalization, *Recents Progres en Genie des Procedes, Numero 110-2017 ISSN: 1775-335X; ISBN: 978-2-910239-85-5, Ed. SFGP, Paris, France.*
N°2. Investigation of new modification strategies for PVA membranes to improve their dehydration properties by pervaporation, *Applied Surface Science 450 (2018) 527537*
N°3. Investigation of OSN properties of PDMS membrane for the retention of dilute solutes with potential industrial applications, *J. APPL. POLYM. SCI. 2019, DOI: 10.1002/APP.48359*
N°4. PDMS membranes modified by polyelectrolyte multilayer deposition to improve OSN separation of diluted solutes in toluene, *Manuscript submitted for publication.*

Seminars and Conferences

N°1. Poster presentation in Journee des Doctorants, organized by CFM (club francais des membranes), April7 2016, Paris.
N°2. Oral presentation in SFGP2017, 11-13 July, Nancy.
N°3. Oral presentation in 6th International Conference on Organic Solvent Nanofiltration Saint Petersburg, Russia, 04-06 June 2017.
N°4. Poster presentation in the 11th International Congress on Membranes and Membrane Processes (ICOM 2017), 29th July 4th August 2017, San Francisco, CA, USA.
N°5. Oral presentation in 4th International conference on membranes (ICM-2017), Kerala, India, Sept.30-Oct.3 2017.
N°6. Seminar Journee OSN (Organic Solvent Nanofiltration), Paris, 23 November 2018.
N°7. Technical Meeting ANR n°002, Paris, 8th July 2015.
N°8. Technical Meeting ANR n°003, Rennes, 29th January 2016.
N°9. Technical Meeting ANR n°004, Rennes, 29th June 2016.
N°10. Technical Meeting ANR n°005, Nancy 13th April 2017.
N°11. Technical Meeting ANR n°006, Paris 26th September 2017.

Contents

Summary of the manuscript in French xi

List of Abbreviations xxix

List of Figures xxxi

List of Tables xxxvii

0.1 Introduction . . . 1
0.1.1 Graphical abstract of OSN study plan and organization of the manuscript 3
0.1.2 Context of the project . . . 4
0.2 Ph.D. Objectives and tasks . . . 6
0.2.1 Objectives . . . 7
0.2.2 Tasks to obtain the objectives . . . 8
0.2.2.1 PHASE 1 . . . 8
0.2.2.2 PHASE 2 . . . 9
0.2.2.3 PHASE 3 . . . 9

1 LITERATURE REVIEW 11
1.1 General Introduction . . . 13
1.2 OSN main feature . . . 14
1.2.1 OSN performance parameters . . . 16
1.2.1.1 Flux . . . 16
1.2.1.2 Permeability/Permeance . . . 16
1.2.1.3 Retention or rejection and transmission . . . 16
1.3 Operating modes of OSN: dead-end and cross-flow . . . 17
1.4 OSN membrane materials . . . 18
1.5 OSN Commercial membranes . . . 20
1.5.1 Prominent OSN membranes based on Polyimide (PI) . . . 22
1.5.2 Prominent OSN membranes based on Polydimethylsiloxane (PDMS) . 22
1.5.2.1 Comparison of toluene permeance in PDMS and PI membranes from literature . . . 22
1.5.3 Prominent OSN membranes based on other polymers . . . 23
1.6 Applications of OSN . . . 23
1.7 Solute rejection by PDMS and PI in toluene media . . . 24
1.8 Homogeneous catalyst recovery by OSN in toluene media . . . 27
1.9 Mass transport mechanisms . . . 30
1.9.1 Fundamentals of mass transport in membranes . . . 30
1.9.1.1 Transport through porous membranes . . . 30

1.9.1.2 Transport through dense membranes 30
1.9.1.3 Solution-diffusion model 31
1.9.1.4 Free volume diffusion model 31
1.9.2 Molecular transport in polymeric systems 34
1.9.2.1 Diffusion in rubbery polymer 34
1.9.2.2 Diffusion in glassy polymer 35
1.9.2.3 Diffusion in polymer blend 35
1.10 OSN parameters 35
1.11 Modification of OSN membranes and expected properties after modification . 38
1.11.1 Plasma assisted activation and/or modification 42
1.11.1.1 Surface modification by plasma 43
1.11.1.2 Inert gas plasmas 43
1.11.1.3 Oxygen-containing plasmas 45
1.11.1.4 Other plasmas 45
1.11.1.5 Plasma effect 45
1.11.2 Polyelectrolytes multilayer (PEM) by Layer by Layer (LbL) 46
1.11.2.1 General feature 46
1.11.2.2 Fundamentals of polyelectrolytes multilayer (PEM) 47
1.11.2.3 Formation of PEM complexes 47
1.11.2.4 Parameters affecting the multilayer thickness and mechanism of conformational changes 48
1.11.2.5 Application of polyelectrolytes in membrane modification . 48
1.11.2.6 Polyelectrolytes on OSN membrane and layer growth model 49
1.11.2.7 Permeability in OSN membranes after PEMs modification . 50
1.11.2.8 Bilayers number and rejection in OSN 51
1.11.2.9 Cross-linking by PEM affecting OSN performance 52

2 Performance of OSN Commercial membranes 55
2.1 Characterization of OSN commercial membranes 56
2.1.1 Characterization by Water Contact Angles (WCA) 56
2.1.2 Characterization by scanning electron microscope 57
2.1.2.1 Dense OSN membrane 57
2.1.2.2 Porous OSN membranes 58
2.1.3 Gas permeation in OSN membranes 59
2.1.4 Summary of membrane characterization 60
2.2 Solvent fluxes and solutes rejection in commercial OSN membranes 61
2.2.1 The effect of transmembrane pressure on toluene fluxes in dense and porous OSN membranes 61
2.2.2 Rejection of diluted R-BINAP and C44 by commercial dense and porous membranes in toluene 61
2.2.3 Rejection of hydroformylation catalyst and ligand by the commercial dense and porous membranes in toluene 62
2.3 Complimentary experiment: Investigation on the oxidation possibility of dilute R-BINAP in toluene under OSN condition 63
2.4 Conclusion and perspective 64
2.5 Article 1: Published in Journal of Applied Polymer Science 66

3 Dense system: PDMS membrane and modification of PDMS by plasma and polyelectrolytes 79
3.1 Background . . . 79
3.2 Abstract . . . 80
3.3 Article 2: Published in Applied Surface Science . . . 81
3.4 Article 3: Manuscript submitted for publication . . . 93
3.5 Transport mechanism through PEM composite membrane . . . 113
3.6 Characterization of modified PDMS . . . 114
3.6.1 Water contact angle before and after OSN in PDMS based PERVAP 4060 . . . 114
3.6.2 Effect of plasma and polyelectrolytes multilayer by water contact angles 115
3.6.2.1 Plasma effect by surface hydrophilicity . . . 115
3.6.2.2 Polyelectrolytes choice and water contact angles after the deposition of multilayers on PDMS . . . 117
3.7 Ellipsometric thickness of polyelectrolytes multilayer . . . 119
3.8 Permeability of pure gases . . . 121
3.9 Polyelectrolytes chain mobility by Fluorescence recovery after photobleaching (FRAP) . . . 126
3.10 Membrane characterization before and after OSN . . . 127
3.11 Performance of modified PERVAP 4060 (PDMS) membrane . . . 130
3.11.1 Effect of plasma exposure time on solvent permeation . . . 130
3.11.2 Effect of toluene permeation in PEM prepared without plasma . . . 130
3.11.3 Effect of number of bilayers of PEM on toluene permeation . . . 131
3.11.4 Toluene and ethanol permeation in modified membranes . . . 132
3.11.4.1 Tentative prediction of solubility parameters of polyelectrolyte multilayers by Hansen solubility parameter and Fedor group contribution . . . 132
3.11.4.2 The effect of polyelectrolyte multilayers (PEMs) properties of swelling, charge density and thickness for the permeation of toluene and ethanol . . . 133
3.11.4.3 Estimation of the toluene and ethanol diffusion coefficient in polyelectrolytes multilayer (PEM) . . . 134
3.12 Solute rejection in polyelectrolytes multilayer (PEMs) modified PERVAP 4060 (PDMS) . . . 135
3.12.1 Effect of transmembrane pressure (TMP) on toluene flux and R-BINAP rejection in (PAH/PSS) modified PERVAP 4060 . . . 135
3.12.2 Effect of the number of PAH/PSS bilayers on PERVAP4060 for the toluene flux and R-BINAP rejection . . . 136
3.12.3 Effect of salt on the polyelectrolyte multilayer for toluene flux and R-BINAP rejection . . . 137
3.12.4 Evolution of toluene flux and R-BINAP rejection in PAH/PSS modified PERVAP4060 (PDMS) membranes having different bilayers number . 138
3.12.5 Intrinsic permeance in polyelectrolyte multilayers by resistance in series while PEM is deposited on PERVAP4060 (PDMS) . . . 139
3.13 Study on the rejection of R-BINAP from EtOH-Toluene mixture using the PERVAP 4060 (PDMS) . . . 140
3.14 Conclusion . . . 141

4 OSN study on porous systems modified by polyelectrolytes multilayers 143
4.1 Abstract . . . 144
4.2 Characterization of the porous membranes . . . 144
4.2.1 Surface hydrophilicity of PAN after PEM modification . . . 146
4.3 Performance of pristine porous membranes by solvent fluxes . . . 146
4.3.1 Investigation on TMP in pristine PAN for steady flux and rejection . 148
4.3.2 Investigation on transmembrane pressure effect on flux and rejection in pristine PAN . . . 149
4.3.3 Long term study of pristine PAN on toluene flux and R-BINAP rejection at 10 and 20 bar . . . 150
4.4 Rejection of diluted R-BINAP and C44 by pristine PAN and AMS 3012 in toluene at 10 bar . . . 152
4.4.1 Hagen Poiseuille (H-P) model for solvent fluxes at 10 bar . . . 153
4.5 Performance of PEM modified AMS 3012 by toluene fluxes and C44 rejection 154
4.6 Permeation of pure solvents in PEM modified PAN membranes . . . 156
4.6.1 Air permeability in modified PAN . . . 157
4.6.2 Porosity by the mercury porosimetry . . . 158
4.7 OSN study for the solute rejection in PAN . . . 160
4.7.1 Solute rejection by pristine and modified PAN from the diluted binary feed in toluene . . . 160
4.8 Solute rejection by pristine and modified PAN from ternary feed mixtures . . 162
4.9 Effect of concentration in C16 wt.% in the ternary mixture of R-BINAP, C16 in toluene . . . 163
4.10 Conclusion . . . 163

5 Study of process parameters on OSN results and their perspectives 165
5.1 Abstract . . . 166
5.2 Effect of cross-flow feed conditions on OSN membrane performance . . . 166
5.2.1 Effect of cross-flow velocity on solvent flux and solute rejection . . . 166
5.3 Determination of concentration polarization from cross-flow velocity . . . 168
5.3.1 Theory (Baker et al., 1997) (Baker, 2000) . . . 168
5.3.2 Determination of concentration modulus: R-BINAP-toluene. . . . 170
5.4 Effect of hydrodynamic flow on flux and rejection in pristine and modified PERVAP4060(PDMS) . . . 171
5.5 Effect of pressure in OSN process for solvent transport and solute rejection in dense PERVAP4060(PDMS) . . . 174
5.5.1 Effect of pressure on flux and rejection though PERVAP4060 for R-BINAP in toluene . . . 175
5.5.2 Effect of pressure on flux and rejection though PERVAP4060 for ToABr in toluene and ethanol . . . 175
5.6 Advantages of OSN over distillation in energy saving . . . 176
5.7 Improving OSN separation by the multi-stage cascades . . . 178
5.8 Hybrid processes . . . 181
5.8.1 OSN with distillation . . . 181
5.8.2 Hybrid of OSN with pervaporation (PV) or dual stage OSN . . . 182
5.9 Conclusion . . . 184

6 Materials and methodologies **185**
6.1 Materials . . . 185
6.1.1 Commercial membranes used for OSN study . . . 185
6.1.2 Polyelectrolytes (PELs), solvent and solutes used for OSN membrane performance . . . 186
6.2 Part 1: Characterization methods . . . 187
6.2.1 Contact angle . . . 187
6.2.2 Scanning electron microscope (SEM) . . . 188
6.2.3 Atomic force microscope (AFM) . . . 188
6.2.4 Fluorescence Recovery After Photobleaching (FRAP) . . . 189
6.2.5 Gas permeability measurement . . . 190
6.2.6 Mercury porosimetry . . . 191
6.2.7 Air permeability . . . 192
6.3 Part 2: modification and performance methods . . . 192
6.3.1 Plasma modification . . . 192
6.3.2 Layer by Layer(LbL)modification by Polyelectrolytes . . . 193
6.3.3 LRGP- OSN set-up . . . 194
6.4 Part 3: Analytical method . . . 197
6.4.1 Analysis by Gas Chromatograph (GC) . . . 197

7 Conclusion **201**
7.1 Literature review . . . 201
7.2 Investigation of the OSN mass transfer properties of dense and porous polymeric membranes . . . 202
7.3 Modification and characterization of dense membranes . . . 203
7.4 Modification and characterization of porous membranes . . . 207
7.4.1 Protocol for the characterization of unknown membrane structure and potential mass transport model: . . . 207
7.5 Perspective . . . 208

Appendix **211**

Bibliography **221**

Index **244**

Avis de Soutenance **247**

Summary of the manuscript in French

Ecole Doctorale Sciences et Ingénierie des Molécules Procédés Produits et Énergie

Résumé français de du manuscrit de thèse

Fractionnement par nanofiltration organique de mélanges liquides modèles de milieux de métathèse. Etude de membranes commerciales, denses et poreuses, et de leurs dérivés obtenues par dépôt de nanocouches de polyélectrolytes

M. Mahbub MORSHED

Directeur de Thèse: Dr. Denis ROIZARD

Co-Directeur de Thèse: Halima ALEM-MARCHAND

Composition du jury:

Rapporteurs

Bart VAN DER BRUGGEN, Professeur, Université Catholique de Louvain (Belgique)
Boris LAKARD, Professeur, Institut UTINAM Besançon Cedex

Examinateurs

Eric FAVRE, Professeur, Université de Lorraine.
Murielle RABILLER-BAUDRY, Professeur, Université de Rennes 1
Denis ROIZARD, DR CNRS, Université de Lorraine
Halima ALEM-MARCHAND, Maître de conférences, Université de Lorraine

Introduction et contexte du projet

Le manuscrit **“ Fractionnement par nanofiltration organique de mélanges liquides modèles de milieux de métathèse. Etude de membranes commerciales, denses et poreuses, et de leurs dérivés obtenues par dépôt de nanocouches de polyélectrolytes”** intétègre les aspects suivants:

- Revue bibliographique sur les membranes de nanofiltration organique (OSN) commerciales denses et poreuses, leur disponibilité commerciale et leurs performances en milieu organique.
- Etude et modification des membranes commerciales pour améliorer leurs performances.
- Caractérisation de ces membranes et des mécanismes de transfert pour la séparation de mélanges liquides modèles de catalyseurs homogènes de métathèse.

L'objectif global du doctorat est de réaliser la tâche de séparation prévue dans le projet ANR MemChem (http://www.agence-nationale-recherche.fr/Project-ANR-14-CE06-0022). Dans le cadre de l'ANR, l'hydroformylation a été considérée comme la réaction modèle (Figure 1, a). Une fois la réaction terminée, il faut séparer le produit catalyseur et le solvant. À l'heure actuelle, la technologie utilisée est la distillation, qui consomme beaucoup d'énergie et provoque une dégradation irréversible du catalyseur. La vision du doctorat consiste à remplacer la distillation par OSN (figure 1b), ce qui devrait permettre d'obtenir un rejet élevé du catalyseur avec une perméation élevée du produit dans des conditions de fonctionnement douces. En cas de succès, OSN constituera une alternative intéressante à la séparation des catalyseurs, qui apportera un avantage considérable en termes d'économie d'énergie et d'environnement.

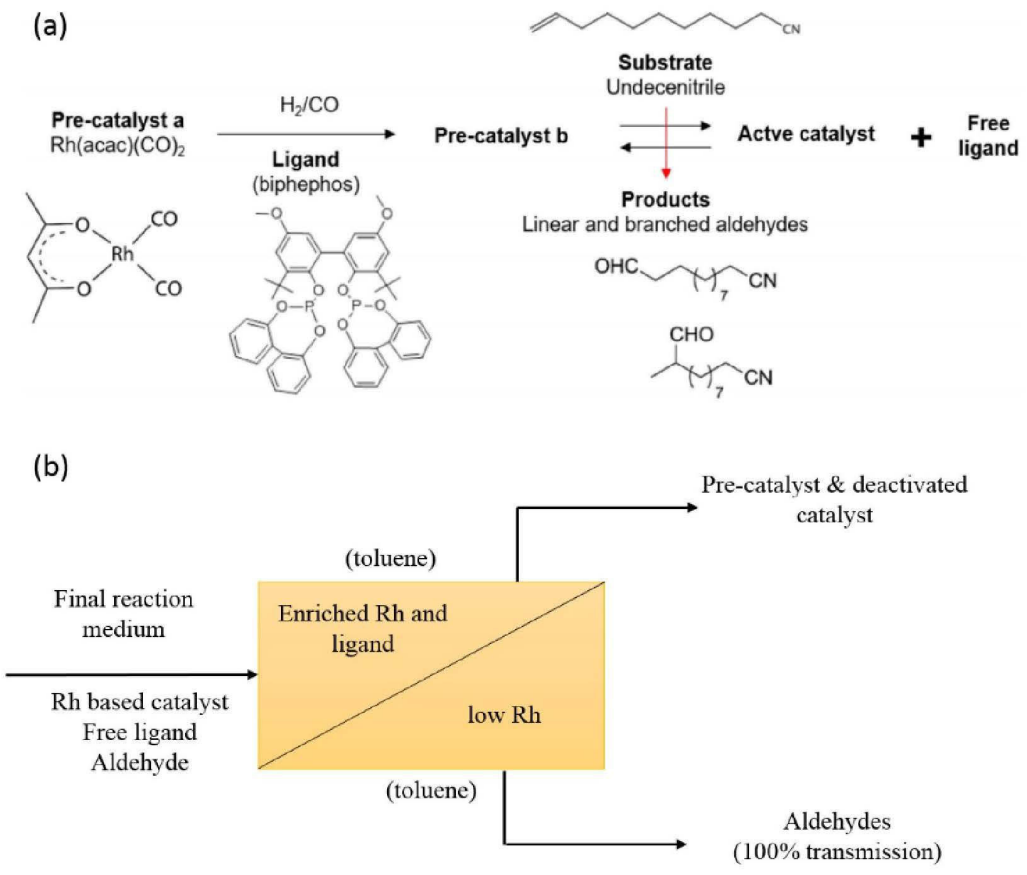

Figure 1: (a) Réaction d'hydroformylation (adoptée à partir du cadre de l'ANR) (b) Séparation proposée basée sur l'OSN (schéma).

L'objectif du doctorat est de développer une séparation OSN qui pourrait retenir en amont de la membrane un catalyseur coûteux à base de rhodium tout en permettant au produit et au solvant de traverser la membrane. Le projet ANR MemChem est divisé en 3 tâches de travaux interconnectés (WP) (Figure 2) Ce doctorat est centré sur la partie WP3 :

- WP 1: Etude de la synthèse des réacteurs batch.
- WP 2: Études fondamentales de la nanofiltration utilisant des milieux organiques.
- **WP 3: Matériaux membranaires pour l'hydroformylation.**

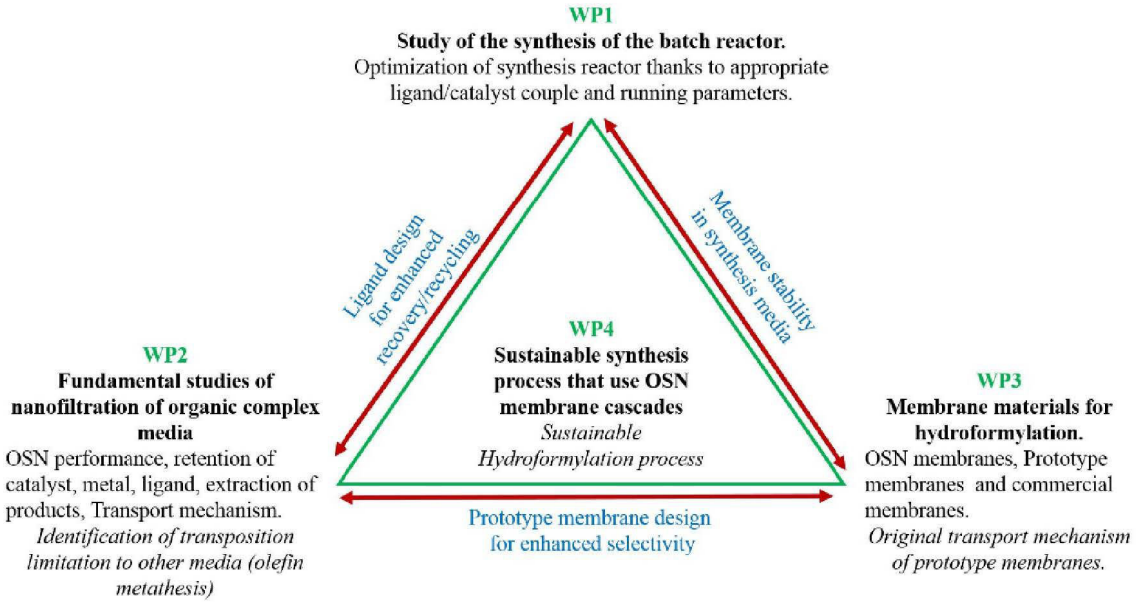

Figure 2: Programme de travail du projet ANR et interconnexions R & D

Objectifs de la thèse

1. Le premier objectif de ce travail était de trouver une membrane commerciale appropriée qui serait stable dans des conditions OSN et conduirait à un rejet important du catalyseur du toluène tout en permettant la perméation du produit de la réaction, une condition pré-établie de l'ANR. .

2. Le deuxième objectif consistait à appliquer une stratégie de modification permettant d'optimiser les propriétés de transfert de masse de la membrane commerciale vierge afin d'améliorer les performances de séparation.

3. Le troisième objectif était d'analyser les résultats expérimentaux afin de comprendre les relations structure-propriétés et d'étudier le mécanisme de séparation qui peut être un sujet assez controversé dans OSN.

Organisation des chapitres

Le manuscrit est divisé en plusieurs chapitres:

Chapitre 1: Revue de littérature.

Points forts

Étude de la disponibilité des membranes OSN du commerce et de leurs performances de rejet dans du toluène.
Obtenir des membranes commerciales crédibles adaptées à l'objectif ANR.
Étude de différentes approches de modification pour les nouvelles membranes OSN.
Effet du plasma et du polyélectrolyte sur la surface du polymère.

Chapitre 2: Performances des membranes commerciales OSN.

Points forts

Examen primaire de certaines membranes commerciales par OSN pour trouver la membrane la plus performante.
Développement de la stratégie expérimentale et de la priorité de la membrane la plus performante, obtenue à partir du test primaire OSN.

Chapitre 3: Membranes de PDMS denses et membranes modifiées associées par dépôt de plasma et de polyélectrolytes par la méthode LbL.

Points forts

Préparation de prototypes de membranes par polyélectrolytes multicouches (PEM) par approche de modification couche par couche (LbL).
Sélection des polyélectrolytes (PEL), du nombre de bicouches et de la condition de dépôt pour développer un nouveau protocole OSN.
Appliquer ces prototypes de membranes pour la séparation du catalyseur dilué dans le toluène.
Étudiez les flux OSN binaires et ternaires pour trouver le PEM le plus performant pour les objectifs ANR.

Chapitre 4: Etude OSN de systèmes poreux modifiés par des polyélectrolytes multicouches

Points forts

Etude des membranes OSN poreuses et de leurs performances après dépôt de PEM.
Comparaison des performances avec des membranes denses après application du même protocole PEM.
Décision rationnelle sur les membranes denses / poreuses à prendre en compte pour l'objectif ANR.

Chapitre 5: Influence des paramètres opératoires

Points forts

Étude de paramètres de procédé tels que l'effet de l'hydrodynamique, du débit tangentiel et de la polarisation de concentration (CP) en utilisant la membrane la plus performante
Faisabilité de la membrane à l'échelle du procédé.
Possibilité d'appliquer OSN en cascade et comparaison entre le droit sur l'énergie de l'OSN et la distillation
Procédé OSN hybrids

Chapitre 6: Matériels et methods

Chapitre 7: Conclusion

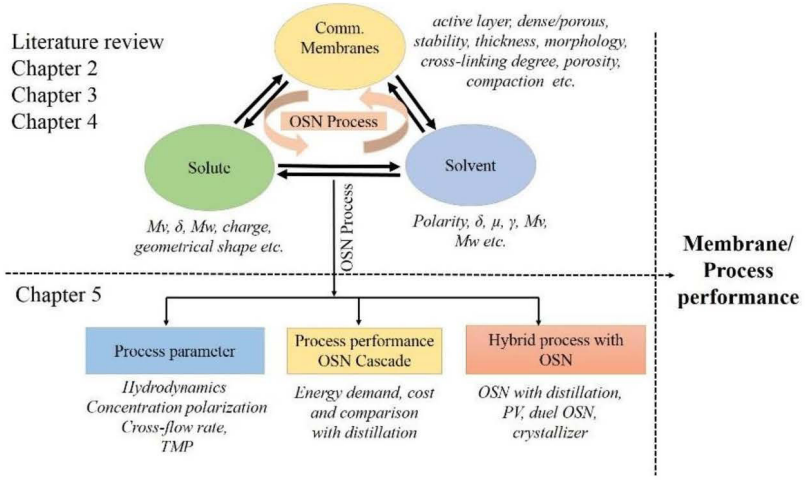

Figure 3: Aperçu du doctorat manuscrit organisé en différents chapitres.

Chapitre 1: Revue de la littérature.

La revue de la littérature se concentre sur les articles d'OSN publiée entre 2000 et 2019 pour identifier les membranes commerciales disponibles en OSN (Tableau 1). Cette étude a été poursuivie en tenant compte des performances de ces membranes OSN dans différents milieux organiques, du mécanisme de transport de masse, du mode de fonctionnement OSN, du processus de fabrication de la membrane et de la comparaison entre membranes céramiques et polymères.

La revue de littérature se concentre sur les articles scientifiques OSN publiés principalement au cours des deux dernières décennies.

Nom commercial / fabricant	Couche de séparation	Dense / poreux
Pervap 4060 / Sulzer	PDMS	Dense
MPF 44 / Koch membrane	PDMS	Dense
MPF 50 / Koch membrane	PDMS	Dense
GMT-oNF-2/GMT	PDMS	Dense
SolSep NF 070706 / SolSep	PA/PDMS	Dense
SolSep NF 010306 / SolSep	PA/PDMS	Dense
SolSep NF 010206 / SolSep	PA/PDMS	Dense
SolSep NF 030306 / SolSep	PA/PDMS	Dense
SolSep NF 030306F / SolSep	PA/PDMS	Dense
SolSep NF 030105 / SolSep	PA/PDMS	Dense
Starmem 120 / MET	PI	Dense
Starmem 122 / MET	PI	Dense
Starmem 240 / MET	PI	Dense
Starmem 400 / MET	PI	Dense
DuraMem 200 / MET	PI	Dense
DuraMem 400 / MET	PI	Dense
PuraMem 280 / MET	PI (enduit de silicone)	Dense
PuraMem 600 / MET	PI (enduit de silicone)	Dense
NanoPro S 3012 / AMS	PAN	poreux
NanoPro S 3014 / AMS	PAN	poreux
Desal 5 / Osmonics	PA	inconnu
Desal 5-DK / Osmonics	PA	inconnu
N3oF /Nadir	PES	inconnu
NF PES 010/Nadir	PES	inconnu

Tableau 1: Membranes OSN commerciales, leurs matériaux de couche actifs et leur nature dense / poreuse.

Les membranes céramiques présentent une limite de masse moléculaire élevée et un coût de matériau élevé ; de plus, ces membranes sont difficiles à produire à échelle industrielle par rapport aux membranes polymères. Par conséquent, ce type de membrane a été exclu de la sélection du matériau.

Sur la base de la disponibilité, il n'existe que quelques membranes commerciales présentant des performances de séparation élevées dans les milieux organiques; parmi eux, STARMEM, MPF, GMT-onF et SOLSEP. Ces membranes polymères OSN présentent des caractéristiques attrayantes telles que la facilité d'application, une stabilité dans les produits organiques, une résistance aux contraintes mécaniques et des caractéristiques de séparation élevées dans différents milieux organiques. La préoccupation essentielle est que ces membranes sont peu disponibles ou difficiles à obtenir du fournisseur. Même si le fournisseur fournit la membrane, souvent, les informations primaires sur ces membranes ne sont pas divulguées, telles que les matériaux des couches actives, le support et la nature de la surface (dense / poreuse). En outre, le fournisseur interdit souvent les recherches complémentaires pour étudier la caractérisation des matériaux. Il n'y a pas d'indication claire sur le type de couche active dans les membranes commerciales : si la membrane est constituée avec une couche active dense ou poreuse, son mécanisme de transport de matière peut être très différent. Dans la littérature, des mécanismes de transport de matière souvent contradictoires sont rapportés. Le choix du polymère pour les membranes OSN est limité en nombre. La plupart des fabricants du commerce ont recours à deux polymères principaux pour la fabrication de la couche active de séparation de la membrane: le polyimide (PI) et le polydiméthylsiloxane (PDMS).

Ensuite, le rejet de solutés par le PDMS et l'IP dans le toluène est axé sur la littérature et le masse moléculaire des solutés par rapport au rejet signalé est tracé séparément (Figure 4). Aucune corrélation claire n'a été obtenue.

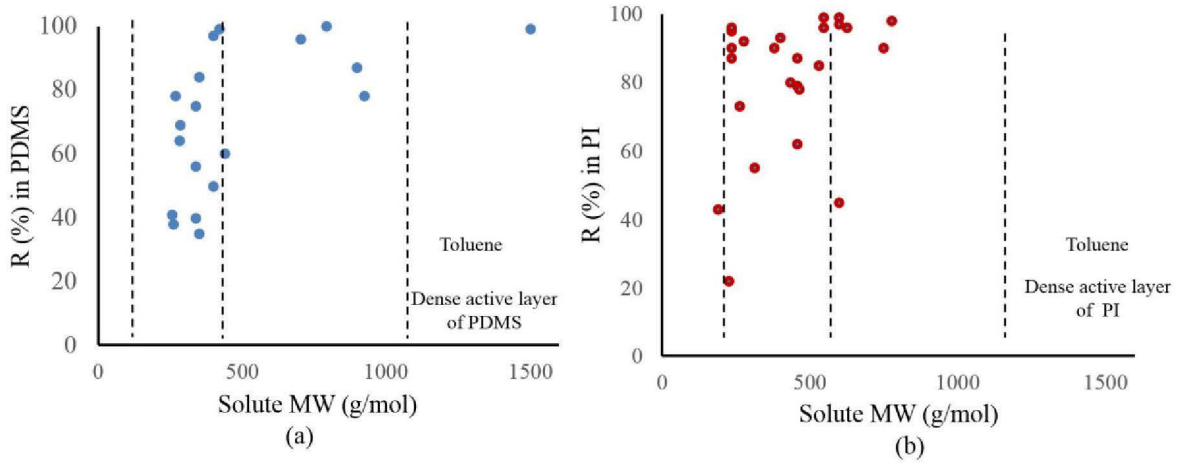

Figure 4: Performance de rejet de la membrane OSN en fonction du masse moléculaire (MW) du toluène: (a) PDMS (b) PI.

Il est donc plutôt difficile de choisir une seule membrane OSN pour la tâche ANR, car les membranes OSN potentielles sont peu nombreuses et la prévision de leurs performances vis-à-vis d'un système soluté-solvant n'est pas encore possible. C'est pourquoi deux types de membranes, denses et poreuses, ont été choisies pour une étude expérimentale préliminaire.

Quatre membranes OSN ont été sélectionnées en fonction de leur disponibilité commerciale et de leur couche active. Ces membranes comprennent deux membranes denses : PERVAP4060, une base de PDMS principalement utilisée dans la pervaporation, SOLSEP 010206, principalement utilisée dans la nanofiltration, et deux membranes poreuses : AMS S3012, une membrane nanoporeuse et PAN, un support microporeux.

L'un des principaux défis des membranes OSN est de maintenir une stabilité élevée de ces membranes dans différentes conditions d'alimentation. La modification de la couche sélective de membranes OSN est la principale approche pour développer des membranes fonctionnalisées qui présentent des sélectivités élevées stables et des perméabilités sans compromettre la nature fondamentale des stabilités dans une large gamme de solvants. Des méthodes telles que le greffage, la modification induite par la lumière, le traitement au plasma et la modification de polyélectrolytes pourraient être la clé pour obtenir des membranes OSN de nouvelle génération. La modification de la surface des membranes a été choisie comme une approche rapide et rationnelle pour obtenir de nouveaux prototypes de membranes OSN à partir de matériaux disponibles dans le commerce.

Chapitre 2: Performances des membranes commerciales OSN.

Ce chapitre présente les performances des membranes commerciales d'intérêt pour l'OSN. Les membranes OSN choisies sur la base de la revue de littérature sont PERVAP 4060 (dese, PDMS), SOLSEP 010206 (dense, supposé PDMS), AMS S3012 (nanoporeux, PAN), support de PAN (poreux, PAN). Les performances de ces membranes ont été mesurées par flux de toluène et rejet du catalyseur soluble dilué 2,2'-bis (diphénylphosphino) -1,1'-binaphtyle (R-BINAP, masse moléculaire 622 g.mol-1) dans le toluène, de structure moléculaire similaire du catalyseur-ligand d'hydroformylation. Le rejet de n-tétratétracontane dilué (C44H90 ou C44, MW 619 g.mol-1) dans le toluène a également été considéré pour expliquer le mécanisme de transport de masse.

Le flux de toluène et le rejet de R-BINAP et de C44 dilués (figures 5 et 6) dans ces membranes commerciales indiquent que PERVAP 4060 est la membrane dense la plus performante pour la séparation de catalyseurs.

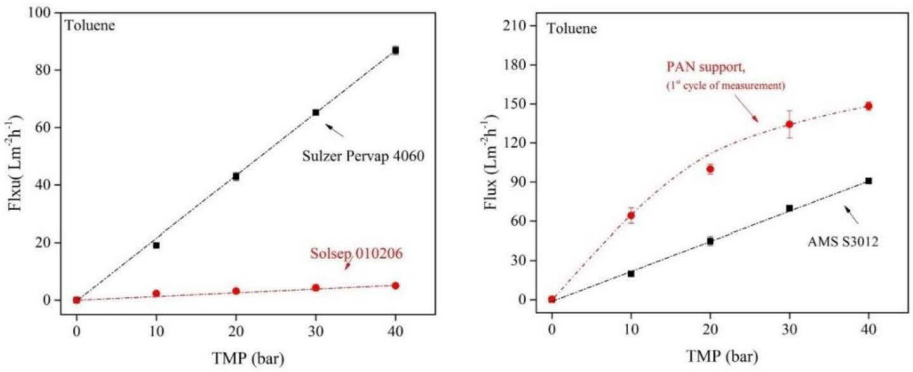

Figure 5: Effet de la pression transmembranaire sur les flux de toluène dans les membranes OSN denses (à gauche) et poreuses (à droite), à 30 ° C et à un débit d'alimentation tangentielle de 7 à 10 kg / h.

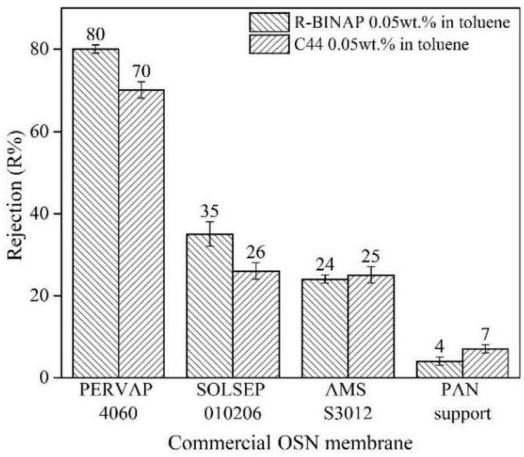

Figure 6: Performances des membranes commerciales en termes de rejet dilué de R-BINAP et de C44 dans le toluène, à 10 bar et 30 ° C.

Ensuite, PERVAP 4060 a été envisagé pour une étude détaillée de la séparation du R-BINAP dilué, du catalyseur de transfert de phase bromure de tétraoctylammonium (ToABr) et du n-hexadécane (C16H34 ou C16) dans du toluène. Les aliments OSN binaires et ternaires ont été utilisés pour se conformer aux objectifs ANR du système de métathèse / hydroformylation. Les résultats détaillés de l'étude sur PERVAP 4060 sont présentés dans l'article 1 soumis, intitulé

“Investigation of OSN properties of PDMS membrane for the retention of dilute solutes with potential industrial applications”

Ce chapitre met également en évidence la décision stratégique de la prochaine étude expérimentale.

1. Dans OSN, les nouveaux prototypes de membranes sont une demande réelle pour se conformer à la séparation du catalyseur d'hydroformylation. La modification de la membrane commerciale OSN est une approche potentielle pour de nouveaux prototypes de membranes.

2. En prévision du nouveau prototype de membrane, le PERVAP 4060 existant constitue le premier choix.

3. Les supports poreux AMS S3012 et PAN sont également pris en compte pour la recherche si la modification peut apporter de meilleures propriétés de séparation dans la matrice poreuse.

Chapitre 3: Membranes de PDMS denses et membranes modifiées par dépôt de plasma et de polyélectrolytes par la méthode LbL.

Dans l'étude du système dense, la modification de surface a été réalisée en utilisant quatre polyélectrolytes: PDDA, PSS, PAH et PAA. Ces polyélectrolytes ont été combinés en fonction de leur nature cationique et anionique pour former des polyélectrolytes multicouches par couche par couche (LbL). Ces polyélectrolytes et leurs configurations différentes sont illustrés à la figure 7.

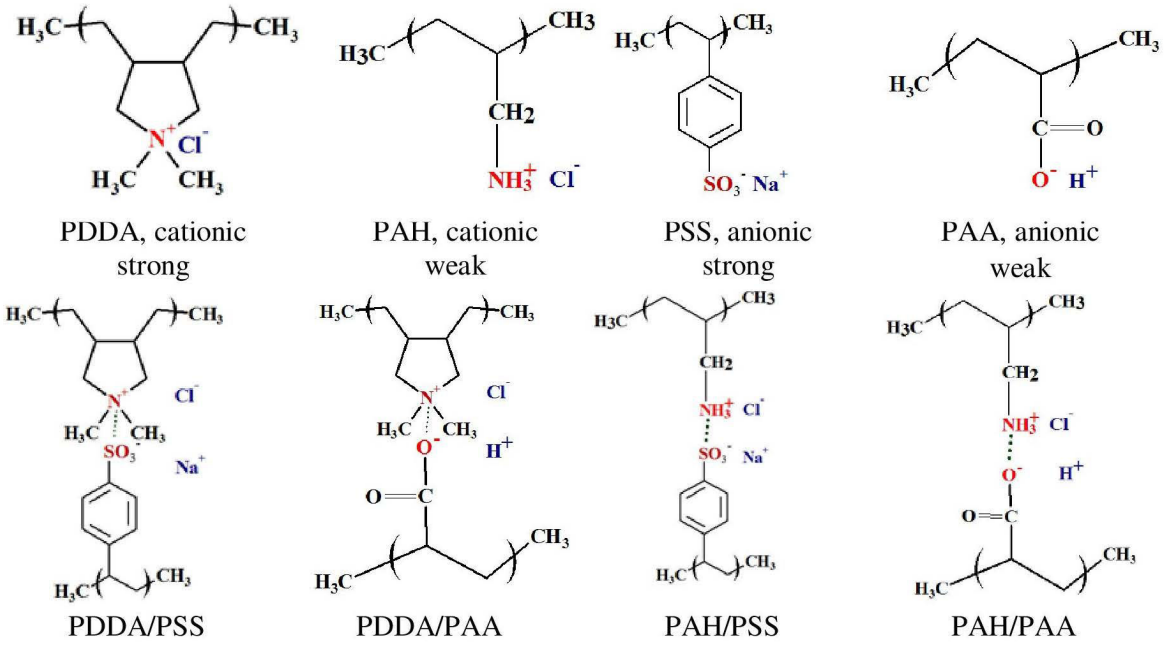

Figure 7: Structures chimiques des polyélectrolytes (en haut) et de leurs multicouches (en bas) formées.

Le premier protocole PEM utilisant PAH/PSS a été appliqué pour modifier la membrane hydrophile de PVA utilisée pour la pervaporation afin d'améliorer les propriétés de déshydratation du mélange d'alcool et d'eau. Dix bicouches de PAH/PSS (PEM) ont été jugées efficaces pour favoriser la perméation de l'eau et améliorer la déshydratation de l'alcool isopropylique-eau (80/20% m /m). Les résultats sont discutés en détail dans l'article 2 intitulé:

"Investigation of new modification strategies for PVA membranes to improve their dehydration properties by pervaporation."

Ensuite, le même protocole utilisant quatre paires de PEM a été appliqué pour modifier PERVAP4060. Les performances des membranes modifiées en termes de flux de solvant et de rejet des solutés sont présentées à la figure 8 et au tableau 2.

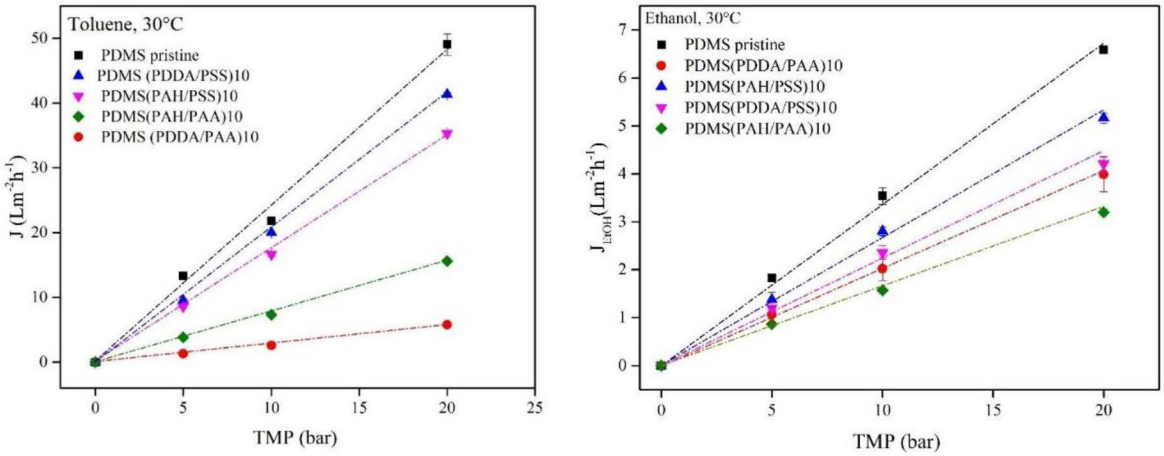

Figure 8: Flux de toluène et d'EtOH dans une membrane de PDMS modifié à 30 ° C, débit tangentiel de 7 à 10 kg / h

Échantillon de membrane	Flux global ($Lm^{-2}h^{-1}$ ±10%)	Rejets de solutés (% ±2)				Densité de charge[c]
		R-BINAP[a] C16[b]	C44[a]	ToABr[a]		
PDMS pristine	24	80	70	93	7	NA
PDMS (PDDA/PSS)10	22,9	82	88	92	6,5	1
PDMS (PAH/PSS10	14	88,5	93	97	7	1,3
PDMS (PAH/PAA) 10	7,6	66,3	80	84	10	2,4
PDMS (PDDA/PAA)10	3,8	80,5	82	92	10	1,6

[a]Concentration de soluté: 0,05 wt%. [b]Concentration de soluté: 0,1 wt%. [c]Densité de charge réduite.

Tableau 2: Résultats des expériences OSN avec des mélanges binaires utilisant des membranes modifiées par LBL (10 bar, 30 ° C, aliments dilués en toluène)

Clairement, ces résultats montrent que chaque PEM présente des propriétés structurelles différentes, une densité de charge qui soulève des résistances différentes à la perméation de solvant. D'autre part, l'amélioration du rejet n'a été obtenue que pour les PAH / PSS.

L'étude sur les PAH / PSS a été étendue en modifiant le nombre de bicouches et l'effet correspondant sur les flux de toluène et le rejet de R-BINAP par la TMP. Il a été observé que l'augmentation du nombre de bicouches diminuait la perméance au toluène et augmentait le rejet (figure 9).

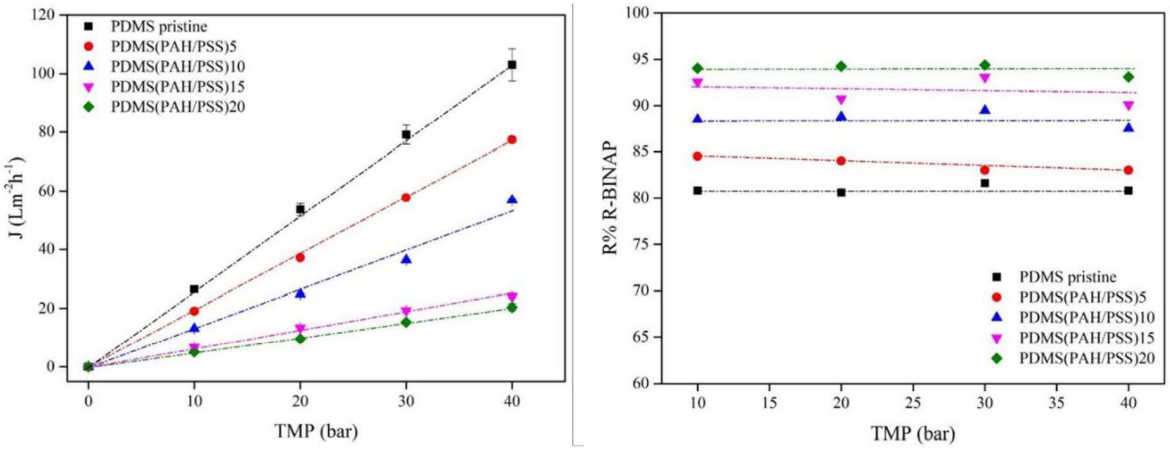

Figure 9: Effet du nombre de bicouches sur les flux de toluène (en haut) et le rejet de R-BINAP (en bas) à 30 ° C et à un flux tangentiel de 7 à 10 kg / h.

L'étude suivante d'OSN a été envisagée pour le rejet du catalyseur dans une alimentation ternaire contenant 0,05% en masse de R-BINAP, jusqu'à 10% en masse de C16 dans du toluène à 10 bar et à 30 °C. Lorsque la concentration de C16 augmentait dans le mélange d'aliments, le rejet de R-BINAP restent stables et le rejet de C16 diminue légèrement avec une légère augmentation des flux globaux (Figure 10). Ces résultats sont très prometteurs pour des applications liées à l'objectif de ANR.

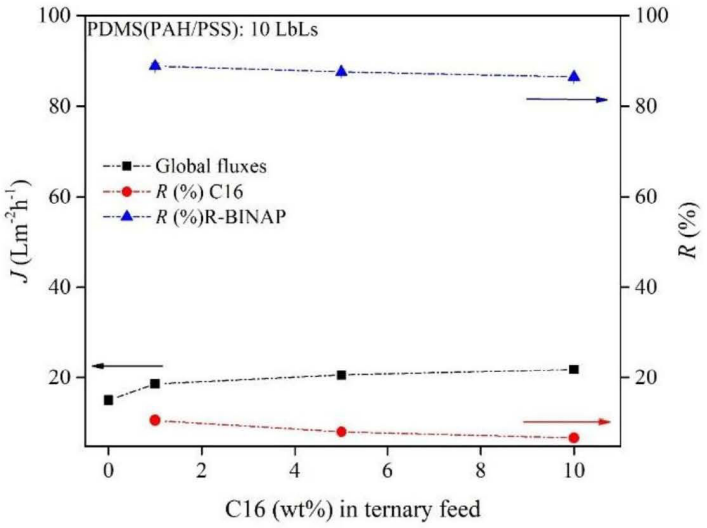

Figure 10: Performances OSN de PAH-PSS: PERVAP4060 modifié de 10 LbL pour la séparation d'un mélange ternaire modèle constitué de C16 (1 à 10% en masse) et de R-BINAP (0,05% en masse) dans du toluène (10 bar, 30 ° C).

L'étude détaillée sur PEM sur PERVAP est mise en évidence à l'article 3, intitulé:

"PDMS membranes modified by polyelectrolyte multilayer deposition to improve OSN separation of diluted solutes in toluene"

Chapitre 4: Etude par OSN de systèmes poreux modifiés par des polyélectrolytes multicouches

La modification de la surface de l'AMS et du PAN a été réalisée selon le même protocole que celui utilisé pour les membranes denses.

Premièrement, les performances des membranes immaculées et modifiées de MGS ont été testées en utilisant du C44 dilué dans du toluène. Les performances de la membrane du tableau 3 montrent une diminution de 96 à 99% du flux dans les membranes modifiées au PEM par rapport au flux dans le AMS vierge.

Membrane	Flux de toluène (L. m-2.h-1) ± 5%	C44 Rejet (0,05% en masse dans l'alimentation ± 5%)
AMS Pristine	20	25
AMS (PDDA/PSS)10	0,07	75
AMS (PAH/PSS)10	0,11	65
AMS (PAH/PAA)10	0,2	42
AMS (PDDA/PAA)10	0,6	25

Tableau 3: Performances des membranes immaculées et modifiées AMS à 10 bar et à 30 ° C.

Même si le rejet s'améliore de PEM, la perte de flux extrême rend cette membrane moins intéressante dans le contexte de l'ANR. De plus, le rejet dans le PEM modifié est inférieur aux performances obtenues dans le PDMS.

Les flux de solvant suivants dans les membranes de PAN modifiées ont été mesurés. Sur la figure 11, les résultats de flux de solvant indiquent que, en fonction de la paire de PEM utilisée pour la modification, le flux de solvant peut différer, ce qui suggère un degré différent de réduction de la taille des pores lors du dépôt de PEM.

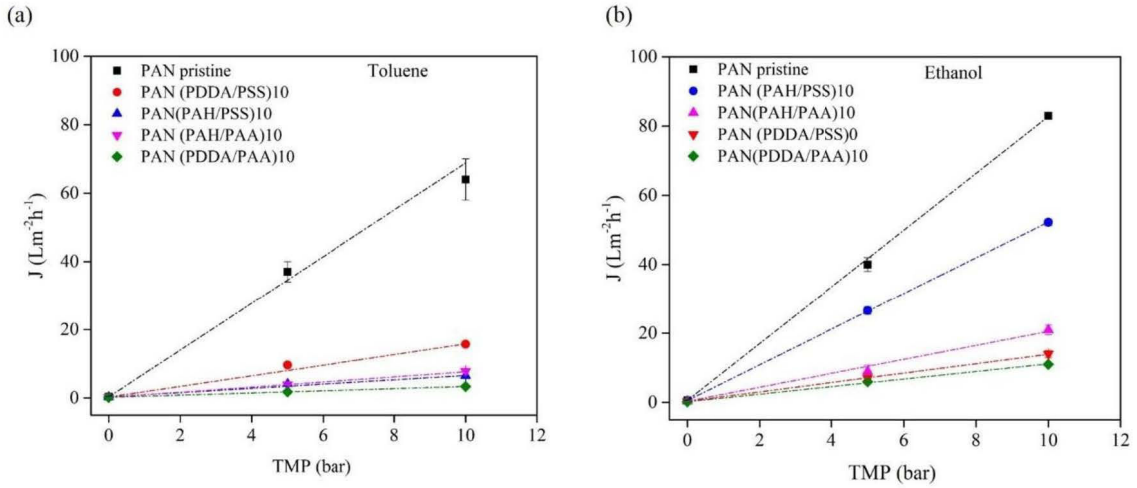

Figure 11: Flux de toluène et d'EtOH à travers le PAN et dans des membranes de PAN modifiées à 30 ° C, à un débit tangentiel de 7 à 10 kg / h.

Ensuite, le rejet de R-BINAP, C44 et C16 ont été mesurés en utilisant des alimentations binaires et ternaires. Le tableau 4 montre que la membrane la plus performante est le PAN modifié par PDDA / PSS.

	0,05% en masse de R-BINAP dans le toluène		0,05% en masse de C44 dans le toluène		0,05% en masse de C16 dans le toluène	
Membrane	Flux de toluène ± 2 L/(h.m2)	R% ±2 (R)-BINAP	Flux de toluène ±2 L/(h.m2)	R% ±2 of C44	Flux de toluène ±2 L/(h.m2)	R% ±1 of C16
PAN pristine	62	4	57	7	60	3
PAN PDDA/PSS)10	14	37	13	55	15	6
PAN (PAH/PSS)10	6	10	6	22	7	5
PAN (PAH/PAA)10	8	17	7	37	7	6
PAN(PDDA/PAA)10	4	38	3	35	5	10

Tableau 4: Flux et rejet dans le système binaire. 0,05 wt. % dans le toluène à 10 bar, 30 C. Débit d'alimentation: 7-10 kg / h

Pour l'alimentation ternaire, le flux et le rejet sont mis en évidence dans le tableau 5.

Mélange ternaire d'alimentation avec du toluène	Alimentation: Toluène avec 0,05% en masse de R-BINAP, 0,05% en masse de C16 ou de C44	Alimentation: RBINAP (0,05% + C16 (0,5-0,1%)		Alimentation: RBINAP (0,05% + C44 (0,5%)	
Membranes	Flux global L / (h.m2) en ternaire	R% RBINAP	R% C16	R% RB	R% C44
PAN pristine	60	5	2	4	7
PAN (PDDA/PSS)10	15,7	32	7	36	50
PAN (PAH/PSS)10	5	10	5	21	15
PAN (PAH/PAA)10	5	17	5	29	37
PAN (PDDA/PAA)10	1.5	37	12	27	35

Tableau 5: Flux et rejet des mélanges ternaires 10 bars, 30 ° C, flux tangentiel d'alimentation: 7-10 kg / h.

Encore une fois la membrane la plus performante a été PDDA / PSS modifié PAN. Bien que la modification apporte une certaine amélioration au niveau du rejet, elle est loin d'être envisageable pour la tâche ANR. Outre la membrane doit respecter une limitation de la pression de fonctionnement pour éviter le compactage. Le flux de solvant diminue lorsque le TMP est supérieur à 10 bars.

La perte de flux extrême pour l'AMS indique un blocage de pores et, éventuellement, la formation d'une une couche dense sur le dessus de la membrane. Pour le PAN, cependant, la simple réduction du diamètre des pore est probable pour expliquer les résultats. Un compromis entre le nombre de couches et la taille des pores de la membrane a été réalisé.

Chapitre 5: Influence des paramètres opératoires

Parmi toutes les membranes étudiées, les PERVAP 4060 vierge et modifiée par PAH / PSS ont été les membranes les plus performantes identifiées. Les paramètres du procédé, tel que l'effet du débit tangentiel, l'hydrodynamique et la polarisation de la concentration, ont été étudiés en utilisant à la fois le R-BINAP et le C16.

Le débit tangentiel dans la cellule à membrane a été modifié dans la plage de 1 à 28 kg/h et le rejet de R-BINAP a été mesuré pour chaque débit d'alimentation utilisé. Le rejet était inchangé dans toute la gamme des débits (Figure 12).

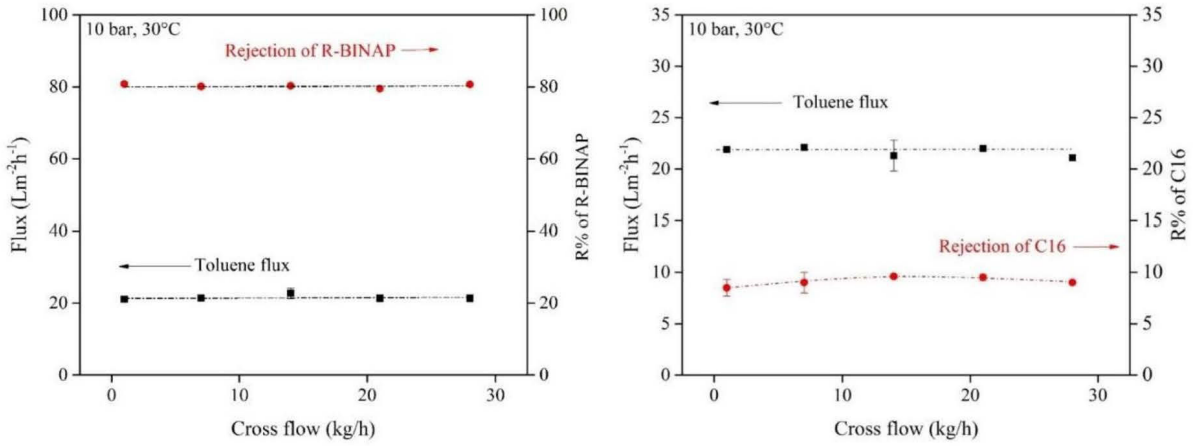

Figure 12: Effet de la vitesse d'écoulement tangentiel sur le flux de toluène, le taux de rejet du R-BINAP (à gauche) et du C16 (à droite) avec PERVAP 4060 vierge à 10 bar, 30 ° C. Alimentation: 0,05% en masse de R-BINAP dans du toluène.

Ensuite, il était possible de calculer le nombre de Reynolds en utilisant la géométrie de la cellule à membrane et le débit p. La figure 13 montre qu'il n'y a pas de changement de flux ni de rejet lorsque OSN opère dans la plage du nombre de Reynolds correspondant au régime d'écoulement laminaire et turbulent.

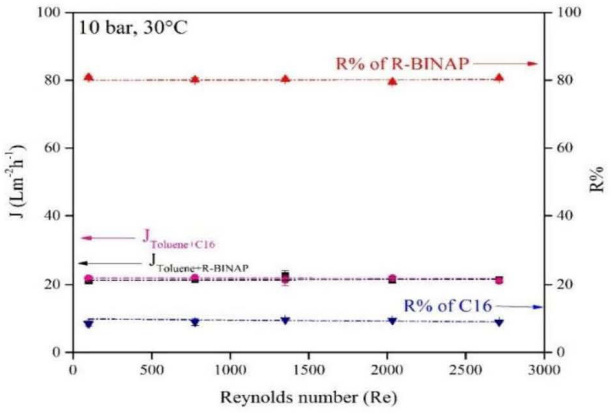

Figure 13: Effet du nombre de Reynolds sur le rejet de R-BINAP (0,05% en masse) et de C16 (0,05% en masse) de toluène à 10 bars, 30 °C, à l'aide de PERVAP 4060 vierge.

Ensuite, nous avons étudié la polarisation de la concentration en calculant le nombre de Pecklet et en utilisant le modèle de film de couche limite illustré à la figure 14. Le rejet à une vitesse de surface différente n'a pas été modifié, ce qui prouve qu'il n'ya pas de concentration de polarisation dans cette plage de vitesse.

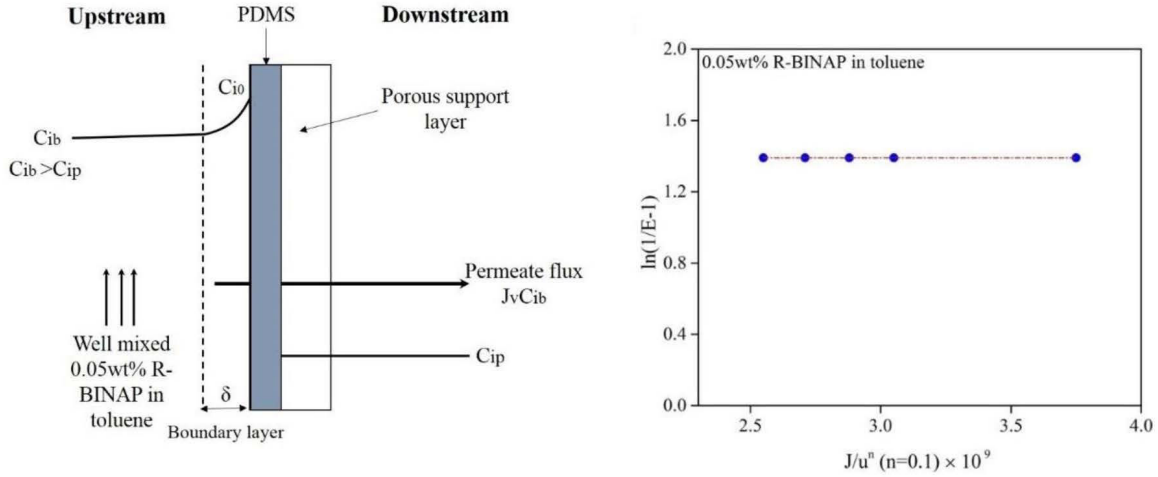

Figure 14: Les enrichissements en R-BINAP dans le PDMS vierge sont tracés en fonction de la vitesse superficielle de la solution d'alimentation dans des expériences OSN avec une configuration de membrane plane à 10 bar, 30 ° C et n = 0,1.

Ces résultats attestent du potentiel élevé de PERVAP 4060 pour une application potentielle à une échelle de procédé pour l'objectif ANR de séparation du catalyseur et de permeation du produit.

Les consommations d'énergie de l'OSN et de la distillation ont été calculées et comparées. La distillation demande env. 60 fois plus d'énergie que OSN pour une tâche de séparation donnée.

Le rejet de 80% de R-BINAP indique une perte de catalyseur par le perméat. Plusieurs solutions peuvent être envisagées pour améliorer son rejet. Tout d'abord, on peut simuler une simple cascade en série de modules d'OSN, ce qui permet alors une récupération de catalyseur de 97% sur 3 étages OSN.

Enfin, plusieurs possibilités de procédé hybrides ont été envisagés, combinant comme opération unitaire comme l'OSN, la distillation, la pervaporation ou la cristallisation, qui peuvent être plus ou moins efficaces en fonction de la cible industrielle de l'ANR.

Conclusion

L'objectif de cette étude était d'améliorer les performances de séparation OSN de membranes commerciales en vue d'applications en métathèse dans laquelle des catalyseurs hautement dilués sont utilisés.

Dans ce travail, des membranes polymères commerciales ont d'abord été étudiéespour caractériser leurs performances dans des milieux organiques en utilisant des mélanges binaires très dilués solvant-solvant. Sur la base d'une revue de la littérature, il a été montré que la membrane PERVAP4060, dont le PDMS est la couche active dense, était un candidat prometteur pour la nanofiltration milieu organique (OSN).

La membrane commerciale Sulzer PERVAP4060 est une membrane composite ayant une mince couche active de 1 à 2 µm ; elle a fait l'objet d'une étude préliminaire détaillée. Le PDMS est un polymère bien connu ayant une structure dense et déjà largement utilisé en perméation gazeuse et en pervaporation.

En tant que membrane poreuse, les supports commerciaux AMS et PAN ont également été pris en compte afin d'étudier les performances et de comprendre le mécanisme de transport de matière, de façon analogue au travail réalisé avec le PDMS.

En général, l'amélioration des performances de séparation par modification peut être réalisée selon deux approches, à savoir : la modification de la matrice du polymère ou bien de la couche active par modification contrôlée de sa surface. Dans cette étude, nous avons considéré la modification sur la surface pour conserver les propriétés de matrice polymère. Les multicouches de plasma Ar/O_2 et/ou de polyélectrolytes ont été utilisées pour la préparation de membranes prototypes comportant des nanocouches minces (quelques nanomètres) à la surface du PDMS. Une exposition contrôlée du PDMS dans le plasma peut modifier la nature de la surface et, par exemple, la rendre hydrophile à partir d'une surface hydrophobe initiale. Dans une étape suivante, des multicouches de polyélectrolytes ont été déposées par une technique couche par couche (LbL) en utilisant des polyélectrolytes cationiques et anioniques. Quatre paires de multicouches de polyélectrolytes différentes ont été utilisées. Cette modification a pour résultat la préparation de nouveaux prototypes de membranes ayant des nanocouches bien ancrées sur la surface active. D'autre part, des membranes de polyacrylonitrile (PAN) poreuses ont été modifiées, simplement par des dépôts de multicouches de polyélectrolytes.

Les membranes non modifiées et modifiées ont été testées dans des conditions OSN en utilisant des mélanges d'alimentation biniares. Plusieurs solutés très dilués, le ligand organophosphoré R-BINAP, un catalyseur de transfert de phase (ToABR) et des alcanes linéaires ont été étudiés pour déterminer le taux de rejet en OSN à partir de solution de toluène. Le R-BINAP et le ToABR ont tous deux été utilisés dans la plage de 0,0001 à 0,5% en masse et la plupart des expériences ont été réalisées ensuite avec des concentrations de 0,05% en masse de soluté dans le toluène. Également dans quelques cas, des alcanes linéaires, C16, C44 ont été utilisés de 0-20wt. % dans le toluène. Il a été montré que le PDMS était capable de retenir 80% de R-BINAP et environ 93% de ToABr dans du toluène. Le taux de rejet de ToABR dans EtOH a atteint environ 95%.

Après modification par les dépôt LBL, le taux de rejet est amélioré avec les membranes modifiées PERVAP4060, conduisant à une rétention de 88% du R-BINAP avec un dépôt de 10 bicouches de polyélectrolytes PAH / PSS en surface, ce taux de rejet pouvant atteindre 95% lorsque le nombre de bicouches est de 20. Le taux de rejet de ToABr augmente à 97%. en utilisant la même paire de

polyélectrolytes. Les performances de la membrane ont été étudiées sous différentes pressions comprises entre 1 et 40 bars; le haut rejet, encore observé dans ces conditions OSN, plaide résolument en faveur d'un mécanisme de transfert de type solution-diffusion à travers le PDMS. Les performances de la membrane pour une expérience de longue durée ont montré une excellente stabilité du PDMS ainsi que de ses performances, ce qui est prometteur pour une application ultérieure. On a également étudié le traitement des mélanges ternaires mimant le mélange catalyseur / solutés / solvant, correspondant à l'hydroformylation ; aucun signe de couplage n'a été détectée et le taux rejet du soluté de masse molaire la plus forte est resté inchangé.

D'autre part, l'amélioration du taux de rejet a également observée à partir des membranes poreuses après modification. Le taux de rétention du C44 dans l'AMS a été atteint 75% après modification par 10 bicouches de PDDA / PSS, alors qu'il n'était que de 25% avant modification. Dans le PAN modifié, le taux de rejet des solutés obtenus est dans la plage de 37 à 50%, en utilisant 10 bicouches de PDDA / PSS, alors qu'il n'était que de 3 à 7% en masse avant modification. L'inconvénient de la membrane poreuse est toutefois la forte diminution du flux après le dépôt des couches multiples.

En comparant les résultats OSN, le système PDMS dense présente des performances supérieures à celles du système AMS ou du PAN poreux. Cette membrane commerciale PERVAP4060 peut être considérée comme un bon candidat pour une application industrielle malgré le fort taux de gonflement de la membrane initiale. Un traitement au plasma suivi d'une modification d'un polyélectrolyte peut améliorer ses performances et permettre la séparation d'un catalyseur homogène coûteux par rétention sélection en amont de la membrane. Une analyse portant sur des modules en cascade et une étude pilote industrielle pourraient être la prochaine étape pour transférer cette technologie à une échelle industrielle.

List of Abbreviations

ANR	Agence Nationale de la Recherche
OSN	Organic Solvent Nanofiltration
NF	Nanofiltration
SRNF	Solvent Resistant Nanofiltration
BAT	Best Available technology
UF	Ultrafiltration
TMP	Transmembrane Pressure
MWCO	Molecular Weight Cut-off
PDMS	Polydimethylsiloxane
PI	Polyimide
PAN	Polyacrylonitrile
PP	Polypropylene
PES	Polyethersulfone
PEI	Polyethylamine
PTMSP	Poly(1trimethylsilyl1propyne)
CA	Cellulose Acetate
IPA	Isopropanol
THF	Tetrahydrofuran
MIBK	Methyl Isobutyl ketone
SD	Solution-diffusion
PF	Pore-flow
PEL	Polyelectrolytes
PEM	Polyelectrolytes multilayer
LbL	Layer-by-Layer
TFC	Thin Film Composite
TFN	Thin film nanocomposites
ISA	Integrally Skinned Asymmetric

MMM	Mixed Matrix Membrane
MEK	Methyl Ethyl Ketone
WCA	Water contact angle
PDDA	poly(diallyl dimethyl ammonium chloride)
PSS	poly(styrene sulfonate)
PAH	poly(allylamine hydrochloride)
PAA	poly(acrylic acid)
TON	Turn Over Number
PEG	Polyethylene glycol
ToABr	Tetraoctylammonium Bromide
API	Active Pharmaceutical Ingredient
SO	Styrene Oligomer
HPB	Hexaphenylbenzene
DMF	Dimethylformamide
PTMSP	poly [1-(trimethylsilyl)-1-propyne]
CS	Chitosan
RO	Reverse osmosis
FO	Forward osmosis

List of Figures

1 (a) Hydroformylation reaction (Adopted from ANR framework) (b) Proposed OSN based separation.(scheme) . . . 1
2 Overview of the Ph.D. manuscript organized in different chapters . . . 3
3 Alkane hydroformylation. Adopted from(Ojima et al., 2000) . . . 4
4 ANR project-work program and R&D inter-connections . . . 6

1.1 Separation techniques and their maturity. Adopted and redrawn from Adler et al. (2000). . . . 13
1.2 (a)Energy duty in distillation (b) Energy duty by OSN. Adopted from Marchetti et al. (2013) . . . 14
1.3 Scheme of a typical OSN membrane . . . 15
1.4 (a) Dead end OSN. Adopted and combined from MacHado et al. (1999), Joseph et al. (2014b), (b) Cross-flow OSN. Adopted and combined from Ben Soltane et al. (2016), Joseph et al. (2014b). . . . 17
1.5 OSN membrane types and their preparation techniques. . . . 18
1.6 (a) Integrally skinned asymmetric (ISA) (b) Thin film composite (TFC) membranes. . . . 19
1.7 Brief desciption of OSN materials mostly used commercially Cheng et al. (2014b) (Drioli et al., 2017). . . . 21
1.8 Solute rejection map for PDMS and PI in toluene media. . . . 26
1.9 Homogeneous catalyst rejection map for PDMS and PI in toluene media. . . . 29
1.10 Schematic of OSN separation process with different driving process . . . 30
1.11 Resistance-in-series model . . . 31
1.12 Configuration, transport and permselectivity employed in the active layer of OSN membranes, adopted from George and Thomas (2001). . . . 32
1.13 Pressure driven permeation of one component solution though OSN membrane according to SD and PF model. . . . 32
1.14 OSN Membrane- solvent-solute properties . . . 36
1.15 Plasma processes. . . . 42
1.16 (a) LbL deposition via dip coating (Decher, 1997). (b)Scheme of intrinsic and extrinsic charge balance in the polyelectrolytes multilayer (PEM) , adopted from (Ghostine et al., 2013) . . . 46
1.17 Polyelectrolytes complexes formation via (a) mixing method and (b) interfacial complexation method (Zhao et al., 2011b) . . . 47
1.18 Chemical structures of common polyelectrolytes (Zhao et al., 2011b) . . . 49
1.19 Layer-by-layer through amine coupling and silane coupling (Saeki et al., 2013) 50
1.20 Schematic representation of three zones in polyelectrolytes OSN membranes (Cheng et al., 2014a) (Ladam et al., 2000) . . . 50

2.1 Water contact angles of commercial OSN membranes. 56
2.2 Microscopic images of dense membranes: (a) Cross-section and (b) surface of PERVAP 4060 (c) Cross-section and (d) surface of SOLSEP 010206. 58
2.3 Microscopic images of porous membranes: (a) Cross-section and (b) surface of AMS 3012 (c) Cross-section and (d) surface of PAN support. 59
2.4 Evolution of toluene fluxes with transmembrane pressure up to 40 bar in (a) dense OSN membranes and (b) porous OSN membranes. Toluene feed at 30 $°C$ and $7-10$ kg/h tangential flow. 61
2.5 Rejection of diluted R-BINAP and C44 by dense and porous commercial OSN membranes, using the OSN feed of 0.05 wt% solute dissolved in toluene at 10 bar, 30° C, and 7-10 kg/h cross-flow rate. 62
2.6 $^{31}P-NMR$ of 2 wt.% R-BINAP dissolved in toluene, before and after five days of solution preparation. 63
2.7 $^{31}P-NMR$ of 2 wt.% R-BINAP dissolved in toluene(with sensitivity correction), before and after five days of solution preparation. 64

3.1 Scheme of molecular permeation (a) in a PEM layer having a porous sublayer. (b) in PEM nanolayer followed by a dense sublayer with porous support. . . 113
3.2 Effect of a gutter layer on the permeance of a composite membrane as a function of the thickness of the gutter layer. Adopted from (Wijmans and Hao, 2015). 114
3.3 Stability of PERVAP 4060 in terms of contact angles and OSN toluene permeance, measured randomly using the same test membrane coupon over three years at 30°C with 10-14 kg/h cross-flow rate. Apart from the OSN test, these membrane coupon stored in room condition. 116
3.4 Effect of Ar/O_2 plasma on PDMS and recovery of hydrophobicity with time. 116
3.5 Chemical structures of polyelectrolytes (top) and their multilayers (bottom). 118
3.6 Chemical structures of polyelectrolytes (top) and their multilayers (bottom). 119
3.7 Number of bilayers and their thickness in different PEM using ellipsometry data obtained from thickness measurement, compared and completed with the data reported by (Francius et al., 2016)(Schönhoff et al., 2007) (Nestler et al., 2013) 120
3.8 Explanation of the polyelectrolytes multilayer (PEMs) thickness when associated with different PELs having low to high charge density and molecular weight. 120
3.9 Effect of gas permeability in PEM modified PERVAP 4060 at 20°C: (a) CO_2, N_2, and He (b) Enlarged view for N_2 and He permeability. 121
3.10 Scheme of PDMS (PEM) and resistance-in-series model. 123
3.11 Selectivity of CO_2/N_2 in PEM modified PDMS, prepared by plasma and polyelectrolyte modification. 124
3.12 Sketch of a possible CO_2 repulsion phenomena by charged polyelectrolytes multilayer that affects the CO_2/O_2 selectivity. 125
3.13 (a) Polyelectrolytes multilayer with 10 bilayers and its effect on the increase of resistance (b)PEM thickness with bilayers number and effect of PEM in OSN performance. 125
3.14 Example of a PEM before (a) and after (b) bleaching of the central circular area. The three areas along the left side of the images serve as references. . . 126

3.15 Surface images of pristine PDMS (a) before and (b) after OSN; at 30° C, 10-40 bar and 7-10 kg/h cross-flow. 127
3.16 Surface image of PDMS (PDDA/PSS)10: (a) before and (b) after OSN; at 30° C, $10-40$ bar and $7-10$ kg/h cross-flow. 128
3.17 Surface image of PDMS (PAH/PSS)10: (a) before and (b) after OSN; at 30°C, $10-40$ bar and $7-10$ kg/h cross-flow. 128
3.18 Surface image of PDMS (PAH/PAA) 10: (a) before and (b) after OSN; at 30°C, $10-40$ bar and $7-10$ kg/h cross-flow. 129
3.19 Surface image of PDMS (PDDA/PAA) 10: (a) before and (b) after OSN; at at 30°C, $10-40$ bar and $7-10$ kg/h cross-flow. 129
3.20 Optical image of PDMS (PAH/PAA) 10 surface before and after immersing in toluene for 24 hours, followed by the image after drying. 129
3.21 Effect of plasma exposure time in PERVAP 4060: (a) ethanol flux up to 40 bar at 30°C and $10-14$ kg/h. (b) Water contact angles. 130
3.22 Effect of PDDA/PSS of 10 bilayers deposited on PDMS based PERVAP4060 without any plasma: (a) toluene permeation up to 40 bar at 30°C with $10-14$ kg/h tangential flow. (b) Water contact angles before and after modification without using any intermediate plasma. 131
3.23 Effect of bilayers number on toluene permeation using (a) PDDA/PSS (b) PAH/PAA on PERVAP4060 at 30°C and $10-14$ kg/h tangential flow. . . . 131
3.24 Effect of transmembrane pressure on solvent fluxes in polyelectrolytes multilayer (PEMs) modified PERVAP 4060: (a) Toluene (b) EtOH fluxes at 30°C, $7-10$ kg/h cross flow rate. 132
3.25 Global swelling of prototype membranes in (a) Toluene (b) EtOH. The swelling of PAH/PSS in toluene is adopted from (Ferrell et al., 2017), considering the PSS swelling. 133
3.26 Effect of transmembrane pressure on (a) toluene flux (b) R-BINAP rejection at 30°C and $7-10$ kg/h cross-flow of diluted R-BINAP ($0.05wt.\%$) in toluene. 135
3.27 Effect of the number of the bilayer of PAH/PSS on (a) toluene fluxes (b) R-BINAP rejection at 30°C and $7-10$ kg/h cross flow of diluted R-BINAP ($0.05wt\%$ in toluene.) 136
3.28 Effect of the number of bilayers on toluene flux, and R-BINAP rejection at 10 bar, 30°C and $7-10$ kg/h cross-flow of diluted R-BINAP ($0.05wt\%$) in toluene. 137
3.29 Effect of using salt in polyelectrolyte multilayer PEM preparation on PERVAP 4060; in terms of (a) toluene flux (b) R-BINAP rejection, at 10 bar, 30°C and $7-10$ kg/h cross-flow of dilute R-BINAP ($0.05wt\%$) in toluene. 137
3.30 (a) PDMS(PAH-PSS) scheme with 5 and 15 bilayers. (b) Diffusion in PEM reported by (Fares and Schlenoff, 2017) 138
3.31 Effect of toluene mass fraction in toluene-ethanol feed with diluted R-BINAP ($\approx 0.05wt\%$) on the performance of PERVAP 4060 (PDMS) : (a) Global fluxes with toluene mass fraction in the feed. (b) R-BINAP rejection with the toluene mass fraction in the feed at 10 bar, 30°C and $7-10$ kg/h tangential feed flow. 140
3.32 Experimental points (o) and predicted curves of ethanol volume fractions in the PDMS network at 40 °C vs. calculated solvent activities; Ethanol in ethanol/toluene/PDMS mixture. (copied from (Favre et al., 1995)). 141

4.1 Modification of porous OSN membrane by polyelectrolyte multilayers and expected effect after modification based on pore sizes of the pristine membrane: (a) Nanopores: before and after PEM. (b) UF pores: before and after PEM. (c) Mixed pores: before and after PEM. 143
4.2 (a) AMS cross-section (b) AMS surface (c) PAN cross-section (d) PAN porous surface. (e) Surface hydrophilicity of AMS and PAN (f) Gas selectivity in AMS. 145
4.3 (top) Chemical structures of polyelectrolytes (PELs). Strong and weak PELs correspond to respective high and low degree of dissociation. (bottom) Chemical structures of polyelectrolytes multilayers (PEMs). The dotted line indicates the complexation. 145
4.4 Water contact angles after modification of the membrane by different PEM on PAN. 146
4.5 The effect of transmembrane pressure (TMP) on toluene (pure) fluxes in AMS S3012, PAN, and PDMS at $30°C$ with a feed cross flow of $7-10$ kg/h. . . . 147
4.6 Surface image analysis by imageJ for the pore size and the number of pores in (a) PAN surface (b) AMS surface. 148
4.7 Effect of TMP in pristine PAN: (a) Toluene flux. (b) R-BINAP rejection, at $30°C$ and $7-10$ kg/h cross-flow rate. 149
4.8 Effect of TMP in pristine PAN: (a) Toluene flux. (b) R-BINAP rejection, at $30°C$ and $7-10$ kg/h cross-flow rate 150
4.9 Toluene flux and R-BINAP rejection by pristine PAN in a long run study at 10 and 20 bar, $30°C$ and $7-10$ kg/h cross-flow rate: (a) OSN measurement at 10 bar in day 1 (b) OSN measurement at 10 and 20 bar up to day 3 . . . 151
4.10 Surface of pristine PAN membrane: (a) and (c) before OSN (b) after OSN at 10 bar(d) after OSN at 20 bar; at $30°C$ and $7-10$ kg/h cross-flow rate. . . . 151
4.11 Hypothesis for AMS top layer with the smaller pores inside the membrane originating rejection of R-BINAP and C44. Δx is the membrane thickness. . 153
4.12 H-P laminar flow through channels. 153
4.13 Factors affecting the transport mechanism of toluene and C44 in PEM modified AMS membrane having a dense-glassy nanolayer of PEM on the top of a porous substrate 155
4.14 Comparison of pure solvent fluxes in pristine and PEM modified PAN membranes at $30°C$, up to 10 bar using feed cross-flow $7-10$ kg/h : (a) Toluene fluxes (b) EtOH fluxes. 156
4.15 Swelling of PEM in different solvent and its effect on the pore reduction to govern the solvent fluxes, when PEM deposited on the porous substrate having a pore range of nanopore to UF-pore. 157
4.16 Air permeability measurement in PAN modified membranes. 158
4.17 Mercury porosimetry for pristine PAN (a) Cumulative intrusion vs pressure plot. (b) Cumulative intrusion vs pore size (diameter). (c) Incremental volume and pore diameter (d) Differential intrusion vs diameter distribution. 159
4.18 Scheme for mass transport in the porous system after PEM modification. . . 162
4.19 Effect of concentration in the ternary feed mixture using PAN(PDDA/PSS)10 at $30°C$, 10 bar TMP under $7-10$ kg/h cross-flow rate. 163

5.1 Overview of the most critical parameters and operating parameters influencing the process performance. 165

5.2 Effect of cross-flow velocity on the performance of pristine PERVAP4060 at 10 bar, 30°C. (a) pure toluene flux (b) toluene flux and R-BINAP rejection using the feed of 0.05wt% R-BINAP in toluene . . . 167
5.3 Effect of cross-flow velocity on the performance of pristine PERVAP4060 at 10 bar, 30°C. (a) pure toluene flux (b) toluene flux and C16 rejection using the feed of 0.05wt% C16 in toluene. . . . 167
5.4 Concentration gradient can form when a membrane separates two solutions with different concentrations . . . 168
5.5 R-BINAP concentration gradient adjacent to the OSN membrane PERVAP4060. The mass balance equation for solute flux across the boundary layer is the basis of the film model description of concentration polarization. . . . 169
5.6 R-BINAP enrichments in pristine PDMS are plotted as a function of feed solution superficial velocity in OSN experiments of flat sheet membrane configuration at 10 bar, 30°C: (a) n=1 (b) n=0.1 . . . 171
5.7 (a) the membrane holding cell used in OSN. (b) the dimension of the cell . . 172
5.8 Effect of Reynolds number on the rejection of R-BINAP (0.05wt.%) and C16 (0.05wt.%) from toluene at 10 bar, 30 °C using pristine PERVAP4060. . . . 173
5.9 Effect of Reynolds number on the rejection of R-BINAP (0.05wt.%) and C16 (0.05wt.%) from toluene at 10 bar, 30 °C using pristine PERVAP4060. . . . 173
5.10 Solvent transport through a dense-swollen system as a function of TMP at room temperature. . . . 174
5.11 Effect of pressure in toluene flux and R-BINAP rejection in PERVAP4060 from a feed of 0.05wt.% R-BINAP in toluene at 30 °C and 7-10 kg/h cross-flow. . 175
5.12 Effect of pressure in toluene flux and R-BINAP rejection in PERVAP4060 from a feed of 0.05wt.% ToABr in toluene and EtOH at 30 °C and 7-10 kg/h cross-flow. . . . 176
5.13 Large scale OSN: energy required from two pumps (feed and bleed) (b) Batch distillation: Energy of evaporation and condensation. . . . 177
5.14 Separation of catalyst and permeation of products by single stage OSN process and relevant cost impact, using PERVAP 4060 for the processing of 5-ton feed. 179
5.15 Separation of catalyst and permeation of products by three-stage OSN process and relevant cost impact, using PERVAP 4060. . . . 180
5.16 Hybrid process with distillation using cascade up to three stages OSN. . . . 181
5.17 Scheme of OSN hybrids for the separation of catalyst and product from a hydroformylation system: (a) Hybrid OSN with PV. (b) Hybrid OSN using a dual membrane in series. . . . 183
5.18 Toluene flux in pervaporation by PERVAP 4060. . . . 183

6.1 Polyelectrolytes used in OSN experiments . . . 187
6.2 Solutes used in OSN experiments . . . 187
6.3 (a) Digidrop contact angle meter (b) An image of water drop on membrane during the measurement . . . 187
6.4 (a) SEM Quanta 600 (b) An example of surface and cross section of PDMS membrane . . . 188
6.5 (a) AFM set-up at LRGP (b) An example of AFM surface image . . . 189

6.6 (a) Confocal microscope: Zeiss LSM 510 (b) Membrane sample before photo-bleaching.(c) after photo-bleaching. 189
6.7 (a) Gas permeation (Time-Lag)set-up at LRGP (b) Detail Scheme 190
6.8 (a) Scheme of air permeability unit (b) membrane mounting cell (c) ALMEMO precision pressure measuring device. 192
6.9 (a) Plasma set-up (b) $Ar - O_2$ glow during modification. 193
6.10 (a) LbL modification scheme (b) Nadatech ND-3D multi-axis robot. (c) Scheme of the polyelectrolyte multilayer expected after modification. 194
6.11 OSN experimental scheme 195
6.12 OSN equipment and their specifications. 195
6.13 (a) Agilan 6890 (b)Example of a chromatogram: (R)-BINAP peak with external standard C44 (tetratetracontane). 197
6.14 Calibration of the GC column for (a) RBINAP in toluene (b)ToABr in toluene (c) R-BINAP with C16 in toluene (ternary). 199

7.1 Mass transport mechanism and solute retention in PERVAP4060 under transmembrane pressure of 10-40 bar, at 30°C with 7-10 kg/h cross-flow. . . 203
7.2 Mass transport mechanism in PAH/PSS modified PDMS for the improved rejection of catalyst from toluene at 30°C and 10-40 bar. Feed cross-flow: 7-10 kg/h. 205
7.3 OSN membrane characterization for the first evaluation of the mass transport model. 207
7.4 Toluene flux and R-BINAP rejection in PEM modified porous membranes in comparison to the performance at their pristine state (a) Modified AMS (b) Modified PAN. Data correspond to the OSN measurement carried at 10 bar, 30°C with cross-flow of 7-10 kg/h feed. 208

List of Tables

1.1 OSN review papers, published from 1999-2019, and their focused investigation areas . . . 12
1.2 Commercial OSN membranes. Summarised from Scarpello et al. (2002a), Ben Soltane et al. (2013), Ben Soltane et al. (2016), Hendrix et al. (2012), Darvishmanesh et al. (2011a), Buonomenna and Bae (2015a) . . . 20
1.3 Deviation in toluene permeance in the active layer of PDMS and PI based commercial membranes. . . . 23
1.4 Application of OSN in separation (Priske et al., 2016). . . . 24
1.5 Solutes rejection in commercial membrane in toluene. . . . 26
1.6 Homogeneous catalyst retention by OSN membranes in toluene media . . . 29
1.7 OSN parameters for dense membrane. . . . 36
1.8 OSN parameters for porous membrane. . . . 36
1.9 Process parameters and their effect on flux and retention. . . . 37
1.10 Transport mechanism to known-unknown-critical governing parameters. . . . 38
1.11 Expected surface properties and OSN characteristics after modification. . . . 40
1.12 Techniques for OSN membrane modifications and their brief description. . . . 42
1.13 Brief properties of plasma (Chan et al., 1996) . . . 44
1.14 PEL in OSN . . . 53

2.1 Examples from literature reporting water contact angles of both commercial and laboratory-made PDMS based OSN membranes. . . . 56
2.2 Commercial OSN membranes and their active surface materials. . . . 57
2.3 Pure gases permeability (Barrer) in commercial membranes by time-lag. . . . 60
2.4 Characterization summary of OSN commercial membranes. . . . 60
2.5 Rejection of hydroformylation catalyst-ligand by commercial dense and porous membranes in toluene at 10 bar, 30°C, and 7-10 kg/h cross-flow rate. . . . 62

3.1 Contact angles and surface energy of pristine PERVAP 4060. . . . 115
3.2 Water contact angle of PERVAP4060 before and after OSN test performed at 30°C, 10-40 bar and 10-14 Kg/h tangential feed flow rate. . . . 115
3.3 Properties of N_2 and CO_2 and permeability and 20° C, solubility and diffusivity in PDMS. Adopted from (Merkel et al., 2000) . . . 122
3.4 Resistance contribution of PEM when deposited on PERVAP4060. . . . 123
3.5 Comparison of permeability values obtained from resistance in series using experimental data. . . . 124
3.6 Polyelectrolytes chain diffusion coefficient by FRAP and comparison with literature. . . . 127

3.7 Tentative evaluation of solubility parameter and molar volume of polyelectrolytes and their multilayers. 133
3.8 Toluene and EtOH diffusion coefficient in PEM systems. 134
3.9 Toluene and R-BINAP diffusion coefficient in PDMS and PAH-PSS. 139
3.10 Intrinsic permeance in PEM by resistance in series 139
3.11 Differences of solubility parameters in solute-solvent-membrane system. . . . 140

4.1 Rejection of R-BINAP and Tetratetracontane (C44) at 10 bar, 30°C and $7-10$ kg/h cross-flow condition. 152
4.2 Comparison of measured and calculated (Hagen-Poseuille) flux and parameters adjustment to reproduce the experimental flux. (Actual data $\Delta x \approx 25\mu m$, $\tau=$ unknown, $d_p = 18.5nm$ in PAN and 11.5 in AMS. $\varepsilon = 7\%$ in PAN and 15% in AMS) 154
4.3 Performance of AMS pristine and modified membranes at 10 bar and 30°C, and feed cross-flow $7-10$ kg/h. 155
4.4 Air permeability in modified PAN from 0.5-3 bar 157
4.5 Characterization parameters obtained from mercury porosimetry 159
4.6 Flux and rejection in the binary system of 0.05 wt.% solutes (R-BINAP, C44, and C16) in toluene at 10 bar, 30°C. Feed cross-flow: $7-10$ kg/h 160
4.7 Solute and solvent properties for mass transport in the porous system. 161
4.8 Flux and rejection in pristine and PEM modified PAN from ternary feed mixtures at 10 bar, 30°C and feed cross-flow: $7-10$ kg/h. 162

5.1 Effect of feed flow and Reynolds number (Re) on toluene flux and rejection of R-BINAP and C16 at 10 bar, 30 °C. 172
5.2 Context of the OSN for process using PERAP 4060 179
5.3 Energy demand: OSN, distillation, and hybrid process. 182
5.4 Properties of decanal and toluene. 184

6.1 Selected membranes for OSN experiments 185
6.2 Selected polyelectrolytes for OSN experiments 186
6.3 Organic solvents used. Toluene has the chosen following ANR objective. . . . 186
6.4 Solutes used in OSN experiments 186
6.5 List of GC oven temperature for the detection of solutes and external standard. 198

0.1 Introduction

The Ph.D. manuscript, entitled as ***Study of the separation by organic solvent nanofiltration of diluted solutes using commercial, dense and porous membranes and their derivatives by deposition of polyelectrolyte nanolayers***, aims to describe following aspects:

(1) Investigation of commercial dense and porous OSN membranes, their market availability, and performance in organic media.
(2) Modification of OSN membranes to enhance their separation properties.
(3) Investigation of applying OSN membranes for the separation of homogeneous catalyst.

The global aim of the Ph.D. is to integrate the separation task to the ANR project, ANR MemChem (http://www.agence-nationale-recherche.fr/Project-ANR-14-CE06-0022), which focuses on developing an innovative membrane process for sustainable production of fine chemistry. In ANR MemChem framework, hydroformylation has been considered as the model reaction, according to the **Figure** 1a. Once the reaction is complete, it requires the separation of catalyst, product, and solvent. At present, the applied technology is highly energy-intensive distillation, causing a partial degradation of the expensive catalyst due to high temperature. The vision of the Ph.D. is to replace distillation to OSN, according to (**Figure** 1b), by which, it has been envisioned to obtain high catalyst rejection with high product permeation. Also, OSN favors preventing degradation, thanks to its mild operating condition. If successful with the ANR project tasks, OSN will be an attractive alternative of hydroformylation or metathesis catalyst separation, ensuring high benefit in energy, economy, and environment.

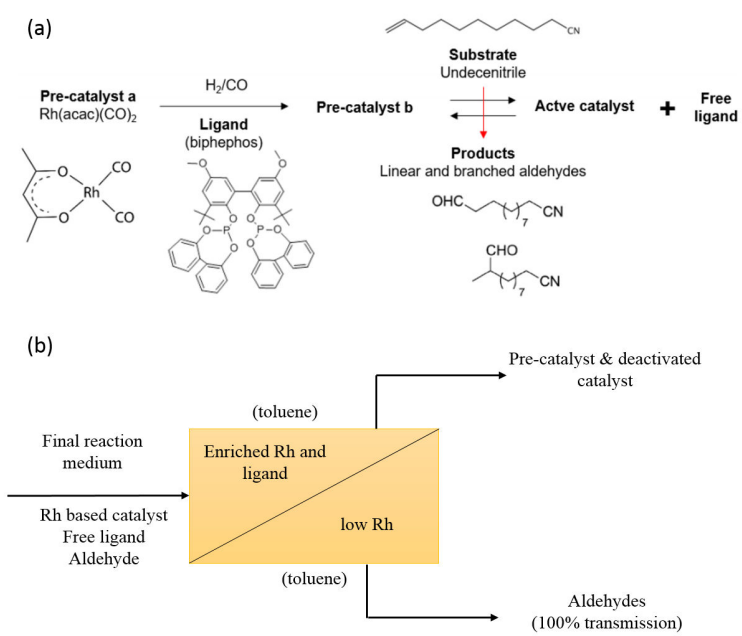

Figure 1: (a) Hydroformylation reaction (Adopted from ANR framework) (b) Proposed OSN based separation.(scheme)

The mission of the Ph.D., first, to find suitable OSN membrane/s for the ANR task of separating rhodium based catalyst while ensuring high product permeation. Next, the development of new generation OSN membrane by suitable modification/s to enhance the existing separation performance.

The manuscript is divided into several chapters.

▶ **Chapter 1: Literature review**.
Highlights
Investigation of the availability of commercial OSN membranes and their rejection performance in toluene media.
Credible OSN membranes for ANR tasks
Modification of commercial OSN membranes is a potential route to obtain new OSN membranes
Plasma and polyelectrolytes assisted modification could be a possible way to modify commercial OSN membranes

▶ **Chapter 2: Performance of OSN commercial membranes**.
Highlights
OSN test of four commercial polymeric membranes using the feed of diluted R-BINAP and C44, dissolved in toluene
PDMS-based membrane exhibits high retention of dilute organic solutes in toluene
PERVAP4060 is stable in toluene under OSN operating conditions
ToABr is more rejected (R=95%) than R-BINAP
Similar rejections were observed for binary and ternary feed mixtures

▶ **Chapter 3: Dense system-PDMS membrane and modification of PDMS by plasma and polyelectrolytes**.
Highlights
Synthesis of PEL-modified PDMS membranes by LBL method for application in OSN
Intrinsic permeance of CO_2, N_2 *and* He *in PDDA/PSS by resistance-in-series model*
Intrinsic permeance of toluene in polyelectrolyte multilayer by resistance-in-series model
Improved rejection of R-BINAP is obtained with PAH/PSS modified membranes
C16 alkanes can be eliminated through the membrane, whereas the R-BINAP is mostly rejected
Investigation of the separation of binary and ternary mixtures by OSN under tangential flow

▶ **Chapter 4: OSN study on porous systems modified by polyelectrolytes multilayer**
Highlights
Synthesis of PEL-modified AMS and PAN membranes by LBL method for application in OSN
Rejection improves in PDDA/PSS modified AMS membrane but exhibit an extreme decline of toluene flux
Rejection in PEL modified PAN membrane is much lower than modified AMS
A trade-off between layer number and flux-rejection in PEL modified porous membranes
Overall, dense systems exhibit high separation performance than porous systems

▶ **Chapter 5: Study of process parameters on OSN results and their perspectives**
Highlights
Both pristine and PEL modified PERVAP 4060 exhibits steady separation performances under laminar and turbulent hydrodynamic conditions
No concentration polarization have been detected from the studied catalyst-product-solvent systems
For a given separation task, energy duty of OSN is much lower than the benchmark distillation process
A simple OSN cascade can improve the overall catalyst yield and product loss

▶ **Chapter 6: Materials and method**.
Highlights
Catalysts, solvents and polyelectrolytes properties
Detail procedures for the characterization of membranes and materials
Description of the plasma activation process, Layer-by-Layer (LbL) deposition and protocol of cross-flow OSN with automatic pressure control
Description of analytical procedures and experimental accuracy

▶ **Chapter 7: Conclusion and perspectives**.
Highlights
Overview, future strategy, scope and opportunities, added values and critical remarks on obtained results.

0.1.1 Graphical abstract of OSN study plan and organization of the manuscript

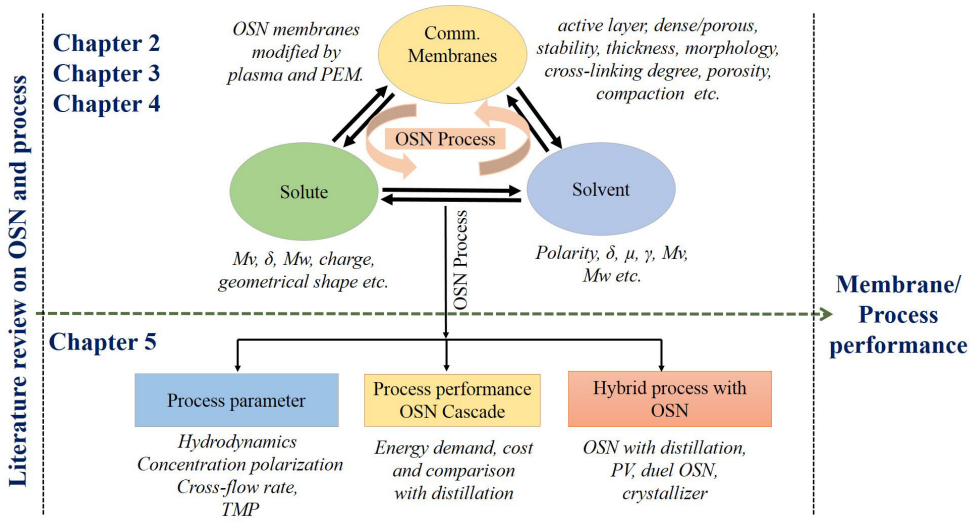

Figure 2: Overview of the Ph.D. manuscript organized in different chapters

0.1.2 Context of the project

Renewable or eco-compatible chemical engineering process is a present demand in terms of **energy**, **economy** and **environment**. An ideal process is expected to display equal balance among these three axes to ensure sustainability and efficiency. Up to now, separation/purification at industrial scale represents from 40 - 70% of the operational cost. Also, they contribute almost 45 % of the total energy consumption, performed mainly by distillation, liquid-liquid extraction, and chromatography.

Distillation is associated with high energy consumption and not well adapted for the molecule that is temperature sensitive. It also results in irreversible degradation of sensitive catalysts.

Liquid-liquid extraction requires a high volume of organic solvents, often followed by a precipitation step which causes the inactivation of some components during the phase change.

Finally, Chromatography is efficient but rarely used because it requires a re-concentrating step which makes it one of the highest energy consuming techniques.

Replacing these classical Chemical Engineering processes to a new generation separation process is a scientific challenge.
Organic Solvent Nanofiltration (OSN), a membrane-based separation technique could be one promising alternative. The separation by OSN takes place at room temperature without any change of state, providing a minimal impact on energy and environment. It is a low waste generating and non-destructive technique towards catalyst and product.

The project **ANR MemChem** entitled ***Innovative Membrane processes for a sustainable production of fine Chemistry*** which focuses on integrating OSN in the process of **hydroformylation** reaction. Hydroformylation, also known as oxo synthesis or oxo process; in a homogeneous catalyzed reaction for the production of aldehydes from alkanes, as shown in **Figure** 3 (Ojima et al., 2000) .

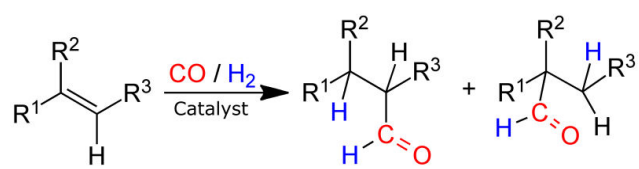

Figure 3: Alkane hydroformylation. Adopted from(Ojima et al., 2000)

The hydroformylation reaction was developed in 1938 by the German chemist Otto Roelen at Ruhrchemie (Germany). The reaction of an alkene with synthesis gas ($CO + H_2$ mixture) in the presence of a suitable metal catalyst leads to the addition of hydrogen and a formyl group on the carbon-carbon double bond of the alkene. As a result, the functionalization of an olefin to aldehyde can be achieved.
Hydroformylation includes the addition of synthesis gas (syngas) , a mixture of CO and H_2, to olefin in the process of a catalytic reaction under the formation of aldehydes. Hydrogen and a formyl group are added in an atom-economical manner. The reaction finally leads to a mixture of isomeric products (unless ethylene is used as a substrate),n-aldehydes (linear), and

isoaldehydes (branched). Different branched aldehydes can be formed Because double-bond isomerization of the substrate may occur before the hydroformylation, even when a single terminal olefin has been subjected to the reaction. The promising catalyst system in this reaction involves a rhodium precursor, $Rh(acac)(CO_2)$ complexed by ***biphosphite ligand*** namely ***biphephos***. The final reaction medium is composed of metal entities in a different form, uncreated pre-catalyst, active catalyst, ligand, and a mixture of products (**Figure** 1a).

The catalyst and ligands for hydroformylation are temperature sensitive and expensive. The main problem for such system is the downstream processing of the reaction products; typically done by thermal separation, by which the catalyst system deactivates, and a significant part is lost by clustering. In contrast, organophilic nanofiltration (**Figure** 1b) allows the separation of the catalyst under stabilizing conditions in a gentle and energy saving way, resulting in an added advantage of preventing irreversible degradation or clustering of catalyst.

The main objective in ANR framework is to retain maximum catalyst-ligand complex while allowing reaction products to pass through the membrane. The bottleneck is to find a suitable membrane to perform the given tasks, which is the beginning work to be done in this Ph.D.

The criteria for the selection of the membrane include the following:

1. The commercial membrane to select over laboratory prepared membrane in order to avoid complexities associated with membrane fabrication. Besides, scaling up with the right commercial membrane is rather straight forward compared to the laboratory prepared membranes.
2. The membranes have to be resistant to organic solvents exhibiting long term stability in separation-permeation performance.
3. The membrane must exhibit high rejection of catalyst-ligand and high permeation of products.

The ANR MemChem project is divided into several inter-connected work packages (WP) managed by different partner laboratories and industries.

- **WP 1:** Study of the synthesis of the batch reactors.
- **WP 2:** Fundamental studies of nanofiltration using organic media.
- **WP 3:** ***Membrane materials for hydroformylation.***

This Ph.D. focuses on WP 3 that includes investigation on the availability of commercial OSN membranes followed by the modification of the suitable OSN membrane/s to improve the performance.
The detail performances of these membranes have been targeted to evaluate by the rejection of model molecules (solutes) from organic media, which are comparable to the hydroformylation catalyst-ligand-products systems.

It has been envisioned that the OSN study of similar characteristic molecules would provide valuable insight into the membrane performance when applied in the real catalytic system

0.2 Ph.D. Objectives and tasks

My Ph.D. has been addressed in the frame an R&D project funded by the French National Agency, ANR, entitled **Innovative membrane process for sustainable production in fine chemistry**, ANR # 14-CE06-0022-03 (2015-2018).

This R&D contract involved three academic partners and one major French chemical company:

• *Chemical and Process Engineering (CIP) team, University of Rennes 1, ISCR-CIP, CNRS-6226.*
• *Organometallic: Materials and catalysis (OMC) team, University of Rennes 1, ISCR-OMC, CNRS-6226.*
• ***Membranes, Separations, Processes (EMSP) team, Laboratory Reactions and Process Engineering(LRGP), University of Lorraine, CNRS 7274 Institute Jean Lamour (IJL), Campus Artem,Departement N2EV, UMR 7198 CNRS, University of Lorraine.***
• *Arkema-CRRA.*

My Ph.D. work carried out in **Membranes, Separations, Processes** team of the Reactions and Process Engineering Laboratory (LRGP) and in Institut Jean Lamour (IJL), which focuses on the Work Packages 2 and 3 (WP2 and WP3), as presented in **Figure** 4.

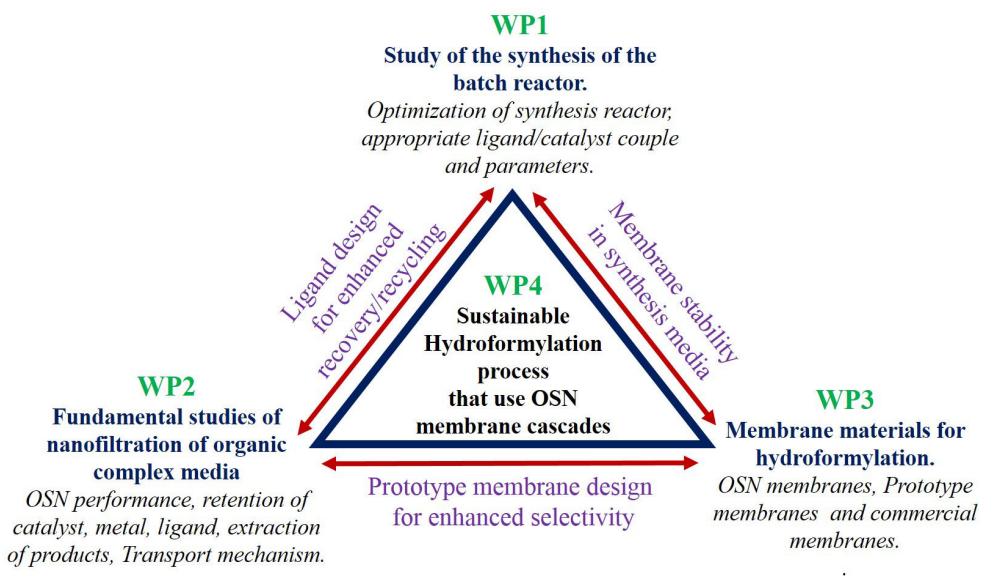

Figure 4: ANR project-work program and R&D inter-connections

In addition to my Ph.D., two other Ph.D. have been launched; one dedicated to OSN study using hydroformylation of olefin in toluene, and the other for the optimization of the hydroformylation reaction.

The main role of my Ph.D. focuses on several aspects:

• Investigation of the availability of commercial OSN membrane/s that exhibit high potentiality to meet ANR MemChem objectives of the separation of soluble metal complexes from organic media, such as toluene or alcohol (MeOH, EtOH)
• Performance improvement of potential commercial membranes by adopting modification in order to obtain a new generation of efficient OSN membranes.(polyelectrolytes multilayer (PEM) deposition by layer-by-layer(LbL) have been chosen.)
• Performance evaluation of these membranes using model mixtures consisting of binary and ternary feed using diluted soluble catalysts.

Both dense and porous polymeric membranes have been considered for the modifications because their mass transport mechanisms fundamentally vary from each other. The validity of these newly prepared membranes has been tested under OSN, with diluted soluble metal complexes, mimicking hydroformylation, and metathesis system.
Besides OSN tests, the modification protocol has been applied to modify polyvinyl alcohol (PVA) membrane and used it in pervaporation to cross-validate the modification approach. The Article entitled ***Investigation of new modification strategies for PVA membranes to improve their dehydration properties by pervaporation***, is the outcome of those study, presented in **Chapter** 3.

0.2.1 Objectives

Global objective

The global objective is to favor the solvent transport and to decrease, as much as possible, the solute permeability under OSN conditions, using commercially available membranes as raw materials. In the frame of the ANR project, final membranes must be stable in toluene.

Establish the OSN state of the art

Establishing the OSN state of the art by illustrating the potential of OSN as an eco-friendly and sustainable membrane separation process for different solute-solvent systems, including homogeneous catalyst recovery.
The feasibility of OSN, when separation is carried out from a highly diluted catalyst-solvent systems.
Identification of the potential routes that can be applied to modify/create OSN membranes to improve the performances.

Investigate the potential of the layer-by-layer (LbL) strategy to get thin polyelectrolytes (PELs) coatings

The first investigation point is to know if PEL layers are dense or porous. Next, main investigation points are the compatibility of PELs layers (some nanometers) on the relatively thick (μm) dense membrane, PELs stability, sorption(S) and diffusion(D) in PEL as well as in composite membranes.
Also, the PELs deposition in porous membranes consist of two possibilities: PELs can

deposit only inside the pore resulting in pore reduction or PEL blocks the pore and add a thin layer on the surface.

Finally, the investigation of PELs performance and comparisons, whether PELs on the dense or porous membrane is useful for improving the membrane separation.
In parallel, the choice of polyelectrolytes, number of LbL bilayers are crucial for achieving the expected properties after modification.

Stability of PELs coating in OSN conditions

Polyelectrolytes (PELs) stability in organic solvents (chemical hazard), high feed flow rates in tangential conditions (mechanical stress), PEL behavior (if any) at elevated temperature and pressure are critical points. The stability tests of PEL under OSN condition also includes, if a systematic protocol can be applied to control or guarantee their stability in the long run.

Controlled surface modification and performance of prototype membranes

The control of the surface modification in a nanometric level is targeted by developing protocols of polyelectrolyte modification.
Evaluation of OSN conditions for the best promising prototype membrane/s, to deliver optimum separation performance from a model feed. This objective mainly concerns the choice of model solutes, binary and multicomponent mixtures to test, developing OSN experimental procedure, and the choice of analytical methods to be identified and performed.

Influence of process parameters

Effect of hydrodynamic conditions, concentration polarization, and transmembrane pressure (TMP).
Interpretation of the mass transport results in terms of transfer mechanisms
Comparison of the best results with distillation, which is the benchmark technology.

0.2.2 Tasks to obtain the objectives

0.2.2.1 PHASE 1

(1) Investigation of the availability of commercial OSN membranes and their separation performances in different organic media, especially in toluene (Literature review, **Chapter** 1).

(2) Selection of OSN membranes, solutes, binary feeds of solvent and solute systems and ternary feeds of solvent, solute 1 (low MW, representative to hydroformylation product) and solute 2 (high MW, representative to catalyst-ligand)(**Chapter** 1 and **Chapter** 2).

(3) Performance evaluation of selected OSN membranes in terms of solvents fluxes and solutes rejection (**Chapter** 2).

0.2.2.2 PHASE 2

(1) Selection of best OSN membrane/s based on their performances and prioritize the selected membrane/s for the modification (**Chapter** 2).

(2) Investigation of modification techniques and selection of suitable modification methods (Literature review, **Chapter** 1).

(3) Preparation of new prototype membranes by surface modification and establish preparation protocols (**Chapter** 3, **Chapter** 4). Provide samples to partner team to carry out the test in a real hydroformylation system.

(4) OSN test of modified membranes in terms of solutes rejection and solvent permeation from different binary and ternary feeds (**Chapter** 3, **Chapter** 4).

0.2.2.3 PHASE 3

(1) Study of mass transport mechanism/s in both pristine and modified membranes (**Chapter** 2, **Chapter** 3, **Chapter** 4 **Chapter** 5).

(2) Feasibility tests for the technology transfer to separate hydroformylation catalyst and ligand from products and solvent (**Chapter** 5).

Chapter 1

LITERATURE REVIEW

The literature review reports the study of Organic Solvent Nanofiltration (OSN), preparation of prototype membranes by surface modification and their performances in organic media. In the beginning, investigation of OSN review papers, published from 1999 through 2019, and their main investigation areas are presented in **Table** 1.1. These review papers are used throughout the literature review and linked with other publications related to OSN.

Review Papers	**Key focus area of review**
Galizia and Bye (2018)	OSN sorption and diffusion, mass transport phenomena, polymers.
Shi et al. (2017)	Molecular separation, intrinsic membrane permeance, ultra high permeance membrane and concentration polarization.
Lim et al. (2017)	Polymeric OSN membranes, nanomaterials and cross-linking, industrial application.
Tul Muntha et al. (2017)	Layer-by-Layer, fouling, membrane preparation and methods, nanoparticles (NP's) and OSN.
Paul and Jons (2016)	Chemistry and fabrication of NF membrane, Interfacial polymerization.
Amirilargani et al. (2016)	membrane separation, modification, functionalized membranes, effect of modification and surface chemistry.
Mohammad et al. (2015)	State of the art overview of NF membrane, fabrication and modification, fouling and fouling mitigation and future direction of NF membrane development.
Lau et al. (2015)	Thin film composite (TFC) membrane, polyamide, nanomaterials and thin film nanocomposites (TFN).
Hermans et al. (2015)	Recent development of TFC for OSN and TFN.
Vural Gürsel et al. (2015)	Separation and recycling of transition metal catalyst by different methods, OSN-Industrial applications, an overview of separation and recycling homogeneous metal catalysts.
Buonomenna and Bae (2015a)	OSN in API's (Active Pharmaceutical Ingredients), solvent exchange, product purification, hybrid processes, polymeric materials for OSN, commercial OSN membranes and their stability in organic media, multi-stage OSN and catalyst (ToABr) recovery.

Table 1.1 continued from previous page

Szekely et al. (2014)	OSN sustainability assessment as a green technology, OSN challenges, and improvement of material fabrication and application, carbon footprint of OSN membranes, the concept of quality by design, process development and improvement.
Marchetti et al. (2014a)	A critical review of molecular separation, OSN membrane preparation, and performance and commercial membranes and their performance in both lab and industrial scale, mechanism of transport.
Joseph et al. (2014a)	Polyelectrolytes multilayer for membranes, Layer-by-layer preparation, separation, OSN, overview of fabrication and separation, potential applications.
Cheng et al. (2014b)	Advances in OSN polymeric membranes and their fabrication, cross-linking, polyelectrolytes, polyimides, transport mechanisms.
Vanherck et al. (2013)	Crosslinking methods for polyimide membranes and main applications and crosslinking chemistry and techniques.
Buonomenna (2013)	Sustainability of different membrane processes including RO, FO, OSN, membrane contactors, gas separation, and their materials, hybrid processes.
Cheng et al. (2011)	Positively charged NF membranes, fabrication methods, and surface modification, membrane characterization techniques.
Volkov et al. (2008)	OSN membranes, applications in petrochemicals, homogeneous catalysis, ionic liquid separations, solvent exchanges, multi-step organic synthesis.
Vandezande et al. (2008a)	Molecular separation in aqueous and organic phase, OSN, and related membrane processes, exhaustive review in OSN industrial applications.
Van der Bruggen et al. (2008)	Drawbacks of NF, fouling improvement, improving separation, chemical resistance and limited lifetime of membranes, insufficient rejection to overcome, modeling and simulation.
Hilal et al. (2004)	NF membrane, pretreatment, fouling, modeling.

Table 1.1: OSN review papers, published from 1999-2019, and their focused investigation areas

The general introduction of the literature review begins with an overview of the separation science of the last 100 years, which highlights the position of membrane separation compared to traditional separation processes. Next, a short comparison between ceramic and polymeric membranes, dead-end, and cross-flow systems are presented, including the main features of OSN.

Next, commercial polymeric membranes for OSN are focused based on actual market availability and their performance in catalyst recovery from toluene media. It has the importance to narrow down the list of the commercial OSN membranes that are high performing. Afterward, OSN mass transport mechanisms, critical parameters, and solute rejections are summarised and briefly discussed.

Finally, the literature review presents OSN membrane modification, including the use of different plasmas and polyelectrolytes in OSN membranes modification.

1.1 General Introduction

Separations processes account for $40 - 70\%$ of both the capital and operating costs in industry (Humphrey, 1997). Application of separation technologies are broad and involve numerous methods. Their application not only impacts costs and energy but also contributes to waste generation in the future. **Figure** 1.1 shows the maturity of different separation technologies over the last century and the position of membrane separation compared to others.

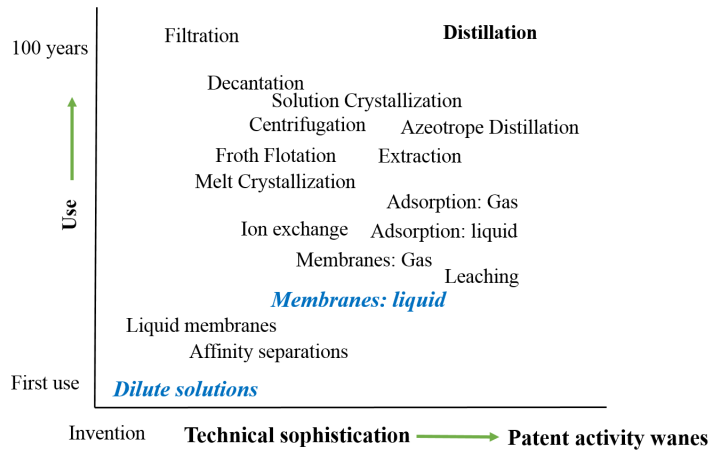

Figure 1.1: Separation techniques and their maturity. Adopted and redrawn from Adler et al. (2000).

Although some technologies have been used longer than other (**Figure** 1.1), no separation has reached its full maturity, i.e., not everything is known about the process, and further improvement is possible in each separation techniques. In the development of new research, two mainstream ways are often reported; first, the possibility of combining individual separation process to revitalize the separation industry (Adler et al., 2000) and second, new separation methods to develop, which is essentially non-distillation type but need to be as predictable as distillation.

The sustainability assessment of separation processes (**Figure** 1.1), conducted by DuPont®, refer to Organic Solvent Nanofiltration (OSN) as a Best Available Technology (BAT) when compared with other separation techniques such as preparative chromatography, distillation, extraction or crystallization.

OSN is relatively more energy-efficient, featuring low waste generation and operated at a mild condition (Szekely et al., 2014). It is, therefore, highly attractive in terms of energy, economy, environment, and safety (Vandezande et al., 2008a) (Geens et al., 2007).

The added advantage of OSN is simplicity in operation and application, which frequently involves three simple modes: concentration, solvent exchange, and purification. These modes are frequently used with a different combination that gives a wide range of application (Marchetti et al., 2014b).

The energy-saving aspect of OSN compared to distillation is presented in **Figure**1.2, showing that OSN only involves pump energy to operate while distillation requires evaporation and condensation, resulting in a significant energy difference. For a given task of concentrating m^3 ethanol, distillation demand much higher energy duty compared to OSN.

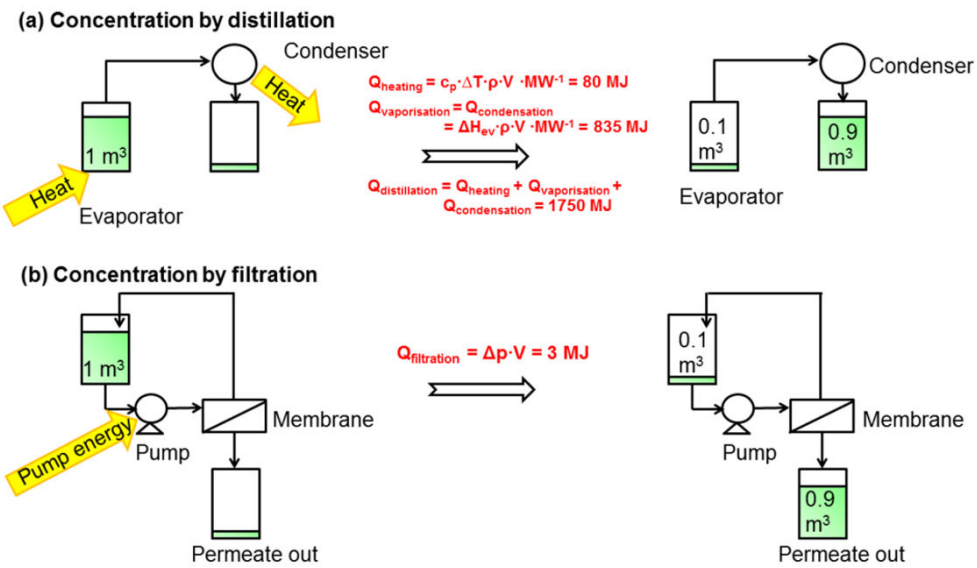

Figure 1.2: (a)Energy duty in distillation (b) Energy duty by OSN. Adopted from Marchetti et al. (2013)

.

This exciting technology, historically dated back to 1964, reporting separation of hydrocarbon solvents using a cellulose acetate membrane Sourirajan (1964). Later a pressure-driven solvent separation are reported in the1965 Loeb (1965). The term **Nanofiltration** was proposed for the first time during FilmTec® meeting in 1984 .

The potentiality of OSN is largely explored during last two decades, which makes it a recent technology. The first commercial success at an industrial scale is the MAX-DEWAX process by ExxonMobil® (Gould et al., 2001). First set of commercial OSN membranes appear in market during mid 1990's , manufactured by Grace division (White and Nitsch, 2000), Koch®, Solsep® and GMT® .

1.2 OSN main feature

Organic Solvent Nanofiltration (OSN) is a pressure-driven, membrane-based technique in which separation is carried out at the molecular level. In literature, OSN is often synonymously termed as Solvent Resistant Nanofiltration (SRNF) .
One of the most compelling features of OSN is that OSN membranes undergo a physical change due to the influence of the solvents. Often, the same membrane exhibit different permeation properties in different solvents, due to the variation in swelling degree (SD) (Vandezande et al., 2008a). Membranes having high swelling degree means that they are not totally solvent resistant; more accurately, they show good tolerance in some solvents. In terminology, using OSN, instead of SRNF, is more logical.

These membranes, either prepared in the laboratory or from the commercial origin, are mostly asymmetric composites , having a top selective layer of small thickness, supported by one or more mesoporous under-layer, as shown in **Figure** 1.3.
The top layer of OSN membrane (**Figure** 1.3) drives the separation properties such as flux and retention, whereas the support layer provides mechanical resistance, generated by transmembrane

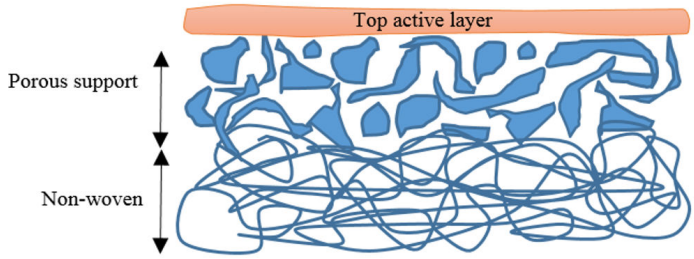

Figure 1.3: Scheme of a typical OSN membrane

pressure, applied on the upstream side of the membrane. The top layer of the membrane can be dense or porous, while the support layer is almost always porous.

Taking a few insights from the review papers listed in **Table** 1.1, the following statements are seemingly logical for OSN:

Under the influence of organic media and high transmembrane pressure, the compaction of the membrane can occur in the support layers. It gives potential challenges to maintain the functional integrity of both the active and support layers, along with high separation performance. In preparation, finding a suitable active layer with the right combination of support is also challenging. While most of the research focuses on the active layer and its performance, the role of support is somewhat ignored. Long term stability of these membranes under organic solvent is also significant to step-up the level of OSN research.

However, when separation task is based on size exclusion, it is readily understood that smaller pore of the membrane allows passing smaller particle but not bigger ones. If not, separation at the molecular level requires an advanced understanding of solute-solvent-membrane systems, swelling or non-swelling phenomena and solvent-solute-membrane affinities. Such complexity rule out the most straightforward size-dependent definition given by IUPAC 1996 nomenclature, which states Nanofiltration (NF) range to separate molecule is < 2nm (Vandezande et al., 2008a).

Next, Molecular Weight Cut-off (MWCO, is defined as the minimum molecular weight of a solute that is 90% retained by the membrane) is often used to describe the OSN membrane; however, MWCO of a membrane varies significantly depending on the swelling degree of the membrane. Solvents that contribute to higher membrane swelling exhibits high MWCO, compared to low swelling solvents. As a result, a single OSN membrane can exhibit different MWCO depending on solvents (Sammells and Mundschau, 2006) (Hermans et al., 2015). Indeed, it is a unique strength of a given OSN membrane that can be used in different solvents for different separation objectives.

In OSN feature, Applied pressure or transmembrane Pressure (TMP) is one of the main parameters. The operating pressure of OSN is reported $10 - 25$bar in Mulder (1998), whereas, numbers of literature report 10-40 bar or even more (Marchetti et al., 2014a). In practice, the highest applicable transmembrane pressure depends on active and support layers, their structural configuration, and solvents effects on the membrane, namely swelling. Besides, the same membrane can be operated at different pressure depending on the swelling and non-swelling solvent and can be termed as UF or NF membrane altogether (Vandezande et al., 2008b).
Taking the above discussion as a reference, an advance definition of OSN is:

OSN is an emerging membrane technology, based on dense or porous membranes, which usually consists of a thin active layer with one or two support layers. These membranes are stable in various organic solvents, and under pressure, molecular separation occurs based on the molar volume, size, and shape of molecules, including interaction among solvent-solute- membrane.

1.2.1 OSN performance parameters

The performance of OSN membranes is defined by the measurement of flux, rejection, permanence, and transmission of solutes.

1.2.1.1 Flux

Flux (J) is defined as the permeate volume (V_m) flow divided by the active membrane surface area (A) per unit time (t), as shown in the formula below.

$$J = \frac{V_m}{A.t} \tag{1.1}$$

1.2.1.2 Permeability/Permeance

The permeate flow per unit pressure defines membrane permeance and permeability is the flow normalized with the thickness of active layer. The relation between permeability and permeance can be expressed according to formula (1.2).

$$Permeance = \frac{Permeability}{Thickness(membrane)} \tag{1.2}$$

In OSN, permeance is more pronounced than permeability because it gives a direct indication of performance. Also, accurate thickness data of commercial membranes are rarely given by supplier and can vary depending on the swelling degree in different solvents. The formula (1.3) expresses the relation between flux and permeance.

$$J = L_p.TMP \tag{1.3}$$

Where, TMP is transmembrane pressure.
In other way permeation of solvents, i.e., hydraulic permeability (L_p) depends on the swelling of the membrane as well as the viscosity of permeate (η) which are related to the hydraulic resistance (R_m) of the membrane; expressed according to equation (1.4).

$$L_p = \frac{1}{\eta.R_m} \tag{1.4}$$

1.2.1.3 Retention or rejection and transmission

Retention or rejection (R%) is the percentage of the molecules retained by the membrane, according to the equation (1.5).

$$R = (1 - \frac{C_P}{C_R}).100 \tag{1.5}$$

Where, C_P is the concentration of solute in permeate and C_R concentration of solute in the retentate. Accordingly, transmission of solutes T_r (%) can be expressed according to equation (1.6).

$$T_r = \frac{C_P}{C_R}.100 = 1 - R \tag{1.6}$$

1.3 Operating modes of OSN: dead-end and cross-flow

The operating modes of OSN, namely dead-end and cross-flow configuration are schematically presented in **Figure** 1.4

The dead-end nanofiltration (**Figure** 1.4a), consists of a cylindrical, high-pressure batch cell, in which fixed feed volume is in contact with the membrane under stirring. The transmembrane pressure is applied in the upstream side by compressed gas (often nitrogen), that forces the feed to the downstream side. The rejected solutes accumulate on the upstream side; as a result, solute concentration increases in the feed.

In cross-flow or tangential flow nanofiltration (**Figure** 1.4b), feed solution passes along the surface of the membrane, which provides a continuous recirculation of feed throughout the upstream side. Often, a back pressure regulator valve is used to apply the desired pressure. As a result, the solvent passes through the membrane (permeate), while retained solute continue to pass along the membrane surface (retentate).

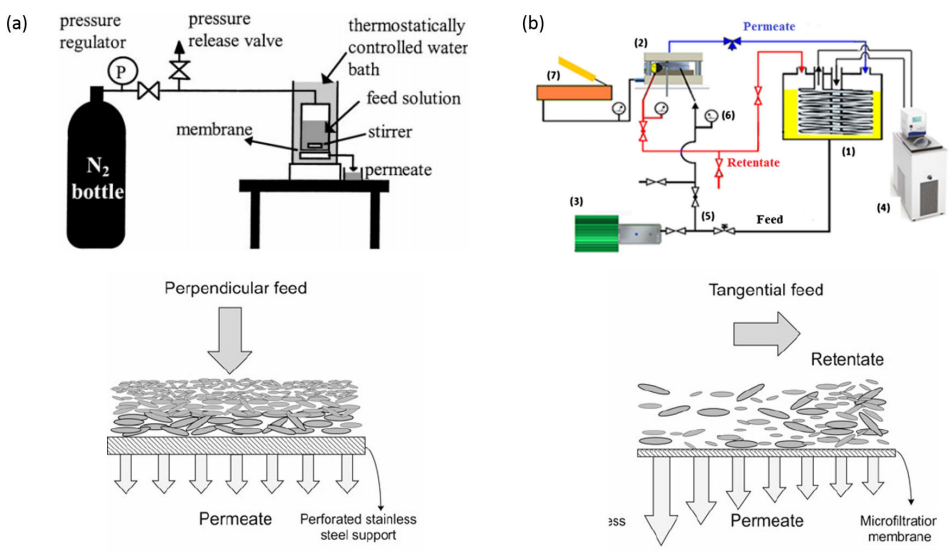

Figure 1.4: (a) Dead end OSN. Adopted and combined from MacHado et al. (1999), Joseph et al. (2014b), (b) Cross-flow OSN. Adopted and combined from Ben Soltane et al. (2016), Joseph et al. (2014b).

At first glance, cross-flow OSN is beneficial over dead-end due to the feed recirculation, allowing it to operate with high volume feed with high solute concentration and less solute accumulation. As a result, the membrane performs longer in the cross-flow rig.

However, the performance of a given membrane differ, when applied in the dead-end, and cross-flow using the same feed (Bhongsuwan et al., 2002) (Patterson et al., 2008). It is somewhat logical due to the faster solutes accumulation on the upstream side of the dead end. Therefore, regular and consistent performance is expected from cross-flow (Van der Bruggen et al., 2008). Indeed,

for both modes, fouling remains an essential limitation to be understood and controlled. Even though, relatively low fouling is reported for cross-flow, compared to dead-end (Bessiere et al., 2005).

Taking few examples from literature, OSN study of concentrating ethanolic extracts using dense PI-based Duramem in both dead end and cross-flow (Peshev et al., 2011) (Mello et al., 2010), (Tsibranska and Tylkowski, 2013), shows that the higher fluxes decline occurs in dead-end over cross-flow, upon increasing the concentration. (Koltuniewicz et al., 1995) reports a cross-flow rate, less than $0.8ms^{-1}$, flux decline is similar in both modes of OSN having the same oil-water emulsion in the feed. A steady flux obtained when cross-flow is $\geqslant 0.8ms^{-1}$.

Next, the rejection of a given solute by a dense membrane in both dead-end and cross-flow is reported to be similar, (Peshev et al., 2011) (Mello et al., 2010), (Tsibranska and Tylkowski, 2013), though (Tansel et al., 2006) reports higher ion permeation occurs in dead-end compared to cross-flow, causing lower rejection in dead-end OSN.

1.4 OSN membrane materials

The fabrication of OSN membranes fundamentally begins with three different materials- organic polymers, inorganics such as oxides, ceramics, and metals; and organic-inorganic hybrids. The various route to obtain OSN membrane in **Figure** 1.5 shows vast possibilities of fabricating OSN membranes, including porous ceramic, dense or porous polymeric, and Mixed Matrix Membrane (MMM).

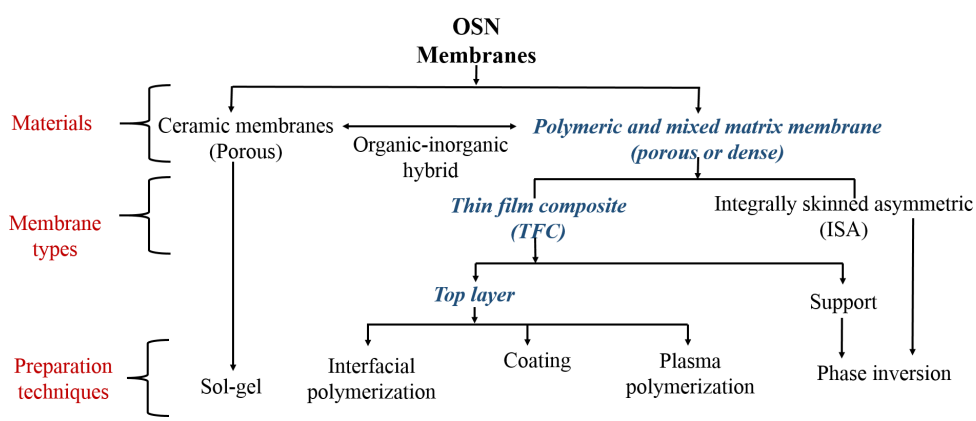

Figure 1.5: OSN membrane types and their preparation techniques.

Ceramic membranes possess asymmetric structures of at least two porous layers. While preparing, a suspension coating process applies a thin layer on a porous ceramic support. This process gives a pore size of 30nm (Ultra-filtration range) (Mishra, 2018). The smaller pore size of 2-3nm is reported via sol-gel process (Voigt et al., 2001). The smallest pore size of ceramic membranes is reported 0.9nm, exhibiting MWCO 450 $g.mole^{-1}$, commercialized by HITK® (Germany) under the name of Inopor(Mishra, 2018).
One of the potential challenges with ceramic membranes are their intrinsic hydrophilicity, which causes intrinsic high water flux (Hosseinabadi et al., 2014) but poor apolar solvents fluxes (Tsuru et al., 2004). Pore surface modification by silanation (Mishra, 2018) and functional membrane preparation by Grignard chemistry (Rezaei Hosseinabadi et al., 2014) are reported to overcome this challenge.
On the other hand, polymeric OSN membranes consist of a top active layer and underneath, a non-woven backing material. There are two well-pronounced types of membranes are reported in

literature- Integrally skinned asymmetric membrane (**Figure** 1.6a) and Thin-film composite (TFC) (**Figure** 1.6b).

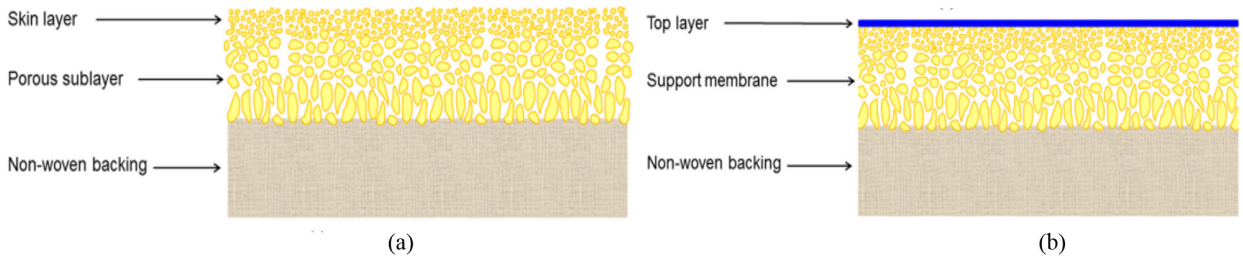

Figure 1.6: (a) Integrally skinned asymmetric (ISA) (b) Thin film composite (TFC) membranes.

Integrally skinned asymmetric membrane (**Figure** 1.6a) have a thin layer supported by porous sub-layers. The thin top layer is the main selective layer, typically prepared by phase inversion technique, developed by Loeb and Sourirajan (Loeb and Sourirajan, 1963). Phase inversion is an immersion-precipitation technique in which the casting solution undergoes to a non-solvent bath. Inside the bath, the polymer-rich phase forms the membrane and the poor polymer phase forms the pore due to the thermodynamics and kinetics of non-solvent exchange (Vandezande et al., 2008a) (Mulder, 1998).

On the other hand, Thin Film Composite (TFC)(**Figure** 1.6b) consist of an ultra-thin separating layer (usually in sub-micron range), cast on a top of a porous support. The dip-coating process fabricates the separating layer followed by interfacial polymerization on the support. In TFC membrane, support and barrier layer properties can be optimized independently, which add competitive advantages over Integrally Skinned Asymmetric (ISA) membranes (Vankelecom and Gevers, 2005), (Petersen, 1993) (Vandezande et al., 2008b).
Both ISA and TFC membranes further can be combined to obtain organic-inorganic hybrids, i.e., Mixed Matrix Membranes (MMM) (Soroko and Livingston, 2009). Several challenges and opportunities of these OSN membranes are summarised in the following comparison points:

(1) Ceramic membranes exhibit excellent mechanical, thermal, and chemical stability compare to polymeric membranes; they neither compact under pressure nor swell in organic solvents, easy to clean and requires low operating pressure. They do not have any pore filler; therefore, leaching possibilities do not exist. Membrane sealing is secure, and the spiral element does not require any spacer and glues. In contrary, up-scaling of the ceramic membrane is more complicated, and they are more brittle than polymeric membranes. Less selectivity and high cost of the material are significant drawbacks. Compare to polymers; choice of ceramic materials are limited. Metal hydroxide membranes are inherently hydrophilic; therefore, less favorable for apolar solvents.

(2) At first glance, polymeric membranes are attractive because of their low material price, ease of fabrication, and high potential of up-scaling. Next, polymeric TFC membranes exhibit higher polar and apolar solvents permeance than ISA membranes. For TFC thin barrier layers, a large variety of chemical compositions are available (linear and cross-linked polymers), whereas ISA is limited to linear, soluble polymers. Only a few of such linear polymers have the right combination of flux and solute rejection characteristics to generate commercially attractive ISA membranes (Petersen, 1993) (Marchetti et al., 2014a).

(3) Finally, composite organic-inorganic membranes, known as mixed-matrix membranes are

attractive in terms of swelling reduction as well as flux decline due to compaction (if any), and exhibits improved mechanical stability (e.g., they are less brittle than ceramic membranes). Mixed matrix membranes (MMMs) can combine the properties of both polymeric and inorganic materials to tailor a membrane with desirable properties such as excellent solvent stability, high rejection, high flux, and anti-fouling properties.

1.5 OSN Commercial membranes

Commercially available polymeric membranes are mostly composite membranes, often exhibit the structure,shown in **Figure** 1.3. Even though the choice of polymer is broad, right properties of the polymer for OSN membrane makes the OSN material choice limited in a few. Up to the moment, the most popular active layer materials are polyimide (PI), polydimethylsiloxane (PDMS), polyamide (PA) and Polyethersulfone (PES). When cross-linked, these polymers exhibit broad stability in organic solvents Cheng et al. (2014b), Drioli et al. (2017). The support materials are typically polyacrylonitrile (PAN), polypropylene (PP), and PI. A list of commercial OSN membranes is presented in **Table** 1.2 and a brief descriptions of mostly used polymers are summarised in **Figure** 1.7.

Commercial name /manufacturer	**Separating layer**	**Dense/Porous**
PERVAP 4060 / Sulzer	PDMS	Dense
MPF 44 / Koch membrane	PDMS	Dense
MPF 50 / Koch membrane	PDMS	Dense
GMT-oNF-2/GMT	PDMS	Dense
SolSep NF 070706 / SolSep	PA/PDMS	Dense
SolSep NF 010306 / SolSep	PA/PDMS	Dense
SolSep NF 010206 / SolSep	PA/PDMS	Dense
SolSep NF 030306 / SolSep	PA/PDMS	Dense
SolSep NF 030306F / SolSep	PA/PDMS	Dense
SolSep NF 030105 / SolSep	PA/PDMS	Dense
Starmem 120 / MET	PI	Dense
Starmem 122 / MET	PI	Dense
Starmem 240 / MET	PI	Dense
Starmem 400 / MET	PI	Dense
DuraMem 200 / MET	PI	Dense
DuraMem 400 / MET	PI	Dense
PuraMem 280 / MET	PI(silicone coated)	Dense
PuraMem 600 / MET	PI(silicone coated)	Dense
NanoPro S 3012 / AMS	PAN	Porous
NanoPro S 3014 / AMS	PAN	Porous
Desal 5 / Osmonics	PA	Unknown
Desal 5-DK / Osmonics	PA	Unknown
N3oF /Nadir	PES	Unknown
NF PES 010/Nadir	PES	Unknown

Table 1.2: Commercial OSN membranes. Summarised from Scarpello et al. (2002a), Ben Soltane et al. (2013), Ben Soltane et al. (2016), Hendrix et al. (2012), Darvishmanesh et al. (2011a), Buonomenna and Bae (2015a) .

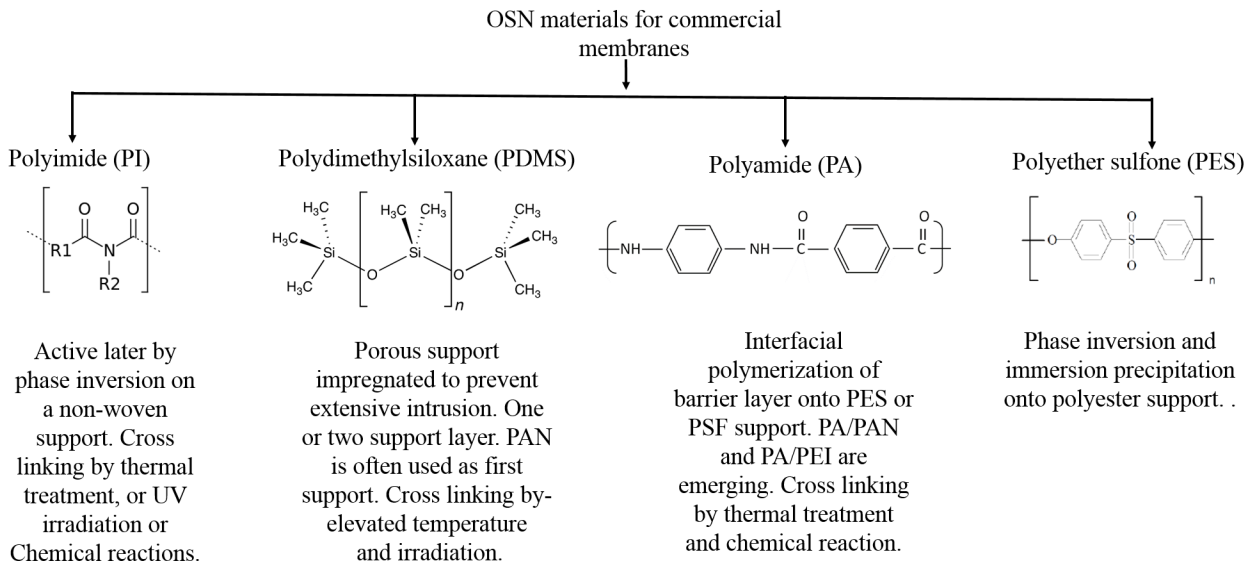

Figure 1.7: Brief desciption of OSN materials mostly used commercially Cheng et al. (2014b) (Drioli et al., 2017).

Initially, these materials (**Table** 1.2) were used to fabricate NF membranes for aqueous media. When applied in aqueous NF, these polymers typically did not need cross-linking. However, for OSN membrane, cross-linking is a key step to ensure their chemical and thermal stability (Hayes, 1988), (Kita et al., 1994), (Jiang et al., 2009) (Shao et al., 2004).
Apart from cross-linking, the mixed-matrix approach often catches the commercial interest, for example, impregnation of rigid nanofiller in PDMS results in a swelling reduction.

Among OSN materials (**Figure** 1.7), polyimides represent a very diverse group of materials ranging from homopolymers of various chemical structures to polyimide blends and segmented block copolymers that provides high thermo-oxidative stability and excellent mechanical properties (Volksen, 2001). Next, PDMS is highly interesting because PDMS represents a fully saturated backbone of alternating silicon and oxygen atoms. The $Si-O$ links in the chain have exceptionally high bond energy of 451 kJ/mol (For comparison, bond energy of $C-C$ links is 352 kJ/mol) and very high chain mobility. The organic side groups shield the backbone, so surface energy is low. These characteristics of PDMS provides excellent high-temperature resistance, combined with low-temperature flexibility, high resistance to chemicals, and environmental influence and water repellent surface (Wacker Chemie, 2011). Afterward, the PA membrane exhibits broad stability in organic solvents. The major challenge for PA is the stability of support (Solomon et al., 2012). Finally, PES exhibit somewhat limited stability in organic media.

As newly emerging new OSN materials, polyoxadiazole (high thermal stability), polyoxatriazole, polyketone (high-performance thermoplastic with a high melting point) and Polybenzimidazole (very high melting point, exceptional thermal and chemical stability) exhibit high potentiality but they are still in the exploration phase for using in commercial OSN membrane (Drioli et al., 2017).

1.5.1 Prominent OSN membranes based on Polyimide (PI)

Polyimides (PI) refers to high-performance polymers because of their exceptionally high thermo-oxidative stability (Critchley et al., 2013). Structural composition of aromatic polyimides consist of heterocyclic imide and aryl groups, which are linked sequentially. Such rigid structures of PIs result in high glass transition temperature ($T_g > 300°C$) and excellent mechanical strength. The linearity and stiffness of the cyclic backbone allow for molecular ordering. This phenomenon results in lower Coefficients of Thermal Expansion (CTE) than those found for thermoplastic polymers having coiled, flexible chains (Hedrick et al., 1997), and stable in most of the organic solvent, showing high potential for catalyst recycling, product separations and, solvent exchange (Vandezande et al., 2008a). Examples of commonly used PI products are P84 and Matrimid (Vanherck et al., 2010) (Van der Bruggen et al., 2008) (Soroko et al., 2011) and commercially fabricated PI membranes are reported ISA types, prepared by phase inversion (Scarpello et al., 2002a).
Most studied PI-based membrane came from Membrane Extraction Technology (MET). Unfortunately, some of their high potential OSN membranes are no longer available in the market. The first OSN membrane applied in a large industrial scale was PI-based Starmemem membrane (in Max-Dewax process)(White and Nitsch, 2000). Relatively new PI membranes from MET are DuraMem and PuraMem (http://duramem.evonik.com/product/duramem-puramem/en/).

1.5.2 Prominent OSN membranes based on Polydimethylsiloxane (PDMS)

PDMS is an organosiloxane elastomeric polymer often termed as **silicone rubber**. It consists of a siloxane (Si-O) backbone substituted with methyl groups that give it a high fraction of free volume, facilitating high diffusion coefficients for solvents and gases (Merkel et al., 2000) (Reijerkerk et al., 2010). When cross-linked, this polymer is stable in most organic solvents.

The first commercialized PDMS based OSN membrane is MPF 50 and MPF 60 by Koch membrane systems. These membranes exhibit high rejection of phase transfer catalyst (Vandezande et al., 2008a). Next, SolSep OSN membranes believed to possess a silicone top layer (Van der Bruggen et al., 2008), are commercialized by Dutch company SolSep BV. These membranes are stable in alcohols, esters, and ketones, and some of them are also stable in aromatics and chlorinated solvents. PDMS based GMT membranes (https://www.borsig.de/) are commercialized by GMT-GmbH, Germany, (http://www.gmtmem.com), found highly effective to separate $Rh - PPh_3$ type catalyst from n-hexanal-toluene system (Schmidt et al., 2014).
Recently emerged PDMS based commercial OSN membrane is PERVAP® 4060, marketed by Sulzer®. It was applied for the first time in OSN by (Ben Soltane et al., 2016), showing its high potential for the separation from ethanol, toluene, DMC, hexane, and heptane.

1.5.2.1 Comparison of toluene permeance in PDMS and PI membranes from literature

This section intends to compare toluene permeance in different PDMS and PI-based commercial membranes. Toluene permeance data in these two polymers are listed in **Table** 1.3, shows inconsistent permeance data.

Membrane	Active material	Membrane property	Permeance ($L.m^{-2}.h^{-1}.bar^{-1}$)	Reference
Pervap 4060	PDMS	Hydrophobic	2	(Ben Soltane et al., 2013)

Table 1.3 continued from previous page

Membrane	Active material	Membrane property	Permeance ($L.m^{-2}.h^{-1}.bar^{-1}$)	Reference
MPF 44		Hydrophilic	NA	(Zhang et al., 2016)
MPF60	PDMS	Hydrophobic	0.6	(Yang et al., 2001)
MPF50		Hydrophobic	1	(Nair et al., 2002)
GMT-oNF2	PDMS	Hydrophobic	2.8	(Zeidler et al., 2013)
GMT-oNF2	PDMS	Hydrophobic	0.7	(Schmidt et al., 2014)
Starmem120		Hydrophobic	0.4	
Starmem122	PI	Hydrophobic	0.6	(Zhang et al., 2016)
Starmem240		Hydrophobic	0.4	
Puramem280	PI	Hydrophobic	1.5	(Rundquist et al., 2012)
Puramem280	PI	Hydrophobic	0.6	(Schmidt et al., 2014)

Table 1.3: Deviation in toluene permeance in the active layer of PDMS and PI based commercial membranes.

Similar inconsistency in permeance data can be found for other solvent, for instance, MeOH flux in MPF 50® is reported 33 - 37 $Lm^{-2}h^{-1}$ (Zhao and Yuan, 2006b) at 30 bar, whereas (Machado et al., 2000) reports 175 $Lm^{-2}h^{-1}$ at that same transmembrane pressure. In addition, (Whu et al., 2000), (Silva et al., 2005) reports that this membrane does not give any reproducible MeOH flux at 30 bar. Indeed, drawing an apparent reason for such data deviation from one literature to another in **Table** 1.3, was not understood. The only insight has been obtained to establish a standard OSN protocol in order to minimize the deviation.

1.5.3 Prominent OSN membranes based on other polymers

Apart from PDMS and PI, other emerging membranes are porous PAN-based AMS® membrane; stable in acid, alkaline, and organic solvent media (`http://www.amsmembrane.com`), PoroGen® based on polyether ether ketone (PEEK-SEP) with tailored pore size and surface chemistry (`http://www.porogen.com`), PolyAn® recently commercializes membranes with molecular surface engineering and molecular surface imprinting (`http://www.poly-an.de`). These membranes are claimed to be applicable for the separation of aromatics from aliphatics, olefins from aliphatics, and the separation of other organic mixtures.

1.6 Applications of OSN

The most significant and state of the art of OSN application is Max-Dewax ® process by EXXON MOBIL. In this process, waxy feed is mixed with organic solvents such as methyl ethyl ketone (MEK) or methyl isobutyl ketone (MIBK) and toluene. The paraffinic waxes are first separated by crystallization, leaves behind a mixture of lube oil with solvent. The solvent recovery step is replaced by OSN instead of distillation, using Polyimide (PI) based membrane, results in 50% recovery of the solvent with 99% purity at 28-55 bar and 21°C. The return of investment was obtained in one year (Priske et al., 2016).

Other potential applications of OSN are fuel treatment Tarleton et al. (2009), (Tres et al., 2014), natural oil processing (Manjula and Subramanian, 2006), bioactive compound and pesticide separation (Teixeira et al., 2014), API separation (Geens et al., 2007), (Sereewatthanawut et al., 2010), solvent recovery purification (Tres et al., 2014) and catalyst separation (Schoeps et al., 2009).

A comprehensive list (**Table** 1.4) of OSN-application is adopted from (Priske et al., 2016), which shows the potentiality of a given membrane in different separation tasks.

Solvent used	**Application**	**Membrane/s**
Acetone	Vegetable oil deacidification	PA
Chloroform/toluene	Removing metal and carbon residue from heavy oil	PVDF
DMF	Pharmaceuticals, purification of polymer PDMS,	PI
Cyclopentane	Fractionation of hydrocarbon oils	P/carbonate
Ethanol	Flavour, pigment, vegetable oil etc.	Several
n-heptane	Aromatics from heavy oil	P/propylene
Hexane	Vegetable oil refining. regeneration of used lube oils	PDMS, PI
Lube base oil	Concentration of furfurals	PDMS
Methanol	Refining of vegetable oils, pharmaceuticals Composites	ceramics
Methyl esters	Biodiesel, vitamins	Composites
MEK	Removal of dewaxing solvents	CA, PI
Paint	solvents Treatment of paint wastes	PI
n-Paraffins	Lube oil dewaxing	CA, PI
Propane	Oils from organic solvents	P/carbonate, PI
Toluene/DMF/xylene	Removal of low MW compounds in polymer manufacture	PI
Vegetable oil Dewaxing	recovery of dewaxing aids	PES, PI

Table 1.4: Application of OSN in separation (Priske et al., 2016).

1.7 Solute rejection by PDMS and PI in toluene media

At first glance, solutes rejection by OSN membranes is frequently reported and summarised in review papers (**Table** 1.1). However, these papers do not draw any boundary on types of solvent. In this section, toluene was first fixed as the solvent, and solutes rejection by PDMS and PI membranes were investigated, firstly by focusing on review papers, listed in **Table** 1.1 and next, OSN publications mostly from 1999-2019 was reviewed for solutes separation from toluene;in order to make the **Table** 1.5 as much as exhaustive possible. Next, solutes rejection in PDMS and PI membrane are plotted in **Figure** 1.8 against solute molecular weight. No clear correlation was obtained.

Membranes	**Material**	**Solutes**	**MW**	P^1	R^2	**Reference**
MPF 60	PDMS	Solvent blue	350	0.4	84	(Yang et al., 2001)
Starmem 122	PI	ToABr	546	0.5	>99	(Nair et al., 2002)
		Heck Catalyst	749	1	90	
		Iodoheptane	226	0.4	22	
Starmem 122	PI	ToABr	546	1	96	(LIVINGSTON et al., 2003)
Starmem 122	PI	ToABr	546	1.1	99	(Peeva et al., 2004)
PDMS coated on PAN	PDMS/PAN	PEG 400	400		50	(Ebert et al., 2006)
		PEG 900	900	8.2	87	
		PEG 1500	1500		99	

Table 1.5 continued from previous page

Membranes	Material	Solutes	MW	P^1	R^2	Reference
Starmem 122	PI	API	189	1	43	(Geens et al., 2007)
			313		55	
			435		80	
			531		85	
Starmem122	PI	Rhodonile blue	778	1.1	98	(Darvishmanesh et al., 2010a)
		Sudan black	276	1.3	92	
		Sudan II	456	1.3	62	
Starmem 122	PI	Sudan black	456	1.3	79	(Darvishmanesh et al., 2010b)
		Sudan 408	464		78	
Starmem 240	PI	Sudan black	456	2	87	(Darvishmanesh et al., 2010a)
Starmem122	PI	API	600	1.2	99	(Rundquist et al., 2012)
Starmem 240	PI	API	600	2	99	(Rundquist et al., 2012)
Puramem 280	PI	API	600	1.5	45	(Rundquist et al., 2012)
P84 PI	PI	Styrene Oligomer	600	0.9	97	(Solomon et al., 2012)
GMT-oNF 2	PDMS/PAN	tetracosane	338	2.8	75	(Zeidler et al., 2013)
P84+ hydrphobic TFC-Si	PDMS/PI	PEG	400	1.1	97	(Solomon et al., 2012)
Composite PDMS/ PI	PDMS	PEG	282	2	64	(Postel et al., 2013)
		Stearic acid	284		69	
		Polystyrene	269		78	
		Octadecane	256		41	
Starmem 122	PI	Grubbs-Hoveyda II	627		96	(Rabiller-Baudry et al., 2013a)
C8 alkyl chain on ceramic	C8 alkyl chain	Umicore M51 diethyl diallyl malonate	654	0.6	99	(Ormerod et al., 2013)
			240	0.6	40	
Puramem 280	PI	Triphenyl phosphine	262	0.6	73	(Schmidt et al., 2014)
GMT-oNF-2	PDMS	Triphenyl phosphine	262	0.7	38	(Schmidt et al., 2013)
Starmem 122	PI	carbonylhydridotris (triphenylphosphine) rhodium(I)	400	3.6	93	(Gorbunov et al., 2015)
Pervap 4060	PDMS/PAN	Sudan blue	350	2	35	(Ben Soltane et al., 2016)
		n-tetracosane	338		56	
		Red 22	439		60	
		n-triacontane	422		99	
		Alphazurine FG	792		100	
		n-pentacontane	703		96	
Pervap 4060	PDMS/PAN	n-tetracosane	338	2	40	(Ben Soltane et al., 2016)
TFC via IP	PA/P84 PI	SO	236	0.1	96	(Solomon et al., 2012)
TFC via IP	PA/PEEK	SO	236	2	98	(Hermans et al., 2015)

Table 1.5 continued from previous page

Membranes	Material	Solutes	MW	P^1	R^2	Reference
TFC via coating	(PIM-1 /PEI)/PAN	HPB	535	1.3	95	(Fritsch et al., 2012)
Polymeric ISA	P84/PI	SO	236	3.6	95	(Toh et al., 2007)
Polymeric ISA	PI/ Starmenm 122	SO	236	0.6	87	(Solomon et al., 2012)
Polymeric ISA	PI/ Starmenm 122	SO	380	0.7	90	(Fritsch et al., 2012)
Polymeric ISA	PI/ Crosslinked P84	SO	236	0.2	90	(Fritsch et al., 2012)
TFC Via IP	PA/ P84 PI	SO	236	0.3	96	(Jimenez Solomon et al., 2013)
TFC via IP	Hydrophobic PA/P84 PI	SO	236	1.7	97	(Fernanda et al., 2012)
TFC via IP	Hydrophobic PA/PEEK	SO	236	2	98	(Solomon et al., 2012)
TFC via coating	PDMS/PI	Wilkinson Catalyst	925	1.2	78	(Gevers et al., 2005)
TFC via Coating	(PIM-1/PEI) /PAN	HPB	535	1.1	94	(Fritsch et al., 2012)

Table 1.5: Solutes rejection in commercial membrane in toluene.

P^1: Global toluene permeance in $Lm^{-2}h^{-1}bar^{-1}$.
R^2: Rejection (%) in toluene media.

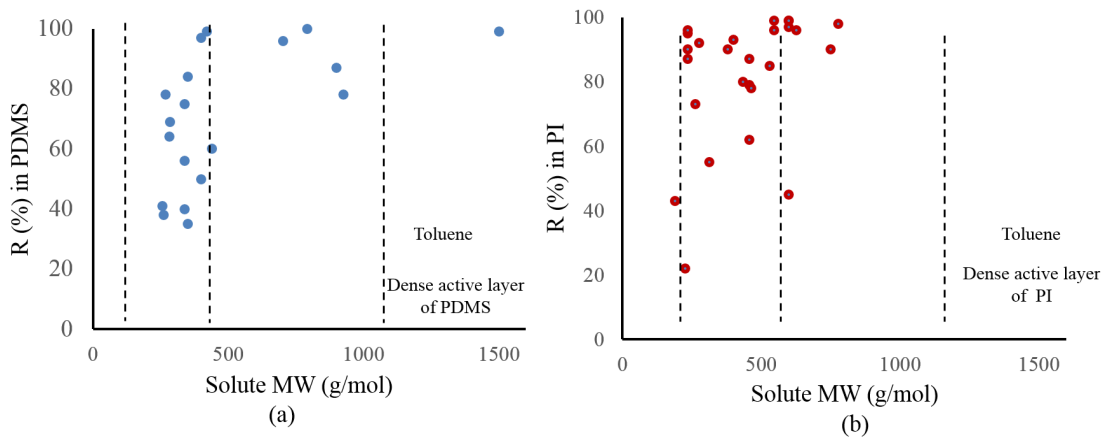

Figure 1.8: Solute rejection map for PDMS and PI in toluene media.

1.8 Homogeneous catalyst recovery by OSN in toluene media

Homogeneous catalysis, by definition, refers to a catalytic system in which substrates for a reaction and catalyst components (in many case organometallic complexes) are brought together in one phase, most often the liquid phase. Organometallic catalysts consist of a central metal surrounded by organic (and inorganic) ligands. Both the metal and the large variety of ligands determine the properties of the catalyst. The success of organometallic catalysts lies in the relative ease of catalyst modification by changing the ligand environment (Cornils et al., 2017).

The application of homogeneous transition metal catalysts offers the chance to create highly efficient processes for chemical industries. Since these tailor-made catalysts show high activity and high selectivity during the reaction, recycle streams of substrates and waste streams of side products can be reduced significantly. Often the separation and recovery of these precious catalysts is the critical operation within a process, as the catalyst and product/s are dissolved both in one single phase. Usually, a homogeneously catalyzed process becomes only economically feasible if an efficient catalyzed recovery is achieved (Behr and Neubert, 2012). In terms of homogeneous transition metal catalysis, the success of the catalyst recovery strongly depends on the stability of the catalytic complex and is distinguished within three types of scenario (Cole-Hamilton and Tooze, 2006).

▶ **Scenario 1 :** Catalyst separation is feasible without direct recycling. Catalyst residues can be concentrated and returned to a precious metal refiner to regain the catalyst metal.

▶ **Scenario 2 :** Catalyst separation at severer conditions (e.g., higher temperatures) which lead to the recovery of the precious metal but than a replenishment of the ligand is necessary to regain the active catalyst species.

▶ **Scenario 3 :**Separation technique/s that preserves the active catalyst and direct recycling to the reactor without any further interference.

The most notable and arguably the most damaging, inherent disadvantage of homogeneous catalysts, and the factor preventing the commercialization, is the difficulty in recovering the catalyst from a reaction medium in both an active and reusable form. It is due to energy and cost-intensive procedures, i.e., distillation, evaporation, adsorption, etc., for the recovery of a homogeneous catalyst which makes the application thereof highly unfavorable from an economic point of view (Cole-Hamilton and Tooze, 2006). Furthermore, current recovery methods employed, especially distillation, use severe conditions to initiate the separation which is usually destructive to the integrity and efficiency of the catalyst and require additional costs to regain the catalytic activity through pretreatment before it can be recycled and reused. These methods are not only destructive but generate large quantities of inactive metal waste, which adds an environmental imperative to the recovery of these catalysts (Cano-Odena et al., 2010). Thus, the availability of robust, efficient and universal unit operations for the recovery of homogeneous catalysts can contribute to the further increase of homogeneously catalyzed processes.

A promising approach for the separation of product and catalyst is the application of OSN. Mild separation conditions and low energy demand distinguish OSN from other separation techniques, e.g., distillation and crystallization. OSN potentiality in catalyst recovery in different solvent media are investigated in in many literature and pioneering work by (Luthra et al., 2002), (Nair et al., 2002), (Peeva et al., 2014), (Scarpello et al., 2002a), (Vanherck et al., 2013), (De Smet et al., 2001),

(Aerts et al., 2006), (Siew et al., 2013); mostly Livingston and Vankelekom group as well as Priske. A critical and comprehensive demonstration of OSN for catalyst recycling was reported in (Cheng et al., 2014a) and (Marchetti et al., 2014a) (Jansen et al., 2013). (Janssen et al., 2011)
Solvents effect on catalyst recovery by OSN is crucial because of the change of the membrane due to the solvent. For example, $HRh(CO)(PPH_3)_3$ catalyst retain only 54% in GMT-oNF (PDMS) membrane with 1-pentanol. When toluene was used, the rejection increased to 90% in the same membrane (Schmidt et al., 2014). Wilkinson catalyst (MW 925) retain 57% in MPF 50 (PDMS) in THF. The same catalyst retains 86% in MPF 50 with EA solvent (Scarpello et al., 2002a)

In bulk chemistry, typical catalytic reactions that have widely considered for OSN are metathesis, suzuki coupling, palladium-catalyzed cross-coupling, hydroformylation, and telomerization. Evonik's membrane reactor is an excellent example of it where PDMS based membrane shows high catalyst rejection for bulky Grubbs complexes in olefin metathesis, olefins, and paraffins (Readiness and Industries, 2010) (Schoeps et al., 2009).

At the industrial scale, it is more likely that homogeneous catalyst separation focuses more on obtaining high purity product rather than recovering the catalyst in their active form. Distillation is, therefore, the first consideration for catalyst removal (Readiness and Industries, 2010), which causes the irreversible deactivation of the catalyst. The loss of the catalyst has a direct impact on cost. The ligand is also a high-cost component temperature-sensitive (Cole-Hamilton and Tooze, 2006) (Vural Gürsel et al., 2015) (Priske et al., 2010) (Buonomenna and Bae, 2015b) Peeva et al. (2014). Evonik shows that switching to membrane-based process for metathesis, Suzuki coupling, palladium-catalyzed cross-coupling, hydroformylation and telomerization reactions results in a 30% lower investment costs, and 75% lower operational costs which corresponds to a saving of 1 million euro per year (Vural Gürsel et al., 2015).

PI-based membrane from MET-Evonik exhibits high rejection, more than 90% of Jacobsen catalyst, Wilkinson catalyst, Hoveyda-Grubbs commercial pre-catalyst, and Pd-BINAP; respectively dissolved in tetrahydrofuran (THF), ethyl acetate (EA) and dichloromethane (DCM). (Rabiller-Baudry et al., 2013b) (Scarpello et al., 2002b). Next, PI-based DuraMem 200 and DuraMem 400 also display high potentiality to recover Rhodium based catalyst (Shaharun et al., 2012). In PDMS/PI composite, Wilkinson catalyst retention was obtained 78% in toluene media (Gevers et al., 2005). Another PDMS based MPF^{TM} membranes are found considerably effective though it suffers from low solvent fluxes. MPF^{TM} 50 shows 92.8% rhodium catalyst retention at a pressure of 27.5 atm (in acetone) whereas MPF^{TM} 60 (MWCO 400) shows 97 to 98% Rh catalyst retention (Volkov et al., 2008) (Micovic et al., 2014).

From the membrane side, both porous and dense membrane can be useful for specific solute-membrane system depending on the targeted application (Volkov et al., 2008), (Tsuru et al., 2003), (Robinson et al., 2005a) (Silva et al., 2005). A porous membrane with tunable pore size could be beneficial to obtain high solvent permeation while small pore size can lead to high rejection. Nevertheless, the challenge is to obtain very low pore size (White and Nitsch, 2000).

Similar to the previous section catalyst rejection by PDMS and PI membranes in toluene media is summarised in **Table** 1.6 and catalyst molecular weight are plotted in **Figure** 1.9 against the rejection data in toluene. Again, no clear correlation was established.

Membrane	Separating layer	Homogeneous catalyst/ ligand	MW (g/mol)	Rejection (R%)	Reference
GMT-oNF-2	PDMS	Triphenylphosphine Biphephos Xantphos	262 787 579	66 98 95	(Dreimanna et al., 2016)
PAN/PDMS	PDMS	Hoveyda-Grubbs complex	1375	>99%	(Schoeps et al., 2009)
GMT-oNF-2	PDMS	HRh(CO)(PPh3)3	920	90	(Schmidt et al., 2014)
GMT-oNF-2	PDMS	HRh(CO)(PPh3)3 Rh-BIPHEPHOS Rh-Xantphos	920 900 680	99 99 99	(Dreimann et al., 2016)
Starmem 228	PI	Hoveyda-Grubbs II Enlarge Hoveyda-Grubbs II	627 2195	70 90	(Keraani et al., 2008)
PDCPD	Polydicyclo-pentadiene	Binol Ligand	286	72	(Long et al., 2011)
Starmem 122 Duramem 300	PI PI	Hoveyda-Grubbs II	627	>96 >46	(Rabiller-Baudry et al., 2013a)
Starmem series	PI	Rh-based	920	>99	(Priske et al., 2010)
Starmem series	PI	Rh-based	200-400	>94	(Fang et al., 2011)
Starmem122 Sratmem240	PI PI	HRh(CO)(PPh3)3	920	81 95	(Pelarut et al., 2013)
Puramem280	PI	HRh(CO)(PPh3)3	920	96	(Schmidt et al., 2014)

Table 1.6: Homogeneous catalyst retention by OSN membranes in toluene media

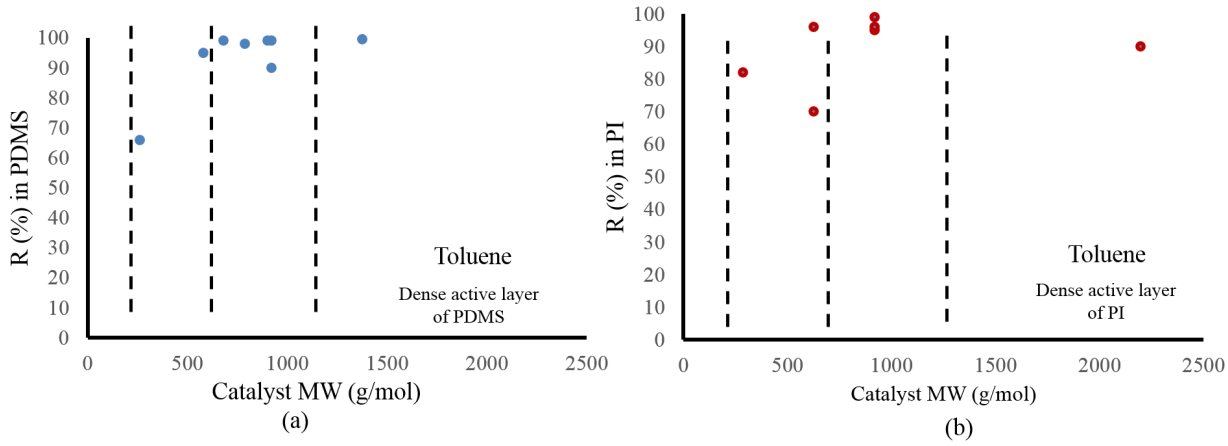

Figure 1.9: Homogeneous catalyst rejection map for PDMS and PI in toluene media.

1.9 Mass transport mechanisms

1.9.1 Fundamentals of mass transport in membranes

The basic principle of membrane mass transport begins with permselective barrier or interface between two phases and transport of a compound through the membrane from one phase to another under specific driving forces (**Figure** 1.10).

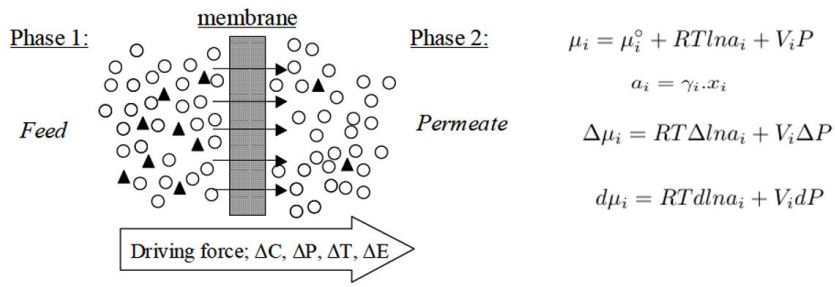

Figure 1.10: Schematic of OSN separation process with different driving process

The performance is described by flux (**Equation** 6.10) and rejection (R) factor (**Equation** 1.5) and transport of molecules from one phase to another depends on force/s that acts on the molecule (Mulder, 1998).

The difference in chemical potential ($\Delta\mu_i$) is caused either by the pressure difference across the membrane (ΔP) or concentration gradient (ΔC) between the two-phase or from temperature (T) difference. The chemical potential (μ) is related to the principle from Gibbs free energy (Wijmans and Baker, 1995) (Mulder, 1998). For isothermal condition, the chemical potential is determined by pressure and concentration, which is related to the activity coefficient and mole fraction. The difference of chemical potential ($\Delta\mu_i$) is therefore determined by concentration term and pressure.

1.9.1.1 Transport through porous membranes

Porous membranes consist of a solid matrix with defined pores which have varying diameters ranging from $< 2nm$ to more than $20\mu m$ (Strathmann et al., 2011). The separation by the porous membrane mainly depends on the molecular size of the solute and membrane pore size distribution, pore geometry, pore continuity, and porosity (Baker, 2007).

Mass transport through pores is typically described by convective flow, Knudsen diffusion, and pore surface diffusion. When pores are much larger than the molecule, transport occurs by the convective flow. If the pore size is smaller than the mean free path (average distance traversed by a molecule between collision) of the molecule (λ) the convective flow is replaced by Knudsen diffusion. Finally, when the molecule is sufficiently small, molecular sieving takes place excluding molecules that are larger than the pore size (Mulder, 1998).

1.9.1.2 Transport through dense membranes

In dense, nonporous membrane, the polymer matrix and molecular chain create global morphology with intrinsic voids. Contrary to porous membranes, mass transport through a dense membrane occurs by the solution-diffusion (SD) mechanism. The solubility and diffusivity of transporting molecules govern the permeability of the membrane according to the equation (**Equation**1.7).

$$Permeability(P) = Solubility(S).Diffusivity(D) \tag{1.7}$$

The solubility is a thermodynamic parameter, depends on the molecule that is dissolving in the membrane. The diffusivity term, on the other hand, is a kinetic parameter that defines how fast a dissolved component is transported through the membrane. The diffusivity is dependent on the molecule being transported and the geometry of the polymer membrane. For dense system, the solution-diffusion model and free volume diffusion model are the most widely accepted models (Wijmans and Baker, 1995).

1.9.1.3 Solution-diffusion model

The solution-diffusion model begins with three assumptions (Wijmans and Baker, 1995) :

1. **Sorption:** Selective uptake of one of the components on the feed side of the membrane.
2. **Diffusion:** Selective transport through the membrane.
3. **Desorption:** Evaporation on the permeate side of the membrane in the vapor phase.

Sometimes modified SD model is reported in OSN literature, namely the solution-diffusion-imperfection model, which takes into account the possibility of fine pores within the membrane matrix. In such case, mass transport includes diffusion terms as well as flow-through pores (Sherwood, 1967) (Yaroshchuk, 1995).

1.9.1.4 Free volume diffusion model

The transport model in dense and porous system, so far based on the mechanistic approach to describe the transport depending on the nature of the membrane. One simplified approach is to apply resistance-in-series model that describes how mass transfer of a given component from one phase to another encounter a resistance according to (**Figure** 1.11).

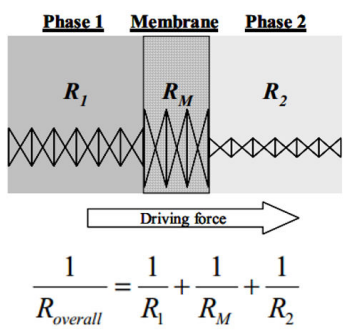

Figure 1.11: Resistance-in-series model

In principle, molecular transport across the membrane needs to overcome a set of stages or resistances. The key to resistance-in-series is, therefore, the identification of different resistances to mass transport and the definition of each resistance.

► **Phase 1** (R_1): In the feed phase, resistance is caused by the formation of a cake layer on the surface of the membrane, or by liquid film boundary layer or gel layer formation.
► **Membrane** (R_M): The resistance as a function of the membrane structure (porous or dense) and various fouling phenomena.
► **Phase 2** (R_2): The resistance is related to the permeate removed from the membrane.

The reciprocal of the overall resistance will be equal to the sum of the reciprocal resistances of each phase and membrane (shown in **Figure** 1.11. In dense membrane, permeability, and thickness, whereas in a porous membrane, pore size and geometry determines the transport. Finally, with the development of the composite membrane, both a dense and porous layer/s together govern the mass transport resistances and overall mass transport phenomena.

When applying this model in membrane transport, the definition of the resistance and incorporating them to an overall resistance term plays a crucial role. If the resistance to mass transfer is due to concentration polarization, resistance-in-series model is referred to a stagnant film model, in which, convective flow transports the solutes to the membrane surface where they are rejected or accumulated. Overall, a summary of mass transport mechanisms is schematically shown in (**Figure** 1.12).

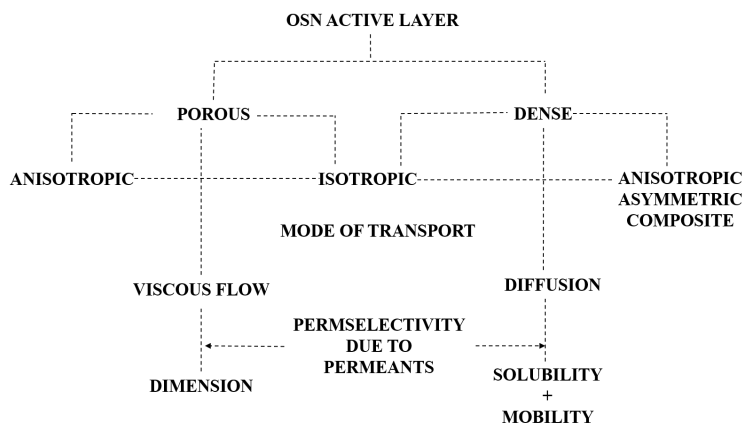

Figure 1.12: Configuration, transport and permselectivity employed in the active layer of OSN membranes, adopted from George and Thomas (2001).

Concentration gradient in the SD model and pressure gradient in the PF model causes an overall driving force for the mass transport to occur, Separation in dense membranes is achieved due to differences in permeants mass transport rate in a given membrane, as one component is more excluded than others (**Figure** 1.13).

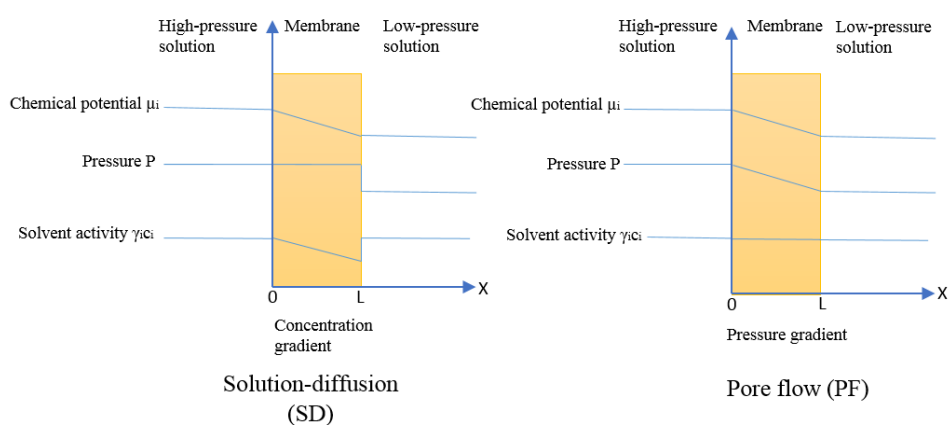

Figure 1.13: Pressure driven permeation of one component solution though OSN membrane according to SD and PF model.

SD model assumes that pressure within the membrane is uniform and chemical potential gradient across the membrane is expressed only as a concentration gradient, whereas, PF model consider the uniform concentration of solutes and solvent in the membrane phase and chemical potential gradient across the membrane is expressed only as a pressure gradient.

Next, the SD model assumes that fluids on both sides of the membrane are in equilibrium with the membrane material at the interface. Thus, there is a continuous gradient in chemical potential from one side of the membrane to another. It is commonly accepted that absorption and desorption rate at membrane interface is much higher than the diffusion rate through the membrane, i.e., diffusion is the rate-limiting step, unless there is no chemical reaction involved in the separation process.
In SD model flux J_i is expressed as the **Equation** 1.8.

$$J_i = -\frac{R.T.L_i}{C_i}.\frac{dC_i}{d_x} = -D_i.\frac{dC_i}{dx} \tag{1.8}$$

Where D_i is the diffusion coefficient. In classical SD model, there is no distinction between solute, solvent, and their transfer. This model is only accurate for diluted solutions.
In PF, separation occurs due to size exclusion. Without concentration gradient, the transport can be described by the Darcys law (**Equation** 1.9)

$$J_i = -k.\frac{(P_\circ - P_l)}{l} \tag{1.9}$$

where, $P_\circ - P_l$ is total pressure and l is for membrane thickness, k is the permeability which depends on structural parameters such as the membrane pore size r_p, tortuosity, τ and the porosity of the membrane, ε. For solvent flux, the Hagen-Poiseuille model is expressed according to the **Equation** 1.10 and 1.11.

$$J_i = \frac{\varepsilon.r_p^2}{8l\tau}.\frac{\Delta P}{\eta} = K_{HP}.\frac{\Delta P}{\eta} \tag{1.10}$$

and

$$K_{HP} = f(r_p, l, \varepsilon, \tau) \tag{1.11}$$

The structural parameters of porous OSN membrane are complex and often unknown because of the size and distribution of pores, presence of non-cylindrical pore in the structure, pore continuity, and tortuosity. These parameters are often estimated for a given membrane. PF known parameters are the thickness of the membrane, viscosity, and total pressure (Robinson et al., 2004)

(Silva and Livingston, 2006) compared SD and PF model for dense PI membrane and suggests that, when solute concentration is low, both models are equivalent. At high solute concentration, SD models exhibit better agreement with experimental results. (Tsuru et al., 2000) addressed the pore size parameter in inorganic nanofiltration membrane of porous silicazirconia showing that, when the membranes pore size is more than 70 nm, PF model shows better agreement with experimental results and does not valid when the pore size is 1 and 5 nm.

(Bhanushali et al., 2001) studied solvent fluxes in porous and dense membranes, showing the relation of molar volume V_m, viscosity, sorption and the interfacial tension $_{SV}$ according to **Equation** 1.12

$$J_{solvent} = K_{BH}\frac{V_m}{\eta}.\frac{1}{\phi^n.\gamma_{sv}} \tag{1.12}$$

Where ϕ correspond to the parameter of SD model and γ_{sv} represents parameter for the PF model.

Next,(Geens et al., 2006) modified the model of Bhanushali, introducing interfacial tension difference between the solvent and the membrane, $\Delta\gamma$ and surface tension of the solvent, γ_{LV}. (**Equation** 1.13, 1.14 and 1.13)

$$J_{solvent} = K_G \frac{V_m}{\eta.\Delta\gamma}. \tag{1.13}$$

where

$$\Delta.\gamma = \gamma_{SV} - \gamma_{LV}. \tag{1.14}$$

And

$$J_{solvent} = \frac{\Delta P}{R_0^S + R_\eta^1 + R_\eta^2} = \frac{\Delta P}{\phi.[(\gamma_{SV} - \gamma_{LV}) + f_1\eta] + f_2\eta} \tag{1.15}$$

Where R_0^S, R_η^1, R_η^2 and are the resistances at the NF skin layer, through the NF sublayer and the UF sublayer, respectively. f_1 and f_2 solvent independent parameter characterizing the NF and UF sublayer. $\gamma_{SV}$and γ_{LV} presents solid-vapour and liquid-vapour surface tension.

Considering viscous flow along with diffusion; SD model has further modified into the solution-diffusion with imperfection model (SD+IM model) which includes viscous flow with diffusion. Transport in SD+IM is governed by diffusion and convection in small cavities, which are termed as imperfections of the membrane (Darvishmanesh et al., 2009) (Fierro et al., 2012).
In OSN, mostly used mass transport models are Solution- diffusion (SD) (Zheng et al., 2008) (Stafie et al., 2004), pore-flow (PF) (Robinson et al., 2004) **Figure** 1.13. Other models are irreversible thermodynamic model such as Kedem-Katchalsky (Kedem and Katchalsky, 1958) and Spiegler-Kedem (Spiegler and Kedem, 1966). These model consider convection and diffusion simultaneously. Semi-empirical models are also reported to explain the transport for specific conditions (Bhanushali et al., 2001) (Geens et al., 2006).
Finally, the following points are essential to consider before to applying OSN mass transport model:

• Dense or porous nature of OSN membranes (active layer) is often not reported in literature.

• Convective and diffusive transport together in a given membrane is a less-likely phenomenon. Even if it occurs, convective transport is much higher than diffusive transport. In such case flux contribution from diffusive transport seems to be negligible compared to the flux from convective transport.

• Role of membrane support/s in mass transport, which is often ignored in literature.

1.9.2 Molecular transport in polymeric systems

1.9.2.1 Diffusion in rubbery polymer

Rubbery polymer bears the characteristics of unsaturation, segmental mobility, and a large amount of free volume between molecules. Thus small molecule can easily diffuse through rubbery polymer(George and Thomas, 2001). Two case study of rubbery polymers is presented below, focusing on molecular transport.

Case 1: Rubbers
Rubbery systems exhibit higher diffusion for molecules that have a lower effective diameter. For example, diffusion coefficient of four solvents follow the order as: chloroform (119 $g.mole^{-1}$) > benzene (78 $g.mole^{-1}$) > ethylbenzene (106 $g.mole^{-1}$) > o-xylene (106 $g.mole^{-1}$). The diffusion in different rubbers follows the trend as silicone > natural rubber > bromobutyl, which may be related to the difference in fractional free volumes and polymer chain flexibilities in these rubbers (Iwai et al., 1993) (Guo et al., 1995). Toluene diffusion in butyl rubber has been investigated by (Schneider et al., 1994) in terms of polymer, mass fixed diffusion, showing that the toluene diffusion (D) exponentially increases with concentration.

Case 2 : Polyurethane(PU)
Polyurethane (PU) is an excellent example of a rubbery system in which a series of aliphatic alcohol permeation show the decrease of diffusion coefficient (D) with the increase of the molecular weight (Hung and Autian, 1972). However, branched alcohol shows lower D values than linear (Zwolinski et al., 1949), which possibly due to the steric hindrance and concentration-dependent diffusivity (Hopfenberg et al., 1969). In contrary, when membrane-solvent interaction was considered for PU membrane, chlorobenzene (MW 112 $g.mole^{-1}$) exhibit a strong affinity for PU, whereas, hexane (MW 86 $g.mole^{-1}$), asymmetrical non-polar solvent shows less interaction. Hence D was found to follow an inverse relationship with the size of the molecule (Hung, 1974).

1.9.2.2 Diffusion in glassy polymer

The glassy polymers are characterized by brittle moiety with restricted chain mobility compared with rubbery polymers. These dense structures have little void space (0.2 -10 %), and therefore diffusion in the glassy polymer is more complicated compared to that in rubbery polymers (George and Thomas, 2001).

Toluene diffusion in glassy polypropylene (PP) was studied by (Choy et al., 1984), in which the authors show that toluene diffusivity increases exponentially with increasing toluene concentration, which is in agreement with the diffusion of benzene, toluene, and ethylbenzene in polystyrene (Zielinski and Duda, 1992a) (Zielinski and Duda, 1992b).

1.9.2.3 Diffusion in polymer blend

Diffusion and transport through polymeric blends (homogeneous and heterogeneous) widely depend on the composition, miscibility, and phase morphology.
In a homogeneous blend, the diffusion process is related to the interaction between the component and polymers (Paul, 1984)(Chiou and Paul, 1986), while in the heterogeneous blend, interfacial phenomena, rubbery or glassy nature of the phase need to be evaluated. In most polymeric blend, one polymeric matrix is embedded by the second polymer, resulting in a high degree of heterogeneity which significantly affects the permeability. It indicates that diffusion in polymeric blends largely depends on the nature of the polymer, and the method of membrane formation (George and Thomas, 2001) (Aminabhavi and Phayde, 1995).

1.10 OSN parameters

OSN parameters arise individually from the membrane, solute, solvent, and process side and highly interlinked to each other, as shown in **Figure** 1.14. Next, the detail range of these parameters are summarised in **Table** 1.7 1.8 and 1.9.

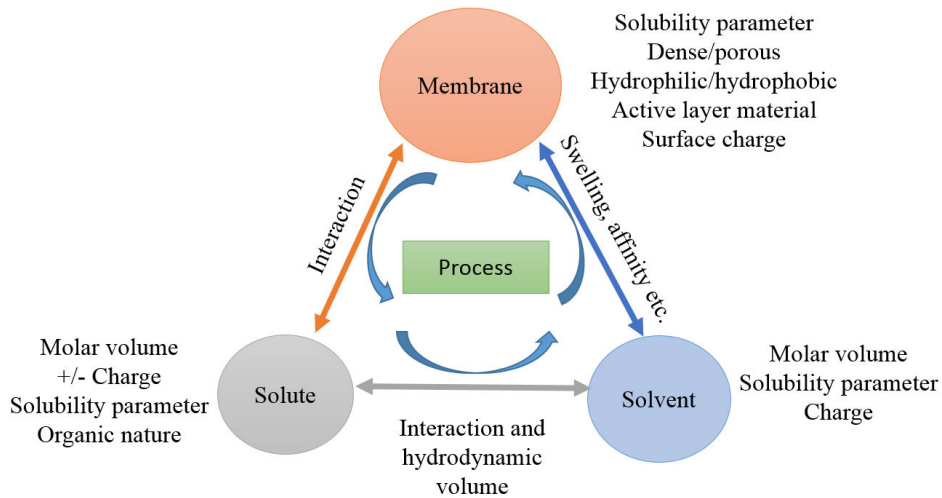

Figure 1.14: OSN Membrane- solvent-solute properties

Also, mass transport in OSN can be influenced by concentration polarization (CP) and osmotic pressure (OP). CP occurs when the convective flow of the solutes due to the applied pressure that cannot be balanced by the back-pressure of the solutes toward the solution in the retentate, result to a difference between concentrations of film layer and bulk. The occurrence of CP is evident but can be minimized. If permeation and selectivity in a given membrane increase, CP effect logically become significant (Marchetti et al., 2014a) (Vandezande et al., 2008a).

Process properties	**Solvent properties**	**Solute properties**	**Membrane properties**
(a)Feed concentration (b) Applied pressure (c) Feed temperature (d) Module type and characteristics. (e) fluid dynamics	(a) Solvent molar volume (size) (b)Polarity of the solvent (c) Viscosity of the solvent	(a) Diffusion co-efficient. (b) Solute geometrical shape (c) Solute solubility in solvent (measure of solutesolvent affinity) and in membrane (d) Solute charge	(a) The degree of crosslinking of the polymeric membrane (resistance to swelling) (b) % intrinsic microvoids. (c) hydrophobic/hydrophilic

Table 1.7: OSN parameters for dense membrane.

Process properties	**Solvent properties**	**Solute properties**	**Membrane properties**
(a)Feed concentration (b) Applied pressure (c) Feed temperature (d) Module type and characteristics. (e) fluid dynamics	(a) Solvent size (b) Solvent surface tension (c) Viscosity of the solvent	(a) Solute size in solvent (b) Solute MW (c) Solute geometric shape (d) Solubility (e) Charge	(a) Pore size and pore size distribution (b) Surface energy (c) Porosity. (d) Tortuosity

Table 1.8: OSN parameters for porous membrane.

Process parameter	Flux and retention characteristics
Effect of pressure (when increase)	1. Driving force increases, therefore, flux increases 2. Membrane compaction may occur which lead to the reduction of permeance as well as the increase in retention.
Effect of temperature (T)	1. The degree of swelling increases as T increases, thus flux and permeance increases as well as retention decreases. 2. Solvent viscosity decreases as well as the diffusion coefficient increases.
Effect of solute concentration	1. Degree swelling decreases, flux decreases. 2. Adsorption of solute on the membrane surface which leads to reducing flux but can make the reverse effect on retention. 3. Aggregation and micelles formation can occur on the membrane active surface.

Table 1.9: Process parameters and their effect on flux and retention.

Among all parameters listed above, few critical parameters that exhibit significant impacts on OSN performance are pointed below, including a list of known/unknown and critical parameters in **Table** 1.10.

• High rejection of apolar solvent is expected in hydrophobic membranes and high polar solvent rejection in hydrophilic membranes.
• Low solubility of a component in membrane results to low permeability.
• Smaller solute-membrane affinity leads to higher rejection of the solute and vice-versa (Ben Soltane et al., 2016) (Darvishmanesh et al., 2011b).
• Smaller difference of solubility parameter between solvent and membrane cause higher sorption due to the high affinity between solvent and membrane (Silva and Livingston, 2006).
• High difference of solubility parameter of solvents and membranes causing low swelling degrees. Using solutes with high sorption in OSN feed, the solvent can be enriched in permeate i.e., negative retention (Bhanushali et al., 2001) (Postel et al., 2016).
• Effective size of molecules are dependent on types of solvent due to the variations in solvation and hydration of a given solute by solvents.
Effective solute diameter is solvent dependent, which can be obtained from stokes diameter but solute diffusivity in different organic solvents are unknown (Darvishmanesh et al., 2010a)
• When ratio of molar volumes $V_{solute}/V_{solvent}$ is, < 7, strong dependence of the molar volume on rejection, however, if $V_{solute}/V_{solvent} > 7$ effect of molar volumes are no longer significant (Volkov et al., 2014) (Bhanushali et al., 2002) (Van der Bruggen et al., 2002).
• In porous membrane, when solute (low polarity and minimally interacting) size is sufficiently small, they pass through the membrane along with solvent causing low rejection of solute (size exclusion mechanism)
• Polymeric chain mobility is highly influenced by organic solvents, which allows to hindered/unhindered solute. Increasing the polarity of a solvent decreases the solvent flux in hydrophobic membranes, but increases in hydrophilic membranes.

Transport model and OSN membrane	**Transport mechanism**	**Membrane-solvent-solute parameter (known)**	**Membrane-solvent-solute parameter (Unknown)**	**Critical parameter**
SD (dense) (classical and Maxwell-Stefan equation)	Sorption-diffusion	1. Solute-solvent concentration, 2. Solubility parameter, 3. Activity.	1. Friction and diffusion co-efficient, 2. Sorption co-efficient (permeate and retentate side). (largely depends on experiments), 3. Molar volume.	1. Molar volume.
PF (porous)	Convention	1. Solute-solvent size. 2. surface tension. 3.viscosity.	1. Mean pore diameter, 2. Tortuosity, 3. Porosity for composite membrane. 4. Reflexion co-efficient, 5. Friction co-efficient. 6. Interfacial forces between solute-solvent.	2. Hydrodynamic radius.
SD+IM (dense)	Diffusion + Convection	combined with SD and PF	1.Permeability of solvent and solute by convention and diffusion together.	combined from SD and PF
Semi empirical (porous and dense)	Diffusion+ Convection	1. Solvent solute size. 2. solvent-solute-membrane interaction.	1. Solvent solute size. 2. Solvent-solute-membrane interaction.	1. Molar volume, 2. Viscosity, 3. Surface tension

Table 1.10: Transport mechanism to known-unknown-critical governing parameters.

1.11 Modification of OSN membranes and expected properties after modification

Over the last two decades, OSN has become a proven technology for molecular separation and purifications. One of the significant challenges, however, is to improve and maintain high performance and stability of these membranes under different feed conditions. Tailoring the selective layer of OSN membranes is the first approach to develop functionalized membranes, which is expected to be highly selective and stable in organics. Methods such as grafting, light-induced modification, plasma treatment, and polyelectrolyte modification are well pronounced to obtain new generation OSN membranes. Up to the moment, extensive references are available for aqueous systems, and integrating these approaches in OSN are in its beginning phase (Solomon et al., 2012) (Jimenez Solomon et al., 2013) (Zhao and Yuan, 2006a).

The approach of OSN membranes modification can be summarised in different groups.

- ► Thin-film composite (TFC) fabrication using high flux materials (existing) for the selective layer.
- ► OSN membrane activation and modification of surface and/or support/s before applying in OSN

separation.
► New generation OSN membrane fabrication by incorporating nano-material into the selective layer.
► Polymer blending for harvesting new separation properties.
► Ultrathin selective layer (nm range), either as free-standing membranes on porous support or nanolayer deposition/formation on existing OSN membrane surface.

Adopting modification for performance improvement are already reported in different membrane separation processes (Zhao et al., 2012). For example, forming aquaporin-based selective layers on polysulfone (Zhao et al., 2012), hydrophilization of RO membranes (Wang et al., 2015) and grafting zwitterionic csarboxybetaine methacrylate (Wang et al., 2015), covalent attachment of PVA (Hu et al., 2016) or supramolecular assembly of chitosan. All these modifications bring interesting separation properties in membranes. Next, modification of support to improve surface porosity or to add small particles into selective layers able to change the membrane morphology. (Chae et al., 2015) (Safarpour et al., 2015) (Ma et al., 2016) (Zhao and Ho, 2014). Indeed, modification of OSN membranes are expected to bring new surface properties by altering the surface properties, as summarised in **Table** 1.11.

Surface property	**OSN characteristics**	**References**
Surface charge	**1.** Surface charge affects the interaction between solute-solvent and membrane. In case of charged solutes, the membrane performance is expected to increase. **2.** The thickness of an electrical double layer around an ion is proportional to the square root of the dielectric constant of the surrounding medium(Debye-Huckel theory. Thus,for solvents with high dielectric constants, the charge effects are exerted over a longer distance. This phenomenon affects the permeation of polar solvent (high dielectric constant) compare to apolar solvents **3.** Membrane sieving effect can be influenced by surface charge. **4.** Solute-membrane affinity can be largely affected by the surface charge.	(Marchetti et al., 2013) (Zhao and Yuan, 2006a) (Atkins et al., 2018) (Gevers et al., 2006) (Bhanushali et al., 2002) (Van der Bruggen et al., 1999)

Table 1.11 continued from previous page

Surface property	OSN characteristics	References
Surface hydrophilicity/ hydrophobicity	**1.** Permeability of the polar solvent in the hydrophilic membrane is 8-10 times higher than non-polar solvent whereas, in hydrophobic membranes permeability of non-polar solvents is 2-3 times higher than that of polar solvent. **2.** The hydration/solvation mechanism: In porous hydrophobic membrane, solvation of the membrane decreases the effective pore size (example MeOH) thus higher rejection is expected in organic media compare to water media. However, in hydrophilic surface, hydration becomes more significant and causes the opposite results. **3.** Surface tension effect: Using solvents with a higher surface tension results in higher fluxes through hydrophilic membranes, but lower fluxes through hydrophobic membranes.	(Bhanushali et al., 2001) (Yang et al., 2001) (Zhao and Yuan, 2006a) (Geens et al., 2006)
Surface roughness	**1.** Increasing the surface roughness of hydrophobic membrane make it more hydrophobic and for hydrophilic membrane more hydrophilic. **2.** Increasing surface roughness increase the effective surface area results in higher permeation. Nevertheless, fouling possibility also increases with surface roughness	(Wenzel, 1936) (Cassie and Baxter, 1944) (Vrijenhoek et al., 2001)

Table 1.11: Expected surface properties and OSN characteristics after modification.

After modification, fundamental characteristics of OSN membrane such as mechanical, chemical, and thermal stability must be preserved, and final separation performance must be improved (Szekely et al., 2014)(Cheng et al., 2014a) (Peeva et al., 2014). Indeed, polymeric OSN membranes (modified or unmodified) must demonstrate continuous long-time operation stability in harsh solvents, while preserving their separation properties (Vandezande et al., 2008a).

Membrane modifications are primarily divided into two principal categories: modification of the surface and modification of bulk (Amirilargani et al., 2016). In the last decade, several techniques were employed to improve the separation properties of OSN membranes (mainly polymeric) without sacrificing their permeation properties. Incorporating active species by plasma (Zhao et al., 2004) (Chen et al., 2007a), polyelectrolyte multilayers, Polymerized thin-film (Amirilargani et al., 2016), Nanoparticle suspended membrane (Peyravi et al., 2014b) (Zhang et al., 2014a), polymer grafting (Pinheiro et al., 2014) and UV cross-linking (Robinson et al., 2005b) (Vanherck et al., 2011) are mostly reported techniques of modification. A brief description of each of these techniques are summarized in **Table** 1.12

Type of Modification	Modification method	Description	Examples	Reference
Plasma induced	Incorporating functional group or nanolayer deposition	Membrane surface is exposed to active plasma to modify the surface. It can be used to modify porous PAN and dense PDMS membrane in order to obtain recovery of solvents and high rejection of dyes.	Ar/O_2 plasma to modify PAN (porous) and Ar, Ar/H_2 plasma for PDMS (dense)	(Zhao et al., 2005) (Chen et al., 2007b)
Polyelectrolyte multilayers	Deposited thin film	Sequential assembly of cationic - anionic polyelectrolytes deposition on charged surface	PDDA/PSS, PDDA/PAA on PAN and PDMS surface	(Amirilargani et al., 2016)
Polymerization	Polymerized thin film	Synthesize a dense and active top-layer on a porous support to prepare composite OSN membranes in order to improve the stability of the membrane in harsh solvent and to separate specific molecular structure .	blend of trimesoylchloride (TMC) with fluoro-alkyl acyl chloride PA membranes	(Amirilargani et al., 2016)
Nanoparticle	Nanoparticles suspended in membrane	Formation of OSN membrane by organic inorganic phase, mixed matrix membranes (MMMs either by in-situ polymerization or by self-assembly.	silica, carbon and zeolites into PA, PDMS membrane	(Peyravi et al., 2014a) (Zhang et al., 2014b)
Grafting	Grafting polymers on the surface (dense) or inside the pore (porous)	Grafting of component by silylation, calcination of alkyl-modified colloidal dispersions, a solgel based sintering method and Grignard chemistry.	PDMS grafted on alumina.	(Pinheiro et al., 2014)

Table 1.12 continued from previous page

Type of Modification	Modification method	Description	Examples	Reference
Light induces	UV cross- linking	Development of a thin polymeric layer by initiating polymerization and cross-linking reactions under the influence of UV-irradiation in both porous and dense membrane	PDMS and blend of polystyrene-b-poly (ethylene oxide) (PS-b-PEO) on CA (porpous)	(Robinson et al., 2005a) (Vanherck et al., 2013)

Table 1.12: Techniques for OSN membrane modifications and their brief description.

Even though each of the modification techniques has their strength to incorporate new separation properties, modification by plasma and polyelectrolytes were prioritized because of their spontaneous applicability and versatility.

1.11.1 Plasma assisted activation and/or modification

Plasmas, by definition, can be created by applying direct or alternating high voltage to a gas. Depending on the gas is at reduced pressure (partial vacuum) or atmospheric pressure, one can thereby obtain either a low-temperature, non-equilibrium glow discharge type of plasma, or an equilibrium thermal plasma, respectively.

In non-equilibrium plasma, gas molecules and ions, **heavy** particles, can be kept **cold** (near ambient temperature, 300 K), while the electron gas can be made very **hot**, well above $1.10^4 K$. These highly energetic electrons are responsible for initiating chemical reactions, by breaking covalent chemical bonds of ground-state gas molecules in the course of collision-induced energy transfer (d'Agostino et al., 2005).

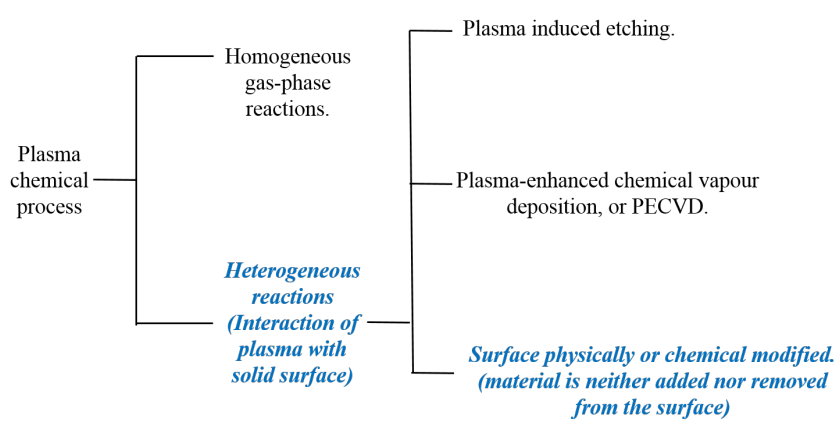

Figure 1.15: Plasma processes.

.

In surface-modification, development of discharge processes at low pressure (10 mtorr to 10 torr) make it highly interesting for rapid and effective surface modification. The application of plasma can be found in microelectronics (Pearton and Norton, 2005) to automotive industries (Lampe et al., 2003), biomedical applications (Bullett et al., 2004) and surface modification of polymer (Chan et al., 1996).

1.11.1.1 Surface modification by plasma

In polymer surface modification by plasma, many advances have been made to alter the chemical and physical properties of polymer surfaces without affecting bulk properties. Plasma modification offers unique surface properties depending on the type of plasma and type of polymers. For example, oxygen-plasma treatment can increase the surface energy of polymers, whereas fluorine-plasma treatment can decrease the surface energy and improve chemical inertness. Next, inert gas plasma plasmas can introduce new cross-linking on the polymer surface. Indeed, modification by plasma is typically confined to the top several hundred angstroms and does not affect the bulk properties, which is, by far, one of the most attractive features of using plasma in polymer surface modification.A summary of plasmas, their reaction with polymer surface with advantages /disadvantages are highlighted in **Table** 1.13.

Plasma treatment, by definition, is a complex state of matter in a gaseous state that consists free radicals, electrons, photons, and ions with a varying lifetime (in nanoseconds) which interact with the membrane surface and modify it. It can be generated by the contiguous discharge of inert or reactive gases. When gaseous organic monomer is used as plasma, it can polymerize and make additional crosslinks on the membrane surface. With proper adjustment, a dense selective polymer coating is also possible to form. For example, plasma by inert gases such as argon or helium (generally long exposure) makes ablation followed by a re-deposition of the substrate material as a highly crosslinked layer. In porous structure, a reduction of pores is frequently occurring phenomena (Petrov et al., 2012). The following effects are expected to obtain from plasma modification of membranes (Nunes and Peinemann, 2006).

(1) Crosslinking of the top layer (dense) and reduction of pore size (porous);
(2) Introduction of functional groups to the surface (dense) or inside the pore wall(porous)
(3) Grafting and deposition of a thin selective layer on a dense/porous substrate.

In membrane modification, three generic types of plasmas are identified: inert gas plasmas, oxygen-containing plasmas, and others such as nitrogen and fluorine-containing plasmas.

1.11.1.2 Inert gas plasmas

Three inert gases, namely helium, neon, and argon, are frequently used in plasma technology. Due to lower cost, Ar is by far the most common inert gas used (Chan et al., 1996) (Guruvenket et al., 2004).
Inert gas plasma induces physical modification of the surface by direct and radiative energy transfer. One of the major use of it in the sputtering processes in semiconductor industries. Besides, it is also used for pretreatment of substrates for cleaning, and in polymers, a major role of plasmas is to improve adhesive characteristics of polymers (exposure1s to several minutes). During this exposure, plasma extracts hydrogen and form free radicals at or near the surface which then interact to form crosslinks and unsaturated groups with chain scission. Plasma also removes low-molecular-weight materials or converts them to a high-molecular-weight by crosslinking reactions. As a result, the weak boundary layer formed by removing the low-molecular-weight materials; consequently, greater adhesive joint strengths develop (Chan et al., 1996).

Types of plasma	Plasma-polymer reactions	Advantages/ disadvantages of plasma
Argon (Ar) Oxygen (O_2) Nitrogen (N_2) Fluorine (F) Carbon - dioxide (CO_2), Water (H_2O) etc.	**1. Surface reactions:** - Reactions between the gas-phase species and surface species. -Reactions between the surface species produce functional groups and crosslinking at the surface. **Examples:** plasma treatment by argon, ammonia, carbon monoxide, carbon dioxide, fluorine, hydrogen, nitrogen, nitrogen - dioxide, oxygen, and water. **2. Plasma polymerization:** The formation of a thin film on the surface of a polymer via polymerization of an organic monomer. **Examples:** CH_4, C_2H_6, C_2F_4 and C_3F_6 in a plasma. **3.Cleaning and etching:** Materials are removed from a polymer surface by chemical reactions and physical etching at the surface to form volatile products. Examples: Oxygen-containing plasmas are used to remove organic contaminants from polymer surfaces, Generally, Oxygen plasmas and oxygen-fluorine plasmas are frequently used for the etching of polymers.	**Advantages:** 1. Modification of the surface without modifying the bulk properties of the polymer. 2. Plasma can modify the surfaces of all polymers, regardless of their structures and chemical reactivity. 3. Chemical modification of polymer surface can be fine-tuned by varying the gas 4. It avoids the problems encountered in wet chemical techniques such as residual solvent on the surface and swelling of the substrate. 5. Modification is fairly uniform over the whole surface. **Disadvantages:** 1. The obligatory requirement of vacuum for plasma includes additional cost of the modification. 2. Process parameter are often system dependent. 3. Complicated scale-up. 4.The process is extremely complex. Often difficult to achieve good understanding of the interaction between surface and plasma. 5. Precise control of functional group on the surface.

Table 1.13: Brief properties of plasma (Chan et al., 1996)

1.11.1.3 Oxygen-containing plasmas

Oxygen and oxygen-containing plasmas react with a wide range of polymers to produce a variety of oxygen functional groups, including $C-O$, $C=O$, $O-C=O$, $C-O-O$, and CO_3 at the surface. Two following processes occur simultaneously (Wavhal and Fisher, 2002) (Abbasi et al., 2001)

► Etching of polymer surface through the reactions of atomic oxygen with surface carbon atoms, giving volatile reaction products.
► Formation of oxygen functional groups at the polymer surface through the reactions between the active species of plasma and surface atoms.

The balance of these two processes depends on the operation parameters of a given experiment. For example, oxygen plasma-treated PTFE, which involves 0.5min-2 min plasma exposure causes to decrease fluorine concentration while increasing oxygen concentration. When the exposure time is high (about 15 min), the trend reverse. The mechanism proposes that short plasma exposure dominates surface modification and long exposure causes surface etching (Morra et al., 1990) and degradation (Chappell et al., 1991). Plasma with low gas pressure, low power, and relatively short treatment time give only surface modification but no degradation. This modified surface exhibit increased wettability and good adhesion (Lee et al., 1991).

(Hettlich et al., 1991) investigated the difference between CO_2 and O_2 plasma in poly(dimethylsiloxane) and found that O_2 plasma induced a faster rate of functional group on PDMS compare to CO_2 plasma.

1.11.1.4 Other plasmas

Nitrogen-containing plasmas are widely used to improve wettability, printability, bondability, and biocompatibility of polymer surfaces (Inagaki, 2014) (Pertile et al., 2010) (Kull et al., 2005).
For example, ammonia-based plasmas improve interfacial strength between polyethylene fibers and epoxy resins by promoting covalent bonding (Chappell et al., 1991). Introduction of amino groups on the surface of polystyrene films by ammonia-plasma treatment improves cell affinity (Nakayama et al., 1988). Fluorine-containing plasma simultaneously induces etching and plasma polymerization. (Liston et al., 1993).

1.11.1.5 Plasma effect

The effect of plasma on poly (1-trimethylsilyl-1-propyne) (PTMSP) membrane makes the surface hydrophilic from hydrophobic (water contact angle decreases from 88° down to 20°) and develops a negative surface with a charge of -5.2 $nC.cm^{-2}$. This treatment creates oxygencarbon and oxygen- silicon bond, which reduce the partition coefficient. As the partition coefficient reduces, the membrane reduces two times the permeability of linear alcohol (methanol and propanol) and acetone, while increases the retention of anionic and cationic dyes. It is assumed that the change of electrostatic interaction due to the plasma-chemical modification influences the retention (Volkov et al., 2014). Using nitrogen plasma on polymer membrane creates nitrogen functional groups that increase hydrophilicity with decreasing fouling (Kim et al., 2011)

Next, Ar plasma can form 40-50 nm thin layer on dense polypropylene surface (Gomathi et al., 2009) whereas, in the porous structure, it changes surface roughness which increases philicity by increasing the liquid viscosity in the vicinity of the philic surface and decreases near to the phobic surface. It creates a defective plasma-assisted layer on the top surface. This layer undergoes a

compression with high pressure and makes the inlet pore smaller which in return, affect flux and retention of cationic and anionic compounds(Volkov et al., 2014).

It is known that, after modification by plasma, the hydrophilic surface trend to regain the hydrophobic surface. Hydrophobicity recovery of O_2 plasma-treated sample is explained in literature by the migration of low molecular weight species from the surface to bulk. For example, native PDMS type membranes are hydrophobic, the water contact angle between 95-110° (Lawton et al., 2005), becomes hydrophilic after exposing to O_2 plasma and next, the hydrophobic characteristics of PDMS return with time (Bodas and Khan-Malek, 2006) (Lawton et al., 2005) (Bodas and Khan-Malek, 2007).

Plasma technique is fast and meets environmental standards for green technology. In OSN, Ar-based, plasma treatment for styrene grafting on porous polyacrylonitrile(PAN)shows high potential for the recovery of toluene and methyl ethyl ketone (MEK) from dewaxed oil (Zhao et al., 2005) (Chen et al., 2007b). Increasing grafting time causes smaller pore sizes and lower pore densities with narrow pore size distribution. In dense PDMS, Ar, $Ar - H_2$ and $Ar - O_2$ plasmas improve rejections of dyes (Aerts et al., 2006).

1.11.2 Polyelectrolytes multilayer (PEM) by Layer by Layer (LbL)

1.11.2.1 General feature

Polyelectrolytes multilayer are formed by alternating sequential exposure of a charged substrate to solutions that contains positive or negative polyelectrolytes (PELs). During this process, adsorbed PELs form electrostatic interaction between polyelectrolytes and the charged surface (Decher, 1997).

Polyelectrolytes, when mixed in water, free polyelectrolyte chains with low molecular counterions are more or less localized near the macroions (counterion condensation in case of high charge densities). The driving force of complex formation is mainly the gain of entropy, due to the liberation of the low molecular counterions (Thünemann et al., 2004). Other interactions, such as hydrogen bonding or hydrophobic, may play an additional part. PELs complex formation could be an endothermic process, because of the elastic energy contributions of the polyelectrolyte chains, impeding the necessary conformational adaptations of the polymer chains during their transition to the much more compact PEL complex structures (Bakeev et al., 1988). Self assembly of PELs complex and their charge balance is schematically presented in **Figure** 1.16.

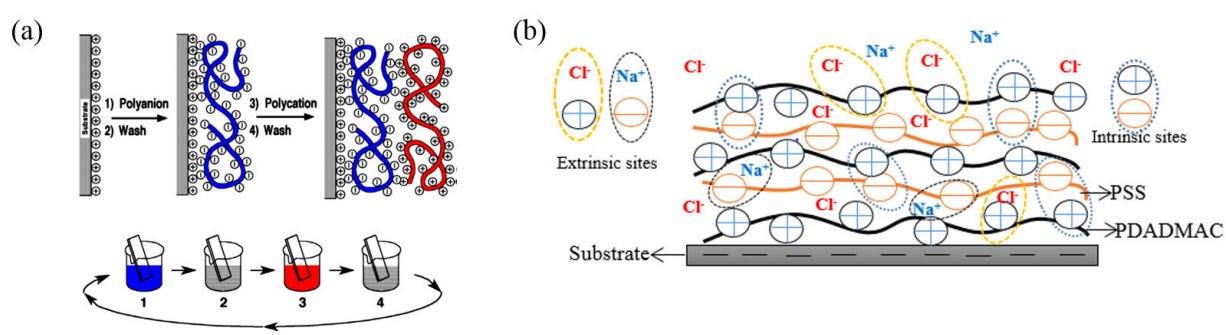

Figure 1.16: (a) LbL deposition via dip coating (Decher, 1997). (b)Scheme of intrinsic and extrinsic charge balance in the polyelectrolytes multilayer (PEM) , adopted from (Ghostine et al., 2013)

.

During the self-assembly process, charge inversion is an inherent feature of PELs deposition. Charge inversion is the reversal of polarity due to excess adsorption of oppositely charged polymer (Decher et al., 1992) (Decher, 1997) and the stability of self-assembled film depends on the electrostatic interactions (Schonnhoff, 2003) (Besteman et al., 2005).

In PELs multilayer deposition, a positively charged substrate is dipped in negatively charged polyelectrolytes. After some time of adsorption, few washing steps are used to remove the excess PELs from the surface. Next, the substrate is sequentially dipped in positively charged PEL and washing baths, which completes one cycle of deposition, i.e., one bilayer of polyelectrolytes multilayer (PEM) (Decher, 1997) (Michel et al., 2012) with intrinsic and extrinsic charge balance (**Figure** 1.16b). This self-assembled bilayer/s are capable of modifying and tuning of surface properties in nanometric level, and a small polyelectrolytes amount can induce significant influence on the surface properties (Dobrynin and Rubinstein, 2005) (Tripathi et al., 2013).

1.11.2.2 Fundamentals of polyelectrolytes multilayer (PEM)

1.11.2.3 Formation of PEM complexes

The formation of PEM complex is guided by fast and robust interactions between two oppositely charged polyelectrolytes, controlled by both thermodynamic and kinetic factors (Thünemann et al., 2004). When two polyelectrolytes chains contact to each other, they combine almost instantaneously due to their electrostatic forces between them. This contact can take place either in bulk such as in mixing solution or the interface of a substrate (Interfacial complexation).

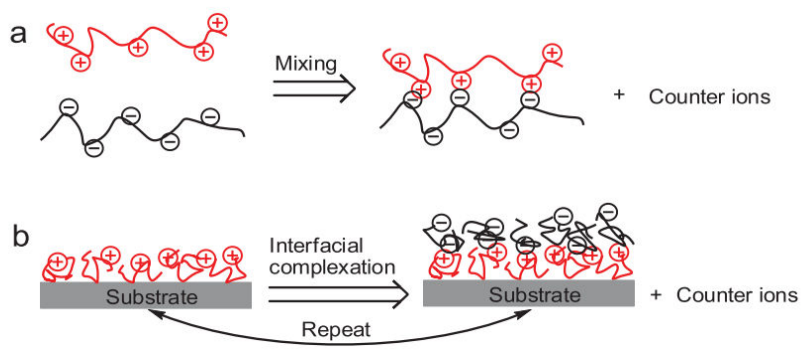

Figure 1.17: Polyelectrolytes complexes formation via (a) mixing method and (b) interfacial complexation method (Zhao et al., 2011b)

.

In the mixing method, oppositely charged polyelectrolytes solution mixed directly. As a result, they immediately combine to form aggregates (Böhme and Scheler, 2007), in less than 5 μs. (Thünemann et al., 2004). These aggregates are either positively or negatively charged depending on their mixing ratios (Böhme and Scheler, 2007) (Hofs et al., 2007). Two models are frequently adopted to describe its structure.

▶ **Ladder like structure:** Polyelectrolytes concentration is very low and contain a limited number of chains.

▶ **Scrambled egg structure:** Polyelectrolytes concentration are high, and each polyelectrolyte is entangled and incorporated to each other.

In contrast, interfacial complexation occurs in the solid-liquid interface via layer-by-layer (LbL) and electrostatic interaction. Dipping a charged substrate into polyelectrolytes solutions forms PELs

complexes on the surface and charge reversal play the key role to obtain bilayers (Schlenoff et al., 1998). The thickness of the PELs depend on the various external conditions such as concentration, pH, and ionic strength of the dipping solution, and assembly temperatures (Dubas and Schlenoff, 1999).

1.11.2.4 Parameters affecting the multilayer thickness and mechanism of conformational changes

▶ **Effect of temperature and relative humidity:** PELs layer thickness increases with increasing temperature and relative humidity. Even small differences in temperature can easily change 5 - 10 % of film thickness depending on the swellability of the film. (Tan et al., 2003)
▶ **Effect of salt concentration:** PELs layer, formed at different salt concentration shows different fluorescence emission intensity. An increase of salt concentration increases the intensity which means, increases of thickness (Sun et al., 2005) (Schlenoff and Dubas, 2001).
▶ **Effect of pH:**The pH of weak polyelectrolytes solutions dramatically affects the film thickness and makes a substantial effect on permeability whereas pH has almost no effect on strong polyelectrolytes (Yoo et al., 1998) (Garg et al., 2008) (Moussallem et al., 2009) (Lulevich and Vinogradova, 2004).

It is well known that polyelectrolytes (PELs) are highly inter-penetrating and electrostatic repulsions mainly govern the conformation of charged polyelectrolytes chain. The persistence length of the charged interpenetrating chain is larger than the uncharged chain. Screening the charges by salt ions (if added to the PEL solution) decreases the electrostatic interaction because the characteristic length (Debye length) of electric potential is shorter in solutions, at higher salt concentration (Schlenoff and Dubas, 2001). As a result, the radius of gyration will be smaller, and the chain will have more coiled and more loopy conformation with lower surface area per chain. Kinetic entrapment of such chains onto a surface will make it to a larger area density of segments and larger layer thickness.

At a very high salt concentration (critical salt concentration), PELs dissociate due to the competition for polymer/polymer ion pairs by external salt ions. Above critical salt concentration, multilayers growth decreases (Dubas and Schlenoff, 2001). Indeed, the net charge neutrality is always conserved within the structure by extrinsic and intrinsic charge balance, as shown in **Figure** 1.16b. Charges of polymer repeat units can be balanced by those on oppositely charged chains or by salt ions (if used) occluded within the film. In any case, the PELs conformation is largely affected by the charge density and salt use. For example, multilayers containing salt ions normally are thicker, less interpenetrating, and individual chains have more mobility, yielding less stable structures. (Schlenoff et al., 1998).

1.11.2.5 Application of polyelectrolytes in membrane modification

The application PELs multilayer, i.e., PEM is well pronounced in pervaporation (PV), ion separation, aqueous nanofiltration, and fuel cell applications, whereas in OSN, few polyelectrolytes have been used to enhance separation (Zhao et al., 2011b). The chemical structure of those PELs are presented in **Figure** 1.18. PELs, by nature, are soluble in water and insoluble in organic media, which make them highly interesting for the application in OSN.

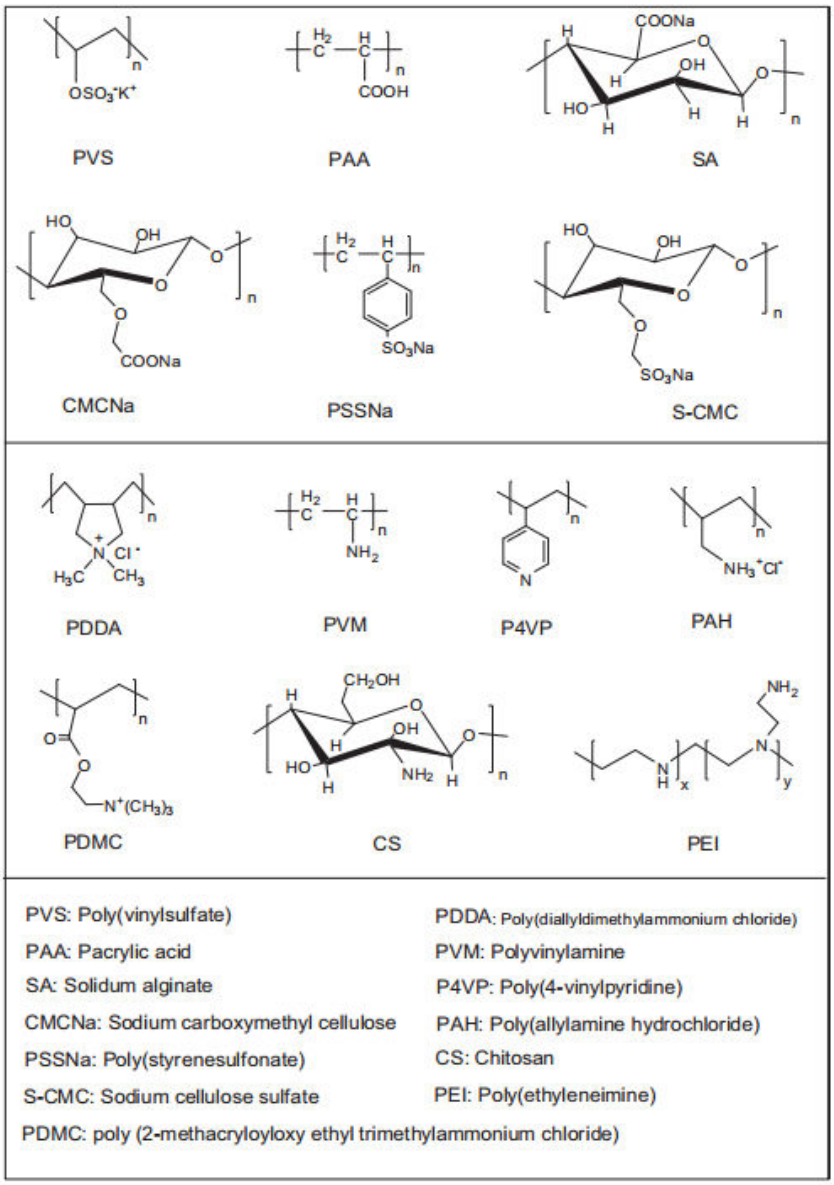

Figure 1.18: Chemical structures of common polyelectrolytes (Zhao et al., 2011b)

.

The insolubility/resistant of PEL complexes in common organic solvents renders them suitable for OSN (Zhao et al., 2011b). The LBL-PEL has two apparent advantages when considered for the modification of OSN membranes.

- ► Thickness of the active layer/s are adjustable.
- ► Charge types on the surface of PELs modified OSN membranes are adjustable.

1.11.2.6 Polyelectrolytes on OSN membrane and layer growth model

Polyelectrolytes on OSN membranes are demonstrated two types of chemical interaction namely amine coupling and silane coupling (**Figure** 1.19) (Saeki et al., 2013) (Ng et al., 2014) (Krasemann and Tieke, 2000).

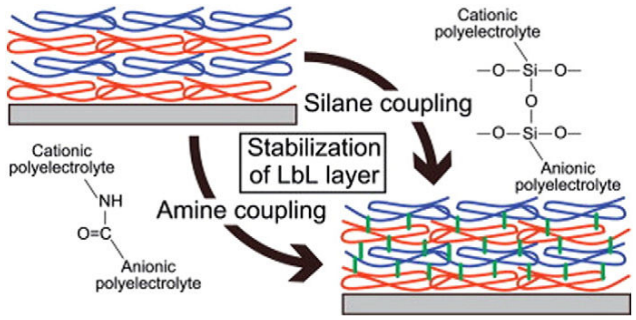

Figure 1.19: Layer-by-layer through amine coupling and silane coupling (Saeki et al., 2013)

.

Amine coupling is cross-linkage between amino groups on cationic polyelectrolytes and carboxyl groups on anionic polyelectrolytes while silane coupling is the reaction between oppositely charged polyelectrolytes on silane groups. Both these chemical interactions ensure the stability of the system (Saeki et al., 2013). When deposited on a given substrate, thickness guided properties of PELs multilayer is presented in **Figure** 1.20, according to the layer zone model.

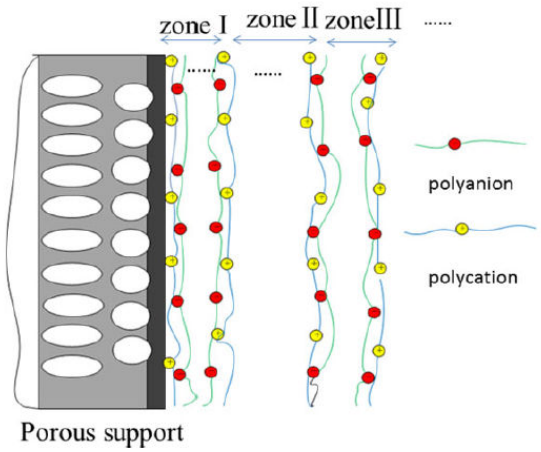

Figure 1.20: Schematic representation of three zones in polyelectrolytes OSN membranes (Cheng et al., 2014a) (Ladam et al., 2000)

.

In this model, Zone I (surface dominated zone) consists only a few layers, starting from the support. The nature of this layer is dependent on the type of surface, initial charge density, type of PELs, and their properties. Next, Zone II is the bulky zone, starts after a few bilayers (frequently 10-12 bilayers) followed by Zone III, as the number of layer formation progresses (Ladam et al., 2000) (Cheng et al., 2014a).

1.11.2.7 Permeability in OSN membranes after PEMs modification

The permeability aspect in PEL modified OSN membrane have only few literature references, namely Ahmadiannamini et al. (2012) Ahmadiannamini et al. (2010) Li et al. (2008) Li et al. (2010) reports PELs multi-layered OSN membrane and their performance . The tested PELs are poly-diallyl dimethylammonium (PDDA), polyacrylic acid (PAA), sulfonated poly(ether ether ketone) (SPEEK), poly(sodium styrene sulfonate) (PSS), and poly(vinyl sulfate)(PVS). Any PELs, as mentioned above, on a given OSN membrane reduces solvent permeability, which is dependent

on the number of deposited layers. The rejection of different dyes, however, are controlled by several factors.

- Type of charges on the membrane top layer,
- Type and quantity of electric charges, and
- Number of deposited layers.

Bilayers of PELs are assumed to be dense and gives a high mass transfer resistance. Therefore, the permeability of membranes decreases as the number of deposited layers increases. Next, the density of electrostatic charges affects the permeability of membranes by adjusting the stretch (conformation) of PELs chains. PELs chains with a higher density of electrostatic charges tend to better match the distances between charged groups in the polycation and the polyanion, leading to a flatter deposition with fewer loops, which accounts for higher retentions (Ahmadiannamini et al., 2012) (Schlenoff et al., 1998).

Multilayered membrane prepared from PDDA, CS, and PEI with anionic counterparts PAA, PSS, and alginic acid shows that the higher the charge density of polyelectrolytes, the higher the selectivity in PV dehydration because of higher charger density causes tighter PELs structures (Zhao et al., 2011b). Next, multilayered membrane prepared from PDDA, CS, and PEI with anionic counterparts PAA, PSS, and alginic acid shows that the higher the charge density of polyelectrolytes, the higher the selectivity in PV dehydration because of higher charger density causes tighter PELs structures (Zhao et al., 2011b). Next, the trend of OSN solvent flux in four different PELs membranes follows the order PSS/PDDA >, PSS/PAH > PAA/PDDA ≫ PAA/PAH. It shows that multilayered PEC membranes made from PELs with higher charger density have a more crosslinking degree, lower swelling, and lower solute permeability. For example, hyaluronic acid (HA)/chitosan films swell four times more than PSS/PAH, due to which the former membrane permitted a higher fractional passage for sucrose (Miller and Bruening, 2005). Also, transport of neutral molecules in PELs are assumed due to size sieving effect, while that of inorganic salts by charge effect.(Liu and Bruening, 2004).

As few exceptions, the PELs of H-boned pair of PVP/PAA on PDMS is reported to form a porous structure which is entirely different from the film produced by other PELs. Another example of H-bonded PELs complex is poly(vinylpyrrolidone) PVPON-PAA/PMMA, which can produce the film with pores of a molecular dimension. For robust film preparation, post chemical reaction also can be involved, for example, Diazoresin (DAR) is reactive and water-soluble which forms a phenyl cationic form under UV irradiation; make it possible to deposit PSS in next deposition step to create DAR/PSS porous film. Finally, newly emerging PELs use in OSN are Sodium alginate (SA), Sodium carboxymethyl Cellulose (CMCNa), Sodium Cellulose sulphate (S-CMC), Poly vinyl amine (PVA), Poly 4 vinylpyridine (P4VP) and Poly ethylamine (PEI) (Dobrynin and Rubinstein, 2005) (Tripathi et al., 2013).

1.11.2.8 Bilayers number and rejection in OSN

The PELs multilayer of PDDA with H-form polyanion PSS, and PVS having 5, 10, 15 and 20 bilayers on PAN show better isopropanol (IPA), and dimethylformamide (DMF) permeability and 99 % RB dye retention compare to the ones in Na-form (Ahmadiannamini et al., 2012) (Marchetti et al., 2014a) (Cheng et al., 2014a). These studies also show that only five bilayers of PDDA/PSS give a smoother surface than PDDA/PVS, which is due to the lower charge density of PSS than PVS. Also, H-form PVS-containing PELs show a rougher surface compared with Na-form PELs.

It is because the adsorption of chains with lower charge densities and smaller intra-chain repulsion forces gives a loopy-structured in the H-form. In both PELs, the distances between charged groups in polycation and the polyanion form flatter deposition with fewer loops having similar bilayer thickness.

In OSN separation, polyanion with H-form shows higher permeability and higher retention than Na-form. However, the retention of neutral dye is smaller than bi-charged dye; assumed due to the electrostatic repulsion. Donnan exclusion effect is reported to play a vital role to govern overall retention. However, when the outer layer of PELs multilayer is positively charged, they can retain both positive and negative dyes. This interesting phenomenon is explained, as if negatively charged dye molecule first, adsorb at the charged surface, neutralize and switch it to negative surface. Later, Donnan exclusion comes to be effective for the separation (Cheng et al., 2014a) (Ahmadiannamini et al., 2012) (Krasemann and Tieke, 2000).

1.11.2.9 Cross-linking by PEM affecting OSN performance

It is known from PELs literature that ionic crosslinking in multilayer depends on the charge density, which is expressed as the number of ion pairs per number of carbon atoms in the repeat unit of polycation-polyanion. The lower ionic crosslinking density in a system likely results in a more open film with higher flux and lower retention (Krasemann and Tieke, 2000).

Lower ionic crosslinking also can be related to the swelling and thus can affect the permeability. PELs prepared by PSS, PDDA, and PAH shows that higher charge density on the polyelectrolytes results in more ionic crosslinking, less swelling, and lower permeabilities (Ahmadiannamini et al., 2012).

When bilayers number increases beyond 15, typically bulky zone II continues to grow, having a fixed zone I and zone III. As the bulky zone increases, in principle it should contribute to giving resistances in mass transport, reducing the solvent flux as well as increase the retention, however; Ahmadiannamini et al. (2012) shows that even a lower bilayer number can contribute higher rejection which suggests that zone II is not the transport rate-determining step in PELs multilayer in PELs multilayer. It is assumed that OSN mass transport through PELs multilayer initially related to the number of bilayers, might have a trade-off between bilayers number and separation. Indeed, the optimum bilayers number is specific for PEM types and depends on their fabricating conditions (Ladam et al., 2000) (Ahmadiannamini et al., 2012) (Cheng et al., 2014a) (Ahmadiannamini et al., 2012).
Finally, a summary of PEL pairs used in OSN and their impact on separation is listed in **Table 1.14**, shows the potentiality of PELs multilayer for new generation OSN membrane.

PEL Pair	**Number of bilayer**	**Substrate**	**Appl.**	**(R%) by PEL**	**Reference**
PSS/ PAH	1-4.5	Porous alumina	Removal of dyes	99.9	(Zhao et al., 2011b)
PDDA/ SPEEK	1-20	PAN	Removal of dyes from IPA, DMF and THF	99	(Li et al., 2008)

Table 1.14 continued from previous page

PEL Pair	**Number of bilayer**	**Substrate**	**application**	**(R%) after PEL**	**Reference**
PDDA/ PSS	1-20	PAN	RB and acid fuchsine from IPA	>99	(Zhao et al., 2011b)
PDDA /PSS	0-20	PMMA PDMS	Improved solvent resistance	after PEL low $ChCl_3$ vapor permeation	(Kumlangdudsana et al., 2011)
Chitosan/ alginate	0-20	PMMA PDMS	Improved solvent resistantance	after PEL low $ChCl_3$ vapor permeation	(Joseph et al., 2014a)
PDDA/ PVS	5-20	PAN	RB and acid fuchsine	>99	(Ahmadiannamini et al., 2012)
PDDA/ SPEEK	5-15	PDMS	RB, CV MO dyes	> 88-99	(Chen, 2013)

Table 1.14: PEL in OSN

Chapter 2

Performance of OSN Commercial membranes

This chapter reports the performance of commercial membranes for organic solvent nanofiltration (OSN). In the literature review, it was shown that few membranes display prominent OSN features for the separation of homogeneous catalysts. Only two polymers, namely, cross-linked polydimethylsiloxane(PDMS) and polyimide(PI), represents the best feature of high catalyst rejection with reasonable solvent permeance to meet ANR objectives of hydroformylation catalyst separation. Up to the moment, most successful commercial OSN membranes for catalyst separation are Starmem (PI-based) and MPF (PDMS based). Unfortunately, these membranes are no longer available in the market.

Based on the OSN membrane availability, the first objective of the Ph.D. is to find suitable commercial membranes that exhibit high OSN separation performance. The initial choices of OSN membranes are, therefore, includes both dense and porous commercial membranes from which the best performing membrane will be selected for the ANR tasks.

Initially selected OSN membranes are PERVAP 4060 (dese, PDMS), SOLSEP 010206 (dense, believed to be PDMS), AMS S3012 (nanoporous, PAN), polyacrylonitrile support (porous, PAN). Characterizations of these membranes were carried out by Water contact angles (WCA), microscopy, and measurement of pure gas permeability. Next, solvent permeation, transmembrane Pressure (TMP) effect and rejection of R-BINAP (Organometallic complex, $C_{44}H_{32}P_2$, (MW 622 $g.mol^{-1}$) and Tetratetracontane (linear alkane $C_{44}H_{90}$, MW 619 $g.mol^{-1}$) were measured and compared.
In addition, Several OSN tests were conducted using the hydroformylation catalytic system, using actual catalyst-ligand concentration in the OSN feed. It links the common Ph.D. objectives in the ANR frame with the target of Chemical and Process Engineering (CIP) team, University of Rennes 1, and Arkema.

Finally, the OSN results, given in this chapter, show that the highest performing OSN membrane is PERVAP 4060. Next, the detailed study on PERVAP 4060 is presented in the published article entitled **Investigation of OSN properties of PDMS membrane for the retention of dilute solutes with potential industrial applications,*J. APPL. POLYM. SCI. 2019, DOI: 10.1002/APP.48359***. The article draft is included by the end of this chapter.

2.1 Characterization of OSN commercial membranes

2.1.1 Characterization by Water Contact Angles (WCA)

The water contact angles of OSN membranes are presented in **Figure** 2.1. Clearly, PERVAP 4060 is hydrophobic, whereas AMS S3012 is highly hydrophilic. Two other membrane exhibits intermediate hydrophilicity.

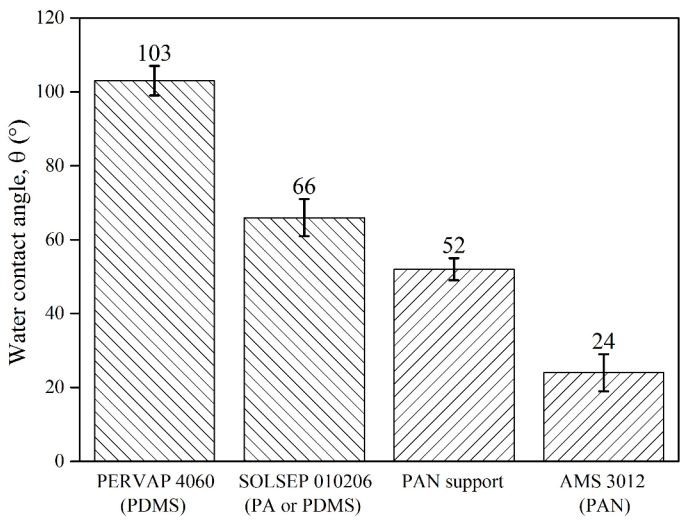

Figure 2.1: Water contact angles of commercial OSN membranes.

Next, WCA of PERVAP 4060 (**Figure** 2.1) is compared with reported WCA values in literature, **Table** 2.1 in which shows that PDMS membranes, both commercial and laboratory-made are hydrophobic.

PDMS (commercial/ lab-made)	**WCA(°)** ± 4 °	**Reference**
PERVAP 4060 (commercial)	103	This study
PERVAP 4060 (commercial)	102	(Bassil et al., 2016b)
SYLGARD 184, Dow Corning Corp.	112	(Kim et al., 2002)
Sylgard-182 with curing agent (10:1)	103	(Lawton et al., 2005)
RTV 615 PDMS with curing agent.	120	(Bodas and Khan-Malek, 2006)
PDMS (Sylgard184)	105	(Haubert et al., 2006)
PDMS prepolymer(Sylgard 184)	110	(Sugiura et al., 2008)
PDMS microchannel	107	(Bashir et al., 2015)

Table 2.1: Examples from literature reporting water contact angles of both commercial and laboratory-made PDMS based OSN membranes.

Next, WCA of SOLSEP 010206 was obtained 60-70° (**Figure** 2.1). According to its supplier, this membrane has an active layer of polyamide (PA), whereas some variant of SOLSEP was believed to have an active layer of PDMS (Marchetti et al., 2014a). In literature, contact angle values of polyamide(PA) surface are reported 70-72° (Extrand, 2002) (Al-Hobaib et al., 2017) which suggest

the active layer of SOLSEP 010206 is more likely to be PA. Finally, WCA of PAN UF surface is reported 55° Zhang et al. (1989), which is comparable to the obtained WCA value of PAN support (**Figure** 2.1). Indeed, WCA of AMS S3012 does not match with the literature data of PAN; however, the PAN origin of this membrane is confirmed by its supplier.

Commercial OSN membranes	Active surface	surface structure
Sulzer PERVAP 4060	PDMS	dense
SOLSEP 010206	PA	dense
PAN support	PAN	porous
AMS S3012	PAN (according to supplier)	porous

Table 2.2: Commercial OSN membranes and their active surface materials.

2.1.2 Characterization by scanning electron microscope

Typically OSN commercial membranes have a multi-layered structure. The top layer has a higher resistance to mass transfer and supposed to determine the performance of the membrane in terms of selectivity and permeance. The bottom layer is mechanical support and compaction can occur in the support layer/s under pressure difference.
Most of the commercial polymeric membranes are integrally skinned asymmetric that possesses a skinned layer on the top of porous sublayer (Marchetti et al., 2014a). Due to their low manufacturing cost, these asymmetric membrane dominates a significant part of the membrane market. The key to high performance is the very thin skin-layer, which enables a high permeability together with high selectivity (Vandezande et al., 2008a). The growing interest in OSN is, therefore, to fabricate nanolayered thin membrane exhibiting high separation performance (Amirilargani et al., 2016).

2.1.2.1 Dense OSN membrane

The surface and cross-sectional images of PERVAP 4060 and SOLSEP 010206 were taken using the scanning electron microscope **Figure** 2.2. Both the membranes exhibit composite structure having a thin top layer and support layer/s.

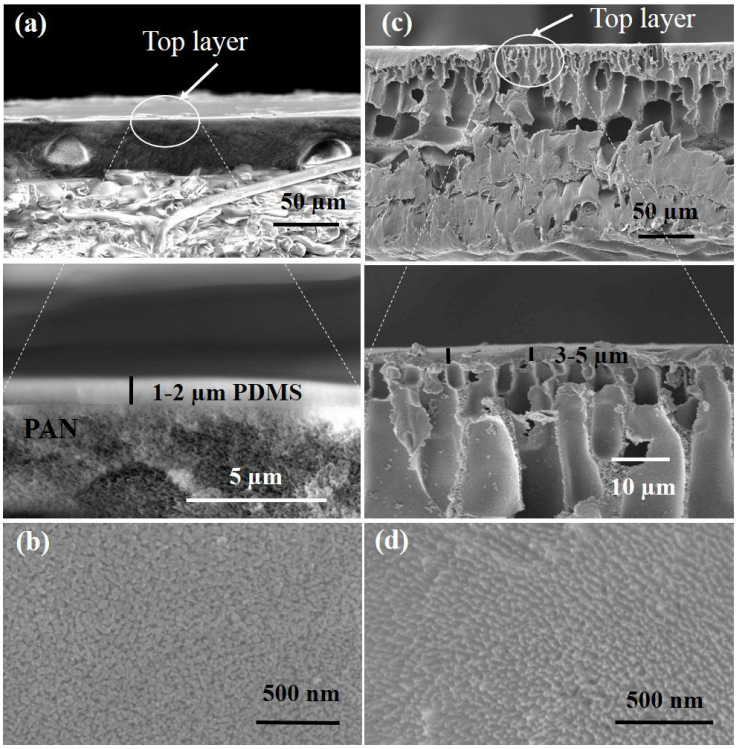

Figure 2.2: Microscopic images of dense membranes: (a) Cross-section and (b) surface of PERVAP 4060 (c) Cross-section and (d) surface of SOLSEP 010206.

Clearly, both PERVAP 4060 and SOLSEP 010206 are composite, displaying $1-2\mu m$ and $3-5\mu m$ of top active layers, having porous supports underneath.
The active layer of PERVAP 4060 is PDMS having porous polyacrylonitrile (PAN) support (Ben Soltane et al., 2013). Initially, this composite was designed to remove Volatile Organic Compounds (VOC) and aroma from aqueous solutions (`https://www.deltamem.ch/pervaporation.html`). By nature, PDMS is an organosiloxane elastomeric polymer having a siloxane ($Si-O$) backbone, substituted with methyl groups that give a high free volume fraction. Therefore, it provides high diffusion coefficients for solvents and gases. When cross-linked, PDMS is chemically stable in most organic solvents (Cheng et al., 2014a), which makes it interesting for OSN application. For instance, rejection of Alphazurine FG from toluene was reported $\simeq 99\%$ using PDMS based PERVAP 4060 (Ben Soltane et al., 2016).
On the other hand, SOLSEP 010206 consists of $3-5\mu m$ PA with a highly porous support layer (**Figure** 2.2). It was believed that SOLSEP membranes are TFC types, and some of them have a silicone top layer (Marchetti et al., 2014a). In another study, the top layer of SOLSEP was reported PA-PI composite (Dutczak et al., 2013). The support of the PA membrane, however, mainly determines its solvent-resistant nature and OSN performance. The cross-linking density in the PA layer is rather high, and under solvent, they often suffer to peel-off from support. Therefore, choosing proper support material is vital to maximizing the performance of this membrane (Cheng et al., 2014a). The support material of SOLSEP 010206 is unknown.

2.1.2.2 Porous OSN membranes

Similar to the dense membrane, the surface and cross-sectional images of AMS 3012 and PAN support were taken using the scanning electron microscope (**Figure** 2.3), showing a composite structure with active layer and support.

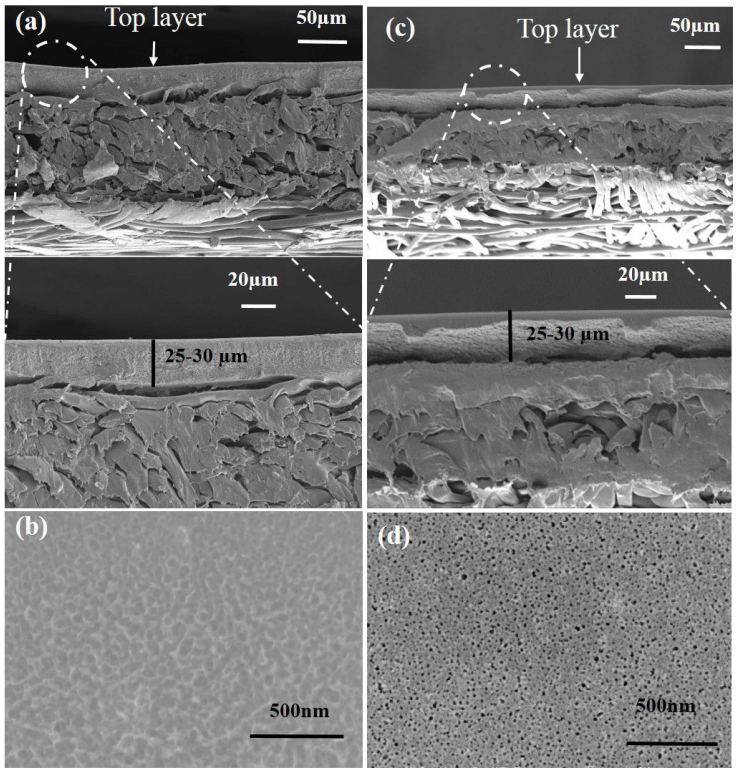

Figure 2.3: Microscopic images of porous membranes: (a) Cross-section and (b) surface of AMS 3012 (c) Cross-section and (d) surface of PAN support.

The active layer thickness of both membranes was obtained 25-30μm. The pores on the PAN surface is clear from **Figure** 2.3d, but for AMS 3012, pores are not clear from the surface image, as shown in **Figure** 2.3d. Though it was known from the supplier that the membrane is nanoporous for OSN application (`http://www.amsmembrane.com/index.php/en/products/ams_membranes`). In porous membranes, the dimension of the pores mainly determines the selectivity, but the choice of the materials affect adsorption and chemical stability (Mulder, 1998). Porous OSN membranes consist of a solid matrix with defined pores, which can go $< 2nm$ and $> 50nm$ (Strathmann et al., 2011). A large variety of pore geometry is evident, and the membrane resistance comes from the asymmetric porous top-layer. The separation of solutes by porous membranes is mainly a function of molecular size and membrane pore size distribution (Baker, 2007). The pore sizes and shape, the structure of the pore and flow through the pore correlated by the mechanism of convective flow, Knudsen diffusion, and pore surface diffusion (Mulder, 1998).

2.1.3 Gas permeation in OSN membranes

The permeation of pure gases in commercial OSN membranes is significant because it can help to define the surface nature of the membrane, whether the membrane is dense or porous. In OSN, it is essential to know if the active layer of the membrane is dense or porous, in order to explain the mass transport mechanism. Therefore, characterization by gas permeability has been adopted to validate the dense/porous structure of the membrane.

Permeability of CO_2, N_2 and He in PERVAP4060, SOLSEP 010206 and AMS 3012 were measured by time-lag method, and then CO_2/N_2 and He/N_2 selectivity were calculated and compared with

Knudsen selectivity (**Table** 2.3). By definition, the Knudsen selectivity of i over j ($\alpha_{i/j}$) is the square root of the molecular weight of J over i, (M_{wj}/M_{wi}). Gas permeability in PAN support was not considered as the SEM image of PAN clearly shows that the membrane is porous (**Figure** 2.3d), The permeability unit in **Table** 2.3 is Barrer. 1 Barrer = $3.35\times10^{-16} mol.m.m^{-2}.s^{-1}.Pa^{-1}$

Membranes	P_{CO_2}	P_{N_2}	P_{He}	**Experimental Selectivity ,** α_{CO_2/N_2} ($\alpha_{CO_2/N_{2_{Knudsen}}}$ = 0.8)	**Experimental Selectivity ,** α_{He/N_2} ($\alpha_{He/N_{2_{Knudsen}}}$ = 2.64)
PERVAP 4060	≈3200	≈ 250	≈ 373	12.8	1.5
AMS S3012	≈ 69453	≈73648	≈185955	≈1	2.5
SOLSEP 010206	≈85	≈86	≈274	1	3.2

Table 2.3: Pure gases permeability (Barrer) in commercial membranes by time-lag.

In pure gas permeation, a high CO_2/N_2 selectivity means that the membrane is dense. On the contrary, when CO_2/N_2 selectivity is ≈1, the membrane is porous. Clearly, the selectivity of CO_2/N_2 in **Table** 2.3 indicates that the active layer of PERVAP 4060 is dense whereas the active layer of AMS 3012 is porous. Comparing the Knudsen CO_2/N_2 and He/N_2 selectivity with experimental values, it is apparent that the AMS 3012 must be a porous membrane.

In SOLSEP 010206, however, the permeability of both CO_2 and N_2 is very low, and the selectivity of CO_2/N_2 is ≈1, suggesting a very low porous structure of the membrane. Also, the selectivity of He/N_2 in SOLSEP 010206 is higher than Knudsen selectivity, suggesting a dense surface of the membrane, which is in agreement with the given information by the supplier.

2.1.4 Summary of membrane characterization

The overall characterizations of OSN commercial membranes are summarised in **Table** 2.4.

Characterization	**PERVAP 4060**	**SOLSEP 010206**	**AMS S3012**	**PAN Support**
Surface type /nature	Dense/ hydrophobic	Dense/ Hydrophilic	Nanoporous/ Highly hydrophilic	Porous/ hydrophilic
Water contact angles (°)	103° ±4°	66° ±5 °	24° ±5 °	55° ±3°
Thickness of top active layer (μm)	1-2	3-5	25±5	25±5
Thickness of porous (middle) layer(μm)	30±5	70±5	–	–
Thickness of Bottom layer (μm) (porous and fibre)	180±10	90±5	140±10	125±10
Global thickness (μm)	210±10	165±15	170±10	150±10
P_{CO_2} at 20°C ($Barrer$)	≈ 3200	≈ 85	≈ 69453	NA
P_{N_2} at 20°C ($Barrer$)	≈260	≈86	≈73648	NA

Table 2.4: Characterization summary of OSN commercial membranes.

2.2 Solvent fluxes and solutes rejection in commercial OSN membranes

2.2.1 The effect of transmembrane pressure on toluene fluxes in dense and porous OSN membranes

Toluene flux evolution with transmembrane pressure was measured using both porous and dense OSN membranes **Figure** 2.4. Comparing the toluene permeation in dense membranes (**Figure** 2.4a), the toluene fluxes in PERVAP 4060 is ≈12 higher than SOLSEP 010206. In porous membranes (**Figure** 2.4b), toluene fluxes in PAN is about three times higher than AMS 3012, showing a flux decline at elevated pressure. Surprisingly, toluene fluxes in dense PERVAP4060 and porous AMS 3012 are almost the same.

Toluene flux evolution in PAN corresponds to the data obtained during the first cycle of OSN measurement among four runs, which will be discussed in **Chapter 4**.

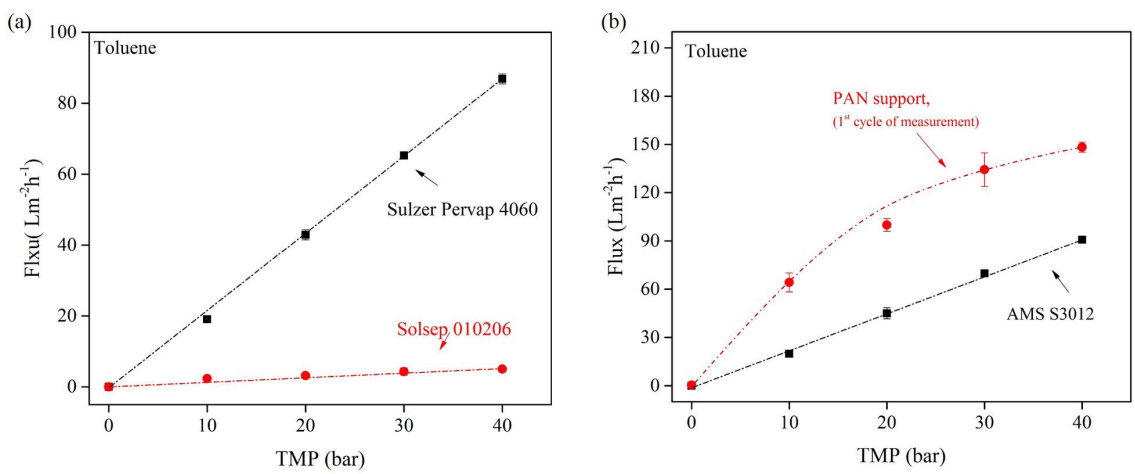

Figure 2.4: Evolution of toluene fluxes with transmembrane pressure up to 40 bar in (a) dense OSN membranes and (b) porous OSN membranes. Toluene feed at 30 $°C$ and $7-10$ kg/h tangential flow.

Except for PAN, toluene fluxes in each of the membranes are linear with transmembrane pressure. In these membranes, the flux evolution was linear and reproducible (data variation ±5%), when transmembrane pressure increased up to 40 bar, followed by the decrease to 10 bar, indicating their high stability in toluene.

2.2.2 Rejection of diluted R-BINAP and C44 by commercial dense and porous membranes in toluene

Rejection of organophosphorus ligand, R-BINAP ($C_{44}H_{32}P_2$, MW 622 $g.mol^{-1}$) and Tetratetracontane ($C_{44}H_{90}$ or $C44$, MW 619 $g.mol^{-1}$) were measured at 10 bar transmembraen pressure using both dense and porous membranes (**Figure** 2.5).
Clearly, PERVAP 4060 exhibits the highest rejection of both solutes among all membranes used. Even though toluene fluxes in dense PERVAP 4060 and porous AMS 3012 are similar (**Figure** 2.4). Rejection in AMS 3012 is obtained much lower than PERVAP 4060; quite logically, due to

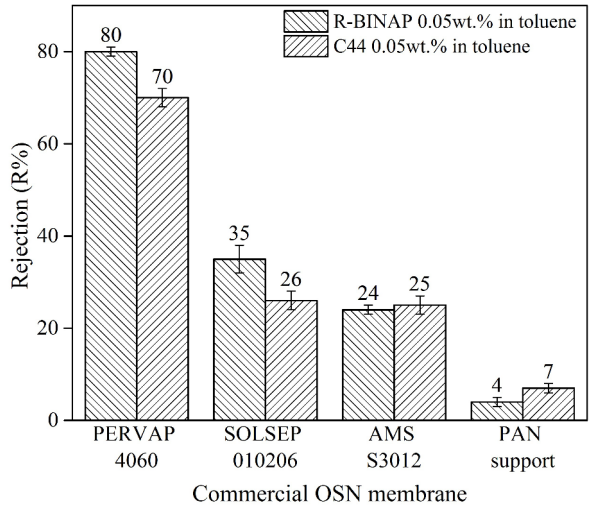

Figure 2.5: Rejection of diluted R-BINAP and C44 by dense and porous commercial OSN membranes, using the OSN feed of 0.05 wt% solute dissolved in toluene at 10 bar, 30° C, and 7-10 kg/h cross-flow rate.

the differences between their mass transport mechanisms. Rejection in dense SOLSEP 010206 and porous AMS 3012 are almost the same but differ significantly in toluene fluxes.

2.2.3 Rejection of hydroformylation catalyst and ligand by the commercial dense and porous membranes in toluene

Rejection of the hydroformylation catalyst-ligand was evaluated using both porous and dense membranes at 10 bar (**Table** 2.5). These experiments were performed in the Chemical and Process Engineering (CIP) team of the University of Rennes 1, reflecting on the common ANR objective of evaluating the best performing OSN membrane. The feed composition was adopted according to the actual solute concentration, used for hydroformylation in toluene: low concentration of a pre-catalyst of $Rh(acac)(CO)_2$, biphephos ligand, and the substrate undecenitrile.

Membranes	**Rh(acac)(CO)2 0.0015 wt %**	**Undecenitrile 19 wt %**	**Biphephos 0.1 wt%**
PERVAP 4060	19	15	88
SOLSEP 010206	31	11	53
AMS S3012	17	36	33
PAN support	5	3	8

Table 2.5: Rejection of hydroformylation catalyst-ligand by commercial dense and porous membranes in toluene at 10 bar, 30°C, and 7-10 kg/h cross-flow rate.

Again, PERVAP 4060 exhibit the highest ligand rejection among all membranes tested. Rejection of $Rh(acac)(CO)_2$ in **Table** 2.5 was not prioritized because, by the end of hydroformylation reaction, the catalyst-ligand complex structurally more resembles bipheohos ligand (See **Figure** 1a in introduction for hydroformylation reaction).

2.3 Complimentary experiment: Investigation on the oxidation possibility of dilute R-BINAP in toluene under OSN condition

The possibility of R-BINAP oxidation was tested following the report of (De Smet et al., 2001), in which the author commented on the possibility of Ru-BINAP deactivation due to the oxidation of phosphine ligand during coupled hydrogenation with OSN. Thus, this test investigates if R-BINAP in toluene undergoes any unexpected oxidation which might influence the OSN results.

First, a fresh solution of 2wt.% R-BINAP in toluene was prepared and used immediately for phosphorous NMR spectrum. Next, the solution kept under stirring at $30°C$ for five days imitating the OSN feed condition followed by taking another $^{31}P-NMR$ spectrum. Both the spectrum were compared for the detection of phosphine ligand oxidation (if any) in **Figure** 2.6.

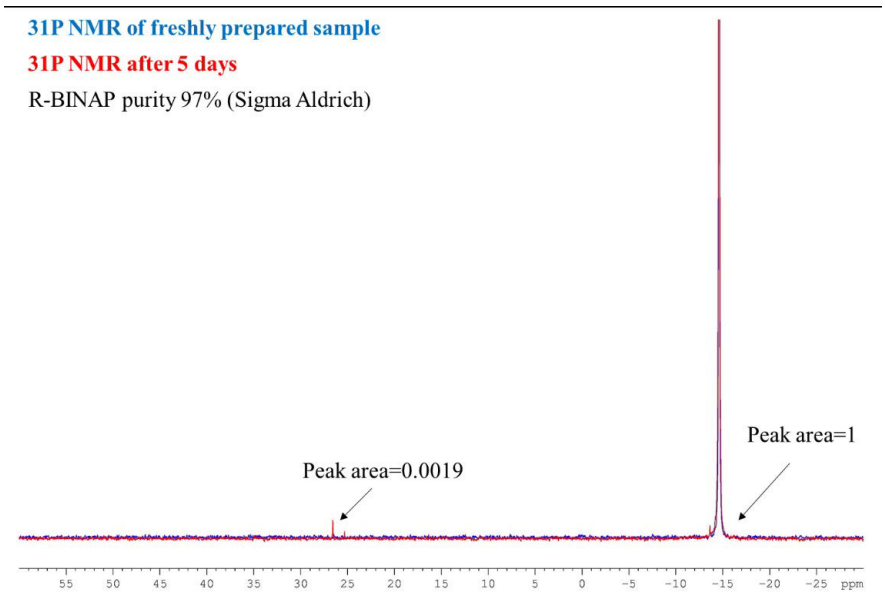

Figure 2.6: $^{31}P-NMR$ of 2 wt.% R-BINAP dissolved in toluene, before and after five days of solution preparation.

The phosphorous NMR of BINAP ligand, reported in Cabello-Sanchez et al. (2007), in which the chemical shift is reported $\delta = -15ppm$. Clearly, in **Figure** 2.6 the peak at $\delta = -15ppm$ correspond to the phosphorous in R-BINAP. At first glance, the main peak is unchanged at $\delta = -15ppm$. The chemical shift of phosphine oxide is reported $29.3ppm$ (Albright et al., 1975). After five days at OSN condition, a tiny peak was found at 26 ppm. This peak disappears when sensibility is adjusted **Figure** 2.7.

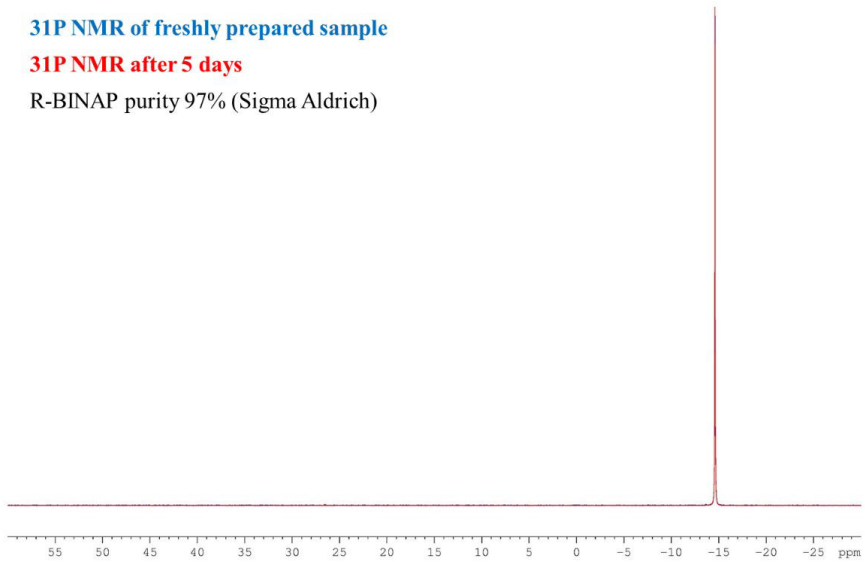

Figure 2.7: $^{31}P-NMR$ of 2 wt.% R-BINAP dissolved in toluene(with sensitivity correction), before and after five days of solution preparation.

The NMR indicates that the phosphine ligand oxidation is highly unlikely, even if it occurs, the amount is too low (estimated about $0.0002wt.\%$ after five days), to make an effect on OSN measurement.

2.4 Conclusion and perspective

Among four commercial membranes investigated in this study, dense PERVAP 4060 (PDMS) exhibits the promising performance of high R-BINAP rejection with reasonable toluene permeance. The dense SOLSEP 010206 and porous AMS 3012 and PAN exhibit both low toluene permeance and rejection compare to PERVAP 4060. High separation performance obtained from PERVAP 4060 makes it a potential candidate for ANR task of separating the active catalyst from toluene. The first objective of the Ph.D. is therefore met by finding the suitable membrane for ANR.

Next, the PERVAP 4060 has been considered for detail experimental investigation on its catalyst separation performance. Those OSN results are presented in the next section followed by supplementary results using PERVAP 4060.

In OSN membrane characterization, gas permeability by time-lag is an excellent tool to investigate the dense/porous structure of the membrane, which is essential for OSN mass transport phenomena. Without time-lag investigation, it would be challenging to know if the commercial membrane is dense/porous.

The OSN study, presented in this chapter, highlights on several following perspectives:

(1) In OSN, few commercial membranes are credible for the separation task of catalyst and ligand separation. New prototype membranes are real demand to comply with such separation objectives. The modification of membrane is proven to be a suitable technique for new prototype membranes (Amirilargani et al., 2016).

(2) Gas permeation is an excellent technique to discriminate porous or dense membrane and to evaluate porosity, permeance qualitatively.

(3) In preparation for the new prototype membrane, the existing PERVAP 4060 is an excellent choice for further modification. A nanolayer formation on the surface could be beneficial to influence the performance while keeping the bulk properties unaltered. For the porous system, both AMS S3012 and PAN support can be considered having the scope of investigation in modifying both nanopore (AMS S3012) and UF pore (PAN).

2.5 Article 1: Published in Journal of Applied Polymer Science

Title

Investigation of OSN properties of PDMS membrane for the retention of dilute solutes with potential industrial applications, *J. APPL. POLYM. SCI. 2019, DOI: 10.1002/APP.48359*

Graphical abstract

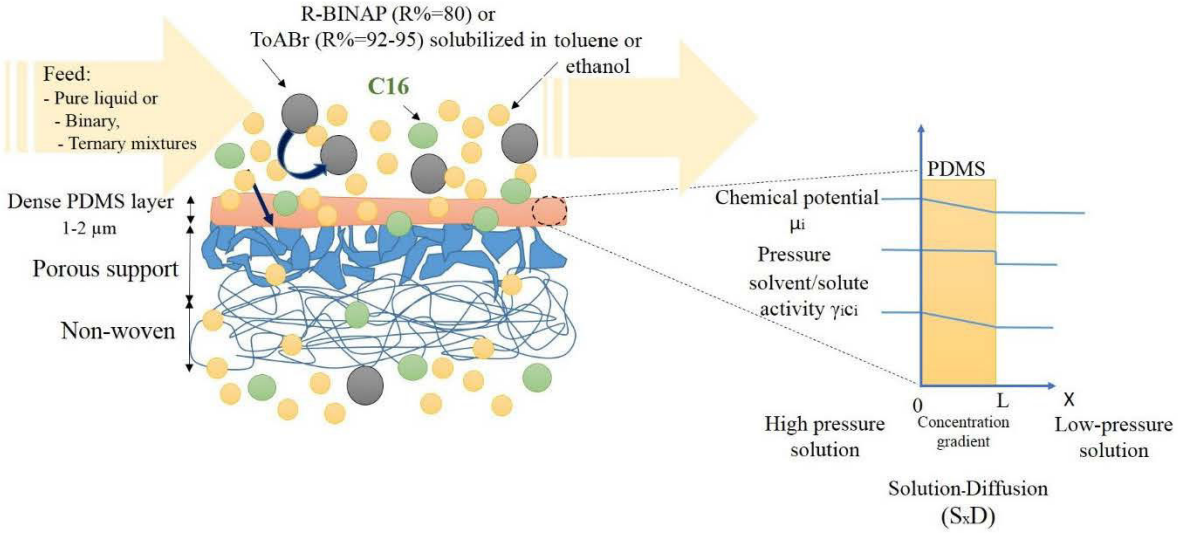

JOURNAL OF Applied Polymer SCIENCE

Investigation of OSN properties of PDMS membrane for the retention of dilute solutes with potential industrial applications

Morshed Mahbub,[1] Simonaire Hervé,[1] Alem-Marchand Halima,[2] Roizard Denis[1]

[1]Laboratoire Réactions et Génie des Procédés (UMR7274 CNRS- Université de Lorraine), ENSIC-1 rue Grandville, BP 20451, 54001 Nancy Cedex, France

[2]Institut Jean Lamour, UMR 7198 CNRS-Université de Lorraine, 2 allée André Guinier—Campus Artem 54011, Nancy Cedex, France

Correspondence to: R. Denis (E-mail: denis.roizard@univ-lorraine.fr) or (E-mail: denis.roizard@ensic.inpl-nancy.fr)

ABSTRACT: Few commercially available membranes can be used for organic solvent nanofiltration (OSN). Applying OSN in chemical industries is nevertheless of high interest to cut with energy consumption linked to solvent recycling and soluble catalysts recovery. A commercial membrane, PERVAP4060, was used to investigate the retention of dilute solutes in toluene feeds and to mimic metathesis medium. The studied solutes were R-BINAP a neutral polyaromatic molecule used in metathesis chemistry, tetraoctylammonium bromide (ToABr), a charged molecule used as a homogeneous catalyst and *n*-hexadecane. Retention of polar ToABr (95%) was higher than that of neutral R-BINAP (80%). The transfer mechanism, either pore flow or solution-diffusion, was discussed. All the results obtained suggested that the transport is governed by the solution-diffusion mechanism. The measured retentions could be explained in terms of solubility affinities and diffusion coefficients. The stability and performances of PERVAP4060 were well established, showing the strong potential for industrial applications. © 2019 Wiley Periodicals, Inc. J. Appl. Polym. Sci. **2019**, *136*, 48359.

KEYWORDS: catalysts; membranes; oil and gas; separation techniques

Received 24 February 2019; accepted 17 July 2019

DOI: 10.1002/app.48359

INTRODUCTION

The application of membrane technologies for the retention of dilute organic solutes, such as soluble catalysts, is an essential target from an industrial viewpoint. An early paper from Gosser[1] and several patents from the late 20th century[2] clearly indicate the interest in and the issues with membrane separation methods, such as pervaporation (PV) or organic solvent nanofiltration (OSN).[3,4] This study aims to investigate the retention of diluted diphosphine ligand R-BINAP and a phase transfer catalyst ToABr from a toluene feed using commercial composite polydimethylsiloxane (PDMS) membrane PERVAP4060 in order to favor industrial catalyst separation by membrane instead of distillation.

From an industrial viewpoint, the availability of membranes that provide a high solvent flux is very important and can be a decisive point in the design of a new process, as they can dramatically reduce capital cost expenditures (CAPEX). OSN is a highly attractive and relatively new method that can be used to purify and recycle low-volatility solvents at low cost or to concentrate valuable solutes, such as homogeneous catalysts dissolved in organic media like alcohols or aromatics. Distillation can also be used for these applications, but this benchmarked technology has two significant drawbacks: the evaporation of large quantity of solvent is very energy demanding, and the temperature increase may alter the properties of the solutes. In such media, it is desirable to extract the reaction products, while preserving the homogeneous catalyst, which is generally a very expensive component based on chelating ligands and specific metallic cations, such as rhodium or ruthenium.

The potential of OSN to increase the catalyst turnover number in such industrial applications[3] has been recognized for approximately two decades since its early industrial application in lube oils upgrading by EXXON.[5] However, the lack of availability of appropriate membranes for OSN with suitable molecular separation performances is a bottleneck. In this work, polymeric membranes were evaluated for the retention of 2,2′-bis(diphenylphosphino)-1,1′-binaphthyl (BINAP) and tetraoctylammonium bromide (ToABr). The neutral molecule BINAP is a ligand that is a key to the activity of many metal complex catalysts,[6] while the charged molecule ToABr is mainly used as a phase transfer catalyst. These two solutes are highly soluble in toluene, which is often used as the reaction media.

Nowadays some studies involving inorganic membranes are emerging.[7] But most of the polymeric membranes that have been

Additional Supporting Information may be found in the online version of this article.

© 2019 Wiley Periodicals, Inc.

used for OSN are highly crosslinked membranes based on rigid polymer backbones, such as the aromatic polyimides P84,[8] Matrimid,[9] PI Starmem,[10] polysulfone, polyether ether ketone, polybenzimidazoles,[11] and more recently PIM.[12] Koch developed the MPF series based on a PDMSactive layer in the 1990s (Koch, 2014; www.kochmembrane.com). However, the number of commercially available OSN membranes is very limited. Currently the leading suppliers are Evonik (http://duramem.evonik.com/product/duramem-puramem/en, 2018), which supplies the Starmem, Duramen, and Puramem series, and Solsep (http://www.solsep.com/OSN.htm, 2018), Koch (http://www.kochmembrane.com/Membrane-Products/Spiral/Nanofiltration.aspx, 2018), and Inopor®, which supply inorganic membranes (Inopor, 2018; http://www.inopor.com).

The retention of some solutes, including soluble catalyst using Starmem and MPF membranes, has reported mainly from EtOH feed. Unfortunately, many of these membranes are no longer available, probably due to their lack of stability over time. Thus, this work was intended to study the retention of diphosphine ligand R-BINAP from a toluene feed using a commercial composite polydimethylsiloxane membrane (PDMS), PERVAP4060.

PDMS is a well-known rubbery polymer that is widely used for liquid, VOC, and gas separations.[13] However, polydimethylsiloxane (PDMS) is often considered to be unstable in nonpolar solvents, as it is a very hydrophobic polymer and can undergo severe swelling in low-polarity solvents, such as alkanes or aromatics, with swelling degrees of well over 100 wt% being observed (g of solvent/g of dry polymer).[14] Nevertheless, this swelling property could be very interesting for OSN applications, because a high degree of polymer swelling induces high solvent permeance, which is desirable in OSN. However, a high degree of swelling is often considered to be detrimental to the high retention of solutes because the solutes could easily flow through the membrane due to the high solvent flux.[15] This issue is even more significant when highly dilute solutes are considered. Hence, the strength of the coupling effect induced by the high solvent flux when using a dense membrane may represent a significant obstacle to their use in OSN.

In order to clarify these points, two series of OSN experiments were carried out under tangential flow to investigate the performance and stability of PERVAP4060 and to determine the retention values of ToABr and BINAP in diluted toluene mixtures. ToABr was studied in toluene as well as in an alcoholic mixture for comparison with literature data. The system was operated in steady-state mode, and the parameters studied were the feed pressure, feed flow, and feed mixture composition.

To the best of our knowledge, this multilayer membrane has never been used under OSN conditions for the retention of these catalysts at low concentration in toluene. R-BINAP is a ligand that is used to form soluble ruthenium complexes for olefin metathesis synthesis, and toluene is a typical solvent for this reaction.[16,17] Before the investigation of the diphosphine ligand R-BINAP retention, we characterized the retention of ToABr from a toluene feed using PERVAP 4060 for comparison with previous results from the literature. By comparing the retention of R-BINAP, a neutral molecule, and ToABr, a charged molecule, under similar OSN conditions, we hoped to obtain further insight into the mechanism of mass transfer through PERVAP4060 and the influence of the solvent.

EXPERIMENTAL

Materials

(R)-BINAP (white powder; purity >94%), ToABr (white powder; purity 98%), and *n*-hexadecane (density 770 kg m^{-3}; purity >99%) were purchased from Sigma Aldrich and used as received. The solvents toluene (purity 99.8%) and ethanol (purity 96%) were also obtained from Sigma Aldrich.

The membrane used for the nanofiltration experiments was PERVAP 4060, which was provided by DeltaMem AG (https://www.deltamem.ch/) in flat A4 sheet form and used as received. PERVAP 4060 is a composite membrane with an active layer of 1–2 μm of PDMS (Figure 1).

Methods

OSN Setup. An OSN setup reported in a previous publication[14] was used. The setup consisted of a rectangular cross-flow cell (GE Osmonics) able to withstand pressures of up to 70 bar. The cell was used in tangential crossflow mode, in which the pressure, feed flow rate, and temperature of the feed can be controlled well [Figure 2(a)].

In addition to the previously reported setup, the applied pressure was regulated using an IP 65 solenoid valve connected to a digital pressure transmitter system and controlled using the Flow DDE Bronchorst software [Figure 2(b)]. This system allowed precise pressure control over the 0–40 bar range with a maximum fluctuation of 10% from the set value. The temperature was controlled using a Thermo Haake K50 with a precision of ±2 °C, and the cross-flow was set to 7–10 kg/h as measured using a Cori flow (digital mass flow) meter.

Membrane Conditioning Procedure

Before the OSN experiments, the membrane was immersed overnight in the solvent at room temperature (preconditioning). The membrane coupons had dimensions of 8 cm × 12 cm (including the area of the O-ring), corresponding to an effective useful membrane area of 34 cm^2.

After quickly wiping the membrane surface, the coupon was mounted into the OSN cell using a double O-ring Viton seal. Next, both the upstream and downstream cells were sealed using an SPX hand pump, which ensured that the unit was free of leaks in the pressure range of 0–40 bar.

The conditioning began with circulating the feed through the circuit at a flow rate of 7–10 kg/h and a temperature of 30 °C. Next, a transmembrane pressure (TMP) of 10 bar was applied in steps of 2/3 bar using the flow DDE software interface. At each step, the set point was compared to the actual value in the OSN, ensuring the stability of the TMP in the upstream. Once a pressure of 10 bar was achieved, the unit was monitored for 10–15 min to confirm that the pressure, cross-flow, and temperature were stable. The same procedure was repeated at 20, 30, and 40 bar. After conditioning at 40 bar, the TMP was gradually decreased to atmospheric pressure following the same conditioning protocol. The aim of this pretreatment was to avoid possible hysteresis effects due to the pressure increase. The same conditioning procedure was followed for the experiments at elevated temperature.

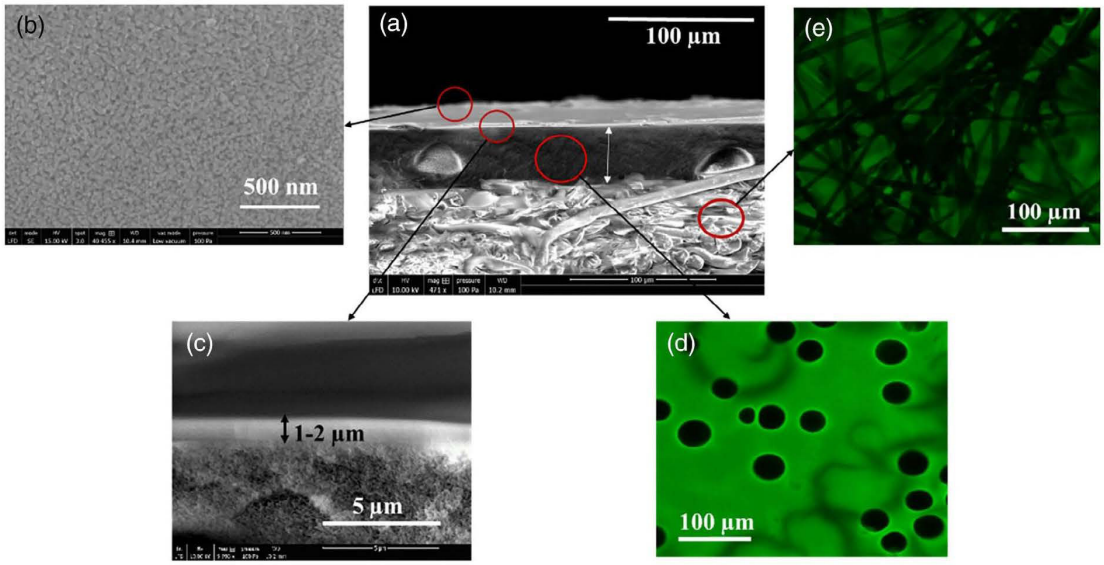

Figure 1. Characterization of the Sulzer PERVAP composite membrane by SEM and confocal microscopic images (a) Cross-sectional view of the membrane (total thickness 200–220 µm). (b) High-resolution image of the PDMS surface. (c) The cross-sectional view of the active layer (PDMS, thickness 1–2 µm). (d) Top view of the PAN porous sub-layer (25–30 µm). (e) PET support layer underneath the PAN sub-layer (170–190 µm). [Color figure can be viewed at wileyonlinelibrary.com]

OSN Procedure

The OSN experiments were performed in a cross-flow rig, in which NF was carried out in continuous mode. The permeate was continuously recycled to ensure a steady-state concentration of the feed.

Approximately 1 L of 0.05 wt% diphosphine ligand R-BINAP and phase transfer catalyst ToABr were separately prepared off-line by dissolving the solutes in toluene. Very low feed concentrations (below 0.05 wt% R-BINAP) were prepared by dilution. High R-BINAP concentrations (higher than 0.07 wt%) were partially achieved inline by concentrating the OSN feed. TMPs of 0–40 bar and temperatures of 30–50 °C were studied in the OSN experiments. The conditioning procedure described above was repeated at each temperature. For the ternary mixture feed, initially, a 0.05 wt% R-BINAP solution was used, and gradually, 1, 5, and 10 wt% *n*-hexadecane (C16) were added to feed.

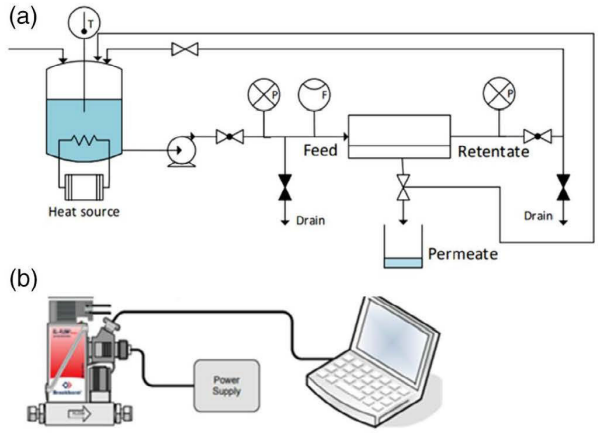

Figure 2. (a) Scheme of the OSN set-up. (b) Digital pressure control system. [Color figure can be viewed at wileyonlinelibrary.com]

After conditioning, an upstream pressure was applied with a stepwise increment of 2/3 bar. At each applied pressure, a 15–20 min blank run (no data point) was conducted to achieve stable permeate flow at the desired temperature and cross-flow. The permeate samples were then collected in a custom-made permeate vial with a small opening on the top to attach the vial to the OSN permeate line. This arrangement minimized evaporation loss of the solvent and ensured better measurement accuracy. At least 3–5 g of the permeate was collected and weighed for each data point, and the corresponding collection time was recorded. At each applied pressure, at least three permeate samples were collected, with an interval of at least 20 min between each sample. The sample size, number of repetitions, and length of the interval between each sample ensured better measurement accuracy and system stability.

In most cases, after the data collection at 40 bar was completed, the permeate flux and retention measurements at 10 bar were repeated. In several experiments, the used membrane was placed in a second OSN unit with a smaller surface area of 20 cm^2, and the reproducibility of the data was verified using a random TMP. The maximum deviation between different OSN units was 10% for the flux. Most of the experiments were repeated more than two or three times using new membrane samples from different batches, obtained at different times.

Analytical Methods

The flux (J) and rejection (R) were calculated according to the formulas (1) and (2) given below:

$$J = \frac{V}{A.t} \quad (1)$$

Where J is the flux ($Lm^{-2}\ h^{-1}$), V is the volume of the collected permeate (L), A is the active surface area (m^2), and t is the time (h).

$$R(\%) = \left(1 - \frac{Cp}{Cf}\right).100 \quad (2)$$

where C_p is the concentration of solute in permeate and C_f is the concentration of the feed.

Quantitative analysis of the solutes was carried out using gas chromatography. The operational conditions of the analysis method were as follows:

- Column: HP-5 phenyl methyl siloxane. Capillary dimensions: 15 m × 320 μm × 0.25 μm.
- Oven program:
  R-BINAP: 325 °C, held for 17 min for R-BINAP using tetratetracontane as the external standard. Retention of R-BINAP at around 13–14 min and retention of the external standard at around 6 min. The calibration and an example chromatogram are provided in the Supporting Information Figures A1 and A2.
  ToABr: 200 °C, held for 10 min for ToABr using *n*-tetracosane ($C_{24}H_{50}$) as the external standard. Retention of ToABr at around 6 min and retention of the external standard at around 8 min. The calibration and an example chromatogram are provided in the Supporting Information.
  n-Hexadecane and R-BINAP: 200 °C, held for 2 min for *n*-hexadecane ($C_{16}H_{34}$), then increased to 325 °C at a rate of 50 °C per minute and held for 17 min to detect R-BINAP. The calibration is given in Supporting Information Figure A2.
- Carrier gas: He, pressure 15 psi.
- Detector: FID (H_2/air: 1/10), 380 °C.

In the dilute feed stream, the peak area of the feed and permeate were significantly lower than that of the solvent peak. Therefore, calibration and measurement were carried out using a suitable external standard and the constant volume addition method. Each sample test was carried out in triplicate, and the results of the individual experiments were compared for the determination of solute retention.

In addition, at very dilute concentrations (as low as 0.0001 wt% of R-BINAP), the feed and permeate samples were first measured directly by GC, and then separate feed and permeate samples were concentrated by a factor of ten using a rotary evaporator. The new concentrations were remeasured using GC and compared with the initial results and were found to be reproducible with no more than 5% deviation. Three separate measurements were conducted using very low feed concentrations, and a new membrane sample was used each time. The retention was reproduced in each measurement. Data are given in Supporting Information Figure A3.

RESULT AND DISCUSSION

At the industrial scale, the use of highly dilute homogeneous catalysts for metathesis synthesis is preferable to the use of immobilized catalysts from an efficiency viewpoint. The current mature technology to recover the reaction products is distillation, but this method has the major drawback of causing the catalyst to lose its catalytic properties. OSN is considered to be a "soft" technology that can allow the separation of the product from the soluble catalyst at room temperature or moderate temperatures, thus avoiding the degradation of the expensive catalytic complex.

An overview of the literature related to the retention of BINAP and ToABr by OSN is given in Table I, and their schematic representations are given in Figure 3. As can be seen, a few OSN studies have dealt with the retention of highly dilute BINAP complexes in MeOH feed solutions with MPF or STARMEM membranes[18–20] but none have utilized toluene, which is one of the preferred solvents for some catalytic reactions, such as olefin metathesis.

Using MPF membranes, de Smet[18] and Vankelecom[19] reported rejection (R%) ranging from 70 to 98% in MeOH and of up to 93% in iPrOH for the complex Ru-BINAP. A flux of ≈1.2 L $m^{-2}\ h^{-1}$ was reported for MPF60, but no stable flux data were reported for the MF50 membrane, while a strong flux decline was observed with MeOH. The transport mechanism was explained using the pore flow model, which is controversial for dense active layers.[14,31,32] The authors suggested that the swollen dense PDMS layer became compacted at an OSN pressure of 16 bars, which was not supported by the work of other authors.[14,31] They cited the work of Paul as a reference, but surprisingly, in the cited paper, Paul did not support the compaction hypothesis in this low-pressure range.

The two other reports of the retention of BINAP from MeOH[10] or ionic liquid (IL)/methanol solutions[21] made use of the Starmem 112 membrane. In both cases, high initial retention values of up to 99% in pure MeOH were obtained. In the IL/MeOH solutions, the retention of the catalytic Ru-BINAP complex was >92%. Interestingly, both papers also reported that the retained catalyst was still active and could be recycled. The retention of the ligand BINAP itself (using the P atom as a marker) was higher than the retention of the Ru-catalyst, indicating the presence of metal species that were able to permeate the membrane more easily.

In the case of ToABr, more OSN studies have been reported (Table I), using both alcohol and toluene media. In each solvent, high solvent retentions in the range of 70–100% were obtained, depending on the type of membrane used. The highest flux was recorded for PMF60, a PDMS-based membrane, along with surprisingly low retention of 48%.[2] The best retention results were obtained in toluene solutions.[25,26] Using a PDMS-PEO composite membrane, Stamatialis showed that concentration polarization occurred when the ToABr feed concentration was below 8 wt%. Peeva analyzed the mass transfer through Starmem122 a polyimide membrane, using the solution-diffusion mechanism[27] and showed concentration polarization at 20 wt% (0.35 M) of ToABr.

Despite the fairly good results shown in Table I, Starmem and MPF membranes are no longer commercially available.

Table II provides information relevant to the feed solutions used for OSN with the commercial membrane PERVAP4060 in this study: EtOH solutions of ToABr (≈0.05 wt%) and toluene solutions of R-BINAP (≈0.05 wt%). C16 has been used as a simple model of an aliphatic linear product that can be produced by metathesis.

Table I. Literature Overview of the Retention of BINAP and ToABr Catalysts by OSN

Membrane (active layer)	Feed T (°C), pressure (bar)	Solutes (wt%)	Flux ($Lm^{-2}h^{-1}$)	Retention (%)	Reference
MPF60	MeOH, 30 °C, 15 bar	0.3% Ru-BINAP	~2	98	18
MPF50	MeOH, 30 °C, 16 bar	0.03% Ru-BINAP	NA	70	19
MPF 50	THF, 30 °C, 25 bar	0.04% Pd-BINAP	166	95.6	20
Starmem 122	THF, 30 °C, 25 bar	0.04% Pd-BINAP	93.6	100	20
Starmem 240	EA, 30 °C, 25 bar	0.04% Pd-BINAP	150.9	95.6	20
Starmem 122	MeOH + ionic liquids (0.01–10 wt%), 35 °C, 20 bar	0.0008% Ru-BINAP	NA	95–99.9	21
Starmem 122	MeOH, 30°C, 30 bar	0.005% Ru-BINAP	40	>97.5	10
Graph.Oxide	MeOH, rt, 5 bar	0.001% Ru BINAP	350	98	22
MPF50	Toluene, 30 bar	3% ToABr	19	48	2
Starmem122	Toluene, 30 bar	3% ToABr	14	>99	23
MPF 50	MeOH, 20 °C, 30 bar	0.3% Quats	NA	~95	24
PDMS-PEO	Toluene, 24 °C, 10 bar	8% ToABr	~16	100	25
Starmem 122	Toluene, 30 °C, 30 bar	20% ToABr	~ 33	100	26
Starmem 122	Toluene, 30 °C, 30 bar	20% ToABr	~35	98	27
Desal 5	Toluene 20 °C, 30 bar	3% ToABr	4	62	28
Starmem122	Toluene, 20–23 °C, 30 bar	3–20% ToABr	70	93–97	29
Starmem122	Toluene and MeOH mixtures, 22 °C, 30 bar	~0.2% ToABr	70	93	30

MPF: PDMS active layer; STARMEM: polyimide top layer.

Study of the Retention of ToABr

The active layer of PERVAP4060 is a dense layer of crosslinked PDMS approximately 1 to 2 μm thick. Despite the thickness and density of this layer, under OSN conditions, PERVAP4060 allowed fairly high toluene permeance of about 2 L m^{-2} h^{-1} bar^{-1} (Table III). Note that while this was the most frequently obtained value, higher values were measured for some coupons without a reduction in retention. This can be explained by variation in the thickness of the active layer from one membrane sample to another without invoking any compaction phenomena. Indeed, for a given coupon, no flux hysteresis was observed when the pressure was varied from 1 to 40 bar (Figure 4). The high permeance was in good agreement with the well-known affinity of dimethyl siloxane networks with toluene; toluene is a low-polarity aromatic solvent, and the active layer is a rubbery polymer that exhibits significant swelling in toluene. The solubility parameters (δ) (SI *units* are $J^{1/2}$ $m^{-3/2}$, equivalent to M $Pa^{1/2}$) of PDMS and toluene are quite similar: 15.4 and 18.2 $MPa^{1/2}$, respectively.

As mentioned above, the permeance was stable at pressures up to 40 bar, indicating that increased pressure does not have any effect on the swelling of the dense layer as previously reported.[14] Moreover, as PERVAP4060 has a composite structure with three layers, that is, polyethylene terephthalate (PET) nonwoven fibers as a mechanical support, polyacrylonitrile (PAN) as an ultrafiltration support, and PDMS as the top layer [Figure 1(a,d,e)] the steady permeance also indicates that this structure has good mechanical resistance that prevents any significant compaction phenomena at pressures of up to 40 bar.

Conversely, the permeance of EtOH was approximately ten times lower than that of toluene. The much higher solubility parameter of EtOH, δ = 26.5 $MPa^{1/2}$, qualitatively explains this result.

As shown in Table III, these results are in good agreement with those obtained by Stamatialis[25] using a composite PDMS-PEO membrane: both the flux and retention are high under analogous experimental conditions. These results demonstrate the good

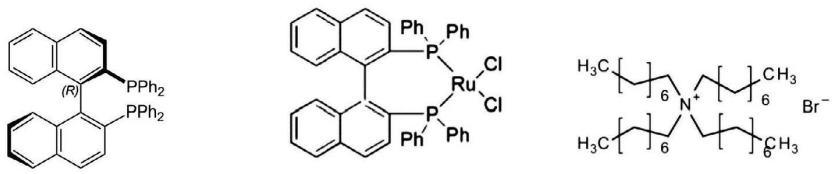

R-BINAP (Mw = 624 g mol^{-1}) Ru-BINAP (Mw = 794.6 g mol^{-1}) ToABr (Mw = 546 g mol^{-1})

Figure 3. Schematic representations of diphosphine ligand R-BINAP, Ru-BINAP, and phase transfer catalyst ToABr.

Table II. Some Specifications of the Used Chemicals

Material	MW g/mol	Molecular diameter (nm) [a]	Molar volume[b] $cm^c\ mol^{-1}$	Diffusion coefficient[c] $(m^b\ s^{-1}) \times 10^{+11}$ in toluene	Diffusion coefficient[c] $(m^b\ s^{-1}) \times 10^{+11}$ in PDMS	Solubility parameter[d] $MPa^{1/2}$
R-BINAP	622.7	NA	511	9.18	3.74	21.5
ToABr	546	NA	761	9.75	4.07	21.9
C16	226	0.845	294.1	14.9	7.26	15.9
Toluene	92.1	0.56	106.8	24	13.1	18.2
EtOH	46	0.52	58.5	26.4	1.7	26.5

[a] From literature.
[b] Molar volumes calculated using HSPiP[33] except for that of ToABr.[27]
[c] Diffusion coefficient of toluene and ethanol,[14] other diffusion coefficient values were calculated using a modified Gierer-Wirtz equation.[34]
[d] Solubility parameters were obtained from HsPiP estimation[33] except for ToABr.[35]

Table III. Solvent Permeance and Retention of ToABr by OSN from Dilute Toluene and EtOH Feeds (10 bar, Toluene, EtOH)

Membrane	Solvent	ToABr wt%	Permeance $\pm 0.1\ L\ m^{-2}\ h^{-1}\ bar^{-1}$	ToABr retention % ± 0.5	Reference
PERVAP4060	toluene	1	2.2 (30 °C)	93.5	This work
PERVAP4060	toluene	0.05	2.2 (30 °C)	93	
PERVAP4060	toluene	0.1	2.2 (30 °C)	92.5	
PERVAP4060	toluene	0.001	2.2 (30 °C)	93	
PERVAP4060	EtOH	0.05	0.35 (30 °C)	95	
PERVAP4060	EtOH	0.1	0.35 (30 °C)	95.6	
PDMS-PEO	toluene	8	1.6 (24 °C)	100	25
MPF 60	toluene	3	0.2 to 1.9 (25 °C)	48 to 86	29
MPF 60	MeOH	0.3	0.13 (30 °C)	98	18

performance of PERVAP4060, which combines high permeance and retention above 92% in toluene and 95% in EtOH. Previous data reported for commercial PDMS-based membranes (MPF series) showed highly variable retention and permeance values in toluene, ranging from 48 to 100% and 0.2 to 1.9 L $m^2\ h^{-1}\ bar^{-1}$, respectively. Clearly, the retention of ToABr from alcoholic feed solutions was superior for both the commercial MPF membranes and PERVAP4060,[18,29] but the permeance in MPF50 was at least 10 times lower. On the other hand, the STARMEM PI-based membrane series showed promising ToABr retention according to the literature data given in Table I; unfortunately, for technical reasons, these membranes are no longer available.

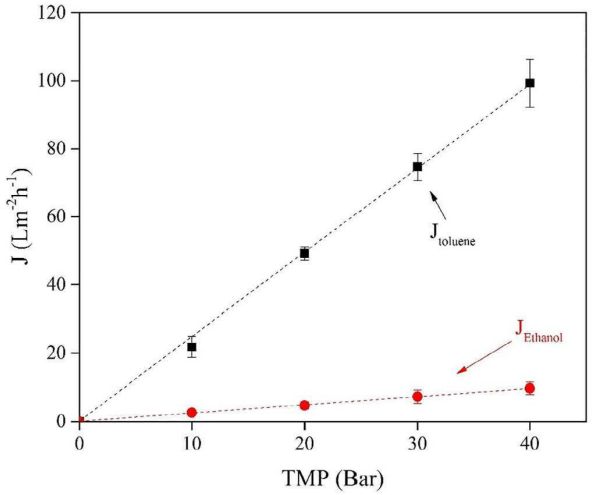

Figure 4. Pure solvent fluxes of EtOH and toluene through PERVAP6040. Deviation ±5%. [Color figure can be viewed at wileyonlinelibrary.com]

Retention of Diphosphine Ligand R-BINAP

The results obtained using BINAP as a dilute solute in toluene are presented in Figures 5–7, which show the effect of the applied pressure on the flux increase, the effect of the applied pressure over time on the OSN flux and BINAP retention, and the effect of temperature, respectively.

Figure 5 shows the OSN fluxes and retention values obtained after the conditioning procedure (feed crossflow 7–10 Kg/h, 15–20 min at each TMP in the range of 0–40 bar). Under these conditions, the retention of R-BINAP was almost constant and was independent of the applied pressure for pressures of up to 40 bar, reaching an average value of 80 ± 1%. The permeate fluxes increased steadily with the applied TMP, corresponding to permeance of ≈2.3 L $m^{-2}\ h^{-1}\ bar^{-1}$, that is, the same value as obtained previously using ToABr as the solute. Even though the two solutes should obviously have distinct mass transfer coefficients due to their different solubility parameters and molecular sizes (Table II), because their molar concentrations are very low, the permeate solute flux, respectively, remains very low compared to the solvent flux. In the case of R-BINAP, a large neutral

aromatic phosphine solute, a difference in its mobility in the PDMS network must be the main reason for the retention. These results also indicated that no significant compaction phenomena occurred with an increase in pressure.

Figure 6 shows the OSN fluxes and retention values obtained after several hours of continuous OSN operation at TMPs of 10 and at 20 bar. To maintain a constant feed concentration, the permeate flux was directly recirculated to the feed reservoir. Under these conditions, the retention of diphosphine ligand R-BINAP was almost constant (80%) and independent of the applied pressure. The permeate fluxes were steady with smooth oscillations related to the temperature and pressure regulation. When the experiments were repeated after 15 or 55 h, the same OSN fluxes were obtained, and the same selectivity was maintained. These experiments showed that the composite membrane was highly stable in the feed mixture and still gave reproducible results after 4 days.

Effect of Increased Temperature on the OSN Flux and Retention of BINAP

In Figure 7, it can be seen that for all the studied temperatures, the flux increased almost linearly with the pressure, leading to a very high flux of 180 L m^{-2} h^{-1} at 50 °C and 40 bar. The steady increase in the flux with an increase in pressure clearly indicates that the composite membrane was highly stable in the range from 30 to 50 °C: no apparent compaction or flux limitation related to the porous structure was observed. Taking into account the solution-diffusion mechanism through the dense active layer and knowing that the sorption of toluene decreases slightly with temperature, (Ea ≈ −7.3 J mol^{-1}),[36] the strong increase in the flux is clearly related to the increase in the diffusion coefficient of toluene.

The effect of temperature was then investigated using dilute feed mixtures of 0.05 wt% R-BINAP in toluene at a TMP of 10 bar. Data were obtained for three temperatures, 30, 35, and 40 °C, and are given in Table IV. First, the retention of R-BINAP, that is, R ≈ 80%, was not altered by the increased temperature, while the flux more than doubled between 30 and 40 °C. This phenomenon is striking because normally in membrane separations, a tradeoff between selectivity and permeance is observed, with a strong decrease in selectivity (or retention) occurring when the permeance is increased for any reason (temperature, pressure, or membrane thickness). Once again, these results attest to the fact that the mass transfer of toluene and that of the solute were apparently fully independent, despite the active layer being highly swollen by toluene.

In membrane separation, when the mass transfer is increased by temperature or by a pressure effect applied at the upside stream of the membrane, some coupling phenomena is often observed that induces of loss of selectivity. With R-BINAP, the increase in

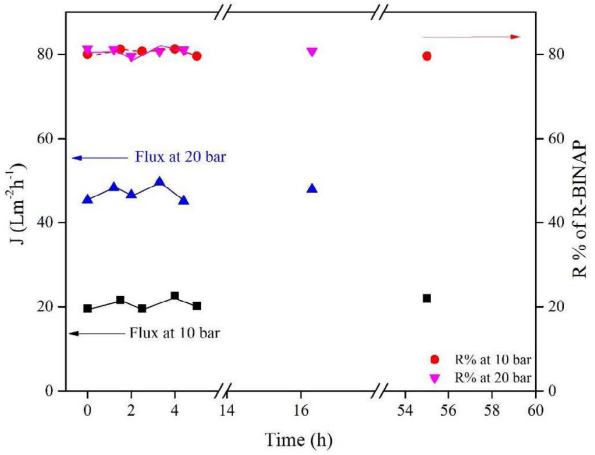

Figure 6. Effect of the applied pressure over time on the OSN flux and R-BINAP retention. Note that the J & R% values at zero correspond to the flux and retention measured after the conditioning procedure (feed cross-flow 8 Kg/h ± 20%, 15–20 min steady results at each studied TMP in the range of 0–40 bar). [Color figure can be viewed at wileyonlinelibrary.com]

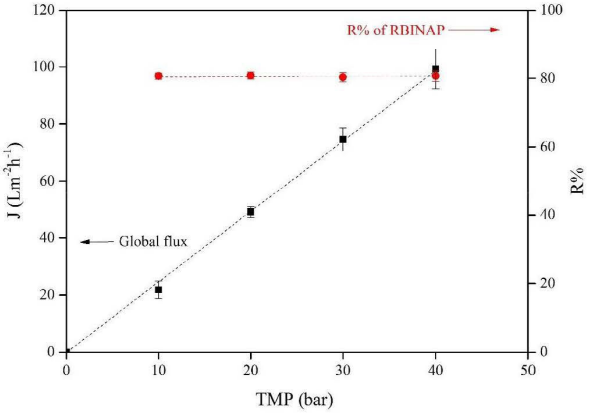

Figure 5. OSN performance of PERVAP4060 for the retention of R-BINAP from a toluene feed solution in the range 1–40 bar. R-BINAP: 0.05 mass%. Note that the J & R% values at different TMP correspond to the flux and retention measured after the conditioning procedure. Continuous black line: OSN permeates flux values. Redline: retention values. Deviation ±5%. [Color figure can be viewed at wileyonlinelibrary.com]

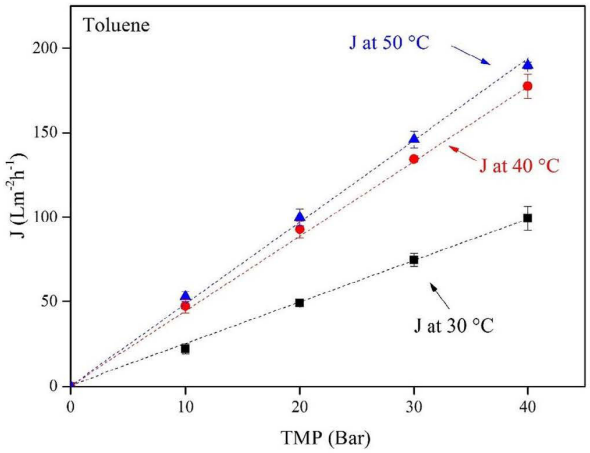

Figure 7. Effect of temperature on the pure toluene fluxes in the OSN system. Deviation ±5%. [Color figure can be viewed at wileyonlinelibrary.com]

temperature did not induce this phenomenon. Thus it means that in the swollen PDMS active layer, the higher toluene flux due to an increase of its diffusion coefficient did not induce a significant increase of the convective force toward the solute. Hence the mass transfer of R-BINAP is not modified by the toluene mass transfer due to the increased temperature, which keeps the same ratio of solvent and solute in permeate, resulting to a constant rejection of R-BINAP from toluene.

Moreover, for porous NF membranes, the opposite situation is usually observed: with an increase in temperature, the molecular cut-off increases, leading a strong reduction in the retention values. This can be explained by an increase in the mean pore size.[37]

Second, the results also indicated that the total OSN flux was unchanged compared to that of the pure solvent series, which in turn demonstrated that the high retention of R-BINAP did not influence the solvent flux and that no significant polarization concentration effect occurred during the experiment. Two factors contributed to this result: first, the concentration of R-BINAP was rather low, and the relative increase in its concentration at the membrane interface could not induce significant osmotic pressure; second, as the permeate was systematically recycled to the upstream reservoir, the average concentration of the solute could not increase in the feed.

The increase in the flux with temperature was not linear but instead followed a power law. This effect is well-known in gas permeation and pervaporation but has rarely been studied in OSN.[38] Figure 8 shows the effect of temperature on the increase of the OSN flux using the Arrhenius law:

$$\ln(J) = A\frac{-Ea}{RT}$$

where J has units of mol m^{-2} h^{-1}, E_a is the activation energy in J mol^{-1}, and R is 8.3141 J mol^{-1} K^{-1}. Both the data obtained for pure toluene and the binary mixtures were used. In the feed mixture, the concentration of BINAP was below 0.05 wt%, and as discussed in the previous paragraph, the OSN flux was the same with and without diphosphine ligand R-BINAP.

The trends at 10 and 40 bar were almost the same in the 30–40 °C range, but a relative flux decline occurred in the 40–50 °C range. Therefore, the regression coefficients (R_c) are below 0.9. In the range 30–40 °C, the observed experimental data exhibit a better linear trend (R_c > 0.97). The calculated E_a values at 10 and 40 bar were 34 and 26 kJ mol^{-1}, respectively. As expected, the highest E_a value was observed at 10 bar. It was well controlled that the flux decline recorded at 50 °C was not due to measurement accuracy. Moreover, no hysteresis was observed, and the previously measured values at 30 °C were easily reproduced after the series of experiments at 50 °C. Hence, the decline in the flux at 50 °C was the result of a specific phenomenon that is not yet clearly understood (Supporting Information Figure A4). Two potential explanations can be suggested:

- First, at higher pressure there is an effect of compaction that affects the porous support layer and hence limits the overall mass transfer;
- Second, as the mass transfer increased a lot at 40 bars, the porosity of the support becomes a physical barrier to the mass transfer and so an additive resistance.

The hypothesis of compaction at 50 °C is unlikely; if any compaction does occur, it seems to be fully reversible, that is fairly not likely. On the other hand, as mentioned above, the sorption of toluene into the PDMS layer is known to be exothermic.[36] Hence, the higher the temperature is, the higher the decrease in sorption. This effect might partially explain the observed phenomenon. Also, such phenomena may occur when the polymer network is in an unsteady state or can rearrange. For PERVAP 4060, the active layer, PDMS, is a chemically crosslink rubbery network and it is unlikely for this network to get a morphological change that would decrease the mass transfer. However, mass transfer can also be dependent on the other sublayer, which supports the active layer. Indeed, as the mass transfer increases sharply at 40 bars between 30 and 50 °C, that is, 80% more, the support itself may become an additive resistance, limiting the overall transmembrane flux.

In conclusion, the combined effect of pressure and temperature strongly increased the OSN solvent flux, while the retention of the solute remained constant.

Looking through OSN literature, the determination of E_a has been reported by Machado[38] for acetone with MPF membranes, giving E_a = 1.1 kJ at 30 bar.

Usually, the relationship between the flux increase, and the temperature is explained in terms of a higher polymer chains mobility and a higher diffusion coefficient of the solvent when the permeation occurs through a dense selective layer. In the present case, having a highly swollen membrane due to toluene, it is interesting to compare the E_a of toluene linked to OSN to the energy of activation (E_μ) only linked to the relationship between the solvent viscosity and the temperature, as calculated by Messaâdi.[39] Hence, it should be underlined that E_μ (9.2 kJ mol^{-1}) is much lower than E_a (26 kJ mol^{-1} at 40 bar) for toluene in PDMS. Once more, this result shows that the transport mechanism through the membrane is far from a viscous flow, even with a highly swollen polymer network. Machado[38] made the same observation in his work with acetone and MPF50 (E_μ = 6.8 *vs* E_a = 13.2 kJ mol^{-1}).[38]

Table IV. Effect of Temperature on the OSN Flux and Diphosphine Ligand R-BINAP Retention at 10 bar. Feed: 0.05% R-BINAP - PERVAP4060

Temperature (°C)	Total flux J (L m^{-2} h^{-1}) ± 10%	R-BINAP retention 0.05 wt% ±2
30	21	80
35	36	81
40	47	79 ± 2

Effect of Dilution on the Retention of Diphosphine Ligand BINAP in Toluene in the Range 0.0001–0.2 wt%

OSN experiments were carried out both at lower and higher R-BINAP concentrations than the reference concentration of 0.05 wt%. The lower concentrations were easily prepared by dilution with an additional solvent and controlled using an external standard by GC. Calibration with an external standard was

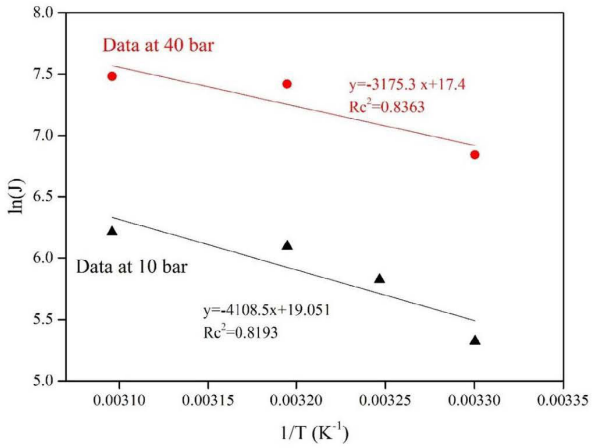

Figure 8. Arrhenius plot of the OSN flux data obtained for PERVAP4060. NB: as the R-BINAP concentration was very low (<0.05 wt%), the solvent flux has been assimilated to the total OSN flux. Deviation on t°: ± 2 °C. [Color figure can be viewed at wileyonlinelibrary.com]

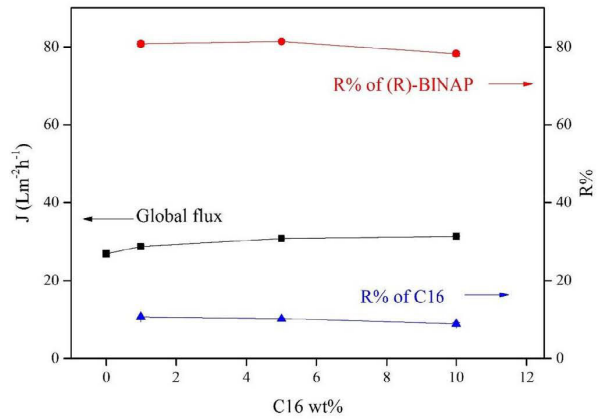

Figure 10. OSN performance of PERVAP4060 for the separation of a model ternary mixture consisting of C16 (1 to 10 wt%) and R-BINAP (0.05 wt%) in toluene (10 bar, 30 °C). Deviation on J: ± 10%. [Color figure can be viewed at wileyonlinelibrary.com]

necessary at the very low concentration of 100 ppm. The results are shown in Figure 9.

Within the studied range of R-BINAP concentrations, the retention of the solute was almost constant with respect to the measurement accuracy. This indicates that no strong dragging effect could be detected even at high dilution.

OSN Performance with a Model Ternary Mixture

A set of experiments was carried out to investigate the retention of diphosphine ligand R-BINAP (constant feed concentration: 0.05 wt %) from a ternary mixture containing a linear saturated hydrocarbon C16 (feed range: 1 to 10 wt%) and toluene. This mixture was intended as a very simple model of a metathesis reaction of linear alkenes.

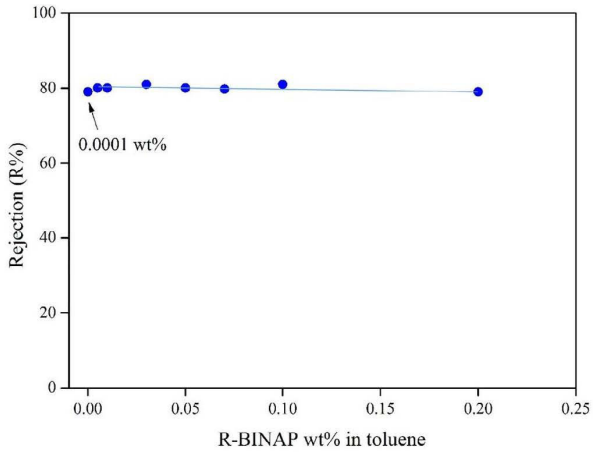

Figure 9. Evaluation of the effect of the concentration of the solute in toluene on its retention by PERVAP4060 (10 bar, 30 °C, concentration range: 0.0001–0.2 wt%). Deviation on rejection data: ± 2%. [Color figure can be viewed at wileyonlinelibrary.com]

In Figure 10, the influence of varying the concentration of the linear C16 on the OSN flux and the retentions of R-BINAP and C16 is shown. Interestingly, the retention of R-BINAP remained almost constant at 80%, with only a slight decrease (77%) occurring at the highest concentration of C16. A similar observation can be made for C16; its retention slightly decreases. The difference between R-BINAP and C16 can be explained by the higher diffusion coefficient, which is in relation with the lower molecular weight of the aliphatic solute (226 g) compared to that of R-BINAP (622 g) and with the correspondingly lower C16 molar volume (Table II). Another potentially relevant parameter is the lower solubility parameter of C16 compared to that of R-BINAP, which favors its sorption in the active PDMS layer ($\Delta\delta \approx 1$).

Finally, the results show that the global OSN flux was markedly increased by the presence of the aliphatic solute, up to about 15% at a C16 feed concentration of 10 wt%. Aliphatic solute contributes to increasing the swelling of the active layer of the membrane, which favors, in turn, the increase of the global-flux of the membrane. Clearly, this flux increase was greater than the simple flux contribution of the linear hydrocarbon.

Moreover, from a process point of view, these results indicate that the OSN method allows easy separation of the linear C16 molecule from R-BINAP in a toluene feed mixture. This is a promising result for its application in olefin metathesis.

CONCLUSIONS

The retentions of the tested solutes, phase transfer catalyst ToABr and diphosphine ligand R-BINAP, were high even at high solute dilutions in toluene, with values of up to 92 and 80%, respectively. Despite the significant swelling of the PDMS active layer in toluene, there was no indication that the mass transfer obeyed a pore flow mechanism. Conversely, all the results obtained indicate that a solution-diffusion mechanism seems to prevail.

In summary, the main findings related to the use of PERVAP4060 in OSN in this work are:

- The stability of the composite membrane was shown to be excellent under the range of pressures tested (10 to 40 bar), regardless of the degree of solvent-induced swelling of the active layer, that is, with both ethanol and toluene. A linear increase in the OSN flux was recorded over the tested pressure range at temperatures of up to 50 °C without any hysteresis effect.
- The retention of dilute solutes (0.05 wt%), such as ToABr and R-BINAP, which have molecular weights of 546 and 622 g, respectively, were above 80% for the neutral aromatic solute and above 92% for the alkyl ammonium salt. This demonstrates that the retention of the solutes was clearly not related to their molecular weights (or molar volume) but was more likely related to the relative affinity of the solute for the membrane active layer and, perhaps most importantly, to the solute mobility.
- In the range of dilutions studied (100 ppm to 0.2 wt%) in the toluene feed mixtures, the retention of R-BINAP was constant (80%). No coupling effect could be detected.
- The OSN flux followed an Arrhenius law with an increase in feed temperature. The energy of activation at 10 bar was higher than at 40 bar, while the retention remained steady. The effect looks very interesting in terms of application.
- Finally, it was shown that a ternary mixture of the solutes R-BINAP and linear C16 in toluene could easily be fractionated. Most of the C16 alkane was eliminated through the membrane, while the R-BINAP was mainly retained in the feed.

These results highlight the promising OSN potential of PERVAP4060 for the rejection of dilute solutes in metathesis synthesis. All the obtained data were in good agreement with a simple solution-diffusion mechanism through the composite membrane. The high retention level of the R-BINAP solute remained steady even at high dilution. Apparently, the transports of the solute and solvent were not coupled.

ACKNOWLEDGMENTS

This work was achieved in the frame of a collaborative project, ANR-14-CE06-0022, thanks to the financial support of the French National Research Agency and the support of ARKEMA. Professor S. Abbott is also greatly acknowledged for discussion about the Hansen solubility parameters of R-BINAP and ToABr.

REFERENCES

1. Gosser, L.; Knoth, W. H.; Parshall, G. W. *J. Mol. Catal.* **1977**, *2*, 253.
2. Livingston, A.G. US 2004/0099603 A1, 2004.
3. Marchetti, P.; Jimenez Solomon, M. F.; Szekely, G.; Livingston, A. G. *Chem. Rev.* **2014**, *114*, 10735.
4. Patterson, D. A.; Lau, L. Y.; Roengpithya, C.; Gibbins, E. J.; Livingston, A. G. *Desalination*. **2008**, *218*, 248.
5. White, L. S. *J. Membr. Sci.* **2006**, *286*, 26.
6. Noyori, R.; Takaya, H. *Acc. Chem. Res.* **1990**, *23*, 345.
7. Andecochea Saiz, C.; Darvishmanesh, S.; Buekenhoudt, A.; Van der Bruggen, B. *J. Membr. Sci.* **2018**, *546*, 120.
8. White, L. S. *J. Membr. Sci.* **2002**, *205*, 191.
9. Cheng, X. Q.; Zhang, Y. L.; Wang, Z. X.; Guo, Z. H.; Bai, Y. P.; Shao, L. *Adv. Polym. Technol.* **2014**, *33* (S1), https://doi.org/10.1002/adv.21455.
10. Nair, D.; Wong, H.-T.; Han, S.; Vankelecom, I. F. J.; White, L. S.; Livingston, A. G.; Boam, A. T. *Org. Process Res. Dev.* **2009**, *13*, 863.
11. Székely, G.; Valtcheva, I. B.; Kim, J. F.; Livingston, A. G. *React. Funct. Polym.* **2015**, *86*, 215.
12. McKeown, N. B.; Budd, P. M. *Macromolecules*. **2010**, *43*, 5163.
13. Alqaheem, Y.; Alomair, A.; Vinoba, M.; Pérez, A. *Int. J. Polym. Sci. 2017*, 1.
14. Ben Soltane, H.; Roizard, D.; Favre, E. *J. Membr. Sci.* **2013**, *435*, 110.
15. Wijmans, J. G.; Baker, R. W. J. *Membr. Sci.* **1995**, *107*, 1.
16. Chen, A.S.C.; Laneman, S.A. 1993/US005202473A, 1993.
17. Mashima, K.; Kusano, K.; Ohta, T.; Noyori, R.; Takaya, H. *J. Chem. Soc. Chem. Commun.* **1989**, *17*, 1208, https://pubs.rsc.org/-/content/articlelanding/1989/c3/c39890001208/unauth#!divAbstract
18. De Smet, K.; Aert, S.; Ceulemans, E.; Vankelecom, I. F. J.; Jacobs, P. A. *Chem. Commun.* **2001**, 597, https://doi.org/10.1039/B009898L.
19. Vankelecom, I. F. J.; De Smet, K.; Gevers, L. E.; Livingston, A. G.; Nair, D.; Aerts, S.; Kuypers, S.; Jacobs, P. A. *J. Membr. Sci.* **2004**, *231*, 99.
20. Scarpello, J. T.; Nair, D.; Freitas dos Santos, L. M.; White, L. S.; Livingston, A. G. *J. Membr. Sci.* **2001**, *203*, 71.
21. Wong, H.-T.; See-Toh, Y. H.; Ferreira, F. C.; Crook, R.; Livingston, A. G. *Chem. Commun.* **2006**, *2063*, https://doi.org/10.1039/B602184K.
22. Huang, L.; Chen, J.; Gao, T.; Zhang, M.; Li, Y.; Dai, L.; Qu, L.; Shi, G. *Adv. Mater.* **2016**, *28*, 8669.
23. Nair, D.; Luthra, S. S.; Scarpello, J. T.; White, L. S.; Freitas dos Santos, L. M.; Livingston, A. G. *Desalination*. **2002**, *147*, 301.
24. Gibbins, E.; D' Antonio, M.; Nair, D.; White, L. S.; Freitas dos Santos, L. M.; Vankelecom, I. F. J.; Livingston, A. G. *Desalination*. **2002**, *147*, 307.
25. Stamatialis, D. F.; Stafie, N.; Buadu, K.; Hempenius, M.; Wessling, M. *J. Membr. Sci.* **2006**, *279*, 424.
26. Silva, P.; Peeva, L. G.; Livingston, A. G. J. *Membr. Sci.* **2010**, *349*, 167.
27. Peeva, L. G.; Gibbins, E.; Luthra, S. S.; White, L. S.; Stateva, R.; P; Livingston, A. G. *J. Membr. Sci.* **2004**, *236*, 121.
28. Luthra, S. S.; Yang, X.; Freitas Dos Santos, L. M.; White, L. S.; Livingston, A. G. *J. Membr. Sci.* **2002**, *201*, 65.
29. Livingston, A. G.; Peeva, L.; Han, S.; Nair, D.; Luthra, S. S.; White, L. S.; Freitas Dos Santos, L. M. *Ann. N. Y. Acad. Sci.* **2003**, *984*, 123.
30. Lin, J. C.-T.; Livingston, A. G. *Chem. Eng. Sci.* **2007**, *62*, 2728.

31. Paul, D. R.; Paciotti, J. D.; Ebra-Lima, O. M. *J. Appl. Polym. Sci.* **1975**, *19*, 1837.
32. Stafie, N.; Stamatialis, D. F.; Wessling, M. *Sep. Purif. Technol.* **2005**, *45*, 220.
33. Hansen, C. M. Hansen Solubility Parameters: A User's Handbook. 2nd ed.; Boca Raton: CRC Press, **2007**, https://www.taylorfrancis.com/books/9780429127526.
34. Evans, R.; Deng, Z.; Rogerson, A. K.; McLachlan, A. S.; Richards, J. J.; Nilsson, M.; Morris, G. A. *Angew. Chem. Int. Ed.* **2013**, *52*, 3199.
35. Boucher-Sharma, A. P.; Chowdhury, G.; Matsuura, T. J. *Appl. Polym. Sci.* **1999**, *74*, 47.
36. Favre, E. *Eur. Polym. J.* **1996**, *32*, 1183.
37. Sharma, R. R.; Agrawal, R.; Chellam, S. *J. Membr. Sci.* **2003**, *223*, 69.
38. Machado, D. R.; Hasson, D.; Semiat, R. *J. Membr. Sci.* **1999**, *163*, 93.
39. Messaâdi, A.; Dhouibi, N.; Hamda, H.; Belgacem, F. B. M.,. Y.; Adbelkader, H.; Ouerfelli, N.; Hamzaoui, H. *J.Chem.* **2015**, Article ID 163262, 1, http://dx.doi.org/10.1155/2015/163262.

Chapter 3

Dense system: PDMS membrane and modification of PDMS by plasma and polyelectrolytes

3.1 Background

The background of this study relies on previously published articles specifically on (Ben Soltane et al., 2013) (Ben Soltane et al., 2016) (Bassil et al., 2016a), including the OSN study presented in the previous chapter.

(Ben Soltane et al., 2013) titled ***Effect of pressure on the swelling and fluxes of dense PDMS membranes in nanofiltration: An experimental study.*** This study investigates the pressure-swelling effect on a highly swollen PDMS based rubbery network. While OSN literature hypothetically reports a compaction phenomenon of highly swollen PDMS network at high pressure, this study experimentally shows an unmodified upstream equilibrium at high pressure. If the swelling extent at atmospheric pressure is known, the solvent concentration at the upstream side of the membrane can be precisely calculated which rules out the compaction possibility in the PDMS network. In mass transport, the authors report no evidence of porous or pseudo porous structures in the swollen gels under equilibrium conditions, even at a very high solvent volume fraction. Instead, the transport behavior likely follows the SD mechanism in PDMS. Finally, OSN fluxes were recorded using Sulzer PERVAP4060, a commercial PDMS composite. OSN fluxes for the three solvents (swelling range varied 5-163%) showed linear relationships with the applied pressure, which correspond to a solvent concentration gradient, thus follow solution-diffusion (SD) mechanism denying the possibility of pore-flow in swollen PDMS rubbery network.

Next, (Ben Soltane et al., 2016) titled ***Study of the rejection of various solutes in OSN by a composite polydimethylsiloxane membrane: Investigation of the role of solute affinity.*** This study reports the OSN separation results of small aliphatic molecules from diluted feed solutions in PDMS based Sulzer PERVAP4060. The retention of the solutes was found highly solvent dependent; contrary to some favourite ideas of retention governs by the swelling extent of PDMS, the membranesolute affinity was found to be a decisive parameter for the mass transport of the solute together with its diffusion ability. Negative retention could be obtained with a low swelling degree, whereas high retention rates with a high swelling degree. The authors explain that the increase in rejection corresponds to the decrease of solutemembrane affinity. Depending on the solvent-solute-membrane affinities, negative to positive (as well as low to high) retention were achieved.

Next, (Bassil et al., 2016a) have published a paper entitled as ***Tailored adhesion behaviour of polyelectrolyte thin films deposited on plasma-treated poly (dimethylsiloxane) for functionalized membranes.*** This study reports the formation of entirely homogenous films on plasma treated Sulzer PERVAP 4060 via layer-by-layer assembly of poly(diallyldimethylammonium chloride) (PDDA) and the poly(styrene sulfonate) (PSS). This study shows that the polyelectrolytes multilayer (PEM) is highly stable on PDMS and adhesion of the polyelectrolytes multilayer was greatly enhanced when the deposition was completed on an activated PDMS surface using plasma treatment.

These studies, as mentioned above, including the experimental findings presented in the previous chapter, are the fundamental standpoint for the modification approach of the dense system and hereafter, modification of PDMS draw the first attention.

The critical concern, however, is the stability of PEM in organic media and if PEM can induce new separation characteristics in OSN. Polyelectrolytes multilayer (PEMs) regarded as a high potential candidate featuring highly tunable thickness in nanometer, which makes PEM as a good fit for OSN (Cheng et al., 2014a). The PEM composed PDDA/PAA (Ahmadiannamini et al., 2012) and PDDA/SPEEK (Li et al., 2008) (Li et al., 2010) was reported highly stable in harsh solvents such as THF and DMF, exhibiting high dye rejection (Ahmadiannamini et al., 2012) (Marchetti et al., 2014a).

3.2 Abstract

This chapter is dedicated to the preparation of the prototype membranes by polyelectrolytes multilayer, their characterization, and finally performance under OSN conditions. Two dense OSN membranes: PVA and PDMS were considered and further modified by deposition polyelectrolytes multilayer using different pairs of cationic and anionic polyelectrolytes. Several key points are highlighted below in order to clarify the objectives out of PVA and PDMS membranes while employing PVA in pervaporation and PDMS in nanofiltration.

1. The PVA is hydrophilic polymer exhibit high selectivity to water and dehydration properties by pervaporation (PV) (Zhao et al., 2011b) (Bolto et al., 2011) whereas PDMS is hydrophobic exhibit high selectivity to solutes even at high swollen condition (Ben Soltane et al., 2013) (Ben Soltane et al., 2016).

2. When cross-linked, PVA is glassy like polymer and mass transport phenomena is well established to follow the SD mechanism. In contrary, PDMS is rubbery, and mass transport phenomena in OSN literature are often contradicting in terms of the transport mechanism.

3. PVA exhibit low to medium permeance characteristics, whereas PDMS is highly permeable.

4. Study on pervaporation (PV) deals with liquid-liquid separation with a phase change, whereas OSN deals with solute-solvent systems without any phase change.

Worth to mention that the PEM deposition protocol remained unaltered in preparation of all prototype membranes. Consecutively, the choice of Polyelectrolytes (PE's), cationic and anionic systems, mass transport phenomena in PEM have been considered to investigate.

The following articles report the objectives, protocol used for the modification,and discuss experimental results. The rest of the chapter highlights the complementary OSN results obtained with PDMS.

3.3 Article 2: Published in Applied Surface Science

Title

Investigation of new modification strategies for PVA membranes to improve their dehydration properties by pervaporation, ***Volume 450, 30 August 2018, Pages 527-537***

Applied Surface Science 450 (2018) 527–537

Contents lists available at ScienceDirect

Applied Surface Science

journal homepage: www.elsevier.com/locate/apsusc

Full Length Article

Investigation of new modification strategies for PVA membranes to improve their dehydration properties by pervaporation

M.E. Dmitrenko [a], A.V. Penkova [a,*], A.I. Kuzminova [a], M. Morshed [b], M.I. Larionov [a], H. Alem [c], A.A. Zolotarev [a], S.S. Ermakov [a], D. Roizard [b]

[a] St. Petersburg State University, 7/9 Universitetskaya nab., St. Petersburg 199034, Russia
[b] Laboratoire Réactions et Génie des Procédés, CNRS, Université de Lorraine, ENSIC, 1 rue Granville, 54000 Nancy, France
[c] Université de Lorraine, CNRS, Institut Jean Lamour (IJL), UMR 7198, Nancy, France

ARTICLE INFO

Article history:
Received 10 January 2018
Revised 6 April 2018
Accepted 18 April 2018
Available online 22 April 2018

Keywords:
PVA
Pervaporation
Fullerenol
Bulk modification
Polyelectrolyte
Layer-by-layer deposition

ABSTRACT

Novel supported membranes based on polyvinyl alcohol (PVA) were developed using two strategies: first, by the modification of the PVA network, via so-called bulk modification, with the formation of the selective layer accomplished through the introduction of fullerenol and/or poly(allylamine hydrochloride), and second, by the functionalization of the surface with successive depositions of multilayered films of polyelectrolytes, such as poly(allylamine hydrochloride) and poly(sodium 4-styrenesulfonate) on the PVA surface. The membrane surface modification was characterized by scanning electron microscopy and contact angle measurements. The modified PVA membranes were examined for their dehydration transport properties by the pervaporation of isopropyl alcohol-water (80/20% w/w), which was chosen as a model mixture. Compared with the pristine PVA membrane, the main improvement was a marked increase in permeability. It was found that the surface modification mainly gave rise to a higher permeation flux but with a strong reduction in selectivity. Only the combination of both bulk and surface modifications with PEL could significantly increase the flux with a high water content in the permeate (over 98%). Lastly, it should be noted that this study developed a green procedure to prepare innovative membrane layers for dehydration, making use of only water as a working medium.

© 2018 Elsevier B.V. All rights reserved.

1. Introduction

PVA is a reference hydrophilic polymer known for its economic advantages, high selectivity to water and dehydration properties by pervaporation because of its good film-forming properties [1,2]. These reasons account for why PVA has already been used to prepare several series of commercial membranes [3]. Improving the properties of PVA membranes nevertheless remains a challenging task [4–7]. In this work, two distinct strategies to this end were investigated, i.e., bulk and surface modifications. Indeed, surface and bulk functionalizations can allow for the tailoring of the properties of polymer materials [8–10]. These modification methods have already been applied in the field of membrane technology, since they help in developing membranes with improved parameters, such as anti-fouling properties and/or improved transport characteristics (flux, selectivity, permeance, barrier and mechanical properties) [11–14]. In particular, nonporous membranes are very sensitive to these modification procedures, which can affect the solution-diffusion mechanism behind gas separation and pervaporation.

The most suitable and prospective way to study and evaluate the effects of internal and surface modifications of a pervaporation membrane is to quantify the membrane mass-transfer. According to the solution-diffusion mechanism, there are three steps in membrane mass transfer:

(1) The upstream-side sorption, preferably favoring one of the components of the mixture in the membrane network. In this step, the membrane coating or surface functionalization can play a significant role.
(2) The diffusion of the components through the membrane. In this step, the available free volume linked to the bulk membrane modification can play a major role.

* Corresponding author.
E-mail addresses: m.dmitrienko@spbu.ru (M.E. Dmitrenko), a.penkova@spbu.ru (A.V. Penkova), ai.kuzminova@mail.ru (A.I. Kuzminova), Mahbub.morshed@univ-lorraine.fr (M. Morshed), Gra-viton@mail.ru (M.I. Larionov), halima.alem@univ-lorraine.fr (H. Alem), andrey.zolotarev@spbu.ru (A.A. Zolotarev), s.ermakov@spbu.ru (S.S. Ermakov), denis.roizard@univ-lorraine.fr (D. Roizard).

https://doi.org/10.1016/j.apsusc.2018.04.169
0169-4332/© 2018 Elsevier B.V. All rights reserved.

(3) The desorption of the components from the downstream side at low pressure. Usually, this step is assumed to be very fast; hence, it has a minor effect on the mass transfer.

Pervaporation is a well-known alternative method to classical distillation for the dehydration of alcohols when azeotropes are formed or when close-boiling component mixtures are considered. In such cases, pervaporation can provide substantially higher selectivity and thus a significant reduction in energy consumption [1,2]. The mixture of isopropyl alcohol (i-PrOH)-water is often studied as a model separation system for dehydration by pervaporation, since i-PrOH is an industrial solvent that can be used as a substitute for ethanol. i-PrOH is widely applied in such fields as perfumery, cosmetics, and medicine [15,16]. A 12 wt.% water – 88 wt.% isopropanol mixture forms an azeotropic mixture [17], which makes it difficult to dehydrate the alcohol by traditional separation methods (distillation and rectification). Using traditional separation methods, it is necessary to add harmful organic solvents that form stronger azeotropic mixtures with water, which prohibits the production of a high-purity alcohol. In addition, these separation methods are energetically expensive. Therefore, a promising way of dehydrating isopropanol-water mixtures is pervaporation, which can extract water through a membrane without any additional chemical reagents for dehydration. Various PVA membranes have already been widely used for the dehydration of isopropanol by pervaporation. However, to prevent strong swelling of the PVA in the aqueous solution and improve its stability, various methods for the modification or cross-linking of PVA have been attempted, for example, the creation of mixed-matrix blend membranes based on copolymers PVA/poly(N-isopropylacrylamide) (PNIPAAm) [18], PVA/sodium carboxymethylcellulose (NaCMC)/poly [19,20], and PVA/chitosan [21]; cross-linking with polyacrylic acid (PAA) [22], glutaraldehyde (GA) with concentrated HCl [19,20], oxalic acid (OA), dimethylol urea (DMU) and tetraethyl orthosilicate (TEOS) [23]; and the introduction of a zeolite or hydrophilic aluminosilicate filler into the PVA matrix [19,23]. However, PVA membrane performance still needs improvement for industrial separation processes.

A promising approach to improve the performance of membrane materials is the functionalization of membranes by the deposition of nanoscale layers on the surface of a selective polymer layer of the supported membrane [24,25]. The creation of an ultrathin film on the surface can be realized by such classical methods as the Langmuir–Blodgett technique and the synthesis of self-organizing layers [26]. However, these approaches have significant drawbacks: first, the Langmuir–Blodgett technique requires expensive equipment to create layers, and this method is not applied to all polymers. Second, the self-assembled layer method is not suitable or useful for multi-layer fabrication [26]. To create a multilayer film on the membrane surface, a relatively modern approach is applied, which is layer-by-layer (LbL) deposition [27–30]. This method is simple, inexpensive and suitable for many polymer materials; it is also easily automated. With this approach, various substances can be applied to the membrane material: polyelectrolytes [31], metallic nanoparticles [32], silicon nanoparticles [33] and many others. One of the promising directions to improve the performance of membranes is the deposition of polyelectrolytes onto the polymer film because of the unique properties of the deposited layers. Such a layered deposition leads to a charged film surface with a highly hydrophilic property, and consequently, a stronger affinity for water molecules. A dense electrostatic layer should only cause a moderate swelling of these membranes while in contact with water, which makes polyelectrolytes attractive for the functionalization and coating of pervaporation membranes [31].

The efficiency of pervaporation membranes can be significantly improved by varying the type of polyelectrolyte pairs and the application conditions (the deposited bilayer numbers, ionic strength and pH [34–36]). For example, alcohol/water pervaporation separation by polyelectrolyte multilayer membranes prepared via electrostatic layer-by-layer (LbL) adsorption of cationic (polyvinylamine (PVA)) and anionic (polyvinylsulfonate (PVS), polyvinylsulfate (PVS) and polyacrylate (PAA)) polyelectrolytes has been described [37]. It was shown that the hydrophilic PVA/PVS membrane had optimal transport properties for the separation of a feed with low water content (<20 wt.%), while the less hydrophilic PVA/PAA membrane was suitable for the separation of mixtures with higher water concentrations.

For better adhesion between the dense membrane and polyelectrolytes, an effective method that can be applied is the plasma treatment (e.g., O_2 and Ar) of the pristine membrane surface to create negative charges. Films based on plasma-treated polydimethylsiloxane (PDMS) have been further functionalized by the LbL deposition of more than 5 bilayers of poly (diallyldimethyl ammonium chloride) (PDADMAC) and poly(styrene sulfonate) (PSS) [38]. The optimal plasma treatment conditions for the films were chosen to obtain a full surface coating, resulting in defect-free and hydrophilic PDMS surfaces, as confirmed by SEM images and contact angle measurements.

This work aimed at improving the transport properties of PVA membranes for the dehydration of isopropanol by using two complementary strategies: bulk and surface modifications.

Several types of additives were considered for bulk modification, namely, fullerenol and poly(allylamine hydrochloride). Based on previous studies [39–43], fullerenol was chosen as one of the modifiers and cross-linking agents. During the chemical cross-linking of a membrane based on a PVA-fullerenol composite with maleic acid, the permeability of a membrane increased significantly with a slight decrease in selectivity during the separation of ethanol-water mixtures [42] because of the changes in the degree of crystallinity, surface polarity and free volume [42,41]. Poly(allylamine hydrochloride) has been used to improve the dispersion of carbon nanoparticles as well as to increase the adhesion of nanolayers of polyelectrolytes deposited on a membrane surface by LbL assembly.

The surface modification of mixed-matrix PVA membranes was accomplished by LbL deposition coating with 10 or 20 bilayers of polyelectrolytes: poly(allylamine hydrochloride) as the polycation and poly(sodium 4-styrenesulfonate) as the polyanion. This modification method is very promising for the functionalization of membrane surfaces with thin functionalized layers (10–100 nm) and can lead to significant changes of surface properties, such as an increased hydrophilicity, which can greatly modify the performance and transport characteristics of the membrane.

The transport properties of the membranes were studied with isopropyl alcohol (80 wt.%) – water (20 wt.%) feed mixtures in pervaporation. Scanning electron microscopy and contact angle measurements were used to characterize the membrane surface before and after pervaporation experiments to evaluate the stability of the thin active layers. The transport properties of the developed membrane were compared with a commercially available analogous PVA membrane, i.e., PERVAP™ 1201, for isopropanol dehydration.

2. Materials and methods

2.1. Materials

The membrane material used was PVA with a molecular weight of 141 kDa from ZAO LenReaktiv (certificate of analysis № 553041-3013, date of manufacture 09.2011). The polyhydroxylated

fullerene, $C_{60}(OH)_{12}$ (Fullerene Technologies, Russia), was used for bulk PVA modification. Maleic acid (MA) from Sigma-Aldrich (France) with a purity of >99.0% was used as an additional cross-linking agent for the PVA membranes. Isopropyl alcohol (i-PrOH) obtained from Vekton (Russia) was used without additional treatment. Poly(allylamine hydrochloride) (PAH, M_w ~50,000) and poly (sodium 4-styrenesulfonate) (PSS, M_w ~70,000) purchased from Sigma–Aldrich (France) were used as the cationic and anionic polyelectrolytes, respectively. For all of the experiments, deionized water (MilliQ® water) was used for the polyelectrolyte solutions.

A hydrophilic porous support based on an aromatic polysulfone amide (UPM, pore size 200 Å, from Vladipor, Russia) was chosen to prepare the supported membranes with a thin PVA top layer. The commercial supported membrane "PERVAP™ 1201" (a cross-linked PVA membrane for the dehydration of mixtures containing up to 80 wt.% water) was purchased from Sulzer Chemtec Co. and tested to compare transport parameters.

2.2. Preparation of supported membranes

PVA composites were prepared according to a previously reported procedure [42]: the required quantity of maleic acid (MA) (35% w/w with respect to the weight of the polymer), fullerenol (0 or 5% w/w with respect to the polymer weight) and/or polyelectrolyte (4.7% w/w with respect to the polymer weight) were added in a 2 wt.% PVA water solution using ultrasonic treatment with a frequency of 35 kHz for 40 min. The maximum loading of fullerenol was limited to 5 wt.%, with higher concentrations leading to poor dispersion in membranes and causing defects and inferior mechanical properties.

All studied membranes were produced by casting a 2 wt.% aqueous solution of PVA with 35 wt.% MA or its composite solutions (PVA/polyelectrolyte/MA, PVA/fullerenol/MA, PVA/fullerenol/polyelectrolyte/MA) onto the surface of the commercial ultrafiltration support (UPM-20) and drying at room temperature for 24 h for solvent evaporation. The choice of the UPM-20 support was based on an earlier study [44] and was due to the good mechanical properties (maximum tension 26.52 ± 2.58 MPa, elastic modulus 0.44 ± 0.034 GPa, and maximum deformation 13.34 ± 3.51%) and chemical resistance of UPM-20 since other supports (including polyacrylonitrile (PAN)) could be hydrolyzed at high temperature. The thin-coated PVA layer had a thickness of 1 ± 0.3 μm, as determined by scanning electron microscopy (SEM) measurements, and its cross-linking was achieved by heating the membrane at 110 °C for 120 min [42].

2.3. LbL deposition technique

PAH (10^{-2} mol/L) and PSS (10^{-2} mol/L) were used as the polyelectrolyte solutions. The pH of the PAH solution was adjusted to 4 because this polyelectrolyte is fully ionized at this value.

Multilayer PELs were deposited using a ND Multi Axis Dip Coater ND-3D 11/5 (Nadetech). This dip coater possessed a wide speed immersion range (from 1 to 2000 mm min^{-1}) and ensured good reproducibility of the thin films.

The membrane was clamped and immersed in each PEL solution for 10 min. The polycation solution of PAH was deposited first and then the membrane was removed and rinsed thoroughly with water for 1 s/15 times, 5 s/3 times and 15 s/1 time, successively. After the membrane was immersed in the PSS solution for 10 min, the same water rinsing process of the membrane was repeated. The successive rinsing steps after the PEL deposition ensured the removal of excess polyelectrolyte and prevented cross-contamination of PEL solutions. In this way, one bilayer of polyelectrolyte on the surface of the membrane (or one cycle of self-assembly membrane) was completed. Similarly, additional bilayers were deposited until the required number of bilayers was reached. Because the polycation (PAH) was previously introduced into the polymer matrix, the polyanion (PSS) had been first deposited on the surface. The deposition consisted of 10 to 20 bilayers of polyelectrolytes (PSS/PAH) on the surface of the membrane.

2.4. Plasma treatment

Plasma surface modification was conducted using a microwave post-discharge reactor consisting of a cylindrical glass chamber (3 cm in diameter) pumped through a primary pump. The residual vacuum was 10^{-2} mbar. A 2.45 GHz microwave generator was used to generate the plasma. The plasma atmosphere consisted of an Ar and O_2 gas mixture with a flow rate of 400 sccm and 40 sccm, respectively. Plasma gases were fed into the system via gas flow meters. The PVA sample was placed downstream from the plasma a 30 cm from the plasma outlet (Fig. 1). After the plasma treatment, the system was vented to atmospheric pressure, and then the sample was removed from the reactor. For the present study, the plasma power was 80 W, and the processing time was varied in a range from 30 s to 5 min. The optimum processing time was 2 min.

As shown in Fig. 1, the plasma treatment was carried out using an Ar-O_2 (10:1) plasma created in a 5 mm (id) quartz tube with a 2.45 GHz microwave generator. This microwave power was optimized for effective surface membrane modification at 80 W [38]. All modifications were conducted at 4 mbar. The post-discharge entered a 28 mm (id) Pyrex tube 30 cm downstream from the plasma gap.

2.5. IR spectroscopy

The spectra were recorded at 25 °C with a resolution of 1 cm^{-1} on an IR-Fourier spectrometer (BRUKER-TENSOR 27) from 400–4000 cm^{-1}.

2.6. Pervaporation experiment

A laboratory cell was used under steady-state conditions for the investigation of membrane transport properties at room temperature (20 °C).

The pervaporation setup is presented in Fig. 2. The feed entered the cell (1). After separation by the membrane (2), the permeate (4) was condensed in a trap (3) cooled with liquid nitrogen (5). A downstream pressure of $<10^{-1}$ kPa was achieved by a vacuum pump (7) and controlled by a pressure controller (6). The composition of permeate and feed was analyzed by gas chromatography using a SHIMADZU GC-2010 chromatograph.

The membrane permeation flux, J (kg/(m^2 h)), was calculated as the amount of liquid vaporized through a unit of the membrane area per hour and was calculated as (Eq. (1)) [45]:

$$J = \frac{W}{A \times t} \quad (1)$$

where W (kg) is the mass of the liquid that penetrated the membrane, A (m^2) is the membrane area, and t (h) is the time of the measurement.

Each measurement was carried out at least three times to ensure good accuracy of the transport parameters, i.e., ±0.5% for selectivity and ±2% for flux.

2.7. Scanning electron microscopy

SEM micrographs of the membrane cross-sections were obtained using a Zeiss Merlin scanning electron microscope. The supported membranes were submerged in liquid nitrogen and fractured perpendicular to the surface. The prepared samples were observed using SEM at 1 kV.

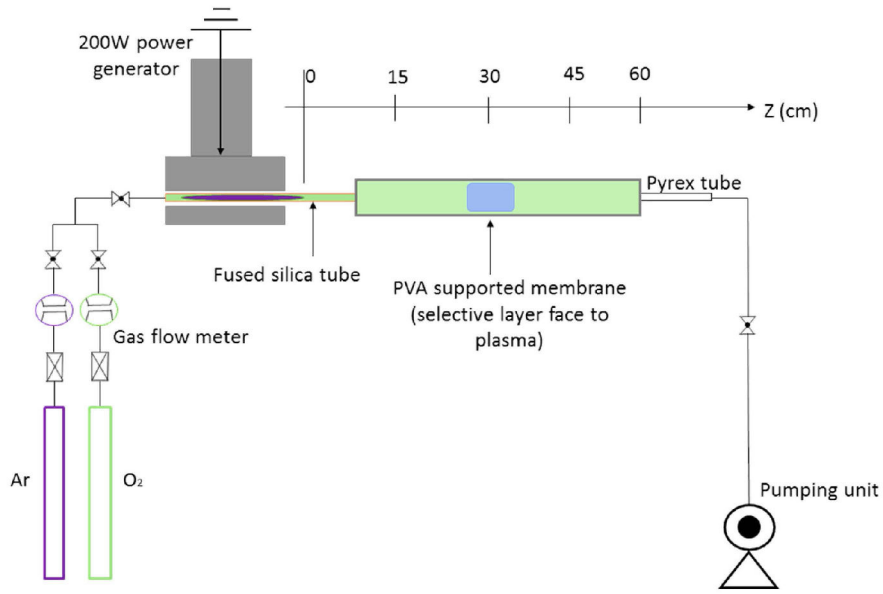

Fig. 1. Schematic representation of the plasma afterglow reactor.

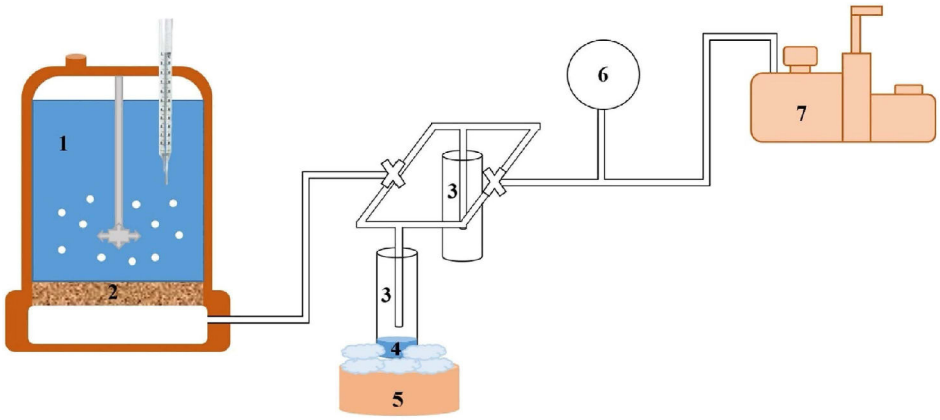

Fig. 2. Scheme of the pervaporation set-up: 1-cell with the feed, 2-membrane, 3-cold trap, 4-permeate, 5-trap with liquid nitrogen, 6-pressure controller, and 7-vacuum pump.

2.8. Contact angle determination

The contact angle measurements of the thin selective layer of the supported membranes were carried out as described in [46] to study the change in the surface properties (hydrophilicity) during modification.

2.9. Total organic carbon (TOC) analysis

The TOC measurements were carried out by a TOC analyzer (Shimadzu TOC-VCSH). The sensitivity of the apparatus was in the 10^{-2} ppm range. The membranes were placed into deionized water to carry out a drip washing test (up to 24 h). Samples of the water were analyzed to measure the carbon concentration (mg/L). The concentration of carbon in water was measured by the combustion of the sample in the combustion gas, followed by carbon dioxide analysis in the IR chamber. Several injections of the sample were made to obtain an average value and to calculate the standard deviation (SD) and the variation coefficient (CV). If the SD was higher than 0.1 or the CV was higher than 2%, then the measurement was repeated.

3. Results and discussion

3.1. Transport properties after membrane modification

The application of bulk and/or surface modifications was expected to significantly improve the membrane separation properties. One of the ways to change the polymer free volume (bulk), and at the same time, to functionalize the selective top surface is

through the creation of a mixed–matrix membrane. In previous studies, we found that the addition of fullerenol to PVA has led to an increase in surface hydrophilicity (shown by contact angle measurements), a decrease in the free volume (shown by pervaporation results) and a change in crystallinity (shown by X-ray) [39,42,41,44].

For this study, the chosen reference membranes were chemically cross-linked supported membranes based on PVA and a PVA-fullerenol (5%) composite. The supported membrane containing fullerenol was found to exhibit the best transport properties for the dehydration process, as shown in previous investigations [39,42,41,44]. For these chemically cross-linked supported membranes, two new modification approaches were developed: surface modification, using plasma treatment and layer-by-layer (LbL) deposition of polyelectrolytes, and bulk modification, which introduces nanoparticles of PAH into the polymer matrix.

3.1.1. Plasma modification

One of the effective and promising methods to increase the adhesion of a polyelectrolyte nanolayer to a membrane surface is plasma modification. This process can be considered as a method of surface pretreatment; in industry, it is widely used for treating surfaces of various materials before printing, gluing, coating or adhesion. Plasma treatment may also remove any contaminants from the surface, and in some cases, change the chemical structure of the surface. Thus, this surface modification by plasma treatment can significantly affect the characteristics of the thin selective PVA layer of the membranes. For this paper, the membrane plasma treatment was performed according to a procedure published previously using plasma obtained from oxygen (O_2) and argon (Ar) gases. The modified membranes were then investigated for the separation of i-PrOH/water mixture (80–20 wt.%) by pervaporation at 20 °C to evaluate the influence of the plasma treatment. The structure of the selective thin PVA layer of the supported membranes treated by plasma was investigated before and after pervaporation by IR spectroscopy to study the stability of membrane surface during the dehydration process of i-PrOH. Additionally, the spectrum of the untreated PVA membrane was obtained for comparison with a plasma-treated membrane to study the change in the structure of PVA under plasma treatment.

In Fig. 3, the IR spectra of the PVA membrane (Fig. 3(a)), and a PVA membrane after plasma treatment for 2 min before and after the pervaporation experiment (Fig. 3(b, c)) are presented to study the changes in the structure of the pristine membrane after plasma treatment.

It was found that the spectra in (b) and (c) are nearly identical, which indicates the stability of the PVA membrane structure treated by plasma during pervaporation.

The following features were observed in the IR spectra of the PVA membranes (Fig. 3):

- The wide bands at 3300 and 1660 cm^{-1} refer to the vibrations of trace H_2O.
- The stretching vibrations of the CH_2 bonds correspond to the absorption in the 2800–3000 cm^{-1} region, the deformation vibrations of the —CH_2 groups appear in the region of 718 cm^{-1} and are located in the spectral region 1150–1350 cm^{-1} [47]. The absorption bands with maxima at 1100 and 1300 cm^{-1}, according to [48], correspond to vibrations associated with the C—O—H group.

Substantial changes in the IR spectra were observed after the plasma treatment of PVA: (1) a consecutive decrease is observed in the intensity of the bands (in the row: PVA membrane (Fig. 3 (a)), PVA membrane treated by plasma before pervaporation (Fig. 3(b)) and after pervaporation (Fig. 3(c))) and (2) the position of individual bands (for untreated and plasma-treated membranes) that are attributed to stretching vibrations of —OH and —CH bonds, leading to their almost complete disappearance due to the dehydration and oxidation of the PVA molecule under O_2/Ar plasma treatment.

The transport properties of the untreated and plasma-treated membranes are presented in the Table 1.

As can be seen from Table 1, the plasma treatment applied to the PVA membrane leads to a marked reduction of the pervaporation flux without any improvement in the selectivity compared with the pristine membrane, which could be caused by the oxidation and dehydration of PVA.

Earlier studies have shown that the introduction of fullerenol to the PVA matrix led to an increase in the membrane selectivity property with respect to water because of changes in membrane structure and crystallinity [39,42,41]. Therefore, the modification of the PVA membrane by fullerenol was carried out in the present work, and the modified membrane was subjected to the plasma treatment. The transport properties of the obtained membranes for the separation of the i-PrOH/water mixture (20 wt.% water, 80 wt.% i-PrOH) at 20 °C are also presented in the Table 1. Similar to the membranes based on pure PVA, a decrease in flux was observed: the composite PVA-fullerenol (5%) membrane after plasma treatment exhibited a flux reduced by a factor ~3 with comparable water selectivity. No significant drop in selectivity was observed compared with those of the PVA membranes without fullerenol, which was due to the change in the surface property of the membranes (increased hydrophilicity of the surface because of the increased number OH-groups), as well as a greater cross-linking of PVA chains because of the fullerenol modification [42].

These results are in good agreement with a previous study on other polymers showing that oxygen plasma treatment can lead to the etching of the polymer surface [49], which could lead to a decrease in the flux and selectivity towards water molecules of PVA membranes. Thus, it is confirmed that the plasma treatment of PVA membranes is not an effective modification method to prepare PEL-modified membranes.

3.1.2. LbL deposition

Taking into account the above results, the layer-by-layer (LbL) technique of polyelectrolyte deposition was applied directly without any plasma treatment to further enhance the charge density of the PVA surface and favor the transport of water molecules. The surface of the mixed-matrix PVA membranes presented in this section were coated with 10 or 20 bilayers of polyelectrolytes: poly (allylamine hydrochloride) as the polycation (noted PAH) and poly(sodium 4-styrenesulfonate) as the polyanion (noted PSS). The pervaporation transport properties of these membranes presented in Fig. 4 were obtained with the model mixture i-PrOH (80 wt.%) – water (20 wt.%) at 20 °C.

The results of Fig. 4 (a) show that the surface modification by deposition of 10 PEL bilayers leads to an increase in flux for the two types of membranes compared with those of the pristine PVA and PVA-fullerenol (5%) membranes. However, the water selectivity is significantly reduced for the supported membranes after the LbL deposition (the water contents in the permeate are 65.7 and 85.6 wt.%) (Fig. 4 (b)). The PVA-fullerenol (5%)/LbL-10 membrane has a high water selectivity compared with that of the PVA/LbL-10 membrane because of the introduction of fullerenol into the polymer matrix, as fullerenol is both a modifier and a cross-linking agent. The increase in the flux for the PVA and PVA-fullerenol (5%) membranes containing 10 PEL layers can be ascribed to the formation of small hydrophilic mashes induced by the higher charge density of PEL that can favor the penetration of water molecules versus the larger, less polar i-PrOH molecules [34]. To further modify the transport properties of the composite

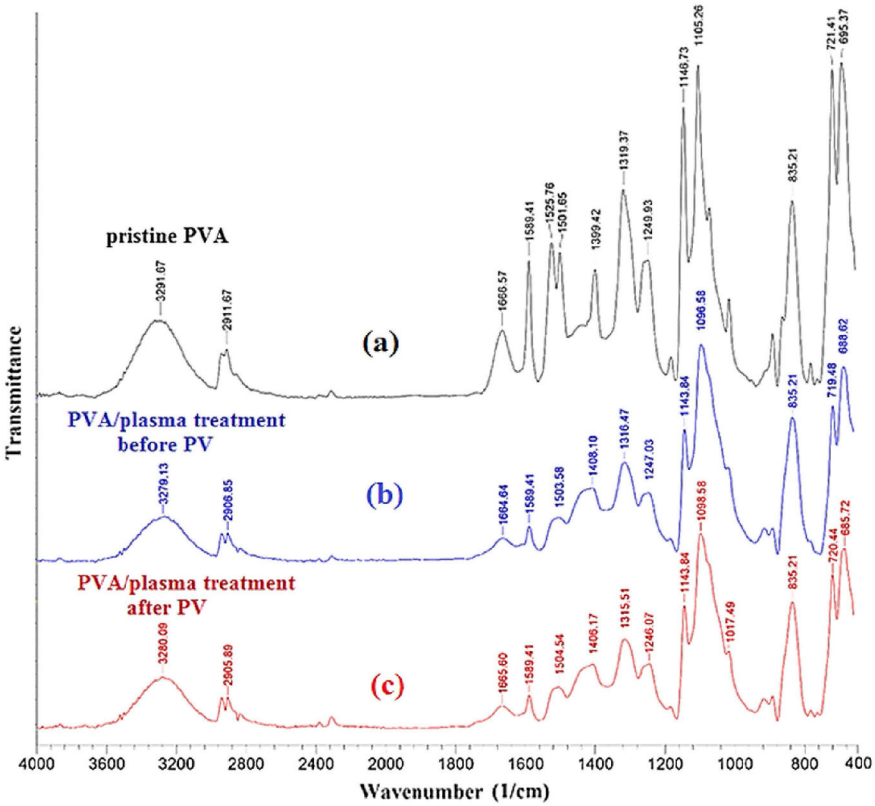

Fig. 3. The IR spectra of the pristine PVA membrane (a), PVA/plasma treatment membrane before pervaporation (b) and the membrane after pervaporation (PV) (c).

Table 1
Pervaporation of the i-PrOH/water mixture (20 wt.% water, 80 wt.% i-PrOH) at 20 °C using pristine and plasma-treated supported membranes.

Supported membrane	Flux, kg/(m^2 h)	Water content in permeate (wt.%)
Pristine PVA	0.102	99.5
PVA/plasma treatment	0.047	95.6
PVA-fullerenol (5%)	0.118	98.9
PVA-fullerenol (5%)/plasma treatment	0.036	98.2

membranes on the UPM support and to investigate the dependence of the i-PrOH/water separation transport characteristics on the bilayer number, the number of polyelectrolyte bilayers was increased up to 20. The data presented in Fig. 4 show that, conversely to the first case, the increase in the number of polyelectrolyte bilayers up to 20 led to a decrease in the PVA-fullerenol (5%)/LbL-20 membrane flux compared with those of the pristine membranes (Fig. 4(A)). Meanwhile, the separation factor for water was not improved over the case of the 10-bilayer sample (a water concentration in the permeate of approximately 71.4 wt.%). Thus, the 10 PEL bilayer coating on the membrane surface obtained by LbL deposition was chosen as the preferred surface modification for testing the strategy of bulk modification by PELs to improve the membrane dehydration properties. The decrease in the transport properties of the membranes with 20 PEL bilayers could be explained by the following factors. It is known that the membrane flux is inversely proportional to the PEL charge density for polar solutes [34]. The deposition of 20 PEL bilayers on the PVA membrane surface led to an increase in the thickness of the PEL layer exceeding 60 nm. This led to an increase in the PEL cross-linking density and to an inhibited diffusion path for the penetrants in the PEL layer to the selective layer based on PVA, ultimately leading to a decrease in the membrane flux. On the other hand, the formation of the polar mashes in the PEL layer facilitated water sorption by the membrane as well as an increase in surface hydrophilicity, leading to increased water content in the PEL layers that simultaneously caused i-PrOH penetration and a decrease in selectivity.

3.1.3. Bulk modification of the PVA network with a polyelectrolyte

The mass transfer through a membrane is closely related to the available free volume in the active layer. Therefore, a way to increase this free volume without overly reducing selectivity is to introduce modifications of the polymer network at the nanoscale, for instance, by introducing nanoparticles or by adding another type of polymer chain to the pristine polymer matrix. The expected effect was a decrease in the strength of the hydrogen bonding of the PVA network while keeping the polar character of the matrix. Therefore, poly(allylamine hydrochloride) (PAH) was chosen for further investigation. In addition, the introduction of PAH should contribute to the stabilization of the PEL bilayer through interactions with the PSS component of the PEL bilayers.

Mixed-matrix membranes based on PVA modified by fullerenol (5 wt.%) and/or PAH (4.7 wt.%) were prepared for this section. The

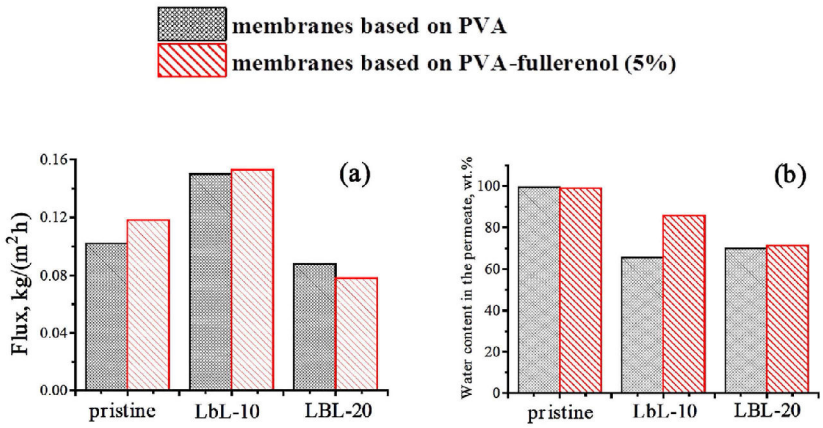

Fig. 4. Dependence of flux (A) and water content in the permeate (B) on the modification method (pristine, LbL deposition of 10 bilayers (LbL-10) or 20 bilayers (LbL-20)) of the supported membrane based on PVA or composite PVA-fullerenol (5%) during the pervaporation of a i-PrOH/water mixture (20 wt.% water, 80 wt.% i-PrOH) at 20 °C.

transport characteristics of the obtained supported membranes based on PVA and its composites were determined by pervaporation of the binary mixture isopropanol (80 wt.%) – water (20 wt.%) at 20 °C. The results are presented in Table 2.

The data presented in the table show that the introduction of PAH into the bulk PVA polymer matrix led to a marked increase in flux (~2 times) compared with that of the pristine PVA membrane; however, at the same time, a significant decrease in the water content in the permeate was observed. This fact is attributed to polar PAH chains that disrupted the H-bonding organization of PVA. Compared with the introduction of fullerenol into PVA (Table 1, Section 3.1.1), the PAH effect on mass transfer appeared to be stronger. The combined dispersion of PAH and fullerenol into the PVA matrix also resulted in an increase in flux compared with the unmodified membrane, as well as an increase in water selectivity (99.1 wt.% in permeate), because of the cross-linking of the PVA matrix by the fullerenol. A surface modification by the LbL deposition was applied to the supported membranes to further improve the transport properties. It was shown that the membranes based on the PVA-PAH and PVA-fullerenol-PAH composites after the LbL modification have higher flux values than those of the PVA/LbL-10 and PVA-fullerenol (5%)/LbL-10 membranes (Fig. 4) with significantly improved water selectivity values, especially for the composite membranes with fullerenol and PAH. Only for the dispersion with two modifiers (fullerenol and PAH) in the polymer matrix and after the LbL deposition of 10 bilayers a high water content in the permeate (98.4 wt.%) and a high flux (0.286 kg/(m^2 h)) could be obtained.

Thus, on the basis of the performed experiments, it was established that the mixed-matrix membrane based on the composite PVA-fullerenol (5%)-PAH (4.7%)-MA (35%) supported on UPM and modified with 10 polyelectrolyte bilayers by LbL deposition (membrane PVA-fullerenol (5%)-PAH/LbL-10) has the best transport properties for the dehydration of i-PrOH (20 wt.% water, 80 wt.% i-PrOH) by pervaporation.

Table 2
Pervaporation of the i-PrOH/water mixture (80 wt.% i-PrOH / 20 wt.% water) at 20 °C using supported membranes after bulk and/or surface modifications.

Supported membrane	Flux, kg/(m^2 h)	Water content in permeate (wt.%)
Pristine PVA	0.102	99.5
PVA-PAH	0.224	92.8
PVA- fullerenol (5%)-PAH	0.213	99.1
PVA-PAH/LbL-10	0.261	68.4
PVA-fullerenol (5%)-PAH/LbL-10	0.286	98.4

3.2. Study of the stability of the supported membrane with the selective PVA-fullerenol (5%)-PAH/LbL-10 layer

To verify the stability of the polyelectrolyte nanosized multilayer in the PVA-fullerenol(5%)-PAH/LbL-10 membrane on the UPM support, contact angles were measured by the static sessile drop method, and the membrane morphology was studied by scanning electron microscopy (SEM).

The optical and SEM images at different magnifications of the PVA-fullerenol (5%)-PAH/LbL-10 membrane are presented in Fig. 5.

The presented images (Fig. 5) demonstrate the absence of defects and continuity of the surface and cross-section of the thin selective layer and PEL layers. It can be seen that PVA-fullerenol (5%)-PAH/LbL-10 membrane has a flat homogeneous membrane surface without any defects or distortions. The pictures of the membrane cross-section demonstrate the continuity and uniformity of the distribution of the thin selective PVA layer and the upper PEL layer.

Additional cross-sectional SEM micrographs were taken for the PVA-fullerenol (5%)-PAH membrane (Fig. 6(a)), as well as the PVA-fullerenol (5%)-PAH/LbL-10 membrane before (Fig. 6(b)) and after pervaporation (Fig. 6(c)), to demonstrate the existence and the stability of the PEL bilayers.

In the cross-sectional SEM micrograph of the supported membrane PVA-fullerenol(5%)-PAH membrane (Fig. 6 (a)), only two distinguished areas were noticed: (1) the region of the porous UPM support and (2) the selective thin non-porous PVA layer; while the PVA-fullerenol(5%)-PAH/LbL-10 membrane modified by 10 PEL bilayers (Fig. 6 (b, c)) contained an additional area (3) that corresponds to the polyelectrolyte layer. A similar white nanosized PEL layer has also been demonstrated by Klitzing et al. [35] (cf. Fig. 12, p. 194). The size of the polyelectrolyte multilayer was determined to be ~60 nm by SEM. The presented images for the PVA-fullerenol(5%)-PAH/LbL-10 membrane before (b) and after (c) pervaporation are identical, which shows that there were no changes to the selective PVA layer and the deposited polyelectrolyte layers before and after pervaporation. As expected, the layer-by-layer assembly is stable upon contact with water-organic solutions.

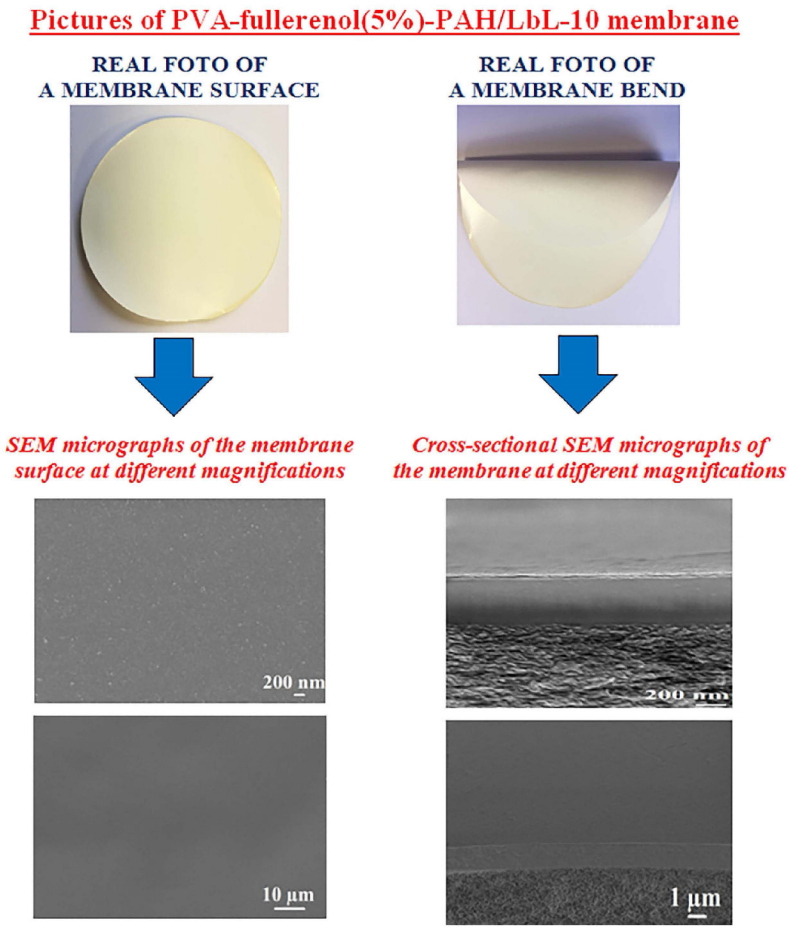

Fig. 5. Optical and SEM images of the PVA-fullerenol (5%)-PAH/LbL-10 membrane.

Another confirmation of the stability of the thin PEL layer was obtained from the unchanged surface properties of the membrane: the contact angle measurements demonstrated the same values for water before and after the pervaporation experiments, equal to (72 ± 3)° and (72 ± 1)°, respectively. These data show that the contact angle of the membrane is not altered by the pervaporation experiment, which proves that the polyelectrolyte layers are anchored onto the surface of the PVA membrane.

Finally, the water stability of the PEL layer created on the PVA was tested in pure water to understand if the water concentration in the feed could be an issue or not. For this purpose, tentative extractions/dissolutions of the PEL layer by immersion in pure water (neutral pH, 24 h in deionized water) were carried out, followed by TOC analysis of the used water. It must be emphasized that these experiments, while simple in theory, are, from a practical point of view, difficult to carry out because of the tedious control of any carbon pollution linked to the experiments and to the pristine PVA-supported membrane as well. However, regardless of the water sample, after immersion, no significant carbon peak could be detected after 10 days. The successive measurements gave an extremely low value of carbon, comparable with those of the blank water samples. The TOC analysis demonstrated that the carbon content in water does not exceed the measurement error (0.013 mg/L), which indicated the stability of the membrane in water. The SEM micrograph of the membrane cross-section, obtained after the immersion experiment and the TOC measurement, is shown in Fig. 7.

The SEM image shows the presence of three layers, i.e., the UPM, the PVA-fullerenol(5%)-PAH and the LbL-10 layer, after aging in water, as described above (Fig. 6).

Additionally, these results allow one to make the conclusion that the stability of the PAH/PSS layers strongly depends on the kind of substrate used for their deposition and on the adjusted pH. Indeed, it has been reported that this pair of polyelectrolytes deposited on a porous substrate based on polyethylene terephthalate fleece with polyacrylonitrile decomposed when the water content in the feed mixture was higher than 20 wt.% [34] at pH = 2.1. However, the high stability of the PAH/PSS layers was sustained when a nonporous polyvinyl alcohol-based system was used as a support layer at pH = 4.

3.3. Comparison of the transport properties of the supported membrane with the selective PVA-fullerenol (5%)-PAH/LbL-10 layer with those of the commercially available analog, Pervap™ 1201

The transport properties of the best supported PVA-fullerenol (5%)-PAH/LbL-10 membrane were compared with the commer-

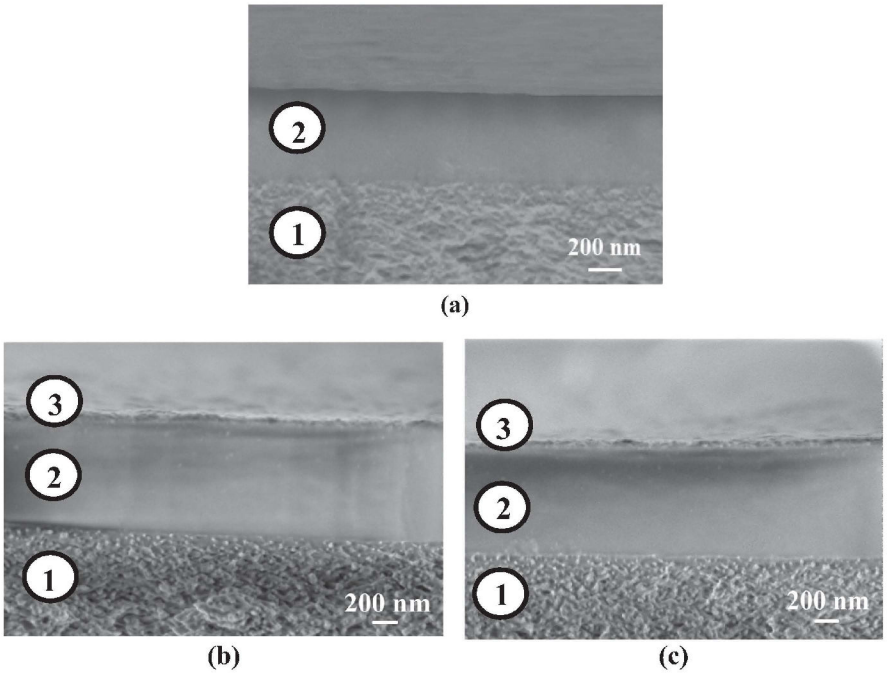

Fig. 6. Cross-sectional SEM micrographs of the supported membranes: PVA-fullerenol(5%)-PAH (a), and PVA-fullerenol(5%)-PAH/LbL-10 before (b) and after (c) pervaporation.

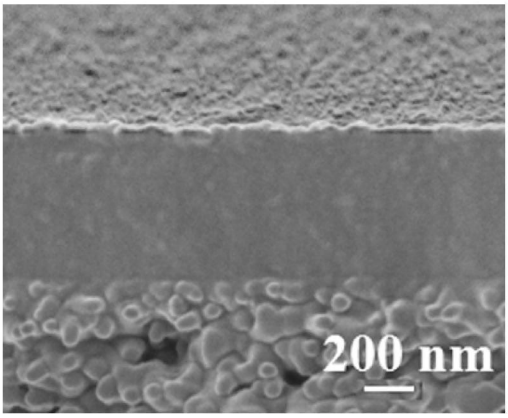

Fig. 7. SEM micrograph of the cross-section of the supported PVA-fullerenol(5%)-PAH/LbL-10 membrane after immersion in water (TOC experiment).

cially available analog – the supported membrane "PERVAP™ 1201" from the company Sulzer Chemtech. The manufacturer reports that this type of membrane allows the dehydration of organic mixtures with a water content up to 80 wt.%. The commercial membrane PERVAP™ 1201 and PERVAP™ 1201/LbL-10 (modified by PEL deposition) were tested for pervaporation of the same i-PrOH/water mixture (80/20 w/w) at 20 °C. A comparison of the transport properties of the obtained membranes during the separation of the isopropanol-water mixture is presented in Table 3.

The PERVAP™ 1201 exhibits a very high selectivity but also a very low flux. The application of the PEL coating on this commercially available membrane did not lead to significant changes in the transport properties of the membrane compared with those of the original membrane (a slight difference in the fluxes with the same water selectivity). This should be linked to the high cross-linking density of the pristine polymer network. These data reveal that the flux of the developed PVA-fullerenol (5%)-PAH/LbL-10 supported membrane exceeds the flux of the PERVAP™ 1201 membrane by 8.5 times and the flux of pristine composite PVA- fullerenol (5%) membrane by 2.4 times while allowing a high selectivity level (a water content in the permeate of 98.4 wt.%).

Accordingly, it can be concluded that the developed PVA-fullerenol (5%)-PAH/LbL-10 supported membrane possesses improved transport characteristics compared with those of PVA and PERVAP™ 1201. The modification strategies are therefore quite promising and give an interesting perspective for developing new green pervaporation membranes.

Table 3
Comparison of the transport properties of the obtained PVA-fullerenol (5%) and PVA-fullerenol(5%)-PAH/LbL-10, PERVAP™ 1201 and PERVAP™ 1201/LbL-10 membranes for the pervaporation of the i-PrOH (80 wt.%) - water (20 wt.%) mixture at 20 °C.

Supported membrane	Flux, kg/(m^2 h)	Water content in permeate (wt.%)
PVA- fullerenol (5%)	0.118	98.9
PVA-fullerenol (5%)-PAH/LbL-10	0.286	98.4
PERVAP™ 1201	0.034	99.9
PERVAP™ 1201/LbL-10	0.039	99.9

4. Conclusions

In this study, it was shown that the simultaneous application of bulk and surface modifications is a promising strategy to create high-performance mixed-matrix membranes for dehydration by pervaporation.

The application of a plasma surface pretreatment to PVA, for improving the adhesion of PEL layers to the membrane surface, should be avoided, because it leads to a significant decrease in the membrane flux. However, even without plasma pretreatment, a thin PEL coating stable to pervaporation conditions could be obtained. This was shown by consistent properties, SEM views and comparable contact angle measurements after PV experiments.

It was found that the preferred number of LbL deposited PEL (PAH/PSS) layers on the surface of composite PVA-supported membranes was 10 bilayers since an increase to 20 PEL bilayers led to a significant decrease in selectivity and flux. The decrease in transport properties was explained by an increase in the surface polarity leading to increased water content in the PEL layers.

It was shown that the best transport characteristics for pervaporation dehydration were achieved through the combination of two modification methods: the use of bulk modification (the introduction of two modifiers, fullerenol and PAH, into the PVA matrix) and surface modification (LbL deposition of 10 PEL bilayers) techniques. The highly effective mixed-matrix supported membrane based on composite PVA-fullerenol (5%)-PAH (4.7%)-MA (35%) with a modified surface coating of 10 PEL bilayers was developed. The obtained membrane had a flux 8.5 times higher than that of the commercially available analog PERVAP™ 1201 (Sulzer) for the pervaporation separation of the i-PrOH-water mixture.

Acknowledgment

This work was supported by the Russian Science Foundation [Grant No. 17-73-20060]. The experimental work of this study was facilitated by CNRS resources and equipment from the Resource Centers of GEOMODEL, Center for X-ray Diffraction Methods, Centre for Innovative Technologies of Composite Nanomaterials, the Chemical Analysis and Materials Research Centre, and the Interdisciplinary Resource Center for Nanotechnology at St. Petersburg State University.

References:

[1] B. Bolto, M. Hoang, Z. Xie, A review of membrane selection for the dehydration of aqueous ethanol by pervaporation, Chem. Eng. Process. Process Intensif. 50 (2011) 227–235, https://doi.org/10.1016/j.cep.2011.01.003.
[2] X. Zhao, L. Lv, W. Zhang, S. Zhang, Q. Zhang, Polymer-supported nanocomposites for environmental application: a review, Chem. Eng. J. 170 (2011) 381–394, https://doi.org/10.1016/j.cej.2011.02.071.
[3] S. Chemtech, Membrane Technol. (2006), https://doi.org/10.1002/3527608788.
[4] W. Yave, The improved pervaporation PERVAP membranes, Filtr. Sep. 54 (2017) 14–15, https://doi.org/10.1016/S0015-1882(17)30126-X.
[5] A. Khazaei, V. Mohebbi, R.M. Behbahani, A. Ramazani, S.A., Pervaporation of toluene and iso-octane through poly(vinyl alcohol)/graphene oxide nanoplate mixed matrix membranes: Comparison of crosslinked and noncrosslinked membranes, J. Appl. Polym. Sci. 135 (2018) 45853, https://doi.org/10.1002/app.45853.
[6] S.G. Chaudhri, J.C. Chaudhari, P.S. Singh, Fabrication of efficient pervaporation desalination membrane by reinforcement of poly(vinyl alcohol)-silica film on porous polysulfone hollow fiber, J. Appl. Polym. Sci. 135 (2018) 45718, https://doi.org/10.1002/app.45718.
[7] A. Malekpour, B. Mostajeran, G.A. Koohmareh, Pervaporation dehydration of binary and ternary mixtures of acetone, isopropanol and water using polyvinyl alcohol/zeolite membranes, Chem. Eng. Process. Process Intensif. 118 (2017) 47–53, https://doi.org/10.1016/j.cep.2017.04.019.
[8] Y. Zhao, K.W.K. Yeung, P.K. Chu, Functionalization of biomedical materials using plasma and related technologies, Appl. Surf. Sci. 310 (2014) 11–18, https://doi.org/10.1016/j.apsusc.2014.02.168.
[9] F. Asvadi, A. Raisi, A. Aroujalian, Preparation of multi-layer pervaporation membrane by electro-spraying of nano zeolite X, Microporous Mesoporous Mater. 251 (2017) 135–145, https://doi.org/10.1016/j.micromeso.2017.05.060.
[10] D. Hetemi, J. Pinson, Surface functionalisation of polymers, Chem. Soc. Rev. 46 (2017) 5701–5713, https://doi.org/10.1039/C7CS00150A.
[11] Q. Nan, P. Li, B. Cao, Applied Surface Science Fabrication of positively charged nanofiltration membrane via the layer-by-layer assembly of graphene oxide and polyethylenimine for desalination, Appl. Surf. Sci. 387 (2016) 521–528, https://doi.org/10.1016/j.apsusc.2016.06.150.
[12] W. Zhang, Z. Yu, Q. Qian, Z. Zhang, X. Wang, Improving the pervaporation performance of the glutaraldehyde crosslinked chitosan membrane by simultaneously changing its surface and bulk structure, J. Membr. Sci. 348 (2010) 213–223, https://doi.org/10.1016/j.memsci.2009.11.003.
[13] Q.W. Yeang, S.H.S. Zein, A.B. Sulong, S.H. Tan, Comparison of the pervaporation performance of various types of carbon nanotube-based nanocomposites in the dehydration of acetone, Sep. Purif. Technol. 107 (2013) 252–263, https://doi.org/10.1016/j.seppur.2013.01.031.
[14] D. Hua, T.-S. Chung, Polyelectrolyte functionalized lamellar graphene oxide membranes on polypropylene support for organic solvent nanofiltration, Carbon N. Y. 122 (2017) 604–613, https://doi.org/10.1016/j.carbon.2017.07.011.
[15] E. Fu, K. McCue, D. Boesenberg, Chemical Disinfection of Hard Surfaces – Household, Industrial and Institutional Settings, Handb. Cleaning/Decontamination Surfaces, Elsevier, 2007, pp. 573–592, https://doi.org/10.1016/B978-044451664-0/50017-6.
[16] R.P. Mlcak, S.D. Hegde, D.N. Herndon, Respiratory Care, Total Burn Care e2, Elsevier, 2012, pp. 239–248, https://doi.org/10.1016/B978-1-4377-2786-9.00020-5.
[17] S.K. Ogorodnikov, T.M. Lesteva, V.B. Kogan, Azeotrope mixtures, Chemistry, St. Petersburg, 1971.
[18] F. Kurşun, N. Işıklan, Development of thermo-responsive poly(vinyl alcohol)-g-poly(N-isopropylacrylamide) copolymeric membranes for separation of isopropyl alcohol/water mixtures via pervaporation, J. Ind. Eng. Chem. 41 (2016) 91–104, https://doi.org/10.1016/j.jiec.2016.07.011.
[19] C.V. Prasad, B. Yeriswamy, H. Sudhakar, P. Sudhakara, M.C.S. Subha, J.I. Song, et al., Preparation and characterization of nanoparticle-filled, mixed-matrix membranes for the pervaporation dehydration of isopropyl alcohol, J. Appl. Polym. Sci. 125 (2012) 3351–3360, https://doi.org/10.1002/app.35658.
[20] C.V. Prasad, H. Sudhakar, B. Yerri Swamy, G.V. Reddy, C.L.N. Reddy, C. Suryanarayana, et al., Miscibility studies of sodium carboxymethylcellulose/poly(vinyl alcohol) blend membranes for pervaporation dehydration of isopropyl alcohol, J. Appl. Polym. Sci. 120 (2011) 2271–2281, https://doi.org/10.1002/app.33418.
[21] N. Ghobadi, T. Mohammadi, N. Kasiri, M. Kazemimoghadam, Modified poly (vinyl alcohol)/chitosan blended membranes for isopropanol dehydration via pervaporation: synthesis optimization and modeling by response surface methodology, J. Appl. Polym. Sci. 134 (2017), https://doi.org/10.1002/app.44587.
[22] N.D. Hilmioglu, S. Tulbentci, Pervaporative separation of isopropyl alcohol/water mixtures: effects of the operation conditions, Desalin. Water Treat. 48 (2012) 191–198, https://doi.org/10.1080/19443994.2012.698812.
[23] P. Das, S.K. Ray, S.B. Kuila, H.S. Samanta, N.R. Singha, Systematic choice of crosslinker and filler for pervaporation membrane: a case study with dehydration of isopropyl alcohol–water mixtures by polyvinyl alcohol membranes, Sep. Purif. Technol. 81 (2011) 159–173, https://doi.org/10.1016/j.seppur.2011.07.020.
[24] J.-Y. Lee, Q. She, F. Huo, C.Y. Tang, Metal–organic framework-based porous matrix membranes for improving mass transfer in forward osmosis membranes, J. Membr. Sci. 492 (2015) 392–399, https://doi.org/10.1016/j.memsci.2015.06.003.
[25] J. Zhao, Y. Zhu, F. Pan, G. He, C. Fang, K. Cao, et al., Fabricating graphene oxide-based ultrathin hybrid membrane for pervaporation dehydration via layer-by-layer self-assembly driven by multiple interactions, J. Membr. Sci. 487 (2015) 162–172, https://doi.org/10.1016/j.memsci.2015.03.073.
[26] K. Ariga, J.P. Hill, Q. Ji, Layer-by-layer assembly as a versatile bottom-up nanofabrication technique for exploratory research and realistic application, PCCP 9 (2007), https://doi.org/10.1039/b700410a.
[27] J. Yu, S. Cheng, Q. Che, Preparation and characterization of layer-by-layer self-assembly membrane based on sulfonated polyetheretherketone and polyurethane for high-temperature proton exchange membrane, J. Polym. Sci., Part A: Polym. Chem. 55 (2017) 3446–3454, https://doi.org/10.1002/pola.28725.
[28] C.J. Lefaux, B.-S. Kim, N. Venkat, P.T. Mather, Molecular composite coatings on nafion using layer-by-layer self-assembly, ACS Appl. Mater. Interfaces. 7 (2015) 10365–10373, https://doi.org/10.1021/acsami.5b01371.
[29] S. Zuin, P. Scanferla, A. Brunelli, A. Marcomini, J.E. Wong, W. Wennekes, et al., Layer-by-layer deposition of titanium dioxide nanoparticles on polymeric membranes: a life cycle assessment study, Ind. Eng. Chem. Res. 52 (2013) 13979–13990, https://doi.org/10.1021/ie302979d.
[30] E.S. Dragan, M. Mihai, J. Schauer, L. Ghimici, PAN composite membrane with different solvent affinities controlled by surface modification methods, J. Polym. Sci., Part A: Polym. Chem. 43 (2005) 4161–4171, https://doi.org/10.1002/pola.20869.
[31] N. Joseph, P. Ahmadiannamini, R. Hoogenboom, I.F.J. Vankelecom, Layer-by-layer preparation of polyelectrolyte multilayer membranes for separation, Polym. Chem. 5 (2014) 1817–1831, https://doi.org/10.1039/C3PY01262J.

[32] H. Xu, H. Shi, Y. Yang, X. Liu, Synthesis and characterization of nanocomposites Fe_3O_4–SiO_2–chitosan based on lbl technology, Glass. Phys. Chem. 42 (2016) 312–321, https://doi.org/10.1134/S1087659616030056.
[33] H. Gao, O.A. Goriacheva, N.V. Tarakina, G.B. Sukhorukov, Intracellularly biodegradable polyelectrolyte/silica composite microcapsules as carriers for small molecules, ACS Appl. Mater. Interfaces. 8 (2016) 9651–9661, https://doi.org/10.1021/acsami.6b01921.
[34] B. Tieke, F. van Ackern, L. Krasemann, A. Toutianoush, Ultrathin self-assembled polyelectrolyte multilayer membranes, Eur. Phys. J. E. 5 (2001) 29–39, https://doi.org/10.1007/s101890170084.
[35] R. Klitzing, B. Tieke, Polyelectrolyte Membranes, in: Springer Berlin Heidelberg, 2004, pp. 177–210. doi: 10.1007/b11270.
[36] L. Krasemann, B. Tieke, Ultrathin self-assembled polyelectrolyte membranes for pervaporation, J. Membr. Sci. 150 (1998) 23–30, https://doi.org/10.1016/S0376-7388(98)00212-9.
[37] B. Toutianoush, A., Tieke, Pervaporation separation of alcohol/water mixtures using self-assembled polyelectrolyte multilayer membranes of high charge density, Mater. Sci. Eng., C. 22 (2002) 459–463, https://doi.org/10.1016/S0928-4931(02)00189-3.
[38] J. Bassil, H. Alem, G. Henrion, D. Roizard, Tailored adhesion behavior of polyelectrolyte thin films deposited on plasma-treated poly(dimethylsiloxane) for functionalized membranes, Appl. Surf. Sci. 369 (2016) 482–491, https://doi.org/10.1016/j.apsusc.2016.01.146.
[39] A.V. Penkova, S.F.A. Acquah, M.E. Dmitrenko, M.P. Sokolova, M.E. Mikhailova, E. S. Polyakov, et al., Improvement of pervaporation PVA membranes by the controlled incorporation of fullerenol nanoparticles, Mater. Des. 96 (2016) 416–423, https://doi.org/10.1016/j.matdes.2016.02.046.
[40] M.E. Dmitrenko, A.V. Penkova, A.B. Missyul, A.I. Kuzminova, D.A. Markelov, S.S. Ermakov, et al., Development and investigation of mixed-matrix PVA-fullerenol membranes for acetic acid dehydration by pervaporation, Sep. Purif. Technol. 187 (2017) 285–293, https://doi.org/10.1016/j.seppur.2017.06.061.
[41] A.V. Penkova, S.F.A. Acquah, M.P. Sokolova, M.E. Dmitrenko, A.M. Toikka, Polyvinyl alcohol membranes modified by low-hydroxylated fullerenol C60 (OH)12, J. Membr. Sci. 491 (2015) 22–27, https://doi.org/10.1016/j.memsci.2015.05.011.
[42] A.V. Penkova, S.F.A. Acquah, M.E. Dmitrenko, B. Chen, K.N. Semenov, H.W. Kroto, Transport properties of cross-linked fullerenol–PVA membranes, Carbon N. Y. 76 (2014) 446–450, https://doi.org/10.1016/j.carbon.2014.04.053.
[43] A.V. Penkova, S.F. Acquah, L.B. Piotrovskiy, D.A. Markelov, A.S. Semisalova, H. W. Kroto, Fullerene derivatives as nano-additives in polymer composites, Russ. Chem. Rev. 86 (2017) 530–566, https://doi.org/10.1070/RCR4712.
[44] A.V. Penkova, M.E. Dmitrenko, S.S. Ermakov, A.M. Toikka, D. Roizard, Novel green PVA-fullerenol mixed matrix supported membranes for separating water-THF mixtures by pervaporation, Environ. Sci. Pollut. Res. (2017) 1–9, https://doi.org/10.1007/s11356-017-9063-9.
[45] R.W. Baker, Membrane Technology and Applications, Wiley, 2004.
[46] E.V. Gribanova, M.I. Larionov, Application of contact angle dependence on pH for estimation of acid-base properties of oxide surfaces, Vestn. Saint-Petersbg. Univ. Ser. 4, Phy. Chem., 1401, 2014.
[47] I.Iu. Prosanov, A.A. Matvienko, Investigation of the thermal decomposition of PVA by IR and Raman spectroscopy, Phys. Solid State. 52 (2010) 2056–2059.
[48] L.A. Kazitsina, N.B. Kupletskaia, Application of UV, IR and NMR Spectroscopy in Organic Chemistry, Higher School, Moscow, 1971.
[49] D.J. Upadhyay, N.V. Bhat, Pervaporation studies of gaseous plasma treated PVA membrane, J. Membr. Sci. 239 (2004) 255–263, https://doi.org/10.1016/j.memsci.2004.03.041.

3.4 Article 3: Manuscript submitted for publication

Title

PDMS membranes modified by polyelectrolyte multilayer deposition to improve OSN separation of diluted solutes in toluene

Graphical abstract

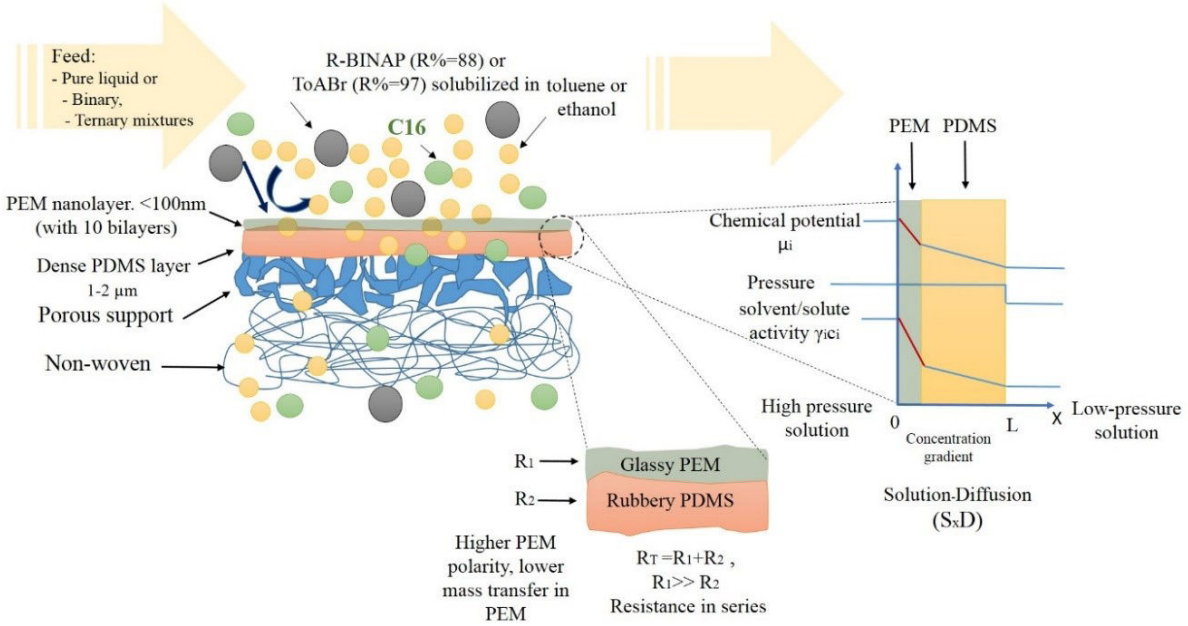

PDMS membranes modified by polyelectrolyte multilayer deposition to improve OSN separation of diluted solutes in toluene

Mahbub Morshed[a], Alexandre Zimmer[bc], Laurent Broch[c], Halima Alem[b], Denis Roizard[*a]

[*a] *Laboratoire Reactions et Genie des Procedes (UMR7274 CNRS-UL) ENSIC-1,rue Grandville-BP 20451-54001 NANCY cedex, France.*
[b] *Institut Jean Lamour, UMR 7198 CNRS-Universite de Lorraine, 2 allee Andre Guinier-Campus Artem Bureau 2-038 F-54000 NANCY CEDEX (FRANCE)*
[c] *LCP-A2MC, Universite de Lorraine, 54000 Nancy, France*
[*] *Denis Roizard, Phone:+33 (3) 72 74 37 95, E-mail: denis.roizard@univ-lorraine.fr*

Abstract

New functionalized poly(dimethylsiloxane)(PDMS)membranes were prepared by the surface modification of the commercially available PERVAP4060 membrane (Sulzer) through cold plasma activation followed by the layer-by-layer assembly method. Four different pairs of polyelectrolytes, i.e., poly(allylamine hydrochloride)(PAH)/poly(acrylic acid) (PAA), PAH/poly(sodium 4-styrene sulfonate) (PSS), poly(diallyldimethylammonium chloride) (PDDA)/PAA, and PDDA/PSS, were used to coat the PDMS layer by the controlled deposition of successive nanolayers(2050 nm).
PERVAP4060 was systematically modified by the deposition of 10 bilayers of polyelectrolyte pairs. These membranes were characterized by contact angle measurements, scanning electron microscopy (SEM), ellipsometry, and atomic force microscopy (AFM). The nanofiltration membrane performance for the rejection of four diluted solutestwo soluble catalysts 2,2-bis(diphenylphosphino)-1,1-binaphthyl (R-BINAP) and tetraoctylammonium bromide (ToABr) and two linear aliphatic molecules n-Tetratetracontane ($C_{44}H_{90}$ or C44) and n-Hexadecane ($C_{16}H_{34}$ or C16) was studied in the toluene feed solution at up to 40 bar pressure. It was shown that the organic solvent nanofiltration (OSN) mass transfer properties differ clearly depended on the layer-by-layer chemical structure and the characteristics of the solutes. Despite the highly diluted concentrations of the solutes, i.e., <1 wt% for R-BINAP and ToABr, and the high solvent permeate flux, the ToABr, R-BINAP, and C44 solutes were markedly rejected by all the membranes. ToABr had the highest rejection coefficient, up to 97%. As a trend, higher the polarity of the bilayer assembly, lower was the mass transfer of the solvent compared to that of the pristine membrane. The results indicated that a solutiondiffusion mechanism is likely to apply. The best rejection of R-BINAP (up to 88%) was obtained when the membrane was coated with 10 bilayers of PAH/PSS. Thus, these prepared polyelectrolyte (PEL)-modified membranes have potential applications in homogeneous catalysis industry, for example in olefin metathesis for expanding the lifetime of soluble catalysts by separating them at mild OSN condition while ensuring the permeation of products.

Keywords

Polyelectrolytes, nanolayer, organic solvent nanofiltration (OSN), PDMS, R-BINAP, C44

Highlights:
- Synthesis of PEL-modified PDMS membranes by LBL method for application in OSN
- Investigation of the separation of binary and ternary mixtures by OSN under tangential flow
- Highly dilute solutes (0.05 wt%) in toluene can be strongly rejected by PDMS membrane
- Polar solutes are more easily rejected by the pristine PDMS membrane
- Improved rejection of R-BINAP is obtained with PAH/PSS modified membranes.
- C16 alkanes can be eliminated through the membrane, whereas the R-BINAP is mostly rejected

1. Introduction

Organic solvent nanofiltration (OSN) is a promising membrane technology for the purification of liquid mixtures. In this process, a pressure gradient is applied to the liquid feed to enable the solute/solvent separation by selective permeation through a membrane. The biggest molecule is expected to be rejected from the permeate flux. The most successful application of this process was carried out by Exxon Mobil in the 2000s, when they recycled the solvent used for the purification of lube oils. The main challenge nowadays is the development of membranes that would demonstrate both high permeance and high rejection performance in organic media for application in diverse industries such as fine chemistry, soluble catalyst recycling, oil and solvent purification, and solvent exchange [1]. In that sense, approximately two decades ago, Mulder et al. [2] classified nanofiltration membranes based on the pressure required to achieve the target separation, i.e., between 5 and 20 bar. Currently, the major challenge is to maintain the time operating stability of the membrane performance at up to 40 bar under different feed conditions as well as other harsh conditions. Therefore, polymeric membranes with high resistance towards solvents, i.e., enhanced stability toward organic solvents and compaction, were developed [24]. The most well-known membranes are polyimides, poly(ether-ether-ketone), poly(dimethylsiloxane) (PDMS), and polybenzimidazoles. The number of membranes is limited owing to the required chemical, mechanical, and thermal membrane stabilities, which are crucial for the targeted application. However, the biggest challenge up to now is that OSN membrane performance is not predictable from one organic solvent to another.

It has been shown that a good alternative to avoid new material synthesis and development is to alter the membrane surface to tailor the interactions between the membrane and the solvent and/or solute [57]. The past decades have, therefore, witnessed the growth of surface functionalization processes such as plasma treatment [8], UV light treatment [9], and covalent and supramolecular grafting of macromolecules [5,10,11]. The layer-by-layer assembly (LBL) of polyelectrolytes (PELs) is one of the most promising processes owing to its versatility and the fact that it can be conducted under environment-friendly conditions, both for aqueous and organic nanofiltration. Moreover, the LBL method is inexpensive and enables the building of thin films with a nanometer scale control [12,13][14].

Further, recent works have shown that the layer-by-layer assembly of polyelectrolytes can create stable nanofiltration membranes that are well-resistant to organic solvents with very high flux and selectivity [57] [15] [16]. The LBL process, developed by G. Decher [12] [17], consists of the alternating deposition of polyelectrolytes with opposite charges in water media. The complex presents unique properties owing to the strong internal Coulomb interactions and the possibility of tuning the final deposited film just by modifying the chemical nature of the polyelectrolyte or more simply the pH, the ionic strength, or layer number. Moreover, the final complex is insoluble in a wide range of organic solvents.

To the best of our knowledge, PDMS has been rarely used as support for PEL deposition and has never been used in OSN as a composite-PEL membrane. As PDMS is highly hydrophobic and PEL highly hydrophilic, it is rather counterintuitive to associate them in a composite film. Nevertheless, the PDMS surface is slightly negative and favors the initial adsorption of poly(diallyldimethylammonium chloride) (PDDA). Benavidez [18] reported the preparation and use of PDDA/poly(sodium 4-styrene sulfonate) (PSS)-modified PDMS films for application in capillary electrophoresis. Kumlangdudsana also reported the use of PDDA/PSS on a PDMS substrate to improve organic resistance in microfluidic applications [19].

To ensure the stability of the LBLs on PDMS and resistance to the mechanical shear stress under the cross-flow OSN operating conditions, a plasma-activating procedure has been used. Indeed it has been shown in previous work [5] that very stable polyelectrolyte layers could be obtained even on PDMS by combining cold plasma activation followed by the layer-by-layer assembly of PDDA

and PSS. In this work, we transposed this plasma-activated process to the layer-by-layer assembly of three other pairs of polyelectrolytes, i.e., poly(allylamine hydrochloride) (PAH)/poly(acrylic acid) (PAA), PAH/PSS, and PDDA/PAA, on a PDMS-based commercial membrane, PERVAP4060 (Sulzer).
The objective of this work was to study the rejection by OSN of four solutestwo soluble catalysts, R-BINAP and ToABr, and two linear aliphatic molecules, C44 and C16, diluted in tolueneand to compare the outcome with the rejection results of pristine PERVAP4060 [20]. It was envisioned that the deposition of bilayers at the nanometer scale on PERVAP4060 could help to improve the rejection of solutes, first, by decreasing the swelling of the PDMS layer and, second, by increasing and tuning the charge density of the top layer in contact with the feed, whereas the total flux would remain rather high in relation to the very small thickness of the polyelectrolyte layer.

2. Materials and Methods

2.1.1 Chemicals

R-BINAP (white powder; purity > 94%), ToABr (white powder; purity 98%), n-hexadecane (purity > 99%), and tetratetracontane (C44, purity 99%) were purchased from Sigma-Aldrich and used as received. Toluene (purity 99.8%) was also obtained from Sigma-Aldrich.
Commercial PERVAP4060 is a composite membrane having a dense top layer made of PDMS (thickness: 1-2 μm) obtained from DeltaMem AG (www.deltamem.ch). The modified membranes were obtained from the deposition of multilayered films from a couple each of strong and weak polyelectrolytes purchased from Sigma-Aldrich, namely, PDDA (molecular weight Mw =100 000-200 000 $g.mol^{-1}$) and PAH (Mw=150 000 $g.mol^{-1}$) as cationic polyelectrolytes and PSS (Mw =70 000 $g.mol^{-1}$) and PAA (Mw =1 250 000 $g.mol^{-1}$) as anionic polyelectrolytes. They were used as received. Deionized water (MilliQ water, $18M\Omega$) was used for all the experiments, polyelectrolyte solutions, and cleaning steps.

2.1.2 Plasma treatment

A microwave post-discharge reactor consisting of a cylindrical glass chamber (3 cm in diameter), pumped through a primary pump, was used; the plasma was generated by a 2.45 GHz microwave generator. The PDMS was placed into the plasma glass tube at 30 cm from the gas inlet at a residual vacuum of 10^{-2} mbar. The plasma atmosphere consists of an argon and oxygen gas mixture with a flow rate of 400 standard cubic centimeters per minute (sccm) and 40 sccm, respectively. It is critical to carefully control the exposure time to avoid any surface ablation. Under these conditions, a short period of plasma exposure, 30 s, was sufficient. Then the system was vented up to atmospheric pressure and the sample was immediately removed from the reactor and used for the LBL deposition steps. The details of the plasma surface modification have been reported previously by Bassil et al. [5].

2.1.3 LBL membrane modification technique

A concentration of 10^{-2} $mol.L^{-1}$ was used for all the polyelectrolyte aqueous solutions (PDDA, PAH, PAA, and PSS). The pH of the PAA and PAH solutions and the rinsing bath were adjusted at 6.5 to ensure maximum ionization of these weak polyelectrolytes as shown by Choi et al. [21].
The layer-by-layer deposition was conducted in static mode by using the ND-3D, which is a three-axis controlled system developed by Nadatech Innovations. Bilayers were created only on the top surface of the PDMS. First, the PDMS membrane positioned by clamps was immersed in the polycation solutions for 10 min, followed by three rinsing steps (15 dips of 1s each, 3 dips of 5s

each, and 1 dip of 15s). Finally, the membrane was immersed in the polyanion solutions for 10 min, followed by the same rinsing steps. Thereby, one bilayer or one cycle of self-assembly membrane was deposited. Additional bilayers were deposited similarly until the target number of bilayers was achieved.

2.1.4 Membrane characterizations

Scanning electron microscopy for original PDMS, plasma-treated PDMS, and polyelectrolyte-modified PDMS

The surfaces of the plasma-modified PDMS and the polyelectrolyte-modified PDMS, prepared by LBL self-assembly, were investigated by scanning electron microscopy (SEM; JEOL 6490LV) at a high vacuum mode (pressure = 10^{-4} Pa).

Atomic Force Microscopy

The morphologies of the PDMS and the polyelectrolyte-modified PDMS were characterized by atomic force microscopy (AFM) in intermittent-contact mode (tapping mode) on an Asylum Research MFP-3D Infinity equipped with a 100-μm close-loop scanner. AFM probes (from Asylum Research) were used in this characterization. The cantilevers had a resonance frequency of approximately 270 kHz and spring constant value of approximately 26 $N.m^{-1}$. Images were acquired in the air at ambient temperature with a drive amplitude of 15 mV and an attenuation set-point of 0.7-0.8. At least five different zones were scanned on each sample and images at different magnifications were acquired (we have only shown the 1×1 μm^2 images). The images were treated and analyzed using procedures developed under Igor Pro (Wavemetrics) by Asylum software.

2.1.5 Ellipsometry

Silicon wafers, boron-doped, type-p, Si(1 0 0), were used for thickness measurements by ellipsometry. First, the wafers were cleaned by Piranha solution (30% hydrogen peroxide and sulfuric acid in 1/1 v/v) for 20 min and followed by three MilliQ rinsing steps. Ex situ variable angle spectroscopic ellipsometry measurements were carried out using a phase-modulated spectroscopic ellipsometer (UVISEL, Horiba Jobin Yvon). Multiple sample analysis [22] was performed using the commercially available DeltaPsi 2 software. Typical (I_s, I_c) measurements were done for incidence angles between 60° and 70° in steps of 5°, and the wavelength range of the spectrum was 260-860 nm in steps of 5 nm.

2.1.6 Water Contact angle measurements

The water contact angles (WCAs) were measured by using a Digidrop contact angle meter. The setup consists of a white light source, a sample holder (a flat surface), and a camera in the same horizontal plane. The syringe-type milliQ drop dispenser was mounted perpendicular to the flat surface. The setup allows one to see a 10× magnification of the dispensed droplet of water and, finally, the WinDrop software was used for data acquisition with an accuracy of ± 0.7°.
Both the pristine and polyelectrolyte-modified PDMS samples were dried with a hand drier prior to placing them on the horizontal flat surface of the contact angle meter. Approximately, 1-2 μL of milliQ water was dispensed on the surface and the contact angle was measured within 5-7 s. At least five data points were taken from the different positions of the same sample and a minimum of five different samples were tested for reproducibility.
The optimization of plasma exposure time and hydrophilicity changes of PDMS before and after modification were recorded.

2.1.7 Cross-flow nanofiltration experiments

The OSN setup consists of a rectangular cross-flow cell (GE Osmonics) that is used in the tangential cross-flow mode, in which the pressure, feed flow rate, and temperature of feed can be well-controlled. This setup has already been reported in the previous papers of Ben Soltane et al. [23,24]. The applied pressure was regulated by using an IP 65 solenoid valve connected with the digital pressure transmitter system and controlled by the Flow DDE Bronchorst software [20]. The system allows a precise pressure control over the 1-40 bar range with fluctuation of 0.5-1% to the set value. The temperature was controlled by a Thermo Haake K50 with a precision of ± 1 °C and the cross-flow was set to 7-10 kg/h, measured by a Cori flow (digital mass flow) meter. Prior to the OSN experiments, the membrane coupons were immersed overnight in the solvent at room temperature as a pre-conditioning step. The membrane coupons used measured 8 cm × 12 cm (including the area of the O-ring), corresponding to the effective useful membrane area of $2.8 \times 10^{-3}\ m^2$. The coupon was mounted wet into the OSN cell for pressure conditioning. Then the feed flow was maintained at 10 kg/h at 30 °C. Next, a transmembrane pressure (TMP) of 10 bar was applied with a step increase of 2-3 bar using the flow DDE software interface. At each step, the set point with respect to the actual value in the OSN was monitored for the stability of TMP in the upstream. As soon as the pressure of 10 bar was achieved, the unit was monitored for 10-15 min, ensuring stable pressure, cross-flow, and temperature. The same procedure was repeated at 20 bar, 30 bar, and 40 bar. The overall pressure-conditioning cycle was applied systematically to all the used coupons. After conditioning at 40 bar, the TMP was gradually decreased to atmospheric pressure. The aim of this step was to check possible hysteresis effects owing to the increase in pressure. Organic solvent nanofiltration experiments were then performed in a cross-flow rig and in a continuous mode. The permeate was continuously recycled to ensure the steady-state concentration of the feed, i.e., initially 0.05 wt% of the solute.

Permeate measurements

At least 3-5 g of permeate were collected and weighed for each data point and the corresponding time was recorded. At each applied pressure, at least three permeate samples were collected at intervals of a minimum of 20 min. The sample size, number of repetitions, and interval between each sample collection confirm the accuracy of the measurement and stability of the system. Most experiments were repeated more than two or three times using new membrane coupons from different batches. The flux (J) and rejection (R) were calculated according to the formulas given below:

$$J = \frac{V}{A.t} \tag{3.1}$$

Where J is the flux ($Lm^{-2}h^{-1}$), V is the volume of the collected permeate (L), A is the active surface area (m^2) and t is the time (h).

$$R(= (1 - \frac{C_P}{C_f}).100 \tag{3.2}$$

where C_p is the concentration of solute in permeate and C_f is the concentration of the feed.

Gas chromatography as analytical method for concentration determination

The quantitative analysis of the solutes was carried out using gas chromatography. The operational conditions of the analysis method were as follows:
- Column: HP-5 phenyl methyl siloxane ($15m \times 320\mu m \times 0.25\mu m$). Flame Ionization Detector

(FID): 380 °C, Helium (He): 1 bar.
- Oven program temperature of 325°C for R-BINAP using tetratetracontane ($C_{40}H_{82}$) as an external standard. The calibration and one typical chromatogram are illustrated in [20].
- Oven program temperature of 200°C for ToABr and n-hexadecane using n-tetracosane ($C_{24}H_{50}$) as an external standard.
As the solutes had low concentrations (0.1-0.05 wt%), the calibration curve and measurements were carried out using suitable external standards and the constant volume addition method. Each sample test was triplicated and the different experimental results were compared for the determination of solute rejection.

3. Results and discussion

3.1.1 Choice and characteristics of PELs

Hundreds of PELs are commercially available. Up to now, there has been no guideline to choose the PEL according to the type of separation being studied. In this work, only four PELs have been used, two cationic and two anionic, to give rise to the LBLs of various charge density. Indeed, in organic media, charge density acts as a physical cross-linker and it has been expected that the average charge concentration could influence the mass transfer by tuning the local network mobility and hence the diffusion coefficient of the permeant. The data collected to characterize the PELs are presented in Table 1. Using either the Fedor group contribution method or the HsPiP software, it has not been possible to obtain coherent values of the Hansen solubility parameters for the PEL because the ionic part of the PEL could not be considered. Instead, the average charge density of the structure was calculated for each PEL. It was found that the charge density varied within a wide range, from 1 to 3, referring to the molar weight of the PEL repeating unit. PSS has the lowest charge density whereas PAA and PAH are endowed with higher values, up to three times for PAH compared to PSS. Giving rise to physical cross-linking via ionic interactions, these charge densities might explain partly the high glass transition temperatures reported in the literature for the PELs (Table 1) [25-30].

3.1.2 PDMS surface modification

As previously shown by Bassil et al. [5], to ensure good stability and homogeneity of the polyelectrolyte depositions, the PDMS surface was activated by cold plasma post-discharge of Ar/O_2 to generate negative charges at the polymer surface to make it able to anchor the first layer of the cationic polyelectrolyte. Subsequently, the four different couples of polyelectrolytes were assembled layer by layer, up to 10 bilayers, to guarantee good coverage, using an automatic coater to ensure good reproducibility:

- PDDA/PSS-one LBL built with strong polyelectrolytes;
- PAH/PSS and PDDA/PAA-two LBLs associating the strong and weak polyelectrolytes; during the procedure, the pH was adjusted to a value of 6.5 to ensure strong dissociation of PAH and PAA; and
- PAH/PAA-one LBL associating two weak PELs. The pH of the coating solution was also adjusted to 6.5 for PAA to enhance the ionization of both PELs.

These composite LBL-modified PDMS membranes were characterized by several techniques to determine the properties of the LBL surface. The results are reported in Table 2.
After plasma exposure, the PDMS membrane exhibits a very low water contact angle (WCA), 19°(± 2), compared to that of the pristine membrane, 100°, in relation with the negative charge

Table 1: Main characteristics of PDMS and the PEL employed

Polymer	Monomer unit	MW unit (g. mol^{-1})	Mn[b] (g)	pKa[c]	T_g[d] (°C)
PDMS	$(Me_2OSi)_n$	74	NA	NA	-123
PDDA	$(C_8H_{16}N)_n$	125.5	≈200 000	7	67
PAH	C_3H_8N	57.5	150 000	9.5	> 190
PSS	$[C_8H_7SO_3^-]_n$	183	70 000	1	180
PAA	$(C_3H_3O_2)_n$	71	1 250 000	4.25	80–128

	PDDA, cationic strong	PAH, cationic weak	PSS, anionic strong	PAA, anionic weak
PEL structure	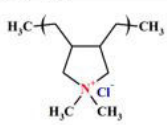	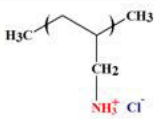	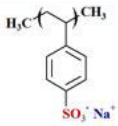	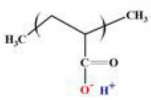
Charge density[a] by weight (× 10^3)	8.01	17.49	5.55	14.17
Reduced value	1.45	3.18	1	2.57

[a]Calculated according to the formula Charge Density = $1/MW_{monomer}$

[b]Number Average Molecular Weight (M_n)

[c]Acid dissociation constant (K_a) of a solution.

[d]Glass Transition Temperature (T_g)

created on the PDMS surface. It was shown that when the plasma-treated membrane is maintained under room temperature, the WCA slowly increases (see Supplementary Figure SM1). To avoid the drawbacks of the PDMS hydrophobicity recovery [5], the PEL depositions were conducted soon after the plasma activation, within 45 min. The WCAs measured after the LBL deposition are shown in Table 2. In all cases, the WCA was markedly increased while, however, remaining lower than the virgin WCA of the pristine membrane, as expected. It should be noted that the contact angles of the PEL-modified PERVAP4060 were stable with respect to time. Repeated measurements after OSN experiments also confirmed the stability. The LBLs prepared gave rise to two types of contact angles, i.e.,$\alpha \approx 78°$ or $\alpha < 56°$. It may be noted that the two higher WCAs characterize the LBLs whose last layer is PSS, whereas the two lower ones characterize the LBLs having PAA as a final deposited layer. This difference is well in agreement with the charge density that characterized each PELthe highest one (PAA) corresponds to the lowest WCA.

Table 2: Main characteristics of the composite LBL formed on PERVAP4060 modified with 10 bilayers. The root-mean-square value as calculated from AFM images (10 × 10 µm^2).

Surface modification	Pristine PDMS	Plasma activation	PDDA/ PSS	PDDA/ PAA	PAH/ PSS	PAH/ PAA
α (°) (±2) [a]	103	19	77	55	79	47
rms (nm) [b]	1.6	1.6	3.4	25.2	3.9	NA
T_g (°C) [c]	-123		90	NA	167	45
Thickness (nm ±0.5) [d]	1500		25	51	25	62

[a]Water contact angle.

[b]Rugosity measured by AFM.

[c][25] [31], [28] [32] [33].

[d]Measured by ellipsometry, except PDMS layer [24] .

The LBLs built with PAA also have another peculiaritythey are thicker (50/60 nm) than the two

others LBLs (approximately 25 nm). As a rule, any phenomenon that has the potential to slow down the chain relaxation process and limit chain spreading when adsorbing the PEL can favor the formation of thicker layers [34]. The high molecular weight of PAA (M_w = 1 250 000 Da) used in this work might generate entanglements and, thus, be the reason for the higher thickness of the LBL containing PAA.
The homogeneity of surface was studied by combining SEM for the large-scale investigation (see Supplementary Figure SM2) and AFM (in the tapping mode) for the nanometric scale.
As shown in Figure 1 with some AFM examples, the modified surfaces are quite different from the pristine PDMS surface; tuning the chemical structure of the PDMS layer also translates into a different root-mean-square (rms) roughness, which increases by up to 3.3 nm for the PDDA/PSS, to reach 25.2 nm for the PDDA/PAA (Table 1). The PDDA/PAA assembly led to thicker and rougher surfaces compared to the PDDA/PSS, which is consistent with the highly coiled chains conforming to the behavior of well-known weak polyelectrolytes [10,35,36].

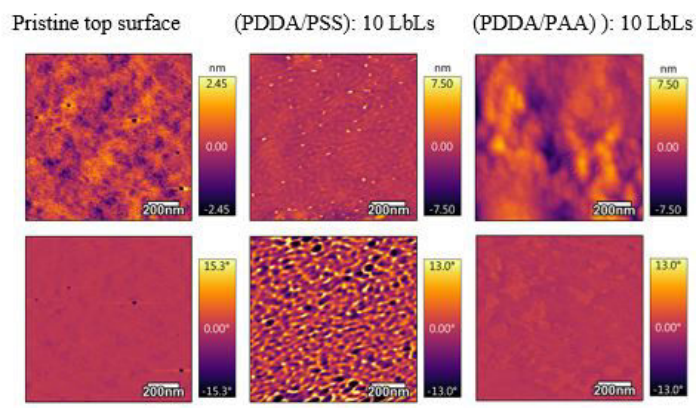

Figure 1: Topographic (top) and phase (bottom) AC-mode images of PERVAP4060 and related modified LbL multilayer (10 cycles).

The local charge density of each bilayer unit has also been calculated as in the case of the PEL unit, using the molar mass PEL pairs forming the LBL. As expected from the PEL properties, the four deposited LBLs cover a large range of charge density, going from 1 to 2.4 times in the increasing order PDA/PSS < PAH/PSS < PDDA/PAA < PAH/PAA (see Table 3).

4. Investigation of the OSN properties of the modified PERVAP4060

4.1.1 Effect of plasma treatment on OSN flux

In the first step, the potential effect of the plasma treatment on the OSN mass transfer was investigated only with toluene as the feed. The results shown in Figure 2 indicate that the plasma procedure used does not modify the permeability of the active layer. It means that no significant cross-linking of the network occurred, neither was there any ablation. Indeed, these two drawbacks can be observed when inadequate plasma parameters are used.

4.1.2 Investigation of the number of LBLs on OSN flux

In the second step, the influence of the number of deposited LBLs on the toluene flux was investigated. Indeed, the PELs used to deposit the LBLs are all characterized in the dry state by a high glassy transition temperature up to 190°C for PAA (Table 1). The reported Tg data of the corresponding LBLs are also characterized by glassy structures (Table 2) [31] [32]. Hence, it was

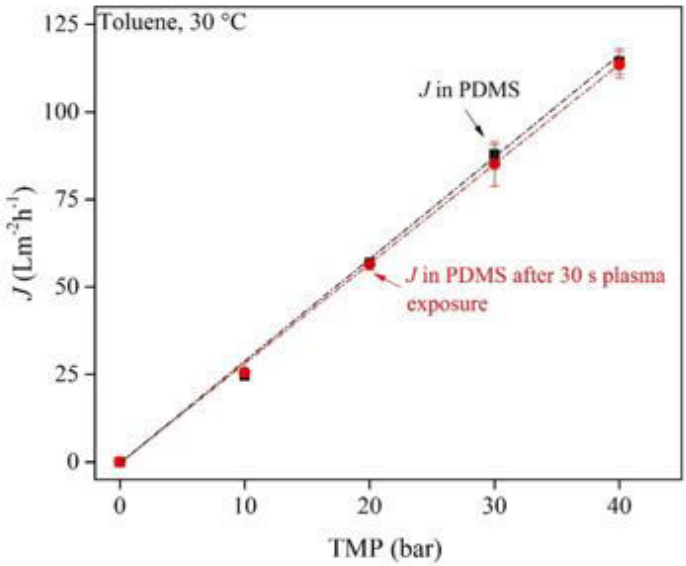

Figure 2: Evaluation of plasma treatment on toluene OSN flux (30 °C)

expected that the modified LBL membranes would have much lower permeances than the pristine PERVAP4060, whose selective layer, PDMS, is known to have a rubbery structure characterized by a very low T_g(-123 °C). As shown in Figure 3, the flux with 5 LBLs of PDDA/PSS was almost unchanged, whereas the flux with 10 LBLs was decreased by approximately 20%. Therefore, in the further LBL deposition, this number, of 10 bilayers, was maintained as a standard to ensure full PDMS surface coverage.

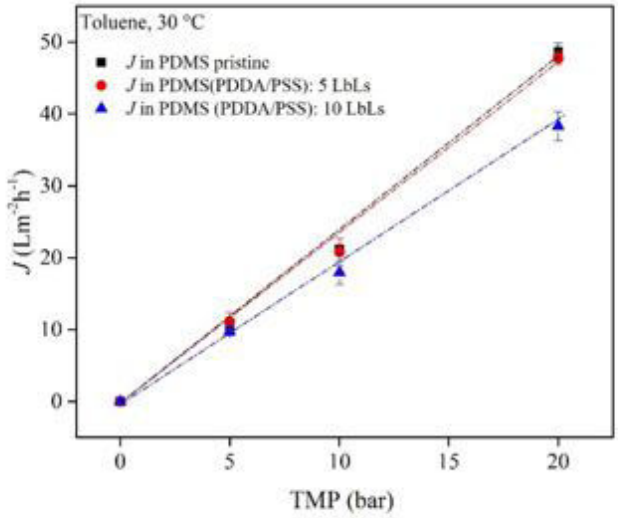

Figure 3. Effect of number of bilayers (PDDA/PSS) in toluene OSN fluxes (30 °C)

4.1.3 Study of effect of LBL composition (10 bilayers) on toluene OSN flux

Prior to the study of the binary and ternary feed mixtures, the toluene mass transport was characterized for the four membranes up to 20 bar. The data presented in Figure 4 show a linear increase of the flux with the transmembrane pressure (TMP) for each LBL type, leading to very different values of toluene fluxes, which vary in the proportion 1 to 7. On the other hand, no hysteresis effect could be detected with respect to time. This indicates that the modified membranes were well stable with respect to the pressure and the shear stress induced by the tangential feed flow, tested up to 20 L/h.

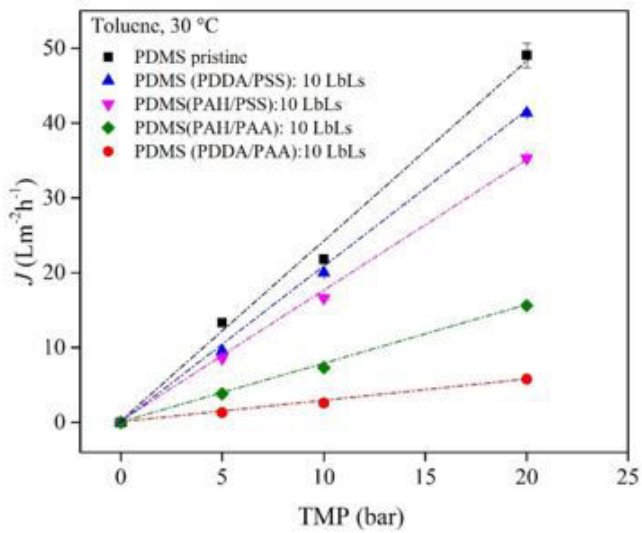

Figure 4. Effect of PEL modification of PERVAP4060 on toluene flux (30 °C) recorded in tangential mode (20 L/h)

To explain the flux variation, the LBL composition was considered first. However, no simple relationship could be drawn between the occurrence of each PEL and the measured fluxes. Indeed, PDDA is, for instance, a part of the modified membrane having the higher flux (PDDA/PSS) and a part also of the modified membrane having the lowest flux.

Table 3: Calculated parameters of the LBLs to address interactions with the solute

LBL structural unit		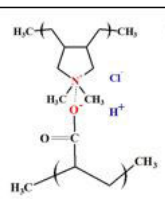	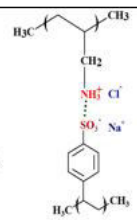	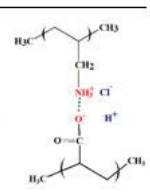
Charge density[a]	PDDA/PSS	PDDA/PAA	PAH/PSS	PAH/PAA
by weight (× 10^3)	3.24	5.09	4.15	7.7
Reduced value	1	1.6	1.3	2.4
Toluene flux (kg/(h/m²))	42	7	35	16
Predicted flux (20 bar, 30 °C)	42	23	33	17

[a]Charge density calculated as $1/MW_{monomer}$

Therefore, another way to evaluate the intrinsic permeability of each LBL has been researched. For a dense network, it is well-known that two major factors determine the permeability: the affinity

properties with the penetrant, the toluene molecules in this study, and the diffusion coefficient of the penetrant, which is controlled by the stiffness of the network. Usually, the affinities can be evaluated using the Hansen solubility parameters (HSP). Unfortunately, with ionic species, HSP cannot be calculated with the Fedor contribution group method (Table 3). The charge density (CD) of the LBLs was considered in turn and calculated, as done previously, to be equal to $1/(\sum M_w)$. Indeed, the charge density accounts for the cross-linking degree of the LBL structure and, thus, for the chain mobility that can tune the diffusion coefficient of a penetrant. First, it was found that the higher solvent fluxes correspond to the LBLs having smaller charge density, i.e., PDDA/PSS and PAH/PSS. Second, it was observed that the fluxes of these two LBL membranes could be predicted by dividing the flux obtained for CD = 1 (reduced value) by the charge density of each LBL (Table 3). Only the flux of the PDDA/PAA was not predicted.

4.1.4 Study of solutes rejection by OSN in toluene solutions

Several series of OSN experiments were carried out with binary feed solutions to mimic the industrial context where catalysts are always used under very high dilution. The chemicals used are reported in Table 4. Besides the experiments with R-BINAP and ToABr, the rejection of the two linear alkanes, C44 (n-tetratetracontane) and C16 (n-hexadecane) have also been studied to evaluate the effect of the molecular size and chemical nature of the solute. In all experiments, high dilutions of the solutes were used in the range 0.050.1 wt% in toluene. Gas chromatography was used to determine solute concentrations in the feed and in the permeate solutions with the help of calibration curves using external references (see the Materials and Methods section). R-BINAP, ToABr, and C44 are bulky molecules having the same range of molecular weight, i.e., 546-622 g/mole, but ToABr is a charged molecule, a quaternary alkyl ammonium bromide. C44, a linear alkane, and ToABr have higher molar volumes (V_m) because of their linear alkyl structure. Indeed R-BINAP, which has a polyaromatic structure, is a more rigid and more compact molecule, i.e., approximately 30% more.

Table 4: Chemicals used to prepare feed solutions and their specifications

Chemicals	Chemical structure	Mw (gmol^{-1}) V_m (cm^{3}mol^{-1})	δHSP (MPa$^{1/2}$)
Toluene	Ph-CH_3	Mw = 92 V_m = 106	18.2
(*R*)- BINAP	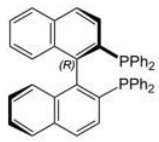	Mw= 622 V_m = 511	21.5
C44	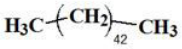	Mw = 619 V_m = 754	16.2
ToABr	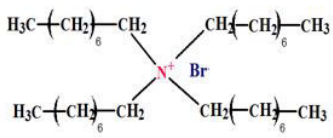	Mw = 546 V_m = 761	21.9
C16	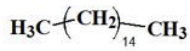	Mw = 226 V_m = 294	15.9

Referring to the Hansen solubility parameters (HSP), the relative affinities for the pristine PDMS

membrane are in the increasing order: ToABr < R-BINAP << C44 < C16. The same order also occurs with toluene. Referring to the LBL-modified PDMS membranes, HSP cannot be used to predict affinities, as already explained in the previous paragraph. However, ToABr being a charged molecule, strong repulsions with the non-polar siloxane network and with the cationic PEL embedded in the LBL structure can be expected.
At this step, before examining the OSN rejection results in detail, it is worth recalling that for a composite membrane, the fluxes and rejection values are the result of the two distinct, dense, and consecutive layers, and each of them has their own intrinsic properties. According to the model of the resistance-in-series [37], for a given component i, the effective mass transfer Q_i through the composite membrane is given by:

$$Q_i = Pe_i \Delta a_i A \tag{3.3}$$

where Pe_i is the permeance ($Pe_i = P_i/l$), Δa_i is the activity gradient, and A is the membrane area. Hence the equivalent mass transfer resistance R_m of the composite membrane can be written as:

$$R_m = \frac{1}{K} = \frac{1}{k_{m1}} + \frac{1}{k_{m2}} \tag{3.4}$$

or

$$K = \frac{1}{\frac{1}{k_{m1}} + \frac{1}{k_{m1}}} \tag{3.5}$$

where K is the total mass transfer coefficient of a given component, k_{m1} and k_{m2} are the mass transfer coefficients, respectively, through the top layer 1, here the PEL pairs, and through the support layer 2, here the PDMS. The porous support polyacrylonitrile (PAN) layer was not considered here as a resistant layer.
Evidently, the application of this model is valid only under some strict assumptions, postulating steady permeability, no coupling effects between the permeants, and a linear relationship between the permeability and membrane thickness. If these assumptions are likely to hold in gas permeation, some deviations from this mechanism can occur at high swelling.
However, equation 4 and 5 shows that the effect of the top layer on the effective mass transfer will strongly depend on the relative values of k_{m1} and k_{m2}: the lower mass transfer coefficient will govern the effective permeance and, thus, the rejection of the composite membrane when a mixture of two components is considered.

Overall, this means that six parameters will control the effective permeance and rejection values:
- the permeability of the solvent and of the solute,
- the activity gradient of each permeant, and
- the real thickness for each layer.

In addition to the OSN case, if the mass transfer coefficient of the top layer k_{m1} is the lowest, as expected with the rigid PEL pairs in toluene, the mass transfer coefficient of the PDMS layer is likely to be reduced owing to the lower swelling degrees of the PDMS network. Clearly, under OSN conditions, the effective permeance of the composite membrane cannot be predicted in a simpler way.
The general trend observed for the rejection of solutes is demonstrated by the pristine PDMS membrane. The solute ToABr, i.e., the charged molecule, has the highest rejection (93%) and the solute C16, being also the smallest molecule, has the lowest rejection (7%). This trend is valid for all the membranes. These results are in agreement both with the HSP and with the size of the molecules (Table 4).
Next, when the rejections of R-BINAP and C44 are considered, the values are much closer to each

Table 5: Results of OSN experiments with binary mixtures using LBL-modified membranes (10 bar, 30 °C, diluted toluene feeds)

Membrane sample	Global flux ($Lm^{-2}h^{-1}$ ±10%)	Rejections of solutes (% ±2)				Charge density[c]
		R-BINAP[a]	C44[a]	ToABr[a]	C16[b]	
PDMS pristine	24	80	70	93	7	NA
PDMS (PDDA/PSS): 10 LBLs	22.9	82	88	92	6.5	1
PDMS (PAH/PSS): 10 LBLs	14	88.5	93	97	7	1.3
PDMS (PAH/PAA): 10 LBLs	7.6	66.3	80	84	10	2.4
PDMS (PDDA/PAA): 10 LBLs	3.8	80.5	82	92	10	1.6

[a]Solute concentration: 0.05 wt%.
[b]Solute concentration: 0.1 wt%.
[c]Reduced charge density.

other. For the pristine PDMS, the C44 alkane molecule is less rejected, in agreement with the lower HSP (δ =16.2) close to the PDMS value (δ =15.4)[38]. However, with all the LBL-modified membranes, the rejection values of these two solutes are reversed. This clearly seems to be an effect induced by the charged LBL layer, which repels the non-polar C44 alkane molecule. This effect is also observed to some extent with the C16 molecule, with the two LBL membranes having the higher charge density, i.e., PDDA/PAA and PAH/PAA.
With respect to R-BINAP rejection, the LBL with 10 layers of (PAH/PSS) exhibits a marked improved rejection, up to 88.5%. The same result is also obtained for the rejection of ToABr and C44. It is, of course, difficult to explain these three results in detail because they are owing to several parameters that are able to affect both the solubility and the diffusion of the solutes, such as the charge density, the LBLs T_g, and the activity and mobility of the solutes. Nevertheless, as a marked rejection improvement is obtained for the three types of solutes (polyaromatic, charged, and alkane molecules), the reason more likely seems to be a relative decrease of the diffusion of the solute versus toluene diffusion.
Another interesting result is linked to the use of the LBL formed by the PEL pair PAH/PAA, the pair that has the highest charge density (Table 4). Indeed, despite a strong global flux reduction, converse to the results obtained with the previous LBL (PAH/PSS), the rejection values of the two polar solutes, R-BINAP and ToABr, are smaller compared to the rejection values obtained with the reference pristine PDMS membrane. Therefore, it seems that this LBL structure is less repulsive for polar solutes than for the others. The reason for this effect is not yet clearly understood but might be linked to the presence of PAA.

4.1.5 Evaluation of potential aging of (PAH-PSS): 10 LbLs -modified PDMS

After conditioning the LBL-modified membranes as usual for 30min, the long-term stability of the multilayered PAH/PSS film was studied for several days. First, the OSN conditions were applied for several hours at 20 bar and 30°C under the tangential feed flow mode. The rejection and the fluxes were measured every hour. The related results are shown in Figure 5, which depicts the relationship of the flux (J) and rejection (R%) with time. Clearly, no deviation was observed and the R-BINAP rejection value remained steady at approximately 88%. Thereafter, the pressure was released for two days and reapplied the third day, along with tangential feed flow. Under these operating conditions, the measured flux and rejection values were found to be the same as they

were three days before, i.e., 38 $L.m^{-2}.h^{-1}$ (TMP = 20 bar) and 88.6%, respectively. This series of experiments confirmed the stability of the LBL-modified membrane under OSN conditions and tangential feed flow, and the absence of any fast aging owing to some delamination of the top layer of the LBL.

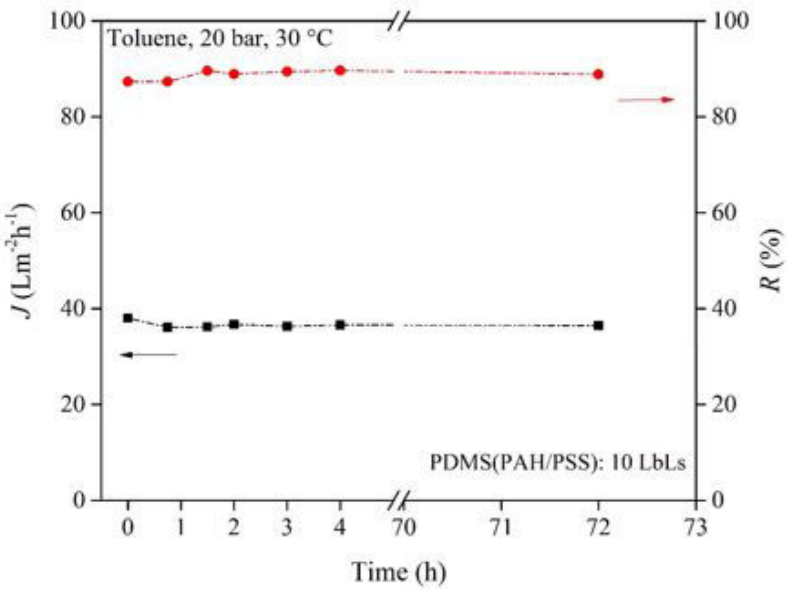

Figure 5. Performance stability with the PAH/PSS-modified PERVAP4060: Rejection of *R*-BINAP in toluene at 20 bar and 30 °C over three days in tangential mode.

4.1.6 Study of OSN performance with a model ternary mixture

Finally, a ternary feed mixture was studied to mimic an industrial case with a simple multicomponent system composed of dilute catalytic ligand (0.05 wt%), the linear saturated hydrocarbon C16 (feed range: 1-10 wt%), and toluene. The results are shown in Figure 6. It can be seen that the rejection of C16, close to 9%, is much lower than that for R-BINAP and similar to the rejection value previously observed at the feed concentration of 0.1 wt%. This big difference can be easily explained by the higher diffusion coefficient of C16 linked to its smaller size, both in the PEL and PDMS layers.

With the increase in the C16 concentration from 1wt% to 10wt%, a small decrease in the R-BINAP rejection value was also observed. However, a much significant effect on C16 rejection can be underlined as well as on the global NF flux, which increased by approximately 40%. Clearly, this flux increase was greater than the simple flux contribution of the linear hydrocarbon. This indicates that the permeability coefficients are likely to increase in the presence of C16.

Finally, from a process point of view, these OSN results are quite interesting because this membrane technique would allow easy separation of the linear C16 molecule from R-BINAP in a toluene feed mixture. This is a promising result for application in metathesis synthesis.

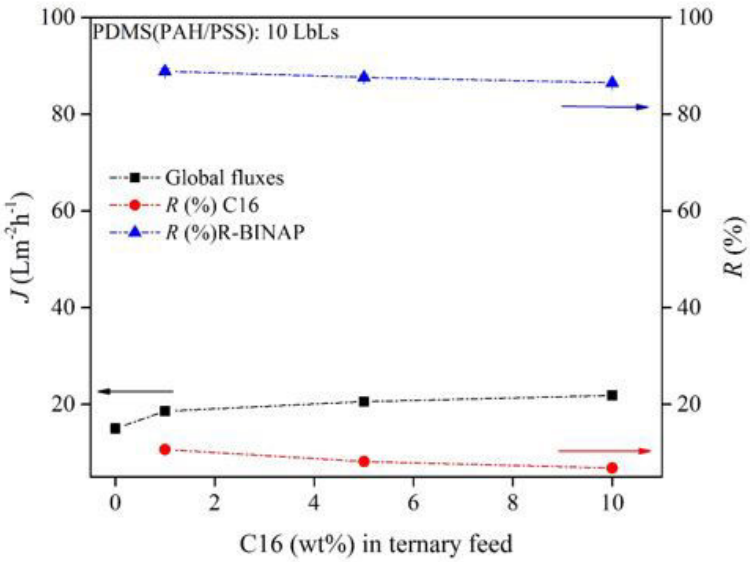

Figure 6: OSN performance of PAH-PSS: 10 LbLs modified PERVAP4060 for the separation of a model ternary mixture consisting of C16 (1–10 wt%) and *R*-BINAP (0.05 wt%) in toluene (10 bar, 30 °C).

5. Conclusion

The layer-by-layer method allowed an easy modification of the commercial PERVAP4060 membrane. Using a cold plasma pretreatment, four new composite membranes, well-stable in OSN, were obtained with top dense nanolayers allowing the solvent mass transfer and solutes rejection values to be tuned. Based on the investigations carried out with these membranes using neutral or charged solutes, the following points can be underlined:

- In the range 10-40 bar, well-reproducible results were obtained from toluene feeds, i.e., either binary or ternary mixtures of diluted solutes;
- Except for the smallest molecule, i.e., the alkane C16, high rejection values of the solutes (>80%) were obtained together with high solvent fluxes (7-21 $kg/(h.m^2)$) at 10 bar and 30 °C;
- The four polyelectrolytes used led to the formation of LBLs endowed with various charge densities, which seemed to govern solvent permeation and solute rejection;
- Using 10 bilayers of PEL to functionalize the top surface facilitated distinct OSN performance from the pristine PDMS membrane;
- Higher solvent mass transfer was obtained with the composite membranes having smaller charge density, i.e., PDDA/PSS and PAH/PSS;
- Interestingly, R-BINAP, ToABr, and C44 were highly rejected even at very low feed concentration (0.05wt%); clearly, these results indicate that the transport of the solute must be almost independent of the solvent transport;
- Irrespective of the membrane used, the charged solute ToABr was always the more rejected solute;
- The PAH/PSS pair improved the rejection value of R-BINAP compared to the pristine PDMS membrane, up to 88%;
- The total mass transfer and rejection values can be explained in terms of a resistance-in-series model;

- Experiments recorded with a ternary mixture indicate a significant effect of the C16 concentration, which tends to increase the global flux and decrease the C16 rejection. This result seems to be very promising in the context of the potential application of OSN to olefin metathesis;
- Finally, no aging effect could be detected over several days: both the flux and the rejection values appeared to be steady.

To conclude, the charge density of the LBLs and, hence, the LBL rigidity in organic media, seems to be a key parameter that controls the molecular diffusion and, thus, the permeation through the top nanolayers.

ACKNOWLEDGMENTS

This work is a part of the collaborative project, **ANR-14-CE06-0022**, thanks to the financial support of the French National Research Agency and the support of ARKEMA. Professor S. Abbott is also sincerely acknowledged for the discussion on the Hansen solubility parameters calculations of R-BINAP and ToABr.

References

[1] P. Marchetti, M.F. Jimenez Solomon, G. Szekely, A.G. Livingston, Molecular Separation with Organic Solvent Nanofiltration: A Critical Review, Chem. Rev. 114 (2014) 1073510806. doi:10.1021/cr500006j.
[2] L.Y. Ng, A.W. Mohammad, C.Y. Ng, A review on nanofiltration membrane fabrication and modification using polyelectrolytes: Effective ways to develop membrane selective barriers and rejection capability, Adv. Colloid Interface Sci. 197198 (2013) 85107. doi:10.1016/j.cis.2013.04.004.
[3] D.L. Oatley-Radcliffe, M. Walters, T.J. Ainscough, P.M. Williams, A.W. Mohammad, N. Hilal, Nanofiltration membranes and processes: A review of research trends over the past decade, J. Water Process Eng. 19 (2017) 164171. doi:10.1016/j.jwpe.2017.07.026.
[4] A.W. Mohammad, Y.H. Teow, W.L. Ang, Y.T. Chung, D.L. Oatley-Radcliffe, N. Hilal, Nanofiltration membranes review: Recent advances and future prospects, Desalination. 356 (2015) 226254. doi:10.1016/j.desal.2014.10.043.
[5] J. Bassil, H. Alem, G. Henrion, D. Roizard, Tailored adhesion behavior of polyelectrolyte thin films deposited on plasma-treated poly(dimethylsiloxane) for functionalized membranes, Appl. Surf. Sci. 369 (2016) 482491. doi:10.1016/j.apsusc.2016.01.146.
[6] P. Ahmadiannamini, X. Li, W. Goyens, B. Meesschaert, W. Vanderlinden, S. De Feyter, I.F.J. Vankelecom, Influence of polyanion type and cationic counter ion on the SRNF performance of polyelectrolyte membranes, J. Membr. Sci. 403404 (2012) 216226. doi:10.1016/j.memsci.2012.02.052.
[7] X. Li, W. Goyens, P. Ahmadiannamini, W. Vanderlinden, S. De Feyter, I. Vankelecom, Morphology and performance of solvent-resistant nanofiltration membranes based on multilayered polyelectrolytes: Study of preparation conditions, J. Membr. Sci. 358 (2010) 150157. doi:10.1016/j.memsci.2010.04.039.
[8] E.M. Liston, L. Martinu, M.R. Wertheimer, Plasma surface modification of polymers for improved adhesion: a critical review, J. Adhes. Sci. Technol. 7 (1993) 10911127. doi:10.1163/156856193X00600.
[9] S. Lazare, V. Granier, Ultraviolet Laser Photoablation of Polymers: A Review and Recent Results, Laser Chem. (1989). doi:10.1155/1989/18750.
[10] H. Alem, F. Blondeau, K. Glinel, S. Demoustier-Champagne, A.M. Jonas, Layer-by-Layer Assembly of Polyelectrolytes in Nanopores, Macromolecules. 40 (2007) 33663372. doi:10.1021/ma0703251.

[11] H. Alem, A.-S. Duwez, P. Lussis, P. Lipnik, A.M. Jonas, S. Demoustier-Champagne, Microstructure and thermo-responsive behavior of poly(N-isopropylacrylamide) brushes grafted in nanopores of track-etched membranes, J. Membr. Sci. 308 (2008) 7586. doi:10.1016/j.memsci.2007.09.036.
[12] G. Decher, Fuzzy Nanoassemblies: Toward Layered Polymeric Multicomposites, Science. 277 (1997) 12321237. doi:10.1126/science.277.5330.1232.
[13] H. Alem, F. Blondeau, K. Glinel, S. Demoustier-Champagne, A.M. Jonas, Layer-by-Layer Assembly of Polyelectrolytes in Nanopores, Macromolecules. 40 (2007) 33663372. doi:10.1021/ma0703251.
[14] W. Lenk, J. Meier-Haack, Polyelectrolyte multilayer membranes for pervaporation separation of aqueous-organic mixtures, Desalination. 148 (2002) 1116. doi:10.1016/S0011-9164(02)00645-8.
[15] P. Ahmadiannamini, X. Li, W. Goyens, N. Joseph, B. Meesschaert, I.F.J. Vankelecom, Multilayered polyelectrolyte complex based solvent resistant nanofiltration membranes prepared from weak polyacids, J. Membr. Sci. 394395 (2012) 98106. doi:10.1016/j.memsci.2011.12.032.
[16] X. Li, S. De Feyter, D. Chen, S. Aldea, P. Vandezande, F. Du Prez, I.F.J. Vankelecom, Solvent-Resistant Nanofiltration Membranes Based on Multilayered Polyelectrolyte Complexes, Chem. Mater. 20 (2008) 38763883. doi:10.1021/cm703072k.
[17] J. Ruths, F. Essler, G. Decher, H. Riegler, Polyelectrolytes I: Polyanion/Polycation Multilayers at the Air/Monolayer/Water Interface as Elements for Quantitative Polymer Adsorption Studies and Preparation of Hetero-superlattices on Solid Surfaces , Langmuir. 16 (2000) 88718878. doi:10.1021/la000257a.
[18] T.E. Benavidez, C.D. Garcia, Spectroscopic ellipsometry as a complementary tool to characterize coatings on PDMS for CE applications: CE and CEC, Electrophoresis. 37 (2016) 25092516. doi:10.1002/elps.201600143.
[19] P. Kumlangdudsana, A. Tuantranont, S.T. Dubas, L. Dubas, Polyelectrolyte multilayers coating for organic solvent resistant microfluidic chips, Mater. Lett. 65 (2011) 36293632. doi:10.1016/j.matlet.2011.07.038.
[20] M. Morshed, D. Roizard, H. Alem, H. Simonaire, Investigation of OSN properties of PDMS membrane for the retention of dilute solutes with potential industrial applications (submitted article).
[21] J. Choi, M.F. Rubner, Influence of the Degree of Ionization on Weak Polyelectrolyte Multilayer Assembly, Macromolecules. 38 (2005) 116124. doi:10.1021/ma048596o.
[22] K. Jrrendahl, H. Arwin, Multiple sample analysis of spectroscopic ellipsometry data of semi-transparent films, Thin Solid Films. 313314 (1998) 114118. doi:10.1016/S0040-6090(97)00781-5.
[23] H. Ben Soltane, D. Roizard, E. Favre, Effect of pressure on the swelling and fluxes of dense PDMS membranes in nanofiltration: An experimental study, J. Membr. Sci. 435 (2013) 110119. doi:10.1016/j.memsci.2013.01.053.
[24] H. Ben Soltane, D. Roizard, E. Favre, Study of the rejection of various solutes in OSN by a composite polydimethylsiloxane membrane: Investigation of the role of solute affinity, Sep. Purif. Technol. 161 (2016) 193201. doi:10.1016/j.seppur.2016.01.035.
[25] .W. Imre, M. Schnhoff, C. Cramer, A conductivity study and calorimetric analysis of dried poly(sodium 4-styrene sulfonate)/poly(diallyldimethylammonium chloride) polyelectrolyte complexes, J. Chem. Phys. 128 (2008) 134905. doi:10.1063/1.2901048.
[26] A. Akyz, G. Buyukunsal, A. Paril, Online monitoring of diallyldimethylammonium chloride polymerization, Polym. Eng. Sci. 54 (2014) 13501356. doi:10.1002/pen.23683.
[27] S.R. Lewis, S. Datta, M. Gui, E.L. Coker, F.E. Huggins, S. Daunert, L. Bachas, D. Bhattacharyya, Reactive nanostructured membranes for water purification, Proc. Natl. Acad. Sci. 108 (2011) 85778582. doi:10.1073/pnas.1101144108.
[28] A. Vidyasagar, C. Sung, K. Losensky, J.L. Lutkenhaus, pH-Dependent Thermal Transitions

in Hydrated Layer-by-Layer Assemblies Containing Weak Polyelectrolytes, Macromolecules. 45 (2012) 91699176. doi:10.1021/ma3020454.
[29] H.C. Zhao, X.T. Wu, W.W. Tian, S.T. Ren, Synthesis and Thermal Property of Poly(Allylamine Hydrochloride), Adv. Mater. Res. 150151 (2010) 14801483. doi:10.4028/www.scientific.net/AMR.150-151.1480.
[30] W. John, C. Buckley, E. Jacobs, Synthesis and use of polyDADMAC for water purification, in: Water Institute of Southern Africa (WISA), 2002: p. 14.
[31] K. Khler, D.G. Shchukin, H. Mhwald, G.B. Sukhorukov, Thermal Behavior of Polyelectrolyte Multilayer Microcapsules. 1. The Effect of Odd and Even Layer Number, J. Phys. Chem. B. 109 (2005) 1825018259. doi:10.1021/jp052208i.
[32] Y. Zhang, F. Li, L.D. Valenzuela, M. Sammalkorpi, J.L. Lutkenhaus, Effect of Water on the Thermal Transition Observed in Poly(allylamine hydrochloride)Poly(acrylic acid) Complexes, Macromolecules. 49 (2016) 75637570. doi:10.1021/acs.macromol.6b00742.
[33] Y. Zhang, P. Batys, J.T. ONeal, F. Li, M. Sammalkorpi, J.L. Lutkenhaus, Molecular Origin of the Glass Transition in Polyelectrolyte Assemblies, ACS Cent. Sci. 4 (2018) 638644. doi:10.1021/acscentsci.8b00137.
[34] P. Nestler, M. Pavogel, C.A. Helm, Influence of Polymer Molecular Weight on the Parabolic and Linear Growth Regime of PDADMAC/PSS Multilayers, Macromolecules. 46 (2013) 56225629. doi:10.1021/ma400333f.
[35] B. Schoeler, G. Kumaraswamy, F. Caruso, Investigation of the Influence of Polyelectrolyte Charge Density on the Growth of Multilayer Thin Films Prepared by the Layer-by-Layer Technique, Macromolecules. 35 (2002) 889897. doi:10.1021/ma011349p.
[36] M. Schnhoff, Layered polyelectrolyte complexes: physics of formation and molecular properties, J. Phys. Condens. Matter. 15 (2003) R1781. doi:10.1088/0953-8984/15/49/R01.
[37] A.J. Ashworth, Relation between gas permselectivity and permeability in a bilayer composite membrane, J. Membr. Sci. 71 (1992) 169173. doi:10.1016/0376-7388(92)85016-C.
[38] C.M. Hansen, Hansen Solubility Parameters: A Users Handbook, Second Edition, Second, CRC Press, 2007.

Supplementary materials

Figure SM1: Evolution of the water contact angle (WCA) of PERVAP4060 after plasma treatment: evidence of hydrophobic recovery with time.

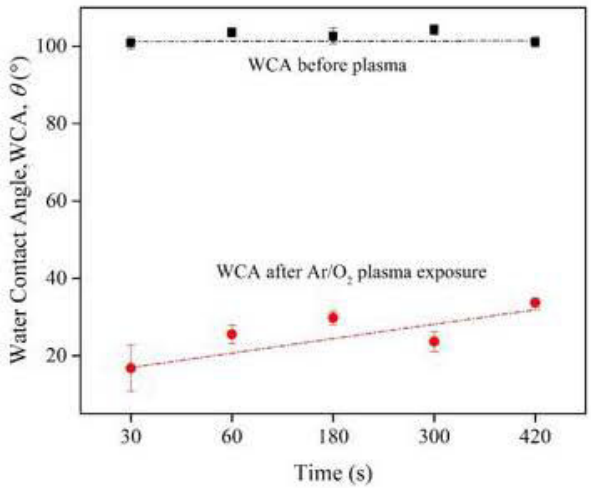

Figure SM2: Defect-free surface after PEL deposition onto PDMS

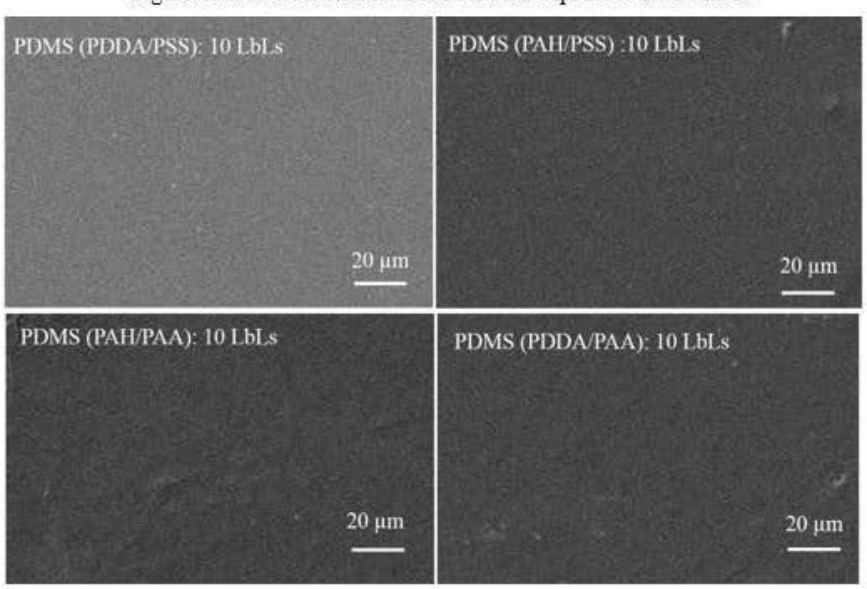

Complimentary results

Concerning the surface modification approach by polyelectrolytes multilayer (PEM), several possible scenarios can be envisioned relating the permeation-separation through PEM-composite membranes.

1. Upon PEM deposition, two possible membrane structure are expected based on the initial substrate used. If the initial substrate is porous, **Figure** 3.1a is likely to occur in which thin PEM layers forms on the surface and permeation of molecule, first, will take place in PEM layer followed by porous sublayer (**Chapter 4**).

2. In contrary, the PEM on the dense layer, in **Figure** 3.1b govern a double dense layer in which permeation of molecule will occur first in the PEM layer followed by the second dense layer, as shown in **Figure** 3.1b, studied in this chapter.

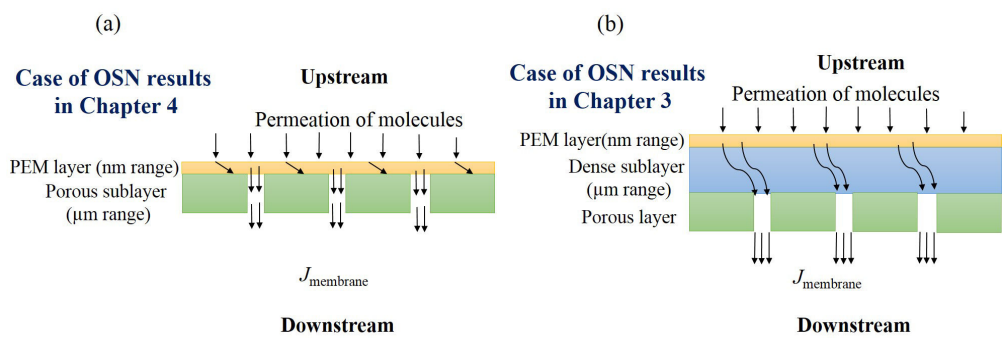

Figure 3.1: Scheme of molecular permeation (a) in a PEM layer having a porous sublayer. (b) in PEM nanolayer followed by a dense sublayer with porous support.

3.5 Transport mechanism through PEM composite membrane

Addition of nanolayers on the membrane, despite porous or dense sublayer/s, could induce additional resistance toward the molecule to pass through the membrane, thereby, resistance in series model would be logical which describes the total resistance to permeation through the membrane is the sum of the resistance to flows in each of the layers.

In molecular transport, as shown in **Figure** 3.1a, when a molecule diffuse through the PEM layer, considering PEM is dense, they only can exit through the pore but restricted to space apart from the pore. When the porosity of the support is low, this phenomenon causes an increase of resistance, affecting the permeance by giving an additional diffusion resistance to intrinsic membrane resistance (Wijmans and Hao, 2015). Such phenomena were previously reported for microfiltration (Davis and Ethier, 1993), UF, and NF (Ramon et al., 2012). This type of transport mechanism will be considered in the next chapter dealing with polyelectrolytes (PELs) deposition on the porous support.

One convenient solution to the above problem is placing a highly permeable dense layer between the porous support and selective top layer, which is often termed as the gutter layer (Cabasso and Lundy, 1986). In **Figure** 3.1b, if the dense sublayer is highly permeable and non-selective, it acts

as a gutter layer. The high permeable gutter layer allows the molecule to passes through smoothly without giving high additional diffusion resistance.

The effect of the gutter layer on permeance is presented in **Figure** 3.2 (Wijmans and Hao, 2015) in which the authors show that the relative permeance is largely affected by the permeability (P) ratio of gutter layer (g) and selective layer (s) (P_g/P_s): For a larger (P_g/P_s), the relative permeance was higher.

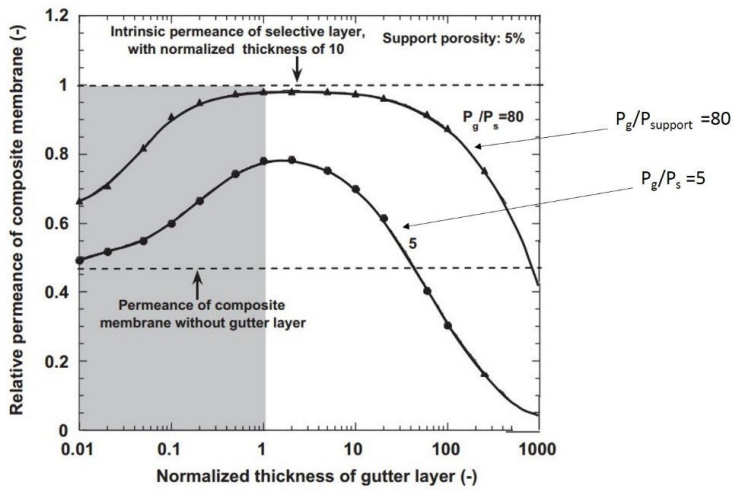

Figure 3.2: Effect of a gutter layer on the permeance of a composite membrane as a function of the thickness of the gutter layer. Adopted from (Wijmans and Hao, 2015).

This example shows very well the combined effect of double-dense layer system within a composite structure.
Clearly, the adopted PEM modification in this study is comparable with the **Figure** 3.1b, adding the following additional advantages over the literature dealing with gutter layer:

1. The PDMS in the polyelectrolytes multilayer (PEM) modified composite will act as a gutter layer, which is highly permeable, thereby, additional mass transport resistance can be avoided. Besides, compared to the **Figure** 3.1b, applying PEM on PDMS with the desired thickness is straight-forward, without complicated nanolayer adhesion procedure.

2. PDMS is highly selective while the gutter layer is generally non-selective, which is expected to be advantageous to obtain an increased selectivity from PEM and PDMS. At least the minimum selectivity would be the same as the selectivity of PDMS.

3. Finally, the PEM layer is expected to reduce the PDMS swelling, which also could be a competitive advantage over conventional PDMS membranes, to limit possible coupling.

3.6 Characterization of modified PDMS

3.6.1 Water contact angle before and after OSN in PDMS based PERVAP 4060

The contact angles of pristine PDMS (PERVAP 4060) have been measured using water, glycerol, and Diiodomethane (Table 1) showing that this commercial membrane has a hydrophobic surface

with moderate surface wettability.

Water contact angle (°)	**Glycerol contact angle** (°)	**Di-iodomethane contact angle** (°)	**Surface free energy** (mJm^{-2})	T_g (°)
103 ± 3	99 ± 2	68 ± 2	$19 - 23$	-123

Table 3.1: Contact angles and surface energy of pristine PERVAP 4060.

Next, the influence of OSN condition on PERVAP 4060 (if any) has been tested by measuring the water contact angles before and after OSN **Table** 3.1. Each data presented in **Table** 3.1, corresponds to the contact angles measured in several coupons of PERVAP 4060 from two different sheets of membranes. These membranes have been pre-conditioned for overnight and then exposed in OSN for $6-8$ hours using toluene and ethanol at $30°C$, $10-40$ bar, $10-14$ kg/h cross-flow rate. After the OSN test, the membrane coupons have been dried overnight at $30°C$, and water contact angles have been measured before and after OSN.

Water contact angle(°), **before OSN**	**Water contact angle**(°), **after OSN (up to 40 bar)**
103 ± 3	104 ± 4 (EtOH)
102 ± 1	99 ± 1 (toluene)

Table 3.2: Water contact angle of PERVAP4060 before and after OSN test performed at $30°C$, 10-40 bar and 10-14 Kg/h tangential feed flow rate.

The contact angle values in **Table** 3.2 indicates that the PERVAP 4060 preserve its surface properties before and after OSN, indicating its compatibility to use under OSN condition up to 40 bar. Initially, PERVAP 4060 was intended to use for pervaporation (PV) application, according to the supplier. For the first time,(Ben Soltane et al., 2013) (Ben Soltane et al., 2016) showed several promising permeation-rejection results using PERVAP 4060 up to 20 bar. In this study, those coupon exposed in OSN condition up-to 40 bar stored as reference membrane and exposed in OSN with toluene up to 40 bar for several times throughout three years. Each time, the membrane exposed to OSN, the water contact angles measured after drying at $30°C$ overnight. The unaltered surface hydrophilicity of PERVAP 4060 over three years **Figure** 3.3 and respective average toluene permeance (P_{avg}) indicates its excellent stability.

3.6.2 Effect of plasma and polyelectrolytes multilayer by water contact angles

This section reports the surface contact angles that correspond to the different stages of surface modification. In this context, an orderly investigation have been performed: the effect of plasma exposure on PERVAP 4060, the effect of storing time after plasma exposure and the effect of plasma and polyelectrolytes on the surface of PERVAP 4060.

3.6.2.1 Plasma effect by surface hydrophilicity

The plasma effect on PERVAP 4060 has been investigated by the evolution of the water contact angles with time; once the membrane exposed to plasma. First, PERVAP 4060 samples (5cm×3cm)

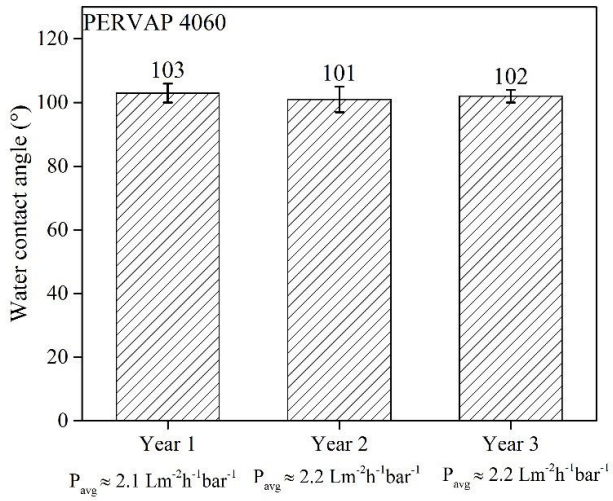

Figure 3.3: Stability of PERVAP 4060 in terms of contact angles and OSN toluene permeance, measured randomly using the same test membrane coupon over three years at 30°C with 10-14 kg/h cross-flow rate. Apart from the OSN test, these membrane coupon stored in room condition.

have been exposed to Ar/O_2 (400/40$sccm$) plasma for five minutes following the contact angles measurement with a time interval of five minutes, 30 minutes and finally after 10 days from the time of exposure. The hydrophilicity change over time has been observed in **Figure** 3.4, which shows an evolution from hydrophilic to hydrophobic changes of PERVAP 4060 surface.

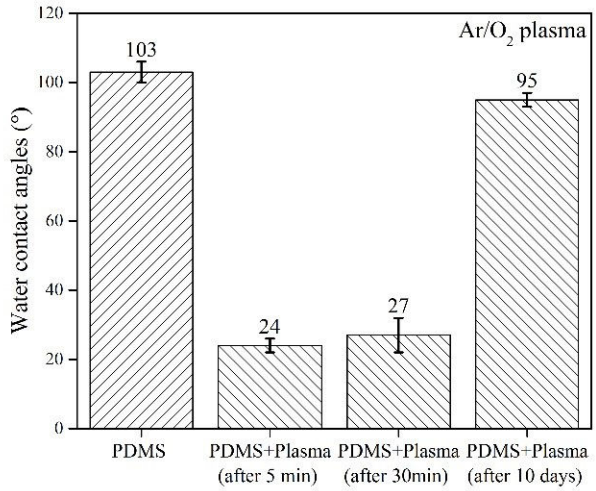

Figure 3.4: Effect of Ar/O_2 plasma on PDMS and recovery of hydrophobicity with time.

Initially, the Ar/O_2 plasma convert the membrane surface to hydrophilic from hydrophobic. Between 5 minutes to 30 minutes, the hydrophilicity change was very small, merely undetectable. However, after ten days, the significant changes in contact angle were obtained, indicating the recovery of the membranes initial state of a hydrophobic surface.

Indeed, the application of plasma for a short exposure introduce functional group on the surface (Nunes and Peinemann, 2006) or ablation and re-deposition of low molecular weight species occurs, when exposed for a long time in the scale of several minutes (Petrov et al., 2012), resulting the surface from hydrophilic to hydrophobic (Nunes and Peinemann, 2006) (Volkov et al., 2014), despite the differences in the exposure time. This recovery of hydrophobicity is caused by the migration of the low molecular weight species on the surface (Lawton et al., 2005), which is well documented for PERVAP 4060 by the (Bassil et al., 2016a), showing the evolution from 25 to 30° in the first 30 min after the exposure.(Bodas and Khan-Malek, 2006) (Bodas and Khan-Malek, 2007) showed the recovery of hydrophobicity of PDMS was more than 90% after 15 days of plasma exposure. In this study, presented in **Figure** 3.4, comparable data have been obtained as found in the literature.

This measurement bears importance on two aspects of OSN protocol development:

- The plasma of Ar/O_2 is highly effective to modify the surface of PERVAP 4060; however, the exposure time needs to be minimum in order to avoid the ablation, i.e., destruction of the surface. The plasma exposure time has been optimized by varying the plasma exposure duration from the 30s to 7 min which concludes that a 30s exposure time is sufficient to activate the surface (Annex of article 3)

- The plasma-modified membrane needs to be used for further modification without a long delay to avoid its hydrophobic recovery. The polyelectrolyte multilayer deposition after plasma activation of PERVAP 4060 needs to be within 30-45 minutes of the exposure.

3.6.2.2 Polyelectrolytes choice and water contact angles after the deposition of multilayers on PDMS

Polyelectrolytes modification have been carried out using four pairs of polyelectrolytes. Among them, two strong (PDDA and PSS) and two weak polyelectrolytes (PAH and PAA) have been used. The strong polyelectrolytes mean their degree of dissociation in water is 100%, and weak polyelectrolytes dissociate partially. A pH of 6.5 was used in each deposition to facilitate a considerable degree of dissociation (Choi and Rubner, 2005) (Yoo et al., 1998).

Several vital aspects have taken into consideration for the choice of polyelectrolytes:

1. In literature, PDDA, PSS, PAH and, PAA are reported as highly stable in organic media including harsh aprotic solvents (Cheng et al., 2014a) (Kumlangdudsana et al., 2011), highly resistant and stable to mechanical stress (Marchetti et al., 2014a) and improve separation characteristics (Imre et al., 2008), (Akyüz et al., 2014), (Lewis et al., 2011), (Vidyasagar et al., 2012) (Zhao et al., 2011b) (Zhao et al., 2011a) (John et al., 2002). These are the properties expected from a right OSN membrane which favors polyelectrolytes multilayer to take into account for the new generation prototype membranes.

2. Different polyelectrolyte means different charge density within the PEM matrix. Also, charge density act as physical cross-linker from which it is expected to obtain improved separation behavior from PEM.

3. Once formed on PDMS, the prototype membrane is expected to obtain as a selective nanolayer

on the top and a rubbery-selective PDMS underneath. Such composite is expected to show high performance in separation.

The polyelectrolytes (PELs) and their multilayers (PEMs) configuration are presented in **Figure** 3.5.

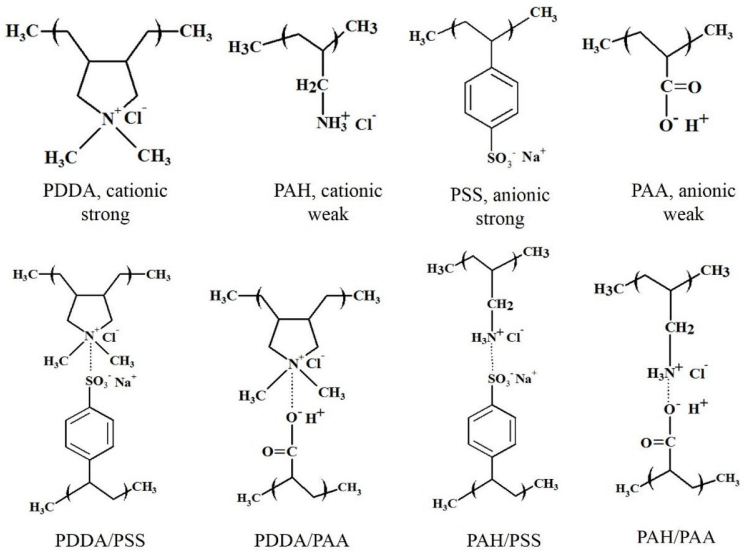

Figure 3.5: Chemical structures of polyelectrolytes (top) and their multilayers (bottom).

After plasma activation of PERVAP 4060, first, polycation has been deposited followed by polyanion deposition having rinsing steps in between and the whole cycle have repeated for desired bilayers number. Ten bilayers of PEM have been taken into account considering that, a higher bilayer number could ensure full surface coverage and minimizes the chance to left uncovered space on the surface.

Though, many works of literature dealing with polyelectrolyte deposition report a formation of 4 to 6 bilayer is satisfactory for defect-free full surface coverage.

The water contact angles of the modified membrane have been then measured and compared with pristine PDMS and plasma modified PDMS (**Figure** 3.6).

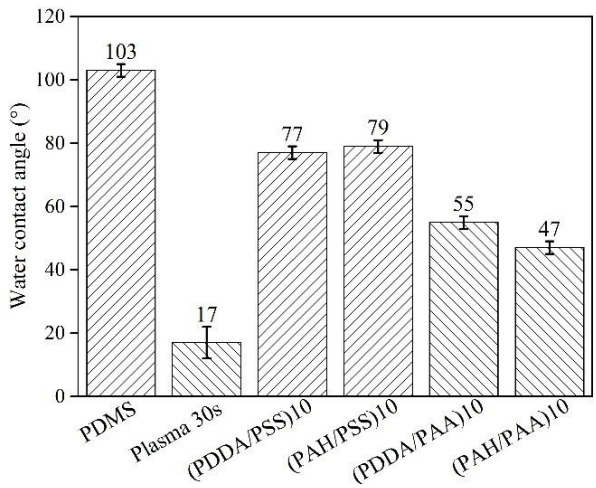

Figure 3.6: Chemical structures of polyelectrolytes (top) and their multilayers (bottom).

As expected, plasma treatment induces very low water contact angle, compared to the pristine PERVAP 4060, due to the negative charges created by the plasma. In all cases, the contact angle values are lower than the contact angle of pristine PDMS and higher than the contact angle of the plasma-modified membrane. The PSS ended multilayers shows higher contact angle than PAA ended ones which could be linked to the high molecular weight and thereby high rugosity of PAA.

The obtained values confirm the successful modification of the PDMS via plasma and polyelectrolytes, and surface hydrophilicity is tunable only by changing the type of polyelectrolytes.

3.7 Ellipsometric thickness of polyelectrolytes multilayer

The thickness of polyelectrolytes multilayers (PEMs) is an important parameter often used in PEM characterization, which to some extent, conveys the information about stability, swellability, and mechanical properties (Picart, 2008).
In this study, the thickness measurement is more targeted to correlate the result in several aspects:

(1) The rejection of solutes could be a result of charge density and thickness.
(2) The bilayer thickness could depend on the charge density of PEM exhibiting a possible correlation between theoretical charge density and thickness.
(3) If the same deposition condition results to achieve different thickness when switching from one polyelectrolyte to another, then the PEM thickness may have a dependence on the permeation under OSN condition.
(4) Charge density to thickness and rejection could also be a function of weak or strong polyelectrolytes pair.

In this context, the theoretical charge density of each PEM have been calculated, and presented in **Article 3**, and the thickness of the PEMs have been measured by ellipsometry in **Figure** 3.7, using 2, 5, and 10 bilayers of each PEM; exhibiting a linear increase of thickness with bilayers number. The experimental data have been compared and completed by some literature data (Francius et al., 2016) (Schönhoff et al., 2007) (Nestler et al., 2013) ensuring a good correlation between the measured

values. Furthermore, the Charge Density (CD) data for each PEM pairs are added for comparison. The details of the charge density perspective are discussed in **Article 3**.

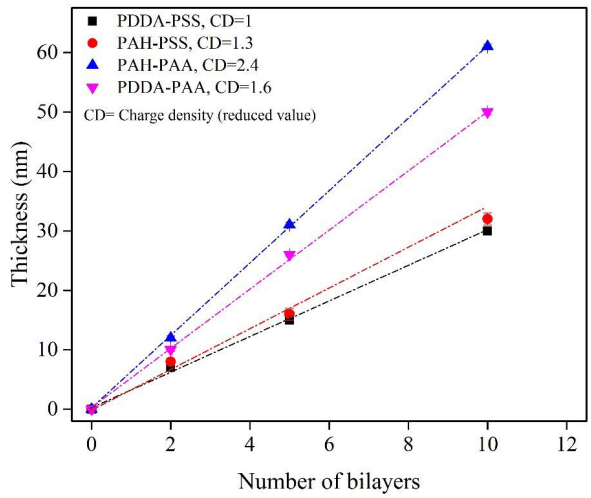

Figure 3.7: Number of bilayers and their thickness in different PEM using ellipsometry data obtained from thickness measurement, compared and completed with the data reported by (Francius et al., 2016)(Schönhoff et al., 2007) (Nestler et al., 2013)

The thickness increment with the number of bilayers is almost linear for each couple of polyelectrolytes multilayer (PEM). The amount of polyelectrolyte mass in PEM increases with the number of bilayers, thus the thickness. However, the PSS ended PEM show lower thickness than PAA ended PEM. The charge density could be one reason for generating the thickness differences from one PEM to another. The highest charge density obtained for PAH-PAA gives the highest thickness per bilayer, whereas the lowest thickness per bilayer for PDDA-PSS exhibiting lowest charge density. As the charge density increases the bilayer thickness also increases due to more complexation point within the PEM (Sun et al., 2005) (Schlenoff and Dubas, 2001).

The thickness differences can be linked with the charge density of each PEM and molecular weight of the PELs, as shown in **Figure** 3.8, providing three cases for low to high thickness of PEM:

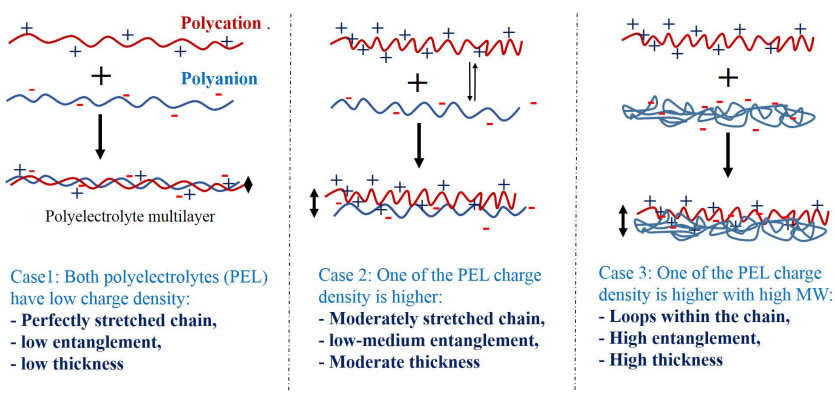

Figure 3.8: Explanation of the polyelectrolytes multilayer (PEMs) thickness when associated with different PELs having low to high charge density and molecular weight.

Case 1: PDDA-PSS: Both polyelectrolytes have low charge density, almost equal which results to a stretched chains conformation due to low complexation point per unit length of PEL without entanglement, and the PEM have low bilayer thickness ($\approx$ 2.5 nm per bilayer).

Case 2: PAH-PSS: PAH charge density is $\approx$ 3 times higher than PSS charge density; thus moderate entanglement occurs due to higher charges, forming relatively a loopy structure within the PEM showing a to a moderate bilayer thickness ($\approx$ 3.5 nm per bilayer).

Case 3: PDDA-PAA and PAH-PAA: The charge density of PAH is $\approx$ 2 times higher than PDDA and $\approx$ 1.5 times higher than PAA. Besides PAA has the highest molecular weight among all PEL; therefore the final PEM most likely to have the coiled conformation within PAA and highly entangled with loops within the PEM, giving a high bilayer thickness ($\approx$ 5nm per bilayer of PDDA/PAA and $\approx$ 6nm per bilayer for PAH-PAA).

3.8 Permeability of pure gases

The permeability of pure CO_2, He and N_2 at 20°C have been measured applying a time-lag method. The aim was to investigate if the PEM on the PERVAP4060 exhibits a dense or porous structure, as well as the nanolayer to be glassy or rubbery.

At first, the permeability of pure gases has been measured in unmodified PERVAP4060. In the following step, the membranes were exposed to Ar/O_2 plasma for less than a minute, and consecutively, 2, 5 and ten bilayers of PDDA/PSS have been deposited on plasma activated PERVAP 4060. The permeability of CO_2, N_2, and He have been measured by time-lag using these prototype membranes (**Figure** 3.9a) and correspondingly the selectivity of CO_2/N_2,(α_{CO_2/N_2}) in **Figure** 3.9. The thickness changes due to polyelectrolytes multilayer (PEMs) were not taken into account for the calculation of permeability from flux measurement as the PEM thickness is significantly lower ($<$ 30 nm for 10 bilayer) than the thickness of the active PDMS layer of the membrane ($\approx 1.5\mu m$).

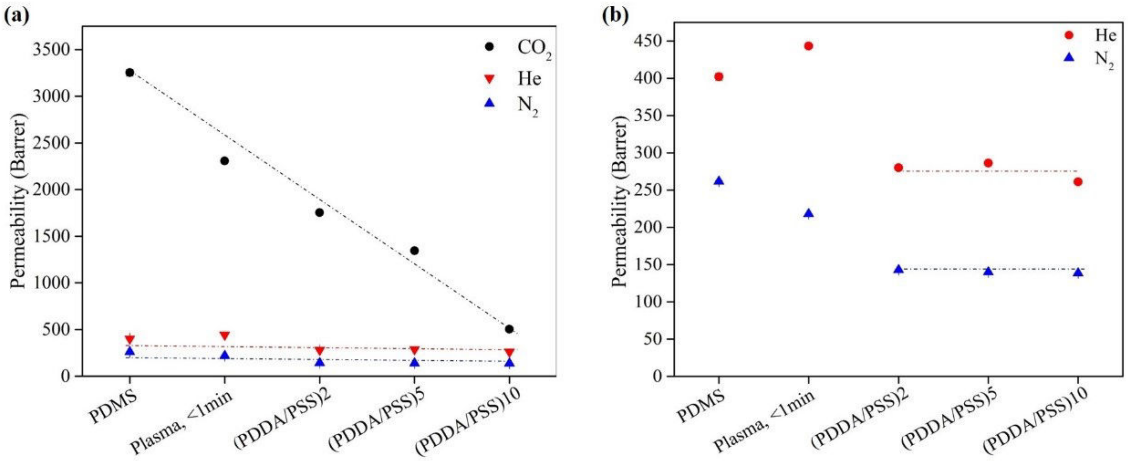

Figure 3.9: Effect of gas permeability in PEM modified PERVAP 4060 at 20°C: (a) CO_2, N_2, and He (b) Enlarged view for N_2 and He permeability.

The results presented in **Figure** 3.9 show that the permeability of CO_2, N_2, and He in PERVAP 4060 is $\approx$ 3200,$\approx$ 260 and $\approx$ 400 Barrer, respectively. (Merkel et al., 2000) (Berean et al., 2014) (Firpo et al., 2015) reported the similar permeability values of CO_2, N_2, and He which validate

the experimental accuracy in the time lag.

The molecular properties of CO_2 and N_2 and their permeability, sorption and diffusion properties are listed in **Table** 3.3 which shows that the sorption of CO_2 in PDMS is ≈ 15 times higher than N_2 giving high CO_2 permeability in PDMS.

Gas molecule	$N \equiv N$	$C(=O)=O$
Unbonded electrons	Two lone pair	Four lone pairs
Lewis acid-base	Neutral, extremely weak	Lewis acid (Polar)
T_c (K)	126	304
S $(cm^3/cm^3.atm)$	0.09	1.29
D (cm^2/s) $\times 10^6$	34	22
P (barrer)	260	3200

Table 3.3: Properties of N_2 and CO_2 and permeability and 20° C, solubility and diffusivity in PDMS. Adopted from (Merkel et al., 2000)

Next, the permeability of CO_2 linearly decreases with plasma and polyelectrolyte bilayers number i.e., with multilayer thickness (**Figure** 3.9a). The CO_2 permeability in plasma activated, 2 and 10 bilayered PERVAP 4060 are ≈ 1.5, ≈ 2 and ≈ 6.5 times lower than in pristine PERVAP 4060.

The N_2 permeability in plasma-activated and two bilayers membrane is about ≈ 1.2, and ≈ 1.5 times lower than the permeability in pristine PERVAP 4060 (**Figure** 3.9b). Afterward, the N_2 permeability in higher bilayer remains fairly constant. The similar trend observed for He permeability. The permeability trend exhibited by the decrease of permeance is very different for CO_2 and for He and N_2. Clearly, it means that the role of the PEM layers is not the same as the composite membranes.

These results indicate several possibilities in explaining the permeability of gases in modified membranes:

(1) The lower CO_2 permeability values in the plasma-activated membrane could be linked to the polar positive charges which repel CO_2, higher than the N_2. Also, plasma assists in the formation of additional crosslinking or incorporate functional groups on the surface (Abetz et al., 2006), which also could affect the T_g; as a result, the permeability of CO_2 decreases significantly.

(2) Once the PEM was introduced, the polar structure of PEM most-likely to play the vital role in reducing the permeability and contributing to add up additional resistance, resulting in lower CO_2 permeability. Also, there might be an effect of the global charge density of PEM. In any PEM system, the global amount of charge increases with the increase of the number of bilayers, which, in return, induces an increased repulsion to CO_2 due to its polar behaviors. As N_2 is a neutral molecule, the permeability of N_2 remains unaltered even when bilayer number is increased whereas the permeability of CO_2 decreased (**Figure** 3.9 and **Table** 3.3).

Indeed, the thickness of PEM (**Figure** 3.7) is much lower than the thickness of the active layer of PERAP4060. At the same time, the total layer number is obtained by the repetition of cationic and anionic layers. In such configuration, the sorption can be assumed to be constant and the only changes made by diffusion. Considering no coupling effect resistance in series can be applied according to the formula:

$$R_i = \frac{l}{P_i} \tag{3.6}$$

The thickness of the bilayers is adopted from **Figure** 3.7, and the thickness of the plasma-treated membrane has been considered to be the same as pristine PERVAP 4060. The conversion factor from Barrer to its SI unit:

$$1Barrer = 3.35 \times 10^{-16} mol.m/(m^2.s.Pa) \tag{3.7}$$

Applying the equation, the resistance of each membrane has been calculated, and the resistance contribution of PEM (% increase compared to unmodified PDMS) at each modification step has been obtained (**Table** 3.4).

PDMS and PEM nanolayers	Permeability $mol.m/(m^2.s.Pa)$ $\times 10^{+13}$	Resistance (%) increase by plasma or bilayers deposited on PDMS
PDMS	11	-
Plasma treated PDMS	7.7	30
PDMS (PDDA/PSS) 2	5.9	46
PDMS(PDDA/PSS) 5	4.5	59
PDMS (PDDA/PSS)10	1.7	84

Table 3.4: Resistance contribution of PEM when deposited on PERVAP4060.

Using the resistance in series model for a bilayer composite membrane (Ashworth, 1992) **figure** 3.10 demonstrates a scheme of a PEM modified PDMS membrane.

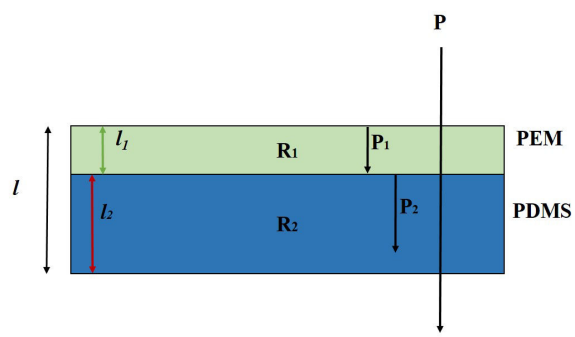

Figure 3.10: Scheme of PDMS (PEM) and resistance-in-series model.

As shown in **figure** 3.10 the overall resistance of the membrane(R)can be expressed as:

$$R = R_1 + R_2 \tag{3.8}$$

$$\frac{l}{P.A} = \frac{l_1}{P_1.A} + \frac{l_2}{P_2.A} \tag{3.9}$$

$$\frac{l}{P} = \frac{l_1}{P_1} + \frac{l_2}{P_2} \tag{3.10}$$

R_1 and R_2 present resistance in PEM and PDMS whereas R is overall resistance. Similarly, P_1, P_2, and P are permeability in PEM, PDMS, and overall permeability coefficient. The overall thickness

l is $1\mu m$, and the thickness of PDDA-PSS is 25 nm for 10 bilayers (as shown in **Figure** 3.7), the surface area of the membrane used for time lag set-up was $3.14 \times 10^{-4} m^2$.

Using the values from **Table** 3.4 in the **Equation** (3.10) , the CO_2 permeability coefficient in (PDDA/PSS)10 was obtained as $5.82 \times 10^{-15} mol.m/(m^2.s.Pa)$, in Barrer, which is 17.4. Next, the permeability values from resistance in series and experimental data are compared in **Table** 3.5.

CO_2	N_2
$P_{PEM} = 17$	$P_{PEM} = 17$
$P_{PDMS} = 3200$	$P_{PDMS} = 260$
Ratio,$(P_{PDMS}/P_{PEM}) \approx 200$	Ratio,(P_{PDMS}/P_{PEM}) $(CO_2/N_2) \approx 15$

Table 3.5: Comparison of permeability values obtained from resistance in series using experimental data.

For CO_2, permeance is well related to the number of bilayers. As bilayer is very thin, $\approx 3nm$ and as the growth is regular, means that the intrinsic resistance of the bilayer is very high compared to PDMS. For He and N_2, the effect of the thickness is less pronounced because the difference of the intrinsic resistance of PDMS and PEM must be smaller. The permeability (P) and the resistance (R) of CO_2 can be compared with He and N_2 as:

$P_{PDMS(He)} << P_{PDMS(CO_2)}$, and $P_{PDMS(N_2)} << P_{PDMS(CO_2)}$
Also, the resistance $R_{PDMS(HeorN_2)} >> R_{PDMS(CO_2)}$
Which indicates to the less influence of R_{PEM} versus the R_{PDMS} for N_2 and He.

The CO_2 permeability in PEM is compared with the different glassy polymers (Minelli and Sarti, 2013), which gives similar values indicating the possibility of PEM to exhibit a glassy structure. The selectivity CO_2/N_2 in PEM, in Figure 11, certainly indicates that the PEM behaves as a dense structure. $\alpha_{CO_2/N_2} > 3$.

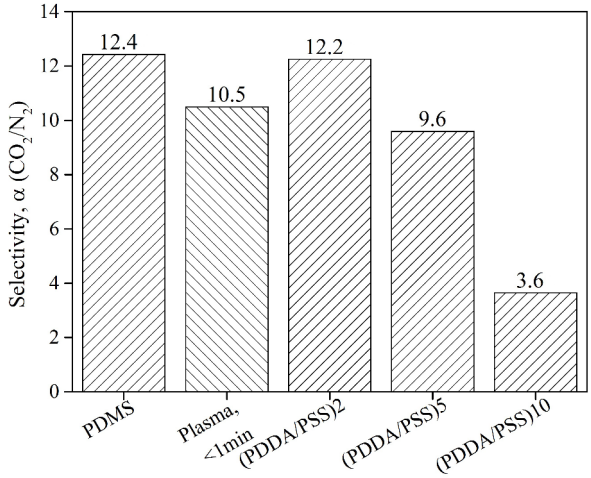

Figure 3.11: Selectivity of CO_2/N_2 in PEM modified PDMS, prepared by plasma and polyelectrolyte modification.

The selectivity of CO_2/N_2 in pristine PERVAP 4060 is ≈ 12.4 (**Figure** 3.11), which in literature reported be in the the range of 11-14 (Selyanchyn et al., 2018). In PEM modified membrane, it

is striking to observe that the selectivity of CO_2/N_2 is reduced with the number of polyelectrolyte (PEL) layers. Hence an specific phenomena should occur with PEL as shown in **Figure** 3.12.

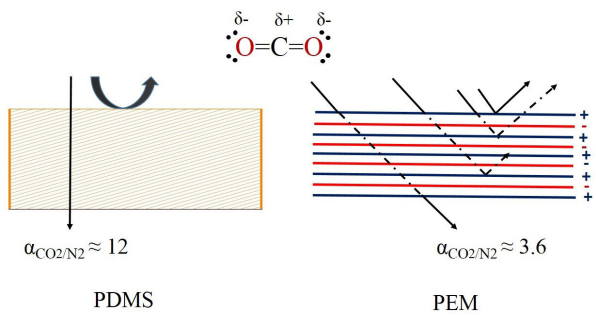

Figure 3.12: Sketch of a possible CO_2 repulsion phenomena by charged polyelectrolytes multilayer that affects the CO_2/O_2 selectivity.

As shown in the **Figure** 3.12, a repulsive interaction between partially charged CO_2 (act as a Lewis acid) to the charged polyelectrolyte multilayers; causing lower selectivity of (CO_2/N_2). The selectivity trend in PEM with bilayer number(**Figure** 3.11) also suggests that at a higher PEM bilayer or in standalone PEM, one may expect to obtain selectivity of N_2/CO_2, which could be highly interesting for the gas separation application.

Next, the PEM thickness and its contribution to the increase of resistance towards CO_2, He and N_2 are showed in **Figure** 3.9 which also indicate to the thickness effect of PEM within the composite, as shown in **Figure** 3.13.

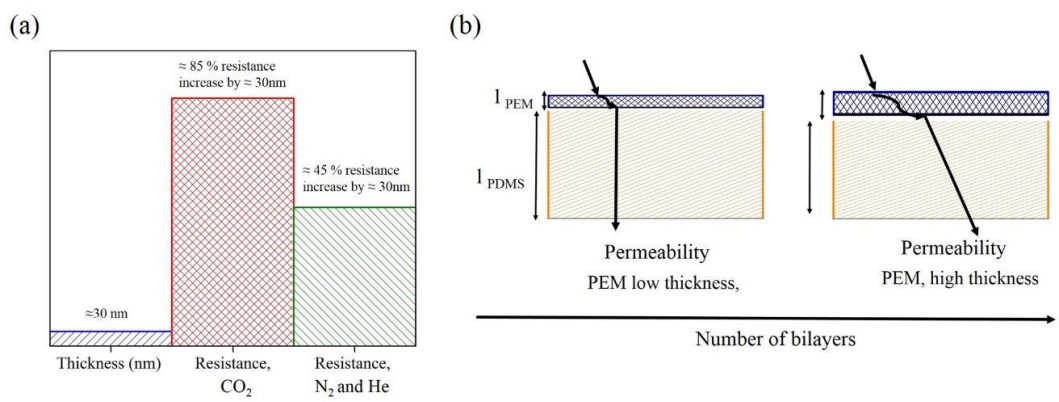

Figure 3.13: (a) Polyelectrolytes multilayer with 10 bilayers and its effect on the increase of resistance (b)PEM thickness with bilayers number and effect of PEM in OSN performance.

Once the thickness of the PEM is increased by adding new bilayers, higher resistance is expected, and at some point, the performance of pristine PDMS will be lost due to the extreme increase of resistance by adding new layers. Therefore a trade-off between the layer number to the highest possible performance can be envisioned.

3.9 Polyelectrolytes chain mobility by Fluorescence recovery after photobleaching (FRAP)

The main interest of the study of polyelectrolytes multilayer (PEMs) chain mobility was to evaluate the PEMs structural property of glassy /rubbery polymer and, next, the molecular diffusion aspect in PEM to explain the OSN result by chain mobility. The glass transition (T_g) temperature of PDMS is $-123°C$ whereas the T_g of PDDA/PSS, PAH/PSS, and PAH/PAA are reported 90, 167, and 45 $°C$ (Imre et al., 2008), (Akyüz et al., 2014), (Lewis et al., 2011), (Vidyasagar et al., 2012) (Zhao et al., 2011b) (Zhao et al., 2011a) (John et al., 2002) indicating to the nature of the PEM to be glassy in structure.

Polyelectrolytes multilayer have been prepared on PERVAP 4060 for FRAP test of chain mobility, which is a method for determining the kinetics of diffusion, capable of quantifying the two-dimensional lateral diffusion of a molecularly thin film containing fluorescently labeled probes. Initially, PDADMAC and PAH were modified by the marker molecule, followed by the deposition of multilayers. Few drops of toluene have been added on the surface (approximately for 1-3 minute) to mimic the condition when PEM is exposed to toluene during OSN, Then, the PEM samples placed under a confocal microscope and bleached in the region of interest (ROI), as shown in **Figure** 3.14, the bigger circle before (a) and after (b) photo-bleaching. Three small unbleached circles near to ROI have been used as a reference area. After bleaching, the intensity recovery or change in the bleached region is monitored continuously.

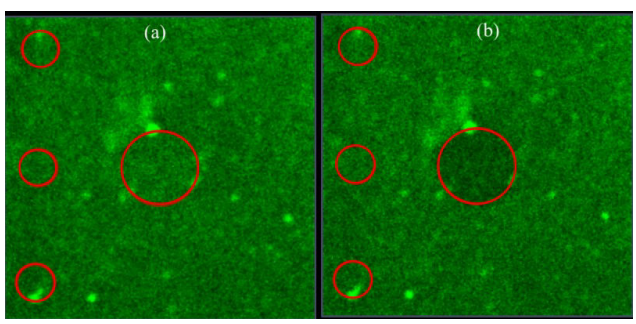

Figure 3.14: Example of a PEM before (a) and after (b) bleaching of the central circular area. The three areas along the left side of the images serve as references.

The evolution of intensities difference between the bleached and unbleached area with the function of time establishes the Fluorescence recovery trend with time. These data enable to determine the chain mobility of the probed polyelectrolyte with the help of simultaneous calculation of mobile fraction and, an immobile fraction (Zheng et al., 2011) (Pincet et al., 2016). The standard protocol for FRAP was adopted (Kang et al., 2012) (Picart et al., 2005) and a details description for the result extraction protocol can be found in **Annex 1**.

Table 3.6 presents the polyelectrolytes chain mobility, often termed as the diffusion coefficient of labeled polyelectrolytes in the multilayer (PEM).

PDMS and PEM	$D(m^2/s) \times 10^{+12}$	$D(m^2/s) \times 10^{+19}$ (literature)
PDMS	0.35-7 (Wong et al., 2010).	
(PDDA/PSS)10	0.43	3 ± 1.5 (Nazaran et al., 2007) 0.5 (Fares and Schlenoff, 2017)
(PAH/PSS)10	77	<1 (Nazaran et al., 2007) (Fares and Schlenoff, 2017)
(PAH/PAA)10	7.9	-
(PDDA/PAA)10	0.56	-

Table 3.6: Polyelectrolytes chain diffusion coefficient by FRAP and comparison with literature.

The experimental data in **Table** 3.6 falls far beyond the comparison with the literature data, indeed, the chain mobility of PEM cannot be same as PDMS or higher than PDMS due to their glassy structure. The reason for obtaining high chain mobility values are not properly understood. It is suspected that, The tested sample may contain free dye molecule that introduces unbound dye diffusion (much larger than the PE chain diffusion).

Also, the experimental procedure in (Nazaran et al., 2007) have been carried out in H_2O, with a spot illumination for 5 min having a bleached area of 60 m. In contrary, the experimental data showed in Table 4 have been carried in toluene media with spot illumination $<$ 1min and the bleached area of $10 - 20\mu m$. Nevertheless, (Nazaran et al., 2007) reports the sample preparation in $0.5MNaCl$, whereas the sample preparation in this study maintained in no salt condition.
However, frequent observation of chain mobility in PEM suggests that the D values increased when polyelectrolytes prepared in salt, which addresses even further complication to rationalize the results from the FRAP experiment.

3.10 Membrane characterization before and after OSN

The characterization of PERVAP 4060 by surface and cross-sectional images are presented in **Article 1**. In **Figure** 3.15, the PERVAP 4060 surface is shown, before and after organic solvent nanofiltration (OSN), showing the unaltered surface of the membrane ensure its preserved surface condition before and after OSN. All the images after OSN test correspond to the membrane that has been exposed to OSN up-to 40 bar using the binary and ternary feed at $30°C$ up to two-week exposure to OSN cell. Worth to mention that the membranes after OSN was stored in a paper folder and no further cleaning step added before SEM observation.

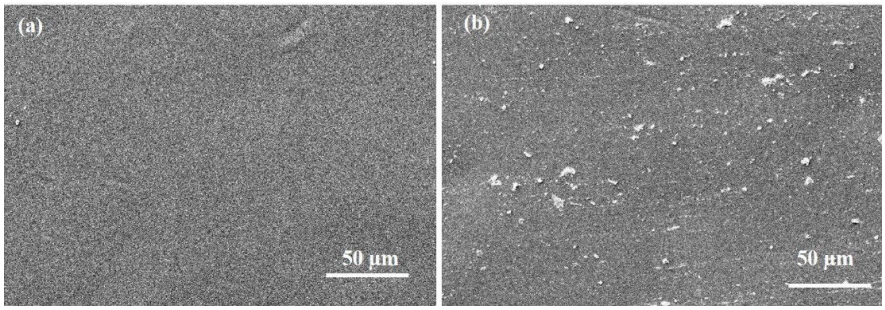

Figure 3.15: Surface images of pristine PDMS (a) before and (b) after OSN; at 30° C, 10-40 bar and 7-10 kg/h cross-flow.

In **Figure** 3.15b, one can notice the presence of pollution on the membrane surface. The origin of this pollution from feed mixture (as if undissolved solute) is less likely because the diluted solute was dissolved offline and observed before and after organic solvent nanofiltration (OSN). However, it seems two possibilities for the origin of pollution in **Figure** 3.15b:

- Each membrane exposed to OSN cell for two weeks while six different OSN measurement has been performed. Afterward, the membrane changeover procedure includes changing the inner gasket from which small particle possibly entered in the circulation system and finally on the membrane surface.

- The pollution can be from the paper folder where the membrane has been stored after the experiment.

Next, the modified membranes have been observed before and after OSN. The **Figure** 3.16- 3.19 shows the surface images of each modified membranes; before and after modification.

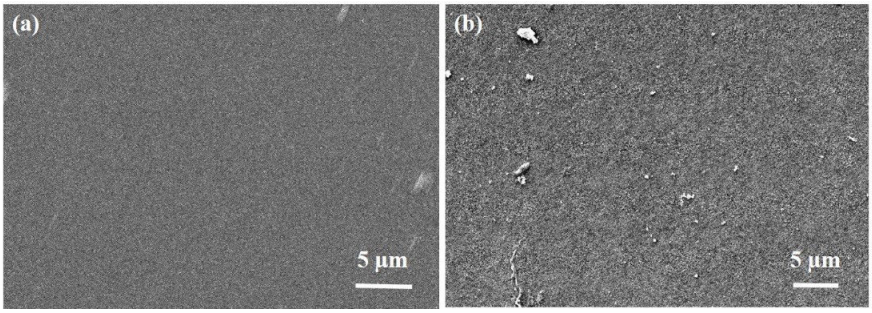

Figure 3.16: Surface image of PDMS (PDDA/PSS)10: (a) before and (b) after OSN; at 30° C, $10-40$ bar and $7-10$ kg/h cross-flow.

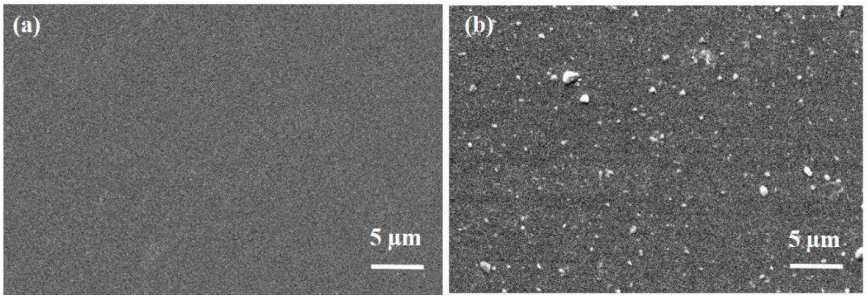

Figure 3.17: Surface image of PDMS (PAH/PSS)10: (a) before and (b) after OSN; at 30°C, $10-40$ bar and $7-10$ kg/h cross-flow.

The similar pollution observed in each membrane after OSN. In **Figure** 3.18 and 3.19, several cracks like lining can be seen in the PEM prepared with PAA. If they are continuous crack or defect, then one can expect the solvent fluxes in prototype membrane to be the same as the fluxes through pristine PERVAP 4060. In reality, much lower toluene permeance ($\approx 0.35 Lm^{-2}h^{-1}bar^{-1}$ in PAH/PAA and ($\approx 0.8 Lm^{-2}h^{-1}bar^{-1}$ in PDDA/PAA) have been observed compared to the toluene permeance in pristine ($\approx 2.1 Lm^{-2}h^{-1}bar^{-1}$. (Discussed in **Article 3**). One hypothesis is, PAA exhibit significant uneven swelling with PDMS, once exposed in toluene. Swelling of PDMS in toluene $\approx$ 114% (Ben Soltane et al., 2013) and PAA swelling in toluene is unknown. If the PEM swelling in toluene is much higher than PDMS, it may induce these crack-like linings. In

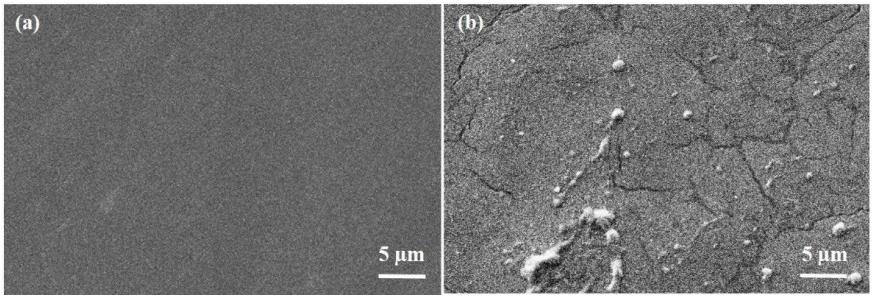

Figure 3.18: Surface image of PDMS (PAH/PAA) 10: (a) before and (b) after OSN; at 30°C, $10-40$ bar and $7-10$ kg/h cross-flow.

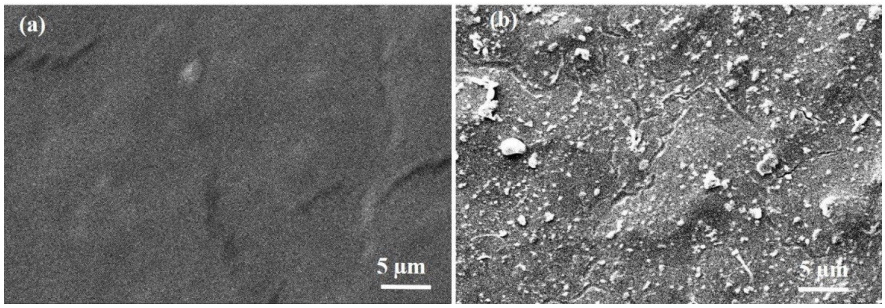

Figure 3.19: Surface image of PDMS (PDDA/PAA) 10: (a) before and (b) after OSN; at at 30°C, $10-40$ bar and $7-10$ kg/h cross-flow.

another way, if PDMS swelling in toluene is higher than swelling of PAA, the same result is expected.

This hypothesis was tested by viewing the PDMS(PAH/PAA)10 membrane in toluene by optical microscope Dino-Lite Edge AM73915MZT (resolution $\times 133-\times 139$). Initially, the surface image has been captured before adding toluene. Next, the samples immersed in toluene overnight, and their surface image was captured from the beginning of immersion to the end of 24 hours, which shows no deformation of the surface. The optical image re-captured again after two days of drying at room temperature, and the sample exhibited its initial surface.

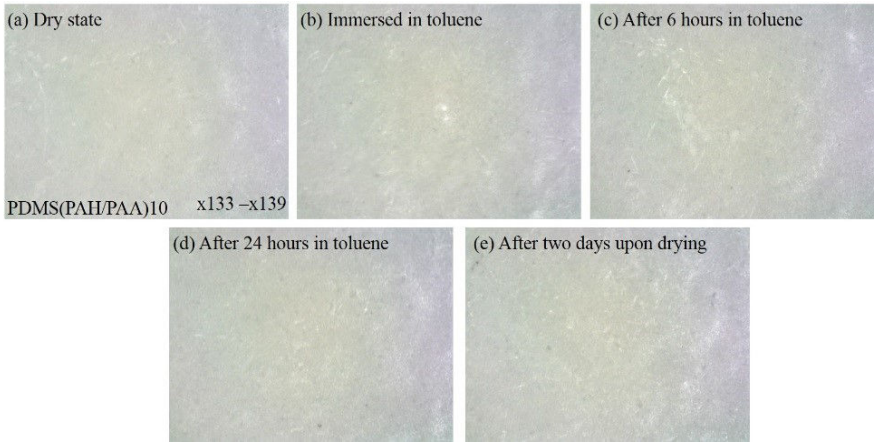

Figure 3.20: Optical image of PDMS (PAH/PAA) 10 surface before and after immersing in toluene for 24 hours, followed by the image after drying.

This test does not justify if the PEM deformation has originated due to the solvent and the deformation observed in **Figure** 3.18 and 3.19 was not fully understood except that these crack-like deformations are not continuous throughout the PEM. Indeed, the relevant question remains as if this deformation occurred due to strong cross-flow at high pressure, which is a subject to investigate.

3.11 Performance of modified PERVAP 4060 (PDMS) membrane

3.11.1 Effect of plasma exposure time on solvent permeation

The effect of plasma on PERVAP 4060 have been studied by ethanol flux measurement in membranes, that exposed to Ar/O_2 plasma for different duration of the 30s and 5 min (**Figure** 3.21a) and their surface contact angles (**Figure** 3.21b).

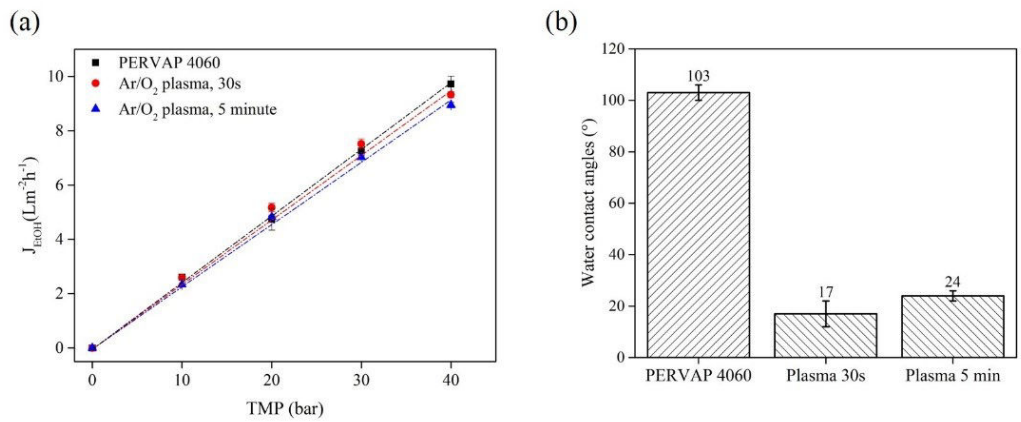

Figure 3.21: Effect of plasma exposure time in PERVAP 4060: (a) ethanol flux up to 40 bar at $30°C$ and $10-14$ kg/h. (b) Water contact angles.

The plasma exposure time has a rather low impact on ethanol flux, $\approx 5-10\%$ lower solvent fluxes, which indicate the low possibility of ablation according to (Lawton et al., 2005) (Bodas and Khan-Malek, 2007). In both cases, the membrane become hydrophilic despite exposure time.
The optimization of plasma exposure is reported in the **Annex of Article 3**, where it was shown that the plasma exposure time could be as low as the 30s in order to activate the surface.

3.11.2 Effect of toluene permeation in PEM prepared without plasma

This study presents the effect of polyelectrolyte multilayer on PERVAP 4060 when deposited without using any plasma. The toluene flux (**Figure** 3.22a) shows no impact on flux; however, the water contact angle values in **Figure** 3.22b shows that the surface hydrophilicity changes slightly.
Clearly, toluene flux presents no effect of the multilayers, but lower contact angle after the modification indicates to the deposition. Indeed, PERVAP 4060 is hydrophobic, and the deposition of polyelectrolytes by LbL on a hydrophobic surface is less favorable due to water-mediated layer-by-layer (LbL). Therefore, even if polyelectrolytes may partially be deposited, it is likely that without plasma, incomplete and irregular surface coverage occurs showing no impact on toluene flux. Besides, (Bassil et al., 2016a) reported a better adhesion phenomena of multilayers on PERVAP 4060 when plasma is used to activate the surface.

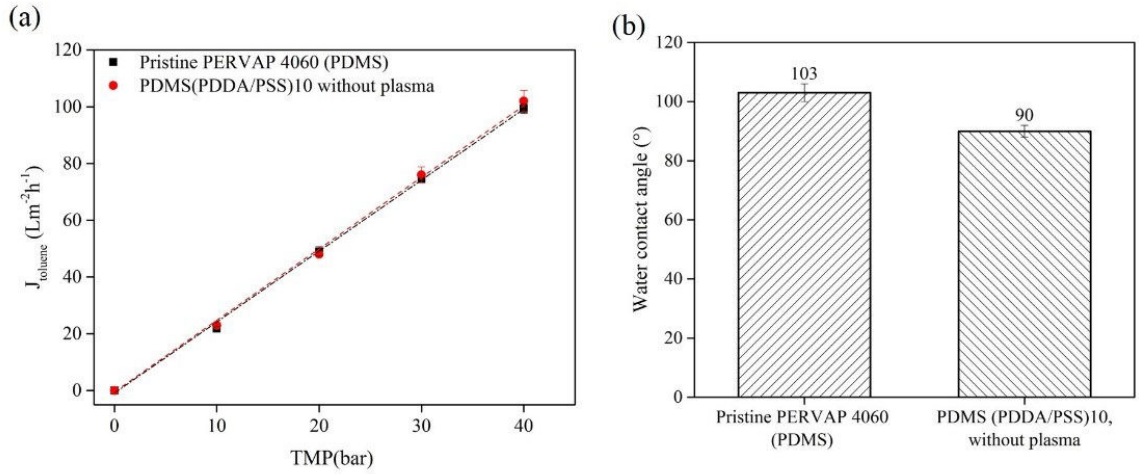

Figure 3.22: Effect of PDDA/PSS of 10 bilayers deposited on PDMS based PERVAP4060 without any plasma: (a) toluene permeation up to 40 bar at 30°C with 10−14 kg/h tangential flow. (b) Water contact angles before and after modification without using any intermediate plasma.

3.11.3 Effect of number of bilayers of PEM on toluene permeation

The effect of bilayers on toluene fluxes has been measured using PDDA-PSS and PAH/PSS on PERVAP 4060 having 5 and 10 bilayers (**Figure** 3.23). This study highlights that the toluene flux in modified membraned is dependent on the type of PEM; while PDDA/PSS with five bilayers has no impact on toluene flux, PAH/PAA induces ≈ 33% lower toluene flux than in pristine.

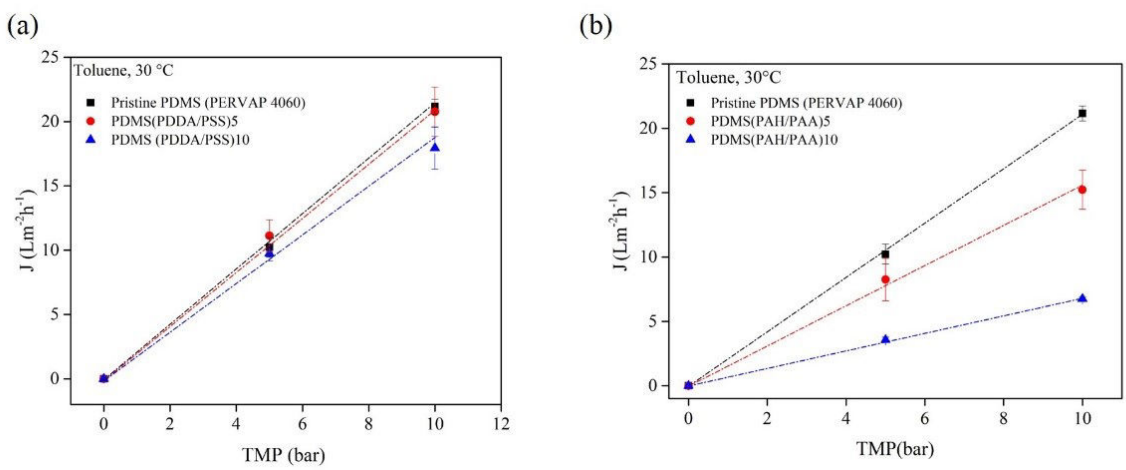

Figure 3.23: Effect of bilayers number on toluene permeation using (a) PDDA/PSS (b) PAH/PAA on PERVAP4060 at 30°C and 10 − 14 kg/h tangential flow.

This study indicates to the choice of bilayers number, as if five bilayers is considered, some PEM such as PDDA/PSS does not ensure full surface coverage based on toluene flux, whereas, PAH/PAA full surface coverage is likely to obtain when bilayers number is even less than five. To keep the homogeneity in the experiment, ten bilayered samples are considered for the rest of the experiment.

3.11.4 Toluene and ethanol permeation in modified membranes

Both toluene and ethanol permeation in pristine and modified PERVAP 4060 have been measured up to 20 bar transmembrane pressure(TMP) (**Figure** 3.24). As expected, each modified membrane exhibits lower flux than pristine with linear evolution of flux with TMP, showing different order based on types of PEM pair as well as the types of solvent used.

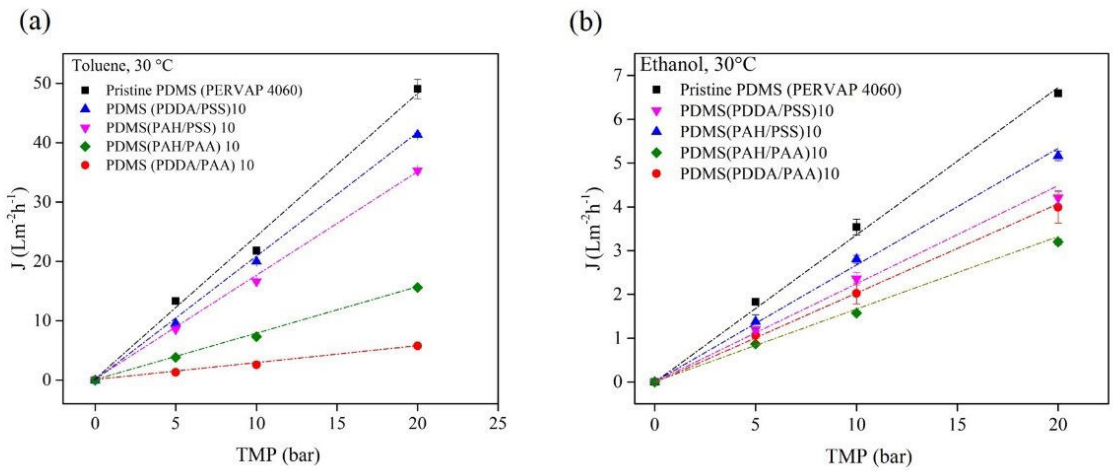

Figure 3.24: Effect of transmembrane pressure on solvent fluxes in polyelectrolytes multilayer (PEMs) modified PERVAP 4060: (a) Toluene (b) EtOH fluxes at $30°C$, $7-10$ kg/h cross flow rate.

The toluene flux in PERVAP 4060 is ≈ 10 fold higher then EtOH flux, which is clearly related to the high PDMS swelling $\approx 114\%$ in toluene than the swelling in EtOH $\approx 5\%$, in a good agreement with the fluxes data reported in (Ben Soltane et al., 2013) (Ben Soltane et al., 2016). As mentioned above, the fluxes in the modified membrane are dependent on the type of PEM, thereby, their interaction with PEM under toluene or EtOH. Different order of flux reduction could be related to:

- The solubility parameter of polyelectrolyte complexes, i.e., PEMs.
- PEMs Charge density and their swelling behavior in toluene and ethanol.
- Finally, toluene and ethanol diffusion coefficient in different PEMs.

3.11.4.1 Tentative prediction of solubility parameters of polyelectrolyte multilayers by Hansen solubility parameter and Fedor group contribution

The estimation of solubility parameter is calculated by group contribution and HsPiP tool. The solubility parameters and molar volume of the polyelectrolytes and their PEM were evaluated by using Hansen solubility parameter approach (HsPiP) (Hansen, 2004) and Fedor group contribution (Fedors, 1974) (**Table** 3.7).

	Group contribution (Fedors, 1974)		HsPiP (Hansen, 2004)	
	δ	M_v	δ	M_v
Unit	$(Mpa)^{1/2}$	(cm^3/mol)	$((Mpa)^{1/2}$	(cm^3/mol)
PDADMAC	17.6	173.4	15.9	151.0
PSS	25.2	84.7	29.5	139.0
PAH	20.0	90.9	19.8	74.0
PAA	22.5	73.1	23.8	70.1
PDDA/PSS	20.4	258.1	24.3	262.0
PAH/PSS	22.6	175.0	19.7	193.0
PAH/PAA	21.1	164.0	22.1	122.0
PDDA/PAA	19.1	246.0	19.7	193.6

Table 3.7: Tentative evaluation of solubility parameter and molar volume of polyelectrolytes and their multilayers.

However, it should be underlined that neither HsPiP nor the group contribution takes into account the charges of the polyelectrolytes system, sometime counter-ion associated with PEM pairs. Therefore, these values possibly do not comply with the real situation of charged chemical species, and using them to explain the OSN results could be misleading. One particular example is (Ferrell et al., 2017), in which the authors show that PSS in H form gives the solubility parameter 40-44 $MPa^{1/2}$, whereas other estimation shows 34 $MPa^{1/2}$ and finally Hidelbrand solubility value for PSS-H is reported 28.8 $MPa^{1/2}$.
In the following part, this evaluation was not used to explain the OSN result.

3.11.4.2 The effect of polyelectrolyte multilayers (PEMs) properties of swelling, charge density and thickness for the permeation of toluene and ethanol

The swelling of polyelectrolyte multilayers in the organic solvent is rarely reported in the literature. (Ferrell et al., 2017) reports the swelling of PSS in toluene and ethanol are ≈ 25% and ≈ 27%, respectively. When PSS combines with PDADMAC, the swelling of PDDA/PSS in EtOH increases to ≈ 112% (Miller and Bruening, 2004); similarly, swelling of PAH/PSS in ethanol is ≈ 92% (Tristan et al., 2008). However, the Ethanol flux thought PDDA(PAH/PSS)10 have been measured higher than the ethanol flux in PDMS(PDDA/PSS)10 despite PEMs higher swelling, which does not explain their flux reduction order, as shown **Figure** 3.24b. Indeed, swelling of the composite membrane must be linked to the individual swelling of PDMS and PEM. For a given PAH/PSS pairs on PDMS, the swelling aspect in toluene and EtOH are shown **Figure** 3.25, which clearly explains high toluene flux in PAH/PSS than low EtOH flux, could be one of the reasons to obtain different flux reduction order.

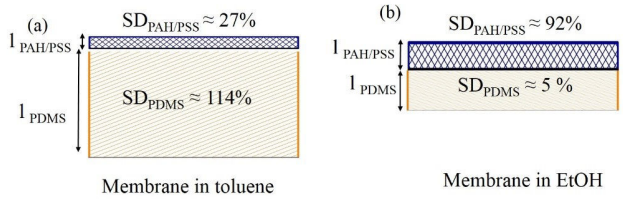

Figure 3.25: Global swelling of prototype membranes in (a) Toluene (b) EtOH. The swelling of PAH/PSS in toluene is adopted from (Ferrell et al., 2017), considering the PSS swelling.

Now, taking the thickness (t) from ellipsometry, charge density (CD) and fluxes of EtOH and

toluene shows that:

$l_{PDDA/PSS} < l_{PAH-PSS}$
$CD_{PDDA/PSS} < CD_{PAH/PSS}$
$J_{PDDA/PSS(toluene)} > J_{PAH/PSS(ethanol)}$

The thickness of PDDA/PSS is lower than the thickness of PAH/PSS which may agree for the first instance to the toluene flux in **Figure** 3.24 but contradict to the EtOH fluxes.

Commonly, the PSS ended PEM shows higher EtOH and toluene fluxes than the PAA ended PEM, which seems to be linked to the charge density, and thereby the high thickness of PEM and low swelling.

3.11.4.3 Estimation of the toluene and ethanol diffusion coefficient in polyelectrolytes multilayer (PEM)

EtOH and toluene diffusion coefficient in PEMs have been estimated using a modified Gierer-Wirtz equation (Evans et al., 2013), which describes the diffusion of a small molecule in the solvent.

$$D = \frac{K_B T(\frac{3\alpha}{2} + \frac{1}{1+\alpha})}{6\pi\eta\sqrt[3]{\frac{3MW}{4\pi\rho_{eff}N_A}}} \tag{3.11}$$

$$\alpha = \sqrt[3]{\frac{MW_s}{MW}} \tag{3.12}$$

where viscosity, η, the effective density of a small molecule, ρ_{eff}, the molecular weight MW_S of the solvent used, and NA, the Avogadro number, to give an estimate of D for a given solute MW.

In this calculation, EtOH and toluene are small molecules, and PEM is considered as highly swollen gel state under the influence of the solvent.
The molecular weight (MW) of polyelectrolytes multilayer has been used as the average MW of polycationic and polyanionic, which is often reported to be valid, according to the literature dealing with polyelectrolytes multilayer. This MW was used to calculate viscosity by using the Mark-Houwink equation, in which Mark-Houwink parameters α is 0.731 and K is 0.0000624 dl/g (reference values for PDMS in toluene) http://www.ampolymer.com/Mark-Houwink.html. These parameters are considered as the same for polyelectrolyte multilayers (PEM). Finally using these values in Gierer-Wirtz equation, both EtOH and toluene diffusion coefficient have been estimated for comparison (**Table** 3.8) among different PEM system. Ethanol and toluene diffusion coefficient in pristine PDMS are taken from (Ben Soltane et al., 2013).

Membrane with PEM	Toluene diffusion coefficient $D_{Toluenen}$ (m^2s^{-1})	EtOH diffusion coefficient D_{EtOH} (m^2s^{-1})
PDMS	1.3×10^{-10}	1.7×10^{-11}
PDDA-PSS	3.2×10^{-13}	5.1×10^{-13}
PAH-PSS	3×10^{-13}	4.7×10^{-13}
PAH-PAA	5.6×10^{-13}	8.9×10^{-13}
PDDA-PAA	5.5×10^{-13}	8.8×10^{-13}

Table 3.8: Toluene and EtOH diffusion coefficient in PEM systems.

Toluene diffusion in PEM is upto 400 times lower, and EtOH diffusion is about 20-40 times lower compare to PDMS. The calculated diffusion coefficient values also presents a clear difference between the diffusion in PSS ended PEM and in PAA ended PEM. However, the order of the solvents diffusion coefficient in different PEM contradict with permeation result due to their apparent differences in sorption.

3.12 Solute rejection in polyelectrolytes multilayer (PEMs) modified PERVAP 4060 (PDMS)

This section presents the OSN results in the continuation of the results presented in **Article 3**. It was shown in the Article that the rejection improved when PAH/PSS modifies PERVAP 4060. This section includes a further study on this membrane including the transmembrane pressure effect up to 40 bar, number of bilayer effect up to 20 bilayers, and salt effect including one study in the ternary system dealing with two solvents and one solute.

3.12.1 Effect of transmembrane pressure (TMP) on toluene flux and R-BINAP rejection in (PAH/PSS) modified PERVAP 4060

The toluene flux and the rejection of R-BINAP have been measured using 10 bilayers of PAH/PSS modified PERVAP 4060, i.e., PDMS (PAH/PSS) 10 in the pressure range of 10-40 bar (**Figure** 3.26a). The flux evolution in both membranes is linear, showing lower flux in PDMS (PAH/PSS) 10 and steady R-BINAP rejection up to 40 bar (**Figure** 3.26b). After a complete run up to 40 bar, the measurement repeated at 10 bar, and indicating of hysteresis. Thus the membranes are well stable in the pressure range and the steady rejection indicates the mass transfer mechanism to be solution-diffusion.

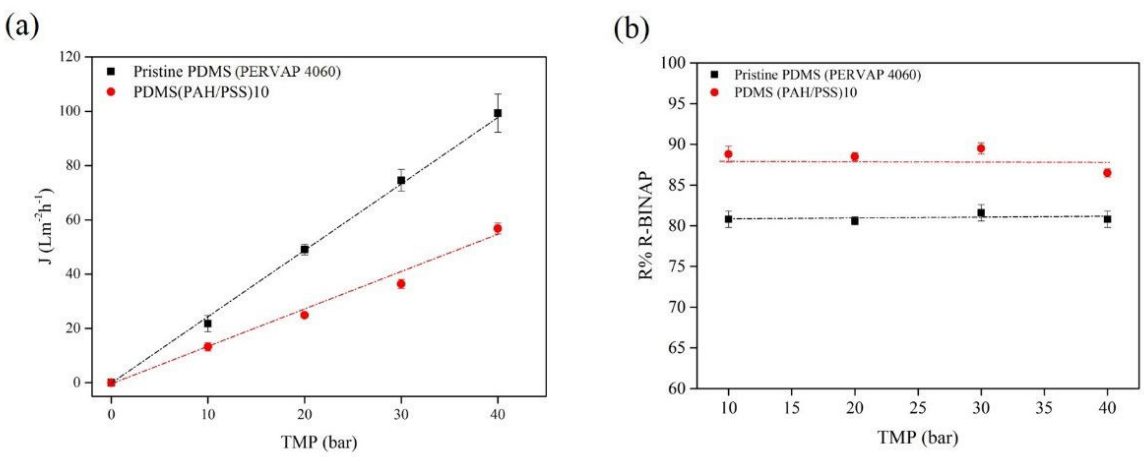

Figure 3.26: Effect of transmembrane pressure on (a) toluene flux (b) R-BINAP rejection at $30°C$ and $7-10$ kg/h cross-flow of diluted R-BINAP ($0.05wt.\%$) in toluene.

The nanolayer of PAH-PSS clearly gives additional mass transfer resistance, which governs both flux and rejection differences in the prototype membrane. Assuming that under steady state, the swelling of PDMS layer is the same, then it is possible to calculate the intrinsic permeance and permeability of the PEM layer for toluene as it was done previously for CO_2 using the resistance model.

3.12.2 Effect of the number of PAH/PSS bilayers on PERVAP4060 for the toluene flux and R-BINAP rejection

In this study, toluene flux and R-BINAP rejection have been measured up to 40 bar using PERVAP 4060 modified by PAH/PSS having 5-20 bilayers on the top. The toluene fluxes in these membranes (**Figure** 3.27a) exhibits linear evolution with transmembrane pressure and steady rejection of R-BINAP, up to 40 bar.(**Figure** 3.27b).

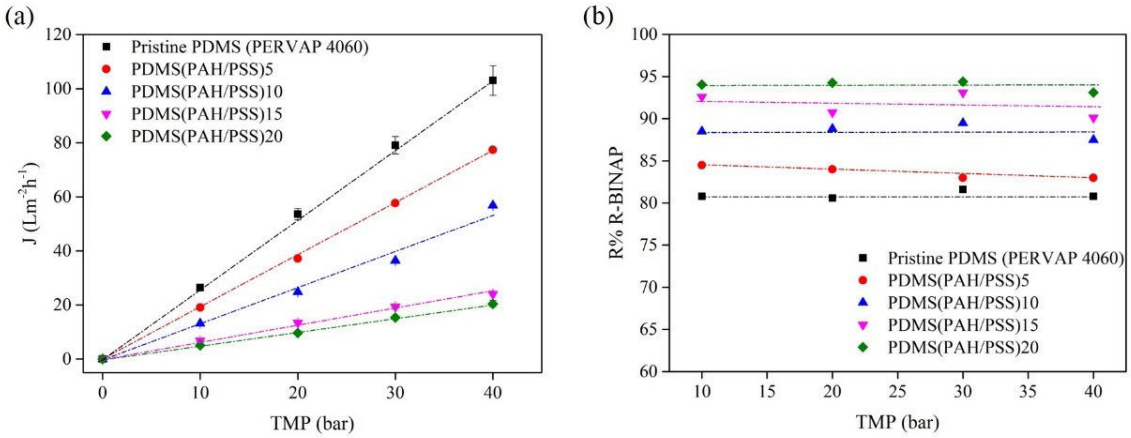

Figure 3.27: Effect of the number of the bilayer of PAH/PSS on (a) toluene fluxes (b) R-BINAP rejection at 30°C and $7-10$ kg/h cross flow of diluted R-BINAP (0.05wt% in toluene.)

As the layer number increases, the decline of flux is caused by the additional mass transfer resistance given by the new layer. In all cases, the flux evolution with transmembrane pressure is linear with different slopes without showing any evidence of compaction or flux hysteresis based on the repeated flux and rejection measurement in the pressure range 10-40 bar.

The R-BINAP rejection in these membranes is well stable up to 40 bar, showing the increase of rejection with the number of bilayers, reaching as high as $\approx 95\%$ in a 20 bilayered PAH/PSS on PERVAP 4060.

The relative decrease of flux and increase of R-BINAP rejection between bilayers 15-20 are smaller than in bilayers 0-5, 10 or 15. This phenomenon seems to correlate the Zone model of PEM in which multilayers are distributed to three zones having a bulk zone in between. Once such bulk zone forms in PEM (often after deposition of 10-12 bilayers), the PEM property does not exhibit significant changes upon addition of new bilayers. (Ladam et al., 2000).

Next, the toluene flux and R-BINAP rejection at 10 bar are plotted against the number of bilayers (0-20), in **Figure** 3.28 which shows almost a linear relation between toluene flux decrease and R-BINAP rejection increase with the number of bilayers.

These results show that the mass transfer resistance of the PEM layer becomes the critical point and governs the properties of the dense composite membrane. Hence, it shows that the bilayers of PAH/PSS exhibit high rejection properties for R-BINAP.

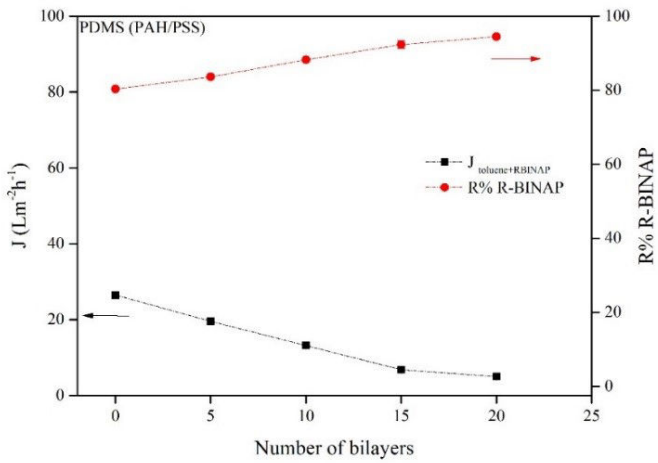

Figure 3.28: Effect of the number of bilayers on toluene flux, and R-BINAP rejection at 10 bar, 30°C and $7-10$ kg/h cross-flow of diluted R-BINAP ($0.05wt\%$) in toluene.

3.12.3 Effect of salt on the polyelectrolyte multilayer for toluene flux and R-BINAP rejection

The salt effect in polyelectrolyte multilayer (PEM) is a well-known phenomenon; the addition of salt during PEM preparation gives additional charges inside the multilayer which causes a more loopy structure compared to the PEM prepared with no salt. As a result of salt, a thicker PEM layer forms. Initially, it was expected that the salt in PEM might induce additional rejection properties in the PEM membrane under OSN. The toluene flux and R-BINAP rejection have been measured using 10 bilayers of PAH/PSS deposited on PERVAP 4060, under 0.5M NaCl salt environment (**Figure** 3.29), and compared with the performance obtained with the same sample prepared without using any salt.

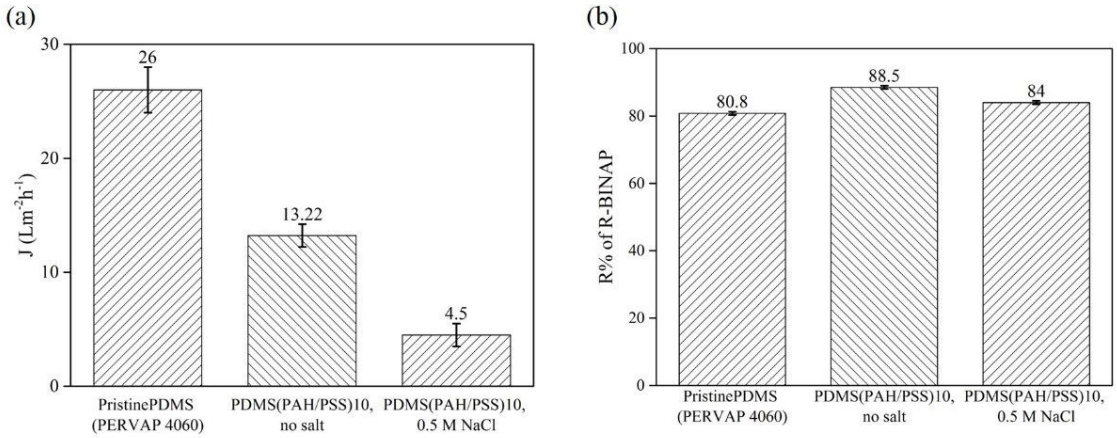

Figure 3.29: Effect of using salt in polyelectrolyte multilayer PEM preparation on PERVAP 4060; in terms of (a) toluene flux (b) R-BINAP rejection, at 10 bar, 30°C and $7-10$ kg/h cross-flow of dilute R-BINAP ($0.05wt\%$) in toluene.

The obtained results show a strong flux decline in the sample prepared under salt, while the rejection slightly decreased. It is obvious that the salt addition during PEM preparation induces additional charges in the multilayer. However, increasing the salt concentration will increase the extrinsic charge compensation, which reduces the number of complexation points between two polyelectrolytes, allowing the more possibilities to coil or to move through the film which gives rougher and thicker structures (Sun et al., 2005) (Schlenoff and Dubas, 2001) (Dubas and Schlenoff, 1999). The thicker structure causes a strong flux decline in the PEM prepared in the presence of salt.

The rejection, however, decreased slightly, which is not clearly understood; however, it seems that the R-BINAP rejection occurs in PAH/PSS when they are more stretched on the surface.

The study on PAH/PSS prepared under salt have no longer considered for further study based on its poor toluene permeance and unsatisfactory improvement on R-BINAP rejection.

3.12.4 Evolution of toluene flux and R-BINAP rejection in PAH/PSS modified PERVAP4060 (PDMS) membranes having different bilayers number

The effect of the number of bilayers on toluene flux and R-BINAP rejection is schematically shown in **Figure** 3.30a and relevant aspect of diffusion in **Figure** 3.30b.

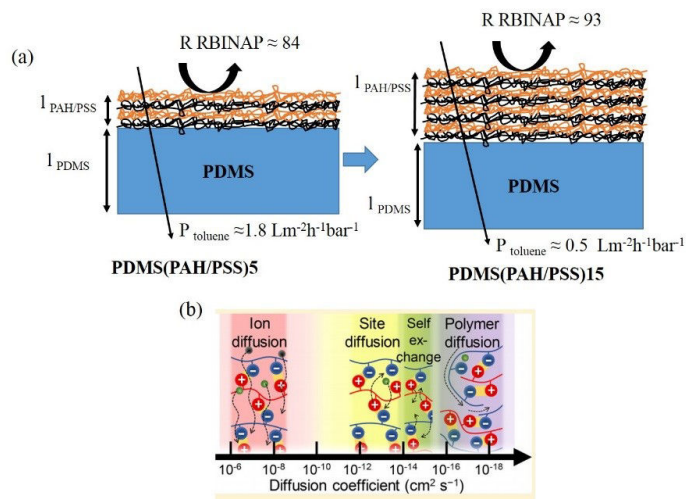

Figure 3.30: (a) PDMS(PAH-PSS) scheme with 5 and 15 bilayers. (b) Diffusion in PEM reported by (Fares and Schlenoff, 2017)

The first changes upon the increase of bilayer are the increase of the thickness, which found linear with the number of bilayers. The swelling of PAH/PSS on PDMS have been discussed previously in **Figure** 3.25, which adopt the hypothesis of swelling difference between PEM and PDMS in a different solvent. However, once PEM covers the PDMS surface, sorption in PDMS is expected to be hindered by the PEM. Thus increasing of bilayers by the same polyelectrolyte pairs does not alter the sorption but necessarily changes the diffusion in PEM. Hence the solute diffusion in PEM could be controlled by both site diffusion (diffusion within charged sites) and polymer diffusion (diffusion of polyelectrolytes) (Fares and Schlenoff, 2017), as shown in **Figure** 3.30b.

Both site and polymer diffusion create an essential structural difference when bilayer number increases, adding up an incremental resistance to the mass transport. Thus the mass transport

resistance increases when the layer number increases. Nevertheless, increasing the bilayer number increases the diffusion length, which may affect the transport of the molecule.

Next, the R-BINAP diffusion coefficient in PAH-PSS have been estimated using the Gierer-Wirtz equation (Evans et al., 2013); the same approach applied previously for the estimation of solvent diffusion coefficient. The solutes diffusion coefficient in PDMS and PAH/PSS modified PDMS is listed in **Table** 3.8, and, toluene diffusion coefficient in PDMS is taken from (Ben Soltane et al., 2016).

Diffusing species in membrane	Diffusion coefficient (m^2/s)	Ratio
Toluene in PDMS	1.31×10^{-10}	$D_{tol(PEM)}$ /$D_{tol(PDMS}$ =432
R-BINAP in PDMS	3.74×10^{-11}	$D_{R-BINAP(PEM)}$ /$D_{R-BINAP(PDMS)}$ =436
Toluene in PDMS (PAH/PSS)	3.03×10^{-13}	
R-BINAP in PDMS (PAH/PSS)	8.57×10^{-14}	

Table 3.9: Toluene and R-BINAP diffusion coefficient in PDMS and PAH-PSS.

Concerning the mobility, The R-BINAP rejection in PDMS (PAH/PSS)10 were obtained as 88% from a diluted feed (0.05$wt.$% in toluene). The majority part of the total flux is toluene ($C_{permeate}Toluene > 99.9wt\%$) and adding diluted solutes does not induce any effect on fluxes.
The rejection of R-BINAP by PDMS (PAH/PSS)10 is 88 %. It corresponds to a decrease of the R-BINAP concentration in the permeate to 0.006 wt%. As the feed concentration is 0.05wt%, it means that the solute mobility in PDMS (PAH/PSS) 10 is about 8 times smaller than the mobility of toluene through the membrane.

3.12.5 Intrinsic permeance in polyelectrolyte multilayers by resistance in series while PEM is deposited on PERVAP4060 (PDMS)

The intrinsic permeance in polyelectrolyte multilayer (PEM) has been calculated by applying the resistance in series model (Ashworth, 1992). The thickness of each PEM is known from ellipsometry, including the thickness of PDMS. The experimental results give both toluene and EtOH permeance in both pristine PDMS and PEM modified PDMS, thereby the intrinsic permeance of toluene and ethanol in PEM have been calculated (**Table** 3.10) using the **Equation** (3.10).

PEM, 10 bilayer	Toluene permeance in PEM ($Lm^{-2}h^{-1}bar^{-1}$)	Ethanol permeance in PEM ($Lm^{-2}h^{-1}bar^{-1}$)
PDMS	2.1	0.2
PDDA-PSS	0.45	0.024
PAH-PSS	0.14	0.014
PAH-PAA	0.03	0.006
PDDA-PAA	0.01	0.013

Table 3.10: Intrinsic permeance in PEM by resistance in series

3.13 Study on the rejection of R-BINAP from EtOH-Toluene mixture using the PERVAP 4060 (PDMS)

This study aims to investigate the rejection of R-BINAP by PERVAP 4060 (PDMS) having diluted R-BINAP in EtOH-toluene feed using a different mass fraction of toluene. It is known that PDMS swells ≈ 114% in toluene and ≈ 5% in EtOH (Ben Soltane et al., 2013). The interest of this experiment is to change the sorption of PDMS by using solvents blend and then monitor the effect of sorption on R-BINAP rejection.

At first, R-BINAP found insoluble in pure EtOH as well as, up to ≈ 25% ethanol in ethanol-toluene mixture. To ensure the complete solubility of R-BINAP, 28/68 (w/w) EtOH-toluene have been used as the starting point for global flux and R-BINAP rejection using PERVAP 4060. Next, EtOH-Toluene composition has been changed while keeping the R-BINAP concentration ≈ 0.05wt% over the range of solvent mass fraction used for the feed. The flux data up to 28wt% does not use R-BINAP in the feed. Finally, global fluxes and R-BINAP rejection have been plotted against the toluene $wt.$% in the feed (**figure** 3.31).

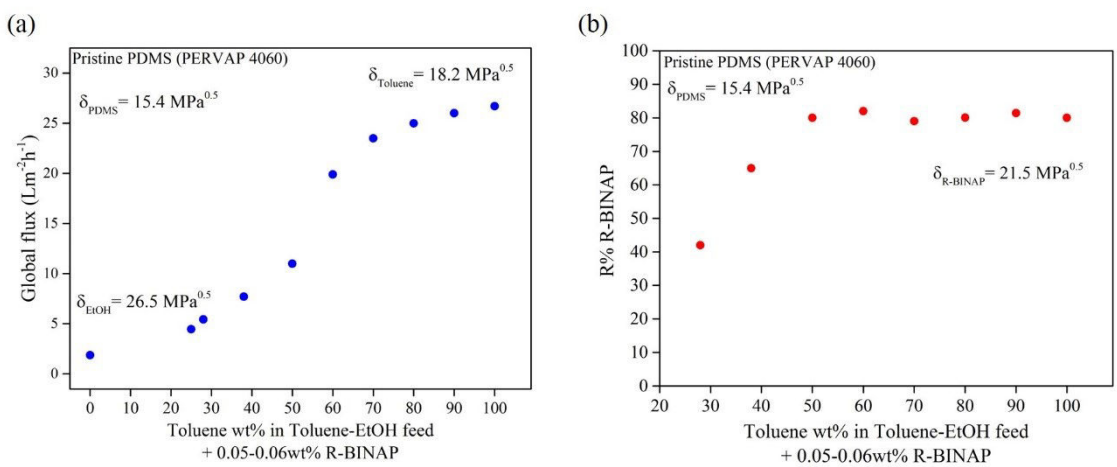

Figure 3.31: Effect of toluene mass fraction in toluene-ethanol feed with diluted R-BINAP (≈ 0.05wt%) on the performance of PERVAP 4060 (PDMS) : (a) Global fluxes with toluene mass fraction in the feed. (b) R-BINAP rejection with the toluene mass fraction in the feed at 10 bar, 30°C and $7-10$ kg/h tangential feed flow.

The solubility parameters of associating R-BINAP, toluene, ethanol and PDMS are summarized in **Table** 3.11:

$\lvert(\delta_{PDMS}-\delta_{EtOH})\rvert$ $MPa^{1/2}$	$\lvert(\delta_{PDMS}-\delta_{Toluene})\rvert$ $MPa^{1/2}$	$\lvert(\delta_{R-BINAP}-\delta_{EtOH})\rvert$ $MPa^{1/2}$	$\lvert(\delta_{R-BINAP}-\delta_{Toluene})\rvert$ $MPa^{1/2}$	$\lvert(\delta_{EtOH}-\delta_{Toluene})\rvert$ $MPa^{1/2}$
11.1	2.8	5	3.2	8.3

Table 3.11: Differences of solubility parameters in solute-solvent-membrane system.

Increase of toluene in the feed increases the swelling of PDMS, and improves the solubility of

R-BINAP in feed, causing high solvent flux and high R-BINAP rejection. Indeed, both flux and rejection are affected by the activity changes when the mass fraction of toluene changes in the feed. Having high EtOH in feed induces low swelling of the membrane, which leads to a low toluene flux. Also, at low EtOH concentration, the activity of R-BINAP is high, which gives a high R-BINAP flux resulting in a low rejection. In contrary, the feed with low EtOH concentration, the swelling is relatively high results a high solvent flux. The activity of R-BINAP at this stage is low, causing lower R-BINAP flux giving a high rejection. The change of ethanol activity applying EtOH-Toluene mixture and their effect on volume fraction in PDMS is presented in **Figure** 3.32 (Favre et al., 1995), which explains the fluxes obtained in **Figure** 3.31 due to the changes of feed activity.

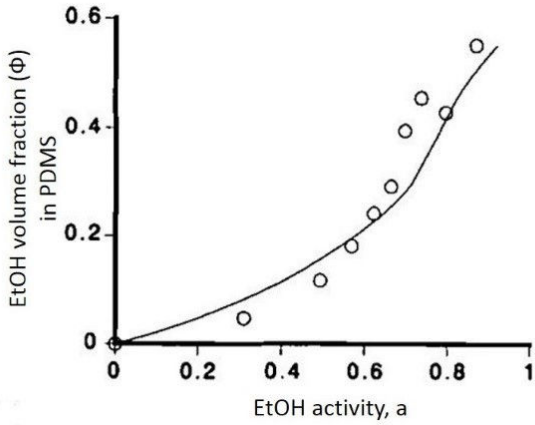

Figure 3.32: Experimental points (o) and predicted curves of ethanol volume fractions in the PDMS network at 40 $°C$ vs. calculated solvent activities; Ethanol in ethanol/toluene/PDMS mixture. (copied from (Favre et al., 1995)).

3.14 Conclusion

This chapter demonstrates that the plasma and polyelectrolytes multilayer deposition is an effective route for prototype membrane fabrication. Both hydrophilic and hydrophobic membrane can be modified effectively for potential new generation membrane to be applied in pervaporation and organic solvent nanofiltration.

Before and after OSN up to 40 bar, the membrane preserves their original surface, which is highly promising for industry concerning the high stability. Spontaneous plasma exposure improves the polyelectrolytes adhesion on the membrane and assists in the deposition of a smooth defect-free nanolayer. The controllability on this nanolayer thickness goes as low as $\approx 3nm$, which is highly interesting for the fabrication.

The gas selectivity (CO_2/N_2), clearly shows these polyelectrolyte multilayers are dense in their structure. Besides, the intrinsic permeability values are quite the same as found for the common glassy polymers. The T_g values of these polyelectrolytes along with permeability values, indicates PEM to be glassy in structure. Surprisingly, the (CO_2/N_2) selectivity decreases linearly with the increase of bilayers number which suggests that there might be a chance to fabricate PEM standalone membrane to obtain N_2/CO_2 selective membrane due to the charged PEM layers and their possible interaction with CO_2, as it acts as a Lewis acid with partial positive charge. The intrinsic permeability of PEM has been obtained by applying resistance in series model, which

explains the mass transport mechanism. The PEM seems to have a very high prospect in gas separation application due to its charge properties.

Regarding the Solvent transport in these prototype membranes, the flux decreases in each PEM following a different order. The rejection has been improved when PAH/PSS was used to form bilayers on PERVAP 4060. The PAH/PSS modified membrane is highly stable in toluene, exhibiting steady high rejection up to 40 bar, which makes this membrane highly prospective for ANR application for the separation of catalyst at an industrial scale. The layer number can be increased to improve the rejection but,then the solvent flux decreases. Therefore a trade-off between the permeation and rejection have been found while using the prototype made of PAH/PSS. The mass transport in these PEM modified membranes follows a solution-diffusion mechanism. The diffusion coefficient and intrinsic toluene permeability have been calculated in the PEM modified membrane. Finally, the activity of solution has been changed by changing the solvent mass fraction in the feed, which could be a design point for OSN to forecast the success from the OSN separation task.

Chapter 4

OSN study on porous systems modified by polyelectrolytes multilayers

This chapter aims to investigate the modification of porous OSN membranes by Polyelectrolyte Multilayer (PEM) deposition. Upon deposition of PEM on porous PAN membrane, having ultrafiltration (UF) pore range or on porous AMS membrane, having nanopores, new separation properties have been expected, according to the scheme shown in **Figure** 4.1.

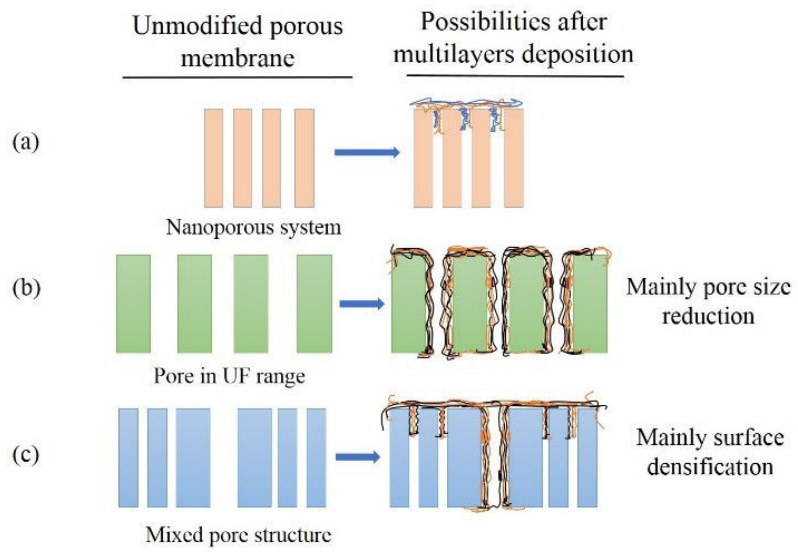

Figure 4.1: Modification of porous OSN membrane by polyelectrolyte multilayers and expected effect after modification based on pore sizes of the pristine membrane: (a) Nanopores: before and after PEM. (b) UF pores: before and after PEM. (c) Mixed pores: before and after PEM.

If the membrane has nanopore (**Figure** 4.1a), the modification can occur inside the pore, may result in a pore block, including a thin nanolayer on the top of the membrane. On the contrary, **Figure** 4.1b shows a different modification aspect in which the PEM resulting in a reduced pore diameters with the possibility to obtain nanopores. Finally, mixed pore system in **Figure** 4.1c consists both nanopore and UF-pore, leading to a surface densification.

In this chapter, two porous systems: AMS S3012 (nanoporous) and PAN have been considered for the modification by polyelectrolytes multilayer (PEM). The first understanding point for this study, if the PEM can be deposited on the porous system following the same protocol used in **Chapter 3** for the dense membrane while expecting improvement in OSN separation from completely different mass transport mechanism than in dense. In this aspect, the second fundamental point to understand if the porous membrane after modification is still porous or PEM has formed a dense nanolayer on the top of the membrane.
The related concerns of PEM modifications are PEM types to consider, the choice of the number of bilayers, PEM stability under OSN condition and mass transport mechanism. The choice of polyelectrolytes, OSN protocol, are adopted from (Ben Soltane et al., 2016), and PEM preparation protocol from (Bassil et al., 2016a). The experimental conditions, including the feed compositions, are kept the same as presented in **Chapter 3**.

4.1 Abstract

This chapter gathers the result obtained with porous AMS and PAN membranes. In the beginning, it has been found that pristine AMS 3012 exhibit higher rejection of R-BINAP ($\approx 24\%$) and C44 ($\approx 24\%$) than in pristine PAN, showing only $3-5\%$ rejection of R-BINAP and 7% rejection of C44. Next, polyelectrolyte multilayers (PEMs) deposition have been carried out on both AMS 3012 and PAN membranes by successive Layer-by-Layer (LbL) deposition of polycation and polyanion polyelectrolytes (PELs), dissolved in milliQ water at room condition. The desired number of bilayers have achieved simply by repeating the deposition cycle of oppositely charged PELs.

After the deposition of PEMs on AMS via LbL, using 10 bilayers, the rejection of C44 reached to 75%, when PDDA/PSS was used. The same deposition on PAN gave 37% R-BINAP rejection and 50% C44 rejection in toluene.

The modified AMS suffers an extreme flux decline, $> 99\%$ compared to pristine, indicating to pore block and dense nanolayer formation on the top. The PAN, on the other hand, exhibit irreversible compaction when applied transmembrane pressure (TMP) was more than 10 bar. After PEM deposition, a porous structure with reduced pore diameter seems to exist on modified PAN. The rejection of R-BINAP, C44, and C16 in PDDA/PSS modified PAN remains unaltered despite their rejection from a binary or ternary feed, indicating that the permeation of each component is independent.

4.2 Characterization of the porous membranes

The characterization of the pristine porous membranes have been discussed previously in **Chapter 2**, presenting the thickness of active surface, their water contact angles on the surface and gas permeability by the time-lag. The summary of those characterizations is presented in **Figure** 4.2.

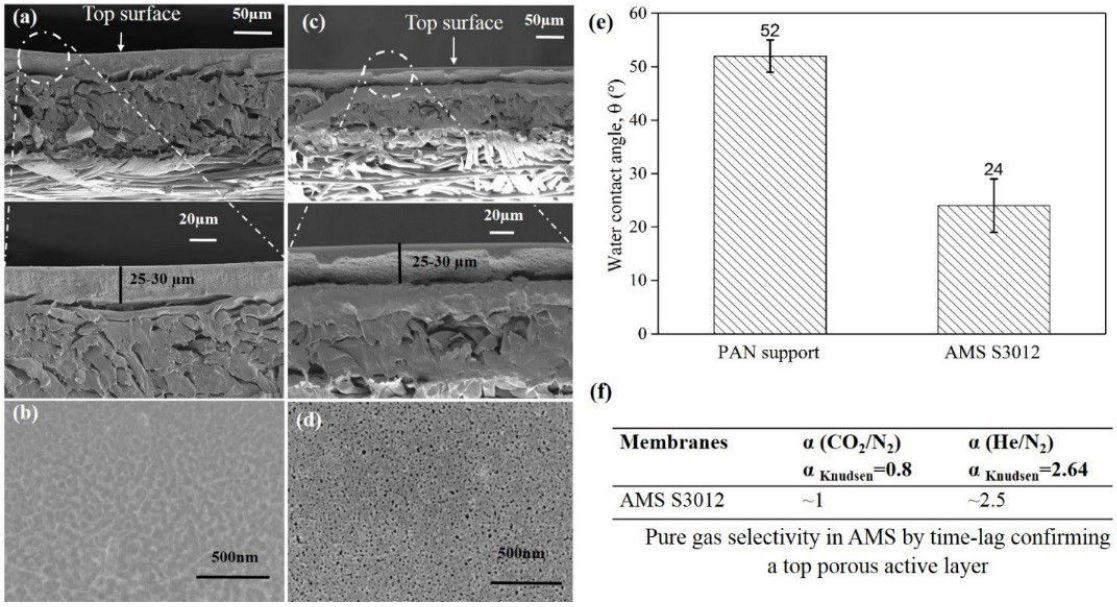

Figure 4.2: (a) AMS cross-section (b) AMS surface (c) PAN cross-section (d) PAN porous surface. (e) Surface hydrophilicity of AMS and PAN (f) Gas selectivity in AMS.

Clearly, both the membrane exhibit a smooth, defect-free hydrophilic surface. The overall thickness of both PAN and AMS lies in between 140-170 m having an average top surface of 25-30 m thick. The porous surface of the PAN is evident from its surface image (**Figure** 4.2d). In contrary, no clear pore can be seen from the AMS surface image; however, the selectivity data (**Figure** 4.2f) confirms its porous surface. Next, the modification of the AMS and PAN membrane have been carried out following the same procedure of modifying dense membranes by using cationic and anionic polyelectrolytes (PELs) via LbL, resulting four pairs of polyelectrolyte multilayers (PEMs), as shown in the **Figure** 4.3.

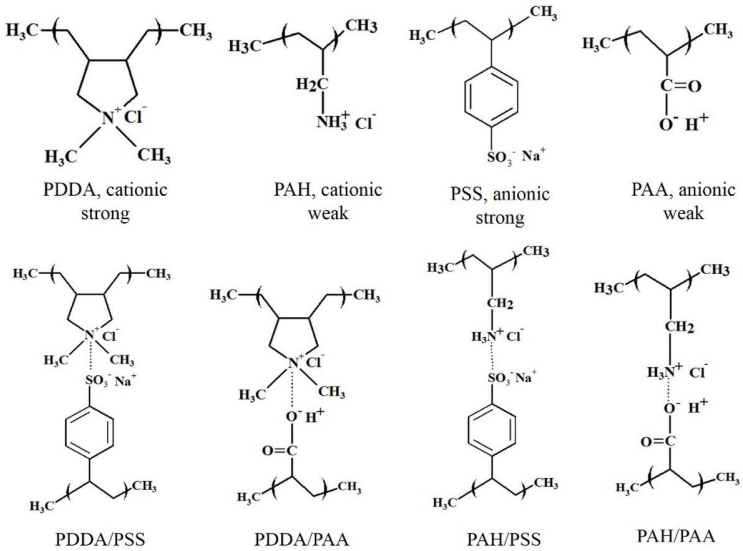

Figure 4.3: (top) Chemical structures of polyelectrolytes (PELs). Strong and weak PELs correspond to respective high and low degree of dissociation. (bottom) Chemical structures of polyelectrolytes multilayers (PEMs). The dotted line indicates the complexation.

Each cycle of deposition is repeated to obtain the desired number of bilayers. For example, AMS (PDDA/PSS) 10 correspond to the deposition of PDDA followed by the deposition of PSS on AMS membrane using ten cycles of deposition, which gives ten bilayers of PEM. Similarly, each PEM deposition on both the pristine membranes gives four prototypes of AMS and four prototypes of PAN

4.2.1 Surface hydrophilicity of PAN after PEM modification

After PEM modification, the water contact angle (WCA) of each PEM modified PAN in **Figure** 4.4, shows different hydrophilicity of each membrane, assuring to successful deposition of PEM while producing new prototypes with different surface properties.

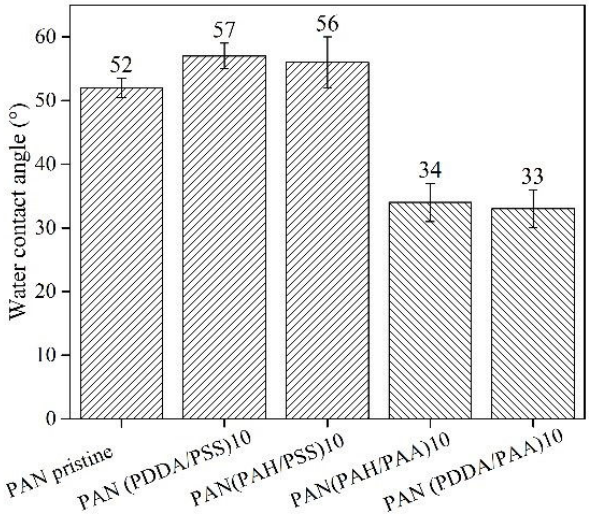

Figure 4.4: Water contact angles after modification of the membrane by different PEM on PAN.

Water contact angle values in modified PAN indicate two groups of new prototypes: PSS ended, which exhibits higher WCA (lower hydrophilicity) than the PAA ended.

4.3 Performance of pristine porous membranes by solvent fluxes

Toluene fluxes in both PAN (run 1 and 4) and AMS 3012 have been measured up to 40 bar and compared with fluxes obtained for dense PERVAP4060 (**Figure** 4.5). In the beginning, the OSN fluxes in PAN has been observed to be declining at higher transmembrane pressure (TMP), therefore, repeated for several runs using the same membrane inside the OSN cell. The results of run1 and 4 are included in **Figure** 4.5 for the comparison with other membranes.

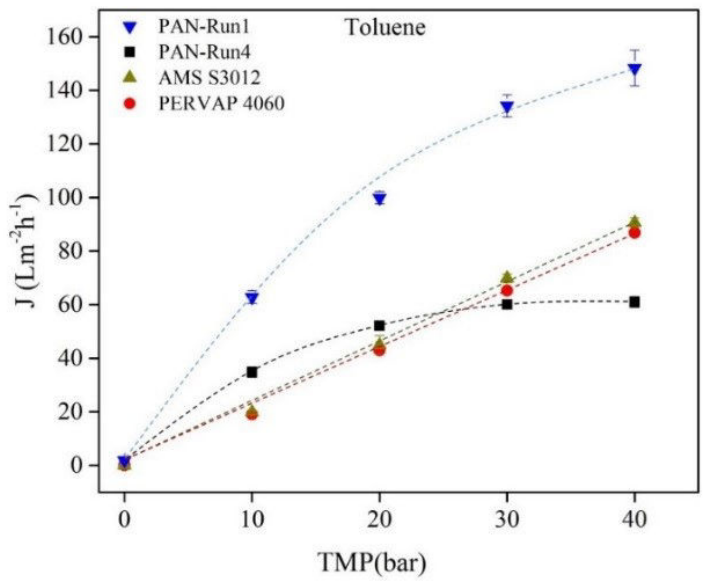

Figure 4.5: The effect of transmembrane pressure (TMP) on toluene (pure) fluxes in AMS S3012, PAN, and PDMS at $30°C$ with a feed cross flow of $7 - 10$ kg/h.

Toluene fluxes in AMS S3012 and PERVAP 4060 increased linearly with TMP, and they are stable in the pressure range up to 40 bar. The flux in pristine PAN was higher initially but exhibited a non-linear trend with applied transmembrane pressure. At 10 bar, toluene flux in PAN-Run1 was ≈ 3 times higher than AMS, which is related to the differences in pore size of these membranes. The surface images of these membranes in **Figure** 4.2b and d, indicates that PAN consists of much larger pores than AMS.

These two surface images have been further analyzed by imageJ (**Figure** 4.6) using the protocol described in `https://www.academia.edu/24152953/Porosity_Analysis_Procedure_with_ImageJ` (AlMarzooqi et al., 2016)

First, the image of **Figure** 4.2 b and d was treated using imageJ-split channel command to obtain the images in RGB(Red, Green and, Blue) colour in order to find the best image; though the split channels did not produce any significant difference in the image obtained from scanning electron microscope (SEM). However, after selecting the best image, a rectangular section was cropped from the main image and threshold tool was used to fill the dark region (**Figure** 4.6) using the contrast difference, which can be adjusted manually to fill all the possible dark region of the image. Then the binary image was extracted, and particles were analyzed by analyze particle command. The size of these particles, their distribution for the given surface then used to obtain the distribution of pore size and area as well as surface porosity.

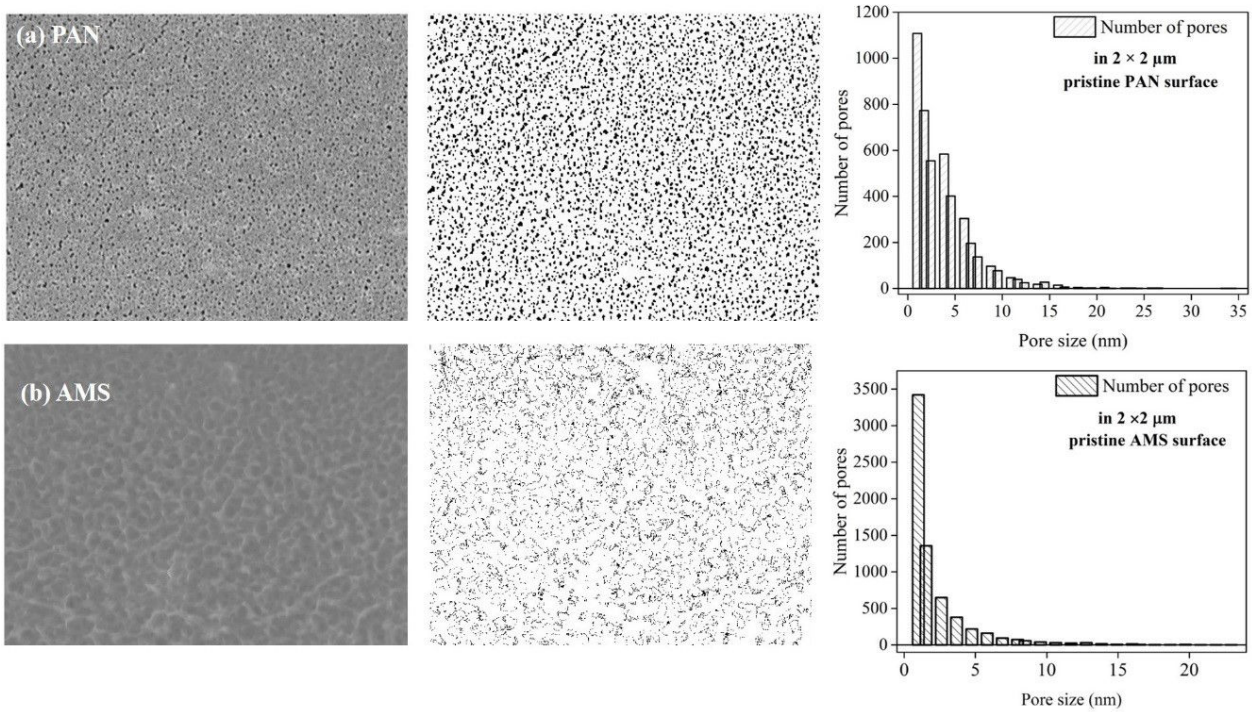

Figure 4.6: Surface image analysis by imageJ for the pore size and the number of pores in (a) PAN surface (b) AMS surface.

The analysis by imageJ, only distinguish the pores on the surface, which can give information based on the surface images and the image treatment procedure. However, the distribution of pores on the surface with their respective sizes, as shown in **Figure** 4.6 indicates three factors that are responsible for the high toluene flux in PAN than in AMS, as presented in **Figure** 4.5.

- The highest pore size in PAN is $37nm$, which is larger than the highest pore size obtained for AMS ($23nm$).
- The total number of the pores in 2×2 μm surface of AMS is about 1.5 times higher than PAN.
- The pore area per unit surface in PAN ($\approx 15\%$) is double than the pore area in AMS ($\approx 7\%$).

Next, flux decline in pristine PAN at elevated pressure in **Figure** 4.5, showing a severe decline after the fourth run repeated of the experiment which is suspected due to compaction or pore collapse of the membrane at an elevated pressure which is most likely occurs when $TMP > 10bar$. This assumption put into test by measuring the flux in several TMP below 10 bar and corresponding rejection of R-BINAP, from a feed of diluted R-BINAP ($0.05wt\%$) in toluene.

4.3.1 Investigation on TMP in pristine PAN for steady flux and rejection

In this measurement, at first, toluene flux and R-BINAP ($0.05wt.\%$ in toluene) rejection were measured at a transmembrane pressure, $TMP = 0$. A small toluene flux of $\approx 0.35L/m^2h$ and about 4% R-BINAP rejection were obtained. Next, the transmembrane pressure was increased stepwise up to 40 bar having several measurements with short-step increase and decrease of TMP up to 10 bar, and corresponding flux and rejection in **Figure** 4.7, indicates that both flux and rejection changes significantly above 10 bar.

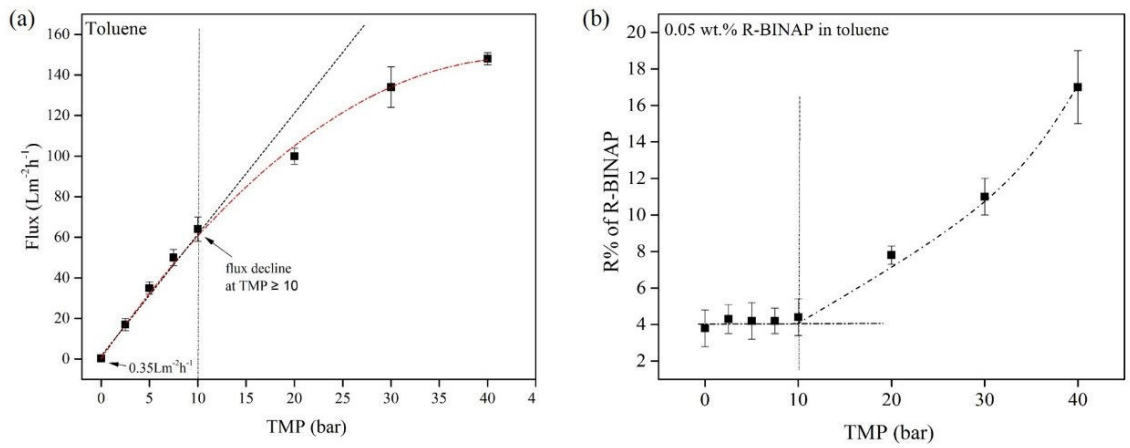

Figure 4.7: Effect of TMP in pristine PAN: (a) Toluene flux. (b) R-BINAP rejection, at $30°C$ and $7-10$ kg/h cross-flow rate.

Both flux decline with the increase of rejection at transmembrane pressure, more than 10 bar helps to assume two possibilities: compaction occurs in the active layer or the support, and/or pore collapse at high transmembrane pressure. It is also evident that both flux and rejection are steady below 10 bar.

To understand these phenomena, three consecutive experiments have been designed to determine the maximum pressure, at which PAN can be taken into consideration for OSN without sacrificing its flux:

- Flux hysteresis (if any) by applying transmembrane pressure (TMP) up to 20 bar using back and forth pressure increase and decrease.
- Long term OSN study on toluene flux and rejection in PAN at 10 and 20 bar for determining if the performance is steady.
- Capturing microscopic images of PAN surface before and after applying 10 and 20 bar to see if there is a pore collapse.

4.3.2 Investigation on transmembrane pressure effect on flux and rejection in pristine PAN

The performance of pristine PAN has been investigated up-to 20 bar using its flux and rejection. Both flux and rejection have been measured while transmembrane pressure (TMP) increased from 0 to 20 bar (forward). Afterward, flux and rejection have been re-measured while TMP decreased from 20 -0 bar (backward). An apparent hysteresis can be seen in **Figure** 4.8.

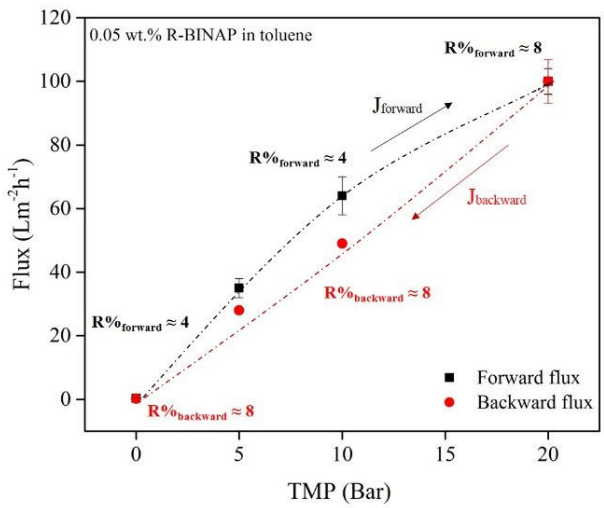

Figure 4.8: Effect of TMP in pristine PAN: (a) Toluene flux. (b) R-BINAP rejection, at $30°C$ and $7-10$ kg/h cross-flow rate

In addition, the same measurement repeated for four times (forward and backward runs) using the same membrane sample, and in every repeated run, flux was declining then the previous run. Finally, at run 4, R-BINAP rejection at 20 bar was increased about ≈ 4 times while toluene flux reduced $\approx 50\%$ compared to run 1. Worth to mention that the toluene flux at the beginning was 0.35 $Lm^{-2}h^{-1}$ at $TMP = 0$, which decreased to 0.20 $Lm^{-2}h^{-1}$ after the 4th run.

4.3.3 Long term study of pristine PAN on toluene flux and R-BINAP rejection at 10 and 20 bar

The toluene flux and R-BINAP rejection have been measured in pristine PAN at constant 10 bar using a total OSN runtime of eight hours (**Figure** 4.9a) in which data taken during the first hour of measurement is the conditioning step. Afterward, the OSN unit stopped overnight following the flux and rejection measurement in the following day using the same membrane at 10 bar (1 data point) and at 20 bar for several hours (**Figure** 4.9b).

Next, TMP decreases to 10 bar, and the measurement of flux and rejection continued until day 3, having the OSN unit stopped overnight.

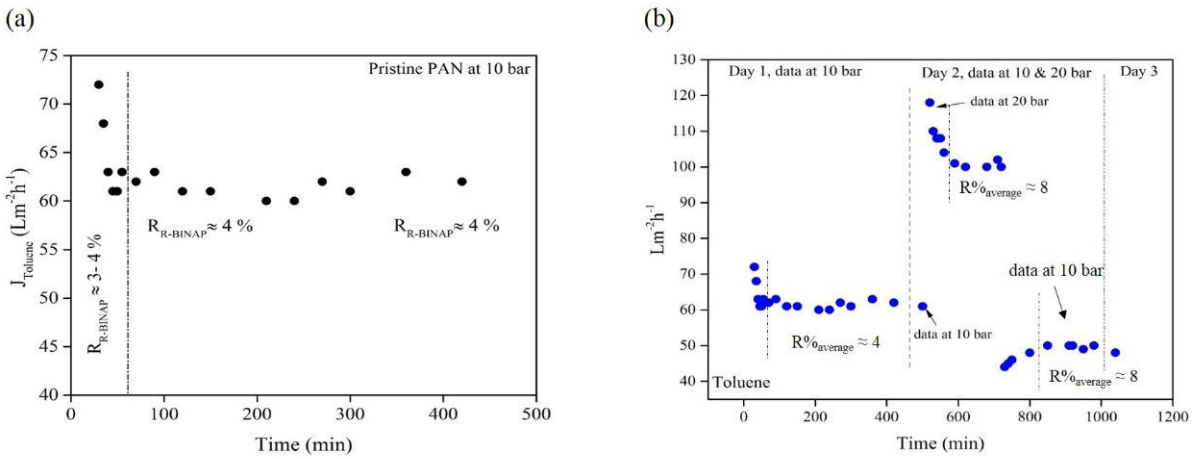

Figure 4.9: Toluene flux and R-BINAP rejection by pristine PAN in a long run study at 10 and 20 bar, 30°C and $7-10$ kg/h cross-flow rate: (a) OSN measurement at 10 bar in day 1 (b) OSN measurement at 10 and 20 bar up to day 3

Flux decline at $TMP > 10$ bar is evident from **Figure** 4.8 and 4.9, while rejection of R-BINAP increases.

Next, the surface images have been captured before and after OSN flux measurement at 10 and 20 bar (**Figure** 4.10) using two different samples in two separate OSN measurement.

Initially, one pristine PAN sample has been used in OSN test for toluene flux at 10 bar for 4-5 hours. Afterward, another coupon of the membrane was exposed at 20 bar. The SEM images of both membranes were captured before and after OSN.

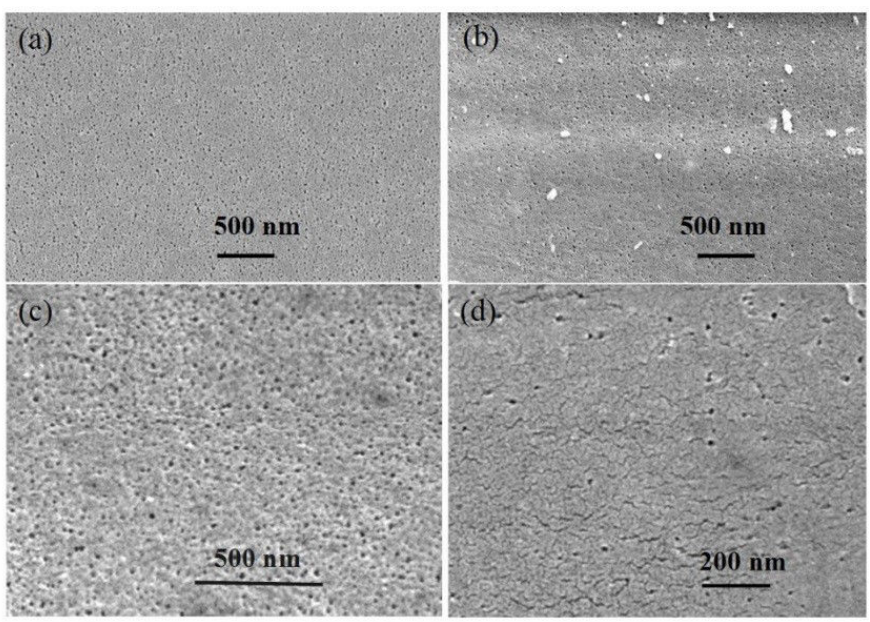

Figure 4.10: Surface of pristine PAN membrane: (a) and (c) before OSN (b) after OSN at 10 bar(d) after OSN at 20 bar; at 30°C and $7-10$ kg/h cross-flow rate.

Clearly, PAN surface is relatively unchanged after OSN test at 10 bar; while comparing **Figure**

4.10a and b. A slight surface change in **Figure** 4.10b indicates the effect of the conditioning step, as shown in **Figure** 4.9a, which shows a flux decline at the beginning of the experiment until the OSN stabilize.

On the other hand, **Figure** 4.10c and d indicates a significant surface change once the membrane is exposed to 20 bar, showing only a few random pores that indicate to the pore collapse due to the high TMP. Indeed, the pore collapse in PAN was unexpected and thereby causing the flux decline as well as hysteresis effect in PAN flux and rejection. At this phase, the OSN test with PAN limited to 10 bar, as its pressure threshold limit. For comparison, OSN study on AMS S3012 membrane also carried out at 10 bar.

4.4 Rejection of diluted R-BINAP and C44 by pristine PAN and AMS 3012 in toluene at 10 bar

Toluene flux and rejection of R-BINAP ($MW622gmol^{-1}$) and C44 ($MW619gmol^{-1}$) in both PAN and AMS 3012 was measured at 10 bar and compared in **Table** 4.1. Clearly, the AMS 3012 exhibit higher rejection of both solutes than in PAN.

Membrane	$J_{toluene+R-BINAP}$ $(Lm^{-2}h^{-1}) \pm 2$	$R\%_{RBINAP} \pm 1$, 0.05$wt.\%$ in toluene	$J_{toluene+C44}$ $(Lm^{-2}h^{-1}) \pm 2$	$R\%_{C44} \pm 1$, 0.05$wt.\%$ in toluene
AMS S3012	62	24	61	25
PAN	19	4	20	7

Table 4.1: Rejection of R-BINAP and Tetratetracontane (C44) at 10 bar, 30°C and $7-10$ kg/h cross-flow condition.

Relating the pore size and pore area, as discussed previously, it primarily distinguish the differences of toluene flux due to pore size differences in both membranes, but the rejection of R-BINAP and C44 in AMS is surprising because the pore sizes, whether for AMS (up to 23nm) or PAN (up to 37nm) ideally should not give any rejection. Hypothetically, it indicates that:

- The pore size inside the membrane matrix is much smaller than the surface pore size.
- According to the pore size distribution presented previously, the part of the membrane consisting nanopores gives the rejection while the part having bigger pores give the bulk permeation, causing the final low rejection performance of the membrane.

For the given rejection in AMS, the pore size needs to be much smaller; thus, the hypothesis on smaller pore radius inside the membrane is presented in **Figure** 4.11 in which the smaller pore size is located inside the membrane having a large pore opening on the top.

This hypothesis (if correct) must contradict to the surface porosity and pore size, obtained from imageJ. Indeed, a high tortuous path inside the membrane matrix is most likely, and having continuous pores of average $13nm$ (AMS) or $18nm$ (PAN) diameter throughout $25\mu m$ is highly unlikely.

In the following section, the Hagen Poiseuille ($H-P$) model have been applied to determine the theoretical flux of the membrane. Based on the OSN experiment with low TMP and low feed concentration with high feed velocity, the HP model is applicable for the given system.

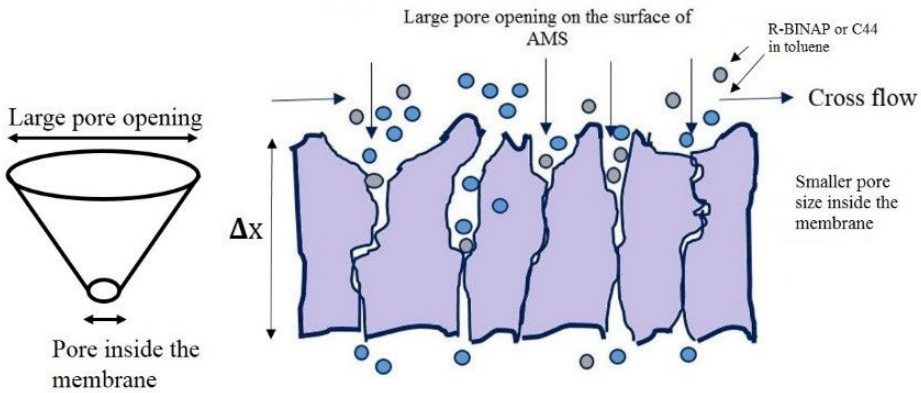

Figure 4.11: Hypothesis for AMS top layer with the smaller pores inside the membrane originating rejection of R-BINAP and C44. Δx is the membrane thickness.

4.4.1 Hagen Poiseuille (H-P) model for solvent fluxes at 10 bar

The Hagen Poiseuille (H-P), laminar flow through channels, is schematically shown in **Figure** 4.12, in which the accessible pore site is shown having the diameter (d_P) through which the permeation occurs.

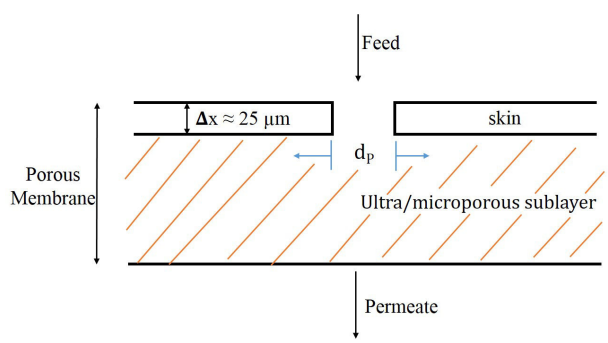

Figure 4.12: H-P laminar flow through channels.

Indeed the skin layer is also highly porous (not shown in **Figure** 4.12) having a large number of small pores which together results in the global performance of the membrane, can be expressed a function of different parameters and $H-P$ equation.

$$J = f(d_p, \varepsilon, \Delta P, \eta, \Delta x, \tau) \tag{4.1}$$

$$J = \frac{\varepsilon d_p^2}{32\eta\tau} . \frac{\Delta P}{\Delta x} \tag{4.2}$$

where ε is the surface porosity ($\approx 7\%$ surface porosity for PAN and $\approx 15\%$ for AMS), d_p is the pore diameter (Average pore diameter in PAN and AMS are considered as $18.5nm$ and $11.5nm$, according to **Figure** 4.6, surface pores), ΔP is the transmmembrane pressure (10 bar), η is the viscosity of toluene ($0.53mPa.s$), Δx is the thickness ($25\mu m$ for each membrane), and τ is the tortuosity factor (actual pore length/cylinder length) which is considered as 1.
Applying these values in the equation, the $H-P$ flux has been calculated and presented in **Table** 4.2, column C2. In both membranes, the calculated HP flux is higher than the experimentally measured flux. Indeed this model considers the pore sizes to be distributed evenly, which is not

possible. However, using HP equation, the experimental flux can be reproduced changing several parameters.

(1) Adjustment of Δx while τ, ε , and ΔP are unchanged: Column C3.
(2) Adjustment of τ while Δx,ε, and ΔP are unchanged: column C4.
(3) Adjustment of ΔP when τ, Δx, and ε are unaltered: Column C5.
(4) Adjustment of ε when τ, ΔP and Δx are unaltered: Column C6

Membranes	C1: Toluene $J_{experiment}$ $(L/m^2h) \pm 2$	C2: Toluene J_{H-P} $(L/m^2.h)$	C3: Δx (μm) to reproduce $J_{experiment}$	C4: τx to reproduce $J_{experiment}$	C5: $d_P(nm)$ to reproduce $J_{experiment}$	C6: ε (%) to reproduce $J_{experiment}$
PAN	62	203	80	3.2	10	2
AMS	20	169	210	9	4	1.8

Table 4.2: Comparison of measured and calculated (Hagen-Poseuille) flux and parameters adjustment to reproduce the experimental flux. (Actual data $\Delta x \approx 25\mu m$, τ= unknown, $d_p = 18.5nm$ in PAN and 11.5 in AMS. ε = 7% in PAN and 15% in AMS)

The thickness in C3 is unrealistic because the thickness of the AMS active layer cannot be higher than the total membrane thickness (140-170 m, from **Figure** 4.2. The porosity in C6 seems to be very low, even though the porosity of top layer can be as low as 5%, reported for the anisotropic polysulfone membrane prepared by Loeb-Sourirajan phase separation process **(Baker, 2000)**.

In column C5, the effective pore diameter was obtained smaller than the surface pore diameter which is logical to give lower flux in AMS with higher rejection of R-BINAP and C44 ($\approx$ 25%), (**Table** 4.1, supporting the hypothesis presented in **Figure** 4.11.

In column C4 the tortuosity value in AMS is much higher which also seems possible because AMS is a nanoporous system, having a much higher active layer thickness (25-30 m) than the pore size (several nm) could give very high τ (actual pore length/cylinder length) showing that smaller pore could be more tortuous. The τ value of 1.5-2.5 is generally acceptable for membranes have UF range pores **(Baker, 2000)**.

However, the H-P equations assume all pores are right circular cylinders, which is highly unlikely. As the pores get smaller in diameter, the number of pores in various sizes increases; thus, the use of average pore diameter in the equation is not an accurate representation of the surface pores distribution.
Hence the H-P approach is not meaningful for fitting the obtained results.

4.5 Performance of PEM modified AMS 3012 by toluene fluxes and C44 rejection

The toluene flux and C44 rejection have been measured using each PEM modified AMS membrane with the feed of $0.05wt\%$ C44 in toluene. The performance of the pristine membrane is compared with the performance of modified membranes in **Table** 4.3, which shows substantial flux loss in prototype AMS membrane while improving the rejection of C44.

Membrane	Toluene flux $(Lm^{-2}h^{-1}) \pm 5\%$	Reducing factor $J_{AMS}/J_{AMS(PEM)}$	C44 Rejection $\pm$ 5% (0.05wt% in feed)
AMS Pristine	20		25
AMS(PDDA/PSS)10	0.07	300	75
AMS(PAH/PSS)10	0.11	200	65
AMS(PAH/PAA)10	0.2	100	42
AMS(PDDA/PAA)10	0.6	33	25

Table 4.3: Performance of AMS pristine and modified membranes at 10 bar and 30°C, and feed cross-flow $7-10$ kg/h.

The highest rejection has been obtained in PDDA/PSS modified AMS with > 99% flux decline compare to pristine. In each PEM membrane, the flux decline is significant that indicates that the PEM deposition on AMS seemingly blocking the pore and possibly, forming a dense-glassy nanolayer on the top, (**Figure** 4.13). (Tang and Besseling, 2016) report a glassy like PDDA/PSS to form when prepared in a no-salt environment.

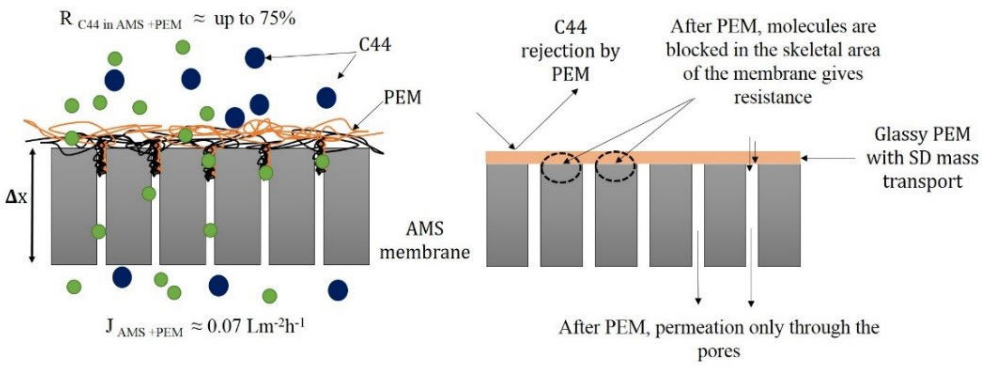

Figure 4.13: Factors affecting the transport mechanism of toluene and C44 in PEM modified AMS membrane having a dense-glassy nanolayer of PEM on the top of a porous substrate

As shown in **Figure** 4.13, the flux in the PEM modified membrane govern by two factors: first, low flux in glassy PEM top layer following an SD mechanism and second, once the molecule pass through the glassy PEM, it receives strong restriction where there is no pore (membrane skeleton) causing a high resistance and blocking the molecule to pass through the porous sublayer. The case of porous substrate under a dense nanolayer has been presented in previous chapter Figure 3.1, according to the phenomena of restriction by porous support in molecular permeation through membrane, described in (Wijmans and Hao, 2015).

In this aspect, note that the surface porosity AMS surface is 15% (**Figure** 4.6). The possible restriction by the porous sublayer under a dense nanolayer is described elaborately in the previous chapter.
Since the toluene flux is extremely low in modified AMS, these prototype membranes have no longer been considered for OSN studies with binary and ternary feed.

4.6 Permeation of pure solvents in PEM modified PAN membranes

Pure solvents, toluene, and ethanol fluxes in modified PAN membranes up-to 10 bar in Figure 4.14 shows that the solvent fluxes in PEM modified PAN is always strongly decreased and varied with the polyelectrolytes multilayer(PEM) type.

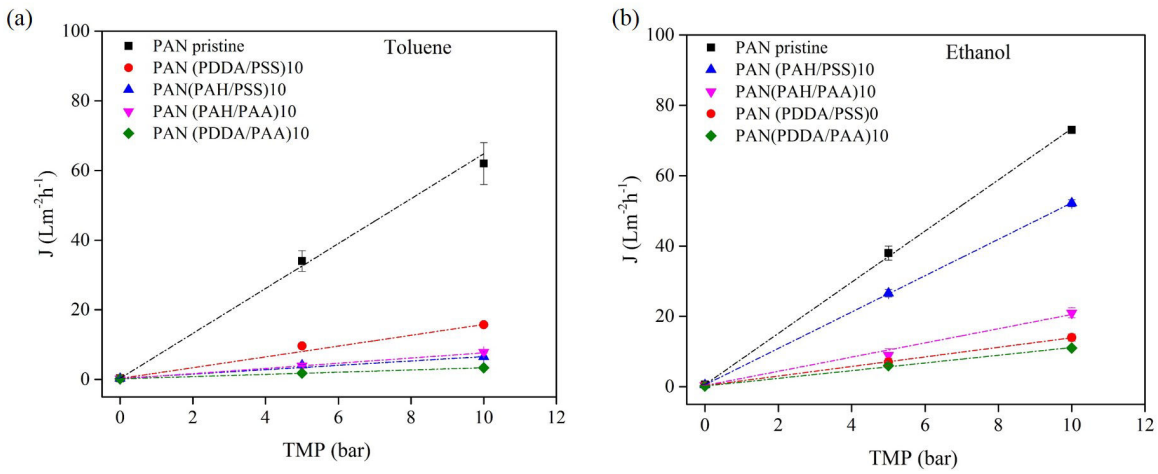

Figure 4.14: Comparison of pure solvent fluxes in pristine and PEM modified PAN membranes at $30°C$, up to 10 bar using feed cross-flow $7-10$ kg/h : (a) Toluene fluxes (b) EtOH fluxes.

In pristine PAN, EtOH flux obtained $\approx$ 10% higher than the toluene flux, mainly caused by their molecular properties such as densities ($\rho_{EtOH} = 0.789gcm^{-3}$, $\rho_{toluene} = 0.867gcm^{-3}$) and viscosities ($\mu_{EtOH} = 0.97mPa.s$, $\mu_{toluene} = 0.53mPa.s$) at $30°C$. Solvent fluxes in modified PAN follow different order depending on PEM and solvents types. The toluene flux follows the order $J_{PAN} > J_{PDDA/PSS} > J_{PAH/PAA} > J_{PAH/PSS} > J_{PDDA/PAA}$ whereas in ethanol $J_{PAN} > J_{PAH/PSS} > J_{PAH/PAA} > J_{PDDA/PSS} > J_{PDDA/PAA}$ The solvent flux order in modified PAN is not clearly understood, however, indicates to the following different possibilities:

- The pore size in the modified PAN is smaller than the pore size of the pristine membrane, which causes the flux reduction despite the solvent type. If reduced pore size would be the only parameter to govern solvent fluxes, then different flux order is not possible indicating to the roles of other parameters such as charge density, dry-wet thickness and PEM swelling in organic media.

- The charge density of each PEM is different, ranging from low to high charge density (shown in **Chapter 3**) which induces some effect on the permeation through tiny pores covered by PEM. The higher charge density of the polyelectrolytes results in more ionic cross-linking, less PEM swelling (Schlenoff and Dubas, 2001).

- The PEM swelling in toluene and EtOH differ significantly. Taking an example, PDDA/PSS swell 112% in EtOH (Miller and Bruening, 2004) and $25-27$% in toluene, estimated value according to PSS swelling reported in (Ferrell et al., 2017) which able induces significant pore structure change once PEM is exposed to solvent. The higher PDDA/PSS swelling (inside the pore wall) in EtOH seems to give lower EtOH flux than toluene flux shown in **Figure** 4.14. The swelling of other PEM in toluene was not obtained from the literature. Hypothetically, the swelling of PEM inside the pore

wall could effect on pore diameter is shown in **Figure** 4.15 that shows low to a very high swelling effect can causes pore reduction to a complete pore block. It also shows that swelling of PEM in different solvent could be a design point for OSN separation along with initial pore size to expected pore size.

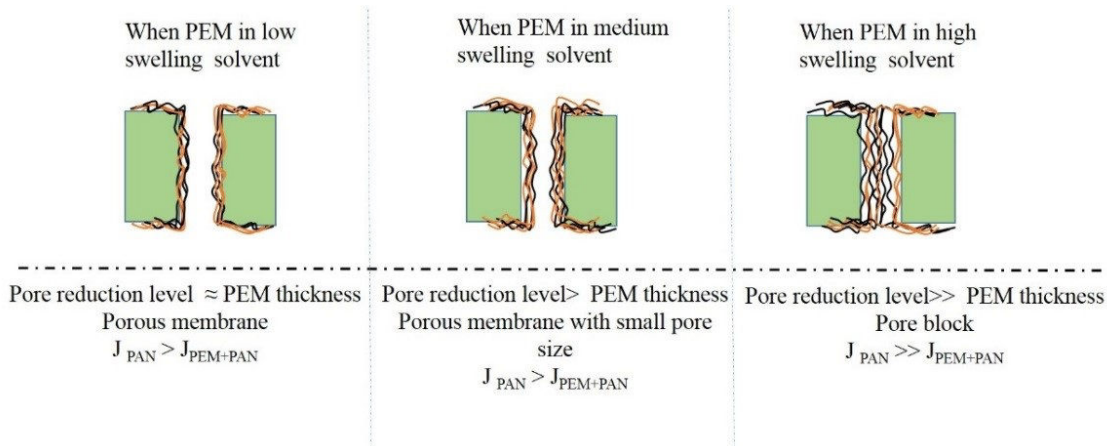

Figure 4.15: Swelling of PEM in different solvent and its effect on the pore reduction to govern the solvent fluxes, when PEM deposited on the porous substrate having a pore range of nanopore to UF-pore.

Nevertheless, the solvent fluxes in modified PAN indicates that the prototype PAN membranes have been porous because the intrinsic toluene permeability of PEM is known from the previous chapter which is much lower than the obtained values in **Figure** 4.14.
A parallel test of air permeability has been measured in PEM modified PAN for cross-examination of its reduced pore by PEM.

4.6.1 Air permeability in modified PAN

Permeability of air in both pristine and modified PAN is presented in **Table** 4.4 followed by the plot of pressure drop vs. total air flow rate in **Figure** 4.16 (for clarity, the pristine PAN is not included). The air permeability values in **Table** 4.4 indicate that the membrane remains porous after PEM modification, and depending on the PEM types, the permeability values differs from each PEM to another.

Membrane	$Airpermeability \times 10^{+9}(m^2.m^{-3})$	Reduction of permeability $P_{PAN}/P_{PAN(PEM)}$
PAN	14.1	
PAN (PDDA/PSS) 10	0.93	≈ 15
PAN(PAH/PSS)10	1.03	≈ 14
PAN (PAH/PAA)10	0.61	≈ 23
PAN (PDDA/PAA)10	0.77	≈ 18

Table 4.4: Air permeability in modified PAN from 0.5-3 bar

The air permeability results show a strong decrease of permeability for all PEM modified membrane by one order of magnitude versus pristine PAN. Clearly the modified PAN exhibit a porous structure. Next, the porosity by Hg-porosimetry has been considered to obtain the new pore size after modification.

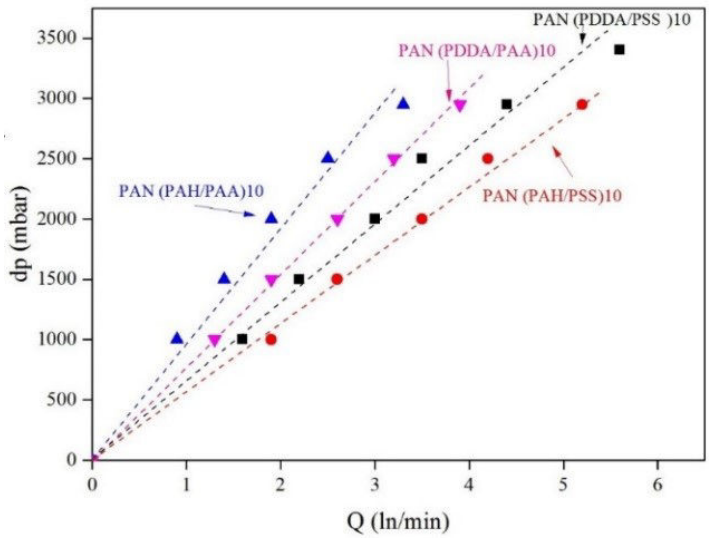

Figure 4.16: Air permeability measurement in PAN modified membranes.

4.6.2 Porosity by the mercury porosimetry

This study was carried out with the composite PAN membrane because it was not possible to peel off the support. In the beginning, mercury intrusion in pristine PAN was measured using $2cm \times 1cm$ PAN sample, which was placed in the penetrometer, and mercury intrusion in the sample was conducted. The most fundamental data obtained pressure vs. cumulative intrusion, which presents the structural demonstration of the membrane sample (**Figure** 4.17a). Next, pressure correlation to the pore size is used according to the Washburn equation, and the cumulative intrusion vs. the pore size plot has been obtained (**Figure** 4.17b). Afterward, the incremental intrusion data was calculated by subtracting the cumulative volume measured at a beginning pressure and the cumulative volume measured at a higher pressure, which gives the distribution characteristics of the membrane. Finally, the differential specific intrusion volume versus diameter was then plotted in figure **Figure** 4.17d, taking only the pressure range D from Figure **Figure** 4.17a and b.
The detailed procedure of mercury porosimetry has been adopted from `http://depts.washington.edu/mseuser/Equipment/RefNotes/Hg%20Porosimetery%20paper.pdf`. The plot presented in Figure **Figure** 4.17a is divided into four regions. Region A indicates to the fibrous support of the membrane, presenting that mercury filled in the voids between fibers. The region B is the breakthrough region, which indicates the void space between the fibrous supports to the middle layer of the membrane. The region C indicates the pore filling of the highly porous layer immediate below the active layer, finally region D presents the active layer (layer of interest in this study).

Almost 90% of the volume intrusion occurred in region A, and B compares to the total intrusion. After region C, a transition can be noticed in **Figure** 4.17a and b, which is the region of interest (the active layer of the membrane). Indeed the transition from region C to D is not very clear, however, according to surface SEM images (**Figure** 4.2) the pore size should be in the UF range (10 to 100 nm), Thus, the intrusion in the active layer begins in the pressure range from 2800 to 3000 psia corresponding the pore diameter 5-60 nm.
Now, obtaining the cumulative volume of mercury in the active layer, mean diameter,and pore area was possible calculated. The porosity of the membrane can be estimated using the ratio of total volume intrusion in the whole sample and total volume intrusion in the active surface.

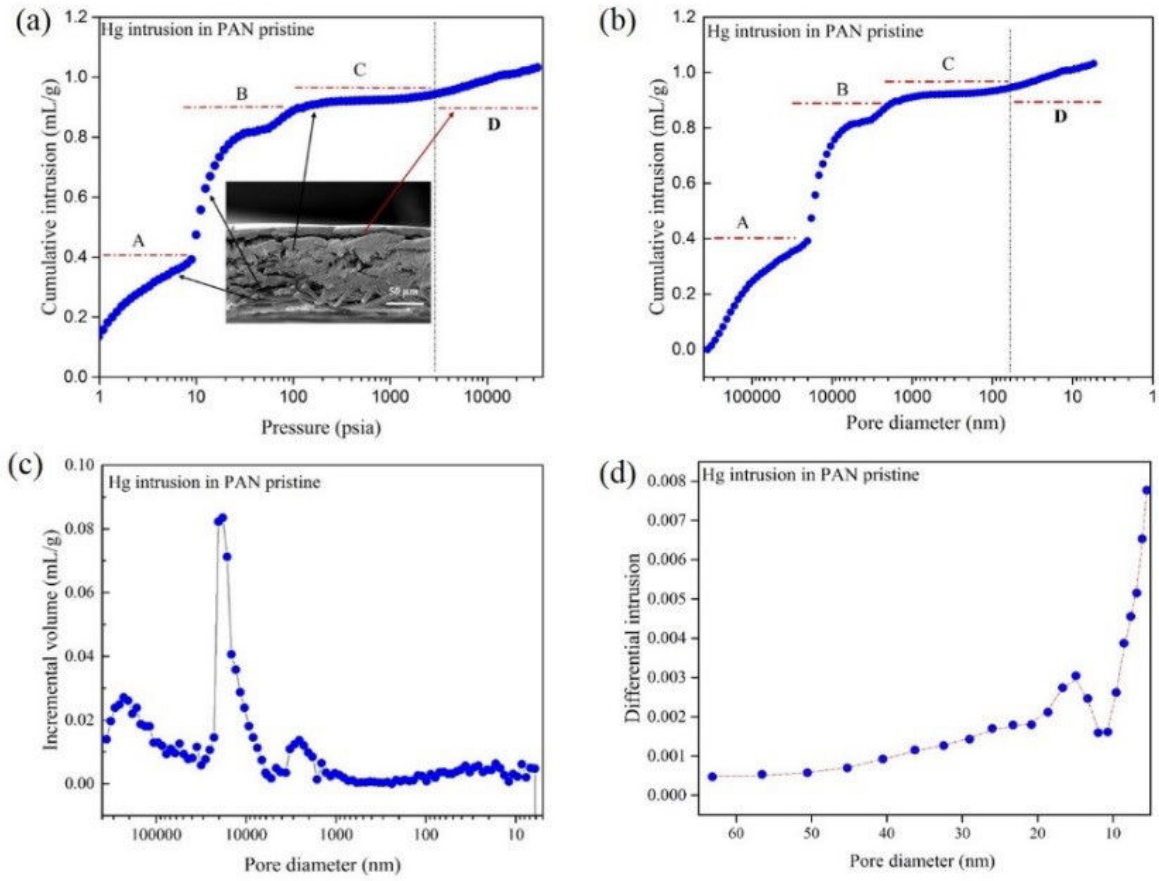

Figure 4.17: Mercury porosimetry for pristine PAN (a) Cumulative intrusion vs pressure plot. (b) Cumulative intrusion vs pore size (diameter). (c) Incremental volume and pore diameter (d) Differential intrusion vs diameter distribution.

The same Hg-porosimetry procedure was followed for each PEM modified PAN membrane and, obtained results are summarised in **Table** 4.5.

Membrane	Cumm. intrusion volume of $(mL/g)Hg$ in top layer	Pore area (m^2/g)	Avg. pore $d, (nm)$	Pore reduction $d_{(PAN)}/$ $d_{PAN(PEM)}$	Estimated porosity of active layer (%)
PAN	0.088728	2.066	34	-	8.61
PAN (PDDA/PSS)10	0.01492	0.5384	7	5	1.7
PAN(PAH/PSS)10	0.0524	1.82	11	3	5.2
PAN(PAH/PAA)10	0.039	1.39	13	2.6	3.9
PAN(PDDA/PAA)10	0.03859	1.21	10.1	3.4	4.26

Table 4.5: Characterization parameters obtained from mercury porosimetry

As expected, the modified membrane exhibit lower pore area and pore diameter than the pristine, which confirms the reduction of pore size after PEM deposition. Among all PEM, PDDA/PSS shows the lowest pore area, and lowest pore diameter.

The pore reduction order by mercury porosimetry is neither comparable with flux reduction order or air permeability results. Therefore a straight-forward link could not be established; however, these results difference can occur if PEM exhibits different swelling behavior under different solvent types which supports the PEM swelling effect on pore reduction hypothesis, as shown previously.

4.7 OSN study for the solute rejection in PAN

4.7.1 Solute rejection by pristine and modified PAN from the diluted binary feed in toluene

Toluene flux and rejection of diluted R-BINAP, C44, and C16 in toluene (**Table** 4.6) have been measured using the pristine and modified PAN membrane.

	0.05 wt% R-BINAP in toluene		0.05wt% C44 in tolune		0.05wt% C16 in tolune	
Membrane	$J \pm 2$ $Lm^{-2}h^{-1}$	$R\% \pm 2$ R-BINAP	$J \pm 2$ $Lm^{-2}h^{-1}$	$R\% \pm 2$ C44	$J \pm 2$ $Lm^{-2}h^{-1}$	$R\% \pm 1$ C16
PAN pristine	62	4	57	7	60	3
PAN (PDDA/PSS)10	14	37	13	55	15	6
PAN(PAH/PSS)10	6	10	6	22	7	5
PAN(PAH/PAA)10	8	17	7	37	7	6
PAN(PDDA/PAA)10	4	38	3	35	5	10

Table 4.6: Flux and rejection in the binary system of 0.05 wt.% solutes (R-BINAP, C44, and C16) in toluene at 10 bar, $30°C$. Feed cross-flow: $7 - 10$ kg/h

The toluene fluxes from binary feed remain the same as the fluxes from pure toluene feed. The low solute feed concentration does not induce a significant effect on flux. The R-BINAP and C44 rejection, however, have improved in PDDA/PSS modified PAN with a reasonable toluene flux. C16 rejection is almost the same in each membrane.

The R-BINAP and C44 rejection compare to C16 rejection in the given porous systems could be related to their molecular diffusion aspect of Knudsen selectivity ($\alpha_{i/j}$) and Knudsen diffusion (D_k), in **Table** 4.7, calculated according to:

$$\alpha_{solute/toluene} = \sqrt{\frac{M_w(toluene)}{M_w(solute)}} \tag{4.3}$$

$$D_{Knudsen} = 0.66r\sqrt{\frac{8RT}{\pi M_w}} \tag{4.4}$$

Molar volume was calculated by HsPiP (Hansen, 2004).

Component	Mw $(gmol^{-1})$	M_v^1 (cm^3mol^{-1})	Knudsen selectivity [2] $\alpha_{solute/toluene}$	Knudsen disffusion [3] $D_{knudsen} \times 10^{+7}$
Toluene	92	106	-	6.90
EtOH	46	58	-	1.38
R-BINAP	622	511	2.6	1.02
C44	619	754	1.5	2.81
C16	226	294	1.5	2.81

Table 4.7: Solute and solvent properties for mass transport in the porous system.

(1) The differences in solute molar volume can partially explain the rejection in PEM modified membranes. Taking the rejection data of PDDA/PSS modified PAN from **Table** 4.6 and molar volumes from (**Table** 4.7), C44 molar volume is ≈ 1.5 times higher than R-BINAP. Similarly, the rejection of C44 is 1.48 times higher than R-BINAP. Similarly, molar volume $M_{v(R-BINAP)}/M_{v(C16)}$ = 2.7 and rejection ratio of these two solutes in PAN (PDDA/PSS)10 is $R_{R-BINAP}/R_{C16}$ =2.5.

(2) The rejection of R-BINAP (R) has been calculated according to:

$$R = 1 - \frac{C_p}{C_f} \tag{4.5}$$

where c_p is the permeate concentration and c_f, is the feed concentration. By the calculation of Knudsen diffusion (D_k) (**Table** 4.7), D_k of toluene is ≈ 6 times higher than D_k of R-BINAP.
For toluene, feed and permeate concentration are equal, which means: $C_{pT} = C_{fT}$;
For R-BINAP, Knudsen diffusion is 6 times smaller than toluene;
Therefore the permeate concentration is also 6 times smaller than the concentration in the feed, which means,

$C_{p(R-BINAP)}$=$C_{f(R-BINAP)}/6$
$C_{p(R-BINAP)}$ / $C_{f(R-BINAP)}$ ≈ 0.16, and
$R_{R-BINAP}$ ≈ 84

The real scenario is the rejection of R-BINAP in pristine PAN was 3-5%, which cannot be explained by the D_k. However, the overall rejection can be primarily affected by the following:

- The pore size of the membrane is widely distributed in which, small pore give the rejection, and large pore causes bulk permeation resulting in overall rejection-permeation performance.

- Once PEM modifies PAN, the reduction of pore depends on specific PEM tape. Each PEM can exhibit different swelling properties once exposed to the solvent. Depending on the solvent type, the swelling level can be different. Once PEM swells in a given solvent, it can cause pore block of small pores, reduce the pore diameter of the larger pores which influence the final rejection in a given porous system, as presented in **Figure** 4.18.

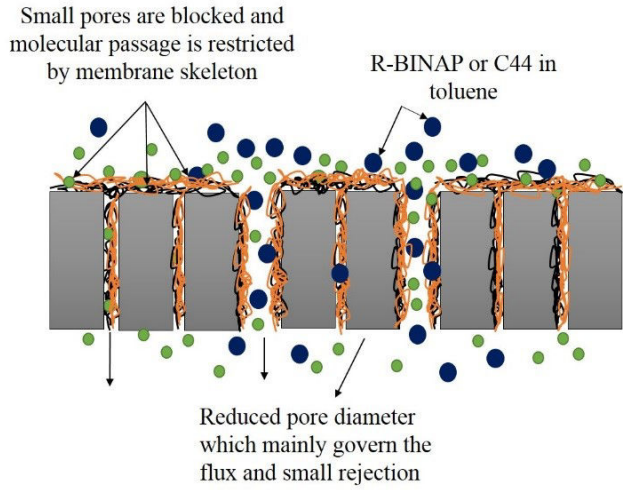

Figure 4.18: Scheme for mass transport in the porous system after PEM modification.

4.8 Solute rejection by pristine and modified PAN from ternary feed mixtures

The permeation-rejection performance of pristine and modified PAN has been measured using ternary feed mixtures. Two ternary systems have been studied:

1. Feed: 0.05wt% R-BINAP, 0.05-0.1wt% C16 in toluene.
2. Feed: 0.05wt% R-BINAP, 0.05wt% C44 in toluene. **Table** 4.8 gives a summary of the results obtained from the ternary OSN feed in prototype PAN membranes.

Ternary Feed	Feed: Ternary 1 & 2	Ternary 1		Ternary 2	
Membranes	J_{global} $(Lm^{-2}h^{-1})$ $\pm 5\%$	R% RBINAP ± 1	R% C16 ± 1	R% RB ± 1	R% C44 ± 1
PAN pristine	60	5	2	4	7
PAN (PDDA/PSS)10	15	32	7	36	50
PAN (PAH/PSS)10	5	10	5	21	15
PAN (PAH/PAA)10	5	17	5	29	37
PAN (PDDA/PAA)10	2	37	12	27	35

Table 4.8: Flux and rejection in pristine and PEM modified PAN from ternary feed mixtures at 10 bar, 30°C and feed cross-flow: $7-10$ kg/h.

The ternary feed has no influence on the global flux i.e., the fluxes are almost the same as the pure solvent fluxes, which seems due to the very low concentration of the solutes (0.05wt %) in the feed, keeping the global solution properties such as viscosity and density are the same as a pure solvent. In most cases, the rejection performance of each solute from binary feed (**Table** 4.6) and ternary feed (**Table** 4.8) are comparable. When ternary 2 was used in the feed, the rejection of R-BINAP slightly increased. In each feed cases, PDDA/PSS modified PAN exhibit the rejection improvement.

4.9 Effect of concentration in C16 wt.% in the ternary mixture of R-BINAP, C16 in toluene

This experiment was dedicated to investigating the retention from a mixture where the concentration of R-BINAP kept constant in the feed mixture while varying the concentration of C16. In **Figure** 4.19, the global flux, rejection of R-BINAP, and C16 are plotted against the C16 concentration, varied from 0-20wt% in the feed.

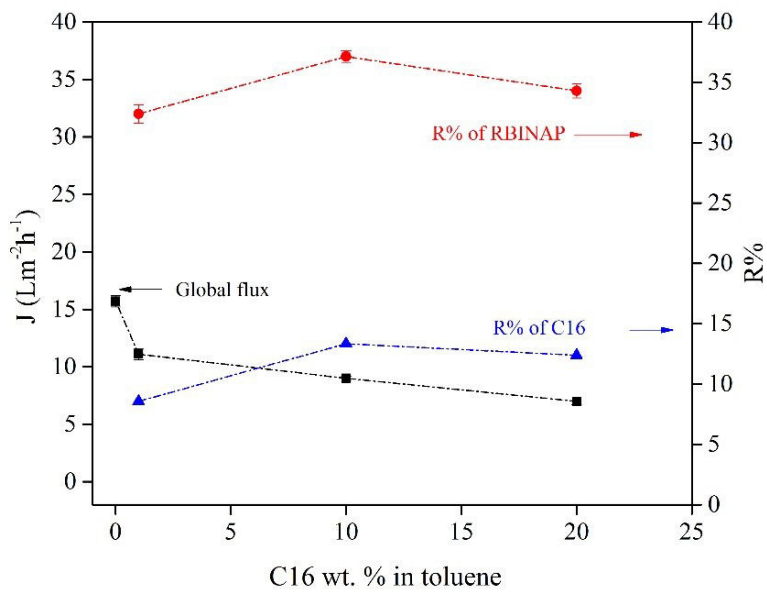

Figure 4.19: Effect of concentration in the ternary feed mixture using PAN(PDDA/PSS)10 at 30°C, 10 bar TMP under $7-10$ kg/h cross-flow rate.

The influence of C16 concentration in **Figure** 4.19 shows that the flux decreases upon increasing C16 in the feed without much of affecting the rejection of R-BINAP and C16. As a simple explanation, one can invoke the lower molar volume of the aliphatic solute, i.e., $Mv = 291cm^3mol^{-1}$, compared to toluene ($Mv = 106cm^3mol^{-1}$).

At last, the results show that the global OSN flux is decreased by 50% when C16 concentration reaches 20wt% in the feed. The addition of C16 increases the viscosity of the feed, which causes the decrease of global flux.

4.10 Conclusion

The OSN study of the porous systems highlights the permeation-rejection results that obtained in AMS 3012 and PAN the first porous system AMS 3012 exhibit a larger number of small pores, high surface porosity when compared with the second porous system PAN. For these apparent reasons, toluene flux in AMS is lower than PAN while the rejection of solute in AMS is higher. However, permeance in PAN is highly affected by the transmembrane pressure, limited the OSN study in the porous system up to 10 bar.

Once modified, two distinct situation rises- in AMS, the flux decline was extreme due to a possible pore block and dense nanolayer formation. In modified PAN, rejection improved but not at an expected level. The trade-off between the pore size and the number of bilayers have been realized for the reduction of pore size and to avoid the formation of dense nanolayer on the top of the membrane. A mixed pore system is apparent in porous system despite modification, in which small pores govern the rejection while larger pores lead to bulk permeation. The permeation of solutes and solvents are independent of each other, and molar volume of solutes play a vital role in the rejection.

Once modified by PEM, the mass transport phenomena in the porous system add new parameters such as charge density and swelling of pore wall by PEM in solvents. The swelling differences of PEM in different solvents is highly promising for designing the new generation nanoporous membrane with tunable pore sizes in different solvents.

However, in the ANR context, the rejection values in the modified porous system are still lower than the rejection obtained in pristine PDMS (80% rejection of R-BINAP). Additionally, the toluene permeance in PEM modified porous systems was also much lower than PDMS. Thus PEM in the porous system is less favorable when considering it for toluene permeation and ligand or catalyst separation.

The interesting fact, however, the EtOH permeation in modified PAN was on average ten times higher than in modified PDMS. Therefore the solute recovery from EtOH media could bear the prospect for PEM modified PAN membrane.

From the above result, the PEL modification of porous structure does not lead to satisfactory rejection result. The OSN flux is sharply reduced without reaching significant improvement for the rejection of the solutes. Also, the detailed characterization of the modification of the prototype membranes is challenging to obtain and do not allow a clear view of the mechanism.

Chapter 5

Study of process parameters on OSN results and their perspectives

Previous chapters focused on OSN performance with dense and porous membranes using diluted feed mixtures of catalyst in toluene and ethanol. The performance was mainly discussed from the viewpoint of the potential interactions between the feed components and the membrane.

The purpose of this chapter is to evaluate the influence of the operating conditions in the obtained results; indeed, it is known that in separations, the results can also be dependent on the operating parameters which may directly influence the performance of the process. Such parameters are the cross-flow velocity, transmembrane pressure (TMP), temperature, and solute concentrations. The effect of these parameters can indeed induce some differences between the properties of the solution in bulk and in close contact with the membrane and, hence, modifies the effective activity gradient of the solutes, the solution viscosity or the feed temperature.

The following scheme (**Figure** 5.1) presents a closely associated membrane-solute-solvent and process parameters. This chapter focuses on the effect of process parameter using dense OSN system.

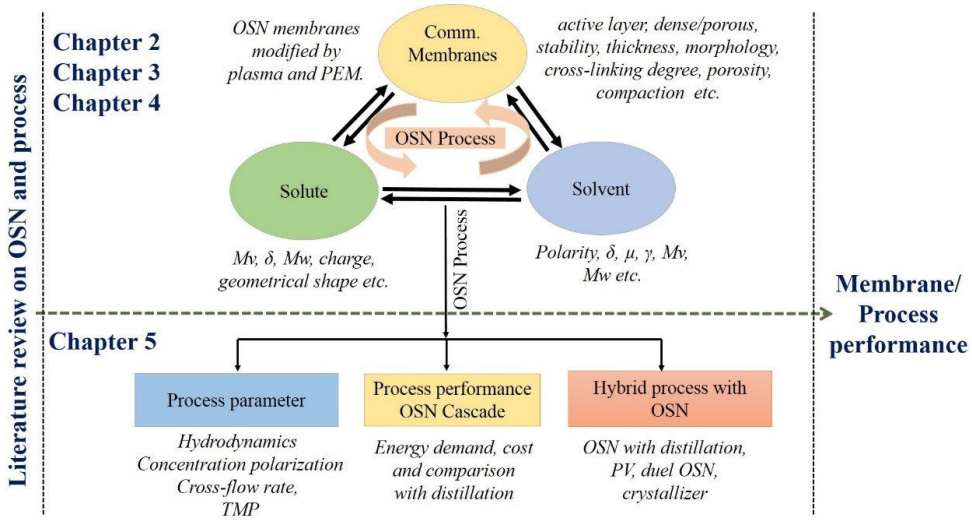

Figure 5.1: Overview of the most critical parameters and operating parameters influencing the process performance.

.

5.1 Abstract

This chapter intends to investigate the effect of process parameters on the observed results using mainly the pristine PERVAP4060. The effect of cross-flow rate, concentration polarization, and flow hydrodynamics have been considered as the critical process parameters. The effect of transmembrane pressure (TMP) in permeation was addressed with the experimental observation in PERVAP4060 using diluted R-BINAP and ToABr in toluene.

The cross-flow rate in OSN cell was varied from 1-28 kg/h, and corresponding toluene flux and R-BINAP rejection were measured in different cross-flow rates. The flux and rejection were obtained fairly constant. Next, the investigation of the concentration polarization (CP) phenomena were conducted by measuring flux and rejection at different cross-flow rate, in the range of 0.1-4 m/s. Applying boundary layer film model and Pecklet number within this cross-flow range, no effect of CP was detected in PERVAP4060 with the feed of diluted R-BINAP and C16 in toluene. Afterward, using the OSN cell dimensions and cross-flow velocities, corresponding Reynolds numbers were calculated, giving a laminar-turbulent flow range in which both flux and rejection of diluted R-BINAP and ToABr in toluene were steady without noticeable fluctuation i.e., no impact of the hydrodynamic condition on permeation-rejection with both pristine and modified PERVAP4060. Next, one cascade in series up to three OSN stages have been investigated using the performance of a single stage OSN and rejection improvement achieved up to 97% with the cascade. In parallel, the price of feed material for a given separation case shows that the highest cost contributing component is the catalyst despite its low feed concentration which also indicates the potentiality of OSN at process scale using PERVAP4060. Also, the energy demand of OSN was calculated ≈ 60 times less than distillation. Other possibilities of hybrid processes such as OSN with distillation, PV, and dual membrane OSN, are briefly addressed.

5.2 Effect of cross-flow feed conditions on OSN membrane performance

In different membrane processes, it is widely reported that hydrodynamic conditions such as cross-flow velocity can affect the performance of the separation. The origin of these observations is often assigned to an uneven distribution of velocities due to the cross-flow conditions that may induce uneven distribution, cake formation, or uneven component concentration. This section investigates if the variation of cross-flow feed velocity would induce any fluctuation in OSN flux or solute rejection. Under low cross-flow feed velocity, the dissolved molecules which are rejected by the membrane can accumulate on the membrane surface, that may reduce the solvent activity and increase of hydraulic resistance.

5.2.1 Effect of cross-flow velocity on solvent flux and solute rejection

The effect of cross-flow velocity from 1 to ≈ 28 kg/h was evaluated, and the results are shown in **Figure** 5.2 and 5.3 through toluene flux and rejection of R-BINAP and C16 at different crossflow rates. The other operating conditions were the same, i.e., TMP = 10 bar and t=30°C.

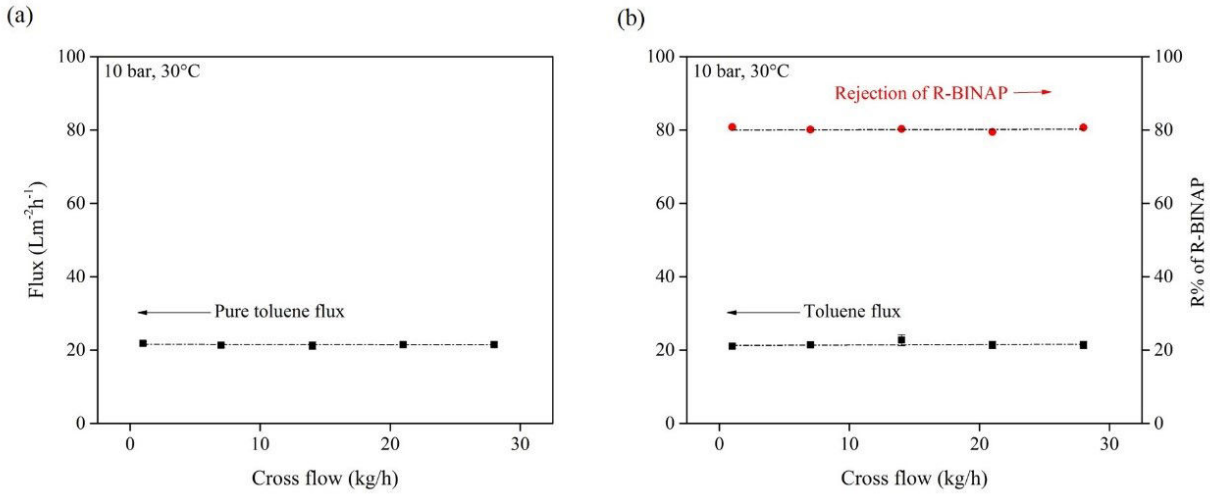

Figure 5.2: Effect of cross-flow velocity on the performance of pristine PERVAP4060 at 10 bar, 30°C. (a) pure toluene flux (b) toluene flux and R-BINAP rejection using the feed of 0.05wt% R-BINAP in toluene

.

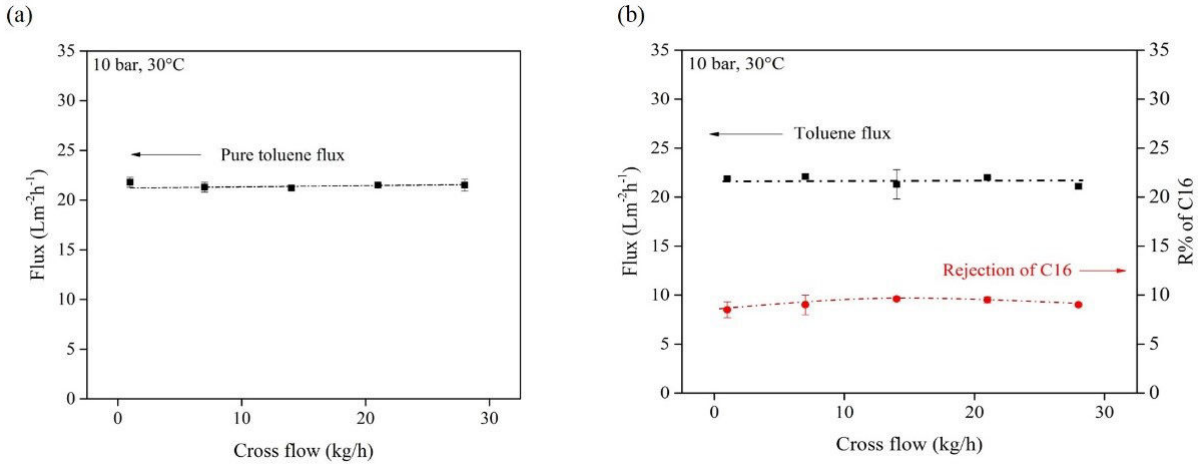

Figure 5.3: Effect of cross-flow velocity on the performance of pristine PERVAP4060 at 10 bar, 30°C. (a) pure toluene flux (b) toluene flux and C16 rejection using the feed of 0.05wt% C16 in toluene.

.

For both feed mixtures, the trends observed are almost the same. Quite logically, the solvent flux is the same and almost equal to the pure toluene flux, whatever the rejection of the solute. As R-BINAP is much rejected than C16, some evolution, if any, was expected. However, the constant flux and rejection indicate that the variation of the cross-flow velocity has no impact on the average flux and rejection when using a highly swollen PDMS.

5.3 Determination of concentration polarization from cross-flow velocity

5.3.1 Theory (Baker et al., 1997) (Baker, 2000)

At a fundamental level, the membrane separation for liquid or gas mixture can be carried out with various objectives: either the separation of one component from a binary mixture or the separation of more than one component from a ternary or multicomponent system.

Thanks to the membrane selectivity, the permeate is enriched in one of the components of the mixture either in one solute, like in pervaporation or in a solvent like in OSN. These different rates of permeation can induce a concentration gradient on both sides of the membrane: the higher the selectivity and the permeance, the more likely CP may occur with low concentrated solutes. Unless the solutions are extremely well stirred, concentration gradients form in the solutions on either side of the membrane. As a result, the layer of the solution adjacent to the membrane surface may become depleted in the permeating solute on the feed side of the membrane and enriched in this component favored on the permeate side.

As a result, the concentration polarization tends to modify the component concentration difference across the membrane, as shown in **Figure** 5.4, according to the two typical cases (a) and (b).

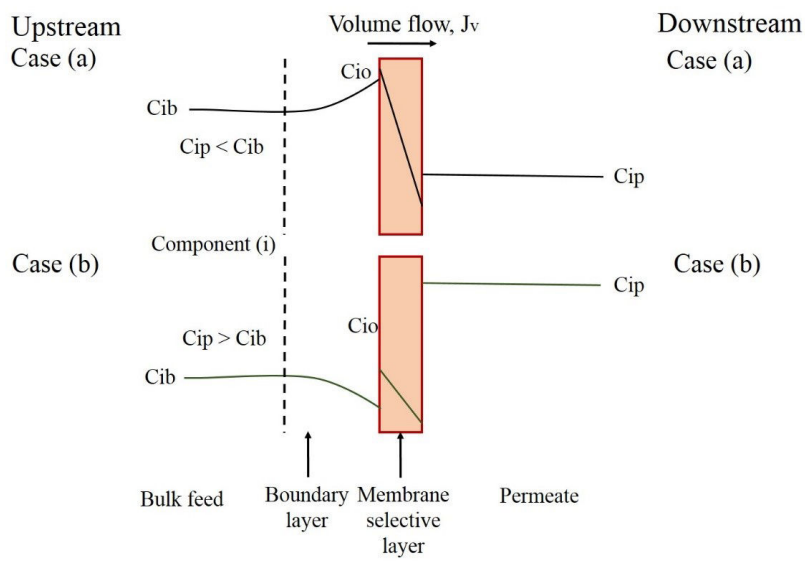

Figure 5.4: Concentration gradient can form when a membrane separates two solutions with different concentrations

.

Figure 5.4 shows the formation of concentration polarization on both sides of the membrane, according to the mass transfer rate through the membrane and the mobility of species in the upstream or downstream phase.

For instance, the case (a) illustrates a rejection situation showing a concentration increase upstream to the membrane. This situation is expected in reverse osmosis and in OSN and may induce osmotic phenomena that can influence the solvent flux.

Conversely, the case (b) illustrates a depletion situation showing a concentration decrease upstream to the membrane, thereby lowering the driving force of the corresponding solute and its mass transfer. This situation can easily occur for components endowed with high membrane permeances, like in pervaporation.

One approach to describe the effect of concentration polarization is to consider the mass transfer resistance to permeation across the membrane and the additional resistance due to the adjacent boundary layer. The mass transfer coefficient on the boundary layer (k_b) and its dependence are empirical.

$$(K_b) = constant.Q^{\alpha}H^{\beta}T^{\delta}.... \tag{5.1}$$

where Q, fluid velocity, H, channel height, D, diffusion coefficient, T, feed solution temperature.

The second approach takes into account the building of concentration polarization is the boundary layer film model, which postulates the formation of a thin boundary layer (δ) adjacent to the membrane. Worth to mention that this model oversimplifies the hydrodynamics, but still contains an adjustable parameter, the boundary layer thickness, which can explain most experimental data.

In any process, if one component is enriched at the membrane surface, then mass balance dictates that a second component is depleted at the surface. By convention, concentration polarization effects are described by considering the concentration gradient of the minor component.
Now considering R-BINAP as a minor component, the flux of R-BINAP is given by the product of permeate volume flux (J_v) and the permeate R-BINAP concentration C_{ip}. Since R-BINAP is used in the feed mixture having a very low concentration of 0.05 wt.% which means that, under steady state, the R-BINAP flux at any point within the boundary layer is equal to the permeate R-BINAP flux ($J_v.C_{ip}$) (**Figure** 5.5).

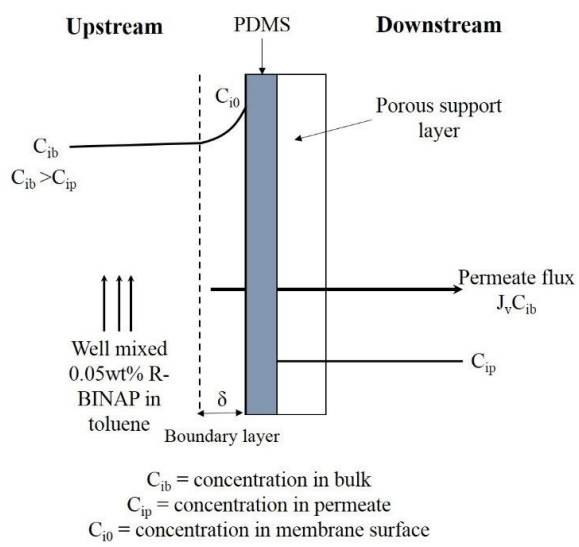

Figure 5.5: R-BINAP concentration gradient adjacent to the OSN membrane PERVAP4060. The mass balance equation for solute flux across the boundary layer is the basis of the film model description of concentration polarization.

In the boundary layer, this net R-BINAP flux is equal to the convective R-BINAP flux towards the membrane ($J_v.C_i$) minus the diffusive R-BINAP flux away from the membrane expressed by Ficks law ($D_i.dc_i/d_x$). So, the simple mass balance, transport of R-BINAP at any point within the boundary layer can be described by the equation:

$$J_v C_i - D_i \frac{dc_i}{d_x} = J_v C_{ip} \tag{5.2}$$

Where D is the diffusion coefficient of R-BINAP, x is the co-ordinate, perpendicular to the membrane surface, J_v is the volumetric flux in the boundary layer generated by permeate flow through the membrane.

The mass balance equation can be integrated over the thickness of the boundary layer δ and the polarization equation written as:

$$\frac{C_{i0} - C_{ip}}{C_{ib} - C_{ip}} = \exp \frac{J_v \delta}{D_i} \tag{5.3}$$

where C_{i0} is the concentration at the membrane surface, C_{ib} is the concentration at the bulk and C_{ip} the concentration in the permeate.

The term $(J_v\delta)/D_i$ is termed as the Pecklet number . Here the increase and decrease of the permeate concentration at the membrane surface C_{i_0}, compare to the bulk concentration (C_{ib}) determines the concentration polarization, and the ratio is termed as the concentration polarization modulus.

5.3.2 Determination of concentration modulus: R-BINAP-toluene.

The equation (5.3), shown in the previous section can be expressed as:

$$\ln(\frac{1}{E} - 1) = \ln(\frac{1}{E_0} - 1) - \frac{J_v \delta}{D_i} \tag{5.4}$$

where this enrichment $E = C_{ip}/C_{ib}$ and $E_0 = C_{ip}/C_{i0}$.
The boundary layer thickness δ (m) is the function of the feed solution velocity in the module feed flow. Thus the term δ/D_i can be expressed as:

$$\frac{D_i}{\delta} = K u^n \tag{5.5}$$

where u is the superficial velocity in the channel and K and n are constants.
The equation (5.5) is thereby expressed as:

$$\ln(\frac{1}{E} - 1) = \ln(\frac{1}{E_0} - 1) - \frac{J_v}{K u^n} \tag{5.6}$$

This equation can be used for the calculation of the membrane system performance on concentration polarization. One method is the data obtained from a single module used operated at various feed solution. Linear regression analysis is then used to fit the data at different feed velocities to obtain an estimate for the concentration polarization. The exponent n is used to adjust to minimize the residual error.
For R-BINAP-toluene system, the flux and rejection of R-BINAP were measured at a different superficial velocity ranging from $0.08m/s$ ($Re \approx 100$) to $3.6m/s$ ($Re \approx 2700$). The feed and permeate R-BINAP concentration gives the enrichment, $E(= 0.2)$ and R-BINAP flux ($m3m^{-2}s^{-1}$) was obtained using the global flux of $21Lm^{-2}h^{-1}$ measured in PDMS. Next, $ln(1/E-1)$ was plotted against J_v/u^n in **Figure** 5.6, using two n values of 1 and 0.1.

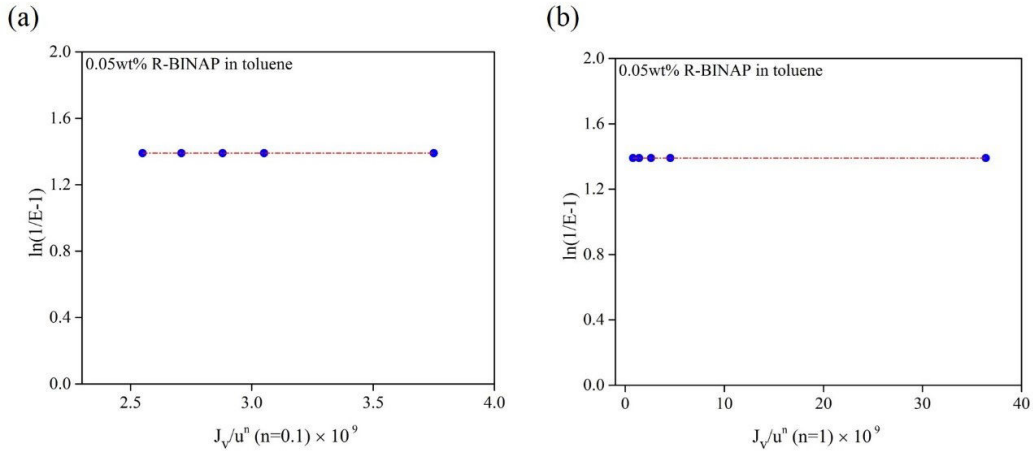

Figure 5.6: R-BINAP enrichments in pristine PDMS are plotted as a function of feed solution superficial velocity in OSN experiments of flat sheet membrane configuration at 10 bar, 30°C: (a) n=1 (b) n=0.1

.

The intrinsic enrichment $E_0(C_{ip}/C_{ib}) = E(C_{ip}/C_{i0})$ =0.2 and C_{io}/C_{ib} =1 which means no concentration polarization occurred.
It is worth to mention that, within the broad range of superficial velocity, the flux and rejection was found nearly constant as such the OSN flux was obtained $\approx 21Lm^{-2}h^{-1}$ and rejection of R-BINAP (R%) was $\approx$ 80 in the whole velocity range. No significant variation were registered in this velocity range.

Similar results of no CP occurrence have been observed for the C16-toluene system with diluted $< 0.1wt\%$C16. The flux remains unaltered while rejection was $\approx$ 10% in the whole velocity range. Thus the diluted C16-toluene system does not either exhibit any concentration polarization phenomena. To go forward with these results, the hydrodynamic regime was evaluated.

5.4 Effect of hydrodynamic flow on flux and rejection in pristine and modified PERVAP4060(PDMS)

The effect of laminar and turbulent regimes (hydrodynamic flow) on the flux and rejection can be quantified by calculating the dimensionless Reynolds number according to the formula:

$$Re = \frac{\rho u D_H}{\mu} \tag{5.7}$$

where ρ, is the density of toluene ($857kg/m^3$) at 30°C, u, is the mean feed velocity (m/s), D_H , is the hydraulic diameter and μ, the dynamic viscosity ($0.53mPas$ at 30°C).)
The hydraulic diameter was calculated according to

$$D_H = \frac{4A}{P} \tag{5.8}$$

where A, cross-sectional area (m^2), P, wetted perimeter (m) of the OSN cell, which was calculated according to the rectangular shape of OSN cell where the membrane was housed (**Figure** 5.7). The dimension of the cell was $7.5cm \times 4.5cm \times 2mm$. Thus, the effective surface area of the membrane $\approx 0.0034m^2$ and the perimeter $\approx 0.5m$ according to the formula

$$P = 4(a + b + c) \tag{5.9}$$

where a, b, and c respectively presents the length, width, and height of the cell.

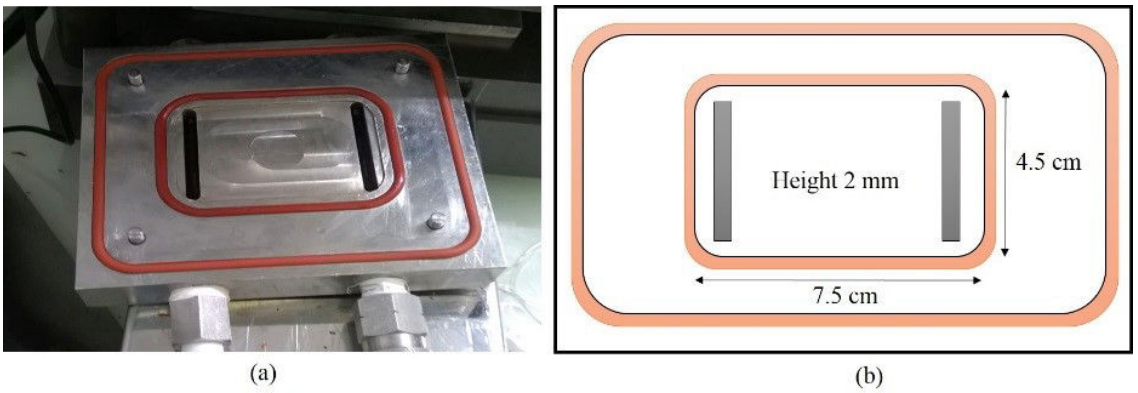

Figure 5.7: (a) the membrane holding cell used in OSN. (b) the dimension of the cell
.

Next, the viscosity (0.53 $mPa.s$) and density (0.857 g/cm^3) of toluene at 30 $°C$ was used for the calculation of mean velocity and Reynolds number. The Reynolds number corresponding to the cross-flow velocity and their effect on membrane performance is summarized in **Table** 5.1.

Feed flow (Kg/h)	Mean velocity (m/s)	Reynolds number (Re)	Average toluene flux ($Lm^{-2}h^{-1}$) ± 5%	Rejection of R-BINAP, 0.05wt.% in toluene ± 5%	Rejection of C16, 0.05wt.% in toluene ± 5%
1	0.08	97	21.5	80.8	8.5
8	0.65	774	21.7	80.1	9
14	1.13	1356	22	80.3	9.6
21	1.70	2034	21.7	79.5	9.5
28	2.27	2712	21.3	80.7	9

Table 5.1: Effect of feed flow and Reynolds number (Re) on toluene flux and rejection of R-BINAP and C16 at 10 bar, 30 $°C$.

The calculations of the Reynolds number indicates that the operating parameters allow running the hydrodynamic flow from laminar to turbulent. **Table** 5.1 shows that the velocity distribution in the cell from a laminar to turbulent does not have any impact on OSN flux and rejection. Worth to mention that the solute feed concentration (0.05wt%) was considerably low. In agreement with the CP presented in **Figure** 5.6, such a trend is assuring of the system stability under different flow velocity. The investigation of the hydrodynamic feed flow via the Reynolds numbers on flux and rejection is also presented in **Figure** 5.8; clearly, no effect could be detected.

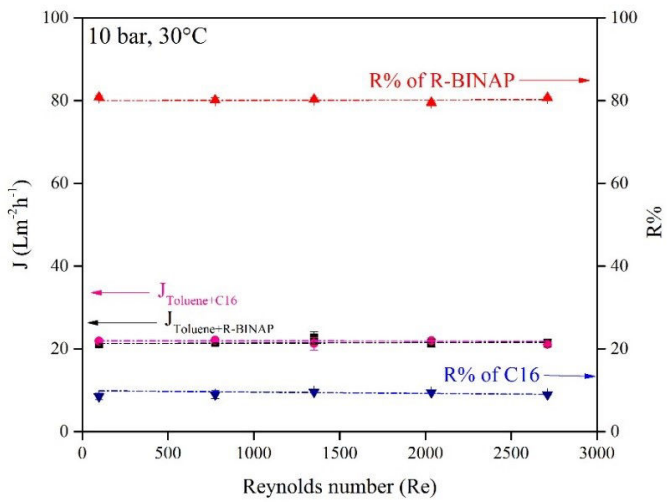

Figure 5.8: Effect of Reynolds number on the rejection of R-BINAP (0.05wt.%) and C16 (0.05wt.%) from toluene at 10 bar, 30 $°C$ using pristine PERVAP4060.

The same experiment was repeated using the PEM modified PDMS (PAH/PSS)10 membrane, and the results presented in **Figure** 5.9 also show no effect of hydrodynamic conditions on flux and rejection. Note that the PEM of PAH/PSS on PDMS provides an improve rejection of R-BINAP and lower flux from a toluene feed when compared with rejection in PDMS.

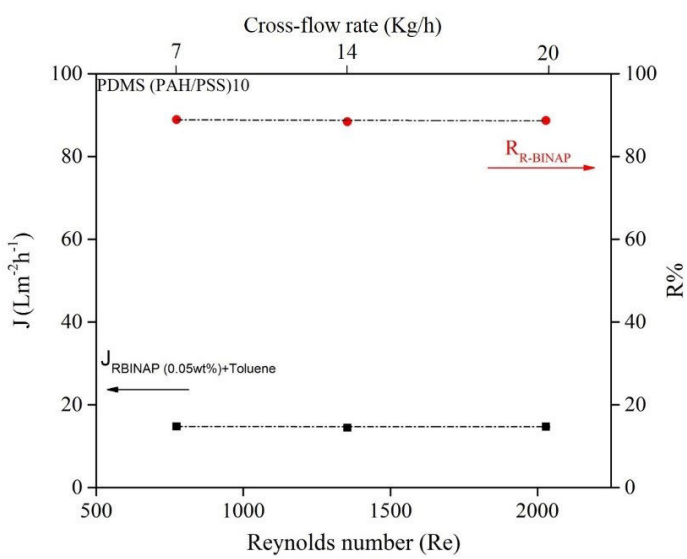

Figure 5.9: Effect of Reynolds number on the rejection of R-BINAP (0.05wt.%) and C16 (0.05wt.%) from toluene at 10 bar, 30 $°C$ using pristine PERVAP4060.

The constant flux and rejection with both pristine and modified PERVAP4060 under different hydrodynamic conditions indicate the high stability of membrane performance.

5.5 Effect of pressure in OSN process for solvent transport and solute rejection in dense PERVAP4060(PDMS)

In pressure driven membrane processes, like in OSN, it can be advantageous to increase the operating pressure to apply high TMP in order to limit the required membrane area and the process capital cost (CAPEX) while increasing the operating costs (OPEX) slightly. However, it is also known that membranes may exhibit lower performances at higher pressures due either to the lack of mechanical stability, i.e., compaction drawbacks, or to the enhanced fouling of porous membranes, resulting in loss of separation performance and shorter lifetime of the membrane. Nevertheless, a linear flux trend with TMP and constant rejection help in the detection of the maximum applicable process pressure.

Compaction phenomena have often been registered in OSN (see Literature Chapter), but getting the right interpretation is very rare. Indeed, whatever the type of membrane, porous or non-porous, distinct origins can induce the same effect, i.e., flux reduction upon pressure increase. That is why compaction phenomena are very controversial in OSN.

Usually, it is wise to know first if the observed flux decrease is reversible or not. If it is not reversible, a mechanical loss of stability can be stated. If the phenomenon is reversible, other hypotheses can be investigated:

- swelling by the organic solvent, deformation of the porous layers and compaction;
- limitation of swelling due to pressure
- ...

Figure 5.10 provides a possible explanation in the dense swollen system adopted from the pioneering work of (Paul, 1973).

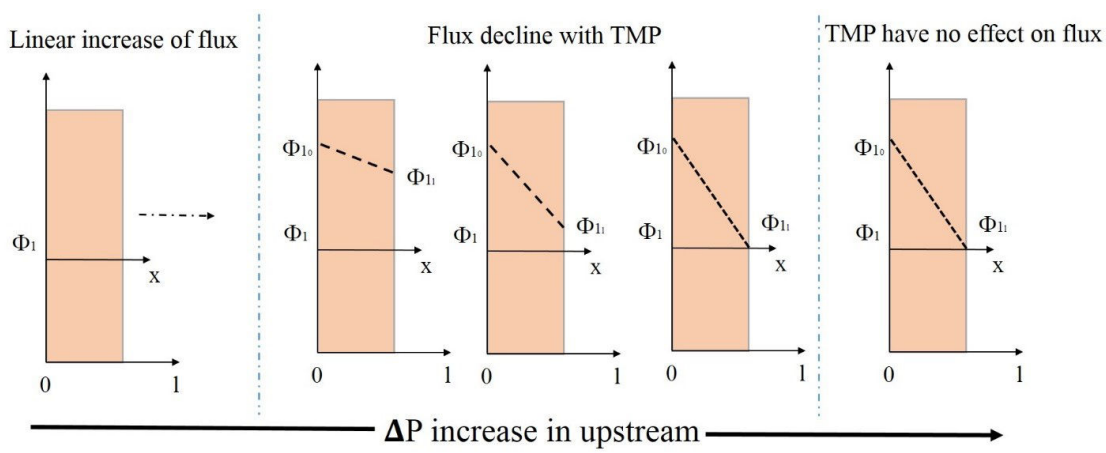

Figure 5.10: Solvent transport through a dense-swollen system as a function of TMP at room temperature.

The driving force for liquid transport through a swollen membrane is the swelling gradient between the upstream and the downstream face of the membrane as denoted ϕ_{l0} ϕ_{l1}, in **Figure** 5.10. ϕ_{l0} is the liquid volume fraction for in the upstream side, ϕ_{l1} is the liquid volume fraction for in the downstream side. The liquid volume fraction in the upstream side is constant, and it does not

depend on the applied pressure. However, as the upstream pressure increases, the liquid volume fraction decreases in the downstream side. At a certain upstream pressure, ϕ_{l1} becomes zero, and the flux cannot be increased further with the increase of upstream pressure.

5.5.1 Effect of pressure on flux and rejection though PERVAP4060 for R-BINAP in toluene

The effect of TMP was studied in pristine PERVAP4060 using a feed of 0.05wt.% R-BINAP in toluene at 30°C and 7-10 Kg/h feed cross-flow.

In **Figure** 5.11, the observed linear flux evolution with TMP is presented up to 40 bar. The corresponding rejection was nearly constant ≈80% within the range of 0-40 bar.

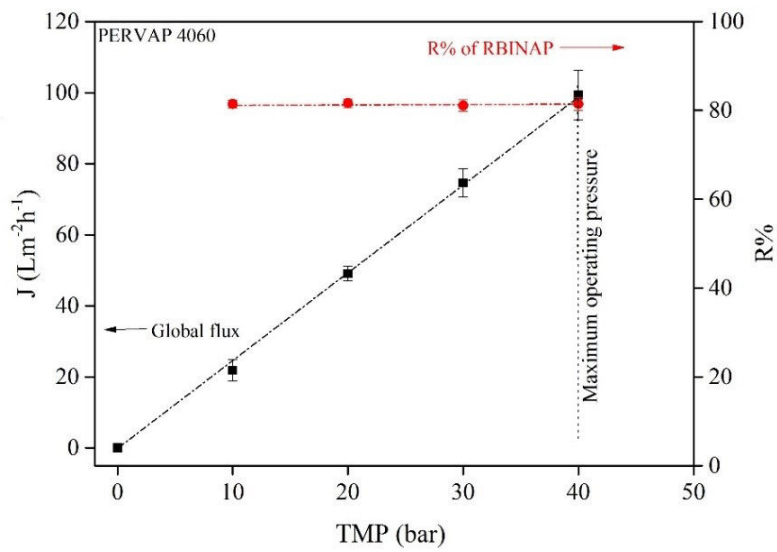

Figure 5.11: Effect of pressure in toluene flux and R-BINAP rejection in PERVAP4060 from a feed of 0.05wt.% R-BINAP in toluene at 30 °C and 7-10 kg/h cross-flow.

The flux result presented in **Figure** 5.11 is in good agreement with the result of (Ben Soltane et al., 2013) (Ben Soltane et al., 2016).

The constant rejection up to 40 bar is highly promising to apply for high yield of the process. Note that the backward flux and rejection (when TMP reduced to 10 bar from 40 bar) was reproducible after several runs which indicate no internal fouling of the system.

5.5.2 Effect of pressure on flux and rejection though PERVAP4060 for ToABr in toluene and ethanol

The rejection of 0.05wt.% ToABr from toluene and EtOH was considered up to 10 bar. This study intended for a cross-check of the flux and rejection trend using a phase transfer catalyst instead of R-BINAP and two completely different solvents in which the catalyst is soluble.

As expected, the linear flux trend was obtained (**Figure** 5.12) in both toluene and ethanol, while the rejection of ToABr was fairly constant.

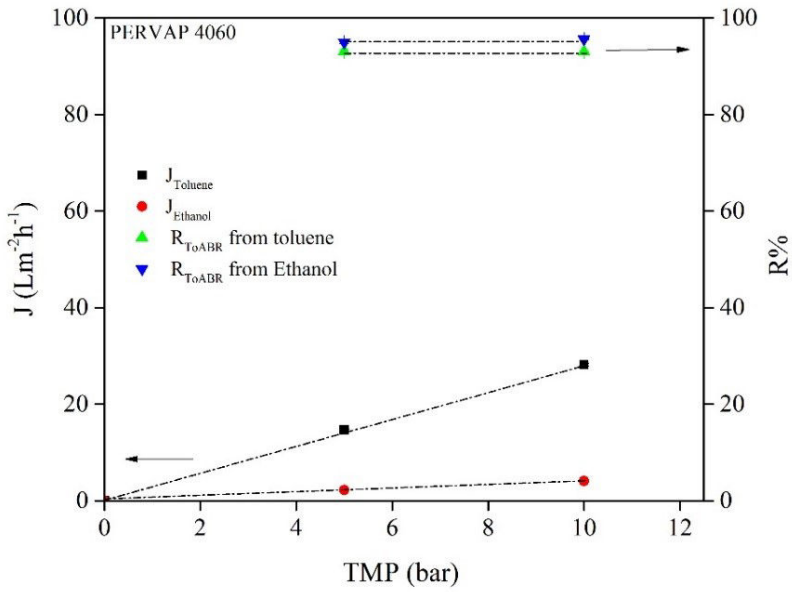

Figure 5.12: Effect of pressure in toluene flux and R-BINAP rejection in PERVAP4060 from a feed of 0.05wt.% ToABr in toluene and EtOH at 30 °C and 7-10 kg/h cross-flow.

The ethanol flux obtained 10 fold lower than the toluene flux. The flux values are related to the difference in PDMS swelling in toluene (≈114%) and in ethanol (≈5%). These flux values are comparable with the finding reported in (Ben Soltane et al., 2013) (Ben Soltane et al., 2016).

5.6 Advantages of OSN over distillation in energy saving

When considering the results reported in previous chapters, and in particular the results corresponding to the capability of OSN to separate post-reaction ternary mixture from a catalytic system, expected advantages are:

- Increase catalyst (R-BINAP) turnover number by continuous recycle and reuse of catalyst.
- Easy permeation of product (C16)
- Lowering the cost of toluene recovery.

Indeed, OSN is commonly mentioned as a more energy-efficient alternative to distillation. An added value of using OSN is to save expensive catalyst from irreversible degradation, which is one commonly referred drawback of using distillation for the separation of homogeneous catalyst. For a process comparison, a simple approach of necessary energy evaluation has been carried out based on batch distillation and a pump pressurized pilot-scale OSN system for a given amount of liquid processing.

The energy source by industrial OSN requires only pump energy generating the required back-pressure while batch distillation considers successive evaporation-condensation as presented in **Figure** 5.13.
A large scale OSN system generally operated by a feed-and-bleed configuration. In such a

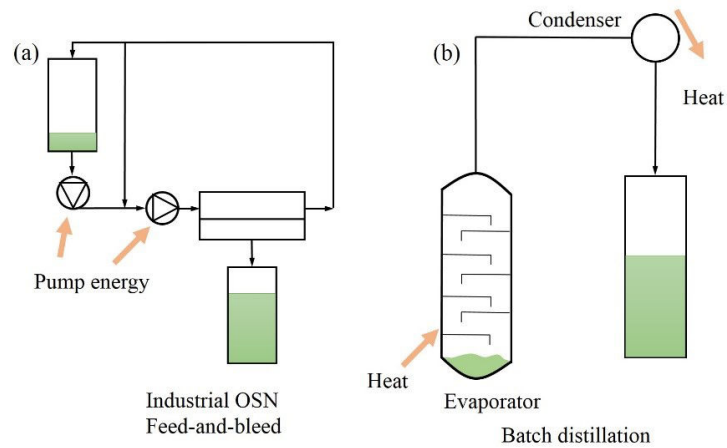

Figure 5.13: Large scale OSN: energy required from two pumps (feed and bleed) (b) Batch distillation: Energy of evaporation and condensation.

system a recirculation loop using a second pump is installed over the membrane. Flow through the recirculation loop is 5 -10 times higher than the feed flow and aims to reduce potential concentration polarisation in the membrane module. Feed-and-bleed operation enables a high-flow rate over the membrane without having to pass the full process volume through the back-pressure valve, hence minimizing the overall energy consumption.

The calculation of energy requirement by OSN processing is adopted from (Rundquist et al., 2012) in which total energy requirement corresponds to two component:

(a) Energy requirement for high pressure ($Q_{\Delta P}$) and
(b) energy requirement for a pressure drop over the module (Q_D). Thus, the total energy Q can be presented:

$$Q = Q_{\Delta P} + Q_D \tag{5.10}$$

$$Q = \frac{F_f \Delta P_{TMP}}{\eta} + \frac{F_r \Delta P_D}{\eta} \tag{5.11}$$

Where F is the pump flow rate of the feed (f) and recirculation (r), ΔP is transmembrane pressure (TM) and the pressure drop over the module (D), and η is the pump efficiency.
For a given 5 ton processing per day by OSN at 25 bar, the flux value of $50L/m2.h$ at 30°C adopted from the experiment. The permeate flow needs to be 150 L/h for the given per day processing target which corresponds to use a $3m^2$ membrane area.

Operating with 50% volume recovery in permeate, F_f=300 L/h (8.33× 10^{-5} m^3/s) and F_r=1500 L/h (F_r is five times higher than F_f) (Rundquist et al., 2012) , ΔP(TMP)= 25 bar, ΔP_D=0.5 bar. The pump efficiency η=0.3 (considered) gives the value of Q_{OSN}=0.76kW.

For the same amount of feed processing by distillation (batch), the energy requirement can be calculated by the equations:

$$Q_{distillation} = Q_{heating} + Q_{vaporization} + Q_{condensation} \tag{5.12}$$

$$Q_{heating} = F_m C \Delta T \tag{5.13}$$

$$Q_{vaporization} = Q_{condensation} = F_m \Delta H \tag{5.14}$$

where Q is the required power, F_m is the molar flow, C is the heat capacity (toluene) at constant pressure, ΔT is the temperature difference between the feed and the boiling point and ΔH is the latent heat of vaporization. Using the same processing amount of feed per day as presented for OSN, F_m=0.62mol/s, C=103.6 $J/mol.k$, ΔT=90K, and δ H=32.3kJ/mol giving a value of $Q_{distillation}$=46 kW for a 24h operating time.

Comparing to OSN, the energy demand for distillation is ≈60 times higher, which makes OSN highly attractive. The similar calculation approach has been presented in (Rundquist et al., 2012) using methanol, reporting ≈30 times less energy requirement by OSN comparing with batch distillation.

Clearly, OSN is advantageous over distillation in the energy demand comparison. As mentioned before, one potential drawback of distillation is the damage to the catalyst due to high-temperature. However, a single stage OSN with the catalyst rejection of 80% does not ensure high purity of the product, given that the product component is preferentially permeated.

One possible route to improve the rejection is operating OSN in a cascade configuration, given that its the same membrane to use at a process scale. In the next section, a case study of OSN cascade with a mass balance and feed material cost is considered.

5.7 Improving OSN separation by the multi-stage cascades

When separation is insufficient by OSN, a multistage cascade can be the route to meet the challenge. For example, a consistent 80% rejection in a single stage OSN indicating further separation need to perform to improve the purity. In cascade, the desired separation is achieved by using several membrane modules arranged in series or parallel using recycle stream with different configurations.

In this context, a model system consisting of 0.05wt.% active catalyst of hydroformylation $H-Rh-(CO)(PPh_3)_2$ (MW 656 $g.mol^{-1}$) and 10wt% decanal ($CH_3(CH_2)_8CHO$) (MW 156 $g.mol^{-1}$) in toluene (**Table** 5.2) can be satisfactory to mimic catalyst, product, and solvent after hydroformylation reaction as presented in ANR objective.

The first concern appears as if the separation of such a diluted catalyst is worthwhile at a process scale, and if it has a significant financial interest. That is why a five-ton per day process has arbitrarily considered, and their price component is listed in **Table** 5.2. The price of each component was taken from `https://www.sigmaaldrich.com/france.html` and reduced to a factor of five considering the price as a bulk. The active catalyst price was the average price of hydroformylation pre-catalyst and ligand, which forms an active catalyst in the product.

Membrane	PERVAP 4060 (PDMS)
Model system: catalyst product- solvent	0.05wt% $H-Rh-(CO)(PPh_3)_2$, 10wt% decanal in toluene
$H-Rh-(CO)(PPh_3)_2$ rejection in PERVAP 4060 (%)	80
Rejection of decanal ($C_{10}H_{20}O$)	10
TMP (bar)	25
Temperature (°C)	30
Toluene permeance in PERVAP4060 ($Lm^{-2}h^{-1}.bar^{-1}$)	2.1
Basis: 5-ton feed per day	5
Amount (kg) $H-Rh-(CO)(PPh_3)_2$	2.5
Amount (kg) decanal($C_{10}H_{20}O$)	500
Amount (kg) toluene	4500
Price (euro per kg) of $H-Rh-(CO)(PPh_3)_2$	87 k
Price (euro per kg) of decanal	248 k
Price(euro per kg) of toluene	4 k
Total price (euro) for catalyst in 5-ton feed	217 k
Total price (euro) for the product in five-ton feed	124 k
Total price (euro)for solvent in five-ton feed	19 k

Table 5.2: Context of the OSN for process using PERAP 4060

Interestingly, the catalyst concentration in the feed is very low, presenting only 0.05wt%, which is the highest cost contributing component. In the five-ton basis (**Table** 5.2), one can notice that the total catalyst price is double than the total product price. Thus, even at a very low concentration, the economic interest is obvious, depending on the efficiency of the catalyst separation for re-use.

Applying the feed composition and rejection, as shown in **Table** 5.2, the performance of a single stage OSN is given in **Figure** 5.14.

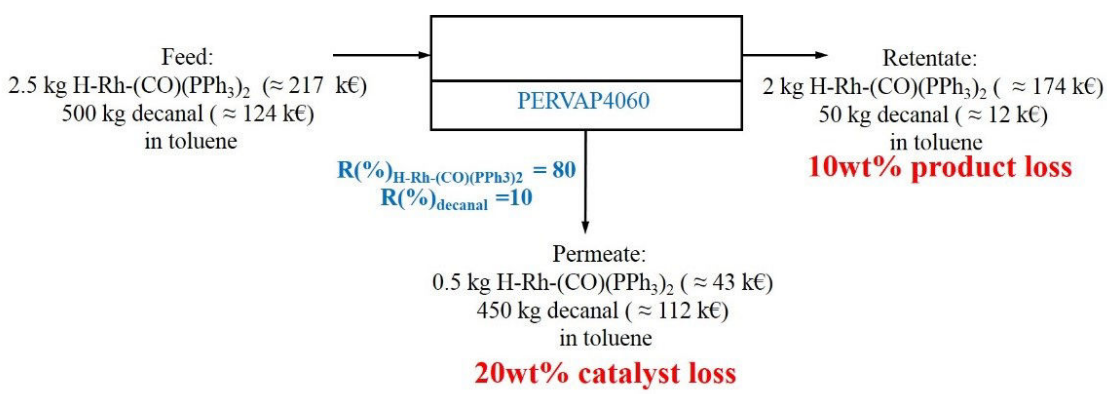

Figure 5.14: Separation of catalyst and permeation of products by single stage OSN process and relevant cost impact, using PERVAP 4060 for the processing of 5-ton feed.

A single stage OSN is capable of recovering a high amount of catalyst while permeating high amount of product. It also presents the possibility of product loss in retentate (if recycled to the reactor) and catalyst loss in permeate (if recovered as a final product). The feasibility largely depends on

the industrial target, which is not present. However, several operational challenges can be estimated:

1. The decanal (10wt% product) in the retentate stream could influence the catalyst turnover number (TON) if recycled to the reaction tank and also can affect the reaction.
2. The $H - Rh - (CO)(PPh_3)_2$ in permeate causes catalyst loss and product impurity, which could be undesirable.
3. The permeate stream needs further treatment to recycle the solvent.

If the industrial objective of product purity and catalyst separation is higher than the separation from a single stage, the multistage cascade could be one route to meet the demand. **Figure** 5.15 presents a three-stage OSN cascade in which the permeate stream is used as the feed in the second stage. For simplicity, the solvent recovery option will be discussed later.

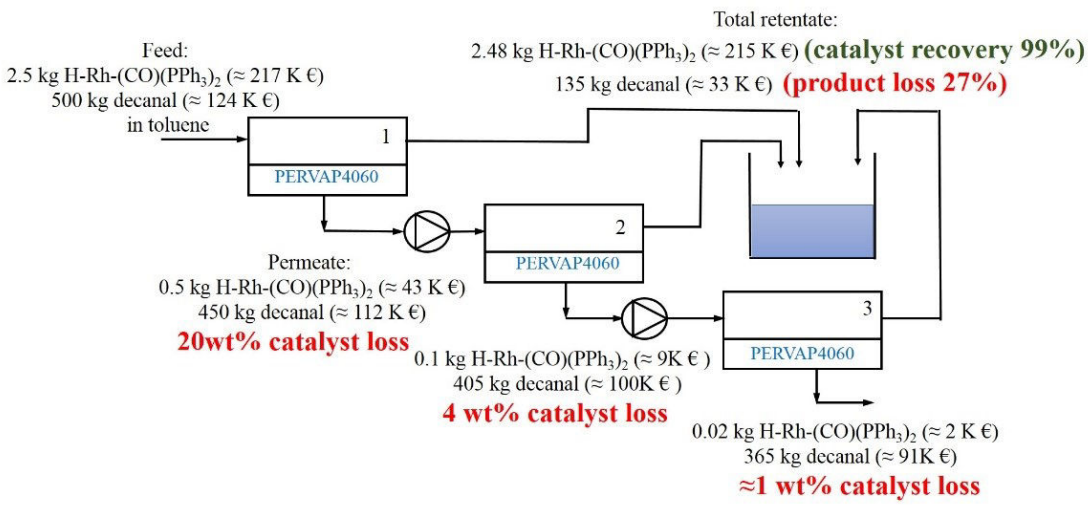

Figure 5.15: Separation of catalyst and permeation of products by three-stage OSN process and relevant cost impact, using PERVAP 4060.

The advantage of a three-stage cascade can be realized from $H - Rh - (CO)(PPh_3)_2$ recovery. The three-stage cascade increases the rejection of $H - Rh - (CO)(PPh_3)_2$ up to $\approx 99\%$ (recovery of 215 k euro equivalents) whereas a single stage rejection is 80% (recovery of 174k euro equivalents). In contrary, three-stage cascade decreases the amount of product in permeate but increase the purity compare to the single stage (**Figure** 5.14). For a given industrial target, if the turnover of a catalyst via retentate stream is tolerated upon recycling, a three-stage cascade can maximize the catalyst loss in permeate. Several trade-off can be realized from cascade:

(a) Single stage OSN ensure high product yield but induces impurity due to a high amount of catalyst in permeate.
(b) Multistage OSN increases catalyst-separation and increase product purity but leads to the loss of overall process yield. It also increases the membrane area and high operating cost.
(c) Additional unit operation with OSN is still necessary with two possibilities: treatment of the permeate stream to recover the solvent or the treatment of retentate stream to recover the product.
(d) The best decision will be mostly dependent on catalytic reaction, industrial objective, and cost to profit analysis.

Next, the solvent recovery from OSN is essential because it represents about $\approx 90\%$ by mass and $\approx 5.3\%$ by cost of the feed (comparing the data from **Table** 5.2). By the end of the process,

this solvent either need to be recycled or separated from the product. Operating the OSN at a moderate 25 bar, an extraction ratio (ratio of volume permeate to volume feed, V_p/V_f) of 0.5 has been considered. If the retentate stream is recycled to the reaction, arithmetically, a single stage OSN allows 50 wt% solvent recovery of total feed (≈2.7% total cost) and a three-stage allows up to ≈ 87.5 wt% solvent recovery (≈ 4.7% of total cost). The rest ≈12.5 wt% solvent remains in permeate after three stages.

As an example, a total feed of total 5000kg toluene in three stages OSN having extraction ratio 0.5 in each stage, recyclable toluene is 4375 kg (retentate) which leaves 625kg (permeate) of toluene to be recovered by other technologies such as distillation, PV or dual OSN.

5.8 Hybrid processes

5.8.1 OSN with distillation

In this section, the hybrid process of OSN up to two stages with distillation is hypothetically assumed using the permeate stream of OSN as the feed of distillation, as shown in **Figure** 5.16. Knowing that the Rh-catalyst is temperature sensitive, and separation of the catalyst by distillation is not desired; the separation task in a hybrid can be distributed as:

- The OSN unit will recover the Rh-catalyst via retentate and transfer it back to the hydroformylation reaction tank.
- The permeate stream will be used in distillation in which toluene will be separated from decanal (product) and transfer back to the reaction tank.
- The number of OSN stage depends on the industrial target of catalyst recovery, which is not known, thereby the multi-stage OSN with high catalyst recovery through retentate is kept as a possibility (**Figure** 5.16b).

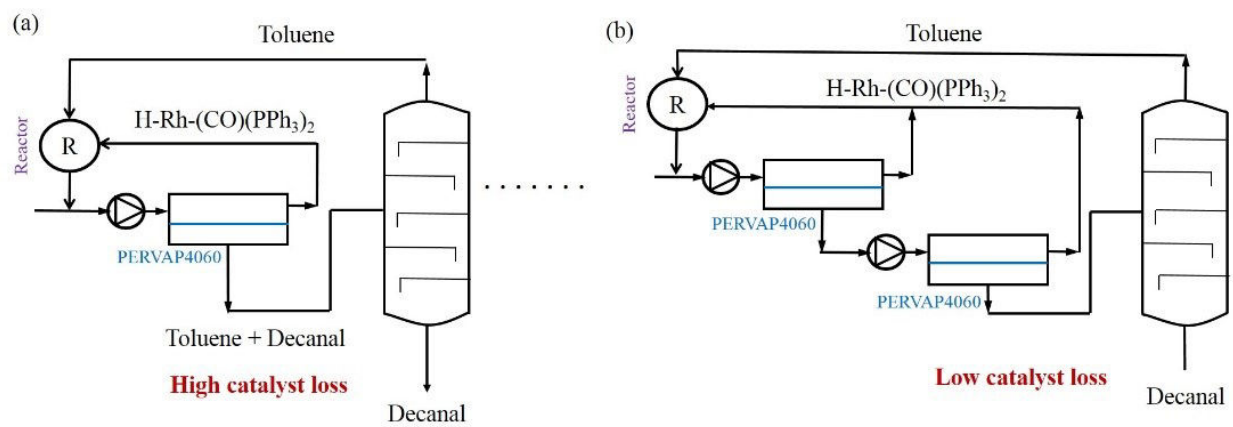

Figure 5.16: Hybrid process with distillation using cascade up to three stages OSN.

Indeed, the drawback of using a single stage is the high catalyst loss through the retentate stream, which can be minimized by increasing the number of OSN stage, as shown in **Figure** 5.15 and 5.16.

The rational decision on OSN hybrid to apply at a process depends on detail CAPEX and OPEX study, which was beyond the scope of this Ph.D.

However, assuming the extraction ratio 0.5 in OSN, the feed volume of distillation in hybrid would be half of the total feed. Accordingly, the energy demand of hybrid is expected to reduce to half when compared with stand-alone distillation for a given separation task.

The energy demand of OSN cascade and hybrid has been calculated according to the formulas presented in the previous section and compared with distillation, and OSN in **Table** 5.3, for a given five-ton feed processing per day.

Technique	Energy requirement (kW)
Distillation	48
OSN	0.8 -1.3
Hybrid OSN+ Distillation (OSN extraction, V_p/V_f =0.5)	24-25

Table 5.3: Energy demand: OSN, distillation, and hybrid process.

Thus hybrid with distillation requires ≈ 50% less energy than standalone distillation using the given configuration for the feed of five-ton feed per day.

5.8.2 Hybrid of OSN with pervaporation (PV) or dual stage OSN

This section presents the hypothetical possibility of applying OSN in a hybrid configuration with pervaporation (**Figure** 5.17a) and dual stage OSN (**Figure** 5.17b), without prior study of CAPEX and OPEX, including unknown separation target of the industry.
As shown in the scheme, the permeate stream of OSN is taken as a feed either in PV using the same PERVAP4060 membrane or in a second OSN stage using Leinzing P84 membrane. Compare to distillation; these hybrids can be operated at a mild temperature condition.

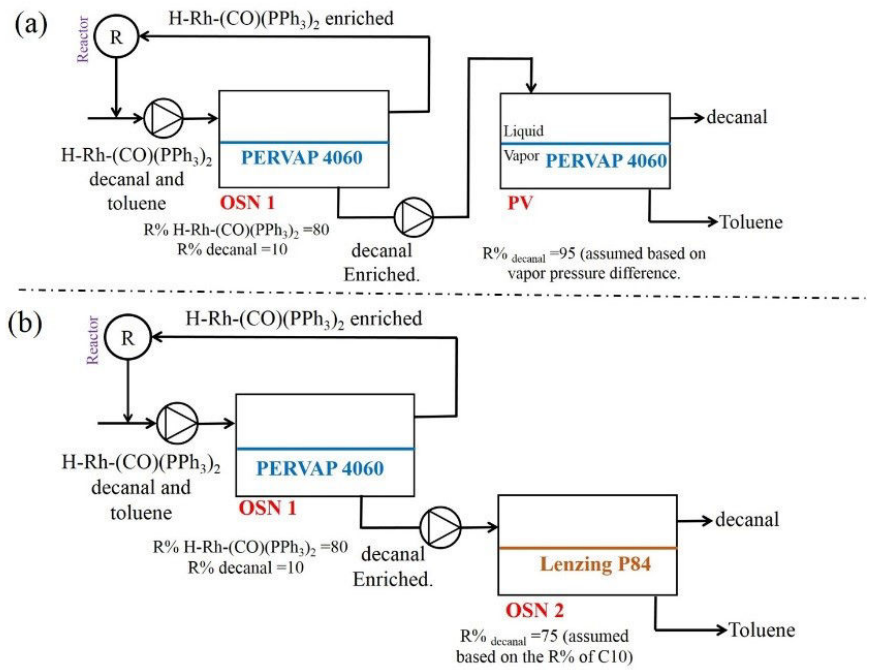

Figure 5.17: Scheme of OSN hybrids for the separation of catalyst and product from a hydroformylation system: (a) Hybrid OSN with PV. (b) Hybrid OSN using a dual membrane in series.

In the hybrid with PV, first, the same PERVAP can be applied based on two factors:

(1) The PERVAP 4060, by origin, is designed for pervaporation application, showing a reasonable PV toluene flux (**Figure** 5.18). The same membrane gives OSN-toluene permeance of 2.1 $Lm^{-2}h^{-1}bar^{-1}$, showing the operational feasibility of PV with OSN, only if, decanal can be separated by PV successfully.

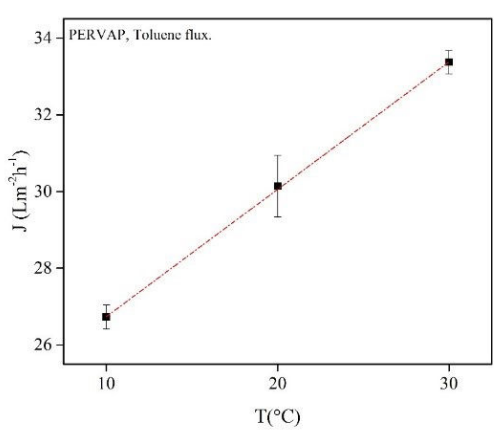

Figure 5.18: Toluene flux in pervaporation by PERVAP 4060.

(2) The vapor pressure of toluene is ≈ 275 times higher than the vapor pressure of decanal (**Table** 5.4) showing the high potentiality of PV with PERVAP4060 for the separation of decanal from toluene, applying a mild vacuum.

Properties	Toluene	Decanal (C10H20O)
Vapor pressure (mmHg) at 25C https://pubchem.ncbi.nlm.nih.gov/	28.4	0.103
Boiling point (C)	110	206-210
Vapor density (relative to air =1)	3.1	>1

Table 5.4: Properties of decanal and toluene.

Indeed, the separation by PV involves additional energy for vacuum, which can be replaced by adding a second OSN stage (**Figure** 5.17b) using Lenzing P84 membrane to avoid the cost of vaporizing toluene.

The interest of dual OSN separation over distillation and PV is that it allows applying same experimental condition throughout the hybrid, i.e., no additional heat (in case of distillation) or phase change (in case of PV) is required. The challenge, however, is to obtain the OSN membrane that can separate decanal from toluene.
As shown in **Figure** 5.17b, annealed Lenzing P84 (HP polymer) could be a potential candidate based on its C10 alkane rejection of 75% from toluene with the global flux of $6L/m^2.h$ from a feed of 2wt% C10 in toluene, at ≈40 bar, 50°C, (Silva, 2007) (White, 2001).

5.9 Conclusion

This chapter reports the effect of process parameter on a cross-flow OSN, dealing with pristine PERVAP4060 and in a few cases, PAH/PSS modified PERVAP4060, for the rejection of diluted catalyst in toluene. The study of process parameters such as cross-flow rate, CP, and hydrodynamic flow suggest that the considered OSN system is highly favorable to apply in a process scale. The linear flux trend and steady-high R-BINAP rejection with TMP indicate to its application in the flexible pressure range from 10-40 bar. The experimental findings from previous chapters show that in a ternary feed of C16 up to 10wt% with 0.05wt% R-BINAP in toluene does not affect the rejection performance of PERVAP4060. These results demonstrate a high potential of PERVAP4060 to apply in hydroformylation or metathesis for their catalyst separation.

Taking these experimental results, a model system of $H-Rh-(CO)(PPh_3)_2$-decanal in toluene is considered for a primary investigation at a process scale. Surprisingly, the catalyst concentration of 0.05wt% accounts for 60% cost of total feed material, which makes it the first target of separation even though the industrial separation objectives are not known. While a single stage OSN can separate 80% of the feed catalyst, three-stage cascade improves the separation of up to >99%. Also, energy duty of OSN is ≈60 times lower than the distillation for a feed.

Quite logically, after the catalyst, the following separation task is to separate the product from toluene and recycle them to the feed. Apparently, the hybrid process could be a possible way depending on the given separation target.

Chapter 6

Materials and methodologies

The materials and methodology chapter consists of two sections. First, the material section includes the information of OSN membranes, polyelectrolytes for modification, and a list of solutes for OSN experiments.
The second section is dedicated to the description of different methodologies, dividing into three parts.

• Part 1 represents the characterization techniques; water contact angle (WCA) measurement, Scanning electron microscope (SEM), Atomic Force Microscopy (AFM), Fluorescence Recovery after Photo-bleaching (FRAP), gas permeability measurement, mercury porosimetry, and air permeability
• Part 2 describes the methodologies of surface modification by plasma and polyelectrolytes, and Organic Solvent Nanofiltration (OSN) protocols,
• Part 3 describes the analytical procedure by gas chromatography.ribes the analytical procedure by gas chromatography.

6.1 Materials

6.1.1 Commercial membranes used for OSN study

Supplier	Material	Primary information
PERVAP 4060	PDMS based	Dense active layer, organophilic membrane.
AMS S3012	PAN based	Nanoporous;
SolSep 010206	PI/PDMS based	Dense active layer.
GmbH	PAN support	micro-porous support

Table 6.1: Selected membranes for OSN experiments

6.1.2 Polyelectrolytes (PELs), solvent and solutes used for OSN membrane performance

PEL	Chemical Structure	Primary information
PDADMAC[1]	$[C_8H_{16}NCl]_n$	Cationic; Avg. MW $\sim 100-200K$
PSS[2]	$[C_8H_7SO^{3-}]_n$	Anionic; Avg. MW $\sim 70K$
PAH [3]	$[CH_2CH(CH_2NH_2.HCl)]_n$	Cationic; Avg MW $\sim 150K$.
PAA[4]	$[C_3H_4O_2]_n$	Anionic; MW $\sim 1250K$

Table 6.2: Selected polyelectrolytes for OSN experiments

[1] Poly(diallyldimethylammonium chloride; 20wt.% in H_2O. solution from Sigma-Aldrich.
[2] Poly(styrenesulfonate); powder from Sigma-Aldrich.
[3] Poly(allylamine hydrochloride; 40wt.% aqueous solution from Polyscience, Inc.
[4] Poly(acrylic acid); powder from Sigma-Aldrich.

Solvent	Chemical formula	Specification
Toluene	$C_6H_5CH_3$	MW=92.14 g/mol; $\rho = 867Kg/m^3$; purity=99.8%
Ethanol	CH_3CH_2OH	MW=46.07 g/mol; $\rho = 789Kg/m^3$; purity=96%

Table 6.3: Organic solvents used. Toluene has the chosen following ANR objective.

Solutes	Chemical formula	Specification
$(R)-BINAP$[1]	$C_{44}H_{32}P_2$	MW=622.67 g/mol; white to beige powder; purity $\geq 94\%$
$ToABr$[2]	$[CH_3(CH_2)_7]_4N^+Br^-$	MW=546.79 g/mol; white powder or flake; purity=98%
n-Hexadecane	$C_{16}H_{34}$	MW= 226.45 g/mol;$\rho = 770Kg/m^3$; purity $\geq 99\%$
n-Tetracosane	$C_{24}H_{50}$	MW= 338.65 g/mol; white powder ; purity = 99 %
n-Triacontane	$C_{30}H_{62}$	MW= 422.82 g/mol; colourless waxy crystal ; purity = 99 %
n-Tetratetracontane	$C_{44}H_{90}$	MW= 619.20 g/mol; powder light yellow ; purity = 99 %

Table 6.4: Solutes used in OSN experiments

[1] (R)-BINAP-(+)-2,2-Bis(diphenylphosphino)-1,1-binaphthyl; organometallic catalyst
[2] Tetraoctylammonium bromide; phase trasfer catalyst.

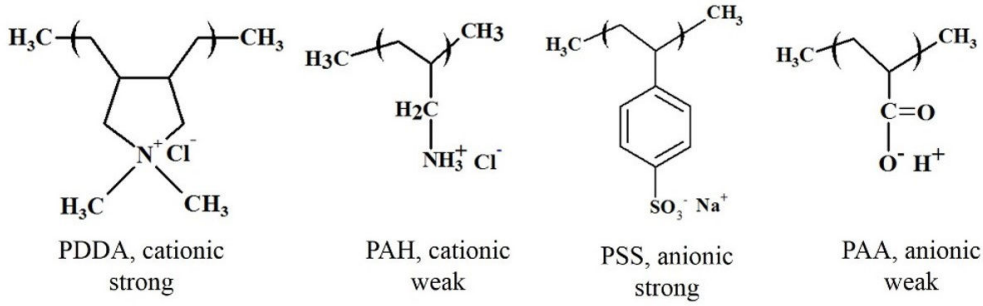

Figure 6.1: Polyelectrolytes used in OSN experiments

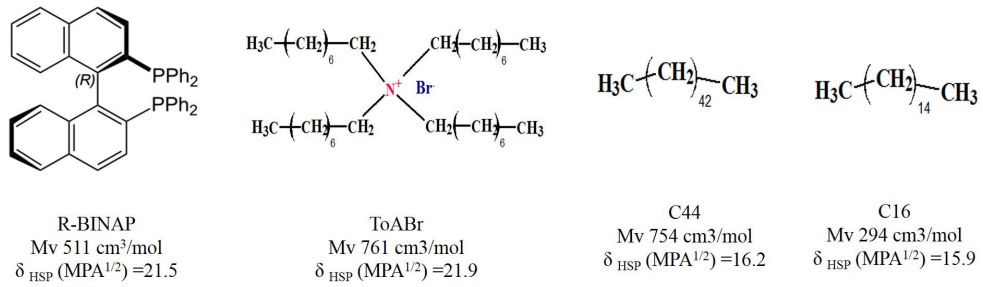

Figure 6.2: Solutes used in OSN experiments

6.2 Part 1: Characterization methods

6.2.1 Contact angle

Water contact angles were measured by Digidrop contact angle meter (GBX Scientific Instruments) The equipment is a telescope-goniometer (**Figure** 6.3), in which a horizontal stage is used to mount a solid sample; a micrometer syringe was used to form a water liquid drop (ultra-pure water as a probe liquid), an illumination source, and a telescope with a camera. The unit allows liquid drop suspension 0.5-10μL. Maximum magnification was 10×, providing an accuracy of ±0.7 degrees.

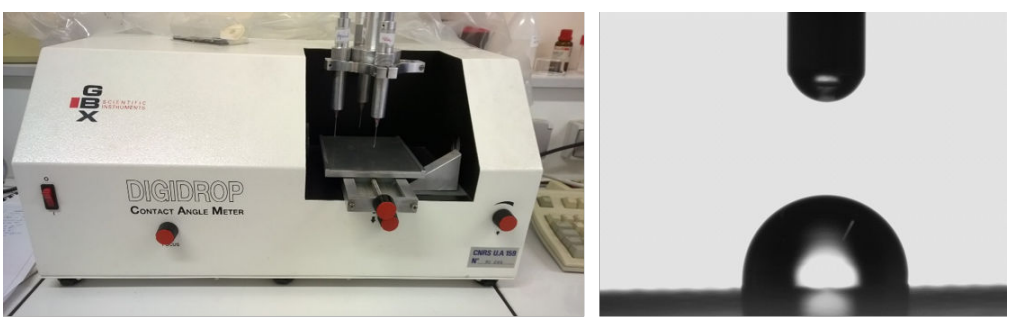

(a) (b)

Figure 6.3: (a) Digidrop contact angle meter (b) An image of water drop on membrane during the measurement

During the contact angle measurement, a small flat membrane sample was dried by a hand drier.

Next, the membrane was mounted on the horizontal stage, and micrometer syringe dispenses a controlled milliQ water on the surface. The Windrop++ software capture the contact angle data. In each sample, at least five data points were taken at random positions of the membrane. At least five samples were tested for the reproducibility.

6.2.2 Scanning electron microscope (SEM)

The scanning electron microscope was used for surfaces and crossectional views of the membrane. Two SEM units were used: for the images, having high magnification, Quanta 600 FEG (FEI) scanning electron microscope (SEM), and for those having relatively low magnification, JEOL 6490LV microscope model was used.

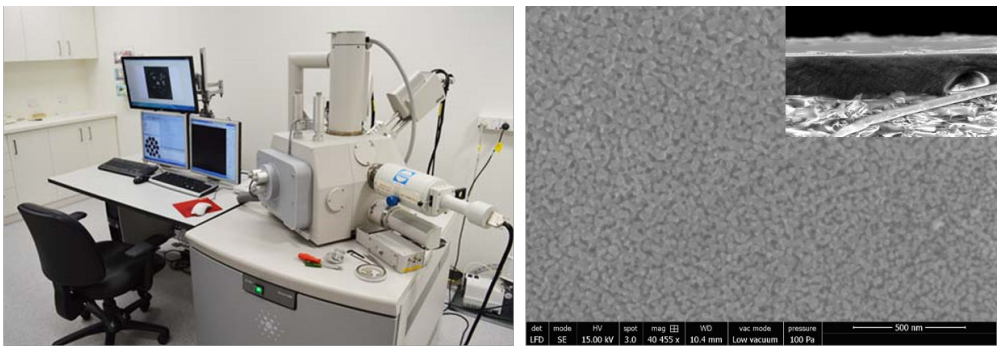

(a) (b)

Figure 6.4: (a) SEM Quanta 600 (b) An example of surface and cross section of PDMS membrane

Approximately 2 mm × 2 mm membrane sample was used for SEM imaging. Minimum five samples from different membrane sheet were viewed for the determination of the average active layer thickness, supports, defect-free surface and overall thickness of the membrane

6.2.3 Atomic force microscope (AFM)

After SEM imaging, the surface topography and mean-square roughness (R_g) were investigated using atomic force microscopy (FastScan, Scan AsystTM, Bruker). FastScan-C probes were used which deliver extreme imaging speed without a loss of resolution.

In AFM measurements, approximately, 2mm×2mm ethanol cleaned membrane sample was attached to a glass slide which is assumed to resist the lateral forces exerted by the scanning tip. The membrane is placed to the AFM sample holder, and then a Fastscan-C probe was used for the imaging.

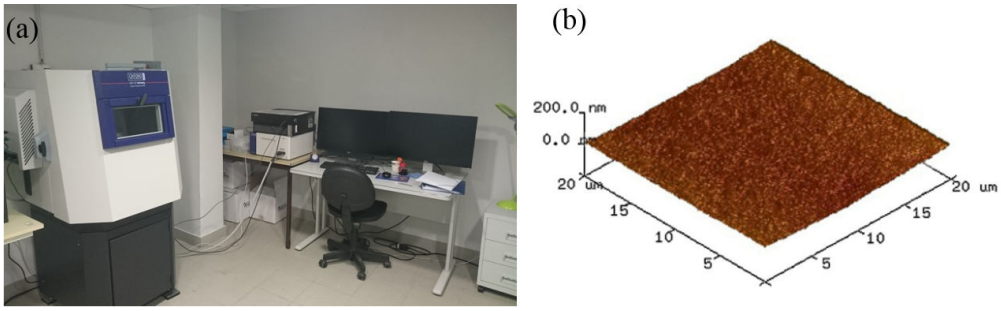

Figure 6.5: (a) AFM set-up at LRGP (b) An example of AFM surface image

Fastscan-C allows obtaining extreme imaging speed without loss of resolution and loss of force control. It also obtains 300 kHz resonant frequency with only a 0.8 N/m force constant with less than 3° cantilever bent assuring accurate information about the surface of the membrane.
At least two samples from each membrane, including pristine and modified, were investigated with the same parameter to ensure reproducibility.

6.2.4 Fluorescence Recovery After Photobleaching (FRAP)

FRAP technique was used to evaluate polyelectrolytes chain mobility, i.e., lateral diffusion of polyelectrolytes within the polyelectrolytes complex layer. This lateral mobility of PELs is connected to their separation properties when deposited on the membrane.

First, one of two polyelectrolytes (PEL's) was modified by attaching an active fluorescence molecule within the backbone of PEL. Next, the bilayer deposition has been carried out on the PDMS membrane using the PEL modified by active fluorescence molecules.

Once the sample is prepared, the membrane is placed under a confocal microscope, and a small section of the membrane undergoes bleaching while microscope observes its surface change.
After bleaching, the non-bleach molecules from surrounding migrates to the beach area, which is easily measurable in terms of intensity difference. Evolution of PELs migration with time then indicates how fast the PEL moves, i.e., the recovery of fluorescence; which can be used to calculate the polyelectrolytes diffusion.

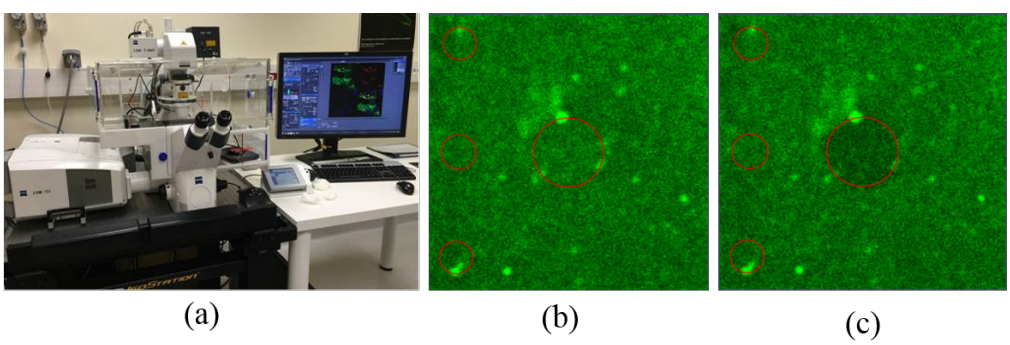

Figure 6.6: (a) Confocal microscope: Zeiss LSM 510 (b) Membrane sample before photo-bleaching.(c) after photo-bleaching.

The bleaching and imaging of PEL films have been performed on a Zeiss LSM 510 confocal microscope equipped with an argon laser (488 nm). During the observation, the PDMS with the

PEL films (on the membrane) was placed in a sample holder. In image capture and intensities evaluation; first, a pre-bleach image was captured **Figure** 6.6b. The selected area then bleached with the laser set at its maximum power. The 10× objective was used for photo-bleaching yields optical sections. The bleaching time was adjusted to achieve sufficient contrast between the bleached and non-bleached regions. After the bleach, images were acquired at times ranging from 10 s up to 1000 s to monitor the recovery process. These images were acquired by scanning the sample with the laser power carefully chosen to have an acceptable signal-to-noise ratio while avoiding strong bleach during image acquisition.
Finally, a set of images with time-lapse have been obtained. The images were analyzed for the intensities of both reference and bleached region vs. time were normalized and plotted for the calculation fo PEL diffusion.

6.2.5 Gas permeability measurement

The permeability of CO_2, N_2 and He in OSN membranes were measured by **Time-Lag method** which is an integral permeation method, based on continuous monitoring of the amount of the penetrant crossing the membrane into a closed vessel, allowing direct determination of the permeability and diffusion coefficient as well as values of solubility coefficient.

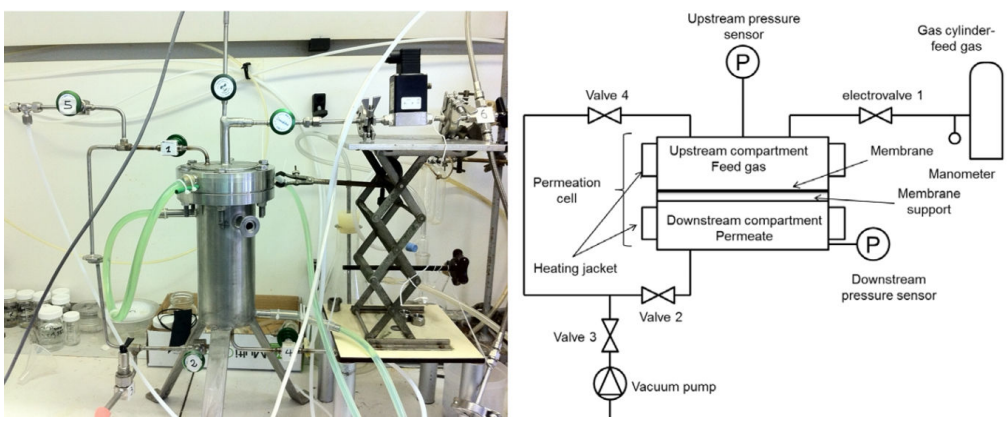

Figure 6.7: (a) Gas permeation (Time-Lag)set-up at LRGP (b) Detail Scheme

As shown in **Figure** 6.7, two compartments (both upstream and downstream) were initially under vacuum and at a constant temperature. The pressure differences in the compartment have recorded by automatic pressure data acquisition device. At a precise time t, the electro-valve opens, allowing the gas molecule to come in contact with the membrane.
Next, Fick's law can define the steady state gas flux across the membrane according to the formula:

$$J = -D\frac{\partial c}{\partial x} \ . \tag{6.1}$$

In ideal cases of elastomer without any gas polymer interaction, D is independent of c and S follows a Henry type law.

$$c = S.p \ . \tag{6.2}$$

The steady state flux ($mol.m^{-2}.s^{-1}$) of the gas across the membrane (dense) can be written as

$$J = \frac{P.(p_{upstream} - p_{downstream})}{l} = \frac{n_{gas}}{A.t} \ . \tag{6.3}$$

where, P is the gas permeability ($mol.m.m^{-2}.s^{-1}.Pa^{-1}$); l, membrane thickness (m); A , membrane surface area (m^2) and n_{gas} is amount of gas (mol) flowing inside the closed vessel.
Since the downstream compartment is maintained under vacuum, the permeability can be expressed as:

$$P = \frac{n_{gas}.l}{A.t.p_{upstream}} = \frac{\partial p_{downstream}}{\partial t}.\frac{V_{downstream}}{RT}.\frac{l}{A.p_{upstream}} \ . \tag{6.4}$$

The unit of permeability obtained from this equation is $mol.m.m^{-2}.s^{-1}.Pa^{-1}$ And usual expression for gas permeability is in Barrer ($= 10^{-10}.cm^3.cm^{-2}.s^{-1}.cm.Hg^{-1}$), having the unit coversion:

$$1mol.m.m^{-2}.s^{-1}.Pa^{-1} == 2.95.10^5 cm^3.cm^{-2}.s^{-1}.cm.Hg^{-1}(Barrer) \tag{6.5}$$

During the permeability measurement by time-lag, a slight pressure increase is almost always, before beginning the experiment, which is due to a small gas leak. In each measurement by time lag, permeation due to leak was deducted.

6.2.6 Mercury porosimetry

Porous membrane samples were characterized by AutoporeIV Mercury porosimeter for the measurement of pore area volume, distribution, the density of the active layer, the porosity of the membranes, which are the critical parameters need to explain mass transport phenomena in porous membranes.

In mercury intrusion porosimetry, the membrane sample is placed in the penetrometer and evacuated for the removal of undesired gases. While evacuating, mercury is addressed to fill the container.

Next, the pressure is increased to fill the pores of the membrane, typically a maximum pressure of about 60,000 psia (414 MPa) can be applied by porosimeter. These powerful forces push mercury into pores down to about 0.003 micrometers in diameter. The volume of mercury that intrudes into the sample due to an increase in pressure from P_i to P_{i+1} is equal to the volume of the pores in the associated size range r_i to r_{i+1}.

The pore sizes being determined by substituting pressure values into Washburns equation, according to:

$$D = \frac{-4\gamma cos\theta}{P} \tag{6.6}$$

Where γ is surface tension, D, pore diameter. Further pore volume was calculated by Hagen-Poiseuille law.

$$Q = \frac{Q}{t} = \frac{\pi.r^4}{8\eta}.\frac{\Delta P}{l} \tag{6.7}$$

where where Q, flow of the liquid, V, the volume of liquid, t time, r the capillary radius, η the liquid viscosity and $\Delta P/l$ the pressure drop per unit length of capillary.
Percent porosity was determined by

$$P\% = \frac{V_{pt}}{V_*}.100 \tag{6.8}$$

Where V_{pt} is for total porosity and V_* is for bulk or envelop volume.

6.2.7 Air permeability

The air permeability in pristine and modified membranes have been measured using the set-up, presented in **Figure** 6.8.

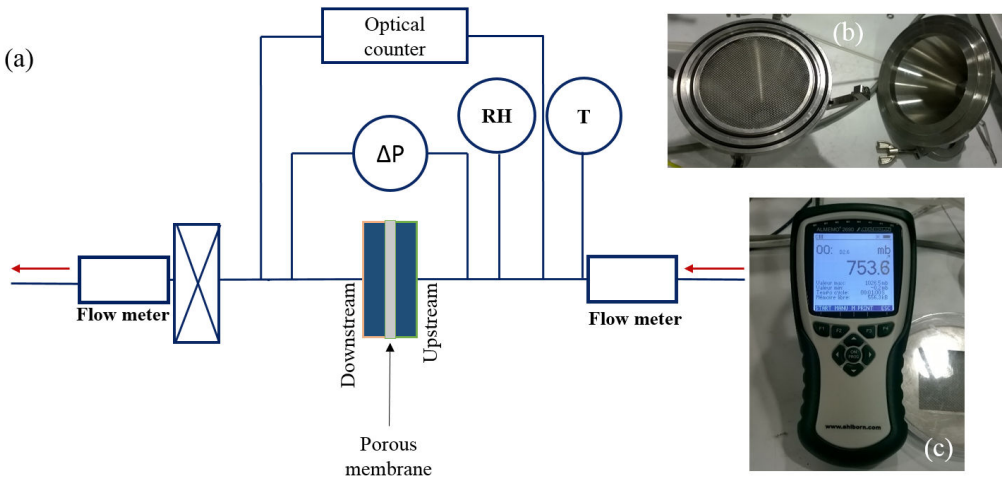

Figure 6.8: (a) Scheme of air permeability unit (b) membrane mounting cell (c) ALMEMO precision pressure measuring device.

This parallel measurement with mercury porosimetry has been considered to see if the modified membrane remains porous after PEL deposition.
During the test, the membrane sample is placed in the call (**Figure** 6.7b), having the top-layer facing the membrane was facing the air-flow direction. Once the membrane is appropriately set in the cell, dry air has been passed for several minutes. Next, the flow rate has been increased stepwise, and the differential pressure drop between the upstream and downstream side is monitored and recorded. The relative change of the Pressure drop and permeability k can have been calculated according to Darcy's law.

$$Q = -\frac{k.A.(P_{dowstream} - P_{upstream})}{\mu.L} \tag{6.9}$$

Q, total discharge, unit volume per time,(m^3/s), k is intrinsic permeability, (m^2), the cross sectional area of flow, A (m^2) and total pressure drop $(P_{dowstream} - P_{upstream}) = \Delta P$, (Pascals), μ is viscosity (Pa/s) and L is length (m) over which the pressure drop occurs.

6.3 Part 2: modification and performance methods

6.3.1 Plasma modification

Plasma surface modifications were carried out in the microwave post-discharge plasma reactor. The reactor was attached to the cylindrical tube, as shown in **Figure** 6.9, in which a flat sheet membrane sample is placed, facing the Ar/O_2 flow, targeting the modification/activation to occur on the active layer of the membrane. Once sealed, the system was pumped to 102 mbar vacuum followed by the ignition to generate a controlled plasma of given composition.

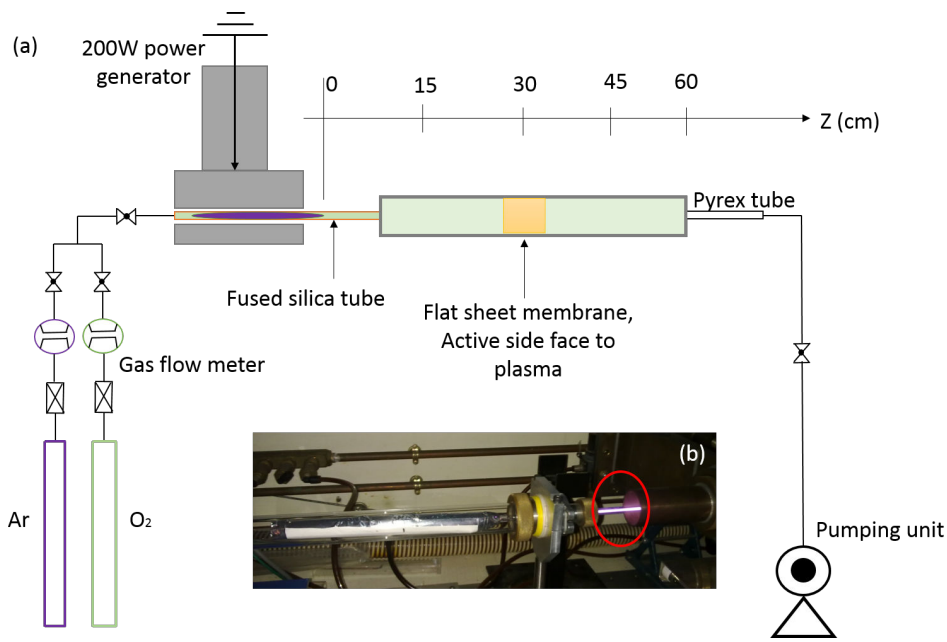

Figure 6.9: (a) Plasma set-up (b) $Ar - O_2$ glow during modification.

In this activation process, a 2.45 GHz microwave generator has been used for creating $Ar/\ O_2$ plasma from a feed flow of 400/40 sccm (standard cubic centimeter per minute, controlled by the gas flow meter.
Membrane sample with the desired dimension is placed downstream in the plasma at 30 cm from the plasma outlet. It is indeed recommended to make a black test (a test without any membrane inside the quartz tube) in order to fix the parameter such as vacuum level, Ar and O_2 flow rate and microwave power setting.
After the blanc test, the modification of membrane is straight-forward exposure of plasma on the membrane surface.
Once the modification is completed, the system is vented, and the sample is removed for the next polyelectrolytes (PEL) deposition.

6.3.2 Layer by Layer(LbL)modification by Polyelectrolytes

Polyelectrolytes (PELs) deposition by Layer-by-Layer (LbL) is the principle modification techniques used in this study. Both dense and porous OSN membranes have been modified by PELs, having an intermediate plasma activation step, only for the dense PERVAP 4060 (PDMS).

In the beginning, the depositing bath is cleaned by piranha solution (hazardous solution, high precaution is required and standard protocol was applied), a mixture of H_2SO_4 and H_2O_2, prepared by adding H_2O_2 in H_2SO_4 which is commonly used to clean organic residues from substrates. In this study, piranha was used to clean the PEL depositing bath.

Once cleaned by piranha followed by milliQ water, both catatonic and anionic polyelectrolytes solution were prepared by dissolving polyelectrolytes in milliQ water ($18.2M\Omega.cm$ at $25°C$). The final PEL concentration obtained $10^-2mol.L^-1$ for each polyelectrolyte solution, based on their monomer molecular weight. The solution baths kept under moderate stirring for 6-8 hours in order to obtain a homogeneous solution. For PDADMAC and PSS, no pH adjustment was required as these two polyelectrolytes are strong and expect to dissociate 100%). In contrary, PAH and PAA

are weak polyelectrolytes, and therefore, an adjustment of $pH \sim 6.5$ were considered. After each polyelectrolyte baths, three rinsing steps were used to remove additional PEL from the sample, to minimizes the possibility of cross-contamination of PELs.

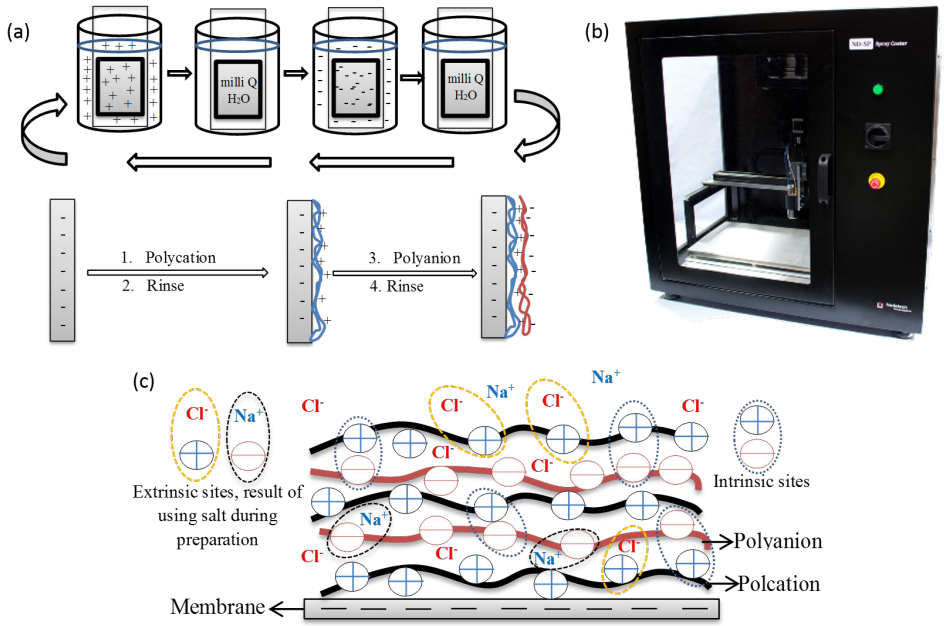

Figure 6.10: (a) LbL modification scheme (b) Nadatech ND-3D multi-axis robot. (c) Scheme of the polyelectrolyte multilayer expected after modification.

Once the PEL baths are ready, membrane sample was attached to flat glass/Teflon and fixed vertically. Nadatech ND-3D dip-coater robot was then used which automatically dips the sample, at a certain immersion speed into the bath having PEL solution. Next, the rinsing steps and deposition of the second PEL were conducted following the same procedure.
The membrane sample immersed in polycation bath for 10 min. Next, three rinsing steps are 1s/15 time, 5s/3 times, and 15s/1 time. Subsequently, the membrane was immersed in a polyanion solution followed by rinsing. Thus, one bilayer, or one cycle of self-assembled membrane was completed. Additional bilayers were deposited by the repetition of the cycles until the required number of bilayers was achieved. Depending on the polyelectrolytes couple; 5-20 bilayer samples have been prepared for the experiment.

The humidity and temperature inside the robot considered as constant throughout the preparation phase. After modification, all these samples have been tested by Organic solvent nanofiltration (OSN) for permeation-separation.

6.3.3 LRGP- OSN set-up

LRGP-OSN set-up consists of three key components: feed reservoir, membrane cell, and flow circulation system. These three key components are interconnected with a hydra cell heavy duty pump, which make it a complete recirculating cross-flow system. (**Figure** 6.11)
In the beginning, the membrane was installed in between the upstream and downstream cell, facing the separating layer to the upstream side. Inside the OSN cell, two rectangular seals are used to make the set-up leak-free under pressure. Both these seals allow an active 34 cm^2 membrane

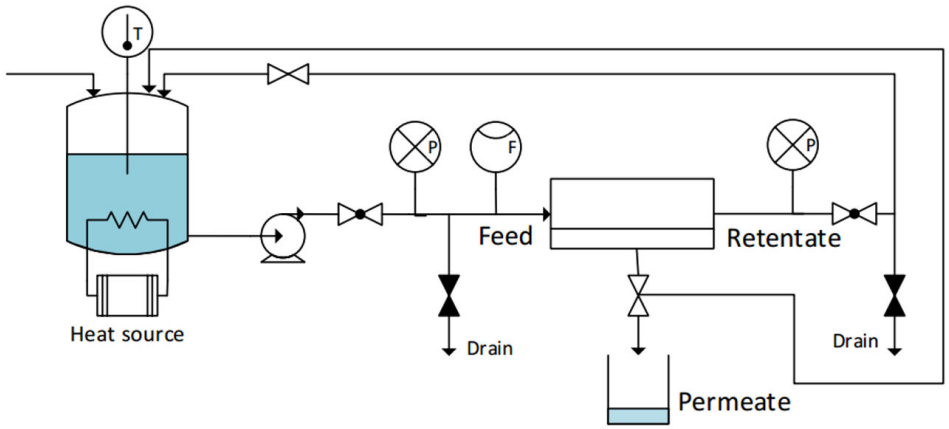

Figure 6.11: OSN experimental scheme

surface. Both upstream and downstream cell is attached and mounted inside the housing, obtained from GE infrastructure.

Next, a hydraulic hand control pump presses the cells and fixes it inside the housing. Once the membrane was fixed inside the cell, the unit was ready for the experiment. Afterward, approximate one liter of feed solution was charged in the reservoir, keeping the adjacent valve open, which allowed the solution passage to the pump head. From the pump head, there are two connection via an intermediate check valve to reduce feed pulsation. One connection then goes to the membrane cell and other to the reservoir. The liquid enters to the upstream side of the membrane through a Coriflow flow control meter, which gives the actual flow rate inside the cell. The variable cross-flow rate can be applied using the valve adjacent to the pump. Next, the temperature is fixed in the continuous feed stream by using THERMO HAAKE BATH CIRCULATOR K50 which allow controlling precise temperature (tested up to 50 ° C) showing actual accuracy of ±1° C in a high recirculation.

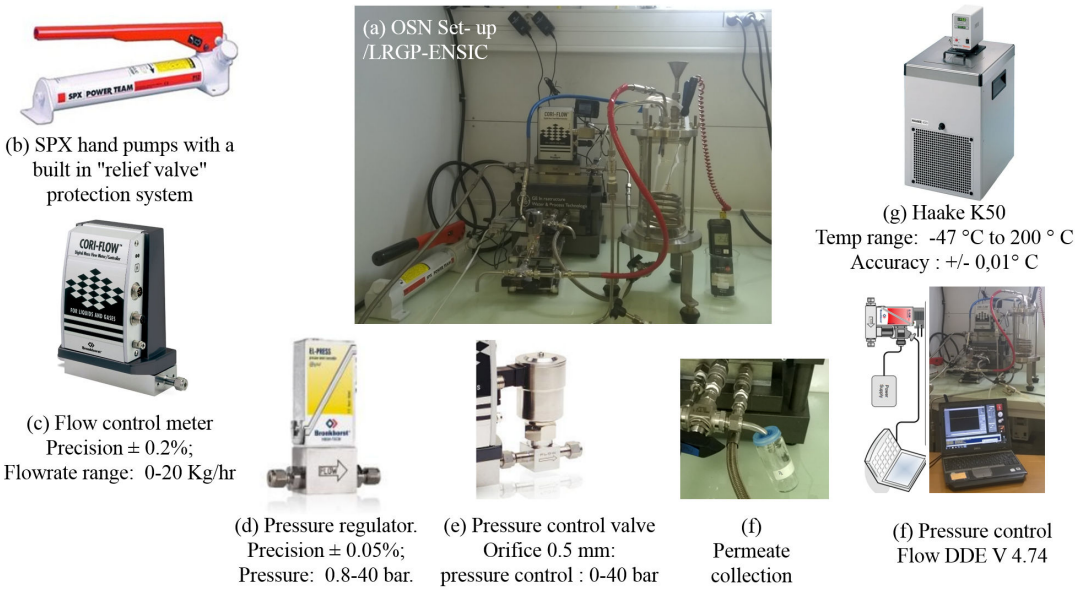

Figure 6.12: OSN equipment and their specifications.

Next, the transmembrane pressure is applied, once the cross flow and temperature in the recirculating system become steady under continuous run. The pressure is applied by pressure regulator and pressure control valve, automatically controlled by FLOW DDE v4.74 software, allowing a fully automatic pressure control system with a precise step-increases of 2/3 bar until the targeted pressure is obtained. This arrangement gives an excellent precision on TMP, applied during the measurement. The increase of pressure, as well as deviation, can be continuously monitored by per second pressure record, generated by FLOW DDE v4.74.
• Membrane pre-conditioning: The membrane is emerged (overnight) to the same solvent used for OSN. In this step, the membrane obtains its stable swollen state.

• Membrane conditioning: At each transmembrane pressure up to 40 bar, the membrane exposed for 10-15 min under OSN condition which eliminates the possibility of flux hysteresis. During the conditioning, no flux or rejection data have been recorded except some random measurement for comparison.

• Performance measurement: At least three data points for flux and rejection have been taken at each transmembrane pressure (TMP) having 15-20 min interval between each recorded data, providing a high accuracy during the measurement.

At one set pressure, the OSN unit runs for 10-15 minute before the data acquisition, which make-sure a stabilized permeate flow. Approximate 3-5 gram permeate sample collected in a vial attached to the permeate line with a Teflon cap allowing only the space required to collect the permeate. This home-made system minimizes the evaporation loss during the measurement. The time (t) required for the sample amount (g) is considerd with the active membrane area to obtain the flux (J) at a given temperature and pressure **Equation** (6.10).

$$J = \frac{V_m}{A.t} \tag{6.10}$$

At least three data points have been taken, before moving to next transmembrane pressure. The same procedure continued up to 40 bar, and flux evolution has been obtained with corresponding rejection.

During flux measurement at one transmembrane pressure (TMP), about one gram of each permeate sample is analyzed by gas chromatography for the solute concentration in the permeate (C_p) and compared with the feed solute concentration (C_f),thereby the rejection (R)can be calculated according to the **Equation** (6.11).

$$R = (1 - \frac{C_P}{C_R}).100 \tag{6.11}$$

At each transmembrane pressure, at least four feed and permeate concentration were measured to obtain reproducible rejection data. Finally, applied transmembrane pressure reduced to 10 bar from 40 bar and flux and rejection was repeated for a cross-check of the possibility of flux hysteresis. At least three OSN membranes were tested to obtain reproducible performance.

Upon completion of one OSN test, quite often, the membrane was removed from the cell and re-tested in a second OSN set-up, applying 10 or 20 bar TMP, having $20cm^2$ effective surface. In this way, both extrinsic and intrinsic performance was ensured for a given membrane. In parallel, the OSN test, using a second membrane, was repeated in both OSN unit following the same procedure described above.

The above mentioned OSN protocol ensures high accuracy in the measurement. Excellent stability of applied transmembrane pressure and strategy on flux and rejection allowed to obtain data with very high accuracy, often data deviation obtained below 5%. Several day-long experiments have been conducted, thanks to the stability if TMP, obtained by FLOW DDE. Several coupons of membrane stored in room condition and OSN performance were re-measured randomly during three years, which supports the long term stability.

6.4 Part 3: Analytical method

6.4.1 Analysis by Gas Chromatograph (GC)

During OSN tests, both feed and permeate samples were collected and analyzed by Agilent 6890 Gas Chromatograph.

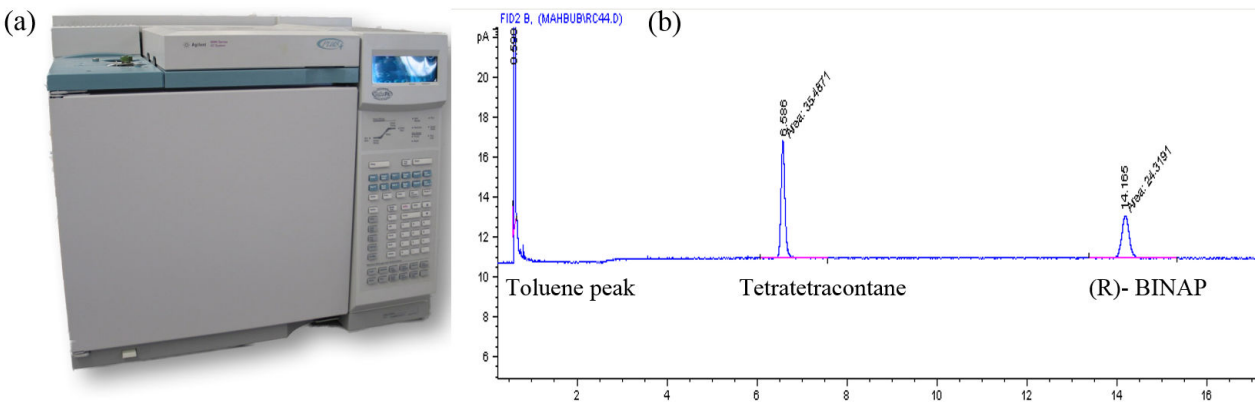

Figure 6.13: (a) Agilan 6890 (b)Example of a chromatogram: (R)-BINAP peak with external standard C44 (tetratetracontane).

Operational conditions for GC:

• Column(capillary): 5% phenyl methyl siloxane, $15m \times 320\mu m \times 0.25\mu m$, thickness of the film = 0.10 m, temperature limit $-60°$ to $325/350°C$
• Oven program:
$325°C$ for 15 min for (R)-BINAP detection,
$250°C$ for 15 min for ToABr peak,
$200°C$ for 15 min for all linear alkanes.
• Carrier gas:helium, pressure = 20 psi
• Constant flow: 2 mL/min,
• Injector: split, split ratio (1:200), temperature = 250° C, volume injection 1μ L.
• Detector: FID (H_2/air : 1/10), 325 $°C$.
$200°C$ Analysis of ternary mixtures:
$200°C$ for 2 min followed by an increase of $50°C/min$ to $325°C$ and a hold for 20 min.

External calibration was performed for each solutes having different concentration of solutes. Depending on the solutes, external standard (constant volume addition)was added for accurate measurement of peak area. In constant volume addition, each feed and permeate sample was added with the external standard at 1:1 mass ration. The sample is then injected to the GC column for analysis.

T ($°C$)	Solute to analyse	External standard
325	(R)-BINAP	Tetratetracontane (C44).
250	ToABr	Tetracosane (C24)
200	Hexadecane (C16)	Tetracosane (C24).
200	Tetracosane (C24)	Hexadecane (C16)
200	Triacontane (C30)	Tetracosane (C24)
325	Tetratetracontane (C44)	(R)-BINAP

Table 6.5: List of GC oven temperature for the detection of solutes and external standard.

The calibration curves (standard peak area/solvent peak area = f (solute concentration)) allowed to establish a linear relationship between the area of the obtained peaks and the concentration of the tested solution.

Each sample injected for three times and at least three sample tested for each data point in order to have a reliable accuracy. Most OSN feed constitutes with highly diluted solutes. The precision of analysis was, therefore, carefully considered by increasing the number of GC test and comparing the data obtained, at least, from three OSN measurement using the same feed composition and the same type of membrane.

One particular test has been performed to cross-check GC data precision. Hence OSN feeds and permeates been separately concentrated by a factor of 10 using a rotary evaporator, and those sample re-tested by GC and rejection have been calculated. The rejection data was unchanged, supporting the validity of all measurement performed for dilutes systems.

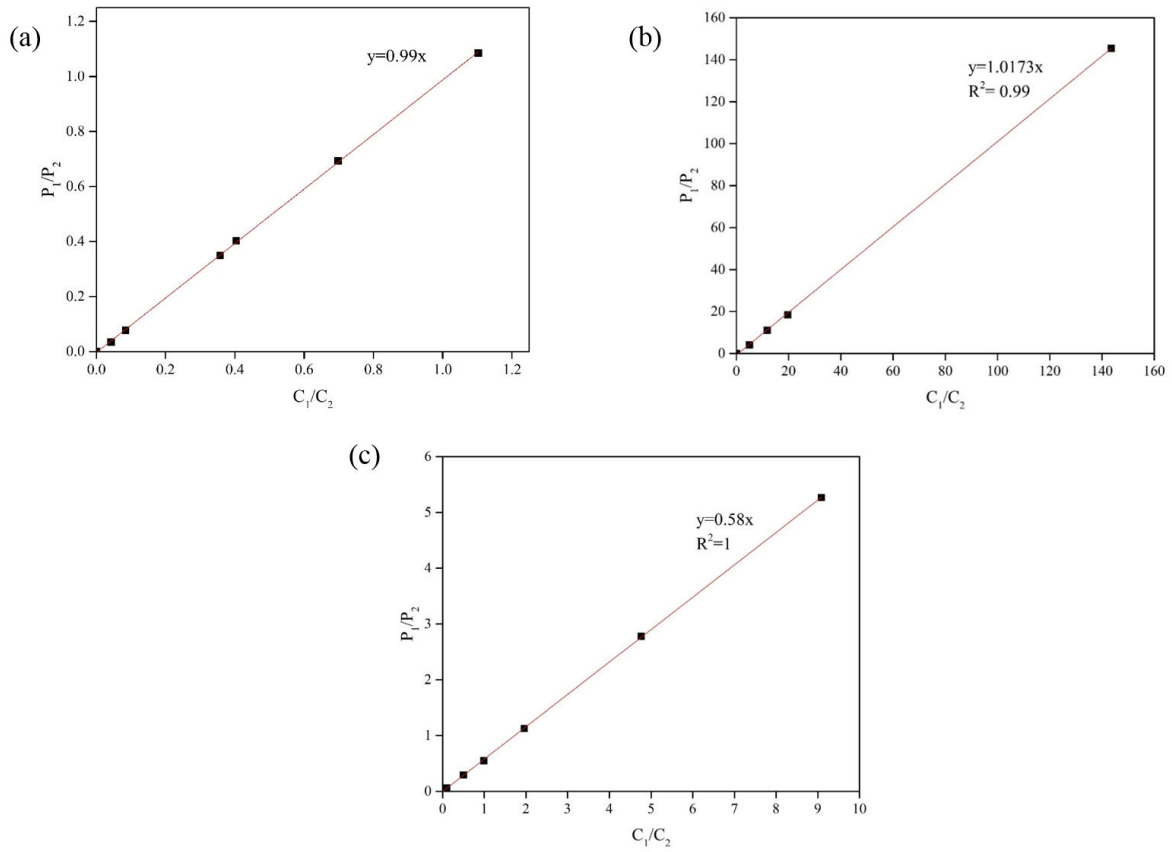

Figure 6.14: Calibration of the GC column for (a) RBINAP in toluene (b)ToABr in toluene (c) R-BINAP with C16 in toluene (ternary).

Chapter 7

Conclusion

This work has been achieved in the frame of the ANR project MemChem with this ambition to improve the current hydroformylation metathesis process by investigating the potential of OSN as separation method to extent life-time of the catalyst and to simplify the recovery of the product and of the solvent.

The first objective was to find a suitable commercial membrane that would be stable in OSN conditions and that would lead to significant rejection of the catalyst from toluene while allowing the permeation of the reaction product, a pre-set condition of ANR. The second objective was to apply a modification strategy able to tune the mass transfer properties of the pristine commercial membrane in order to improve the separation performance. The third objective was to analyze the experimental results to understand the structureproperties relationships and to investigate the separation mechanism, that can be quite a controversial topic in OSN.

To fulfill these objectives, the following steps were followed:

• A literature review, to examine the state of art and establish a modification strategy of commercially available membranes;
• The investigation of the mass transfer properties under OSN conditions of dense and porous commercial polymeric membranes;
• The modification and characterization of dense and porous membranes;
• The investigations of the effect of some key operating conditions on the OSN performance

At last some prospective flowsheets involving the potential of OSN separation were discussed.

7.1 Literature review

It was shown that the most of the ceramic membranes exhibit high molecular weight cut-off and high material cost; in addition these membranes are hard to scale-up compared to the polymeric membranes. Therefore, this type of membrane were excluded from the material selection.
Considering now the commercial polymeric membranes, the market availability and the reported performance underline the following critical points linked to the choice of OSN membranes:

(1) There are only few commercial membranes reported in the literature exhibiting high separation performance in organic media; among them, STARMEM, MPF, GMT-oNF, and SOLSEP.

(2) These OSN polymeric membranes bear quite attractive feature such as readiness to apply,

stable in organics, resistant to mechanical stress and high separation characteristics in different organic media. The critical concern is that these membranes are somewhat unavailable or not easy to obtain from the supplier.

(3) Even if the supplier provides the membrane, often primary information about these membranes are not disclosed such as materials of active layers, support, nature of the surface (dense/porous). Also, supplier often blocks the research to investigate on material characterization.

(4) No clear indication on the type of active layer in commercial membranes: if the membrane constitutes with a dense or porous active layer to dictate their mass transport mechanism. In literature, often contradictory mass transport mechanism is reported.

(5) The choice of polymer for OSN membranes are limited in number. Most of the commercial manufacturer relies on two main polymers for fabricating the active layer/separating layer of the membrane: Polyimide (PI) and polydimethylsiloxane (PDMS).

It can be seen from the literature review that the retention of R-BINAP in toluene has never been studied either with commercial or with lab-made membranes. In addition, the case of the rejection of highly diluted species in organic media has not been often considered. There are very few commercial membranes that are credible for the rejection of a metathesis catalyst, or the related ligand, in order to meet the ANR MemChem objectives. Previously to this work, the performance of Sulzer membrane PERVAP4060 was unknown for the retention of R-BINAP in toluene or in other solvents. Nevertheless the stability of PERVAP4060 under OSN conditions in toluene was known by the LRGP membrane team.

7.2 Investigation of the OSN mass transfer properties of dense and porous polymeric membranes

Four OSN membranes were selected based on their commercial availability and on the nature of their active layers, either dense or porous. These membranes include two dense membranes: PERVAP4060, a PDMS base mainly used in pervaporation, SOLSEP010206, mainly used in nanofiltration, and two porous membranes: AMS S3012, a nanoporous membrane, and PAN, a microporous support.

The initial performance of these pristine membranes was evaluated by measuring separately the retention of diluted organophosphorus ligand R-BINAP (MW 622 $g.mol^{-1}$) and a linear alkane C44 (MW 619 $g.mol^{-1}$) dissolved in toluene. The dense OSN membranes exhibited higher separation performance compared to the ultra and nano porous membranes. The PERVAP4060 exhibited highest rejection performance (R-BINAP:80%; C44:70%) and SOLSEP010206 gave poor solute rejection (R-BINAP: 35%; C44:26%). In addition, the permeance of the toluene 2.1 $L/(m^2.h.bar)$ through PERVAP4060 was quite high (VALUE) These results clearly governed the choice and the use of PERVAP4060 as dense membrane for the ongoing work.

From the detailed study carried out with PERVAP4060 using binary and ternary model toluene feed mixtures composed with R-BINAP and C16 (MW 226 $g.mol^{-1}$), the performance of PERVAP4060 can be schematically illustrated by **Figure** 7.1. It highlights that the retention of R-BINAP was high in PERVAP4060 even at a high dilution of solute (100 ppm-0.2wt%) despite the significant swelling of PDMS active layer in toluene. These results clearly indicate that the solution-diffusion (SD) mass transport mechanism rules the transport.

Analogous results were obtained with ToABr (a phase transfer catalyst, MW 547 $g.mol^{-1}$), confirming also the solution-diffusion transport mechanism with this tetraalkylammonium salt.

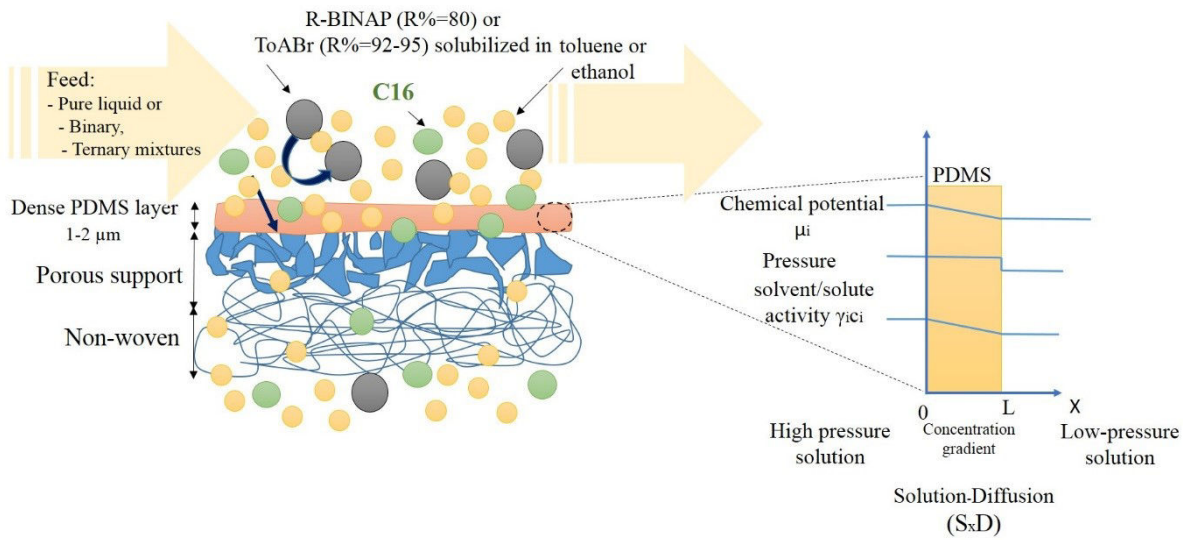

Figure 7.1: Mass transport mechanism and solute retention in PERVAP4060 under transmembrane pressure of 10-40 bar, at 30°C with 7-10 kg/h cross-flow.

PERVAP4060 was found to be highly stable in the transmembrane pressure range of 10-40 bar, regardless of the solvent-induced swelling. When ternary feed mixture was used, it permeated most of the C16 (as a product) while retaining most of the R-BINAP, the bulky ligand, as required to enhanced the turn over number of the metathesis catalyst. Thus PERVAP 4060 gives a promising OSN potential to comply with ANR objective.

7.3 Modification and characterization of dense membranes

In OSN, new prototype membranes are a real demand to comply with hydroformylation catalyst separation. The surface modification of membranes was chosen as a fast and rational approach to get new OSN membrane prototypes from commercially available materials.

First, for the preparation for the new prototype membrane, the existing PERVAP 4060 was the logical choice. It was expected that nanolayers on the PERVAP 4060 surface would help to tailor the separation and allow to improve the separation obtained with the PERVAP 4060 at its pristine condition. The open questions were to design a convenient procedure to guaranty reproducible modified membranes as well as the nanolayer stability, and to know if the created top nanolayer would be dense or porous.

Second, the porous AMS S3012 and the PAN support were also considered for further modification to investigate if the surface modification could also improve separation properties of the porous pristine matrixes. The open questions were to known if the same procedure would induce either a pore size reduction or a the formation of a dense nanolayer.

Thus, one of the critical tasks of this Ph.D. has been to control and develop a convenient procedure to get new membrane prototypes with the target to improve catalyst retention as main goal without reducing too much the solvent permeation.

Initially there were two ways to proceed: either by modification of the bulk matrix or only the membrane surface. The controlled bulk modification of a commercial membrane, i.e. of a multilayer membrane, is obviously difficult to design and to achieve selectively without damaging the integrity of the membrane. In addition, the top layer is often crosslinked. In contrary, surface modifications can add new properties keeping the bulk properties unaltered and this later route was preferred since PERVAP4060 is already a high performing membrane. Literature gives examples of different surface modification routes such as plasma, polyelectrolytes, UV, grafting, and nanoparticles impregnation. Among these methods, plasma and polyelectrolytes (PEL) were considered because of their wide versatility and separation potential along with the possibilities of well-controlled formation of nanolayers.

The surface modification of OSN commercial membranes was carried out by Layer-by-Layer method (LbL) to get polyelectrolytes multilayers (PEM). Both dense and porous membranes were modified using the four polyelectrolytes combination: PDDA/PSS, PAH/PSS, PDDA/PAA, and PAH/PAA. From the characterizations made, the following key features of these PEM layers were identified:

1. With the hydrophobic dense membrane, a short exposure of Ar/O_2 plasma was used to ensure the better PEM anchoring of the initial layer on PDMS. Upon OSN experiments no degradation or delamination of the PEM could be detected.

2. With the porous hydrophilic membranes, PEM was applied without any plasma activation. Upon OSN experiments no degradation or delamination of the PEM could be either detected.

3. The PEM of 10 bilayer forms a thin nanolayer on dense PERVAP4060 with full surface coverage having thickness range from 20 nm to 60 nm depending on the type of PEM.

4. These prototype dense and porous membranes differ from each other having different hydrophilicity, charge density, rugosity and surface morphology of the surface.

All these prototype membranes were provided to the partner laboratory for OSN testing in the frame of the hydroformylation catalyst and product separation.

The selection of the starting polyelectrolytes (PEL) was made based on the most studied PELs reported in different domain of application ranging from aqueous UF to NF and PV. To our best knowledge, these PEM with PERVAP4060 were never applied for the preparation of OSN membranes. Hence the relative interest of the PEL for separation in organic media was difficult to rationalize.

Next, the formation of 10 bilayered PEM holds the assumption of full membrane surface coverage. Indeed, considering the variation of solvent flux between the pristine and the modified membranes, the full surface coverage was not apparent with PEM having a lower bilayer number. Therefore, ten bilayers were considered as the standard choice.

At last, the pH value 6.5 was used for the maximum degree of dissociation of PEL when dissolved in water.

With these prototype membranes, the objective of the experimental work has been to establish the OSN performance and to translate these results in terms of structureproperties relationships for R-BINAP and ToABr as diluted model of catalysts, for the linear C16 alkane as product model and for toluene.

Using binary and then ternary feeds of solutes-solvent of R-BINAP-C16-toluene, it was found that the best rejection was obtained with the PEM nanolayer prepared from the PAH/PSS pair deposited on PERVAP4060. The **Figure** 7.2 intends to present the improved OSN performance and the corresponding mass transport mechanism. Here again the solution-diffusion mechanism seems able to explain the retention of the biggest molecules despite the high flux of the solvent.

(1) The four PEM used on PERVAP4060 led to the formation of LBL endowed of various charge densities which seemed to rule the solvent permeation and the solute rejections.

(2) The overall permeance decreases and the rejection increase linearly with the increase of the bilayer number of PAH/PSS.

(3) Interestingly, R-BINAP, ToABr, and C44 were highly rejected even at a low feed concentration of $0.05wt\%$ in toluene which indicates the transport of the solute must be almost independent of the solvent transport.

The clear decrease of the toluene permeance demonstrates also that the PEM was well covering the whole membrane top surface, i.e. that the PEM layer has a dense nature. This was also in agreement with the gas permeation properties that were measured with PEL modified membranes, showing a permeance decrease while keeping almost constant the ideal selectivity.

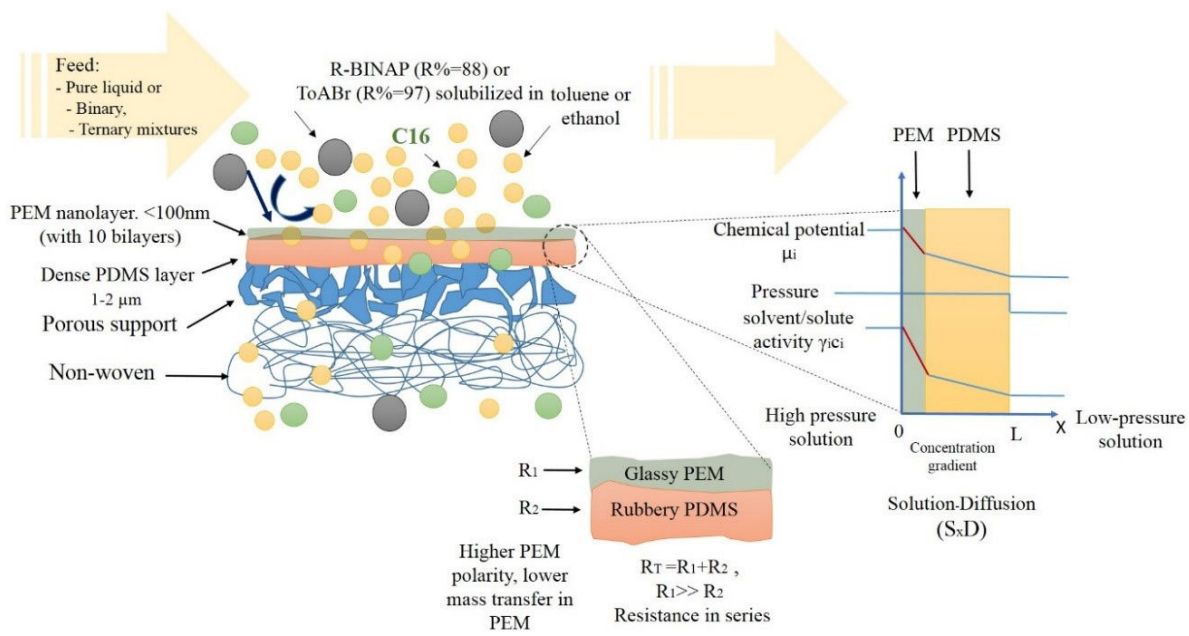

Figure 7.2: Mass transport mechanism in PAH/PSS modified PDMS for the improved rejection of catalyst from toluene at $30°C$ and 10-40 bar. Feed cross-flow: 7-10 kg/h.

(4) While the PDMS is a rubbery matrix, the PEM exhibits a glassy matrix as shown by the decrease of the solvent permeance linked to the presence of these PEM nanolayers.

It was shown also that a correlation seems to hold between the charge density of PEM and the toluene permeance: the higher solvent mass transport was obtained with the composite membranes having the smaller charge density. Indeed, molecular diffusion first takes place in glassy nanolayer and follow through the rubbery PDMS governing dual diffusion system that agrees with an SD mechanism.

The selectivity in PEM, however, is specific to the type polyelectrolyte pair. Among four PEM, PAH/PSS shown to increase the rejection of diluted solutes from toluene. As presented in **Figure** 7.2, the mass transport in modified PEM is governed by the transport in two dense layers: mass transport in the glassy nanolayer on the top followed by mass transport in the rubbery polymer.

To the best of our knowledge, the toluene transport in PEM with PDMS under OSN condition was not previously reported in the literature. It was possible to apply resistance in a series model to determine intrinsic toluene permeance in individual PEM. Such an approach could strengthen the mass transport characterization in PEM-OSN membrane. Also, the solute diffusion coefficient in PEM was calculated.

Indeed, the PEM layer puts an additional resistance to the membrane which can be questioned for a rational decision on the layer number for best possible performance in terms of highest catalyst separation while keeping reasonable permeance of solvent and product. In this argument, the configuration of glassy PEM (low permeability, high resistance) with rubbery PDMS (high permeability, low resistance) makes the PDMS as a gutter, selective layer (permeation facilitating layer) that facilitate high permeation of molecule that already passed through the PEM. Thus, high resistance given by an increased PEM layer number could hinder the actual PDMS performance, and for a low PEM number, the rejection would be the same as PDMS. Such a situation indicates a trade-off between layer number to performance of the membrane and it can differ from one PEM to another. Thus, increasing layer number must have a maximum limit of rejection improvement based on the PEM used.

The proof of concept was obtained when 20 bilayers of PAH/PSS on PDMS was tested for the rejection showing an increase of rejection with drastic flux decline in a way that relative increase of rejection was much lower than the decline of global flux.

(5) The study of the ternary feed mixture in modified PDMS indicates a significant effect of the C16 concentration which tends to increase the global flux and to decrease the C16 retention while no decrease of the R-BINAP rejection was detected. This result seems to be very promising in the frame of the potential application of OSN to olefin metathesis.

In addition, PEM protocol using PAH/PSS was applied to modify the hydrophilic PVA membrane which was used in pervaporation to improve the dehydration properties of alcohol/water mixture (Article 2). Ten bilayered PEM of PAH/PSS was found efficient to favor the water permeation to improve the dehydration of isopropyl alcohol-water (80/20%w/w). This study cross-validate the interest of PEM protocols applied in OSN using PERVAP4060.

7.4 Modification and characterization of porous membranes

7.4.1 Protocol for the characterization of unknown membrane structure and potential mass transport model:

Often the OSN research lacks the necessary information of commercial membrane related to the porous or dense nature of the active surface. Such information is critical to analyze the results and use proper hypothesis to discuss the mass transport mechanism. As shown in this work (Chapter 2), the permeability of pure gases can solve this initial concern of OSN membrane type. Measurements CO_2, N_2 permeability and determination of CO_2/N_2 selectivity are appropriate characterizations to classify the membrane as porous or dense **Figure** 7.3.

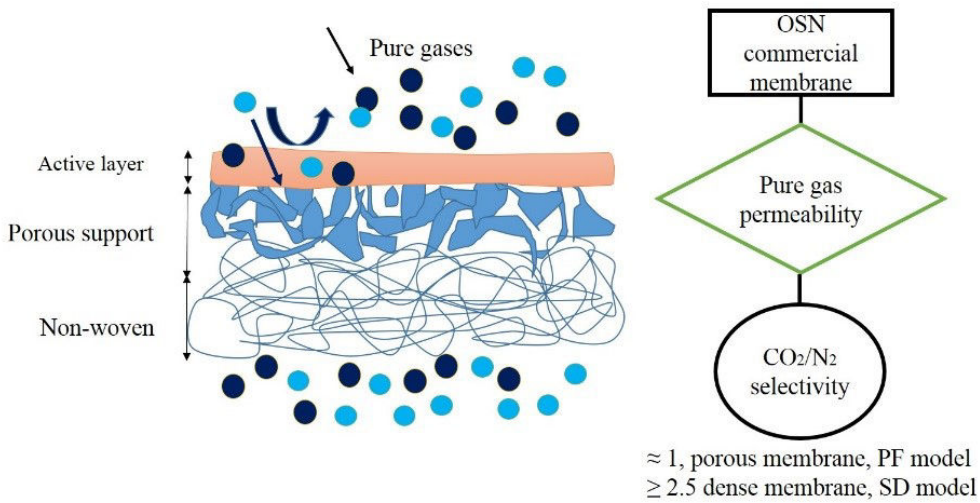

Figure 7.3: OSN membrane characterization for the first evaluation of the mass transport model.

In the porous system, ten bilayers of PDDA/PSS on AMS and PAN gives the highest separation among all prototype porous membranes. However, the rejection of catalyst in the modified porous system was always lower than the rejection in PERVAP4060 which makes the porous system less favorable for ANR tasks.

Interestingly the best performing PEM is different when the dense or the porous membrane was used. Despite differences in mass transport mechanism, there must be a membrane parameter that plays a role in PEM formation to its final configuration and performance. Initially, pore size reduction was expected from PEM on a porous membrane. A parallel possibility is pore blocking and thus the formation of dense nanolayer upon PEM deposition which was undesirable. If pore blocking together with dense layer form on the porous membrane, the permeation first occur in the dense layer and then it will only pass through the pores which are accessible by the molecule, inducing finally a strong porosity reduction. In the non-porous part of the membrane, the molecule will be blocked by the glassy PEL matrix which will raise an additional mass transport resistance resulting in a strong flux-decline.

Indeed, in PEM modified AMS, flux decline was observed >99% when compared with the flux in the pristine membrane which suggests to the pore block in the membrane and possibly a dense

nanolayer formation on the top.

Contrarily, in the modified PAN, it seems that the modification caused a reduction in pore size as presented in **Figure** 7.4. The major drawback of PAN is irreversible compaction when >10 bar TMP is applied.

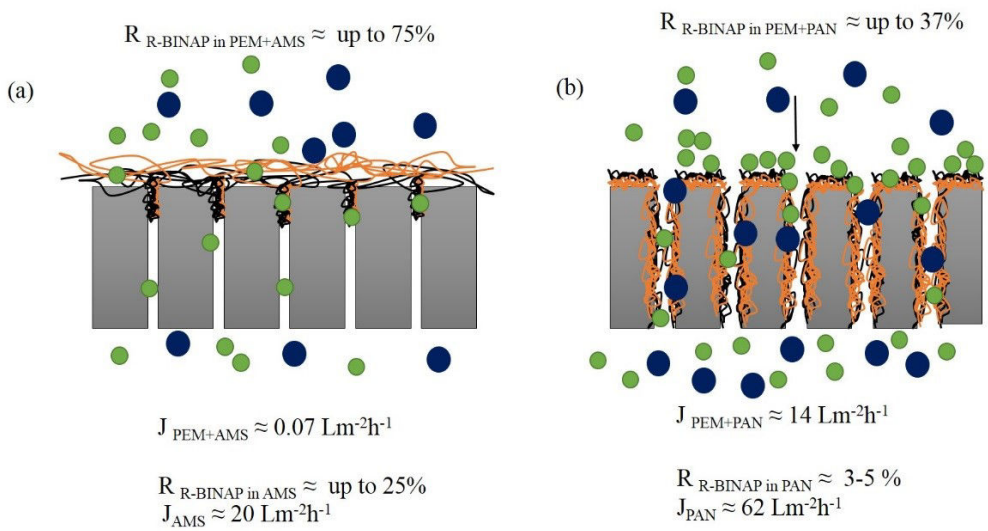

Figure 7.4: Toluene flux and R-BINAP rejection in PEM modified porous membranes in comparison to the performance at their pristine state (a) Modified AMS (b) Modified PAN. Data correspond to the OSN measurement carried at 10 bar, 30°C with cross-flow of 7-10 kg/h feed.

For a given pore size of the membrane, an increased number of bilayer can block the pore and causes performance loss. In contrary, the small number of PEM bilayer would not be sufficient for the desired performance for catalyst recovery. A trade-off can be understood between pore reduction and PEM bilayer to obtain the desired performance.

Though PEM on porous membrane improved the rejection, it always remains below the performance of PERVAP4060. With the ANR objective for the catalyst separation, the dense PERVAP4060, therefore, the first preference.

7.5 Perspective

1. Further OSN study for evaluation of PEL-PDMS interest in catalytic processes

The OSN study takes into account the PDMS membrane in toluene with the diluted ligand R-BINAP, C44 and C16. The real evaluation needs to consider the active catalyst containing the metal moieties such as Pd-BINAP and Ru-BINAP. Such metal moiety would increase the molar volume and so it is expected to lead to higher rejection in OSN. But the possible lifetime increase of the catalyst and its related activity is unknown.
On the other hand, the rejection of other phase transfer catalysts needs also to be tested. One such example could be to test Tetra-n-butylammonium bromide (TBAB). The comparison between ToABr and TBAB could give a clear picture of PEM charge and solute charge contribution to the

rejection.
The solvent range used in this study was limited to toluene ($Mv \approx 106, \delta \approx 18.4$) and ethanol ($M_v \approx 59, \delta \approx 26$). Other organic solvents such as IPA ($Mv \approx 78, \delta \approx 22.3$) and acetone ($Mv \approx 73.3, \delta \approx 19.3$) are the next potential candidate to investigate.

2. Pilot test of pristine and modified PERVAP4060

OSN at a process scale is briefly addressed in this study. A detailed study on the multistage cascade with/without hybrid process needs to take into account the corresponding CAPEX-OPEX. Knowing these benchmark data, the pilot tests of PDMS and PEM modified PDMS would be the next step for the successful valorization at an industrial scale.

3. Improving membrane performance by tuning the PEM structure

In our studies, PEM was prepared from water solutions without any added salt. It is known that the presence of salt can modify the PEM structure. Hence the effect of salt in each PEM could be interested to investigate for the mass transport in glassy PEM under OSN condition and to evaluate the charge effect on permeance and rejection.

4. Characterization of PEM transport properties

Using the resistance in series model, it has been shown that it is possible to determine the intrinsic permeance properties of a given PEM when the transport properties of the support membrane is known. This work could generalize to other PEL pair to rationalize the effect of PEM on mass transport.

5. Optimization of the PEL bilayer number and of the performance of the composite membranes

As long as the composite membrane involved two dense layers, the model in series can be applied to calculate the overall separation performance using the permeability and the thickness of each layer.
Thus for a given permeance of the support, the minimum number of PEL bilayers to be created can be calculated in order to get the mass transport governs by the PEM and not only by the support. On the other hand to improve the effect of the composite membrane, the permeance of the support layer should be maximized by decreasing the support thickness.

6. Effect of PEM on CO_2/N_2 separation.

As far as the gas measurements made with the pure gases CO_2 and N_2 are valid and reproducible, these unexpected results raise many questions. Indeed, as the bilayer number increases the selectivity of CO_2/N_2 decreases. It would be very interesting to know to which point the further increase of the LbL number will decrease the CO_2 selectivity and what is the reason of this phenomena. One of the first series of experiments to carry out would to repeat measurements for CO_2/N_2.

Appendix

FRAP data processing

1. Normalization of the measured intensities

A circular region of interest (ROI), of radius a, has been bleached. Then, the fluorescence intensity has been measured in the ROI and in three reference regions (Ref) as shown in Figure 1. The reference regions allow to follow the bleach due to the imaging. This bleach occurs although the laser is attenuated with respect to the full power used during the initial bleaching step.

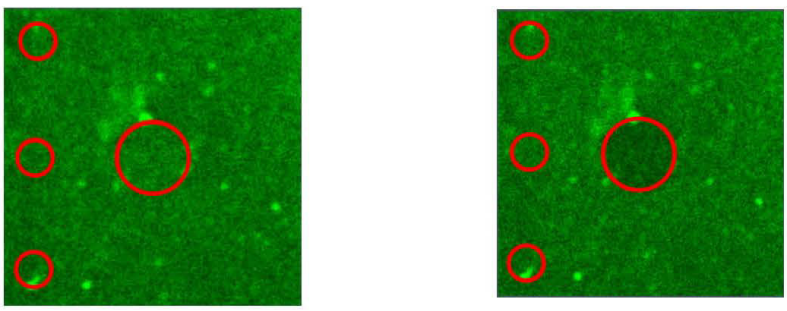

Figure 1. PEM before (left) and after (right) bleaching of the central circular area. The three areas along the left side of the images serve as references.

The intensity at time t (after the end of the initial bleaching taken as $t = 0$) in the ROI is $F_{\mathrm{ROI}}(t)$ and the corresponding reference intensities are $F_{\mathrm{Ref}}(t)$. The pre-bleach intensities are respectively $F_{\mathrm{ROI}}^{\text{pre-bl}}$ and $F_{\mathrm{Ref}}^{\text{pre-bl}}$. For each of the three references used here, the normalized ROI intensity is defined by:

$$f_{\mathrm{ROI}}(t) = \frac{F_{\mathrm{ROI}}(t)}{F_{\mathrm{ROI}}^{\text{pre-bl}}} \times \frac{F_{\mathrm{Ref}}^{\text{pre-bl}}}{F_{\mathrm{Ref}}(t)} \tag{1}$$

2. Extraction of the diffusion coefficient and fraction of mobile labeled molecules

The time evolution of the normalized fluorescence intensity in the ROI, as defined by eq. 1, is aimed at determining the diffusion coefficient, D, of the mobile labeled molecules, as well as their relative amount, p. It is assumed in the present study that all mobile labeled molecules have the same diffusion coefficient. The immobile labeled molecules are either irreversibly bound to the polyelectrolyte meshwork or have a movement that cannot be

detected over the time of observation of the fluorescence recovery. In both (undistinguishable) cases, $D = 0$ is ascribed to these molecules. Let's note in passing that the fluorescence recovery leads in general not to an equilibrium state, unless all labeled molecules are mobile ($p = 1$). The system is in equilibrium before the initial bleaching step. Afterward only the mobile molecules may re-equilibrate through diffusion from the non-bleached region around the ROI to the bleached ROI. In contrast, the immobile molecules cannot.

To extract both D and p, a theoretical expression of the recovery kinetics is desirable. Indeed, the sole examination of the experimental date makes the estimation of these parameters quite delicate, if not impossible. This is particularly true as to the asymptotic value of the florescence, i.e. $f_{\mathrm{ROI}}(\infty)$, either because the recording was interrupted too early or because of the noise. The amplitude of the recovery depends also on the intensity at the end of the initial bleaching step ($t = 0$). Strictly speaking, this intensity is unknown too because the first image, even if its recording starts exactly at $t = 0$, requires a non-zero acquisition time (0.4 s in the present study for all images).

If the fluorescence intensity is uniform over the ROI, if all molecules are mobile ($p = 1$) and if the intensity is zero at $t = 0$, the time evolution of the fluorescence intensity is given by (Soumpasis, 1983):

$$f_{\mathrm{ROI}}(t) = \mathrm{e}^{-\frac{2}{\tau}}\left[\mathbf{I}_0\left(\frac{2}{\tau}\right) + \mathbf{I}_1\left(\frac{2}{\tau}\right)\right] \tag{2}$$

where $\tau = \frac{4Dt}{a^2}$; $\mathbf{I}_0$ and $\mathbf{I}_1$ are the modified Bessel functions of first kind of order 0 and 1, respectively. Because in general $f_{\mathrm{ROI}}(0) \neq 0$, eq. 2 becomes (Picart et al., 2005, where α stands as a short hand notation for $f_{\mathrm{ROI}}(0)$) :

$$f_{\mathrm{ROI}}(t) = f_{\mathrm{ROI}}(0) + [1 - f_{\mathrm{ROI}}(0)]\,\mathrm{e}^{-\frac{2}{\tau}}\left[\mathbf{I}_0\left(\frac{2}{\tau}\right) + \mathbf{I}_1\left(\frac{2}{\tau}\right)\right] \tag{3}$$

Finally, because in general $p < 1$, the recovery kinetics is described by:

$$f_{\mathrm{ROI}}(t) = f_{\mathrm{ROI}}(0) + p[1 - f_{\mathrm{ROI}}(0)]\,\mathrm{e}^{-\frac{2}{\tau}}\left[\mathbf{I}_0\left(\frac{2}{\tau}\right) + \mathbf{I}_1\left(\frac{2}{\tau}\right)\right] \tag{4}$$

It follows from this expression that

2

$$f_{\mathrm{ROI}}(\infty) = f_{\mathrm{ROI}}(0) + p[1 - f_{\mathrm{ROI}}(0)] \tag{5}$$

gives the maximum fluorescence intensity which can eventually be reached. The time required to achieve half of the possible recovery is defined by:

$$f_{\mathrm{ROI}}(t_{1/2}) = f_{\mathrm{ROI}}(0) + \frac{1}{2} p[1 - f_{\mathrm{ROI}}(0)] \tag{6}$$

Comparing with eq. 4 shows that $t_{1/2}$ is the root of:

$$\mathrm{e}^{-\frac{2}{\tau}}\left[\mathbf{I}_0\left(\frac{2}{\tau}\right) + \mathbf{I}_1\left(\frac{2}{\tau}\right)\right] = \frac{1}{2} \tag{7}$$

The solution is $\tau = 0.894\ldots$ It follows that:

$$t_{1/2} \approx 0.224 \frac{a^2}{D} \tag{8a}$$

or, conversely, that (Soumpasis, 1983):

$$D \approx 0.224 \frac{a^2}{t_{1/2}} \tag{8b}$$

3. Results

The values of D and p are listed in Table 1. There appears also the value of $t_{1/2}$ derived from eq. 8a.

Table 1. Value of the diffusion coefficient and the fraction of mobile labeled molecules in various polyelectrolyte multilayer (PEM) films. The time of half-recovery is also given for completeness.

	***a* (µm)**	**$f_{\mathrm{ROI}}(0)$**	***D* (µm² / s)**	***p***	**$t_{1/2}$ *(s)***
PEM on glass					
$(PDDA/PSS)_{10}$	20	0.75	0.54	0.82	165
$(PAH/PSS)_{10}$	10	0.74	2.3	0.09	9.7
$(PAH/PAA)_{10}$	20	0.41	9.3	0.38	9.6
$(PDDA/PAA)_{10}$	20	0.67	65.0	0.26	1.4
PEM on PDMS					
$(PDDA/PSS)_{10}$	20	0.64	0.43	0.40	208
$(PAH/PSS)_{10}$	20	0.58	77.0	0.28	1.2

$(PAH/PAA)_{10}$	20	0.34	7.9	0.15	11.4
$(PDDA/PAA)_{10}$	20	0.82	0.56	0.20	160

4

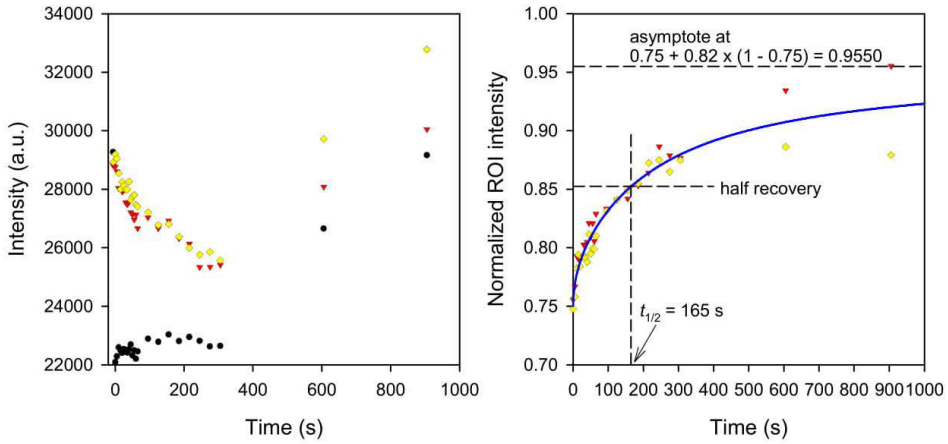

Figure 2. $(PDDA/PSS)_{10}$ film on glass. Left panel: Raw fluorescence intensity in the ROI (black) and the two reference areas (red, yellow). Right panel: Normalized intensity in the ROI and graphical representation of eq. 4 (blue line) with optimized fitting parameters.

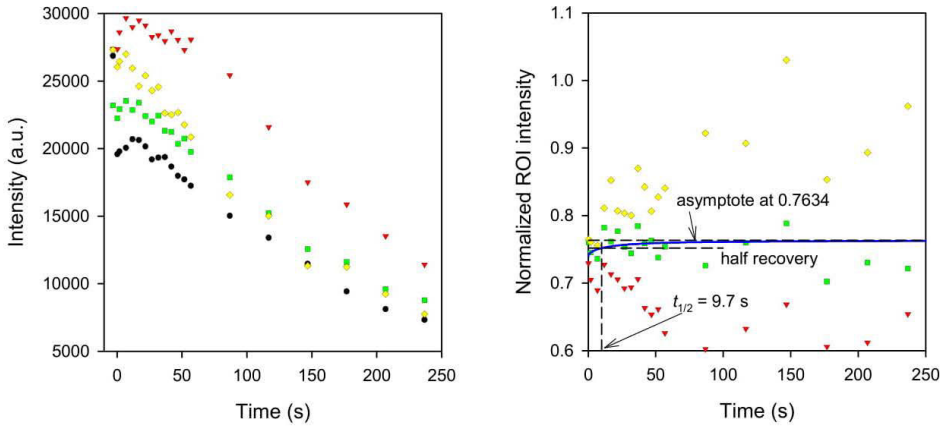

Figure 3. $(PAH/PSS)_{10}$ film on glass. Left panel: Raw fluorescence intensity in the ROI (black) and the three reference areas (red, green, yellow). Right panel: Normalized intensity in the ROI and graphical representation of eq. 4 (blue line) with optimized fitting parameters.

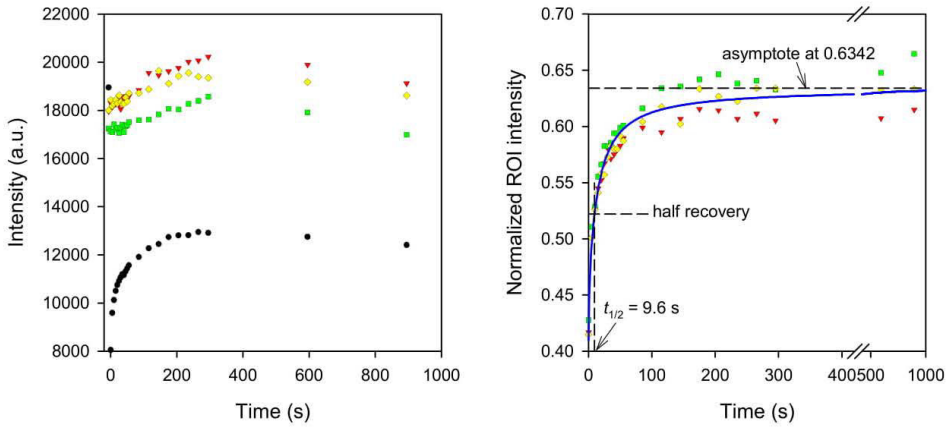

Figure 4. $(PAH/PAA)_{10}$ film on glass. Left panel: Raw fluorescence intensity in the ROI (black) and the three reference areas (red, green, yellow). Right panel: Normalized intensity in the ROI and graphical representation of eq. 4 (blue line) with optimized fitting parameters.

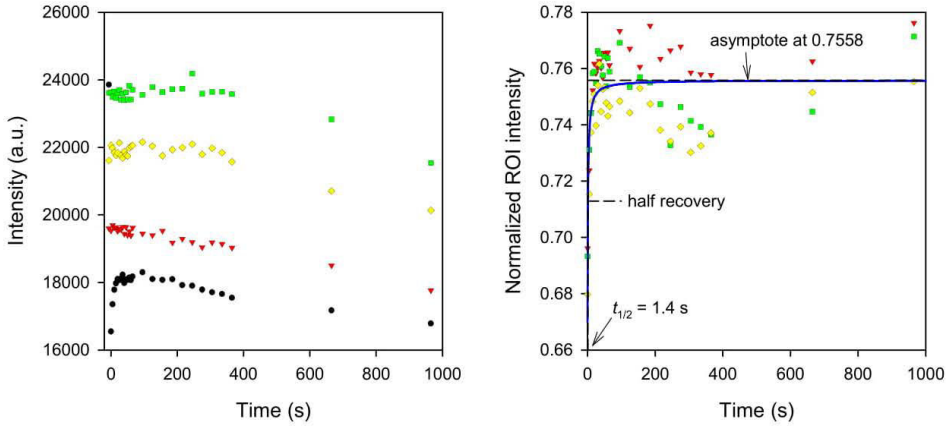

Figure 5. $(PDDA/PAA)_{10}$ film on glass. Left panel: Raw fluorescence intensity in the ROI (black) and the three reference areas (red, green, yellow). Right panel: Normalized intensity in the ROI and graphical representation of eq. 4 (blue line) with optimized fitting parameters.

6

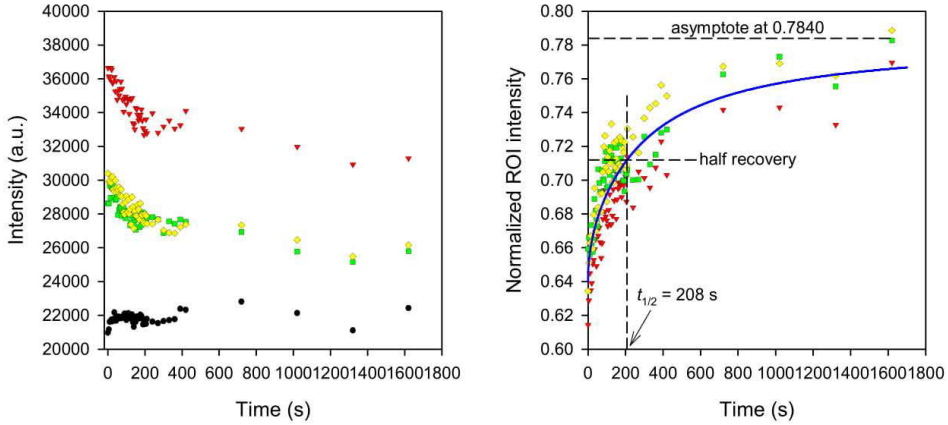

Figure 6. $(PDDA/PSS)_{10}$ film on PDMS. Left panel: Raw fluorescence intensity in the ROI (black) and the three reference areas (red, green, yellow). Right panel: Normalized intensity in the ROI and graphical representation of eq. 4 (blue line) with optimized fitting parameters.

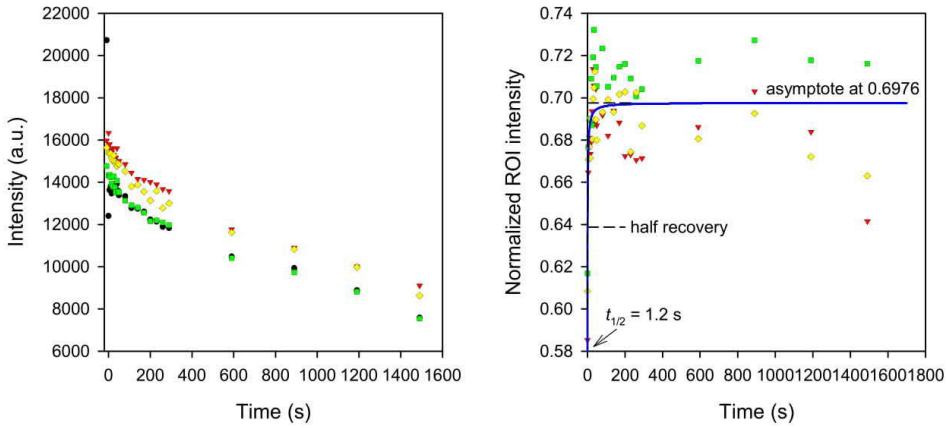

Figure 7. $(PAH/PSS)_{10}$ film on PDMS. Left panel: Raw fluorescence intensity in the ROI (black) and the three reference areas (red, green, yellow). Right panel: Normalized intensity in the ROI and graphical representation of eq. 4 (blue line) with optimized fitting parameters.

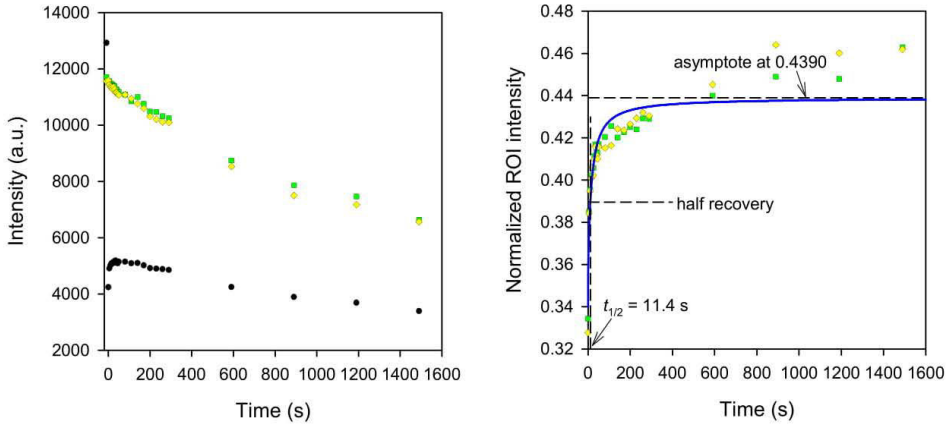

Figure 8. $(PAH/PAA)_{10}$ film on PDMS. Left panel: Raw fluorescence intensity in the ROI (black) and the two reference areas (green, yellow). Right panel: Normalized intensity in the ROI and graphical representation of eq. 4 (blue line) with optimized fitting parameters.

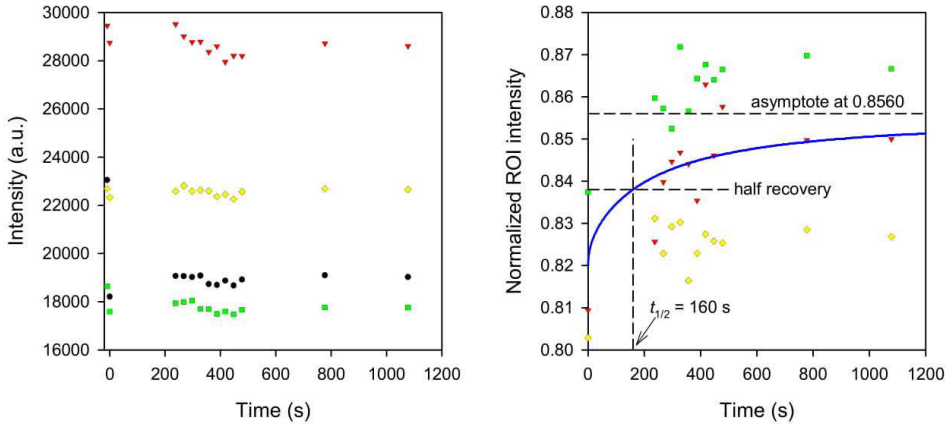

Figure 9. $(PDDA/PAA)_{10}$ film on PDMS. Left panel: Raw fluorescence intensity in the ROI (black) and the three reference areas (red, green, yellow). Right panel: Normalized intensity in the ROI and graphical representation of eq. 4 (blue line) with optimized fitting parameters.

Bibliography

F. Abbasi, H. Mirzadeh, and A.-A. Katbab. Modification of polysiloxane polymers for biomedical applications: a review. *Polymer International*, 50(12):1279–1287, 2001.

V. Abetz, T. Brinkmann, M. Dijkstra, K. Ebert, D. Fritsch, K. Ohlrogge, D. Paul, K.-V. Peinemann, S. Pereira-Nunes, N. Scharnagl, et al. Developments in membrane research: from material via process design to industrial application. *Advanced Engineering Materials*, 8(5):328–358, 2006.

S. Adler, E. Beaver, P. Bryan, S. Robinson, and J. Watson. Vision 2020: 2000 separations roadmap. *New York, NY: AIChE*, 2000.

S. Aerts, A. Vanhulsel, A. Buekenhoudt, H. Weyten, S. Kuypers, H. Chen, M. Bryjak, L. E. M. Gevers, I. F. J. Vankelecom, and P. A. Jacobs. Plasma-treated PDMS-membranes in solvent resistant nanofiltration: Characterization and study of transport mechanism. *Journal of Membrane Science*, 275(1-2):212–219, 2006. ISSN 03767388. doi: 10.1016/j.memsci.2005.09.021.

P. Ahmadiannamini, X. Li, W. Goyens, B. Meesschaert, and I. F. J. Vankelecom. Multilayered PEC nanofiltration membranes based on SPEEK/PDDA for anion separation. *Journal of Membrane Science*, 360(1-2):250–258, 2010. ISSN 03767388. doi: 10.1016/j.memsci.2010.05.021. URL http://dx.doi.org/10.1016/j.memsci.2010.05.021.

P. Ahmadiannamini, X. Li, W. Goyens, N. Joseph, B. Meesschaert, and I. F. J. Vankelecom. Multilayered polyelectrolyte complex based solvent resistant nanofiltration membranes prepared from weak polyacids. *Journal of Membrane Science*, 394-395:98–106, 2012. ISSN 03767388. doi: 10.1016/j.memsci.2011.12.032. URL http://dx.doi.org/10.1016/j.memsci.2011.12.032.

A. Akyüz, G. Buyukunsal, and A. Paril. Online monitoring of diallyldimethylammonium chloride polymerization. *Polymer Engineering & Science*, 54(6):1350–1356, 2014.

A. S. Al-Hobaib, K. M. Al-Sheetan, M. R. Shaik, and M. Al-Suhybani. Modification of thin-film polyamide membrane with multi-walled carbon nanotubes by interfacial polymerization. *Applied Water Science*, 7(8):4341–4350, 2017.

T. A. Albright, W. J. Freeman, and E. E. Schweizer. Nuclear magnetic resonance studies. iv. carbon and phosphorus nuclear magnetic resonance of phosphine oxides and related compounds. *The Journal of Organic Chemistry*, 40(23):3437–3441, 1975.

F. A. AlMarzooqi, M. Bilad, B. Mansoor, and H. A. Arafat. A comparative study of image analysis and porometry techniques for characterization of porous membranes. *Journal of materials science*, 51(4):2017–2032, 2016.

T. M. Aminabhavi and H. T. Phayde. Molecular transport characteristics of santoprene thermoplastic rubber in the presence of aliphatic alkanes over the temperature interval of 25 to 70 c. *Polymer*, 36(5):1023–1033, 1995.

M. Amirilargani, M. Sadrzadeh, E. J. Sudhölter, and L. C. de Smet. Surface modification methods of organic solvent nanofiltration membranes. *Chemical Engineering Journal*, 289:562–582, 2016. ISSN 13858947. doi: 10.1016/j.cej.2015.12.062. URL http://dx.doi.org/10.1016/j.cej.2015.12.062.

A. Ashworth. Relation between gas permselectivity and permeability in a bilayer composite membrane. *Journal of membrane science*, 71(1-2):169–173, 1992.

P. Atkins, J. De Paula, and J. Keeler. *Atkins' physical chemistry*. Oxford university press, 2018.

K. Bakeev, V. Izumrudov, A. Zezin, and V. Kabanov. Kinetics and mechanism of reactions of the formation of polyelectrolytic complexes. *Doklady Akademii Nauk SSSR*, 299(6):1405–1408, 1988.

R. Baker, J. Wijmans, A. Athayde, R. Daniels, J. Ly, and M. Le. The effect of concentration polarization on the separation of volatile organic compounds from water by pervaporation. *Journal of membrane science*, 137(1-2):159–172, 1997.

R. W. Baker. Membrane technology and applications. 2004. *England: John Wiley and Sons*, 2007.

S. Bashir, M. Bashir, J. M. Rees, W. B. Zimmerman, et al. Hydrophilic surface modification of pdms microchannel for o/w and w/o/w emulsions. *Micromachines*, 6(10):1445–1458, 2015.

J. Bassil, H. Alem, G. Henrion, and D. Roizard. Tailored adhesion behavior of polyelectrolyte thin films deposited on plasma-treated poly(dimethylsiloxane) for functionalized membranes. *Applied Surface Science*, 369:482–491, 2016a. ISSN 01694332. doi: 10.1016/j.apsusc.2016.01.146. URL http://dx.doi.org/10.1016/j.apsusc.2016.01.146.

J. Bassil, H. Alem, G. Henrion, and D. Roizard. Tailored adhesion behavior of polyelectrolyte thin films deposited on plasma-treated poly (dimethylsiloxane) for functionalized membranes. *Applied Surface Science*, 369:482–491, 2016b.

A. Behr and P. Neubert. *Applied homogeneous catalysis*. John Wiley & Sons, 2012.

H. Ben Soltane, D. Roizard, and E. Favre. Effect of pressure on the swelling and fluxes of dense PDMS membranes in nanofiltration: An experimental study. *Journal of Membrane Science*, 435: 110–119, 2013. ISSN 03767388. doi: 10.1016/j.memsci.2013.01.053.

H. Ben Soltane, D. Roizard, and E. Favre. Study of the rejection of various solutes in OSN by a composite polydimethylsiloxane membrane: Investigation of the role of solute affinity. *Separation and Purification Technology*, 161:193–201, 2016. ISSN 18733794. doi: 10.1016/j.seppur.2016.01.035.

K. Berean, J. Z. Ou, M. Nour, K. Latham, C. McSweeney, D. Paull, A. Halim, S. Kentish, C. M. Doherty, A. J. Hill, et al. The effect of crosslinking temperature on the permeability of pdms membranes: Evidence of extraordinary co2 and ch4 gas permeation. *Separation and Purification Technology*, 122:96–104, 2014.

Y. Bessiere, N. Abidine, and P. Bacchin. Low fouling conditions in dead-end filtration: evidence for a critical filtered volume and interpretation using critical osmotic pressure. *Journal of membrane science*, 264(1-2):37–47, 2005.

K. Besteman, M. Zevenbergen, and S. Lemay. Charge inversion by multivalent ions: Dependence on dielectric constant and surface-charge density. *Physical Review E*, 72(6):061501, 2005.

D. Bhanushali, S. Kloos, C. Kurth, and D. Bhattacharyya. Performance of solvent-resistant membranes for non-aqueous systems: Solvent permeation results and modeling. *Journal of Membrane Science*, 189(1):1–21, 2001. ISSN 03767388. doi: 10.1016/S0376-7388(01)00356-8.

D. Bhanushali, S. Kloos, and D. Bhattacharyya. Solute transport in solvent-resistant nanofiltration membranes for non-aqueous systems : experimental results and the role of solute solvent coupling. *Journal of Membrane Science*, 208:343–359, 2002. ISSN 03767388. doi: PiiS0376-7388(02)00315-0. URL http://www.sciencedirect.com/science/article/B6TGK-46PBG1D-M/2/02e877801026b385b9577394301ccec5.

D. Bhongsuwan, T. Bhongsuwan, and J. Na-Suwan. Construction of a dead-end type micro-to ro membrane test cell and performance test with the laboratory-made and commercial membranes. *Membr. Sci. Technol.*, pages 999–1007, 2002.

D. Bodas and C. Khan-Malek. Formation of more stable hydrophilic surfaces of PDMS by plasma and chemical treatments. *Microelectronic Engineering*, 83(4-9 SPEC. ISS.):1277–1279, 2006. ISSN 01679317. doi: 10.1016/j.mee.2006.01.195.

D. Bodas and C. Khan-Malek. Hydrophilization and hydrophobic recovery of PDMS by oxygen plasma and chemical treatment-An SEM investigation. *Sensors and Actuators, B: Chemical*, 123 (1):368–373, 2007. ISSN 09254005. doi: 10.1016/j.snb.2006.08.037.

U. Böhme and U. Scheler. Hydrodynamic size and charge of polyelectrolyte complexes. *The Journal of Physical Chemistry B*, 111(29):8348–8350, 2007.

B. Bolto, M. Hoang, and Z. Xie. A review of membrane selection for the dehydration of aqueous ethanol by pervaporation. *Chemical Engineering and Processing: Process Intensification*, 50(3): 227–235, 2011.

N. A. Bullett, D. P. Bullett, F.-E. Truica-Marasescu, S. Lerouge, F. Mwale, and M. R. Wertheimer. Polymer surface micropatterning by plasma and vuv-photochemical modification for controlled cell culture. *Applied Surface Science*, 235(4):395–405, 2004.

M. G. Buonomenna. Membrane processes for a sustainable industrial growth. *RSC Advances*, 3 (17):5694, 2013. ISSN 2046-2069. doi: 10.1039/c2ra22580h. URL http://xlink.rsc.org/?DOI=c2ra22580h.

M. G. Buonomenna and J. Bae. Organic solvent nanofiltration in pharmaceutical industry. *Separation and Purification Reviews*, 44(2):157–182, 2015a. ISSN 15422127. doi: 10.1080/15422119.2014.918884.

M. G. Buonomenna and J. Bae. Organic solvent nanofiltration in pharmaceutical industry. *Separation and Purification Reviews*, 44(2):157–182, 2015b. ISSN 15422127. doi: 10.1080/15422119.2014.918884.

I. Cabasso and K. A. Lundy. Method of making membranes for gas separation and the composite membranes, July 29 1986. US Patent 4,602,922.

N. Cabello-Sanchez, L. Jean, J. Maddaluno, M.-C. Lasne, and J. Rouden. Palladium-mediated n-arylation of heterocyclic diamines: insights into the origin of an unusual chemoselectivity. *The Journal of organic chemistry*, 72(6):2030–2039, 2007.

A. Cano-Odena, P. Vandezande, D. Fournier, W. Van Camp, F. E. Du Prez, and I. F. Vankelecom. Solvent-resistant nanofiltration for product purification and catalyst recovery in click chemistry reactions. *Chemistry–A European Journal*, 16(3):1061–1067, 2010.

A. Cassie and S. Baxter. Wettability of porous surfaces. *Transactions of the Faraday society*, 40: 546–551, 1944.

H.-R. Chae, J. Lee, C.-H. Lee, I.-C. Kim, and P.-K. Park. Graphene oxide-embedded thin-film composite reverse osmosis membrane with high flux, anti-biofouling, and chlorine resistance. *Journal of Membrane Science*, 483:128–135, 2015.

C.-M. Chan, T.-M. Ko, and H. Hiraoka. Polymer surface modification by plasmas and photons. *Surface science reports*, 24(1-2):1–54, 1996.

P. Chappell, J. Brown, G. George, and H. Willis. Surface modification of extended chain polyethylene fibres to improve adhesion to epoxy and unsaturated polyester resins. *Surface and interface analysis*, 17(3):143–150, 1991.

D. Chen. Solvent-resistant nanofiltration membranes based on multilayered polyelectrolytes deposited on silicon composite. *Journal of Applied Polymer Science*, 129(6):3156–3161, 2013. ISSN 00218995. doi: 10.1002/app.39042.

J. Chen, J. Li, Z.-P. Zhao, D. Wang, and C.-X. Chen. Nanofiltration membrane prepared from polyacrylonitrile ultrafiltration membrane by low-temperature plasma: 5. grafting of styrene in vapor phase and its application. *Surface and Coatings Technology*, 201(15):6789–6792, 2007a.

Y. Chen, F. Xiangli, W. Jin, and N. Xu. Organic-inorganic composite pervaporation membranes prepared by self-assembly of polyelectrolyte multilayers on macroporous ceramic supports. *Journal of Membrane Science*, 302(1-2):78–86, 2007b. ISSN 03767388. doi: 10.1016/j.memsci.2007.06.019.

S. Cheng, D. L. Oatley, P. M. Williams, and C. J. Wright. Positively charged nanofiltration membranes: Review of current fabrication methods and introduction of a novel approach. *Advances in Colloid and Interface Science*, 164(1-2):12–20, 2011. ISSN 00018686. doi: 10.1016/j.cis.2010.12.010. URL http://dx.doi.org/10.1016/j.cis.2010.12.010.

X. Q. Cheng, Y. L. Zhang, Z. X. Wang, Z. H. Guo, Y. P. Bai, and L. Shao. Recent advances in polymeric solvent-resistant nanofiltration membranes. *Advances in Polymer Technology*, 33(S1): 1–24, 2014a. ISSN 10982329. doi: 10.1002/adv.21455.

X. Q. Cheng, Y. L. Zhang, Z. X. Wang, Z. H. Guo, Y. P. Bai, and L. Shao. Recent advances in polymeric solvent-resistant nanofiltration membranes. *Advances in Polymer Technology*, 33(S1): 1–24, 2014b. ISSN 10982329. doi: 10.1002/adv.21455.

J. Chiou and D. Paul. Sorption and transport of co2 in pvf2/pmma blends. *Journal of applied polymer science*, 32(1):2897–2918, 1986.

J. Choi and M. F. Rubner. Influence of the degree of ionization on weak polyelectrolyte multilayer assembly. *Macromolecules*, 38(1):116–124, 2005.

C. Choy, W. Leung, and T. Ma. Sorption and diffusion of toluene in highly oriented polypropylene. *Journal of Polymer Science: Polymer Physics Edition*, 22(4):707–719, 1984.

D. J. Cole-Hamilton and R. P. Tooze. *Catalyst separation, recovery and recycling: chemistry and process design*, volume 30. Springer Science & Business Media, 2006.

B. Cornils, W. A. Herrmann, M. Beller, and R. Paciello. *Applied Homogeneous Catalysis with Organometallic Compounds: A Comprehensive Handbook in Four Volumes*, volume 4. John Wiley & Sons, 2017.

J. Critchley, G. Knight, and W. W. Wright. *Heat-resistant polymers: technologically useful materials*. Springer Science & Business Media, 2013.

R. d'Agostino, P. Favia, C. Oehr, and M. R. Wertheimer. Low-temperature plasma processing of materials: past, present, and future. *Plasma Processes and Polymers*, 2(1):7–15, 2005.

S. Darvishmanesh, A. Buekenhoudt, J. Degrève, and B. Van der Bruggen. General model for prediction of solvent permeation through organic and inorganic solvent resistant nanofiltration membranes. *Journal of Membrane Science*, 334(1-2):43–49, 2009. ISSN 03767388. doi: 10.1016/j.memsci.2009.02.013.

S. Darvishmanesh, J. Degrè, and B. V. D. Bruggen. Performance of solvent-pretreated polyimide nanofiltration membranes for separation of dissolved dyes from toluene. *Industrial and Engineering Chemistry Research*, 49(19):9330–9338, 2010a. ISSN 08885885. doi: 10.1021/ie101050k.

S. Darvishmanesh, J. Degrève, and B. Van der Bruggen. Mechanisms of solute rejection in solvent resistant nanofiltration: the effect of solvent on solute rejection. *Physical Chemistry Chemical Physics*, 12(40):13333, 2010b. ISSN 1463-9076. doi: 10.1039/c0cp00230e. URL http://xlink.rsc.org/?DOI=c0cp00230e.

S. Darvishmanesh, T. Robberecht, P. Luis, J. Degrève, and B. Van Der Bruggen. Performance of nanofiltration membranes for solvent purification in the oil industry. *JAOCS, Journal of the American Oil Chemists' Society*, 88(8):1255–1261, 2011a. ISSN 0003021X. doi: 10.1007/s11746-011-1779-y.

S. Darvishmanesh, J. Vanneste, E. Tocci, J. Jansen, F. Tasseli, J. Degr??ve, E. Drioli, and B. Van Der Bruggen. Physicochemical characterization of solute retention in solvent resistant nanofiltration: The effect of solute size, polarity, dipole moment, and solubility parameter. *Journal of Physical Chemistry B*, 115(49):14507–14517, 2011b. ISSN 15205207. doi: 10.1021/jp207569m.

A. Davis and C. R. Ethier. Transport through materials bounded by porous surfaces. *Chemical engineering science*, 48(9):1655–1663, 1993.

K. De Smet, S. Aerts, E. Ceulemans, I. F. J. Vankelecom, and P. A. Jacobs. Nanofiltration-coupled catalysis to combine the advantages of homogeneous and heterogeneous catalysis. *Chemical Communications*, (7):597–598, 2001. ISSN 13597345. doi: 10.1039/b009898l.

G. Decher. Fuzzy nanoassemblies: Toward layered polymeric multicomposites. *Science*, 277(5330):1232–1237, 1997. ISSN 00368075. doi: 10.1126/science.277.5330.1232.

G. Decher, J. Hong, and J. Schmitt. Buildup of ultrathin multilayer films by a self-assembly process: Iii. consecutively alternating adsorption of anionic and cationic polyelectrolytes on charged surfaces. *Thin solid films*, 210:831–835, 1992.

A. V. Dobrynin and M. Rubinstein. Theory of polyelectrolytes in solutions and at surfaces. *Progress in Polymer Science (Oxford)*, 30(11):1049–1118, 2005. ISSN 00796700. doi: 10.1016/j.progpolymsci.2005.07.006.

J. Dreimann, P. Lutze, M. Zagajewski, A. Behr, A. Górak, and A. J. Vorholt. Highly integrated reactor–separator systems for the recycling of homogeneous catalysts. *Chemical Engineering and Processing: Process Intensification*, 99:124–131, 2016.

J. M. Dreimanna, A. J. Vorholta, M. Skiborowskib, and A. Behra. Removal of homogeneous precious metal catalysts via organic solvent nanofiltration. *CHEMICAL ENGINEERING*, 47, 2016.

E. Drioli, L. Giorno, and E. Fontananova. *Comprehensive membrane science and engineering*. Elsevier, 2017.

S. T. Dubas and J. B. Schlenoff. Factors controlling the growth of polyelectrolyte multilayers. *Macromolecules*, 32(24):8153–8160, 1999. ISSN 00249297. doi: 10.1021/ma981927a.

S. T. Dubas and J. B. Schlenoff. Polyelectrolyte multilayers containing a weak polyacid: construction and deconstruction. *Macromolecules*, 34(11):3736–3740, 2001.

S. Dutczak, F. Cuperus, M. Wessling, and D. Stamatialis. New crosslinking method of polyamide–imide membranes for potential application in harsh polar aprotic solvents. *Separation and purification technology*, 102:142–146, 2013.

K. Ebert, J. Koll, M. F. J. Dijkstra, and M. Eggers. Fundamental studies on the performance of a hydrophobic solvent stable membrane in non-aqueous solutions. *Journal of Membrane Science*, 285(1-2):75–80, 2006. ISSN 03767388. doi: 10.1016/j.memsci.2006.07.037.

R. Evans, Z. Deng, A. K. Rogerson, A. S. McLachlan, J. J. Richards, M. Nilsson, and G. A. Morris. Quantitative interpretation of diffusion-ordered nmr spectra: Can we rationalize small molecule diffusion coefficients? *Angewandte Chemie International Edition*, 52(11):3199–3202, 2013.

C. W. Extrand. Model for contact angles and hysteresis on rough and ultraphobic surfaces. *Langmuir*, 18(21):7991–7999, 2002.

J. Fang, R. Jana, J. A. Tunge, and B. Subramaniam. Continuous homogeneous hydroformylation with bulky rhodium catalyst complexes retained by nano-filtration membranes. *Applied Catalysis A: General*, 393(1-2):294–301, 2011.

H. M. Fares and J. B. Schlenoff. Diffusion of sites versus polymers in polyelectrolyte complexes and multilayers. *Journal of the American Chemical Society*, 139(41):14656–14667, 2017.

E. Favre, Q. T. Nguyen, D. Sacco, A. Moncuy, and R. Clement. Multicomponent Polymer/Solvents Equilibria: An Evaluation of Flory-Huggins Theory for Crosslinked Pdms Networks Swelled by Binary Mixtures. *Chemical Engineering Communications*, 140(1):193–205, 1995. ISSN 15635201. doi: 10.1080/00986449608936463.

R. F. Fedors. A method for estimating both the solubility parameters and molar volumes of liquids. *Polymer Engineering & Science*, 14(2):147–154, 1974.

M. Fernanda, J. Solomon, Y. Bhole, and A. Guy. High flux membranes for organic solvent nanofiltration (OSN) Interfacial polymerization with solvent activation. *Journal of Membrane Science*, 423-424:1–12, 2012. ISSN 0376-7388. doi: 10.1016/j.memsci.2012.08.030. URL http://dx.doi.org/10.1016/j.memsci.2012.08.030.

W. H. Ferrell, D. I. Kushner, and M. A. Hickner. Investigation of polymer–solvent interactions in poly (styrene sulfonate) thin films. *Journal of Polymer Science Part B: Polymer Physics*, 55(18): 1365–1372, 2017.

D. Fierro, A. Boschetti-de Fierro, and V. Abetz. The solution-diffusion with imperfections model as a method to understand organic solvent nanofiltration of multicomponent systems. *Journal of Membrane Science*, 413-414:91–101, 2012. ISSN 03767388. doi: 10.1016/j.memsci.2012.04.027. URL http://dx.doi.org/10.1016/j.memsci.2012.04.027.

G. Firpo, E. Angeli, L. Repetto, and U. Valbusa. Permeability thickness dependence of polydimethylsiloxane (pdms) membranes. *Journal of Membrane Science*, 481:1–8, 2015.

G. Francius, A. Razafitianamaharavo, M. Moussa, M. Dossot, E. Andre, J. Bacharouche, B. Senger, V. Ball, and J. F. Duval. Remarkable structure and elasticity relaxation dynamics of poly (diallyldimethylammonium chloride)–poly (acrylic acid) multilayer films. *The Journal of Physical Chemistry C*, 120(10):5599–5612, 2016.

D. Fritsch, P. Merten, K. Heinrich, M. Lazar, and M. Priske. High performance organic solvent nanofiltration membranes: Development and thorough testing of thin film composite membranes made of polymers of intrinsic microporosity (PIMs). *Journal of Membrane Science*, 401-402: 222–231, 2012. ISSN 03767388. doi: 10.1016/j.memsci.2012.02.008. URL http://dx.doi.org/10.1016/j.memsci.2012.02.008.

M. Galizia and K. P. Bye. Advances in organic solvent nanofiltration rely on physical chemistry and polymer chemistry. *Frontiers in chemistry*, 6, 2018.

A. Garg, J. R. Heflin, H. W. Gibson, and R. M. Davis. Study of film structure and adsorption kinetics of polyelectrolyte multilayer films: effect of ph and polymer concentration. *Langmuir*, 24 (19):10887–10894, 2008.

J. Geens, K. Boussu, C. Vandecasteele, and B. Van der Bruggen. Modelling of solute transport in non-aqueous nanofiltration. *Journal of Membrane Science*, 281(1-2):139–148, 2006. ISSN 03767388. doi: 10.1016/j.memsci.2006.03.028.

J. Geens, B. De Witte, and B. Van Der Bruggen. Removal of API's (active pharmaceutical ingredients) from organic solvents by nanofiltration. *Separation Science and Technology*, 42(11): 2435–2449, 2007. ISSN 01496395. doi: 10.1080/01496390701477063.

S. C. George and S. Thomas. Transport phenomena through polymeric systems. *Progress in Polymer Science*, 26(6):985–1017, 2001.

L. E. Gevers, I. F. Vankelecom, and P. A. Jacobs. Zeolite filled polydimethylsiloxane (pdms) as an improved membrane for solvent-resistant nanofiltration (srnf). *Chemical communications*, (19): 2500–2502, 2005.

L. E. Gevers, G. Meyen, K. De Smet, P. Van De Velde, F. Du Prez, I. F. Vankelecom, and P. A. Jacobs. Physico-chemical interpretation of the SRNF transport mechanism for solutes through dense silicone membranes. *Journal of Membrane Science*, 274(1-2):173–182, 2006. ISSN 03767388. doi: 10.1016/j.memsci.2005.08.009.

R. A. Ghostine, M. Z. Markarian, and J. B. Schlenoff. Asymmetric growth in polyelectrolyte multilayers. *Journal of the American Chemical Society*, 135(20):7636–7646, 2013.

N. Gomathi, D. Mishra, T. K. Maiti, and S. Neogi. Surface Modification of Polypropylene using Argon Plasma for Biomedical Applications. *Ispc_19*, pages 2–5, 2009.

D. N. Gorbunov, A. V. Volkov, Y. S. Kardasheva, A. L. Maksimov, and E. A. Karakhanov. Hydroformylation in petroleum chemistry and organic synthesis: Implementation of the process and solving the problem of recycling homogeneous catalysts (Review). *Petroleum Chemistry*, 55(8):587–603, 2015. ISSN 0965-5441. doi: 10.1134/S0965544115080046. URL http://link.springer.com/10.1134/S0965544115080046.

R. M. Gould, L. S. White, and C. R. Wildemuth. Membrane separation in solvent lube dewaxing. *Environmental progress*, 20(1):12–16, 2001.

C. Guo, D. De Kee, and B. Harrison. Free volume model and diffusion of organic solvents in natural rubber. *Journal of applied polymer science*, 56(7):817–822, 1995.

S. Guruvenket, G. M. Rao, M. Komath, and A. M. Raichur. Plasma surface modification of polystyrene and polyethylene. *Applied Surface Science*, 236(1-4):278–284, 2004.

F. Hansen. The measurement of surface energy of polymers by means of contact angles of liquids on solid surfaces. *A short overview of frequently used methods. University ...*, pages 1–12, 2004. URL http://folk.uio.no/fhansen/surface{_}energy.pdf.

K. Haubert, T. Drier, and D. Beebe. Pdms bonding by means of a portable, low-cost corona system. *Lab on a Chip*, 6(12):1548–1549, 2006.

R. A. Hayes. Polyimide gas separation membranes, Jan. 5 1988. US Patent 4,717,393.

J. Hedrick, H. Brown, W. Volksen, M. Sanchez, C. Plummer, and J. Hilborn. Low-stress polyimide block copolymers. *Polymer*, 38(3):605–613, 1997.

K. Hendrix, K. Vanherck, and I. F. Vankelecom. Optimization of solvent resistant nanofiltration membranes prepared by the in-situ diamine crosslinking method. *Journal of Membrane Science*, 421-422:15–24, 2012. ISSN 03767388. doi: 10.1016/j.memsci.2012.06.022. URL http://dx.doi.org/10.1016/j.memsci.2012.06.022.

S. Hermans, H. Mariën, C. Van Goethem, and I. F. Vankelecom. Recent developments in thin film (nano)composite membranes for solvent resistant nanofiltration. *Current Opinion in Chemical Engineering*, 8(Figure 1):45–54, 2015. ISSN 22113398. doi: 10.1016/j.coche.2015.01.009.

H.-J. Hettlich, F. Otterbach, C. Mittermayer, R. Kaufmann, and D. Klee. Plasma-induced surface modifications on suicone intraocular lenses: chemical analysis and in vitro characterization. *Biomaterials*, 12(5):521–524, 1991.

N. Hilal, H. Al-Zoubi, N. A. Darwish, A. W. Mohammad, and M. Abu Arabi. A comprehensive review of nanofiltration membranes: Treatment, pretreatment, modelling, and atomic force microscopy. *Desalination*, 170(3):281–308, 2004. ISSN 00119164. doi: 10.1016/j.desal.2004.01.007.

B. Hofs, A. De Keizer, and M. Cohen Stuart. On the stability of (highly aggregated) polyelectrolyte complexes containing a charged-block-neutral diblock copolymer. *The Journal of Physical Chemistry B*, 111(20):5621–5627, 2007.

H. B. Hopfenberg, N. S. Schneider, and F. Votta. Monohydric alcohol transport in a rubbery poly (urethan). *Journal of Macromolecular Science, Part B: Physics*, 3(4):751–766, 1969.

S. R. Hosseinabadi, K. Wyns, V. Meynen, R. Carleer, P. Adriaensens, A. Buekenhoudt, and B. Van der Bruggen. Organic solvent nanofiltration with grignard functionalised ceramic nanofiltration membranes. *Journal of Membrane Science*, 454:496–504, 2014.

Y. Hu, K. Lu, F. Yan, Y. Shi, P. Yu, S. Yu, S. Li, and C. Gao. Enhancing the performance of aromatic polyamide reverse osmosis membrane by surface modification via covalent attachment of polyvinyl alcohol (pva). *Journal of Membrane Science*, 501:209–219, 2016.

J. L. Humphrey. *Separation process technology.* McGraw-Hill (canada), 1997.

G. Hung. Solvent-polymer interaction: I. molecular transport of some selected organic liquids in polymer membrane. *Microchemical Journal*, 19(2):130–152, 1974.

G. Hung and J. Autian. Use of thermal gravimetric analysis in sorption studies ii: Evaluation of diffusivity and solubility of a series of aliphatic alcohols in polyurethan. *Journal of pharmaceutical sciences*, 61(7):1094–1098, 1972.

Á. W. Imre, M. Schönhoff, and C. Cramer. A conductivity study and calorimetric analysis of dried poly (sodium 4-styrene sulfonate)/poly (diallyldimethylammonium chloride) polyelectrolyte complexes. *The Journal of chemical physics*, 128(13):134905, 2008.

N. Inagaki. *Plasma surface modification and plasma polymerization*. CRC Press, 2014.

Y. Iwai, S. Miyamoto, H. Ikeda, Y. Arai, S. Kobuchi, and Y. Sano. Measurement and correlation of mutual diffusion coefficients for styrene-butadiene rubber (sbr)-n-nonane systems. *Polymer Engineering & Science*, 33(6):322–327, 1993.

J. C. Jansen, S. Darvishmanesh, F. Tasselli, F. Bazzarelli, P. Bernardo, E. Tocci, K. Friess, A. Randova, E. Drioli, and B. Van der Bruggen. Influence of the blend composition on the properties and separation performance of novel solvent resistant polyphenylsulfone/polyimide nanofiltration membranes. *Journal of Membrane Science*, 447:107–118, 2013. ISSN 03767388. doi: 10.1016/j.memsci.2013.07.009. URL http://dx.doi.org/10.1016/j.memsci.2013.07.009.

M. Janssen, C. Mueller, and D. Vogt. Recent advances in the recycling of homogeneous catalysts using membrane separation. *Green Chemistry*, 13(9):2247–2257, 2011.

L. Y. Jiang, Y. Wang, T.-S. Chung, X. Y. Qiao, and J.-Y. Lai. Polyimides membranes for pervaporation and biofuels separation. *Progress in Polymer Science*, 34(11):1135–1160, 2009.

M. F. Jimenez Solomon, Y. Bhole, and A. G. Livingston. High flux hydrophobic membranes for organic solvent nanofiltration (OSN)-Interfacial polymerization, surface modification and solvent activation. *Journal of Membrane Science*, 434:193–203, 2013. ISSN 03767388. doi: 10.1016/j.memsci.2013.01.055. URL http://dx.doi.org/10.1016/j.memsci.2013.01.055.

W. John, C. Buckley, E. Jacobs, and R. Sanderson. Synthesis and use of polydadmac for water purification. In *Biennial Conference of the Water Institute of Southern Africa, Durban, South Africa*, 2002.

N. Joseph, P. Ahmadiannamini, R. Hoogenboom, and I. F. J. Vankelecom. Layer-by-layer preparation of polyelectrolyte multilayer membranes for separation. *Polym. Chem.*, 5(6): 1817–1831, 2014a. ISSN 1759-9954. doi: 10.1039/C3PY01262J. URL http://xlink.rsc.org/?DOI=C3PY01262J.

N. Joseph, P. Ahmadiannamini, R. Hoogenboom, and I. F. J. Vankelecom. Layer-by-layer preparation of polyelectrolyte multilayer membranes for separation. *Polym. Chem.*, 5(6): 1817–1831, 2014b. ISSN 1759-9954. doi: 10.1039/C3PY01262J. URL http://xlink.rsc.org/?DOI=C3PY01262J.

M. Kang, C. A. Day, A. K. Kenworthy, and E. DiBenedetto. Simplified equation to extract diffusion coefficients from confocal FRAP data. *Traffic*, 13(12):1589–1600, 2012. ISSN 13989219. doi: 10.1111/tra.12008.

O. Kedem and A. Katchalsky. Thermodynamic analysis of the permeability of biological membranes to non-electrolytes. *Biochimica et biophysica Acta*, 27:229–246, 1958.

A. Keraani, T. Renouard, C. Fischmeister, C. Bruneau, and M. Rabiller-Baudry. Recovery of enlarged olefin metathesis catalysts by nanofiltration in an eco-friendly solvent. *ChemSusChem*, 1(11):927–933, 2008. ISSN 1864564X. doi: 10.1002/cssc.200800152.

E. S. Kim, Q. Yu, and B. Deng. Plasma surface modification of nanofiltration (NF) thin-film composite (TFC) membranes to improve anti organic fouling. *Applied Surface Science*, 257(23): 9863–9871, 2011. ISSN 01694332. doi: 10.1016/j.apsusc.2011.06.059. URL http://dx.doi.org/10.1016/j.apsusc.2011.06.059.

I. C. Kim, J. Jegal, and K. H. Lee. Effect of aqueous and organic solutions on the performance of polyamide thin-film-composite nanofiltration membranes. *Journal of Polymer Science, Part B: Polymer Physics*, 40(19):2151–2163, 2002. ISSN 08876266. doi: 10.1002/polb.10265.

H. Kita, T. Inada, K. Tanaka, and K.-i. Okamoto. Effect of photocrosslinking on permeability and permselectivity of gases through benzophenone-containing polyimide. *Journal of membrane science*, 87(1-2):139–147, 1994.

A. B. Koltuniewicz, R. Field, and T. Arnot. Cross-flow and dead-end microfiltration of oily-water emulsion. part i: experimental study and analysis of flux decline. *Journal of Membrane Science*, 102:193–207, 1995.

L. Krasemann and B. Tieke. Selective ion transport across self-assembled alternating multilayers of cationic and anionic polyelectrolytes. *Langmuir*, 16(2):287–290, 2000. ISSN 07437463. doi: 10.1021/la991240z.

K. R. Kull, M. L. Steen, and E. R. Fisher. Surface modification with nitrogen-containing plasmas to produce hydrophilic, low-fouling membranes. *Journal of membrane science*, 246(2):203–215, 2005.

P. Kumlangdudsana, A. Tuantranont, S. T. Dubas, and L. Dubas. Polyelectrolyte multilayers coating for organic solvent resistant microfluidic chips. *Materials Letters*, 65(23-24):3629–3632, 2011. ISSN 0167577X. doi: 10.1016/j.matlet.2011.07.038. URL http://dx.doi.org/10.1016/j.matlet.2011.07.038.

G. Ladam, P. Schaad, J. Voegel, P. Schaaf, G. Decher, and F. Cuisinier. In situ determination of the structural properties of initially deposited polyelectrolyte multilayers. *Langmuir*, 16(3): 1249–1255, 2000.

T. Lampe, S. Eisenberg, and E. R. Cabeo. Plasma surface engineering in the automotive industrytrends and future prospectives. *Surface and Coatings Technology*, 174:1–7, 2003.

W. J. Lau, S. Gray, T. Matsuura, D. Emadzadeh, J. Paul Chen, and A. F. Ismail. A review on polyamide thin film nanocomposite (TFN) membranes: History, applications, challenges and approaches. *Water Research*, 80:306–324, 2015. ISSN 18792448. doi: 10.1016/j.watres.2015.04.037. URL http://dx.doi.org/10.1016/j.watres.2015.04.037.

R. A. Lawton, C. R. Price, A. F. Runge, W. J. Doherty, and S. S. Saavedra. Air plasma treatment of submicron thick PDMS polymer films: Effect of oxidation time and storage conditions. *Colloids and Surfaces A: Physicochemical and Engineering Aspects*, 253(1-3):213–215, 2005. ISSN 09277757. doi: 10.1016/j.colsurfa.2004.11.010.

J. H. Lee, J. W. Park, and H. B. Lee. Cell adhesion and growth on polymer surfaces with hydroxyl groups prepared by water vapour plasma treatment. *Biomaterials*, 12(5):443–448, 1991.

S. R. Lewis, S. Datta, M. Gui, E. L. Coker, F. E. Huggins, S. Daunert, L. Bachas, and D. Bhattacharyya. Reactive nanostructured membranes for water purification. *Proceedings of the National Academy of Sciences*, 108(21):8577–8582, 2011.

X. Li, S. D. Feyter, D. Chen, S. Aldea, P. Vandezande, F. D. Prez, and I. F. J. Vankelecom. Solvent-Resistant Nanofiltration Membranes Based on Multilayered\rPolyelectrolyte Complexes. *Chem. Mater.*, 20(3):3876–3883, 2008. ISSN 08974756. doi: 10.1021/cm703072k.

X. Li, W. Goyens, P. Ahmadiannamini, W. Vanderlinden, S. De Feyter, and I. Vankelecom. Morphology and performance of solvent-resistant nanofiltration membranes based on multilayered polyelectrolytes: Study of preparation conditions. *Journal of Membrane Science*, 358(1-2): 150–157, 2010. ISSN 03767388. doi: 10.1016/j.memsci.2010.04.039. URL http://dx.doi.org/10.1016/j.memsci.2010.04.039.

S. K. Lim, K. Goh, T.-H. Bae, and R. Wang. Polymer-based membranes for solvent-resistant nanofiltration: A review. *Chinese journal of chemical engineering*, 2017.

E. Liston, L. Martinu, and M. Wertheimer. Plasma surface modification of polymers for improved adhesion: a critical review. *Journal of adhesion science and technology*, 7(10):1091–1127, 1993.

X. Liu and M. L. Bruening. Size-Selective Transport of Uncharged Solutes through Multilayer Polyelectrolyte Membranes. *Chemistry of Materials*, 16(2):351–357, 2004. ISSN 08974756. doi: 10.1021/cm034559k.

A. LIVINGSTON, L. PEEVA, S. HAN, D. NAIR, S. S. LUTHRA, L. S. WHITE, and L. M. FREITAS DOS SANTOS. Membrane Separation in Green Chemical Processing. *Annals of the New York Academy of Sciences*, 984(1):123–141, 2003. ISSN 00778923. doi: 10.1111/j.1749-6632.2003.tb05996.x. URL http://doi.wiley.com/10.1111/j.1749-6632.2003.tb05996.x.

S. Loeb. Desalination research in california. *Science*, 147(3663):1241–1242, 1965.

S. Loeb and S. Sourirajan. Saline water conversion-ii. *Advances in chemistry series*, 38:117, 1963.

T. R. Long, A. Gupta, A. L. Miller II, D. G. Rethwisch, and N. B. Bowden. Selective flux of organic liquids and solids using nanoporous membranes of polydicyclopentadiene. *Journal of Materials Chemistry*, 21(37):14265–14276, 2011.

V. V. Lulevich and O. I. Vinogradova. Effect of ph and salt on the stiffness of polyelectrolyte multilayer microcapsules. *Langmuir*, 20(7):2874–2878, 2004.

S. S. Luthra, X. Yang, L. M. Freitas Dos Santos, L. S. White, and A. G. Livingston. Homogeneous phase transfer catalyst recovery and re-use using solvent resistant membranes. *Journal of Membrane Science*, 201(1-2):65–75, 2002. ISSN 03767388. doi: 10.1016/S0376-7388(01)00704-9.

R. Ma, Y.-L. Ji, X.-D. Weng, Q.-F. An, and C.-J. Gao. High-flux and fouling-resistant reverse osmosis membrane prepared with incorporating zwitterionic amine monomers via interfacial polymerization. *Desalination*, 381:100–110, 2016.

D. R. MacHado, D. Hasson, and R. Semiat. Effect of solvent properties on permeate flow through nanofiltration membranes. Part I: Investigation of parameters affecting solvent flux. *Journal of Membrane Science*, 163(1):93–102, 1999. ISSN 03767388. doi: 10.1016/S0376-7388(99)00158-1.

R. Machado, D. Hasson, and R. Semiat. Effect of solvent properties on permeate flow through nanofiltration membranes Part II . Transport model. 166:63–69, 2000.

S. Manjula and R. Subramanian. Membrane technology in degumming, dewaxing, deacidifying, and decolorizing edible oils. *Critical reviews in food science and nutrition*, 46(7):569–592, 2006.

P. Marchetti, A. Butté, and A. G. Livingston. NF in organic solvent/water mixtures: Role of preferential solvation. *Journal of Membrane Science*, 444:101–115, 2013. ISSN 03767388. doi: 10.1016/j.memsci.2013.04.069. URL http://dx.doi.org/10.1016/j.memsci.2013.04.069.

P. Marchetti, M. F. Jimenez Solomon, G. Szekely, and A. G. Livingston. Molecular separation with organic solvent nanofiltration: A critical review. *Chemical Reviews*, 114(21):10735–10806, 2014a. ISSN 15206890. doi: 10.1021/cr500006j.

P. Marchetti, M. F. J. Solomon, G. Szekely, and A. G. Livingston. Molecular Separation with Organic Solvent Nano fi ltration : A Critical Review. *Chem. Rev.*, 114:10735–10806, 2014b. ISSN 1520-6890. doi: 10.1021/cr500006j.

B. C. Mello, J. C. C. Petrus, and M. D. Hubinger. Concentration of flavonoids and phenolic compounds in aqueous and ethanolic propolis extracts through nanofiltration. *Journal of Food Engineering*, 96(4):533–539, 2010.

T. Merkel, V. Bondar, K. Nagai, B. Freeman, and I. Pinnau. Gas sorption, diffusion, and permeation in poly (dimethylsiloxane). *Journal of Polymer Science Part B: Polymer Physics*, 38(3):415–434, 2000.

M. Michel, V. Toniazzo, D. Ruch, and V. Ball. Deposition mechanisms in layer-by-layer or step-by-step deposition methods: From elastic and impermeable films to soft membranes with ion exchange properties. *ISRN Materials Science*, 2012, 2012.

J. Micovic, K. Werth, and P. Lutze. Hybrid separations combining distillation and organic solvent nanofiltration for separation of wide boiling mixtures. *Chemical Engineering Research and Design*, 92(11):2131–2147, 2014. ISSN 02638762. doi: 10.1016/j.cherd.2014.02.012. URL http://dx.doi.org/10.1016/j.cherd.2014.02.012.

M. D. Miller and M. L. Bruening. Controlling the nanofiltration properties of multilayer polyelectrolyte membranes through variation of film composition. *Langmuir*, 20(26):11545–11551, 2004. ISSN 07437463. doi: 10.1021/la0479859.

M. D. Miller and M. L. Bruening. Correlation of the swelling and permeability of polyelectrolyte multilayer films. *Chemistry of Materials*, 17(21):5375–5381, 2005. ISSN 08974756. doi: 10.1021/cm0512225.

M. Minelli and G. C. Sarti. Permeability and diffusivity of co2 in glassy polymers with and without plasticization. *Journal of membrane science*, 435:176–185, 2013.

A. K. Mishra. *Smart Ceramics: Preparation, Properties, and Applications*. Pan Stanford, 2018.

A. W. Mohammad, Y. H. Teow, W. L. Ang, Y. T. Chung, D. L. Oatley-Radcliffe, and N. Hilal. Nanofiltration membranes review: Recent advances and future prospects. *Desalination*, 356:226–254, 2015. ISSN 00119164. doi: 10.1016/j.desal.2014.10.043. URL http://dx.doi.org/10.1016/j.desal.2014.10.043.

M. Morra, E. Occhiello, and F. Garbassi. Surface characterization of plasma-treated ptfe. *Surface and Interface Analysis*, 16(1-12):412–417, 1990.

M. D. Moussallem, S. G. Olenych, S. L. Scott, T. C. Keller III, and J. B. Schlenoff. Smooth muscle cell phenotype modulation and contraction on native and cross-linked polyelectrolyte multilayers. *Biomacromolecules*, 10(11):3062–3068, 2009.

M. Mulder. Basic Principles of Membrane Technology, 1998. ISSN 03767388. URL http://linkinghub.elsevier.com/retrieve/pii/037673889285058Q{%}5Cnhttp://scholar.google.com/scholar?hl=en{&}btnG=Search{&}q=intitle:basic+principles+of+membrane+technology{#}1{%}5Cnhttp://scholar.google.com/scholar?hl=en{&}btnG=Search{&}q=intitle:Basic+principles+of+me.

D. Nair, S. S. Luthra, J. T. Scarpello, L. S. White, L. M. Freitas dos Santos, and A. G. Livingston. Homogeneous catalyst separation and re-use through nanofiltration of organic solvents. *Desalination*, 147(1-3):301–306, 2002. ISSN 00119164. doi: 10.1016/S0011-9164(02)00556-8.

Y. Nakayama, T. Takahagi, F. Soeda, K. Hatada, S. Nagaoka, J. Suzuki, and A. Ishitani. Xps analysis of nh3 plasma-treated polystyrene films utilizing gas phase chemical modification. *Journal of Polymer Science Part A: Polymer Chemistry*, 26(2):559–572, 1988.

P. Nazaran, V. Bosio, W. Jaeger, D. F. Anghel, and R. V. Klitzing. Lateral mobility of polyelectrolyte chains in multilayers. *Journal of Physical Chemistry B*, 111(29):8572–8581, 2007. ISSN 15206106. doi: 10.1021/jp068768e.

P. Nestler, M. Paßvogel, and C. A. Helm. Influence of polymer molecular weight on the parabolic and linear growth regime of pdadmac/pss multilayers. *Macromolecules*, 46(14):5622–5629, 2013.

L. Y. Ng, A. W. Mohammad, C. Y. Ng, C. P. Leo, and R. Rohani. Development of nanofiltration membrane with high salt selectivity and performance stability using polyelectrolyte multilayers. *Desalination*, 351:19–26, 2014. ISSN 00119164. doi: 10.1016/j.desal.2014.07.020. URL http://dx.doi.org/10.1016/j.desal.2014.07.020.

S. P. Nunes and K.-V. Peinemann. *Membrane technology: in the chemical industry*. John Wiley & Sons, 2006.

I. Ojima, C.-Y. Tsai, M. Tzamarioudaki, and D. Bonafoux. The hydroformylation reaction. *Organic Reactions*, 2000.

D. Ormerod, B. Sledsens, G. Vercammen, D. Van Gool, T. Linsen, A. Buekenhoudt, and B. Bongers. Demonstration of purification of a pharmaceutical intermediate via organic solvent nanofiltration in the presence of acid. *Separation and Purification Technology*, 115:158–162, 2013. ISSN 13835866. doi: 10.1016/j.seppur.2013.05.007. URL http://dx.doi.org/10.1016/j.seppur.2013.05.007.

D. A. Patterson, L. Y. Lau, C. Roengpithya, E. J. Gibbins, and A. G. Livingston. Membrane selectivity in the organic solvent nanofiltration of trialkylamine bases. *Desalination*, 218(1-3):248–256, 2008.

D. Paul. Gas transport in homogeneous multicomponent polymers. *Journal of membrane Science*, 18:75–86, 1984.

D. R. Paul. Relation between hydraulic permeability and diffusion in homogeneous swollen membranes. *Journal of Polymer Science: Polymer Physics Edition*, 11(2):289–296, 1973.

M. Paul and S. D. Jons. Chemistry and fabrication of polymeric nanofiltration membranes: A review. *Polymer*, 103:417–456, 2016.

S. J. Pearton and D. P. Norton. Dry etching of electronic oxides, polymers, and semiconductors. *Plasma Processes and Polymers*, 2(1):16–37, 2005.

L. Peeva, J. d. S. Burgal, I. Valtcheva, and A. G. Livingston. Continuous purification of active pharmaceutical ingredients using multistage organic solvent nanofiltration membrane cascade. *Chemical Engineering Science*, 116:183–194, 2014. ISSN 00092509. doi: 10.1016/j.ces.2014.04.022. URL http://dx.doi.org/10.1016/j.ces.2014.04.022.

L. G. Peeva, E. Gibbins, S. S. Luthra, L. S. White, R. P. Stateva, and A. G. Livingston. Effect of concentration polarisation and osmotic pressure on flux in organic solvent nanofiltration. *Journal of Membrane Science*, 236(1-2):121–136, 2004. ISSN 03767388. doi: 10.1016/j.memsci.2004.03.004.

M. M. N. T. Pelarut, N. S. RAzAk, M. S. SHAHARuN, and H. M. M. F. TAHA. Separation of hydridocarbonyltris (triphenylphosphine) rhodium (i) catalyst using solvent resistant nanofiltration membrane. *Sains Malaysiana*, 42(4):515–520, 2013.

R. A. Pertile, F. K. Andrade, C. Alves Jr, and M. Gama. Surface modification of bacterial cellulose by nitrogen-containing plasma for improved interaction with cells. *Carbohydrate Polymers*, 82 (3):692–698, 2010.

D. Peshev, L. Peeva, G. Peev, I. Baptista, and A. Boam. Application of organic solvent nanofiltration for concentration of antioxidant extracts of rosemary (rosmarinus officiallis l.). *Chemical engineering research and design*, 89(3):318–327, 2011.

R. J. Petersen. Composite reverse osmosis and nanofiltration membranes. *Journal of membrane science*, 83(1):81–150, 1993.

S. Petrov, P. Atanasova, P. Dineff, and T. Vladkova. Surface modification of polymeric ultrafiltration membranes i. effect of atmospheric pressure barrier discharge in air onto some characteristics of polyacrylonitrile ultrafiltration membranes. *High Energy Chemistry*, 46(4):283–291, 2012.

M. Peyravi, M. Jahanshahi, A. Rahimpour, A. Javadi, and S. Hajavi. Novel thin film nanocomposite membranes incorporated with functionalized TiO2nanoparticles for organic solvent nanofiltration. *Chemical Engineering Journal*, 241:155–166, 2014a. ISSN 13858947. doi: 10.1016/j.cej.2013.12.024. URL http://dx.doi.org/10.1016/j.cej.2013.12.024.

M. Peyravi, M. Jahanshahi, A. Rahimpour, A. Javadi, and S. Hajavi. Novel thin film nanocomposite membranes incorporated with functionalized tio2 nanoparticles for organic solvent nanofiltration. *Chemical Engineering Journal*, 241:155–166, 2014b.

C. Picart. Polyelectrolyte multilayer films: from physico-chemical properties to the control of cellular processes. *Current medicinal chemistry*, 15(7):685–697, 2008.

C. Picart, J. Mutterer, Y. Arntz, J.-C. Voegel, P. Schaaf, and B. Senger. Application of fluorescence recovery after photobleaching to diffusion of a polyelectrolyte in a multilayer film. *Microscopy Research and Technique*, 66(1):43–57, 2005. ISSN 1059-910X. doi: 10.1002/jemt.20142. URL http://doi.wiley.com/10.1002/jemt.20142.

F. Pincet, V. Adrien, R. Yang, J. Delacotte, J. E. Rothman, W. Urbach, and D. Tareste. FRAP to characterize molecular diffusion and interaction in various membrane environments. *PLoS ONE*, 11(7):1–19, 2016. ISSN 19326203. doi: 10.1371/journal.pone.0158457.

A. F. Pinheiro, D. Hoogendoorn, A. Nijmeijer, and L. Winnubst. Development of a pdms-grafted alumina membrane and its evaluation as solvent resistant nanofiltration membrane. *Journal of membrane science*, 463:24–32, 2014.

S. Postel, G. Spalding, M. Chirnside, and M. Wessling. On negative retentions in organic solvent nanofiltration. *Journal of Membrane Science*, 447:57–65, 2013. ISSN 03767388. doi: 10.1016/j.memsci.2013.06.009.

S. Postel, C. Schneider, and M. Wessling. Solvent dependent solute solubility governs retention in silicone based organic solvent nanofiltration. *Journal of Membrane Science*, 497:47–54, 2016. ISSN 18733123. doi: 10.1016/j.memsci.2015.09.014. URL http://dx.doi.org/10.1016/j.memsci.2015.09.014.

M. Priske, K. D. Wiese, A. Drews, M. Kraume, and G. Baumgarten. Reaction integrated separation of homogenous catalysts in the hydroformylation of higher olefins by means of organophilic nanofiltration. *Journal of Membrane Science*, 360(1-2):77–83, 2010. ISSN 03767388. doi: 10.1016/j.memsci.2010.05.002. URL http://dx.doi.org/10.1016/j.memsci.2010.05.002.

M. Priske, M. Lazar, C. Schnitzer, and G. Baumgarten. Recent Applications of Organic Solvent Nanofiltration. *Chemie Ingenieur Technik*, 88(1-2):39–49, 2016. ISSN 0009286X. doi: 10.1002/cite.201500084. URL http://doi.wiley.com/10.1002/cite.201500084.

M. Rabiller-Baudry, G. Nasser, T. Renouard, D. Delaunay, and M. Camus. Comparison of two nanofiltration membrane reactors for a model reaction of olefin metathesis achieved in toluene. *Separation and Purification Technology*, 116:46–60, 2013a. ISSN 13835866. doi: 10.1016/j.seppur.2013.04.052. URL http://dx.doi.org/10.1016/j.seppur.2013.04.052.

M. Rabiller-Baudry, G. Nasser, T. Renouard, D. Delaunay, and M. Camus. Comparison of two nanofiltration membrane reactors for a model reaction of olefin metathesis achieved in toluene. *Separation and Purification Technology*, 116:46–60, 2013b.

G. Z. Ramon, M. C. Wong, and E. M. Hoek. Transport through composite membrane, part 1: Is there an optimal support membrane? *Journal of membrane science*, 415:298–305, 2012.

A. Readiness and F. Industries. Evonik Innovation Award 2009. 2010.

S. R. Reijerkerk, M. H. Knoef, K. Nijmeijer, and M. Wessling. Poly (ethylene glycol) and poly (dimethyl siloxane): Combining their advantages into efficient co2 gas separation membranes. *Journal of membrane science*, 352(1-2):126–135, 2010.

S. Rezaei Hosseinabadi, K. Wyns, V. Meynen, R. Carleer, P. Adriaensens, A. Buekenhoudt, and B. Van der Bruggen. Organic solvent nanofiltration with Grignard functionalised ceramic nanofiltration membranes. *Journal of Membrane Science*, 454:496–504, 2014. ISSN 03767388. doi: 10.1016/j.memsci.2013.12.032.

J. P. Robinson, E. S. Tarleton, C. R. Millington, and A. Nijmeijer. Solvent flux through dense polymeric nanofiltration membranes. *Journal of Membrane Science*, 230(1-2):29–37, 2004. ISSN 03767388. doi: 10.1016/j.memsci.2003.10.027.

J. P. Robinson, E. S. Tarleton, K. Ebert, C. R. Millington, and A. Nijmeijer. Influence of cross-linking and process parameters on the separation performance of poly(dimethylsiloxane) nanofiltration membranes. *Industrial and Engineering Chemistry Research*, 44(9):3238–3248, 2005a. ISSN 08885885. doi: 10.1021/ie0496277.

J. P. Robinson, E. S. Tarleton, K. Ebert, C. R. Millington, and A. Nijmeijer. Influence of cross-linking and process parameters on the separation performance of poly (dimethylsiloxane) nanofiltration membranes. *Industrial & engineering chemistry research*, 44(9):3238–3248, 2005b.

E. M. Rundquist, C. J. Pink, and A. G. Livingston. Organic solvent nanofiltration: a potential alternative to distillation for solvent recovery from crystallisation mother liquors. *Green Chemistry*, 14(8):2197, 2012. ISSN 1463-9262. doi: 10.1039/c2gc35216h. URL http://xlink.rsc.org/?DOI=c2gc35216h.

D. Saeki, M. Imanishi, Y. Ohmukai, T. Maruyama, and H. Matsuyama. Stabilization of layer-by-layer assembled nanofiltration membranes by crosslinking via amide bond formation and siloxane bond formation. *Journal of Membrane Science*, 447:128–133, 2013. ISSN 03767388. doi: 10.1016/j.memsci.2013.07.022. URL http://dx.doi.org/10.1016/j.memsci.2013.07.022.

M. Safarpour, A. Khataee, and V. Vatanpour. Thin film nanocomposite reverse osmosis membrane modified by reduced graphene oxide/tio2 with improved desalination performance. *Journal of Membrane Science*, 489:43–54, 2015.

A. F. Sammells and M. V. Mundschau. *Nonporous inorganic membranes: for chemical processing*. John Wiley & Sons, 2006.

J. T. Scarpello, D. Nair, L. M. Freitas Dos Santos, L. S. White, and A. G. Livingston. The separation of homogeneous organometallic catalysts using solvent resistant nanofiltration. *Journal of Membrane Science*, 203(1-2):71–85, 2002a. ISSN 03767388. doi: 10.1016/S0376-7388(01)00751-7.

J. T. Scarpello, D. Nair, L. M. Freitas Dos Santos, L. S. White, and A. G. Livingston. The separation of homogeneous organometallic catalysts using solvent resistant nanofiltration. *Journal of Membrane Science*, 203(1-2):71–85, 2002b. ISSN 03767388. doi: 10.1016/S0376-7388(01)00751-7.

J. B. Schlenoff and S. T. Dubas. Mechanism of polyelectrolyte multilayer growth: charge overcompensation and distribution. *Macromolecules*, 34(3):592–598, 2001.

J. B. Schlenoff, H. Ly, and M. Li. Charge and mass balance in polyelectrolyte multilayers. *Journal of the American Chemical Society*, 120(30):7626–7634, 1998.

P. Schmidt, T. Köse, and P. Lutze. Characterisation of organic solvent nanofiltration membranes in multi-component mixtures: Membrane rejection maps and membrane selectivity maps for conceptual process design. *Journal of Membrane Science*, 429:103–120, 2013. ISSN 03767388. doi: 10.1016/j.memsci.2012.11.031.

P. Schmidt, E. L. Bednarz, P. Lutze, and A. Górak. Characterisation of Organic Solvent Nanofiltration membranes in multi-component mixtures: Process design workflow for utilising targeted solvent modifications. *Chemical Engineering Science*, 115:115–126, 2014. ISSN 00092509. doi: 10.1016/j.ces.2014.03.029.

N. S. Schneider, J. A. Moseman, and N.-H. Sung. Toluene diffusion in butyl rubber. *Journal of Polymer Science Part B: Polymer Physics*, 32(3):491–499, 1994.

D. Schoeps, K. Buhr, M. Dijkstra, K. Ebert, and H. Plenio. Batchwise and continuous organophilic nanofiltration of Grubbs-type olefin metathesis catalysts. *Chemistry - A European Journal*, 15(12):2960–2965, 2009. ISSN 09476539. doi: 10.1002/chem.200802153.

M. Schönhoff, V. Ball, A. R. Bausch, C. Dejugnat, N. Delorme, K. Glinel, R. v. Klitzing, and R. Steitz. Hydration and internal properties of polyelectrolyte multilayers. *Colloids and Surfaces A: Physicochemical and Engineering Aspects*, 303(1-2):14–29, 2007. ISSN 09277757. doi: 10.1016/j.colsurfa.2007.02.054.

M. Schonnhoff. Layered polyelectrolyte complexes: Physics of formation and molecular properties. *Journal of Physics Condensed Matter*, 15(49), 2003. ISSN 09538984. doi: 10.1088/0953-8984/15/49/R01.

R. Selyanchyn, M. Ariyoshi, and S. Fujikawa. Thickness effect on co2/n2 separation in double layer pebax-1657®/pdms membranes. *Membranes*, 8(4):121, 2018.

I. Sereewatthanawut, F. W. Lim, Y. S. Bhole, D. Ormerod, A. Horvath, A. T. Boam, and A. G. Livingston. Demonstration of molecular purification in polar aprotic solvents by organic solvent nanofiltration. *Organic Process Research and Development*, 14(3):600–611, 2010. ISSN 10836160. doi: 10.1021/op100028p.

M. S. Shaharun, A. K. Mustafa, and M. F. Taha. Nanofiltration of rhodium tris (triphenylphosphine) catalyst in ethyl acetate solution. In *AIP Conference Proceedings*, volume 1482, pages 279–283. AIP, 2012.

L. Shao, T.-S. Chung, S. H. Goh, and K. P. Pramoda. Transport properties of cross-linked polyimide membranes induced by different generations of diaminobutane (dab) dendrimers. *Journal of Membrane Science*, 238(1-2):153–163, 2004.

T. Sherwood. Brian. plt and fisher. re, desalination by reverse osmosis. *Industrial and Engineering Chemistry Fundamental*, 6:2–10, 1967.

B. Shi, P. Marchetti, D. Peshev, S. Zhang, and A. G. Livingston. Will ultra-high permeance membranes lead to ultra-efficient processes? Challenges for molecular separations in liquid systems. *Journal of Membrane Science*, 525(July 2016):35–47, 2017. ISSN 18733123. doi: 10.1016/j.memsci.2016.10.014. URL http://dx.doi.org/10.1016/j.memsci.2016.10.014.

W. E. Siew, A. G. Livingston, C. Ates, and A. Merschaert. Molecular separation with an organic solvent nanofiltration cascade - augmenting membrane selectivity with process engineering. *Chemical Engineering Science*, 90:299–310, 2013. ISSN 00092509. doi: 10.1016/j.ces.2012.10.028.

P. Silva. Organic solvent nanofiltration (osn) modelling-from pure solvents to highly rejected solutes. 2007.

P. Silva and A. G. Livingston. Effect of concentration polarisation in organic solvent nanofiltration - flat sheet and spiral wound systems. *Desalination*, 199(1-3):248–250, 2006. ISSN 00119164. doi: 10.1016/j.desal.2006.03.061.

P. Silva, S. Han, and A. G. Livingston. Solvent transport in organic solvent nanofiltration membranes. *Journal of Membrane Science*, 262(1-2):49–59, 2005. ISSN 03767388. doi: 10.1016/j.memsci.2005.03.052.

M. F. J. Solomon, Y. Bhole, and A. G. Livingston. High flux membranes for organic solvent nanofiltration (osn)interfacial polymerization with solvent activation. *Journal of membrane science*, 423:371–382, 2012.

I. Soroko and A. Livingston. Impact of tio2 nanoparticles on morphology and performance of crosslinked polyimide organic solvent nanofiltration (osn) membranes. *Journal of Membrane Science*, 343(1-2):189–198, 2009.

I. Soroko, Y. Bhole, and A. G. Livingston. Environmentally friendly route for the preparation of solvent resistant polyimide nanofiltration membranes. *Green Chem.*, 13(1):162–168, 2011. ISSN 1463-9262. doi: 10.1039/C0GC00155D. URL http://xlink.rsc.org/?DOI=C0GC00155D.

S. Sourirajan. Separation of hydrocarbon liquids by flow under pressure through porous membranes. Technical report, NATIONAL RESEARCH COUNCIL OF CANADA OTTAWA (ONTARIO) DIV OF APPLIED CHEMISTRY, 1964.

K. Spiegler and O. Kedem. Thermodynamics of hyperfiltration (reverse osmosis): criteria for efficient membranes. *Desalination*, 1(4):311–326, 1966.

N. Stafie, D. F. Stamatialis, and M. Wessling. Insight into the transport of hexane-solute systems through tailor-made composite membranes. *Journal of Membrane Science*, 228(1):103–116, 2004. ISSN 03767388. doi: 10.1016/j.memsci.2003.10.002.

H. Strathmann, L. Giorno, and E. Drioli. *Introduction to membrane science and technology*, volume 544. Wiley-VCH Weinheim, 2011.

S. Sugiura, J.-i. Edahiro, K. Sumaru, and T. Kanamori. Surface modification of polydimethylsiloxane with photo-grafted poly (ethylene glycol) for micropatterned protein adsorption and cell adhesion. *Colloids and Surfaces B: Biointerfaces*, 63(2):301–305, 2008.

Q. Sun, Z. Tong, C. Wang, B. Ren, X. Liu, and F. Zeng. Charge density threshold for lbl self-assembly and small molecule diffusion in polyelectrolyte multilayer films. *Polymer*, 46(13): 4958–4966, 2005.

G. Szekely, M. F. Jimenez-Solomon, P. Marchetti, J. F. Kim, and A. G. Livingston. Sustainability assessment of organic solvent nanofiltration: from fabrication to application. *Green Chem.*, 16 (10):4440–4473, 2014. ISSN 1463-9262. doi: 10.1039/C4GC00701H. URL http://xlink.rsc.org/?DOI=C4GC00701H.

H. L. Tan, M. J. McMurdo, G. Pan, and P. G. Van Patten. Temperature dependence of polyelectrolyte multilayer assembly. *Langmuir*, 19(22):9311–9314, 2003.

B. Tansel, J. Sager, T. Rector, J. Garland, R. F. Strayer, L. Levine, M. Roberts, M. Hummerick, and J. Bauer. Significance of hydrated radius and hydration shells on ionic permeability during nanofiltration in dead end and cross flow modes. *Separation and Purification Technology*, 51(1): 40–47, 2006.

E. S. Tarleton, J. P. Robinson, and J. S. Low. Nanofiltration: A technology for selective solute removal from fuels and solvents. *Chemical Engineering Research and Design*, 87(3):271–279, 2009. ISSN 02638762. doi: 10.1016/j.cherd.2008.09.006.

A. R. Teixeira, J. L. Santos, and J. G. Crespo. Assessment of solvent resistant nanofiltration membranes for valorization of deodorizer distillates. *Journal of Membrane Science*, 470:138–147, 2014. ISSN 18733123. doi: 10.1016/j.memsci.2014.07.032. URL http://dx.doi.org/10.1016/j.memsci.2014.07.032.

A. F. Thünemann, M. Müller, H. Dautzenberg, J.-F. Joanny, and H. Löwen. Polyelectrolyte complexes. In *Polyelectrolytes with defined molecular architecture II*, pages 113–171. Springer, 2004.

Y. S. Toh, F. Lim, and A. Livingston. Polymeric membranes for nanofiltration in polar aprotic solvents. *Journal of Membrane Science*, 301(1-2):3–10, 2007.

M. V. Tres, J. C. Racoski, R. Nobrega, and R. B. Carvalho. Solvent recovery from soybean oil / n- butane mixtures using a hollow fiber ultrafiltration membrane. *Brazilian Journal of Chemical Engineering*, 31(01):243–249, 2014. doi: doi.org/10.1590/S0104-66322014000100022.

B. P. Tripathi, N. C. Dubey, and M. Stamm. Functional polyelectrolyte multilayer membranes for water purification applications. *Journal of hazardous materials*, 252:401–412, 2013.

F. Tristan, J. L. Menchaca, F. Cuisinier, and E. Pérez. Granular structure of self-assembled PAA/PAH and PSS/PAH nascent films imaged in situ by LC-AFM. *Journal of Physical Chemistry B*, 112(20):6322–6330, 2008. ISSN 15206106. doi: 10.1021/jp710195e.

I. Tsibranska and B. Tylkowski. Concentration of ethanolic extracts from sideritis ssp. l. by nanofiltration: Comparison of dead-end and cross-flow modes. *Food and Bioproducts Processing*, 91(2):169–174, 2013.

T. Tsuru, T. Sudou, S. I. Kawahara, T. Yoshioka, and M. Asaeda. Permeation of liquids through inorganic nanofiltration membranes. *Journal of Colloid and Interface Science*, 228(2):292–296, 2000. ISSN 00219797. doi: 10.1006/jcis.2000.6955.

T. Tsuru, M. Miyawaki, H. Kondo, T. Yoshioka, and M. Asaeda. Inorganic porous membranes for nanofiltration of nonaqueous solutions. *Separation and purification technology*, 32(1-3):105–109, 2003.

T. Tsuru, H. Kondo, T. Yoshioka, and M. Asaeda. Permeation of nonaqueous solution through organic/inorganic hybrid nanoporous membranes. *AIChE journal*, 50(5):1080–1087, 2004.

S. Tul Muntha, A. Kausar, and M. Siddiq. Advances in Polymeric Nanofiltration Membrane: A Review. *Polymer - Plastics Technology and Engineering*, 56(8):841–856, 2017. ISSN 15256111. doi: 10.1080/03602559.2016.1233562. URL http://dx.doi.org/10.1080/03602559.2016.1233562.

B. Van der Bruggen, J. Schaep, D. Wilms, and C. Vandecasteele. Influence of molecular size, polarity and charge on the retention of organic molecules by nanofiltration. *Journal of Membrane Science*, 156(1):29–41, 1999.

B. Van der Bruggen, J. Geens, and C. Vandecasteele. Influence of organic solvents on the performance of polymeric nanofiltration membranes. *Separation Science and Technology*, 37(4): 783–797, 2002. ISSN 01496395. doi: 10.1081/SS-120002217.

B. Van der Bruggen, M. Mänttäri, and M. Nyström. Drawbacks of applying nanofiltration and how to avoid them: a review. *Separation and Purification Technology*, 63(2):251–263, 2008.

B. Van der Bruggen, M. M??ntt??ri, and M. Nystr??m. Drawbacks of applying nanofiltration and how to avoid them: A review. *Separation and Purification Technology*, 63(2):251–263, 2008. ISSN 13835866. doi: 10.1016/j.seppur.2008.05.010.

P. Vandezande, L. E. M. Gevers, and I. F. J. Vankelecom. Solvent resistant nanofiltration: separating on a molecular level. *Chem. Soc. Rev.*, 37(2):365–405, 2008a. ISSN 0306-0012. doi: 10.1039/B610848M. URL http://xlink.rsc.org/?DOI=B610848M.

P. Vandezande, L. E. M. Gevers, and I. F. J. Vankelecom. Solvent resistant nanofiltration: separating on a molecular level. *Chem. Soc. Rev.*, 37(2):365–405, 2008b. ISSN 0306-0012. doi: 10.1039/B610848M. URL http://xlink.rsc.org/?DOI=B610848M.

K. Vanherck, A. Aerts, J. Martens, and I. Vankelecom. Hollow filler based mixed matrix membranes. *Chemical communications*, 46(14):2492–2494, 2010.

K. Vanherck, S. Hermans, T. Verbiest, and I. Vankelecom. Using the photothermal effect to improve membrane separations via localized heating. *Journal of Materials Chemistry*, 21(16):6079–6087, 2011.

K. Vanherck, G. Koeckelberghs, and I. F. J. Vankelecom. Crosslinking polyimides for membrane applications: A review. *Progress in Polymer Science*, 38(6):874–896, 2013. ISSN 00796700. doi: 10.1016/j.progpolymsci.2012.11.001. URL http://dx.doi.org/10.1016/j.progpolymsci.2012.11.001.

I. F. Vankelecom and L. E. Gevers. *Membrane processes*. Wiley WCH: Germany, 2005.

A. Vidyasagar, C. Sung, K. Losensky, and J. L. Lutkenhaus. ph-dependent thermal transitions in hydrated layer-by-layer assemblies containing weak polyelectrolytes. *Macromolecules*, 45(22): 9169–9176, 2012.

I. Voigt, M. Stahn, A. Junghans, J. Rost, W. Voigt, et al. Integrated cleaning of coloured waste water by ceramic nf membranes. *Separation and Purification Technology*, 25(1-3):509–512, 2001.

A. Volkov, A. Yushkin, Y. Kachula, V. Khotimsky, and V. Volkov. Application of negative retention in organic solvent nanofiltration for solutes fractionation. *Separation and Purification Technology*, 124:43–48, 2014. ISSN 13835866. doi: 10.1016/j.seppur.2013.12.044. URL http://dx.doi.org/10.1016/j.seppur.2013.12.044.

A. V. Volkov, G. A. Korneeva, and G. F. Tereshchenko. Organic solvent nanofiltration: prospects and application. *Russian Chemical Reviews*, 77(11):983–993, 2008. ISSN 0036-021X. doi: 10.1070/RC2008v077n11ABEH003795. URL http://stacks.iop.org/0036-021X/77/i=11/a=R04?key=crossref.9123fd77e64ed369f574f646a52cadaa.

W. Volksen. Polyimides: Polymerization and properties. 2001.

E. M. Vrijenhoek, S. Hong, and M. Elimelech. Influence of membrane surface properties on initial rate of colloidal fouling of reverse osmosis and nanofiltration membranes. *Journal of membrane science*, 188(1):115–128, 2001.

I. Vural Gürsel, T. Noël, Q. Wang, and V. Hessel. Separation/recycling methods for homogeneous transition metal catalysts in continuous flow. *Green Chem.*, 17(4):2012–2026, 2015. ISSN 1463-9262. doi: 10.1039/C4GC02160F. URL http://xlink.rsc.org/?DOI=C4GC02160F.

A. Wacker Chemie. Solid and liquid silicone rubber-material and processing guidelines, 2011.

J. Wang, Z. Wang, J. Wang, and S. Wang. Improving the water flux and bio-fouling resistance of reverse osmosis (ro) membrane through surface modification by zwitterionic polymer. *Journal of Membrane Science*, 493:188–199, 2015.

D. S. Wavhal and E. R. Fisher. Hydrophilic modification of polyethersulfone membranes by low temperature plasma-induced graft polymerization. *Journal of Membrane Science*, 209(1):255–269, 2002.

R. N. Wenzel. Resistance of solid surfaces to wetting by water. *Industrial & Engineering Chemistry*, 28(8):988–994, 1936.

L. S. White. Polyimide membranes for hyperfiltration recovery of aromatic solvents, Jan. 30 2001. US Patent 6,180,008.

L. S. White and A. R. Nitsch. Solvent recovery from lube oil filtrates with a polyimide membrane. *Journal of Membrane Science*, 179(1-2):267–274, 2000.

J. A. Whu, B. C. Baltzis, and K. K. Sirkar. Nanofiltration studies of larger organic microsolutes in methanol solutions. *Journal of Membrane Science*, 170(2):159–172, 2000. ISSN 03767388. doi: 10.1016/S0376-7388(99)00374-9.

J. Wijmans and P. Hao. Influence of the porous support on diffusion in composite membranes. *Journal of Membrane Science*, 494:78–85, 2015.

J. G. Wijmans and R. W. Baker. The solution-diffusion model: a review. *Journal of Membrane Science*, 107:1–21, 1995. ISSN 0376-7388. doi: 10.1016/0376-7388(95)00102-I. URL https://ac.els-cdn.com/037673889500102I/1-s2.0-037673889500102I-main.pdf?{_}tid=7dc8e370-ad0b-46ca-a774-e8b680eb33f0{&}acdnat=1524568864{_}4108330f9dfcfcd9be60a106b436a8d4.

J. S. Wong, L. Hong, S. C. Bae, and S. Granick. Fluorescence recovery after photobleaching measurements of polymers in a surface forces apparatus. *Journal of Polymer Science, Part B: Polymer Physics*, 48(24):2582–2588, 2010. ISSN 08876266. doi: 10.1002/polb.22118.

X. J. Yang, A. G. Livingston, L. Freitas, S. B. Pharmaceuticals, O. P. Mills, and K. Tn. 2001, Experimental observations of nanoltration with organic solvents .pdf. 190:45–55, 2001.

A. E. Yaroshchuk. Solution-diffusion-imperfection model revised. *Journal of Membrane Science*, 101(1-2):83–87, 1995.

D. Yoo, S. S. Shiratori, and M. F. Rubner. Controlling Bilayer Composition and Surface Wettability of Sequentially Adsorbed Multilayers of Weak Polyelectrolytes. *Macromolecules*, 31 (13):4309–4318, 1998. ISSN 0024-9297. doi: 10.1021/ma9800360. URL http://dx.doi.org/10.1021/ma9800360.

S. Zeidler, U. Kätzel, and P. Kreis. Systematic investigation on the influence of solutes on the separation behavior of a PDMS membrane in organic solvent nanofiltration. *Journal of Membrane Science*, 429:295–303, 2013. ISSN 03767388. doi: 10.1016/j.memsci.2012.11.056.

H. Zhang, H. Mao, J. Wang, R. Ding, Z. Du, J. Liu, and S. Cao. Mineralization-inspired preparation of composite membranes with polyethyleneimine–nanoparticle hybrid active layer for solvent resistant nanofiltration. *Journal of Membrane Science*, 470:70–79, 2014a.

H. Zhang, Y. Zhang, L. Li, S. Zhao, H. Ni, S. Cao, and J. Wang. Cross-linked polyacrylonitrile/polyethyleneimine-polydimethylsiloxane composite membrane for solvent resistant nanofiltration. *Chemical Engineering Science*, 106(100):157–166, 2014b. ISSN 00092509. doi: 10.1016/j.ces.2013.11.043. URL http://dx.doi.org/10.1016/j.ces.2013.11.043.

H. Zhang, Z. Ren, Y. Zhang, Q. Yuan, and X. J. Yang. Comparison Between Polydimethylsiloxane and Polyimide-Based Solvent-Resistant Nanofiltration Membranes. *Chemical Engineering Communications*, 203(7):870–879, 2016. ISSN 15635201. doi: 10.1080/00986445.2014.990632. URL http://dx.doi.org/10.1080/00986445.2014.990632.

W. Zhang, M. Wahlgren, and B. Sivik. Membrane characterization by the contact-angle technique .2. characterization of UF-membranes and comparison between the captive bubble and sessile drop as methodes to obtian water contact angles. *Desalination*, 72(3):263–273, 1989. ISSN 0011-9164. URL http://tugraz.summon.serialssolutions.com/2.0.0/link/0/eLvHCXMw3Z1Lb5tAEMdXlppDqypq-lCTNtIcql5WWOYRYw49LHgdaA24sI6VXiIwS9VDrapyL{_}14{_}WTZBxjstJLP

H. C. Zhao, X. T. Wu, W. W. Tian, and S. T. Ren. Synthesis and thermal property of poly (allylamine hydrochloride). In *Advanced Materials Research*, volume 150, pages 1480–1483. Trans Tech Publ, 2011a.

L. Zhao and W. W. Ho. Novel reverse osmosis membranes incorporated with a hydrophilic additive for seawater desalination. *Journal of Membrane Science*, 455:44–54, 2014.

Q. Zhao, Q. F. An, Y. Ji, J. Qian, and C. Gao. Polyelectrolyte complex membranes for pervaporation, nanofiltration and fuel cell applications. *Journal of Membrane Science*, 379(1-2): 19–45, 2011b. ISSN 03767388. doi: 10.1016/j.memsci.2011.06.016. URL http://dx.doi.org/10.1016/j.memsci.2011.06.016.

Y. Zhao and Q. Yuan. Effect of membrane pretreatment on performance of solvent resistant nanofiltration membranes in methanol solutions. *Journal of Membrane Science*, 280(1-2):195–201, 2006a. ISSN 03767388. doi: 10.1016/j.tsf.2005.08.407.

Y. Zhao and Q. Yuan. A comparison of nanofiltration with aqueous and organic solvents. *Journal of Membrane Science*, 279(1-2):453–458, 2006b. ISSN 03767388. doi: 10.1016/j.memsci.2005.12.040.

Y. Zhao, C. Qiu, X. Li, A. Vararattanavech, W. Shen, J. Torres, C. Helix-Nielsen, R. Wang, X. Hu, A. G. Fane, et al. Synthesis of robust and high-performance aquaporin-based biomimetic membranes by interfacial polymerization-membrane preparation and ro performance characterization. *Journal of Membrane Science*, 423:422–428, 2012.

Z.-P. Zhao, J. Li, D.-X. Zhang, and C.-X. Chen. Nanofiltration membrane prepared from polyacrylonitrile ultrafiltration membrane by low-temperature plasma: I. graft of acrylic acid in gas. *Journal of Membrane Science*, 232(1-2):1–8, 2004.

Z.-P. Zhao, J. Li, J. Chen, and C.-X. Chen. Nanofiltration membrane prepared from polyacrylonitrile ultrafiltration membrane by low-temperature plasma: 2. grafting of styrene in vapor phase. *Journal of membrane science*, 251(1-2):239–245, 2005.

C.-Y. Zheng, R. S. Petralia, Y.-X. Wang, and B. Kachar. Fluorescence Recovery After Photobleaching (FRAP) of Fluorescence Tagged Proteins in Dendritic Spines of Cultured Hippocampal Neurons. *Journal of Visualized Experiments*, 9(50):9–11, 2011. ISSN 1940-087X. doi: 10.3791/2568. URL http://www.jove.com/index/Details.stp?ID=2568.

F. Zheng, C. Li, Q. Yuan, and F. Vriesekoop. Influence of molecular shape on the retention of small molecules by solvent resistant nanofiltration (SRNF) membranes: A suitable molecular size parameter. *Journal of Membrane Science*, 318(1-2):114–122, 2008. ISSN 03767388. doi: 10.1016/j.memsci.2008.02.046.

J. M. Zielinski and J. Duda. Influence of concentration on the activation energy for diffusion in polymer-solvent systems. *Journal of Polymer Science Part B: Polymer Physics*, 30(10): 1081–1088, 1992a.

J. M. Zielinski and J. Duda. Predicting polymer/solvent diffusion coefficients using free-volume theory. *AIChE Journal*, 38(3):405–415, 1992b.

B. J. Zwolinski, H. Eyring, and C. E. Reese. Diffusion and membrane permeability. *The Journal of physical chemistry*, 53(9):1426–1453, 1949.

Index

CO_2/N_2 selectivity, 60

Interfacial complexation, 47

Air permeability, 157
Amine coupling, 49
ANR MemChem, 1, 4
Asymmetric composites, 14

Best Available Technology (BAT), 13

C44, 61
Cascade, 178
Ceramic membranes, 18
Chain mobility, 126
Charge density, 120
charge density, 104
Charge inversion, 47
chemical potential, 30
Compaction, 15
Concentration modulus, 170
Concentration polarization, 168
Concentration polarization (CP), 36
Critical OSN parameters, 38
Cross-flow nanofiltration, 17

Darcys law , 33
Dead-end nanofiltration, 17
Dense OSN membrane, 57
Desorption, 31
Diffusion, 31
Diffusion in Polyurethane(PU, 35
Diffusion in rubbers, 35

Extrinsic-intrinsic charges, 48

Fedor group contribution, 132
Flux,J, 16

Gas Chromatograph, 197
Gierer-Wirtz equation, 134
Glassy polymer, 35
Gutter layer, 113

HagenPoiseuille (H-P), 153
HagenPoiseuille model, 153
Hansen solubility parameter, 132
Hansen solubility parameters, 104
Homogeneous catalysis, 27
Hybrid process, 181
Hydroformylation, 1, 4

imageJ, 148
Integrally skinned asymmetric (ISA), 19
Integrally Skinned Asymmetric (ISA) membrane, 19
Intrinsic permeability in PEL, 124
Intrinsic permeance, 139

Knudsen diffusion, 161
Knudsen selectivity, 60

Mark-Houwink parameters, 134
Max-Dewax, 23
Membrane modification techniques, 42
Membrane-solvent-solute and process parameters., 36
Mercury Porosimetry, 158
Mixed Matrix Membranes (MMM), 19
Modification of membranes, 38
Multilayer numbers and PELs zone model, 50

non-equilibrium plasma, 42

OSN cascades, 178
OSN features, 14
OSN Membrane selection criteria, 5
OSN parameters, 35
OSN support materials, 20
oxo process, 4

PDMS, 21
PDMS membranes for OSN, 22
Pecklet number, 170
Permeability, 16
Permeance, 16

Permselective barrier, 30
Phase inversion, 19
PI membranes for OSN, 22
Plasma effect, 45, 115
Plasma modification, 42
Polyelectrolytes, 119
Polyelectrolytes multilayer, 119
Polyelectrolytes structure, 47
Polymer blend, 35
Polymeric OSN membranes, 20
Pore-Flow (PF), 33
Porous OSN membrane, 58

R-BINAP, 55, 61, 63
Resistance-in-series, 31
resistance-in-series, 105
Retention or rejection (R%), 16
Reynolds number, 172
Rubbery polymer, 34

Separations processes, 13
Silane coupling, 49
Solution-Diffusion (SD), 30
solution-diffusion model, 31
Solvent-Resistant Nanofiltration (SRNF), 14
Sorption, 31
Surface properties after modification, 40
Suspension coating process, 18
swelling degree (SD), 14
syngas, 4

the Hagen-Poiseuille model, 33
Thin film composite, 19
Thin Film Composite (TFC) membrane, 19
transmembrane Pressure (TMP), 15
Transport mechanism in multilayer, 113

Water contact angles, 56

Avis de Soutenance

Monsieur Mahbub MORSHED

Génie des Procédés, des Produits et des Molécules

Soutiendra publiquement ses travaux de thèse intitulés

Fractionnement par nanofiltration organique de mélanges liquides modèles de milieux de métathèse. Etude de membranes commerciales, denses et poreuses, et de leurs dérivés obtenus par dépôt de nanocouches de polyélectrolytes

dirigés par Monsieur Denis ROIZARD

Soutenance prévue le ***mardi 16 juillet 2019*** à 14
Lieu : ENSIC 1 rue Grandville 54000 Nancy
Salle : Amphi Donzelot

Composition du jury proposé

M. Denis ROIZARD	Université de Lorraine	Directeur de thèse
Mme Halima ALEM-MARCHAND	Institut Jean Lamour	Co-directeur de thèse
M. Eric FAVRE	ENSIC Université de Lorraine	Examinateur
Mme Murielle RABILLER-BAUDRY	Université de Rennes 1	Examinateur
M. Bart VAN DER BRUGGEN	Process Engineering for Sustainable Systems, Katholieke Universiteit Leuven	Rapporteur
M. Boris LAKARD	Professeur des Universités (PU1) - Institut UTINAM	Rapporteur

Mots-clés : nanofiltration organique,modification de surface,Polyélectrolyte nanocouche (PEL),PDMS,R-BINAP, Toluene,

Résumé :

L'objectif de cette étude était d'améliorer les performances de séparation OSN de membranes commerciales en vue d'applications en métathèse dans laquelle des catalyseurs hautement dilués sont utilisés. Dans ce travail, des membranes polymères commerciales ont d'abord été étudiéespour caractériser leurs performances dans des milieux organiques en utilisant des mélanges binaires très dilués solute-solvant. Sur la base d'une revue de la littérature, il a été montré que la membrane PERVAP4060, dont le PDMS est la couche active dense, était un candidat prometteur pour la nanofiltration milieu organique (OSN). La membrane commerciale Sulzer PERVAP4060 est une membrane composite ayant une mince couche active de 1 à 2 µm ; elle a fait l'objet d'une étude préliminaire détaillée. Le PDMS est un polymère bien connu ayant une structure dense et déjà largement utilisé en perméation gazeuse et en pervaporation. En tant que membrane poreuse, les supports commerciaux AMS et PAN ont également été pris en compte afin d'étudier les performances et de comprendre le mécanisme de transport de matière, de façon analogue au travail réalisé avec le PDMS. Dans cette étude, nous avons considéré la modification sur la surface pour conserver les

propriétés de matrice polymère. Les multicouches de plasma Ar/O2 et/ou de polyélectrolytes ont été utilisées pour la préparation de membranes prototypes comportant des nanocouches minces (quelques nanomètres) à la surface du PDMS. Les membranes non modifiées et modifiées ont été testées dans des conditions OSN en utilisant des mélanges d'alimentation biniares. Plusieurs solutés très dilués, le ligand organophosphoré R-BINAP, un catalyseur de transfert de phase (ToABR) et des alcanes linéaires ont été étudiés pour déterminer le taux de rejet en OSN à partir de solution de toluène. Le R-BINAP et le ToABR ont tous deux été utilisés dans la plage de 0,0001 à 0,5% en masse et la plupart des expériences ont été réalisées ensuite avec des concentrations de 0,05% en masse de soluté dans le toluène. Également dans quelques cas, des alcanes linéaires, C16, C44 ont été utilisés de 0-20wt. % dans le toluène. Il a été montré que le PDMS était capable de retenir 80% de R-BINAP et environ 93% de ToABr dans du toluène. Le taux de rejet de ToABR dans EtOH a atteint environ 95%. Après modification par les dépôt LBL, le taux de rejet est amélioré avec les membranes modifiées PERVAP4060, conduisant à une rétention de 88% du R-BINAP avec un dépôt de 10 bicouches de polyélectrolytes PAH / PSS en surface, ce taux de rejet pouvant atteindre 95% lorsque le nombre de bicouches est de 20. Le taux de rejet de ToABr augmente à 97%. en utilisant la même paire de polyélectrolytes. Les performances de la membrane ont été étudiées sous différentes pressions comprises entre 1 et 40 bars; le haut rejet, encore observé dans ces conditions OSN, plaide résolument en faveur d'un mécanisme de transfert de type solution-diffusion à travers le PDMS. On a également étudié le traitement des mélanges ternaires mimant le mélange catalyseur / solutés / solvant, correspondant à l'hydroformylation ; aucun signe de couplage n'a été détectée et le taux rejet du soluté de masse molaire la plus forte est resté inchangé. D'autre part, l'amélioration du taux de rejet a également observée à partir des membranes poreuses après modification. Le taux de rétention du C44 dans l'AMS a été atteint 75% après modification par 10 bicouches de PDDA / PSS, alors qu'il n'était que de 25% avant modification. Dans le PAN modifié, le taux de rejet des solutés obtenus est dans la plage de 37 à 50%, en utilisant 10 bicouches de PDDA / PSS, alors qu'il n'était que de 3 à 7% en masse avant modification. L'inconvénient de la membrane poreuse est toutefois la forte diminution du flux après le dépôt des couches multiples.